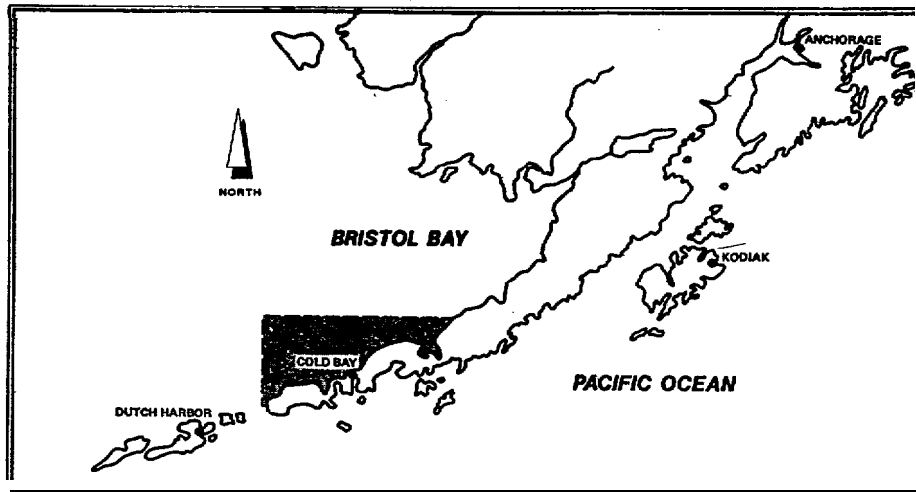


SEAFLOOR GEOLOGIC HAZARDS ON THE NORTHERN ALEUTIAN SHELF



VOLUME 1 TEXT

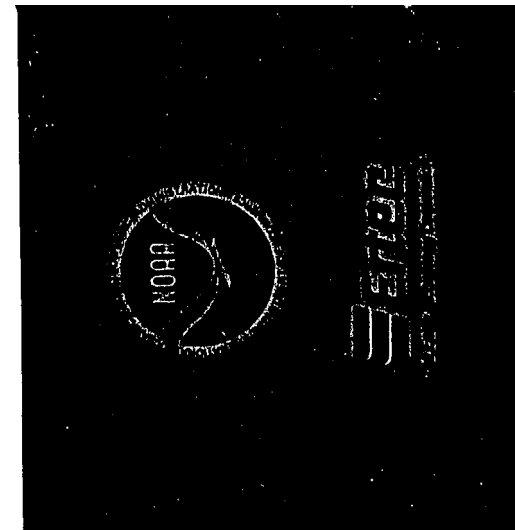
Submitted to
NATIONAL OCEANIC AND ATMOSPHERIC ADMINISTRATION

tte
R W RN N



**SEAFLOOR GEOLOGIC HAZARDS ON
THE NORTHERN ALEUTIAN SHELF**

VOLUME 1 TEXT



SEAFLOOR GEOLOGIC HAZARDS
ON THE
NORTHERN ALEUTIAN SHELF

VOLUME 1 - TEXT

Submitted to:

National Oceanic and Atmospheric Administration
Contracting Office, Room 5532
325 Broadway
Boulder, Colorado 80303

Submitted by:

Ertec Western, Inc.
3777 Long Beach Boulevard
Long Beach, California 90807

Ertec Project No. 80-231

June 1983

Ertec Western, Inc.

3777 Long Beach Boulevard, P.O. Box 7765, Long Beach, California 90807
Telephone: (213) 595-6611/979-1721 • Telex: 656338

July 22, 1983

National Oceanic and Atmospheric
Administration
National Ocean Service
Alaska Office
P.O. Box 1808
Juneau, Alaska 99802

Attention: **Mr. Laurie E. Jarvella**

Subject: Seafloor Geologic Hazards of the
Northern Aleutian Shelf
(Contract No. **NA80-RAC-00167**)

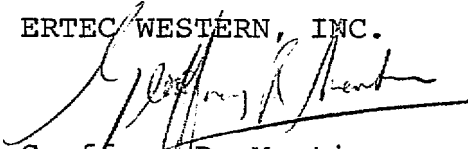
Gentlemen:

Transmitted herewith is **our** final report entitled "Seafloor Geologic Hazards of the Northern Aleutian Shelf". This submittal comprises a camera-ready original, including text, figures, oversize plates and ten bound copies.

This submittal completes our commitments under Contract No. **NA80-RAC-00167**. If there are any questions regarding this report, please do not hesitate to contact us.

Sincerely,

ERTEC WESTERN, INC.


Geoffrey R. Martin
Vice President, Engineering and
Principal-In-Charge

GRM: gn
Attachments

TABLE OF CONTENTS

	<u>Page</u>
LISTOFTABLES	iv
LIST OF FIGURES	v
SUMMARY	ix
1.0 INTRODUCTION	
1.1 BACKGROUND	1-1
1.2 SCOPE OF STUDY	1-2
1.3 ORGANIZATION OF REPORT	1-3
2.0 REGIONAL SETTING	
201 LOCATION AND SETTING OF STUDY AREA	2-1
2.2 OCEANOGRAPHY.	2-2
2.2.1 Hydrography.	2-2
2.2.2 General Circulation	2-3
2.2.3 Waves.	2-4
2.2.4 Tides and Currents	2-5
2.2.5 Longshore Drift	2-6
2.3 METEOROLOGY	2-7
2.3.1 Winds.	2-7
2.3.2 Precipitation.	2-8
2.3.3 Temperatures	2-9
2.4 REGIONAL GEOLOGY.	2-9
2.4.1 Stratigraphy	2-9
2.4.2 Tectonics.	2-14
2.4.3 Seismicity	2-16
2.4.4 Volcanism.	2-17
2.4.5 Magnetics and Metallic Mineral Resources	2-19
3.0 FIELD PROGRAM	
3.1 OPERATIONS	3-1
3.1.1 Vessel and Scientific Crew	3-1
3.1.2 Navigation	3-2

TABLE OF CONTENTS (Cont.)

	<u>Page</u>
3.2 GEOPHYSICAL SURVEY	3-2
3.2.1 Trackline Data...	3-3
3.2.2 Geophysical Equipment	3-3
3.3 SEDIMENT SAMPLING	3-4
3.3.1 Grab and Gravity Core Samples	3-4
3.3.2 Vibracores	3-5
3.3.3 Drop Penetrometer	3-6
4.0 LABORATORY TESTING	4-5
4.1 SAMPLE DISTRIBUTION	4-1
4.2 GEOLOGICAL DESCRIPTION.	4-2
4.2.1 Grain-Size Analyses	4-2
4.2.2 Bulk Mineralogy..	4-3
4.2.3 Total Organic Carbon and Percent CaCO₃	4-3
4.2.4 Age-Dating	4-4
4.3 ENGINEERING CHARACTERISTICS	4-5
4.3.1 Unit Weight and Water Content	4-5
4.3.2 Specific Gravity	4-5
4.3.3 Grain-Size Analyses	4-6
4.3.4 Maximum and Minimum Dry Unit Weights	4-6
4.3.5 Compressibility.	4-7
4.3.6 Permeability	4-7
4.3.7 Static Triaxial Strength	4-8
4.3.8 Liquefaction Resistance	4-8
4.3.9 Shear Modulus and Damping	4-9
4.3.10 Sonic Velocities	4-11
5.0 DATA INTERPRETATION AND RESULTS	
5.1 BATHYMETRIC MAP	5-1
5.2 GEOLOGIC STRUCTURE	5-1
5.2.1 Basement Complex	5-2
5.2.2 Faulting	5-3
5.2.3 Structural Cross-Section A-A'	5-5
5.2.4 Structural Cross-Section B-B'	5-6
5.2.5 Late Quaternary Stratigraphy	5-7

TABLE OF CONTENTS (Cont.)

	<u>Page</u>
5.4 SEISMIC ENVIRONMENT	5-9
5.4.1 Earthquake Sources	5-9
5.4.2 Maximum Earthquakes	5-10
5.4.3 Earthquake Ground Motions	5-18
5.5 SEDIMENT CHARACTERISTICS	5-23
5.5.1 Core Descriptions	5-23
5.5.2 Grain Size	5-24
5.5.3 Mineralogy	5-25
5.5.4 Carbon Content	5-28
5.5.5 Engineering Properties	5-29
5.6 GEOTECHNICAL ANALYSES	5-38
5.6.1 Gravity Loading	5-39
5.6.2 Storm-Wave Loading	5-41
5.6.3 Earthquake Loading	5-46
6.0 POTENTIAL HAZARDS	
6.1 Earthquakes	6-1
6.2 Surface Faulting	6-2
6.3 Volcanoes	6-2
6.4 Soil Instability	6-3
6.5 <i>Shallow</i> Gas and Gas Seeps	6-5
6.6 Sediment Transport	6-5
6.7 Other Possible Hazards	6-6
7.0 CONCLUSIONS AND RECOMMENDATIONS	
7.1 Conclusions	7-1
7.2 Recommendations	7-5
8.0 REFERENCES	

LIST OF APPENDICES

Appendix No.

I	SAMPLE LOCATIONS AND GRAIN-SIZE DISTRIBUTIONS
II	SUMMARY OF LABORATORY TEST RESULTS
III	VIBRACORE DESCRIPTIONS
IV	RESULTS OF LIQUEFACTION ANALYSIS

LIST OF TABLES

<u>Number</u>	<u>Title</u>
2-1	HYDROGRAPHIC DOMAINS - SUMMER CONDITIONS
2-2	MAXIMUM WIND AND WAVE DATA
2-3	ACTIVE VOLCANOES IN THE VICINITY OF THE NORTHERN ALEUTIAN SHELF
3-1	SEISMIC PROFILING SYSTEMS
3-2	NUMBERS OF SAMPLES OBTAINED DURING SEDIMENT SAMPLING PROGRAM
3-3	VIBRACORE SUMMARY
4-1	MINERALOGIC COMPOSITION DETERMINED FROM BULK MINERALOGY ANALYSES
4-2	percentage CARBON (ORGANIC AND INORGANIC) AND CALCIUM CARBONATE CONTENT FOR SELECTED SAMPLES
4-3	MOISTURE CONTENT AND UNIT WEIGHT VALUES FOR SELECTED SAMPLES
4-4	SPECIFIC GRAVITY VALUES FOR SELECTED SAMPLES
4-5	MAXIMUM AND MINIMUM DRY UNIT WEIGHT VALUES FOR SELECTED SAMPLES
4-6	COMPRESSIBILITY PROPERTIES
4-7	PERMEABILITY CHARACTERISTICS OF SELECTED SAMPLES
4-8	SHEARING STRENGTH RESULTS FROM ISOTROPICALLY CONSOLIDATED, DRAIN TRIAxIAL COMPRESSION TESTS (CID)
4-9	CYCLIC SIMPLE SHEAR TEST RESULTS
4-10	LOW AMPLITUDE SHEAR MODULUS FROM RESONANT COLUMN TESTS

LIST OF TABLES (CONT'D)

<u>Number</u>	<u>Title</u>
4-11	CYCLIC TRIAxIAL TEST RESULTS
4-12	SONIC VELOCITY AND OTHER CHARACTERISTICS OF VIBRACORE SAMPLES
5-1	ESTIMATES OF MAXIMUM EARTHQUAKES IN THE NORTHERN ALEUTIAN SHELF REGION
5-2	RECOMMENDED TIME HISTORIES FOR EARTHQUAKE SOURCES
5-3	SUMMARY OF RESULTS FROM DROP PENETROMETER TESTS
5-4	EXPECTED RANGE OF DRY UNIT WEIGHTS
5-5	WAVE HEIGHT HISTOGRAM USED IN LIQUEFACTION STUDIES
5-6	SOIL PROPERTIES FOR LIQUEFACTION ANALYSES
5-7	SUMMARY OF RESULTS FROM LIQUEFACTION ANALYSES

LIST OF FIGURES

<u>Figure No.</u>	<u>Title</u>
2-1	LOCATION MAP OF THE NORTH ALEUTIAN SHELF STUDY AREA
2-2	MAP OF STUDY AREA SHOWING LOCATION OF THE THREE MAJOR SEDIMENTARY BASINS
2-3	HYDROLOGY, GENERAL CIRCULATION, TIDES, BOTTOM CURRENTS AND LONGSHORE DRIFT ON NORTHERN ALEUTIAN SHELF
2-4	COMPOSITE STRATIGRAPHIC COLUMN FOR THE PROPOSED LEASE SALE AREAS 75 AND 92
2-5	LOCATION OF SURFACE SEDIMENT SAMPLING STATIONS
2-6	GENERALIZED GEOLOGY MAP OF WESTERN ALASKA, BERING SEA, AND EASTERN SIBERIA
2-7	REGIONAL SEISMICITY AND RELATIVE MOTION VECTORS ALONG THE ALASKA-ALEUTIAN ARC
2-8	CROSS-SECTIONS SHOWING BENIOFF ZONE OF THE ALASKA-ALEUTIAN SUBDUCTION ZONE

* Also found in Volume 11

LIST OF FIGURES (CONT'D)

<u>Figure No.</u>	<u>Title</u>	
2-9	ACTIVE VOLCANOES IN THE NORTHERN ALEUTIAN SHELF REGION	
3-1	PHOTOGRAPH OF NOAA SHIP DISCOVERER	
3-2	GEOPHYSICAL TRACKLINE-BASELINE REFERENCE SYSTEM	
3-3	VIBRACORE LOCATION MAP	
3-4	PHOTOGRAPH OF DROP PENETROMETER	
3-5	SCHEMATIC DIAGRAM OF DROP PENETROMETER OPERATION	
3-6	DROP PENETROMETER TEST LOCATIONS	
4-1	PHOTOGRAPHS OF CYCLIC SIMPLE SHEAR EQUIPMENT	
4-2	PHOTOGRAPHS OF RESONANT COLUMN EQUIPMENT	
4-3	PHOTOGRAPHS OF RESONANT COLUMN AND CYCLIC TRIAXIAL TEST CHAMBERS	
4-4	PHOTOGRAPHS OF CYCLIC TRIAXIAL EQUIPMENT	
5-1	LOCATION MAP FOR CROSS-SECTIONS A-A' AND B-B'	
5-2	SCHEMATIC GEOLOGIC CROSS-SECTION OF NORTHERN ALEUTIAN SHELF REGION	
5-3	MAP OF MODERATE TO LARGE MAGNITUDE EARTHQUAKES IN THE NORTHERN ALEUTIAN SHELF REGION	
5-4	MAP OF EARTHQUAKES IN THE ST. GEORGE BASIN REGION, 1925 THROUGH 1978	
5-5	SOURCES OF POSTULATED MAXIMUM EARTHQUAKES, NORTHERN ALEUTIAN SHELF REGION	
5-6	PERCENT SAND IN SURFACE SEDIMENTS	*
5-7	MEAN GRAIN SIZE OF SURFACE SEDIMENTS	*
5-8	GRAIN-SIZE STANDARD DEVIATION OF SURFACE SEDIMENTS	*
5-9	SEDIMENT SKEWNESS	*

* Also found in Volume II

LIST OF FIGURES (CONT'D)

<u>Figure No.</u>	<u>Title</u>	
5-10	SEDIMENT KURTOSIS	*
5-11	PERCENT QUARTZ IN SURFACE SEDIMENTS	*
5-12	PERCENT FELDSPAR IN SURFACE SEDIMENTS	*
5-13	RATIO OF QUARTZ TO FELDSPAR IN SURFACE SEDIMENTS	*
5-14	PERCENT HYPERSTHENE IN SURFACE SEDIMENTS	*
5-15	PERCENT HORNBLLENDE IN SURFACE SEDIMENTS	*
5-16	PERCENT OPAQUES IN SURFACE SEDIMENTS	*
5-17	TOTAL ORGANIC CARBON AND PERCENT CALCIUM CARBONATE IN SURFACE SEDIMENTS	*
5-18	DISTRIBUTION OF SOIL TYPES	*
5-19	RANGE OF GRAIN-SIZE CONDITIONS	
5-20	VARIATION OF DRY UNIT WEIGHT WITH MEAN GRAIN SIZE	
5-21	VARIATION OF FRICTION ANGLE AND DRY UNIT WEIGHT	
5-22	RESULTS OF CYCLIC SIMPLE SHEAR TESTS	
5-23	ESTIMATED LIQUEFACTION STRENGTH IN THE FIELD	
5-24	SHEAR MODULUS VALUES USED IN LIQUEFACTION ANALYSES	
5-25	POTENTIAL FOR EARTHQUAKE-INDUCED PORE PRESSURE BUILDUP	

* Also found in Volume II

LIST OF PLATES

Plate No.

I(A) and I(B)	MAP SHOWING LOCATION OF SHALLOW PENETRATION GEOPHYSICAL LINES, BRISTOL BAY EAST AND WEST	**
II(A) and II(B)	MAP SHOWING LOCATION OF DEEP PENETRATION GEOPHYSICAL TRACKLINES , BRISTOL BAY EAST AND WEST	**
III(A) and III(B)	BATHYMETRY MAP, BRISTOL BAY EAST AND WEST	**
IV(A) and IV(B)	MAP OF GEOLOGIC STRUCTURE, BRISTOL BAY EAST AND WEST	**
V(A) and V(B)	MAP OF POTENTIAL GEOLOGIC HAZARDS, BRISTOL BAY EAST AND WEST	**
VI	GEOLOGIC CROSS SECTION A-A'	**
VII	GEOLOGIC CROSS SECTION B-B'	**
VIII(A) and VIII(B)	MAP OF QUATERNARY GEOLOGY, BRISTOL BAY EAST AND WEST	**

** Found in Volume 2

SUMMARY

BACKGROUND

The National Oceanic and Atmospheric Administration (NOAA) contracted the Earth Technology Corporation (Ertec)* to perform a geologic hazards evaluation for the Northern Aleutian Shelf. The objective of this hazards evaluation was to identify geologic conditions which could affect the safe development of lease areas on the shelf. These geologic hazards potentially involved faulting, weak seafloor sediments, slope instabilities and scour.

The area of primary interest in the evaluation was bounded by the Alaskan Peninsula and Unimak Island on the south, latitude 57° 00' on the north, longitude 159° 30' W on the east and longitude 165° W on the west. The eastern and western boundaries roughly intersect Port Moller and Unimak Pass, respectively.

A four-part study involving literature review, field geophysical profiling and sediment sampling, laboratory testing, and data interpretation was initiated to identify these potential hazards. The program was managed by Ertec; significant contributions in the field, laboratory and interpretative phases of the study were made by Mesa², as a subcontractor to Ertec.

REGIONAL SETTING

The Northern Aleutian Shelf comprises a very flat continental shelf with water depths ranging from 0 to 110 m. Oceanographic and meteorologic conditions are a dominant force in the area. Significant wave heights for

* Ertec was formerly called Fugro, Inc.

100-year return periods range from 17 to 23 m, winds can exceed 55 **kts**, tides vary from 2 to 7 m, and currents can exceed 100 **cm/sec**. These conditions affect seafloor soils either **by** direct loading (scour and wave-induced pressure fluctuations) or by loading to structures supported on the soil.

A review of **the** geologic history for the area indicates that the region has undergone several distinct episodes during its formation. The major change occurred during the Late Mesozoic - early Cenozoic, and was presumably associated with abandonment of a regime involving subduction and transform faulting along the continental margin of the Bering Sea and inception of the present day subduction zone along the Aleutian Arc. This transition is represented by a major unconformity between highly deformed basement rocks and relatively undeformed Cenozoic strata, sedimentary rocks and volcanic rocks. These Cenozoic strata are disrupted only by normal faults which indicate a tensional tectonics regime throughout much of the Cenozoic era.

The present geologic and tectonic environment is dominated by seismicity and volcanism. These processes are primarily related to subduction of the Pacific Plate under the Bering - North American **Plate** along the Aleutian Trench. Most earthquakes occur along the trench or in a northerly dipping Benioff zone which dips beneath the Aleutian Arc and the study area. However the presence of scattered earthquakes in the upper crust within the study region and the presence of long, potentially active faults indicates that earthquake hazards are significant within the study region. The Aleutian volcanic arc bounds the study region on the southeast, and at least three of the volcanoes in the portion of the arc adjacent to the study area are **potentially** active.

FIELD PROGRAM

A field program was conducted from the NOAA ship Discoverer in August, September and October of 1980. The objective of the field program was to supplement the existing geologic data base. This objective was accomplished by conducting a geophysical survey and a bottom sampling program. Geophysical equipment included 3.5 kHz, **uniboom**, air **gun**, sparker and side-scan systems. Sediment samples were collected with a Van Veen grab sampler, a gravity corer and a vibracorer. A drop penetrometer was used to obtain in situ soil data.

Over 4000 km of geophysical data were collected. **Tracklines** were oriented approximately north-south and east-west with spacings of 15 to 25 km. Vessel speed ranged from 4 to 5 knots during the survey. The prevalence of crab pots in the area precluded use of side-scan equipment at night, and hence, only partial side-scan coverage was achieved.

Sediment samples and in situ soil resistance data were collected at 60 locations. Only limited sediment penetration (1 to 2 m maximum) **could** be achieved with the gravity corer, the vibracorer and the drop penetrometer. This is attributed to the very dense, **cohesionless** nature of the sediments.

LABORATORY TESTING

Sediment samples recovered during the field program were transported to onshore soil testing facilities at Ertec and California State University, Northridge for detailed analyses. The scope of the testing program included geological descriptions and engineering parameter determinations.

Results of the laboratory studies indicate that **surficial** sediments are very dense silty sands and sands, consisting primarily of quartz, feldspar, hornblende and unidentified opaque minerals. Carbon content is **less** than 1.0 percent. These sediments have wet unit weights ranging from 18 to 21 kN/m^3 ; water contents vary from 20 to 40 percent. The compressibility of the material is low; permeability is relatively high; and effective friction angles range from 37 to 41 degrees. Cyclic strength and stiffness are high.

DATA INTERPRETATION AND RESULTS

Literature, field and laboratory data were interpreted and analyzed collectively to enhance existing information about geologic conditions within the study area. The results of this analysis confirm that the shelf is very flat with slopes generally less than 0.5 percent. The area is underlain by three deep basins (depth to 5000 m) filled with Tertiary sediments. Sediment ages within 1 to 2 m of the seafloor range from 11,000 to 12,000 years **B.P.** Complex faulting occurs at the margins of two basins.

The southeastern portion of the study area is also characterized by earthquakes primarily associated with the subduction of the Pacific Plate beneath the Bering-North American Plate. Based on historic data, a maximum earthquake magnitude of $8 \frac{3}{4}$ is postulated for subduction-related events. The historic record for earthquakes in the crust of the study area is considered to be too short to provide a basis for estimating maximum earthquakes; therefore, worldwide empirical data in similar tectonic environments were analyzed. This analysis indicates that a possibility of

infrequent earthquakes as large as magnitude 7 3/4 exists. Peak ground accelerations from these earthquakes could vary from **0.1g** for the general region to 0.7g near the North Amak Fault Zone.

Sediment stability during static, storm-wave and earthquake loading varies from excellent to poor. The denseness of sediments and the gentleness of slopes should lead to good static stability under normal foundation loading. Storm-wave loading may introduce limited instability due to wave-induced liquefaction in shallow water areas (less than 25 m water depths) or sediment scour. However, the coarseness of **surficial** sediments within this depth regime suggests that the occurrence of these problems will be limited. Large earthquake-induced ground accelerations will likely cause high excess pore-water pressures near earthquake sources. These sources are located near the Amak and Bristol Bay Fault Zones. The effects of high pore pressures are expected to be small because of the denseness of most sediments.

GEOLOGIC HAZARDS

This evaluation documents several potential geologic hazards which must be considered in the design of offshore facilities. These geologic hazards include earthquake-induced ground accelerations, surface faulting, volcanic ejects, soil instabilities, shallow gas and gas seeps, and sediment transport. Earthquake-related hazards (accelerations, faulting and sediment instability) and gas seeps are regarded as the most serious hazards. The severity of these hazards is not regarded as being so great that safe development of the area is precluded. Most of the identified hazards can be accommodated by proper site selection and sound engineering design.

CONCLUSIONS AND RECOMMENDATIONS

This geologic hazards evaluation indicates that geologic hazards exist on the Northern Aleutian Shelf but appear to be manageable within the engineering profession's existing state-of-technology. However, it is also clear from this study that site-specific evaluations will be required before pipelines, platforms or other facilities are installed. Future evaluations must include oceanographic and meteorologic studies to enhance understanding of wave, wind and current conditions. Furthermore, more detailed geophysical and sediment testing programs are essential. Sediment sampling programs for large **fixed-**base structures should include borings to 100 m or more. Future laboratory testing and engineering analyses should quantify soil and foundation behavior under the postulated loading environment.

1.0 INTRODUCTION

1.1 BACKGROUND

This report summarizes the results of a geological hazards evaluation for the southeastern portion of the Northern Aleutian Shelf. The evaluation was conducted by the Earth Technology Corporation (**Ertec**)* for the National Oceanic and Atmospheric Administration (NOAA) under Contract No. NA **80-RAC** 00167. The period of contract performance extended from August 1980 until January 1983.

The geological hazards study was performed in general accordance with a scope of work outlined in NOAA's Request for Proposal (**RFP**) dated April 21, 1980 (Ref NOAA RFP No. 52-80). The general objective of the study, as outlined in the RFP, was to assess the geologic hazards on the Northern Aleutian Shelf by collecting reconnaissance geophysical, geological and **geotechnical** data. These data were to be integrated with all available nonproprietary and existing literature information into a regional geologic and **geotechnical** framework of the study area. Results of the study were to be summarized in a form useable for the Minerals Management Service in lease-sale evaluations. Additional details about the scope of work are presented in Subsection 1.2.

To accomplish this study, Ertec utilized a team of engineers, geologists and consultants. Dr. Donald Anderson of Ertec served as Project Manager. Messrs Charles F. Chamberlain and Bruce A. **Schell** were responsible for field and office geological studies, respectively. Drs. Bill (**T.D.**) Lu and C. B. Crouse of **Ertec** were responsible for **geotechnical** and earthquake engineering studies. Significant phases of the geological studies were conducted by

* At the time of contract award, **Ertec** was called **Fugro** Inc. The name of the company changed in **1981**.

2.0 REGIONAL SETTING

2.1 LOCATION AND SETTING OF STUDY AREA

The study area encompasses approximately 25,000 km in the southeastern section of the Northern Aleutian Shelf in Bristol Bay. It is bounded by the Bering Sea to the north and west and **by** the glaciated, volcanic terrains of the Alaskan Peninsula and Unimak Island to the south, where elevations range from sea level to over 2850 m (Figures 2-1 and 2-2). The area of study extends eastwards along the northern Alaska Peninsula from **Unimak** Pass (165° **W**) to the vicinity of Port **Moller** (159° 30' W) and north to 57° 00' N latitude.

Generally the seafloor within the study area consists of a very flat and shallow continental shelf which deepens to the southwest. The north shelf is regionally flat having a gradient of approximately 0.02 percent (**Sharma**, 1974). Water depths in the study area reach 70 m in the northeast and 110 m in the southwest; the average water depth is about 50 m.

A broad gentle trough paralleling the Alaska Peninsula is the most prominent feature of the bottom topography (Plates 3(A) and 3(B)). The area is also characterized by a series of transverse linear ridges which parallels the trend of the Alaska Peninsula. These ridges occur in a 30 to 50 km wide band, and are oriented in various directions, ranging from east-west to **west-southwest** to east-northeast and exist in maximum water depths which range from 70 to 110 m. The minimum length of the ridges is about 10 km. The area also has three nearly east-west trending structural basins (St. George, Amak and Bristol Bay) (Figure 2-2) which contain sedimentary **stratigraphic** sections in

excess of 4 km thick (Plate VI). These basins are **the** primary areas of interest with respect to future oil and gas production.

2.2 OCEANOGRAPHY

The study area is within a very dynamic and complex oceanographic area. The large shallow portion of the area is recognized as a high latitude estuary characterized by its variability. Water circulation within the area generally comprises a counter-clockwise gyre with normal current velocities of about 5 cm/sec. Semi-diurnal tides average 2 m on the open shelf and 3.3 m at Port **Moller** at the eastern edge of the study area (Brewer and others, 1977). Climatic conditions, intrusions by oceanic water masses, and fresh water inflow contribute to this variability (**Lisitzin**, 1966; U.S. Army Corps of Engineers, 1974; Sharma, 1979). Hydrography, general circulation, tides, bottom currents, and long-shore drift parameters of the area are summarized in Figure 2-3. These are discussed separately below.

2.2.1 Hydrography

Many investigators have studied the hydrography within Bristol Bay and the broader Bering **Shelf** area (**Dodimead** and others, 1963; Arsen'ev, 1967; **Ohtani**, 1973; **Takenouti** and **Ohtani**, 1974; Kinder, 1977; Schumacher and others, 1979; and Kinder and Schumacher, 1980). Early efforts focused on identifying summer water masses in terms of salinity and temperatures.

The results of these studies generally indicate that four distinct water masses occur on the North Aleutian Shelf: 1) oceanic water, 2) outer shelf water, 3) mid-shelf water, and 4) coastal water. The oceanic water originates from the Pacific Ocean and Bering Sea. This water has a temperature 3 to 5

degrees (°) Centigrade (C) and a salinity of 33 to 35 parts per thousand (0/00), respectively. Outer-shelf water is characterized by temperatures of 0.5 to 9.0° C and salinities of 32.7 to 33.0 ‰. Salinities of 31.0 to 32.6 ‰ and temperatures of 1.8 to 9.0° C are typical of mid-shelf waters. Coastal water has salinities **less** than 31.0 ‰ and temperatures between 1.3 and **18.2°** C.

Kinder and Schumacher (1981) describe a three-domain shelf, for the area. The three domains include coastal, middle and outer shelf regions (Table 2-1, Figure 2-3). The coastal domain is **shoreward** of the 50 m isobath and is characterized by generally warm, low salinity, vertically well-mixed water lacking stratification. A strong inner front, defined by an enhanced mean salinity gradient, separates the coastal domain from a middle shelf domain. The middle shelf domain is recognized by a strongly stratified two-layered structure extending to approximately the **100** m isobath. A middle front, at about the 100 m isobath, delineates the third or outer **shelf** domain. The outer shelf domain structure is characterized by a stratified layer with pronounced fine structure, separating surface- and bottom-mixed layers. Beyond the front of the shelf break, ocean water persists. Kinder and Schumacher (1981) suggest that this hydrographic structure is controlled by boundary processes which include tidal and wind stirring, surface cooling, river runoff, and lateral exchange with oceanic water.

2.2.2 General Circulation

The generalized surface circulation pattern for the Northern Aleutian **Shelf** area is a weak counter clockwise gyre with surface current velocities of

5 **cm/sec** or less. Figure 2-3 shows a schematic drawing of the surface circulation pattern for Bristol Bay as modified from Kinder and Schumacher (1981). The counter clockwise gyre does not appear to be a geostrophic current because neither the extreme meteorological conditions nor the shallow water depths, both characteristic of the area, are conducive to the formation of geostrophic circulation. Various investigators have suggested that in the southeastern Bering Sea **thermohaline** effects, tides, and winds are the forces that drive water mass movement during the portion of the year that the sea is ice free. Generally, the study area is ice free all year.

The mechanics of Bristol Bay circulation are thought to be controlled by southerly and southwesterly winds which tend to drive water eastward toward the head of the bay. The incoming tide from the North Pacific further reinforces this eastward flow which parallels the Alaska Peninsula. At the head of Bristol Bay the eastward flow is mixed with brackish coastal waters that result from high seasonal runoff, and is then deflected northward and westward. Offshore of Cape Newenham the major portion of the water moves northward while a minor quantity flows southerly completing the gyre.

2.2.3 Waves

The Northern Aleutian Shelf area is characterized by severe wave conditions. These waves are generated by **local** storms. As noted in the preceding subsection, they have a significant impact on water mass stability and general circulation within Bristol Bay.

According to Brewer and others (1977), the most critical parameters controlling wave climate for the area include fetch, storm duration, and shallow-depth conditions. During the summer months, winds are predominantly

from the south, placing the nearshore portion of Bristol Bay in the lee of the Alaska Peninsula. As a result, most waves are generated locally. During the winter season, winds originate from the northwest in the Bering Sea. Winter storms are significantly more severe than the summer winds from the south. Table 2-2 presents maximum sustained wind velocities and maximum significant and extreme wave heights for the Bristol Bay area.

2.2.4 Tides and Currents

Tides in the study area are dominated by a tidal bulge which enters the Bering Sea through the central and western Aleutian Straits. This bulge progresses as a free wave onto the Bering Shelf. It is dominantly a mixed semi-diurnal tide over the southeastern portion of the shelf. On the open shelf the tidal amplitudes average 2 m. Toward the head of Bristol Bay the largest amplitudes exceed 6 m. The tidal range at Port **Moller** averages 3.3 m, whereas a 6.9 m range occurs at the Naknek River entrance (Brewer and others, 1977).

The natural period of oscillation for the inner bay equals that of the major lunar tide (U.S. Army Corps of Engineers, 1974). This results in a reinforcement of the tidal amplitude toward the head of Bristol Bay. Pearson and others (1981) note that the semi-diurnal tide propagates as a Kelvin Wave along the Alaska Peninsula and appears to be converted to a Sverdrup Wave upon reflection in inner Bristol Bay. Tidal oscillations within the bay trend northeast-southwest (Favorite and others, 1961).

Tidal currents in Bristol Bay are nearly reversing along the Alaskan Peninsula and become more **cyclonic** rotary offshore. Hebard (1961) found tidal currents in the study area having maximum flood velocities exceeding 85 **cm/sec**

at Station D ($55^{\circ} 40' N$, $163^{\circ} 30' W$) and 41 **cm/sec** at Station C ($56^{\circ} 40' N$, $161^{\circ} 15' W$). Outside the study area maximum flood tidal current velocities were recorded as 51 and 77 **cm/sec** at two other stations in central Bristol Bay. Hebard (1959) further noted little difference in direction or speed with depth. Mean tidal values in central Bristol Bay were reported at 22 **cm/sec** (Stations C and D) for the surface and 34 **cm/sec** (Station C) and 18 **cm/sec** (Station D) near the bottom. Favorite and others (1961) reported that **tidal** current velocities exceed 75 to 100 **cm/sec** inshore and 40 to 50 **cm/sec** on the open shelf. These measured tidal currents compare well with calculated maximums for open-water conditions (U.S. Army Corps of Engineers, 1974). This tidal current information represents summer values. No studies have measured average current velocity or maximum tidal current velocity during winter or storm conditions. Erosional evidence suggests that significantly higher velocities must exist.

Another source of currents is general water circulation, as discussed in Section 2.2.2. Hebard (1961) reports average surface current velocities from generalized **arcolation** at Stations C and D as approximately 6 and 3 cm/sec, respectively. Average bottom current velocities are even lower, 2.0 **cm/sec** at Station C and 1.5 **cm/sec** at Station D. Hebard's measurements, which were made in June of 1957, involved measuring current velocities at four depths every hour for 38 hours at each of four stations.

2.2.5 Longshore Drift

Longshore drift on the northern coast of the Alaska Peninsula has been divided into a series of **longshore** drift cells along the coastline (Hunter and others, 1979). Three of these cells occur within the study area. These cells converge at the locations of large bays and diverge a short distance to the

B northeast of each bay. The long-term effect of wave action in this system of cells is erosion of headlands and deposition in bays, thereby ultimately producing a straightened coastline. In general, the net drift direction along this coast is to the northeast with local reversals near the bays (Figure 2-3).

Waves and wave-driven currents are the primary drift agents, but tidal and other currents may be locally important. The rate of longshore drift increases with increasing wave size. Where wave size is constant, the drift rate is maximum when the waves approach the coastline at an angle of about 45 degrees (Komar, 1976).

2.3 METEOROLOGY

The Northern Aleutian Shelf is in the subarctic climatic zone where the annual weather patterns develop as a result of strong seasonal pressure changes. The U.S. Coast Pilot (U.S. Dept. of Commerce, 1979, p. 297) describes weather in the Bering Sea as follows:

"The weather over the Bering Sea is generally bad and very changeable. Good weather is the exception, and it does not last long when it does occur. Wind shifts are both frequent and rapid. The summer season has much fog and considerable rain. In **early** winter, the gales increase, the fogs lessen, and snow is likely any time after mid-September. Winter is the time of almost continuous storminess".

2.3.1 Winds

Southwesterly and southerly winds dominate during the summer; northeasterly winds are common during the winter season. At King Salmon, about 450 km east of the study area, northern winds blow more than 20 percent of the time during the winter. The prevailing wind direction at Port **Moller** is southerly with average speeds of 9 kts (17 **km/hr**) but speeds in excess of

55 kts (102 km/hr) have been recorded. At Cold Bay, the mean wind speed is 15 kts (27 km/hr).

Surface currents, vertical water mixing, and water-mass exchange are all influenced by these seasonal wind patterns. The presence of a major storm track in late summer through early winter introduces an additional mechanism influencing general circulation in Bristol Bay.

2.3.2 Precipitation

Precipitation falls primarily as rain during the summer and autumn months (July through October). Measureable precipitation at Port Moller has been recorded 59 percent of the days and trace amounts during an additional 18 percent (Brewer and others, 1977). At Port Moller precipitation occurs as much as 77 percent of the month of August. At Cold Bay annual cloud cover is 85 percent, relative humidity is 86 percent, and mean annual precipitation is approximately 84 cm falling on 320 days. On a yearly average, Bristol Bay receives precipitation 44 percent of the time; the average annual accumulation is 50 to 60 cm.

Average snowfall totals 100 to 130 cm/yr from November through April, although it has occurred in all months. Mean annual snowfall at Cold Bay is approximately 140 cm, accumulating on 124 days.

Poor visibility can be a problem all year. Visibility is restricted by land fog and snow in winter and by sea fog and rain in summer. For example, there are an average of 192 foggy days per year at Cold Bay. This weather often interferes with and causes cancellation of aircraft and ship operations.

2.3.3 Temperatures

Mean annual maximum and minimum temperatures at Port **Moller** are 5.5° C and -2.9° C, respectively, with extremes ranging from approximately +23° C to -23° C (Brewer and others, 1977). **At** Cold Bay, extreme high and low temperatures have been +25° C and -25° C.

2.4 REGIONAL GEOLOGY

The regional geologic setting for the study area is described in the following five subsections (stratigraphy, tectonics, seismicity, volcanism, and magnetics and metallic resources). These summaries, when combined with data collected during the field phase of this evaluation, provide the **frame-**work for establishing geologic hazards.

2.4.1 Stratigraphy

Existing stratigraphic studies generally have involved evaluations of shallow rather than deep stratigraphy. No deep core holes exist on the Northern Aleutian Shelf; consequently, all deep stratigraphic interpretations are based on projections of data from wells on the adjacent Alaska Peninsula. Three of these deep interpretations have been presented by the Alaska Geological Society (1975) in their Bristol Bay Region "**Stratigraphic** Correlation Section" and by McLean (1979). These interpretations were based on borehole data from nine wells drilled on the **Alaska** Peninsula; four of the wells are located within 15 to 40 km of the study area. Shallow stratigraphy has been investigated in more detail. Generally these investigations involved shallow gravity cores from which sediment composition has been defined. A generalized composite **stratigraphic** section for the Northern **Aleutian** Shelf area is shown in Figure 2-4.

2.4.1.1 Deep Stratigraphy

The **stratigraphic** section for the crust of the Bering and North Aleutian Shelf comprises two major sequences: 1) highly deformed, Mesozoic rocks and 2) slightly deformed Tertiary rocks (Figure 2-4). The lower sequence (Mesozoic rocks) is referred to herein as the basement. These basement rocks were deposited and deformed in conjunction with an ancient phase of plate subduction unrelated to later Tertiary and present tectonic regimes (Cooper and others, 1976; **Marlow** and others, 1976b), and hence are not discussed in great detail within this report. The following discussion is given to provide only a general framework for the tectonic and **geotechnical** discussions in subsequent sections of the report.

Basement deposits are overlain unconformably by the **Tolstoi** Formation (Figure 2-4). The **Tolstoi** Formation is a Paleocene/Eocene unit with a thickness of **1500+** m. Marine fossils are rare within the formation; however, plant fossils are abundant at the base of the unit. The formation also **contains** volcanic sandstone units which have poor porosity, presumably due to **zeolitic** cement (McLean, 1977).

The **Tolstoi** Formation is overlain by the Meshik and Stepovak Formations which form an Oligocene unit as much as 4550 m in thickness composed of **interfingering** layers of **volcanoclastic** and volcanic flow rocks. The **Stepovak** Formation contains lignite seams in the upper part of the section, and carbonaceous layers occur throughout the section (**Marlow** and others, 1980). The Meshik Formation contains volcanic **breccias** and andesitic basalt flows. Both units have marine and non-marine layers.

The Unga Conglomerate of the Bear Lake Formation overlies the Meshik and Stepovak Formations. This basal conglomerate marks the Oligocene-Miocene boundary. The Bear Lake Formation is approximately 1500 m thick and has its upper and lower contacts bounded **by** unconformities. Sands, conglomerates and interbedded mudstones with low grade coal (McLean, 1977) characterize the Bear Lake Formation. This formation is considered to be a good hydrocarbon reservoir (**Marlow** and others, 1976a).

The Milky River Formation overlies the Bear Lake Formation. The base of this formation defines the Miocene-Pliocene boundary. The Milky River Formation is **a** fossiliferous marine and **nonmarine** unit of **conglomeratic** sandstones and mudstones of volcanic origin (**Marlow** and others, 1980).

2.4.1.2 Shallow Stratigraphy

Approximately 300 m **of** undifferentiated and partly indurated Quaternary and Holocene sediments and volcanic rocks overlie the Milky River Formation. Quaternary rocks within the study area include the **volcanics** of Amak Island and the Aleutian Peninsula. Holocene deposits include **fluvial** sediments of glacial and volcanic origin, much of which are still undergoing active transport, erosion, and deposition.

2.4.1.3 Surficial Sediments

The composition and distribution of **surficial** sediment from the southeastern Bering Sea have been described by Lisitzin (1966 and 1972), **Gershanovich** (1968), Askren (1972), **Sharma** (1974 and 1975) and **Sharma** and others (1972), with the work by Askren and Sharma being the most relevant to the **study** area.

Askren suggests that the entire area is covered by at least 3 m of Holocene sediment. According to Askren, all of the study area falls within a "sand province" characterized by a high sand content (greater than 50 percent). He states that the well-sorted character of the **"sand province"** reflects proximity to mainland and island sediment sources and the influence of strong coastal currents. The presence of sand at depths greater than 50 m in Bristol Bay is believed to be due to the contrast of seasonal wind-wave effects and permanent circulation patterns in Bristol Bay and the shelf to the north.

Sharma (1975) and **Sharma** and others (1972) describe a much more complicated shelf situation. They suggest that nearshore sediments consist of very poorly sorted gravelly sands which grade to well-sorted, **fine-grained** sands in the central bay. The far-offshore sediments are very poorly sorted muddy sands. The mean size of the sediments generally decreases with increasing depth and distance from the coast. Two broad depositional environments, an "Inner Continental Shelf" and an "Outer Continental Shelf", are recognized on the basis of silt and clay distribution, the plot of skewness versus kurtosis, and the plot of mean grain size versus sorting coefficient. **Sharma** sees drainages to the north and east, the Alaska Peninsula to the south, and **bio-**genic processes as being the sources of Bristol Bay sediment.

The Bristol Bay Shelf is described by **Sharma** (1974, 1975, and 1979) and **Sharma** and others (1972) as a model contemporary graded shelf. In the sense that mean grain size generally decreases with depth, it is a contemporary graded shelf. However, there is no uniformity in sorting, skewness, or **kurtosis** across the shelf. If an equilibrium shelf (graded shelf) is considered to be a shelf where sediments are in equilibrium with the prevailing wind,

wave, tide, and bottom current conditions; Bristol Bay does not fit this definition in that the only factor that approaches a condition of equilibrium is mean grain size. **All** other sediment parameters have failed to reach a state of **equilibrium**.

Concentration of coarse material in scours adjacent to areas of fine sediment, at numerous locations in the study area, also shows a lack of equilibrium conditions (**Molnia** and others, 1982). It is also uncertain whether the generally graded nature of the shelf may be relict, a carryover from the outwash and **fluvial** plain conditions that existed prior to the Holocene sea level transgression. Reworking of the relict sediment during **post-eustatic** sea level rise may account for the tremendous variability in sorting and **kurtosis**.

Mineralogically, Sharma describes the principal components of the sand fraction as quartz and feldspar in the light fraction; and **hypersthene**, amphibole, magnetite, and **ilmenite**, in the heavy fraction. Other heavy minerals present include diopside, garnet, **sillimanite**, epidote, **staurolite**, **tremolite**, **sphene**, and **uralite**. Small percentages of **illite** and chlorite are **also** present. Sharma uses the composition of the clay fraction to characterize the source area as a region without much chemical weathering. Sharma also observes a decrease in the percentage of heavy minerals with an increase in water depth. Organic carbon content in sediments also increases seaward, coinciding closely with the increase in the clay-size fraction. The maximum organic carbon detected by **Sharma** was about 0.45 percent. Locations of **all** historic samples are shown on Figure 2-5 and are tabulated in Appendix I.

2.4.2 Tectonics

The structure and **stratigraphy** for *the* Northern Aleutian Shelf indicates that the area has had a complex history of **crustal** subduction, folding, faulting, uplift, subsidence, and sedimentation. The similarity of Mesozoic rocks on the Alaska Peninsula, the Bering Sea **Shelf**, and eastern Siberia (Figure 2-6) implies that a continental margin once extended between the Aleutian area and eastern Siberia along the edge of the Bering Shelf (Burk, 1965; Moore, 1972; Cooper and others, 1979; Marlow and Cooper, 1980a).

The basement rocks underlying the area, consisting predominantly of Jurassic and Cretaceous **flysch** type rocks (Nelson and others, 1974), were deposited during convergence and subduction between the **Kula** and North American Plates (Grow and Atwater, 1970). The Alaska region, **like** much of the Pacific margin of North America, may consist of terranes which were tectonically transported (**allochthonous**) many hundreds of kilometers during Mesozoic and early Tertiary plate tectonic events. These **allochthonous** terranes may continue beneath the continental shelf to make up much of the Bering Sea basement (McGeary and Ben-Avraham, 1981). By the end of the Mesozoic or early Tertiary, this episode of convergence and consolidation ended and appears to have been followed by regional subsidence and extensional collapse which created a *series* of submarine ridges and basins. The Bristol Bay, Amak, and St. George basins may have been initiated at that time.

At the end of the Mesozoic or in the early Tertiary, the plate boundary shifted to near the present Aleutian Trench, and the Aleutian arc was formed. Part of the Kula Plate was trapped behind the arc and now forms the **abyssal** floor of the Bering Sea (Cooper and others, 1976). By mid-Tertiary, the

continental shelf was submerged for the first time and the basins continued to subside due to sediment loading and crustal tension. The Aleutian arc continued **to** be platonically and volcanically active.

During the Pliocene, the arc underwent severe structural deformation which led to development of most of the structures seen today (**Burk, 1965**). This **orogeny** seems to correlate with the subduction of a spreading center between the **Kula** and **Farallon lithospheric** plates (Grow and Atwater, 1970).

In addition to the tectonic activity, the Pleistocene was time of intermittent glaciation throughout most of the Alaska Peninsula with at **least** four major glaciation. Sea level rose and fell depending on the amount of water contained as ice in glaciers. The maximum lowering of sea level amounted to about 130 m (Curry, 1965), and this resulted in exposure of most of the Bering Shelf including all of Bristol Bay Basin area.

The present day tectonics of the Bristol Bay area are strongly influenced by subduction of the Pacific Plate under the North American/Bering Plate along the Aleutian Trench. The Alaska-Aleutian Trench has a gently arcuate **con-**figuration that extends from the Kamchatka Peninsula on the west to the Gulf of Alaska on the east (Figure 2-7). The subduction zone is bounded by the **Kuril-Kamchatka** subduction zone on the west and the Queen Charlotte Islands-Fairweather transform fault system on the east. The present rate of subduction of the Pacific Plate along the Aleutian subduction zone varies from about 5.5 **cm/yr** to 7.6 **cm/yr** (Figure 2-7).

Under the present tectonic regime, the Aleutian subduction zone changes from 1) a poorly developed sediment-filled trench adjacent to the mainland, to 2) a well-developed trench adjacent to the Alaska Peninsula involving

subduction of oceanic crust under continental crust, to 3) the well-developed trench west of Unimak Island which involves thrusting of oceanic crust under oceanic crust. These changes indicate that the Aleutian subduction zone comprises several segments each with its own unique combination of tectonic characteristics.

Von **Huene** and Shor (1969) noted distinct differences in morphology and geology along the Aleutian subduction zone and divided the zone into four distinct segments: 1) the Mainland, 2) East Aleutian, 3) **Central** Aleutian, and 4) West Aleutian. The Bristol Bay region **lies** adjacent to the East Segment which occupies the region between the St. Elias and Shumagin Transitions. Along the Aleutian arc other segments can be distinguished based on seismicity characteristics (**Spence**, 1977) which appear to change across transition zones and tend to support the idea of discrete trench segments.

2.4.3 Seismicity

Earthquake epicenters in the Aleutian area form a prominent curvilinear belt primarily between the Aleutian Trench and the *volcanic* arc (Figure 2-7). These earthquakes are shallow near the trench and gradually increase in depth northward forming a Benioff Zone that defines the upper portion of the **under-thrust** Pacific **lithospheric** plate. The angle and the maximum depth of the Benioff Zone changes laterally along the trend of the Arc (Figure 2-8). Near **Amchitka**, the **Benioff** Zone is steep and extends to about 250 km deep. In the study area the maximum depth of the Benioff Zone is about 150 to 200 km with about a 40 degree dip. Eastward the earthquakes are generally no deeper than 100 km and the angle of dip ranges from nearly horizontal near the trench to about 20 degrees under the mainland.

Not all the earthquakes are directly associated with the subduction zone. Earthquakes also occur in the shallow crust behind and on the arc. These earthquakes are particularly common on the Alaska mainland near the eastern end of the **Aleutian** subduction zone. Seismicity is poorly documented in the region of the Bering Sea north of the Aleutian Arc but large earthquakes ($M_s > 7.0$) have occurred in the vicinity of the St. George Basin and the **Pribiloff** Islands (Davies, 1981) (see Section 5.4 for more-detailed discussion).

2.4.4 Volcanism

Much of the Alaska Peninsula is covered by active volcanoes and volcanic rocks. At least 60 of these volcanic centers have erupted during the past 10,000 years. Commonly, the andesitic volcanoes are characterized by violent and explosive eruptions with widespread volcanic ash fall and with moderately large earthquakes.

At least ten potentially active volcanoes line the southern edge of Bristol Bay basin (Figure 2-9; Table 2-3). The major volcanoes adjacent to the study region are **Shishaldin**, **Pavlof**, and Veniaminoff (Plates V(A) and V(B)). None of these have actually erupted in a **major** destructive eruption in recent times, although **Pavlof** frequently has given off steam. Table 2-3 gives the dates of the last eruption.

An example of the potential destruction from a volcanic eruption may be that of Mount Katmai, a volcano located on the Alaska Peninsula east of the study region. Mount **Katmai** erupted in 1912 spreading about 16 cubic km of volcanic debris into the atmosphere. The ash was carried to all parts of the northern hemisphere; near the volcano the ash deposit reached a thickness of more than 15 m and at Kodiak, 160 km to the southeast, it reached a thickness

of about 3 m (Wilcox, 1959). Pumice clogged the nearby Cook Inlet and the skies were darkened several thousand kilometers downwind from the eruption. Hundreds of square kilometers of forestland were converted into an ashy desert and this is still evident today.

Volcanism has also been a dominant process in the past. Volcanic and **volcaniclastic** rocks dominate the Tertiary record, though all units in this area are limited in areal extent and generally cannot be correlated. Detailed investigations of two Tertiary **strato-volcanoes** on the Alaskan Peninsula were conducted by Kennedy and **Waldron** (1955). The volcanoes, **Pavlof** which is 45 km northeast of Cold Bay and **Frosty Peak** which is 15 km southwest of Cold Bay, have a long history of eruptions. This history is characterized by long periods of activity separated by brief periods of relative quiescence. The quiet periods are characterized by erosion, sedimentation and glacier buildup. The earliest events, discernible from the geologic record, occurred during the mid-Tertiary when a long period of intense volcanism took place. During this time, **Belofski** Tuff accumulated to a thickness of more than 1000 m (**Waldron**, 1961). McLean and others (1978), using fossil evidence, have identified this event as Oligocene in age. Following the accumulation of the **Belofski** Tuff, numerous other volcanic eruptions continued into the Quaternary (Table 2-3). Late Pleistocene volcanism built the composite summit cone of **Frosty Peak**. Following the late Pleistocene events, volcanic activity ceased and **Frosty Peak** and its flows were actively eroded and modified by wind, waves, ice and precipitation.

The chemical composition of these extrusive has not been reported in detail. **Waldron** (1961) noted that the extrusive volcanic rocks contain less **olivine** as they become younger. **Wilson** (1981) summarized the **radiometric**

dating of rocks in the Aleutian Islands and Alaska Peninsula; however, there has been no age dating within the study area outside of a 6.2 million year (my.) date of a porphyry copper deposit south of the Herendeen Bay area, 20 km west of Port **Moller** (Armstrong and others, 1976).

2.4.5 Magnetics and Metallic Mineral Resources

Baily and others (1976) compiled a residual magnetic data map of the Bering Sea which included data collected on 18 separate surveys between 1964 and 1973. Part of this 1976 summary overlaps the Northern Aleutian Shelf study area. Numerous east-west trending magnetic anomalies occur on the map; however, none of the anomalies clearly correlate with **basinal** configuration or other structure as mapped from the data evaluated in this survey.

Known metallic mineral resources of the Cold Bay Quadrangle, determined by Cobb (1972) from a survey of historic data, are limited to a single placer occurrence of iron oxide. This site, originally mapped by **Berryhill** (1963), is 7.5 km northeast of Moffet Point. Similar deposits of common metallic opaques can be expected to occur throughout the study area due to the proximity of the source rock (The Aleutian Volcanic Arc) and a depositional environment conducive to concentrations of coarse and heavy particles.

Table 2-1 Hydrographic Domains - Summer Conditions*

<u>Characteristic</u>	<u>Coastal Shelf</u>	<u>Middle Shelf</u>	<u>Outer Shelf</u>
vertical structure	homogeneous	two layer	surface mixed layer, stratified interior fine-structure, with bottom mixed layer
stratification	very low	very high	moderate
water depth	<50 m	<u><50</u> m - 100 m	<u>>100</u> m
temperature	very warm in late summer (8 to 12° C)	very cold bottom temperature throughout summer (-1 to 30° c)	moderate (3 to 6° C)
salinity	generally low (<31.5 ‰)	moderate low (31.5 ‰)	high (>32‰)
influences	river runoff freezing	melting	adjacent water overlying deep basin; Bering Slope Current

*modified from Kinder and Schumacher, 1981

Table 2-2 Maximum Wind and Wave Data

Return period years	Maximum sustained wind (knots) (Thom)*(Q & F)**		Maximum significant wave (meters) (Thorn) (Q & F)		Extreme wave- (meters) (Thorn) (Q & F)	
5	75	75	13.0	10.2	24.0	18.0
10	81	81	15.0	11.2	27.0	20.1
25	90	91	17.5	13.1	31.5	23.8
50	98	98	20.0	14.9	35.5	26.5
100	106	107	22.5	16.8	40.0	29.9

* Thorn (1973)

** Quayle and Fulbright (1975)

Table 2-3 Active Volcanoes in the Vicinity of the Northern Aleutian Shelf

Map No. (#)	Name	Latitude (N)	Longitude (W)	Type of Eruption	Date of Last Eruption
1	* Bogoslof	53° 56'	168° 02'	Normal Explosion	1931
2	* Okmok	53° 25'	168° 03'	Normal Explosion, Lava	1945
3	* Makushin	53° 52'	168° 56'	Normal Explosion	1938
4	* Akutan	54° 08'	165° 59'	Normal Explosion, Lava	1973
5	* Westdahl	54° 31'	164° 39'	Normal Explosion, Lava	1967
6	* pogromni	54° 34'	164° 41'	Normal Explosion, Lava	1830
7	Fisher	54° 35'	164° 26'	Ash	1826
8	* Shishaldin	54° 45'	163° 58'	Lava	1965-76
9	† Isanotski Peaks	54° 47'	163° 13'	Normal Explosion, Ash	1845
10	Roundtop Mt.	54° 48'	163° 35'	---	----
11	Frosty Peak	55° 04'	162° 49'	---	----
12	* Pavlof	55° 25'	161° 53'	Normal Explosion, Lava	1975-76
13	Pavlof Sister	55° 27'	161° 51'	Ash	1786
14	Dana	55° 38'	161° 13'	---	----
15	Veniaminof	55° 12'	159° 24'	Normal Explosion, Ash	1944

Sources: Minerals Management Service, 1982

* high potential for eruption (based on historic activity reports)

† moderate potential for eruption (based on historic activity reports)

Figure 2-9

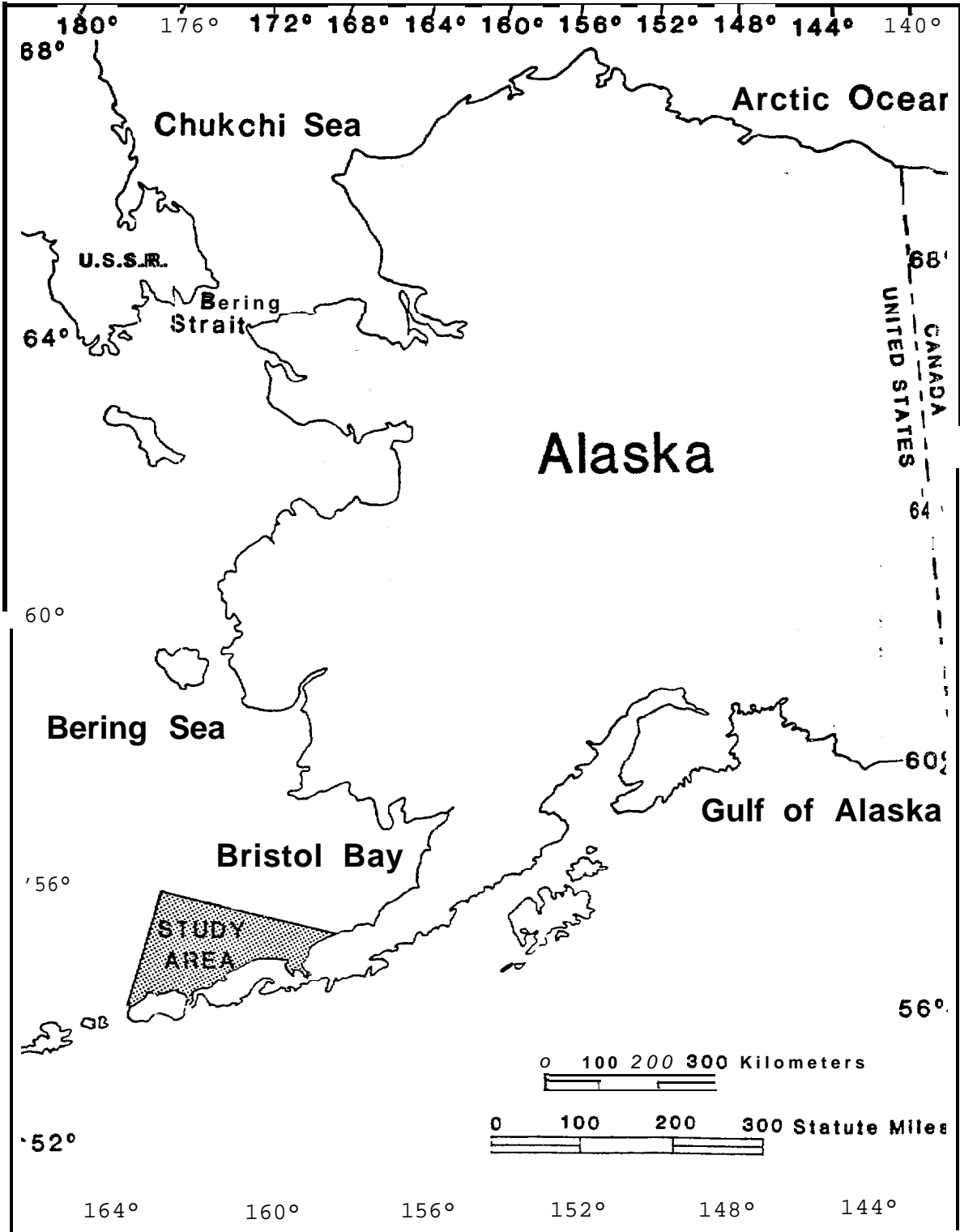


FIGURE 2-1 LOCATION MAP OF THE NORTHERN ALEUTIAN SHELF STUDY AREA

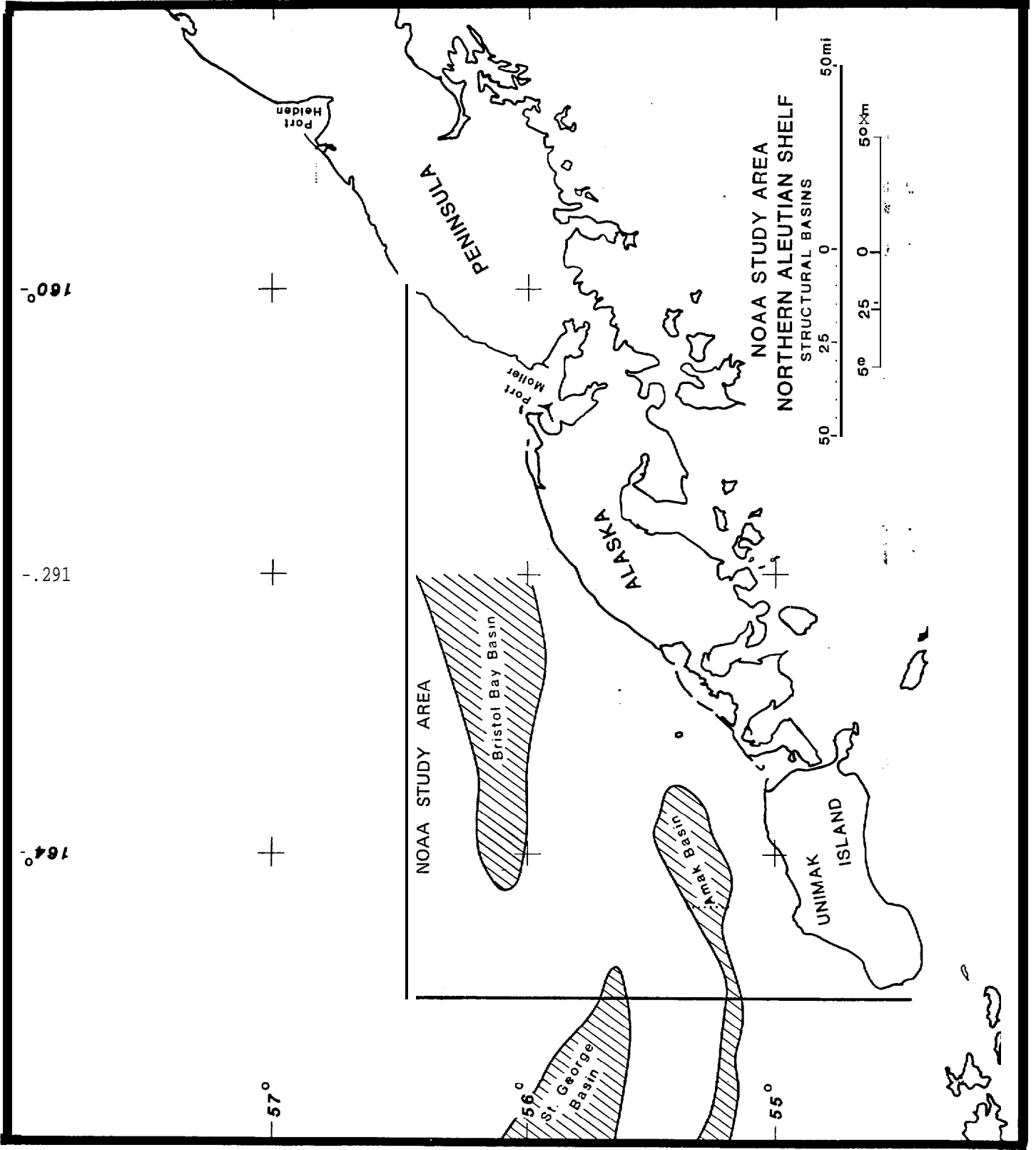


FIGURE 2-2 MAP OF STUDY AREA SHOWING LOCATION OF THE THREE MAJOR SEDIMENTARY BASINS

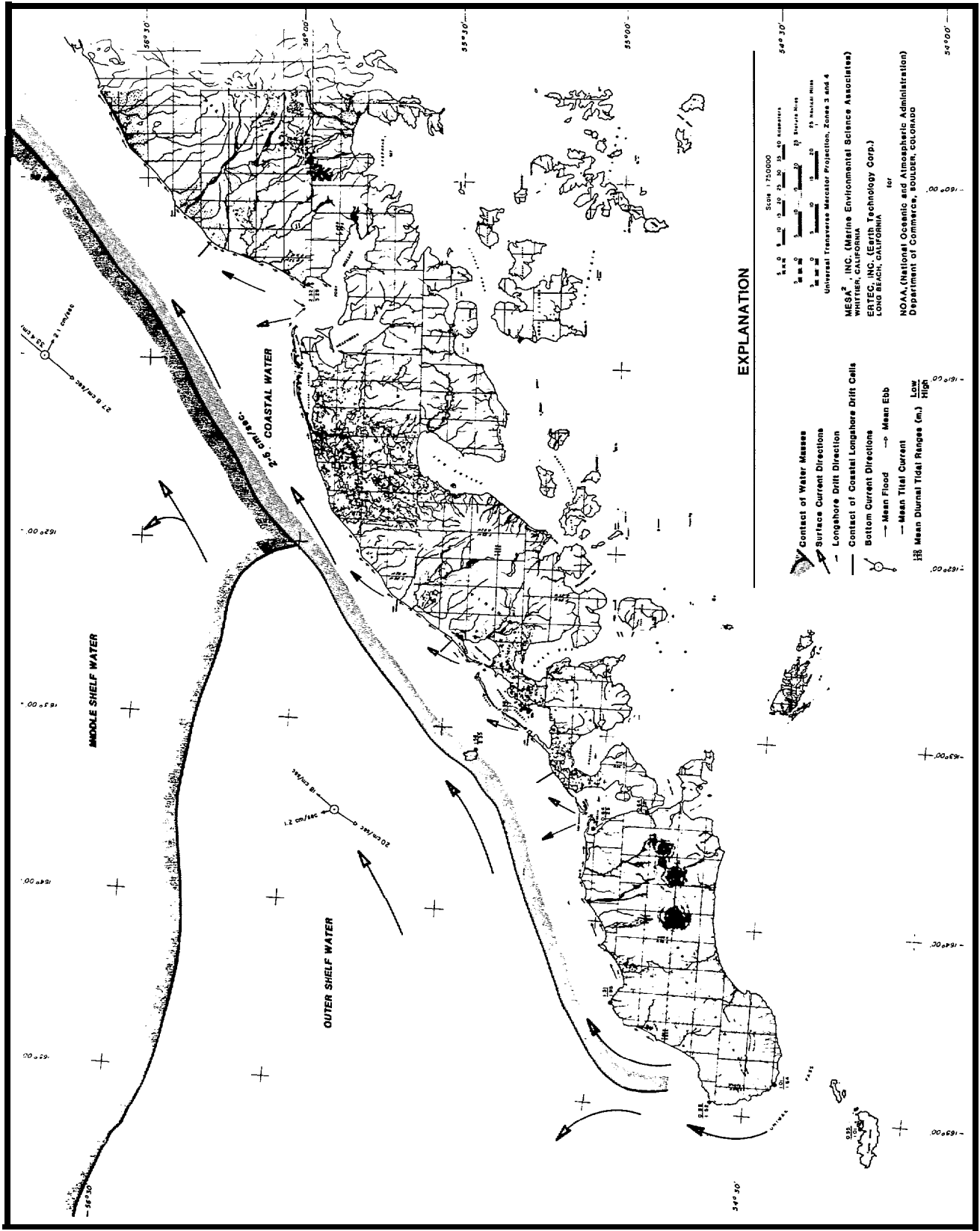


FIGURE 2-3 HYDROLOGY, GENERAL CIRCULATION, TIDES, BOTTOM CURRENTS, AND LONG SHORE DRIFT ON NORTHERN ALEUTIAN SHELF

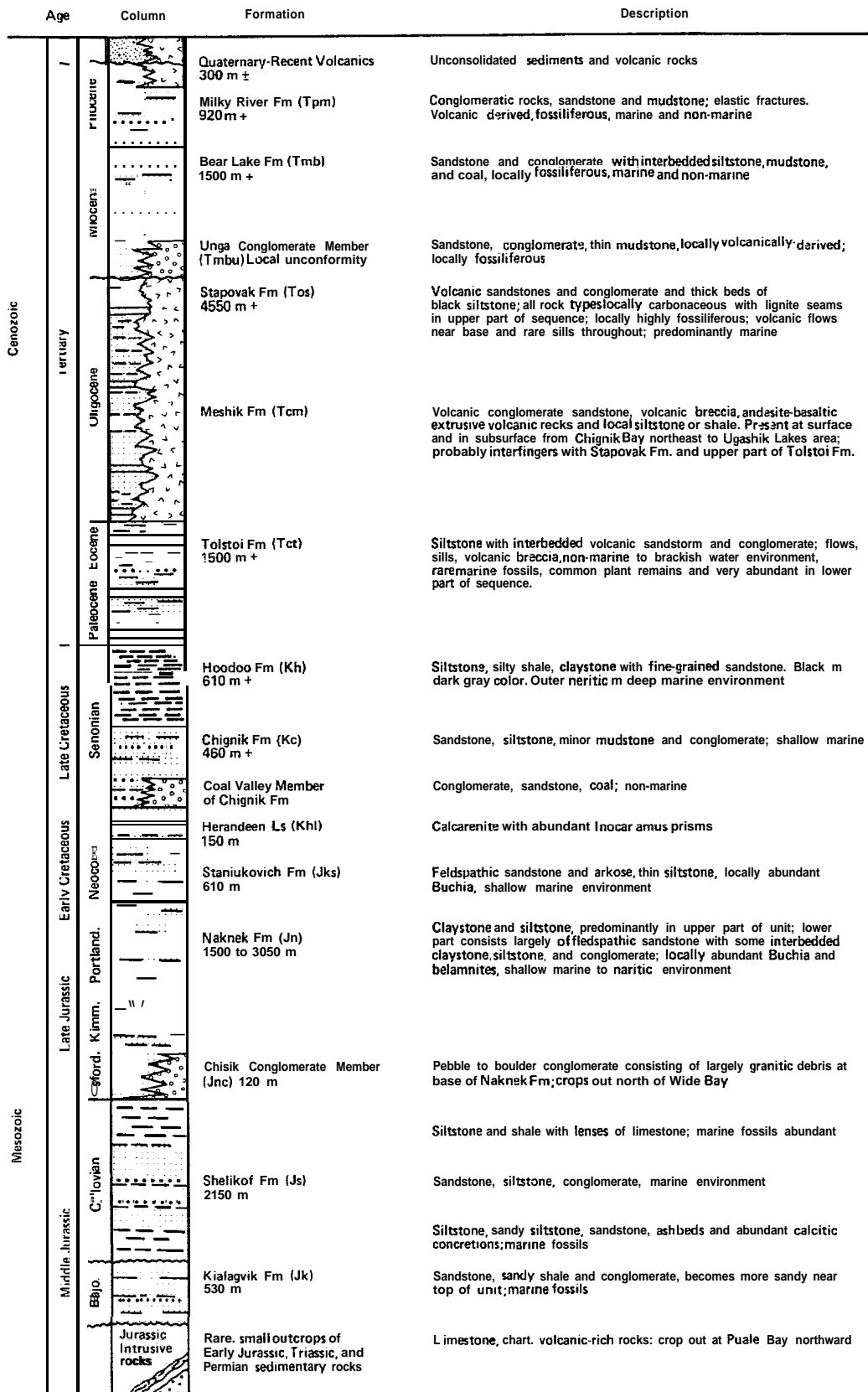


FIGURE 2-4 COMPOSITE STRATIGRAPHIC COLUMN FOR THE PROPOSED LEASE SALE AREAS 75 AND 92

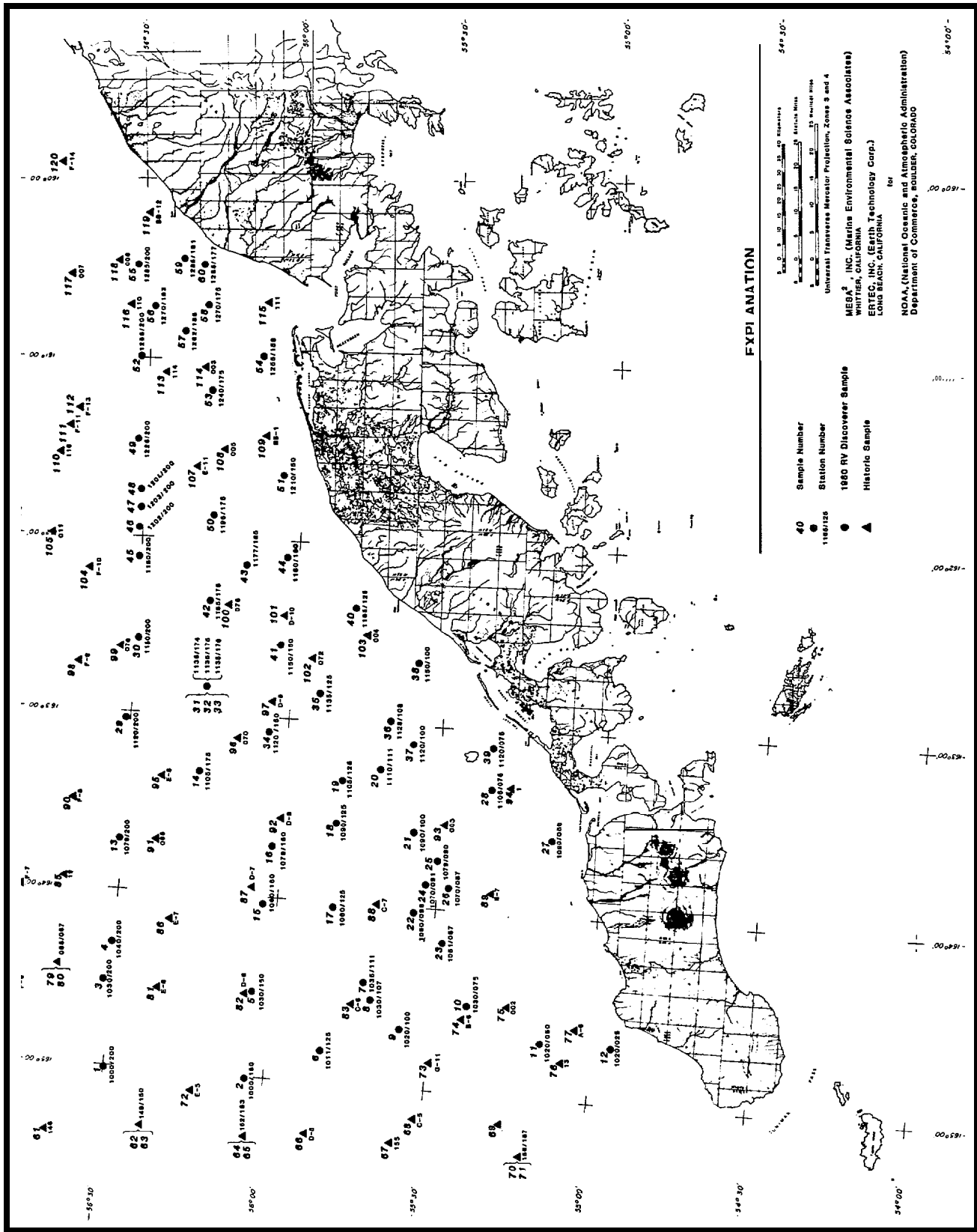


FIGURE 2-5 LOCATION OF SURFACE SEDIMENT SAMPLING STATIONS

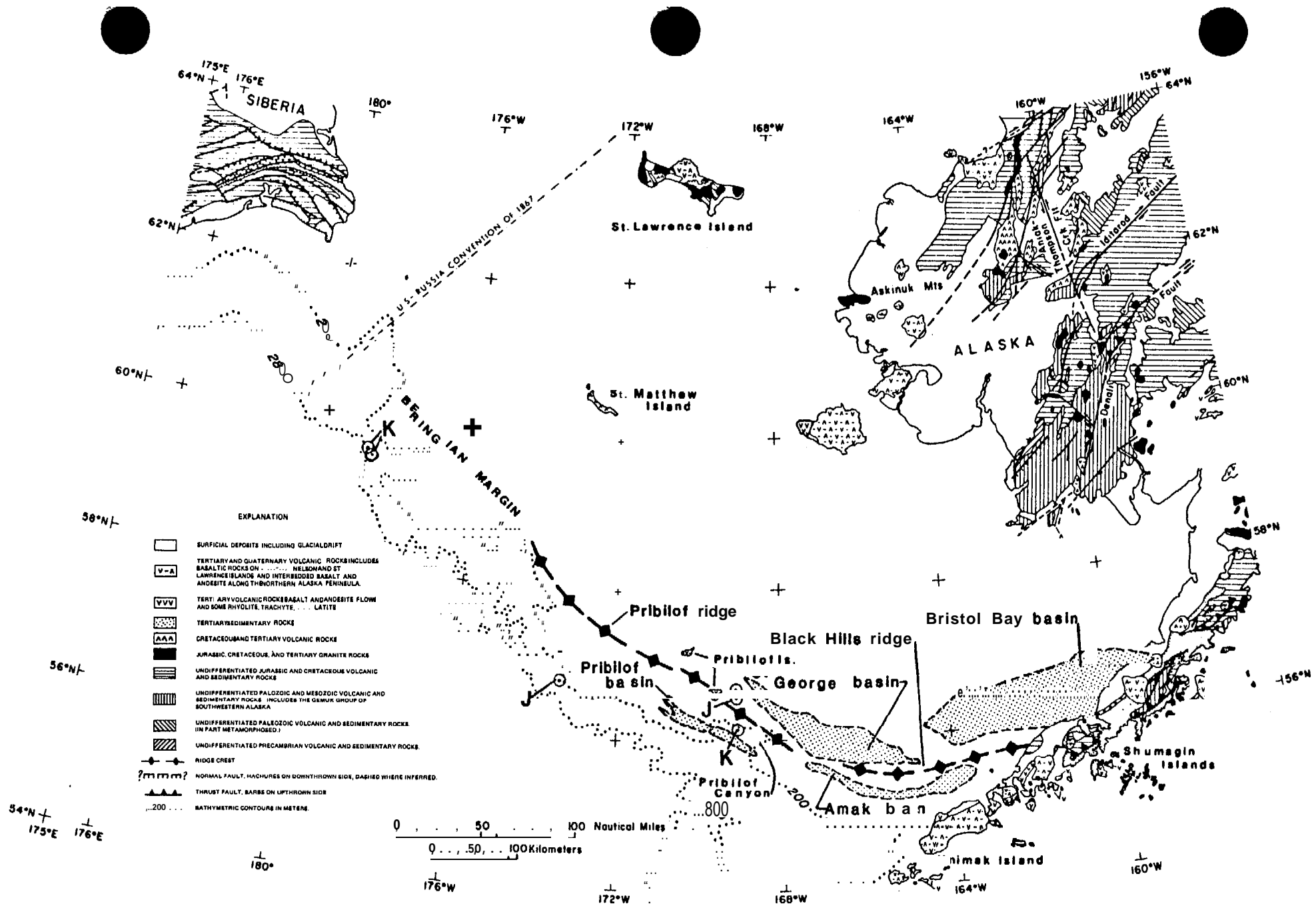


FIGURE 2-6 GENERALIZED GEOLOGY MAP OF WESTERN ALASKA, BERING SEA, AND EASTERN SIBERIA (FROM MARLOW AND COOPER, 1980a)

EXPLANATION

	SURFICIAL DEPOSITS INCLUDING GLACIAL DRIFT.
	TERTIARY AND QUATERNARY VOLCANIC ROCKS. INCLUDES BASALTIC ROCKS ON NUNIVAK, NELSON, AND ST. LAWRENCE ISLANDS. AND INTERBEDDED BASALT AND AN DESITE ALONG THE NORTHERN ALASKA PENINSULA.
	TERTIARY VOLCANIC ROCKS. BASALT AND ANDESITE FLOWS AND SOME RHYOLITE, TRACHYTE, AND LATITE.
	TERTIARY SEDIMENTARY ROCKS.
	CRETACEUS AND TERTIARY VOLCANIC ROCKS.
	JURASSIC, CRETACEUS, AND TERTIARY GRANITE ROCKS.
	UNDIFFERENTIATED JURASSIC AND CRETACEUS VOLCANIC AND SEDIMENTARY ROCKS.
	UNDIFFERENTIATED PALOZOIC AND MESOZOIC VOLCANIC AND SEDIMENTARY ROCKS. INCLUDES THE GEMUK GROUP OF SOUTHWESTERN ALASKA.
	UNDIFFERENTIATED PALEOZOIC VOLCANIC AND SEDIMENTARY ROCKS. (INPART METAMORPHOSED.)
	UNDIFFERENTIATED PRECAMBRIAN VOLCANIC AND SEDIMENTARY ROCKS.
	RIDGE CREST.
	NORMAL FAULT, HACHURES ON DOWNTHROWN SIDE; DASHED WHERE INFERRED.
	THRUST FAULT, BARBS ON UPthrown SIDE.
	BATHYMETRIC CONTOURS IN METERS.

NOTE: DOTTED CIRCLES INDICATE SITES WHERE JURASSIC (J) AND CRETACEUS (K) SEDIMENTARY ROCKS WERE DREDGED FROM CONTINENTAL SLOPE.

FIGURE 2-6 CONTINUED

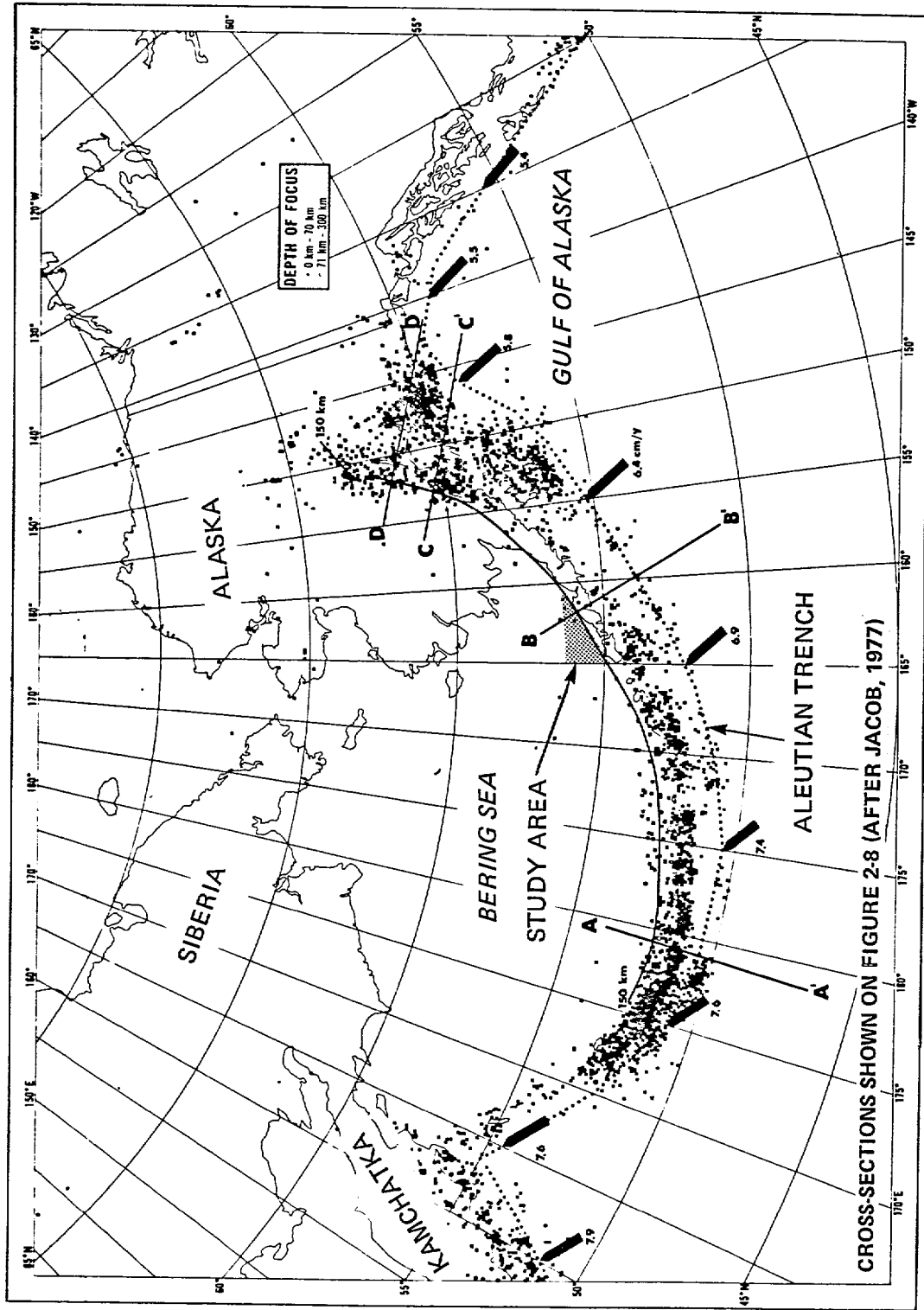


FIGURE 2-7 REGIONAL SEISMICITY AND N^2 RELATIVE MOTION VECTORS ALONG THE ALASKA-ALEUTIAN ARC

LOCATION OF CROSS-SECTIONS SHOWN ON FIGURE 2-7 (FROM JACOB, 1977)

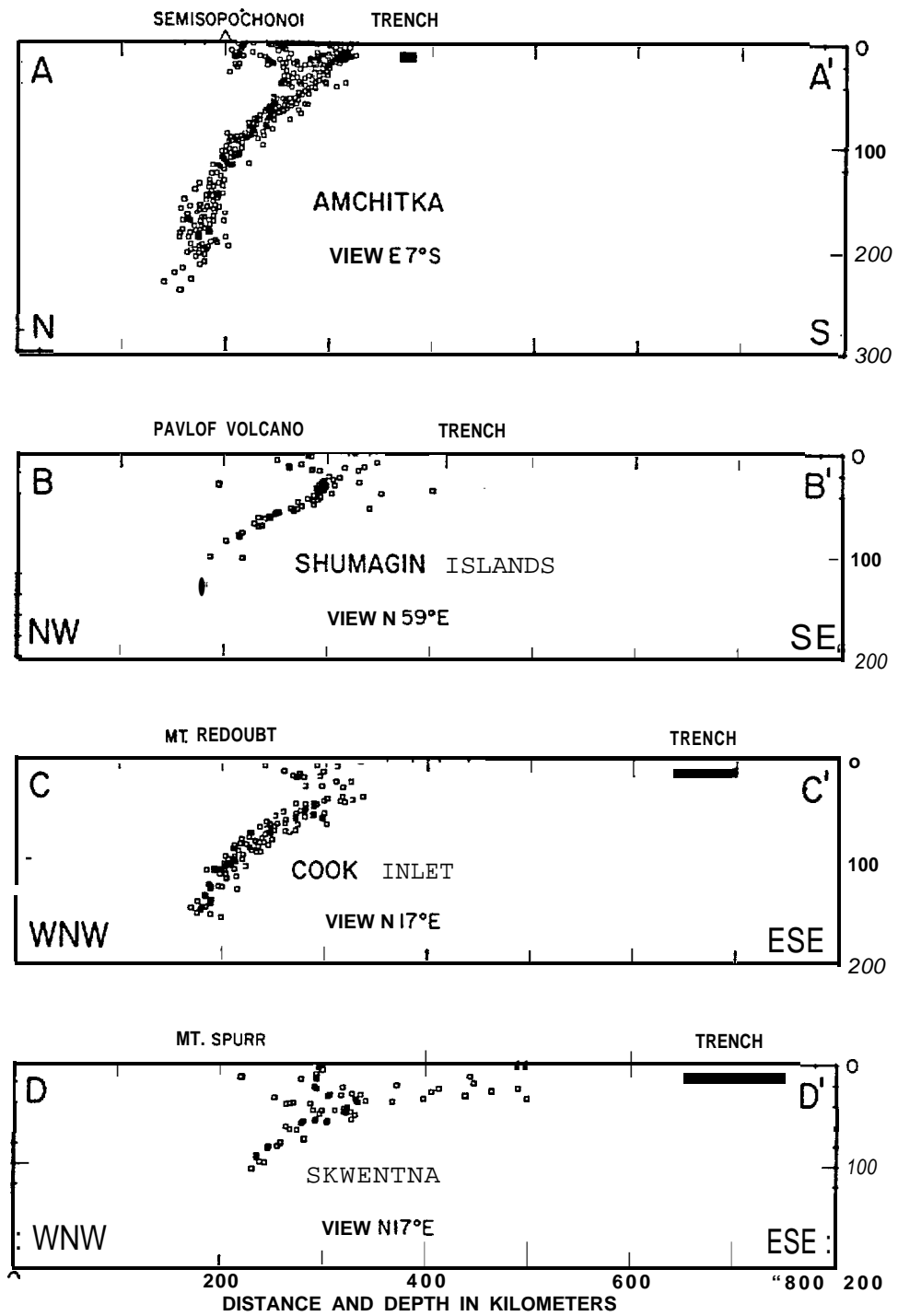


FIGURE 2-8 CROSS-SECTIONS SHOWING BENIOFF ZONE OF THE ALASKA-ALEUTIAN SUBDUCTION ZONE

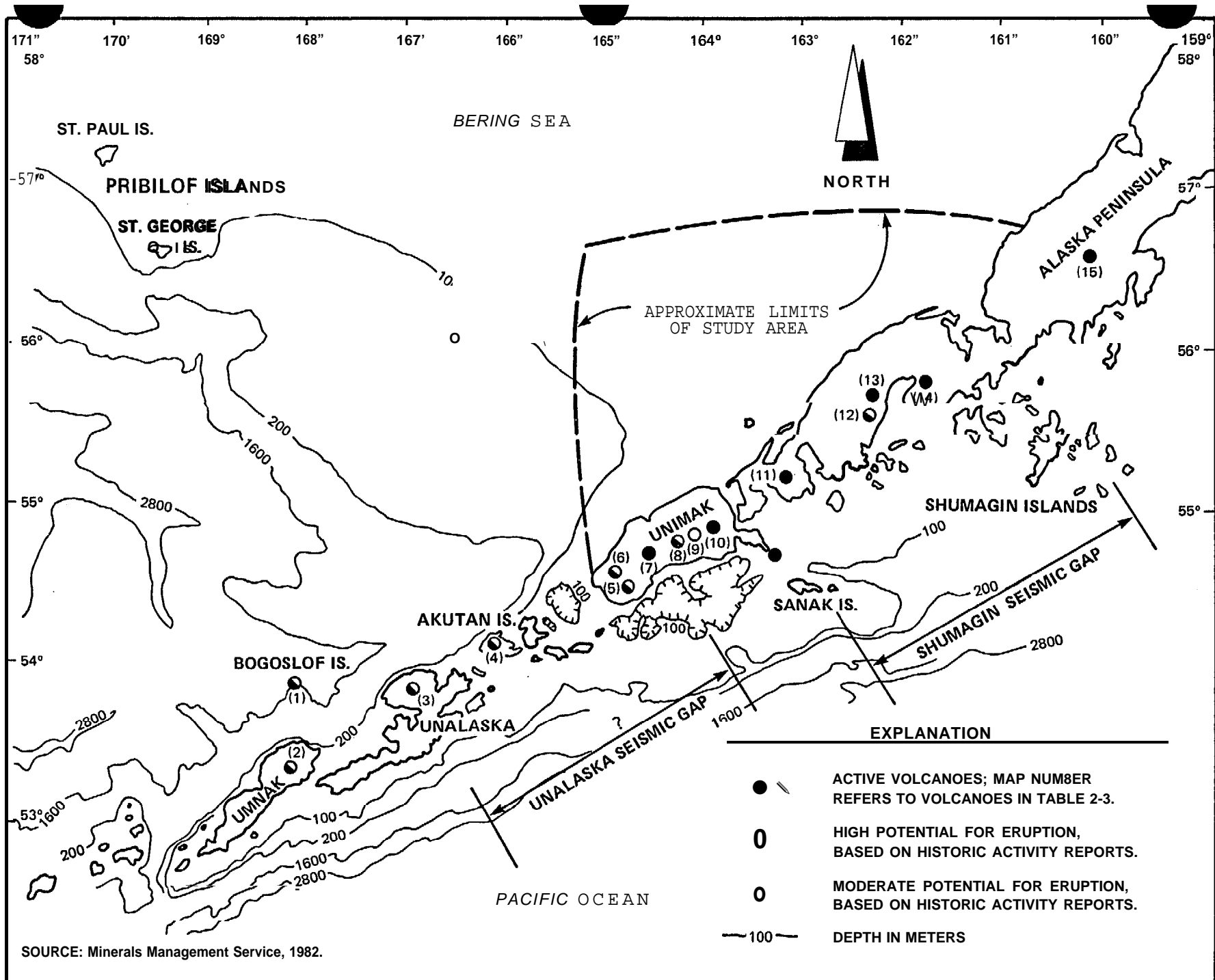


FIGURE 2-0 ACTIVE VOLCANOES IN THE NORTHERN ALEUTIAN SHELF REGION

3.0 FIELD PROGRAM

3.1 OPERATIONS

A field program was conducted from aboard the NOAA ship Discoverer. The purpose of the program was to supplement existing geophysical (seismic reflection profiles) and **geotechnical** data on the Northern Aleutian Shelf. The program was accomplished in two phases. These phases were referred to as **RP-4-DI-80A**, Legs VI and VII. Only 70 percent of sea time during Leg VI and 53 percent of Leg VII were available for field work. The remaining time was spent in transit, transferring equipment, and performing miscellaneous tasks.

During the 24 field days in the study area, 4180 km of seismic profiles were collected on a N-S by E-W grid. Bottom samples and in situ **geotechnical** data were gathered at 60 stations.

3.1.1. Vessel and Scientific Crew

The NOAA ship Discoverer was used during both legs of the cruise. The Discoverer is a 92-m long oceanographic research vessel, with a 16-m beam and a fully loaded draft of 5.5 m. The Discoverer is equipped with an oceanographic laboratory, deck winches and A-frames, and high-resolution navigational systems to facilitate geophysical and **geotechnical** research programs. A photograph of the Discoverer is shown in Figure 3-1.

Field operations were carried out in August, September and October of 1980. All field equipment and scientific personnel were mobilized to Kodiak, Alaska before August 25, 1980. Travel to the study area from Kodiak required approximately 72 hours. Of the 20 days assigned to Leg VI, 14 days of field work were accomplished. The remaining six days involved transit time, a

medical evacuation to Port **Moller**, and downtime while untangling the ship from crab-pot lines. Leg VII was assigned **18** days of which 9 1/2 days of **field** work were accomplished. The remaining time was used in transit, support for another scientific study, and assorted tasks. Demobilization was carried out from Kodiak beginning on October 18, **1982**.

The scientific party for Leg VI of the cruise comprised seven personnel. Dr. Peter J. Fischer, Professor of Geological Sciences at California State University at Northridge and Consultant to Ertec, served as Chief Scientist. Mr. Charles F. Chamberlain, Project Geologist at **Ertec**, was Co-Chief Scientist. During Leg **VII**, the scientific party was increased to eight with Dr. Dwight Sangrey, Professor of Civil Engineering at Carnegie **Mellon** University serving as Co-Chief Scientist. Captain Charles H. Nixon was the commanding officer of the Discoverer.

3.1.2 Navigation

Shipboard navigation was provided by LORAN-C and SATNAV with positions recorded every 5 minutes. These data were key-punched and programmed for a "best-fit" navigation solution. The LORAN-C fixes on N-S lines consistently plotted several tenths of a nautical mile to the west of the SATNAV (**SM-1** and **SM-7**) fixes. No suitable explanation for this difference was provided by the Operations Officer on the Discoverer. For simplicity and consistency, the final positions for **all tracklines** used in this study were based on adjusting the LORAN-C fixes to **SM-1** and **SM-7** SATNAV positions.

3.2 GEOPHYSICAL SURVEY

The study was designed so that all seismic-reflection **trackline** data were collected along a preselected grid pattern (Figure 3-2). During the two legs

of the Discoverer cruise, 4180 km of seismic profiles were collected on a N-S by E-W grid (Plates I(A), I(B), II(A) and II(B)).

3.2.1 Trackline Data

All dip lines (N-S orientation) shown in Figure 3-2 and **two** major strike (E-W orientation) lines were collected. In addition numerous strike-line segments were also collected (Plates **I(A)** and I(B)). The strike **line** grid was not completed due to lack of available work time during the cruise.

The dip lines were orientated slightly west of north-south to reflect the trend of the major offshore structural features (Gardner and others, 1979; **Marlow** and others, 1979; **Marlow** and Cooper, 1980a and **1980b**). The spacing between dip lines was approximately 15 km. The strike lines were oriented at right angles to the dip lines with about a 25 km spacing.

All **tracklines** were collected and numbered **in** relation to the "base **line**" reference system shown in Figure 3-2. This system facilitated easy, identification of the line number and located every line by its approximate distance from a "base line." All short lines collected near the core stations during Legs VI and VII were assigned grid numbers and "standard" shot point numbers. This greatly simplified data access and permitted a simplified computer coding **of** the **tracklines**.

3.2.2 Geophysical Equipment

All lines shown in Figure 3-2 were profiled using dual airguns (495 cm³ and 660 cm³ or 165 and 330 cm³) and 3.5 kHz sub-bottom profiling systems. Side-scan sonar data were collected only during daylight hours to avoid entanglement of the towed instrument with crab pots in the survey area.

A mini-sparker was used on two dip-line segments. Table 3-1 provides a description of these equipment. Vessel speed during geophysical profiling was 4 to 5 knots.

Two of the primary geophysical systems experienced significant operational problems during the cruise. The intermediate resolution mini-sparker **profiling** system became inoperative after the explosion of one of its transformers, early in Leg VI, and remained in-operable during the rest of the cruise. The side-scan tow fish collided with a crab pot early in Leg VI. In view of the downtime required to untangle the fish and crab pots and given the prevalence of crab pots in the survey area, a decision was made to operate the side-scan system only during daylight hours.

3.3 SEDIMENT SAMPLING

Sediment information was collected at 60 stations using grab samplers, gravity corers, **vibracorers**, and a drop penetrometer. **Table** 3-2 summarizes the numbers of samples by each method; Figure 2-5 identifies the locations of the 60 stations; and Appendix I tabulates the position of each station.

3.3.1 Grab and Gravity Core Samples

Grab samples were collected using a Van Veen sampler. If the **lithology** was at least slightly cohesive, a gravity core with a 365 kg weight stand and a 1- to 2-m long barrel was deployed. Van Veen samples were recovered at 55 of the 60 stations. Seven gravity cores were recovered from a total of 22 attempts during both legs of the cruise. The average length of gravity cores was 38 cm. Large volume (25 kg) **surficial** samples were collected at 10 stations during Leg VII of the cruise by taking multiple Van Veen samples.

3.3.2 Vibracores

A small **vibracore** was employed on Leg VII in an attempt to penetrate dense **surficial** sands encountered during the Leg VI gravity coring operations. The **vibracore** (built by Mr. Gordon **Womack** of Sub-Ocean Systems, Inc., Tustin, California) was used when wind and sea state permitted. The **Womack** corer is hydraulically driven and has a **barrel** 6 m in length and 7 cm in diameter. The core barrel is supported in a frame for stability. The total weight of the assembly is approximately 2000 kg.

The **vibracore** was utilized at nine different stations within the study area. These stations were located in areas with potential geologic hazards. Only eight cores were recovered during 17 attempts. The average recovery length was 93 cm with lengths ranging from 15 cm to 216 cm. A summary of **vibracoring** attempts is presented in Table 3-3; locations of the **vibracores** are shown in Figure 3-3.

The maximum depth of penetration of the vibracore was considerably less than anticipated. Typically a very dense fine sand was found at the tips of the successful vibracores. Further penetration apparently ceased when this material or layer was reached. Whether the denseness was introduced by the action of the vibracore or actually represents the in situ condition is not known with certainty. However, the areal distribution of the "more successful" **vibracore** attempts (recovery better than 1 m) coincided with the location of the "more successful" gravity cores, thus suggesting that the hard sediment is an in situ condition.

3.3.3 Drop Penetrometer

Density and strength information was also obtained by the use of a drop penetrometer developed by Professor R. F. Scott of the California Institute of Technology (Scott, 1967). Figure 3-4 shows a photograph of the drop penetrometer. The penetrometer consists of a 3-m long, 2.5-cm diameter rod with a 10 cm diameter conical tip (60° level) on the end. A 100 kg **weightstand** containing a mechanical accelerometer is attached to the other end of the rod.

The penetrometer is operated by lowering the system on a winch line to within 10 to 15 m of the **seabottom**. At this height the penetrometer is allowed to "free-fall" to the seafloor. This sequence is illustrated in Figure 3-5. As the penetrometer falls toward the seafloor and penetrates the bottom, the mechanical accelerometer within the weightstand records the change in acceleration. The acceleration data are subsequently processed to obtain a force-deformation relationship for the soil during the penetration process. This information is then interpreted using conventional **geotechnical** engineering procedures to estimate density and frictional angles of the sediment.

The drop penetrometer was used 46 times during Leg VI and 43 times during Leg VII. Figure 3-6 shows the drop penetrometer test locations. The results of subsequent interpretations suggested that the maximum cone penetration was less than 1 m, which confirmed observations made during sampling operations regarding the denseness of the sediments.

Table 3-1 Seismic Profiling SystemsDescription

EDO-WESTERN (Model 515) - high resolution profiling system (3.5 kHz) low to moderate (with proper booster) penetration (50 m), very high resolution system employing a mounted hull transducer, data are printed on 19 inch graphic recorder. Supplied **by** Mesa⁺.

BOOMER - EPC 200 Joule Boomer - a moderate penetration (up to 75 m), high resolution (30 cm) system employing a towed electromechanical sound source and a towed hydrophore array. **Subbottom** data are printed on a 19 inch graphic recorder. Supplied by Mesa⁺.

BOLT AIR GUN - **a** high energy, low frequency system utilized for deep penetration seismic profiling. The 40 **cubic inch** unit is capable of a resolution of **+3** m; penetration can be varied by changing capacity (1 to 40 cubic inches). Data output presented on 19 inch graphic recorder. Supplied by USGS and Mesa⁺.

EDO-WESTERN Side Scan Sonar System - employed a **dual** channel graphic recorder and transducer towfish to obtain quasi-three-dimensional imagery of sea floor features. The system is complete with 150 m tow cables and power **supply**. Supplied by Mesa⁺.

GEOTECHNICAL SPARKER - **28kJ** maximum power, variable frequency system for intermediate-penetration profiling and resolution (**+ 3** m). Data output can be presented in analog form on a graphic recorder **and/or** on a magnetic tape. Supplied by Mesa⁺.

RECORDERS - 2 supplied by **NOAA**, 1 by Mesa⁺.

HYDROPHORES - 2 supplied by USGS, 2 by Mesa⁺.

SEDIMENT SAMPLING EQUIPMENT

Gravity Core - Supplied by NOAA.

Vibracore - Supplied by Mesa⁺.

Shipek Grab - Supplied by NOAA.

Van Veen Grab - Supplied by NOAA.

Phleger Core - Supplied by NOAA.

Drop Penetrometer - Supplied by Ertec.

Table 3-2 Numbers of Samples Obtained
During Sediment Sampling Program

	Number of Samples		
	Leg VI	Leg VII	<u>Total</u>
Stations	40	20	60
Grab Sampling			
Van Veen	39	16	55
Gravity Core	1	7	8
Vibracoring	(not on board)	8	8
Drop Penetrometer Testing	46	43	89

Table 3-3 Vibracore Summary

<u>Station</u>	<u>Attempts</u>	<u>Recovery</u>	<u>Length Meter</u>
1777/185	1	0	0
1204/200	1	0	0
1202/200	2	1	0.40
1285/181	3	0	0
1070/91	3	1	0.15
			0
			0
1070/87	2	2	0.65
			0.70
1051/87	1	0	0
1020/100	2	2	0.20
			1.05
1000/200	2	2	1.40
			1.95
Totals:	_____	_____	_____
9 Stations	17	8	6.50 m Total Length Recovered

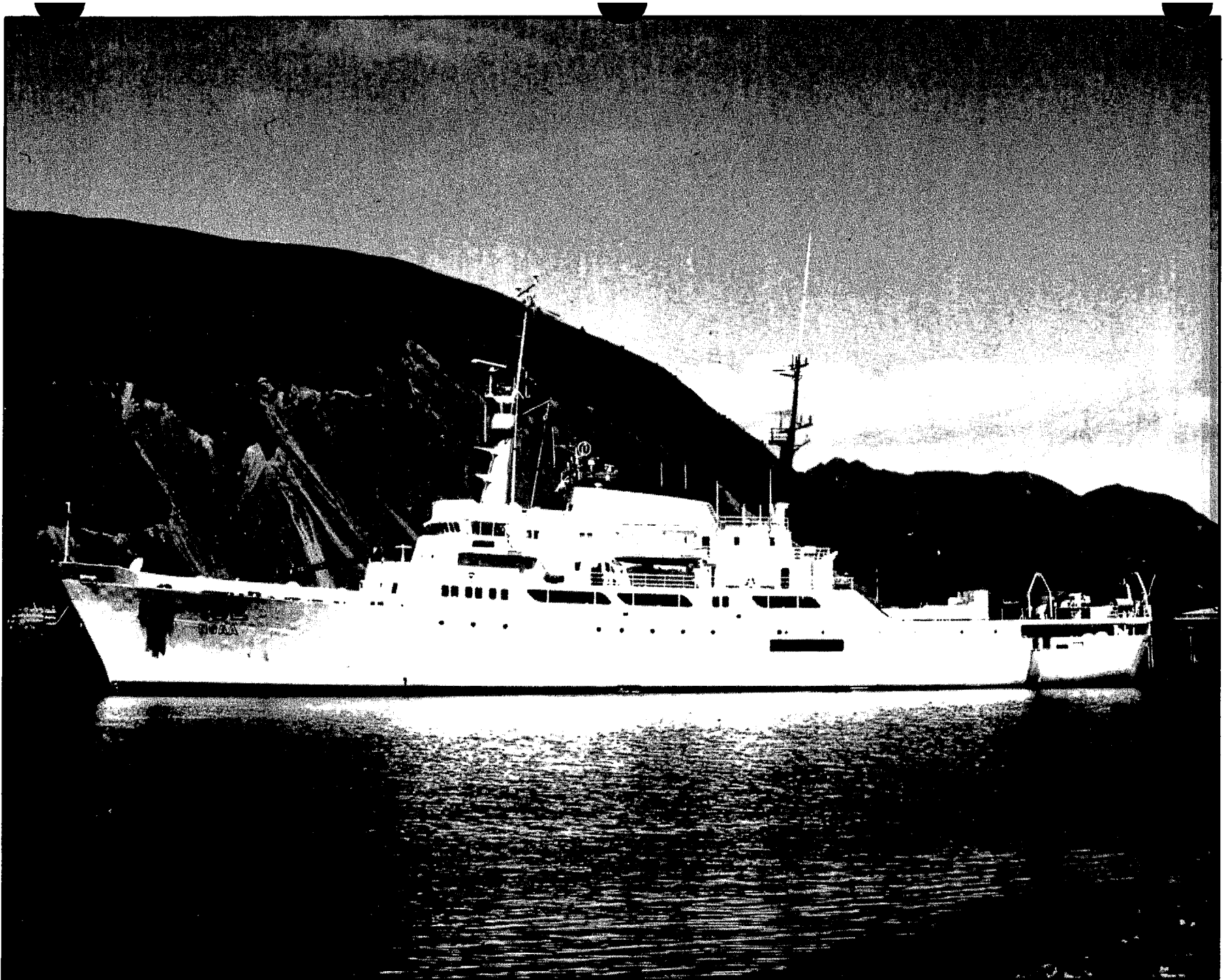


FIGURE 3-1 PHOTOGRAPH OF NOAA SHIP DISCOVERER

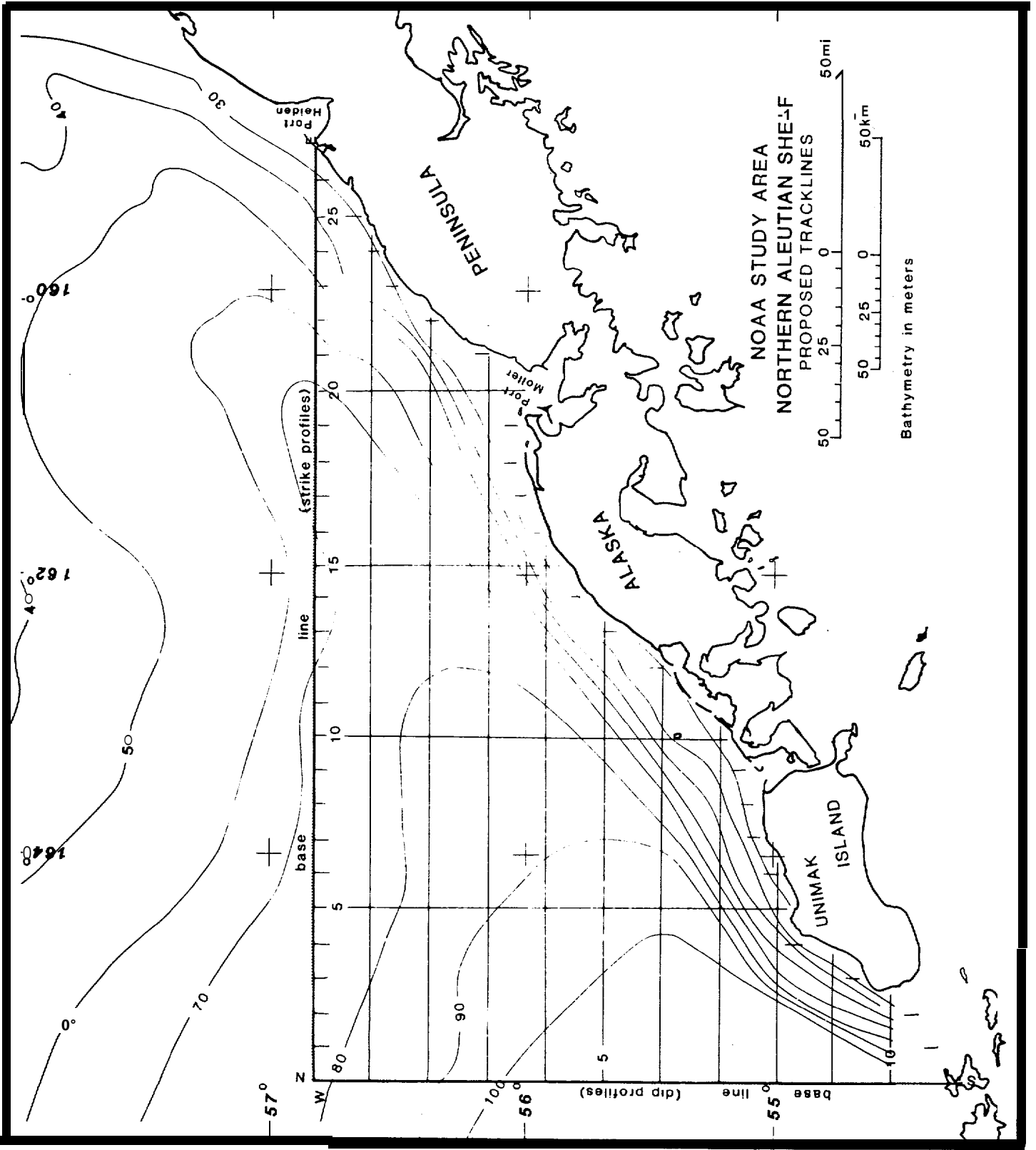


FIGURE 3-2 GEOPHYSICAL TRACKLINE—BASELINE REFERENCE SYSTEM

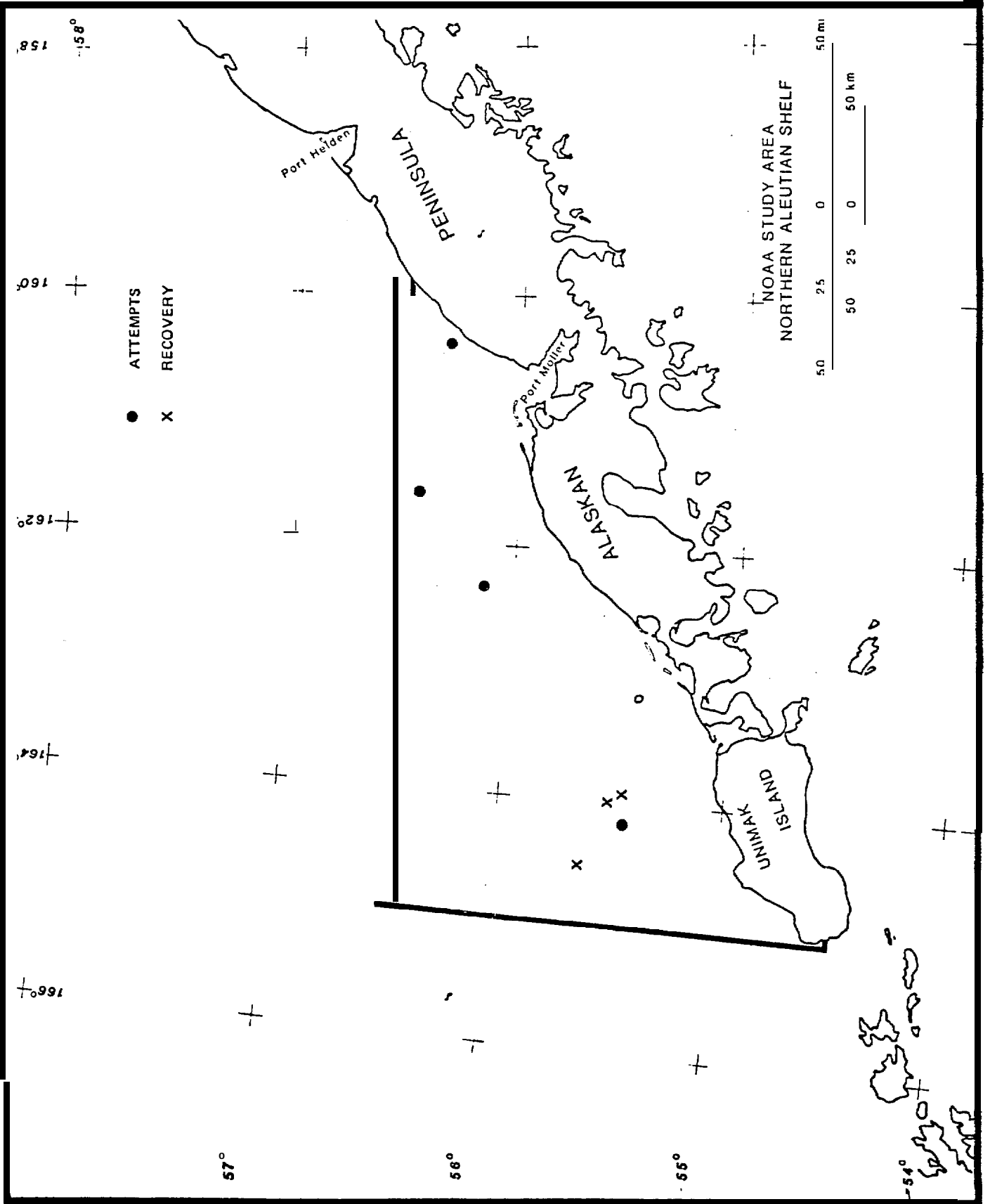
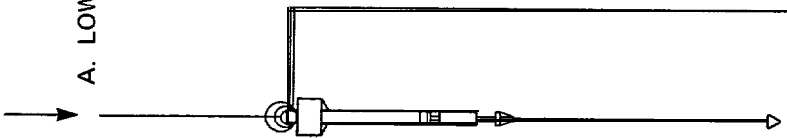


FIGURE 3-3 VIBRACORE LOCATION MAP

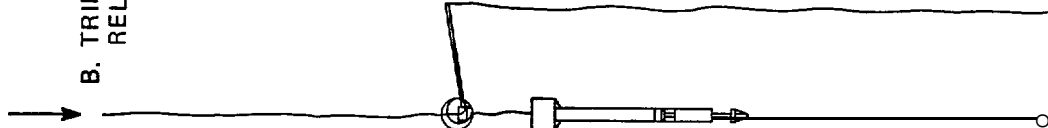


FIGURE 3-4 PHOTOGRAPH OF DROP PENETROMETER

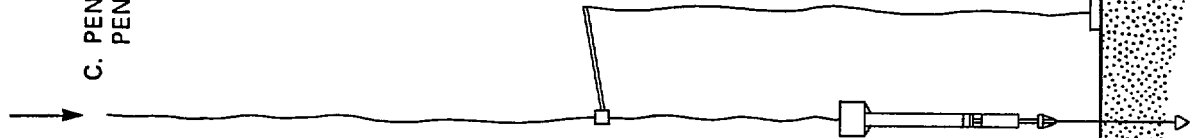
A. LOWERING M



B. TRIP MECHANISM RELEASED



C. PENETROMETER PENETRATED



R 3-5 SCHEMATIC DIAGRAM OF DROP PENETROMETER OPERATION

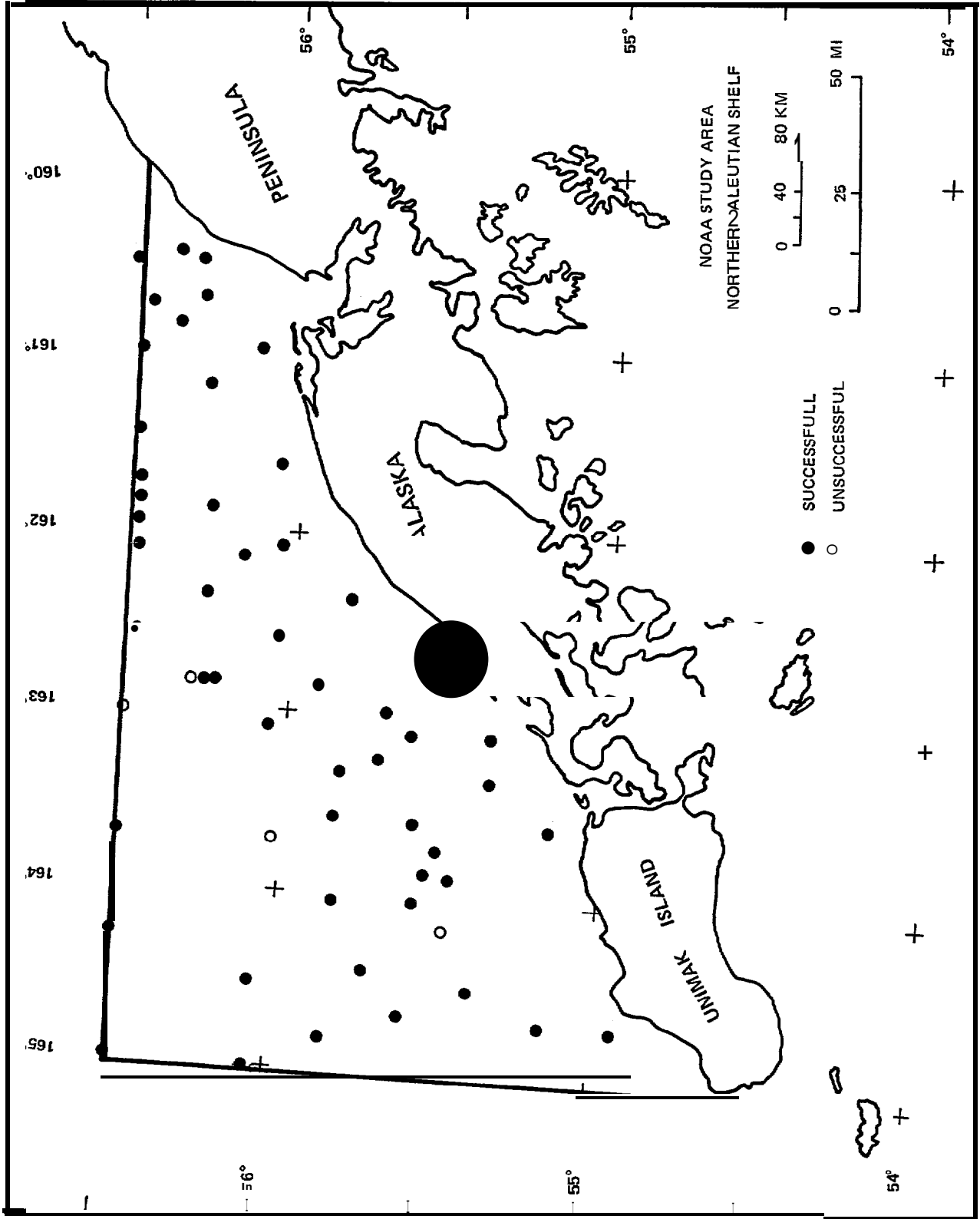


FIGURE 3-6 DROP PENETROMETER TEST LOCATION

4.1 SAMPLE DISTRIBUTION

Sediment samples recovered during the field program were visually classified onboard the survey vessel. From this visual examination, it was determined that all sediments were **cohesionless** (silts and sands), and hence, it was decided that all laboratory testing would be performed in onshore laboratories. Each sample was then sealed and stored for subsequent laboratory testing. If cohesive (clay) samples had been recovered, the scientific crew was prepared **to** conduct limited offshore testing including water content and miniature vane shear strength determinations.

The onshore testing program was conducted at **Ertec's** soil mechanics laboratory located in Long Beach, California and at California State University, Northridge, California. The onshore testing program involved geological description and engineering classification of the sediment samples. The geological description included determination of grain-size distribution, total organic content, carbonate content, bulk mineralogy, X-radiography and radiocarbon dating. Engineering classification included determination of water content, total unit weight, specific gravity, maximum/minimum density, compressibility, permeability, static strength, liquefaction resistance, shear modulus, and material damping properties. Test procedures and results from the tests are described below. Section 5.5 of this report presents a detailed discussion of significant results. Appendix 11 contains a detailed summary of test results.

4.2 GEOLOGICAL DESCRIPTION

The majority of the geological tests were conducted by the Geological Sciences Department at California State University, Northridge. The purpose of these tests was to establish baseline characteristics of existing sediments.

4.2.1 Grain-size Analyses

Grain-size analyses were performed on 60 samples using an Automatic Particle-Size Analyzer (Gibbs, 1974). The Automatic Particle-Size Analyzer (APSA) utilizes settling procedures to compute grain-size distributions (Hand, 1964, and 1967; McIntyre, 1969). Grain sizes were determined in 0.5 phi intervals. The settling method was used because it exhibits several advantages over the conventional sieving technique. For example, it is precise and accurate so that analyses are completely reproducible; it provides a continuous record of sediment grain-size properties, permitting precise increments of measurement; it provides a measure of hydraulic properties rather than possibly extraneous shape distributions; and it is relatively rapid.

Discussion and comparison of sieving and settling techniques using a variety of settling devices are plentiful in the literature (Emery, 1938; Schlee, 1966; Sengupta and Veenstra, 1968; Felix, 1969; Gibbs and others, 1971; Sanford and Swift, 1971; Reed and others, 1976). In general these comparisons indicate that sieves segregate particles on the basis of minimum properties, while the settling tube directly measures the velocity with which a sediment particle settles through a column of water. Settling velocity is a sensitive function of grain shape, size, density, and surface texture, as well as certain properties of the **fluid**. Thus, **small** dense particles may settle with the same velocity as larger, less dense grains.

Twenty-two of the samples were also sieved using methods recommended by the American Society for Testing and Materials (ASTM) to provide comparative data. Samples that contained more than 5 percent silt and clay were further analyzed by standard pipette techniques. **Surficial** sediments at 13 of the 60 stations had more than 5 percent fines.

Average or graphic mean grain size, inclusive graphic standard deviation (sorting), inclusive graphic skewness, and graphic kurtosis were calculated according to Folk and Ward (1957) and Folk (1974) (see definition of terms in Appendix I). Grain-size parameters, as discussed in Section 5.5, are based upon these measures. Individual grain-size data are tabulated in Appendix 1.

4.2.2 Bulk Mineralogy

Sixty samples were examined to determine the bulk mineralogy of the **sediments**. A minimum of 300 grains were counted using a petrographic microscope. Grains were identified under both plain and polarized light and assigned to one of six mineralogical categories. The categories included quartz, feldspar, hornblende, hypersthene, opaques, and others. Results of the mineralogy studies are summarized in Table 4-1.

4.2.3 Total Organic Carbon and Percent CaCO_3

Total organic carbon and percent calcium carbonate (CaCO_3) were determined using a modified Bien gasometric digestion assembly and a LECO total carbon analyzer. These methods are based upon the evolution of carbon dioxide (CO_2) from the sample. The volume of CO_2 evolved is directly related to the amount of carbon contained in the sample. Carbon dioxide evolved from both digestion and combustion of carbon compounds in sediments follows a flow pattern modified after **Kolpack** and Bell (1968). Eleven samples which contained

greater than 5 percent silt and clay were tested. As most resultant numbers were very low, replicates were conducted on each sample to ensure statistical repeatability. Results are summarized in Table 4-2.

4.2.4 Age-Dating

Radiocarbon dating was performed on marine shells from two samples by Dr. R. E. Taylor, Director of the Radiocarbon Laboratory at the University of California, Riverside. No other samples had sufficient carbon to yield useable dates. To determine the dates on the two samples, the outer one-third of the surface of the shell was removed in acid to reduce the chance of contamination. Carbon Dioxide (CO_2) was evolved by 2 normal hydrochloric acid (HCL) in a closed system and collected in **liquid** nitrogen traps. After being purified, this CO_2 was introduced into a 1.5 liter gas proportional detector. The counting activity of the sample was compared to that of 0.95 NBS (National Bureau of Standards) **oxalic** acid standard. The age was then expressed in radiocarbon years before present (**B.P.**) with 5568 used as the ^{14}C half-life and **A.D. 1950 = B.P.**

The results of the two analyses indicate that sediments at a depth of 7 to 10 cm below the surface have an age of about 12,000 years, i.e.

- o Station 1070/91 from 7 cm in 84 m of water 12,390 \pm 250 years
- o Station 1070/87 from 10 cm in 89 m of water 11,720 \pm 245 years

4.3 ENGINEERING CHARACTERISTICS

The engineering phase of the laboratory program was conducted to characterize the engineering properties of the sediments. Information from this phase formed the basis for conducting various geologic hazards analyses.

The laboratory testing program involved determination of 1) index properties and 2) engineering parameters. In general, the engineering laboratory tests were performed in accordance either with American Society for Testing and Materials (ASTM) procedures, or with practices adopted by the **geotechnical** engineering profession. Laboratory tests were performed on selected soil samples as well as reconstituted samples. Reconstituted samples were prepared using a wet-tamping method with the procedures described by Ladd (1978). Reconstituted samples were prepared to best-estimate, in-situ density values (Section 5.5.5.4). The following paragraphs provide a general description of the testing methods and a summary of test results. Detailed results of these tests are presented in Appendix II.

4.3.1 Total Unit Weight and Water Content

The total (or bulk) unit weight and water content were determined for 46 samples using conventional **geotechnical** procedures. The total unit weight was computed by measuring the weight of a known volume of material. **Subcores** of larger samples were made to obtain the unit weight data. Water contents were determined by drying a known weight of sediment and then obtaining the ratio of weight loss to dry weight, in accordance with ASTM **D2216**. No corrections were made for **salt** content. Results of these tests are summarized in Table 4-3.

4.3.2 Specific Gravity

Specific gravity tests were conducted on three samples using procedures set forth in ASTM **D854**. The procedure generally involved determination of the unit weight of the sediment and comparison of this weight to the unit weight of water at 4° C. A dry preparation method was employed. This specific gravity was determined on sediments as they occur naturally (and hence can be referred to as apparent specific gravity). Examination of the sediment particles

suggested that no voids exist within the individual particles; therefore, the apparent specific gravity was probably similar to the true specific gravity **value** of the soil grain. Results of specific gravity tests are summarized in Table 4-4.

4.3.3 Grain-Size Analyses

Grain-size analyses were performed on 34 samples 1) to supplement **grain-** size data obtained during geological classification and 2) to provide direct information on samples subjected to other engineering tests. These latter data provided a basis for drawing correlations between certain engineering properties and sediment size. Procedures given in ASTM **D422** were followed in these tests. In view of the coarseness of the sediments, sieving methods were used on most samples. Test specimens were prepared using a dry preparation method. Results are tabulated in Appendix I.

4.3.4 Maximum and Minimum Dry Unit Weights

Eight maximum and minimum dry unit weight **tests** were conducted in general accordance with ASTM procedure **D2049**. These tests were conducted to obtain 1) a basis for judging the relative denseness of sediment in situ and 2) possible ranges of densities if local materials are used for construction. Minimum dry unit weights were obtained by use of the funneling method; the maximum height of free fall of the soil was maintained constant at 2.5 cm. Maximum dry unit weights were obtained by vibrating a mold containing a sample of soil with a standard vibrator for a specified duration. Results of these tests are summarized in Table 4-5.

4.3.5 Compressibility

The one-dimensional compressibilities of seven samples were measured by conducting oedometer (or consolidation) tests in accordance with procedures

described in ASTM D2435. A standard, dead-load **consolidometer** was used. Three of the test specimens were obtained from gravity cores. These specimens were relatively undisturbed ie., the natural grain structure of the sediment was retained. The other four samples were totally reconstituted to specific density and moisture content values shown in Table 4-6. Information from the oedometer tests provides an indication of the amount of compression the sediment might experience for different stress levels. Results are summarized in Table 4-6 and Appendix II.

4.3.6 Permeability

Six permeability tests were conducted using constant head, **triaxial** testing methods. Two of the tests were performed on gravity core specimens; the others were performed on reconstituted material. These tests were required to quantify the rate at which excess pore-water pressures would dissipate after storm-wave or earthquake-induced pore pressure increases. Samples were consolidated **isotropically** to the estimated in situ effective vertical stress and then back-pressure saturated prior to testing. During the test a constant head was applied to the top of the sample, and the resultant outflow from the bottom was measured for a period of time. Permeability characteristics were obtained by plotting and analyzing the cumulative outflow versus **time** during the **tests**. Results are summarized in Table 4-7.

4.3.7 Static Triaxial Strength

Fourteen **isotropically** consolidated, drained **triaxial** compression **tests** were conducted on 12 reconstituted and 2 gravity core specimens. The purpose of these **tests was to** obtain the effective angle of internal friction for the materials. Reconstituted samples were prepared using a **moist** tamping procedure.

Procedures recommended by the Corps of Engineers (EN11110-2-1906) were used to conduct the **tests**. In general these procedures involved placement of a cylindrical sample of soil in a membrane, consolidation of the sample in a pressure chamber at a specified confining pressure, and shearing by application of an axial load. The rate of loading (0.08 percent per minute) was sufficiently slow to ensure that no excess pore-water pressures developed. Load, **deformation** and volume change were recorded during the tests.

Standard test procedures were modified slightly during tests on the two gravity core samples. For these tests a multistage testing method was employed. This method involved shearing each sample under three confining pressures. The maximum shearing strain was limited to 2 percent under the first two pressures; the last test was carried out to 20 percent strain. Results of these tests are summarized in Table 4-8. Appendix II contains individual test data.

4.3.8 Liquefaction Resistance

Cyclic simple shear tests were conducted on five gravity core specimens and 12 reconstituted samples. The purpose of these tests was to estimate the resistance of **surficial** sediments to liquefaction.

Cyclic simple shear tests were performed using a modified version of the **Geotechnical** Equipment Corporation Model SS-104 cyclic simple shear device (Figure 4-1). Test specimens were confined in wire-bound membranes and consolidated under estimated in situ effective vertical stresses. Pore fluids were back pressured to ensure full saturation. Once saturated, the cylindrical specimens were subjected to a *cyclic* horizontal shearing load at a frequency of 0.5 Hz. Applied shearing stresses were selected so as to generate

failure between 5 and 50 cycles. Load, deformation, and pore-water pressure were monitored on a strip chart recorder. Test results were plotted as pore-water pressure ratio and double-amplitude shearing strain versus number of loading cycles. Liquefaction strength was determined at a cyclic shearing strain of 10 percent or at excess pore-water pressures equal to the axial stress at the beginning of the test, whichever occurred first. Information from these tests was used to predict soil response during earthquake or storm-wave loading. Results of these tests are summarized in Table 4-9; individual test data are presented in Appendix II.

4.3.9 Shear Modulus and Damping

Four sets of resonant column and cyclic **triaxial** tests were conducted on reconstituted samples to define the shear modulus and material damping characteristics of **surficial** sediments. Test procedures involved first testing a sample in the resonant column device to obtain modulus and damping values over the 10^{-4} to 10^{-2} percent shearing strain range, and then carefully transferring the sample to the cyclic **triaxial** device to define modulus and damping values over the 10^{-2} to 1 percent strain range.

The resonant column **tests** were performed using a Hardin-type resonant column device (Figures 4-2 and 4-3). During these tests, the samples were first **isotropically** consolidated under the estimated in situ vertical effective stresses. After consolidation was complete, torsional vibrations were applied to the top of the **sample**; the bottom was rigidly fixed. Resonant frequency, torque and acceleration were recorded. Using a wave equation analysis, dynamic shear modulus and damping of soils for each strain level were determined.

An MTS Model 810 **electro-hydraulic** loading system, operated in the strain-controlled mode at a loading frequency of 1.0 Hz, was used to perform the cyclic **triaxial** tests (Figures 4-3 on 4-4). During these tests, the sample was transferred from the resonant column device, and the same consolidation pressure used in the resonant column test was applied. A back pressure was used to induce full saturation, then 15 cycles of loading were applied. Drainage was not permitted during cyclic loading. After the 15th cycle, drainage was allowed. Upon complete dissipation of generated excess pore-water pressures, the next higher strain level loading was applied. Hysteresis loops of load versus deformation were recorded to facilitate calculation of secant modulus and damping values. These hysteresis loops were digitized; a computer program was used to convert the measured axial characteristics to shear characteristics. The conversion equations used are:

$$\begin{aligned} G &= E/2(1 + \nu) \\ \gamma &= E(1 + \nu) \end{aligned} \quad (4-1)$$

where G is shear modulus, E is Young's modulus, γ is shearing strain and ν is Poisson's Ratio (assumed equal to 0.45). The value of shear modulus obtained at any shearing strain in the cyclic **triaxial** test was normalized by the maximum modulus for that sample as measured in the resonant column device.

Results of these tests are summarized in Tables 4-10 and 4-11; individual test data are presented in Appendix II.

4.3.10 Sonic Velocities

Sonic velocity measurements were performed on eight samples by Dr. Edward L. Hamilton of the Naval Ocean Systems Center, San Diego, California. All measurements were made with a sound **velocimeter**. Results of these tests are summarized in Table 4-12.

Table 4-1 Mineralogic Composition Determined from Bulk* Mineralogic Analyses

Sample Number	Quartz (%)	Feldspar (%)	Hypersthene (%)	Hornblende (%)	Opaque (%)	Other (%)
1	31.0	21.7	8.0	8.7	27.7	3.0
2	36.3	24.7	1.0	4.3	25.0	8.7
3	38.3	22.3	9.3	10.7	18.0	1.3
4	28.7	37.3	1.3	6.8	25.3	1.7
5	38.0	27.7	0.7	3.0	27.3	3.3
6	35.3	33.7	0.7	1.0	27.3	2.0
7	27.7	30.0	2.0	2.7	36.0	1.7
8	34.7	33.0	2.7	1.7	27.7	0.3
9	35.8	25.8	0.3	1.3	36.1	0.8
10	25.3	32.7	3.3	2.0	33.0	3.7
11	23.3	17.7	2.0	8.0	46.3	2.7
12	15.3	20.0	13.0	4.3	45.3	2.0
13	31.0	35.0	1.0	1.0	31.3	0.7
14	23.3	24.7	9.0	8.7	27.7	6.7
15	35.0	25.7	3.0	6.7	26.7	3.0
16	23.0	43.7	4.3	1.7	24.0	3.3
17	21.7	37.0	1.7	2.7	35.7	1.3
18	27.7	31.7	2.7	4.0	32.7	1.3
19	28.3	32.0	1.3	2.3	35.3	0.7
20	32.0	21.3	6.3	4.7	32.3	3.3
21	23.0	41.1	3.7	3.4	27.9	0.9
22	34.0	16.0	2.7	10.0	33.0	4.3
23	21.7	20.3	2.7	8.7	32.3	4.7
24	27.7	22.7	5.0	8.7	43.0	3.7
25	35.0	22.7	4.7	8.3	28.7	0.7
26	30.3	30.7	1.3	6.7	28.0	3.0
27	14.3	13.0	15.7	10.7	43.3	3.0
28	12.3	27.0	3.3	5.7	50.3	1.3
29	29.3	27.0	0.3	11.7	28.7	3.0
30	29.7	40.0	0.7	3.0	26.7	0.0
31	20.3	30.7	2.0	8.7	36.0	2.3
32	29.3	21.3	2.7	7.3	36.3	3.0
33	38.3	19.0	7.3	11.7	22.0	1.7
34	40.3	9*3	3.0	11.0	35.0	1.3
35	24.7	21.3	7.7	18.0	28.3	0.0
36	12.3	27.0	13.3	4.0	42.3	1.0
37	26.3	16.7	9.7	9.3	38.0	1.0
38	15.0	13.3	16.3	18.3	41.0	2.3
39	15.0	15.0	6.3	13.7	46.3	3.7
40	12.0	25.7	15.7	21.0	18.7	7.0

*300 Counts

Table 4-1 **Mineralogic** Composition Determined from Bulk* **Mineralogic** Analysis
(Continued)

Sample Number	Quartz (%)	Feldspar (%)	Hypersthene (%)	Hornblende (%)	Opaque (%)	Other (%)
41	36.3	17.0	9.3	14.3	21.0	2.0
42	26.3	23.0	4.7	9*7	35.0	1.3
43	24.0	27.3	6.7	6.7	32.7	2.7
44	27.7	12.0	16.0	14.3	28.3	1.7
45	32.7	31.3	2.7	5.0	28.0	0.3
46	31.3	26.0	1.7	3.3	37.0	0.7
47	47.0	18.0	3.3	6.3	25.3	0.0
48	26.7	24.7	1.0	7.3	39.7	0.7
49	23.0	27.3	2.7	3.6	41.7	0.7
50	19.7	32.7	6.3	7.7	32.7	1.0
51	17.7	5.3	21.7	22.7	31.3	1.3
52	17.0	22.7	8.7	11.7	34.7	5.3
53	21.3	25.7	6.7	8.0	35.0	3.3
54	17.3	20.7	15.0	12.0	32.3	2.7
55	23.0	21.3	7.3	5.0	39.7	3.7
56	25.7	27.3	3.6	6.7	33.0	3.7
57	19.3	21.3	8.3	14.3	35.0	1.7
58	20.7	24.3	6.0	6.7	41.0	1.3
59	22.7	14.7	15.0	7.3	35.7	4.7
60	24.3	6.3	15.0	8.0	44.3	2.0

* 300 Counts

Table 4-2 Percentage of Carbon (Organic/Inorganic) and Calcium Carbonate Content for Selected Samples Tests

Sample Number	Total Carbon (%)	Total Organic Carbon (%)	Total Inorganic Carbon (%)	Calcium Carbonate (%)
1	0.48	0.44	0.03	0.28
3	0.49	0.46	0.02	0.22
7	0.40	0.37	0.03	0.26
8	0.36	0.35	0.02	0.16
9	0.44	0.43	0.02	0.15
11	0.44	0.42	0.02	0.13
15	0.34	0.33	0.02	0.14
17	0.36	0.35	0.02	0.16
18	0.30	0.28	0.02	0.13
22	0.33	0.31	0.02	0.15
28	0.30	0.29	0.02	0.13

Table 4-3 Moisture Content and Unit Weight Values for Selected Samples

Sample Number	Sample Type ¹⁾	Average Depth (cm) ²⁾	Soil Type ³⁾	Dry Unit Weight (kN/m ³) ⁴⁾	Moisture Content (%)	Total Unit Weight (kN/m ³) ⁴⁾
1	V*V.	s	SM (4)	14	34	18
1A	v	0-8	SM (4)	16	26	20
1A	v	78-86	SM (4)	16	23	20
1B	v	0-8	SM (4)	14	35	18
1B	v	63-71	SM (4)	17	21	20
2	V.V.	s	SM (4)	13	43	18
2	G.C.	8	SM (4)	14	36	19
2	G.C.	22	SM (4)	15	30	19
2	G.C.	32	SM (4)	14	34	19
2	G.C.	38	SM (4)	14	37	19
2	G.C.	50	SM (4)	14	33	19
2	G.C.	66	SM (4)	15	31	19
7	V.V.	s	SM (4)	14	32	19
9	V.V.	s	SM (4)	12	40	17
9	v	0-8	SM (4)	15	29	19
9	v	72-80	SM (4)	17	21	21
11	V.V.	s	SM (4)	13	42	18
11	G.C.	3	SM (4)	14	31	18
11	G.C.	8	SM (4)	16	28	20
11	G.C.	22	SM (4)	15	30	20
15	V.V.	s	SM (4)			
22	V.V.	s	SM (4)	14	34	19
23	V.V.	s	SP/SM (3)	13	39	18
23	G.C.	5	SP/SM (3)	14	31	18
23	G.C.	17	SP/SM (3)	15	26	19
23	G.C.	21	SP/SM (3)	15	28	20
23	G.C.	33	SP/SM (3)	14	35	19
23	G.C.	41	SP/SM (3)	15	29	19
23	G.C.	64	SP/SM (3)	15	28	19

- Notes :
- 1) **V.V.** = Van Veen; **G.C.** = **Gravity Corer**; **V** = **Vibracorer**
 - 2) **S** = Surface sample
 - 3) Number **in** parenthesis denotes **soil** type number described in Section 5.5; letter refers to soil type based on Unified Classification System
 - 4) 1 kN/m³ = 0.102 g/cm³

Table 4-3 Moisture Content and Unit Weight Values for Selected Samples

(Cent'd)

Sample Number	Sample Type ¹⁾	Average Depth (cm) ²⁾	Soil Type ³⁾	Dry Unit Weight (kN/m ³) ⁴⁾	Moisture Content (%)	Total Unit Weight (kN/m ³) ⁴⁾
26	V.V.	s	SP/SM (3)	16	29	21
26A	v	0-8	SP/SM (3)	16	26	20
26A	V	57-65	SP/SM (3)	16	24	20
26B	v	0-8	SP/SM (3)	15	29	19
27	V.V.	s	SP (2)	15	23	19
28	V.V.	s	SP/SM (3)			
35	V.V.	s	SP (2)	16	24	20
37	V.V.	s	SP (2)	16	25	20
39	V.V.	s	SP (1)	15	8	16
41	V.V.	s	SP (2)	17	25	22
43	V.V.	s	SP (2)	17	23	21
49	V.V.	s	SP (2)	16	28	20
50	V.V.	s	SP (2)	17	24	21
54	V.V.	s	SP (1)	18	13	20
55	V.V.	s	SP (1)	15	25	19
279	v	0-8		17	20	21
279	v	83-91		16	24	20

- Notes: 1) V.V. = Van Veen; G.C. = Gravity Corer; v = Vibracorer
 2) s = Surface Sample
 3) Number in parenthesis denotes the soil type number described in Section 5.5; letter refers to soil type on Unified Classification System
 4) 1 kN/m³ = 0.102 g/cm³

Table 4-4 Specific Gravity Values for Selected Samples

Sample Number	Sample Type ¹⁾	Soil Type ²⁾	Specific Gravity
9	V.V	SM(4)	2.69
36	V.V	SP(2)	2.80
48	V*V	SF(1)	2.74

Notes:

1) **V.V.** = Van Veen

2) Refer to Table 4-3

Table 4-5 Maximum and Minimum Dry Unit Weight **Values** for Selected Samples

Sample Number	Soil Type ¹⁾	Maximum Dry Unit Weights (kN/m ³)	Minimum Dry Unit Weights (kN/m ³)
1	SM (4)	14	12
7	SM (4)	14	12
9	SM (4)	15	11
12	SM (4)	14	12
24	SP/SM (3)	16	13
36	SP (2)	20	17
43	SP (2)	17	14
56	SP (2)	17	14
59	SP (1)	19	18

Note:

1) Refer to Table 4-3

Table 4-6 Compressibility Properties

Sample Number	Sample Type ¹⁾	Soil Type ²⁾	Total Unit Weight (kN/m ³)	Moisture Content (%)	Compression Index, C _c	Recompression Index, C _r	Voids Ratio, e.
2	GC	SM (4)	19	36	0.18	0.012	1.00
2	GC	SM (4)	19	34	0.19	0.009	0.96
9	R	SM (4)	19	28	0.04	0.005	0.74
23	cc	SP/SM (3)	19	32	0.15	0.008	0.87
24	R	SP/SM (3)	20	25	0.03	0.005	0.68
43	R	SP (1)	20	24	0.04	0.005	0.65
57	R	SP (2)	20	24	0.03	0.003	0.64

Note:

1) GC = Gravity Corer; R = Reconstituted

2) Refer to Table 4-3

Table 4-7 Permeability Characteristics of Selected Samples

Sample Number	Sample Type ¹⁾	Soil Type ²⁾	D ₁₀ (mm)	D ₅₀ (mm)	Coefficient of Permeability k (cm/see)
2	G.C.	SM (4)	0.005	0.055	1 x 10 ⁻⁶
9	R	SM (4)		0.13	2 x 10 ⁻⁵
23	G.C.	SP/SM (3)		0.12	5 x 10 ⁻⁶
24	R	SP/SM (3)	0.08	0.20	5 x 10 ⁻⁵
43	R	SP (1)	0.20	0.42	1 x 10 ⁻³
57	R	SP (2)	0.21	0.28	5 x 10 ⁻³

Note:

1, **G.C.** = Gravity Corer, R = Reconstituted

2) Refer to Table 4-3

Table 4-8 Shearing Strength Results from **Istropically** Consolidated,
Drained **Triaxial** Compression Tests (CID)

Sample Number	Sample Type ¹⁾	Soil Type ²⁾	Consolidation Stress (kN/m ²)	Dry Unit Weight (kN/m ³)	Initial Moisture Content (%)	Final Moisture Content (%)	Axial Strain (%)	q ³⁾ (kN/m ²)	p ³⁾ (kN/m ²)
2	G.C.	SM (4)	69	14	37	26	2	55	125
2	G.C.	SM (4)	138	14	37	26	2	105	243
2	G.C.	SM (4)	276	14	37	26	18	407	683
23	G.C.	SP/SM (3)	69	15	29		2	72	141
23	G.C.	SP/SM (3)	138	15	29		2	155	293
23	G.C.	SP/SM (3)	276	15	29		18	459	735
9	R	SM (4)	69	15	28	26	4	121	188
9	R	SM (4)	138	15	28	28	7	206	344
9	R	SM (4)	276	15	28	27	9	417	693
24	R	SP/SM (3)	69	16	26	28	2	171	240
24	R	SP/SM (3)	138	16	28	28	3	315	4.53
24	R	SP/SM (3)	276	16	26	27	4	478	754
43	R	SP (1)	69	16	24	25	2	130	199
43	R	SP (1)	138	16	23	26	3	252	390
43	R	SP (1)	276	16	24	25	5	469	744
57	R	SP (2)	69	16	24	27	2	117	186
57	R	SP (2)	138	16	24	27	4	281	419
57	R	SP (2)	276	16	24	26	6	520	796

Notes:

1) R = Reconstituted; G.C. = Gravity Corer

2) Refer to Table 4-3

3) $q = (\sigma_1 - \sigma_3)/2$; $p = (\sigma_1 + \sigma_3)/2$
where σ_1 = major principal stress and σ_3 = minor principal stress

Table 4-9 Cyclic Simple Shear Test Results

Sample Number	Sample Type	Average Depth (cm)	Soil Type	Dry Unit Weight (kN/m ³)	Moisture Content (%)	Vertical Stress (kN/m ²)	Shear ²⁾ Stress Ratio	Cycles at 5% Strain	Cycles to Initial Liquefaction
9	V.V.	s	SM (4)	15.1	29.5	69	0.24	11	14
9	V.V.	s	SM (4)	15.1	29.5	69	0.29	3	6
9	V.V.	s	SM (4)	15.1	29.5	69	0.19	24	24
9	V.V.	s	SM (4)	15.1	29.5	69	0.16	620	630
24	V.V.	s	SP/SM (3)	15.7	26.6	69	0.17	72	75
24	V.V.	s	SP/SM (3)	15.7	26.6	69	0.21	39	30
24	V.V.	s	SP/SM (3)	15.7	26.6	69	0.30	8	15
43	V.V.	s	SP (1)	16.4	24.3	69	0.22	9	10
43	V.V.	s	SP (1)	16.4	24.3	69	0.29	5	7
43	V*V.	s	SP (1)	16.4	24.3	69	0.17	80	80
57	V.V.	s	SP (2)	16.2	23.3	69	0.21	7	6
57	V.V.	s	SP (2)	16.2	23.3	69	0.17	20	26
57	V.V.	s	SP (2)	16.2	23.3	69	0.13	305	330
57	V*V.	s	SP (2)	16.2	23.3	69	0.14	29	30
1	G.C.	49	SM (4)	14.4	32.1	69	0.22	72	
1	G.C.	66	SM (4)	14.4	32.1	69	0.27	5	
1	G.C.	22	SM (4)	14.4	32.1	69	0.22	4	
11	G.C.	8	SM (4)	15.5	28.4	69	0.26	14	45
23	G.C.	33	SM (4)	14.8	29.5	69	0.20	45	60
23	G.C.	64	SM (4)	14.8	29.5	69	0.23	9	
23	G.C.	2	SM (4)	14.8	29.5	69	0.30	9	

Notes:

- 1) Refer to Table 4-3
- 2) Shear stress ratio defined as the ratio of cyclic shearing stress to the vertical stress

Table 4-10 Low Amplitude Shear Modulus From Resonant Column Tests

Sample Number	Sample ¹⁾ Type	Soil ²⁾ Type	Dry Unit Weight (kN/m ³)	Water Content (%)	Maximum Shear Modulus (kN/m ²)
9	R	SM (4)	15	14	7.6×10^4
24	R	SP/SM (3)	16	15	1.1×10^5
43	R	SP (1)	16	11	1.2×10^5
57	R	SP (2)	16	10	1.2×10^5

Notes:

1) R^e Reconstituted

2) Refer to Table 4-3

Table 4-11 Cyclic Triaxial Test Results

Sample Number	Sample Type	Average Depth (cm)	Soil ¹⁾ Type	Dry Unit Weight (kN/m ³)	Moisture Content (%)	Confining Pressure (kN/m ²)	Shearing Strain (%)	Shear Modulus (10 ⁴ k N/m ²)	Damping Ratio (%)
9	V.V.	5	SM (4)	15	27	138	0.02	7.0	18
9	V*V*	5	SM (4)	15	27	138	0.05	4.8	16
9	V*V*	5	SM (4)	15	27	138	0.10	3.9	15
9	V.V.	5	SM (4)	15	27	138	0.20	2.5	18
9	V.V.	5	SM (4)	15	27	138	0.67	0.5	24
24	V.V.	5	SP/SM (3)	18	27	138	0.02	7.0	5
24	V*V.	5	SP/SM (3)	18	27	138	0.05	4.6	24
24	V.V.	5	SP/SM (3)	18	27	138	0.11	4.5	15
24	V*V.	5	SP/SM (3)	18	27	138	0.20	3.6	16
24	V.V.	5	SP/SM (3)	18	27	138	0.68	1.0	18
43	V.V.	5	SF (1)	16	24	138	0.03	6.8	5
43	V*V.	5	SP (1)	16	24	138	0.05	4.3	21
43	V.V.	5	SP (2)	16	24	138	0.12	3.6	18
43	V.V.	5	SP (2)	16	24	138	0.21	2.4	21
43	V.V.	5	SP (2)	16	24	138	0.72	0.5	22
57	V.V.	5	SP (2)	18	25	138	0.02	9.3	3
57	G.C.	5	SM (4)	18	25	138	0.05	7.7	15
57	G.C.	5	SM (4)	18	25	138	0.10	5.6	16
57	G.C.	5	SM (4)	18	25	138	0.19	3.5	18
57	G.C.	5	SM (4)	18	25	138	0.65	0.8	22

Notes:

1) Refer to Table 4-3

Table 4-12 Sonic Velocity and Other Characteristics of Vibracore Samples

Vibracore Sample Number	Interv. (cm)	Sediment Name (1)	Grain Diameter				Sand %	Silt %	clay %	Specific Gravity of Grains (2)	Saturated Unit Weight (g/cm ³)	Porosity %	Velocity (23°C)		Color		Lab. No.
			Mean mm	ϕ	Median mm	Q							m/sec (3)	Ratio (4)	(5)		
VC 70/87A	0-8	Fine Sand	0.1696	2.56	0.1560	2.68	94.2	03.3	02.5	2.666	1.991	4.01	1s05	1.183	5Y 2.5/1	Black	1
VC 70187A	57-65	Very Fine Sand	0.1241	3.01	0.1111	3.17	*8.5	12.9	05.6	2.705	2.039	39.6	1845	1.209	5Y 2.5/1	Black	11
VC 70/87B	0-8	Fine Sand	0.1638	2.61	0.1397	2.84	*88.8	07.2	04.0	2.666	1.954	44.0	1804	1.182	5Y 2.5/1	Black	2
VC 20/100	0-8	Very Fine Sand	0.0934	3.42	0.1022	3.29	76.1	19.7	04.2	2.669	1.947	43.8	1729	1.133	5Y 2.5/1	Black	3
VC 20/100	72-80	Fine Sand	0.1550	2.69	0.1560	2.68	*88.8	06.0	05.2	2.706	2.103	35.8	1875	1.229	5Y 2.5/1	Black	4
VC 279	0-8	Very Fine Sand	0.0825	3.60	0.1001	3.32	76.0	16.8	07.2	2.697	2.117	34.6	1896	1.242	5Y 2.5/1	Black	5
VC 279	83-91	Silty Sand	0.0652	3.94	0.0665	3.91	55.4	37.6	07.0	2.677	2.034	38.8	1804	1.182	5Y 2.5/1	Black	6
VC O/200A	0-8	Silty Sand	0.0728	3.78	0.0764	3.71	57.1	37.8	05.1	2.661	1.995	40.6	1736	1.138	5Y 2.5/1	Black	7
VC O/200A	78-86	Silty Sand	0.0738	3.76	0.9067	3.37	67.2	25.2	07.6	2.688	2.048	38.4	1789	1.172	5Y 2.5/1	Black	8
VC O/200B	0-8	Sandy Silt	0.0367	4.77	0.0451	4.47	39.3	49.1	11.6	2.644	1.862	48.2	1698	1.113	5Y 2.5/1	Black	9
VC O/200B	63-71	Very Fine Sand	0.0921	3.44	0.1081	3.21	*78.2	05.4	05.4	2.655	2.089	35.8	1830	1.199	5Y 2.5/1	Black	10

Notes: (1) Shepard, 1954

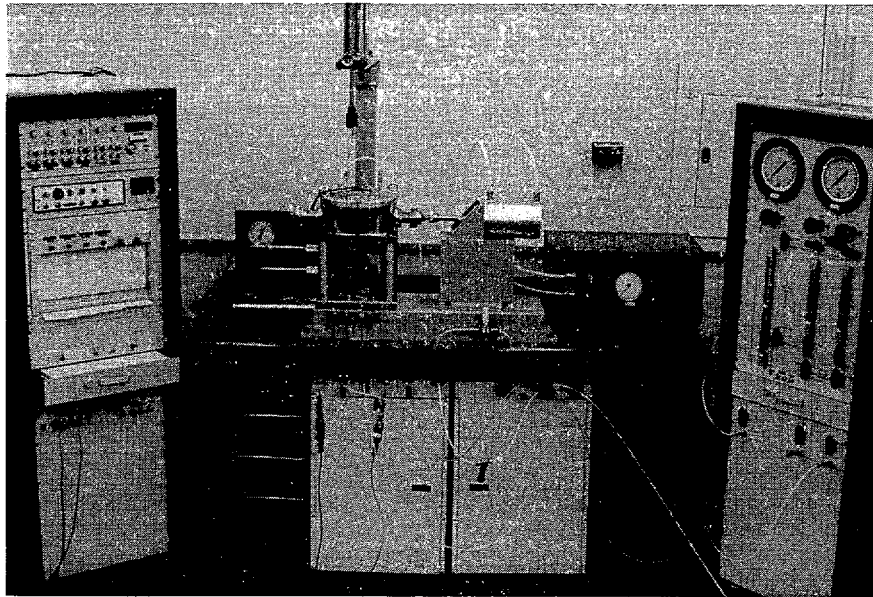
(2) Measured by pycnometer

(3) Ratio: Velocity in sediment/Velocity in sea water at 23° C, 1atm, and salinity of bottom water; in this case velocity is 1526 m/sec and salinity is 31.8 0/00

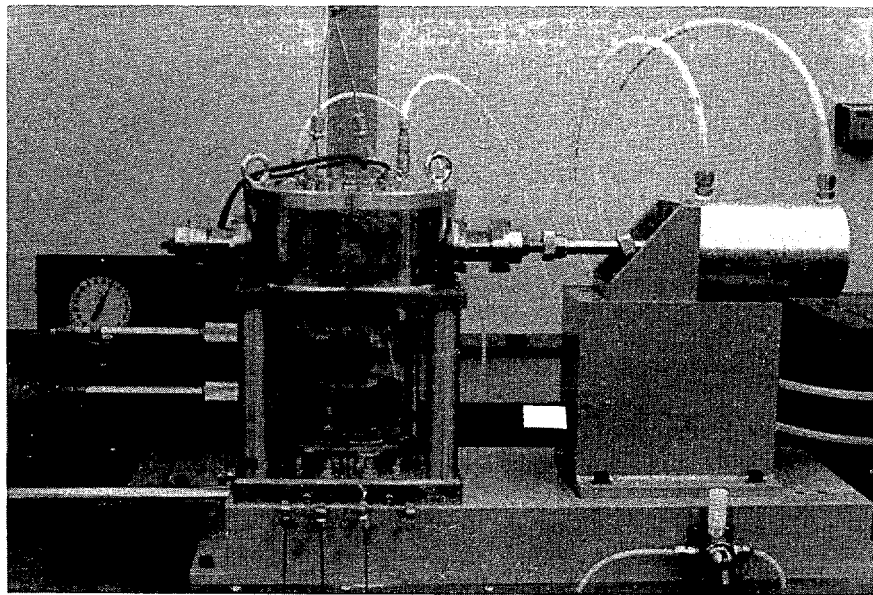
(4) Munsell Soil Color Chart

(5) Black color is due to decomposed organic matter

* Includes gravel fraction

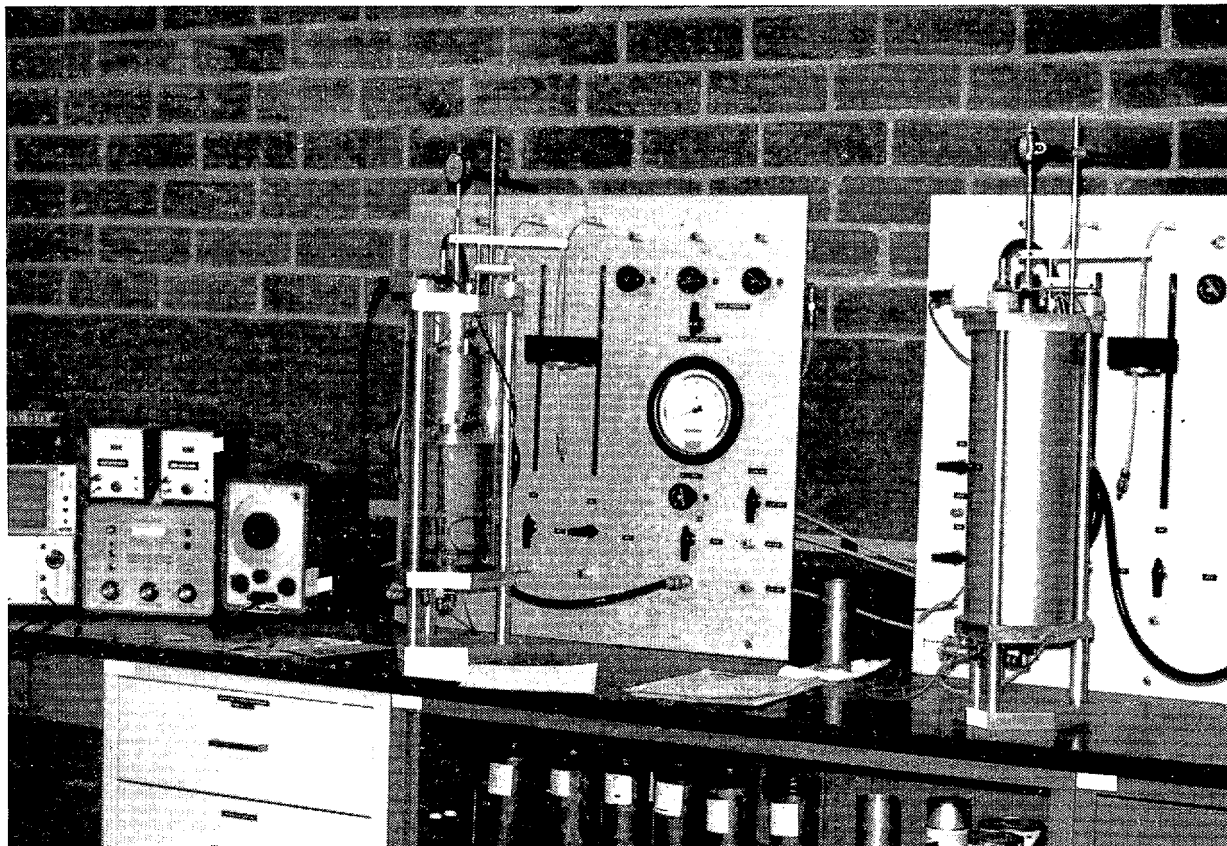


LOADING AND RECORDING SYSTEM



TEST CHAMBER

FIGURE 4-1 PHOTOGRAPHS OF CYCLIC SIMPLE SHEAR EQUIPMENT

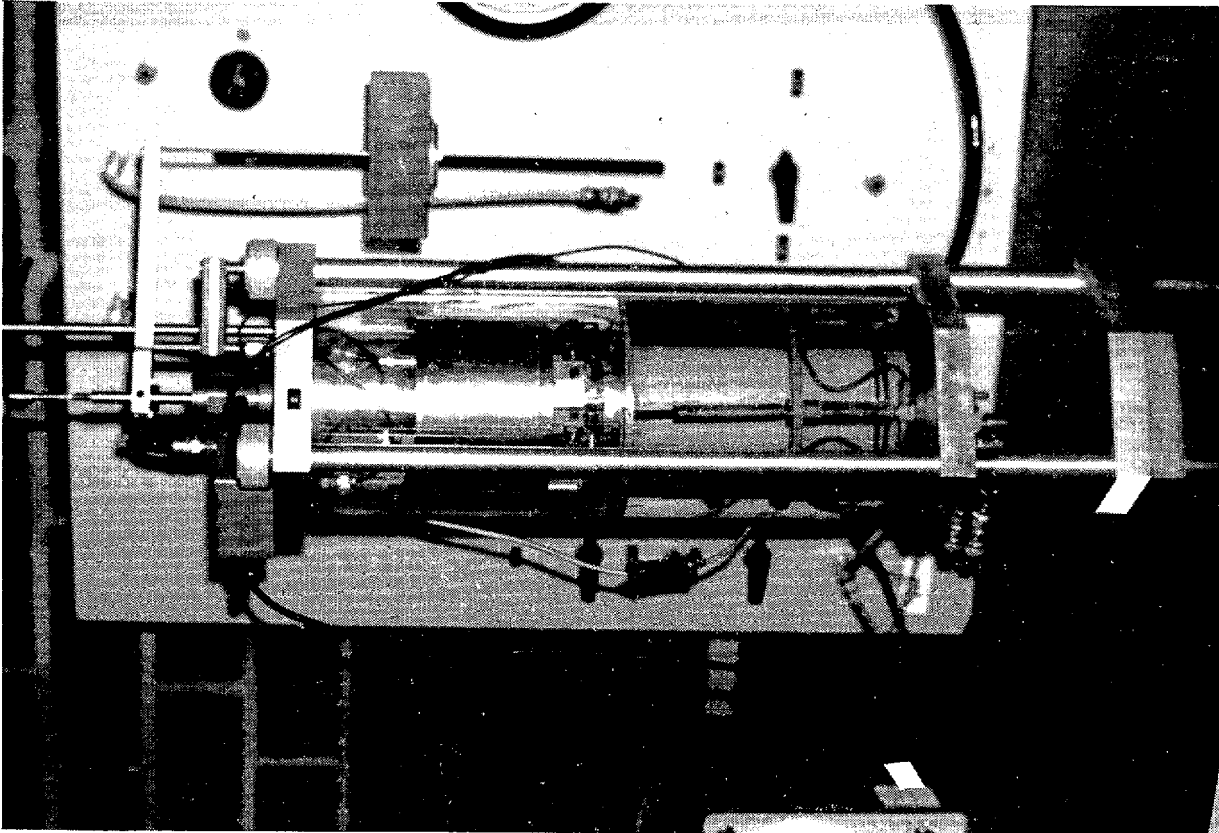


RESONANT' COLUMN TEST SETUP

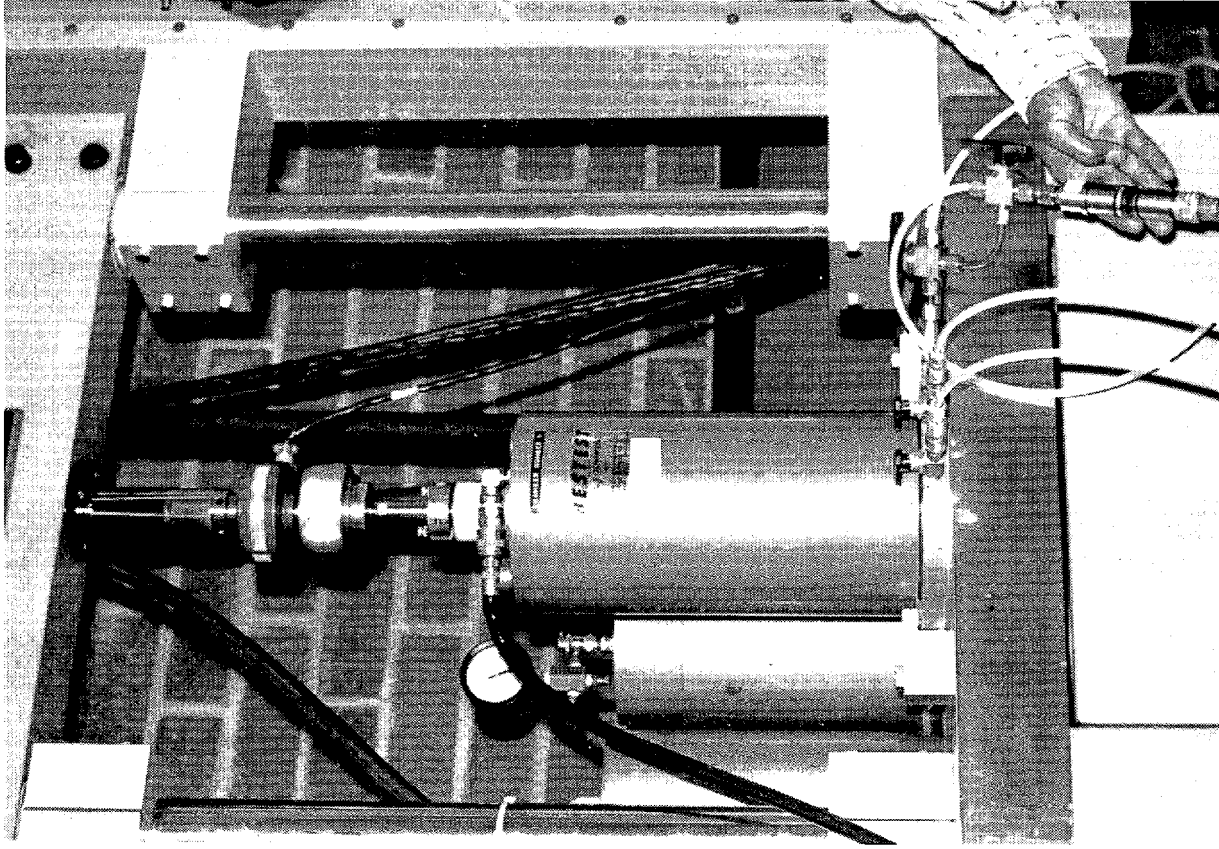


ELECTRONICS FOR RESONANT TEST

FIGURE 4-2 PHOTOGRAPHS OF RESONANT COLUMN EQUIPMENT

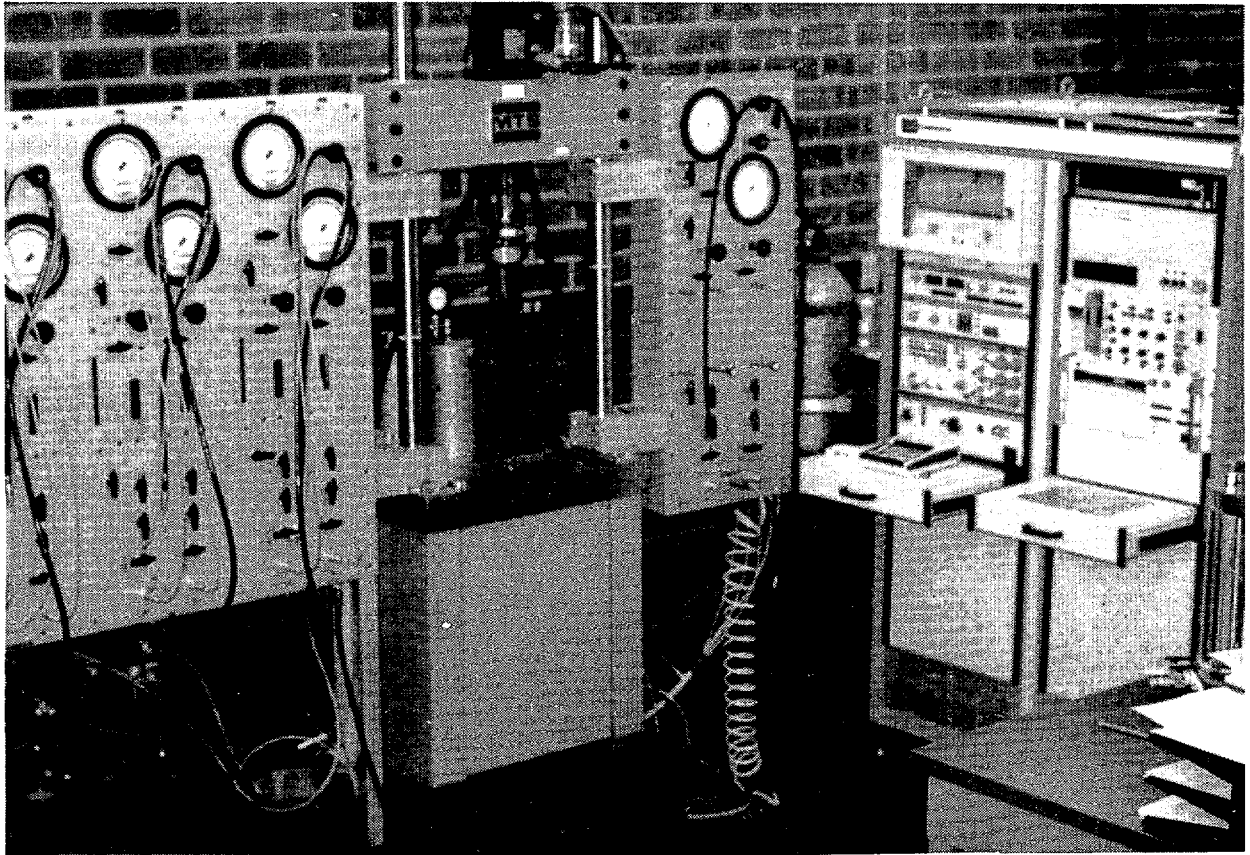


RESONANT COLUMN DEVICE

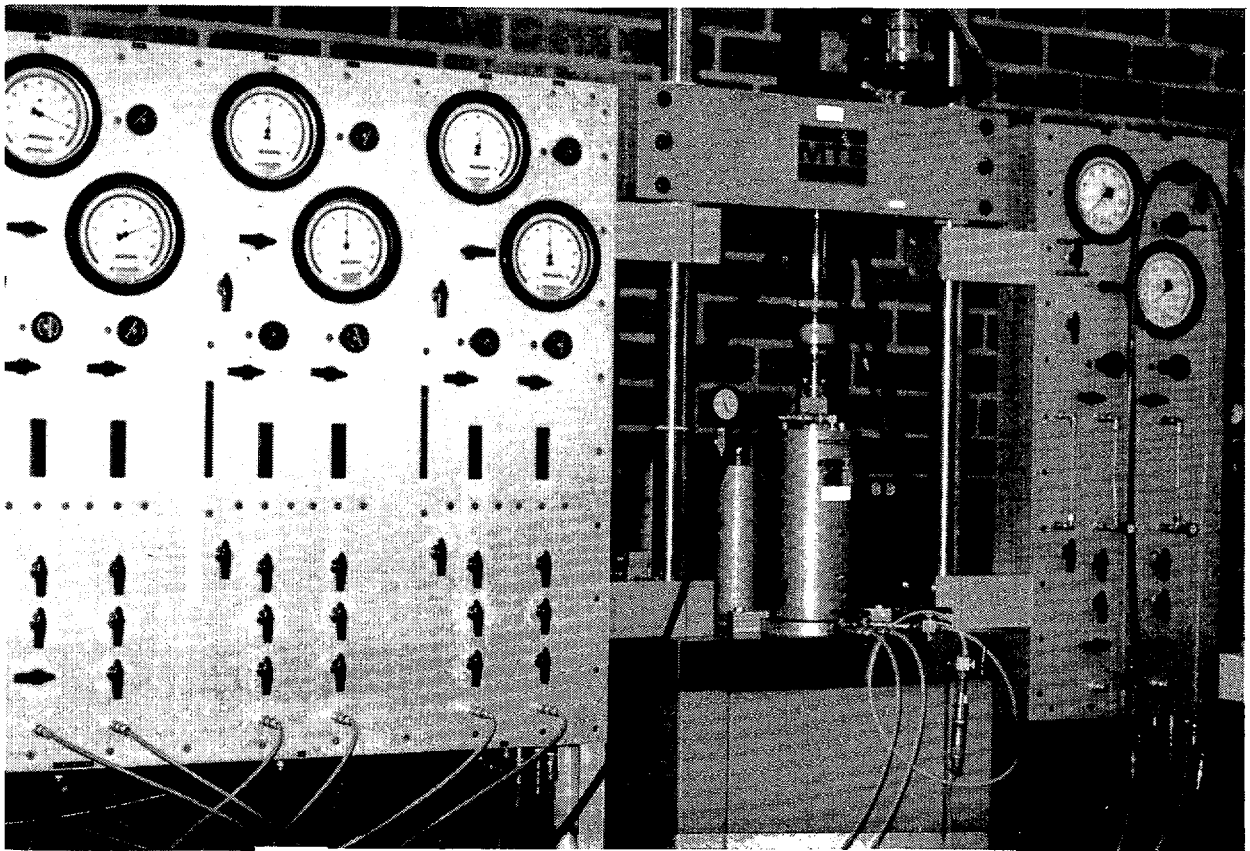


CYCLIC TRIAXIAL CHAMBER

FIGURE 4-3 PHOTOGRAPHS OF RESONANT COLUMN AND CYCLIC TRIAXIAL TEST CHAMBERS



LOADING AND RECORDING SYSTEM



LOADING SYSTEM

FIGURE 4-4 PHOTOGRAPHS OF CYCLIC TRIAXIAL EQUIPMENT

5.0 DATA INTERPRETATION AND RESULTS

5.1 BATHYMETRIC MAP

Bathymetric data compiled during this survey were incorporated with existing bathymetric data (i.e. NOAA Bathymetry Map NOS 1711N-18B) to construct new bathymetric maps (Plates III(A) and III(B)) at a scale of 1:250,000 and with a 5-m contour interval. The new data were based on a sonic velocity of 1580 m/sec. No corrections were made for tides, sea-state, transducer depth, temperature, or salinity.

The new contour map (Plates III(A) and III(B)) confirms the existence of a very flat, shallow continental shelf. Water depths vary from 0 to 110 m; slopes along the coastline are generally less than 0.5 percent. Beyond the 90 m **isobath**, slopes are generally less than 0.02 percent. Although contour lines in the western portion of the study **area** (Plate III(A)) indicate a more irregular seafloor near the shoreline, the seafloor still must be considered very flat and regular.

5.2 GEOLOGIC STRUCTURE

A geologic structure map (Plates IV(A) and IV(B)) and two structural cross-sections (Plates VI and VII) were interpreted from the analysis of shallow and deep-penetration data gathered during the Discoverer program and during similar programs conducted by Marine Technical Services Company (MTS) and the United States Geological Survey (USGS). Cross Sections A-A' and B-B' (Plates VI and VII respectively) were constructed using 1976 USGS **seismic-** reflection records (Marlow and Cooper, 1980b) at a scale of 1:250,000 and the NOAA Discoverer (1980) air gun data.

Depths (D) were calculated using Marlow and Cooper's (1980b) equation

$$D = 1.266t + 1.033t^2 - 0.117t^3 \dots \dots \dots (5-1)$$

where t is the one-way travel time in seconds and D is in kilometers. The following interpretation were made on the basis of these data.

5.2.1 Basement Complex

The surface of the basement complex (Plates VI and VII) was identified and mapped as the interface between the upper well layered sequence (Tertiary (?)), representative of relatively continuous deposition, and the lower sequence (Cretaceous and Jurassic (?)) with a typically noisy signature and few coherent reflectors. A high-amplitude continuous reflector marks this unconformity over most of the study area. Tertiary basin fill within the study area has been previously correlated (Marlow and others, 1980b) to comparably aged elastic and volcanic rock units on the Alaska Peninsula.

The edges of basins were defined at the sharp breaks in slope between the highs and lows in the basement surface. The east-west trending St. George Basin, which lies at the west-central edge of the study area, is the deepest structural basin in the area. The basin floor (basement surface) is approximately 5.1 km deep in the west and rises steeply on its eastern end to approximately 1.2 km. Both Amak Basin, located in the southwest, and Bristol Bay Basin, located in the northeast, are shallower structural basins with maximum depths of approximately 4.8 and 3.8 km, respectively. A basement high, the Black Hills Uplift, separates the Amak Basin from the Bristol Bay and St. George Basins. Shallow-penetration seismic profiles indicate that the Black Hills Uplift extends eastward and rises rapidly from an average depth of 1.0 km to 0.1 km near the Alaska Peninsula. A second basement high

(Plate VI) bounds the northern edge of St. George Basin. This high continues northward as a broad basement platform approximately 1.2 km below the seafloor surface.

5.2.2 Faulting

A number of faults can be identified within the study area. Correlations of fault traces are sometimes approximate because of the widely-spaced reconnaissance grids of the 1976 USGS (90-120 km) and 1980 NOAA Discoverer (10-15 km) cruises, and the lack of detailed coverage in the fault areas of the MTS data (Molnia and others, 1982). Nevertheless, based on the relative magnitude of offset and subsurface extent, the correlation of major fault segments appears good.

Separation on major faults is generally normal and increases with depth indicating that the faults formed early in the history of the area and have grown as time progressed. Many of these faults extend upward to near the seafloor and some are associated with **surficial** sags indicating activity during the Quaternary Period.

The greatest concentration of faults occurs along the southern edge of St. George Basin and the northeastern edge of Amak Basin in the North Amak Fault Zone (Plate IV(A)). These faults are sometimes less than a kilometer apart and form a zone of faults approximately 15 km wide in the area north of Amak Island to about 25 km wide along the western margin of the study area. Along the trace of the North Amak Fault Zone, the sense of displacement changes from downthrown block on the north in the St. George Basin area, to downthrown block on the south in the Amak Basin area. Differential basement **formational** irregularities may account for this rotational sense along the

fault zone. This changing sense of displacement may also be the result of en echelon fault segments which may have geometries unique to each of the two basins and may not be correlative along their length.

Major faults also are present along the southern edge of the **Amak** Basin and just north of the North Amak Fault Zone. These faults are normal faults that strike west-northwest similar to the North Amak fault. Minor faults of limited **areal** extent, which have much lesser offset than the major faults, are distributed over the entire area. The greatest concentrations of these **faults** occur at depth along the contact between the basement complex and sedimentary basin-fill (Plate VI). Minor faults are relatively rare in shallow portions of the basin-fill sequence. Surface faults were observed on both shallow- and intermediate-penetration data sets (Plates VIII(A) and VIII(B)). Rarely were any of these faults expressed by steep-sided **surficial scarps**, but almost all of them had **surficial** sag zones (Plate V). The locations of these relatively rare, **surficial** faults coincide with the greatest concentration of major faults as plotted on Plate IV(A) and IV(B).

Compressional folding was not observed in the study area. However, drape folds were observed in association with many fault elements.

5.2.3 Structural Cross-Section A-A'

Cross-Section A-A' (Plate VI) was prepared from the deep, intermediate and shallow penetration seismic data sets. This cross-section traverses southwest to northeast to south-central Bristol Bay Basin (Figure 5-1) along 1976 USGS CDP Lines 1 and 2 (**Marlow** and Cooper, 1980b), oblique to the major structural trends in the area. Major geologic features along the **cross-section** include Amak Basin, North Amak Fault Zone, Black Hills Uplift and Bristol Bay Basin.

From this cross-section the Amak Basin was interpreted as a Cenozoic (?) graben bounded on the north by the North Amak Fault Zone and Black Hills Uplift. Tertiary sedimentary fill within the **Amak** Basin exceeds 4.7 km (Shot Point 700). The **Black** Hills Uplift is a structural high of the Mesozoic (?) basement. This high rises to within an average depth of 750 m below the sea-floor. **An** intensely faulted 3-km-wide area of the uplift rises to within 550 m of the surface.

The Bristol Bay Basin is a structural depression, 60 km wide, with a maximum Tertiary basin fill of 3.8 km (Shot Point 3600). The regularity and horizontality of the bedding combined with the paucity of large faults and folds, except at the edges of basin, indicate relatively continuous deposition **in** a fairly stable tectonic environment since early Tertiary time.

The apparent abundance of faults throughout the length of Cross-Section A-A' (Plate VI) is more a result of the orientation of the cross-section oblique to the structural fabric than to the actual abundance of faults. The only major faulting in the study region is the normal fault regime of the North Amak Fault Zone which forms the boundary between Amak Basin and the Black Hills Uplift (Plate VII).

5.2.4 Structural Cross-Section B-B'

Cross-Section B-B' (Plate VII) trends north-south (Figure 5-1) along the 1976 USGS Line 4 (**Marlow** and Cooper, 1980b) and 1980 Discoverer Line 1079 normal **to** the major east-west structural trends of the Bristol Bay region.

This cross-section shows the Amak Basin as a graben structure with over 4.7 km of Tertiary basin-fill (Shot Point 2400). The graben is approximately 30 km wide and bounded on the north by a **set** of major normal faults comprising

the North **Amak** Fault Zone. Within the upper kilometer of basin-fill in the **middle** of the basin there are numerous minor normal "growth" faults which do not appear to extend to the basement.

Bristol Bay Basin, 20 km north of Amak Basin, is a **crustal** depression which may be the result of the tensional regime behind the Aleutian Volcanic Arc. However, Bristol Bay Basin is not a simple graben; its geometry appears to be controlled by numerous minor faults along the basement surface. Faulting within the basin appears to have occurred contemporaneously with **desposition**. Like Amak Basin, Bristol Bay Basin appears to have experienced nearly continuous deposition since *early* Tertiary time with Tertiary deposits reaching a maximum thickness of over 2 km (Shot Point 1000).

The cross-section shows that the Black Hills Uplift is covered by an average of about 800 m of Tertiary strata. Major faulting within the Black Hills Uplift is limited to its southern extreme, the North Amak Fault Zone. Other faulting within the area is generally limited to minor tensional faulting extending through basement and mid-Tertiary (?) units only. As noted previously, the Black Hills Uplift represents a Mesozoic basement structural high separating Amak and Bristol Bay Basins.

5.2.5 Late Quaternary Stratigraphy

The Late Quaternary geology of the Bering Sea Shelf, north of Unimak Island, and the southern end of the Alaska Peninsula, is shown on Plates VIII(A) and VIII(B). The upper Quaternary **stratigraphy** is generalized from seismic records and sediment samples. Generally, three stratigraphic units are found above a basal channel-fill unit. These units comprise the Wisconsinan (?) and Holocene (?) (late Quaternary) stratigraphic sequence.

Their combined thickness ranges from 0 to 20 m, as indicated by the isopachs on Plates VIII(A) and VIII(B). Generally, **the** thickest portion (20 m) is located northeast of Amak Island. General thinning occurs radially away from this location. The thickest occurrence and surrounding **isopach** configuration displays a somewhat east-west elongation.

The oldest Quaternary unit is interpreted on **the** basis of seismic signatures as a channel fill sequence. These sediments occur most prominently northwest of Port **Moller**. The thickness of this unit averages 25 m, with a maximum of 33 m. Because the upper surface of this unit is masked by the seismic bubble-pulse on intermediate-penetration seismic data, its thickness is uncertain. The approximate average depth below the surface in the Port **Moller** area is 8 m. An average strike of N 40 E and a dip of 0.6° NW was orthographically derived from the orientations of intersecting bedding planes at eight locations within the unit to give a general **areal** bedding orientation.

A thin, flat-lying, seismically transparent layer believed to be marine sand was recognized only in localized areas unconformably overlying the channel-fill unit described above. Above these two lower units is a thin, locally preserved unit of variable thickness. Core analyses show this layer to consist of moderately dense, very-dark-grey, **medium-grained** sand with thin interbeds of shell hash. An upper **surficial** sediment layer, ranging in thickness from 0 to 3 m, is composed of a seismically "transparent", **nonindurated** grey to **very-dark-grey** sand, representing modern detritus which is actively mixed by waves and currents.

Shell layers at depths of 7 and 10 cm below sea bottom (Sample Nos. 24 and 26; Station Nos. 1070/91 and 1070/87) were dated by ¹⁴C analysis.

Resultant dates were $12,390 \pm 250$ years B.P. and $11,729 \pm 245$ years B.P. The calculated sedimentation rate for these cores, assuming uninterrupted deposition, is less than 1 cm/1000 years. This rate is considerably less than that suggested by Askren (1972), who estimated a sedimentation rate of 9 cm/1000 years, but is more consistent with the lower bound proposed by Gershanovich (1968), who estimated a rate of 2 to 30 cm/1000 year. The apparent low rate of sedimentation could be a result of the dated shell material being washed in from another area, or of removal of a portion of the overlying sediments during times of lowered sea level. Such an interpretation is suggested by the disarticulate broken nature of the shell material.

5.4 SEISMIC ENVIRONMENT

The general nature and distribution of regional seismicity was presented in Section 2. This section presents more detail on seismic aspects in the study region to provide a background for estimation of maximum credible earthquakes. The intent of this analysis is to provide a basis for preliminary evaluation of the possible adverse effects of earthquakes on geotechnical parameters in the study region. This analysis is based on data readily available at the time of the study so a more-detailed analysis of seismicity and engineering design parameters will be necessary for specific facilities as the area is developed.

Potential sources of earthquakes that might affect future facilities within the Northern Aleutian Shelf region are primarily the Benioff zone, the island arc, the back-arc graben-bounding fault zones (Amak, St. George), and other intrabasin faults. These earthquake sources are shown diagrammatically on Figure 5-2. Potential sources of large earthquakes such as the normal faults

seaward of the Aleutian Trench are not considered here because they are clearly not as significant as the nearby features which can generate nearer and larger earthquakes. Based on **seismicity** and geologic characteristics maximum earthquake magnitudes are estimated for each of these sources. The magnitudes of these earthquakes are surface-wave magnitudes (M_s) which tend to saturate above a magnitude of about 7.75. A moment magnitude scale **would** probably be a better indicator of the relative size of earthquakes above 7.75, but it is not used in this report because, as the M_s scale tends to saturate at the larger earthquakes, so does the strong ground motion in the near field. Because attenuation relations for strong ground motion developed by earthquake engineers generally use M_s magnitudes without corrections for magnitude saturation, saturation effects are included implicitly in the attenuation relations.

5.4.1 Earthquake Sources

The regional tectonic setting and seismicity of the study region are discussed in Section 2.4.2 and 2.4.3. In these discussions, it is pointed out that the primary cause of earthquakes and tectonic deformation in the Aleutian Island region is subduction of the Pacific **lithospheric** plate beneath the Bering-North America Plate. Figure 5-2 is a conceptual model of the subduction zone in cross-section and illustrates the geometric relationships of the Amak Basin, **Black Hills Uplift**, and Bristol Bay Basin to the subduction zone.

As discussed in Section 2.4.3, the vast majority of earthquakes are directly related **to** subduction **of** the Pacific **Plate** and **occur** along the subducted plate or in the crust directly adjacent to the trench. However, there are several **shallow** earthquakes on the Aleutian arc and behind the arc (Figure

5-3) which may be only indirectly related to the subduction process or which have no **obvious** relationship to subduction.

According to the NOAA earthquake catalog, in the back-arc area there have been ten shallow earthquakes recorded during the limited time span of the **seismicity** record (1953 to 1977). The largest of these back-arc earthquakes occurred in 1971 and had a magnitude of 5.2 (Figure 5-3). The largest events on the Aleutian arc were **in** the 4 to 5 magnitude range. The largest event in the entire region was the Ms 8.7 ($M_w = 8.2$) magnitude earthquake which occurred east of the **Shumagin** Islands in 1938 and which is believed to have been associated with the subduction zone. **In** 1902, a 7.8 magnitude earthquake occurred in the study region but its location in the back-arc region has been considered by most seismologists to have been only a rough approximation. The location of the event, as shown on Figure 5-3, has great uncertainty which **could** be attributable to minimal seismograph coverage in the **early** part of the century or possibly to seismic-velocity anomalies. It is generally believed that the earthquake was probably associated with the subduction zone. The large, young, normal faults bounding the Amak and St. George Basins documented during this study, however, may provide a potential source for **large-**magnitude earthquakes; consequently, it no longer may be possible to simply dismiss the 1902 event as a dislocated event.

According to Davies (1981), there are several earthquakes in the western part of the study area and the St. George Basin region which are not included in the NOAA catalog. These earthquakes are shown on Figure 5-4. The largest of these earthquakes occur in the vicinity of faults associated with the St. George Basin. The strong geologic similarities **of** the St. **George** Basin and the Amak Basin suggest that the earthquake potential is probably similar in

both basins. The largest historic events in the vicinity of the St. George Basin appear to have been the magnitude 7.2 event which occurred in 1925 and intensity $I_{MM} = X$ event which occurred in 1836 (Davies, 1981). Davies (1981) calculated probabilities based on a 22 years **teleseismic** record and found that the probability is about 11 percent that a randomly selected site within the St. George Basin region will experience strong ground motion in excess of 0.2 g within 40 years and is about 3 percent for 0.5 g.

5.4.2 Maximum Earthquakes

The maximum earthquakes which could be associated with the sources identified in the previous section are listed in Table 5-1. These estimates are based on records which are only about a hundred years long, and this may be too short to characterize, adequately, the earthquake potential. Uncertainties in magnitude estimates arise because the time period between recurrence of the maximum earthquakes for some tectonic features may be longer than the seismic record. To help resolve these uncertainties, empirical fault-length/earthquake-magnitude relationships based on worldwide data and geologic/tectonic relationships in similar tectonic regimes in other areas were examined. In this review it is noted that the maximum earthquake associated with the **Benioff** Zone is well established compared to the other sources and is fairly well restricted **in** location relative to any sites in the study area. However, maximum earthquakes associated with the other features, such as volcanoes, shallow faults on the arc, and behind-the-arc grabens are much more **speculative**.

5.4.2.1 Aleutian Subduction Zone

The maximum earthquakes for the subduction zone are estimated at Ms 8 3/4 and 7 3/4 for shallow and deep source zones, respectively. The 8 3/4 event is

based on the occurrence of a similar-size event in 1938 ($M_s=8.7$). Such **magnitudes** are consistent with earthquakes in other subduction zones throughout the world although they appear to be more frequent in the Alaska-Aleutian zone.

The subduction zone was divided into shallow and deep source zones based on the premise that earthquakes may be characteristically smaller at great depth where there is no direct interface between rigid, brittle crusts of the two colliding plates. The boundary between the two zones is gradational and should be on the order of 40 to 50 km deep (Figure 5-2) based on typical **crustal** thicknesses in the area and throughout the world **in** similar environments. The maximum earthquake in the deeper zone is estimated at $M_s 7 \frac{3}{4}$ because, historically, earthquakes at depth are generally no larger than this magnitude.

5.4.2.2 Major Graben-Bounding Faults

The most significant uncertainty, with respect to earthquake potential in the study region, appears to lie with the normal faults bounding the major structural basins such as the **Amak**, St. George, and **Pribilof** grabens. These features may have originated during the late Mesozoic or early Tertiary in response to rifting along a transform boundary (**Marlow** and Cooper, 1980a), but faults along their margins have moved repeatedly throughout the Cenozoic Era and probably as late as the Holocene Epoch suggesting that they are active at the present time.

These normal-fault-bounded grabens appear to indicate a tensional stress field behind the volcanic arc although a component of lateral movement cannot be ruled out. A tensional stress regime is supported by young **alkalai** basaltic volcanoes in the distant back-arc region which appear to be associated

with normal faults and other tectonic features which suggest regional tension oriented roughly north-south (**Nakamura** and others, 1977). The inference of tensional stresses behind the volcanic arc suggests that the grabens are **back-arc** basins similar to those found behind other volcanic arcs around the globe. If so, earthquake magnitudes should be similar to or compatible with earthquakes in these other back-arc basins.

To determine the characteristics of the back-arc basins, a review of back-arc basins was performed. A complete summary of this review is beyond the scope of this report; however, discussions by Uyeda (1977), Uyeda and **Kanamori** (1979), Zonenshain and Savostin (1981), and Hsui and Toksoz (1981) suggest that back-arc basins throughout the **world** can be grouped into the following five major categories:

- 1) those with continental crust (Peru-Chile, Middle America, Basin and Range province of the western U.S., Alaska-eastern Aleutians, Java-Sumatra);
- 2) those composed of trapped oceanic crust (western Bering Sea, Caribbean);
- 3) those with active back-arc spreading (Lau Basin, Marianas, Scotia Sea);
- 4) those with inactive back-arc spreading (Grenada-Antilles Trough, Sea of Japan, southern **Okhotsk**); and
- 5) those with oblique spreading or "leaky" transform faults (**Andaman** Sea).

Not all investigators agree on which back-arc basins fit into which category, and it seems that several back-arc basins have characteristics of more than one.

In the search for modern analogs of the east Aleutian-Alaska Peninsula region, the following parameters were considered necessary similarities: 1) an active volcanic arc, 2) oceanic crust being subducted under continental

crust, and 3) tensional faulting (grabens) behind the volcanic arc. Review of the subduction regimes throughout the world revealed that there are no exact analogs to the Aleutian regime. Most subduction zones fulfill the first criterion; only a few fulfill the second (Java-Sumatra, Japan, western North America, Middle America, and South America); and none fulfill the third criterion very well. The western United States has elements of back-arc grabens in the Great Basin but no longer has the arc; the extensional back-arc region of Japan may have involved more fundamental **crustal** spreading rather than graben formation, and now appears to be relatively inactive; the tectonic evolution of Java is remarkably similar to the Northern Aleutian Shelf, but Quaternary tectonics in the Java back-arc region are poorly understood and available information is inadequate to construct a soundly based *tectonic model*.

In addition to the above criteria, seismicity characteristics of back-arc regions were also examined. Typically island arcs have shallow **seismicity** behind the island arc which forms trends that may be **subparallel** to the **fore-arc** belt of **seismicity** along the trench. These back-arc seismic events are few in number compared to the **forearc** region, but commonly include events exceeding magnitude 5 (for example, Japan, south **Okhotsk**, Java). Apparently the back-arc seismic belts represents a variety of tectonic regimes. In Japan shallow back-arc earthquakes have exceeded magnitude Ms 7 1/2 but focal **mecha-**nisms and geologic data indicate reverse faulting; in the south **Okhotsk** Basin (**Kuril** back-arc) the focal mechanisms show reverse and normal displacements with strike-slip components (**Baranov** and **Lobkovskii**, 1980); behind Java, earthquakes have reached magnitude 6.8 but the tectonic situation is poorly known and no focal mechanism solutions have been determined. According to

Katili and Soetadi (1971), Pliocene and Pleistocene strata in the Java **back-arc** region are folded and faulted, and a number of the back-arc faults and **flexures** have large vertical displacements of possible Quaternary age. The available data, however, are not sufficient to confirm whether these basins are similar to those in the study area. Although seismicity is not abundant in the Java back-arc region, there have been several events **larger** than magnitude 6. The depths of these earthquakes are poorly known but they are **crustal** events, like those in the Aleutian study area, and most likely are **not associated** with the Benioff Zone, which is 400 to 700 km deep below the crust where these basins occur.

Another possible analog is the Great Basin, located in the western United States. Although there is no modern subduction zone directly associated with the Great Basin, faults there are caused by tensional forces that appear to be generated by mechanisms similar to those behind some island arcs (mantle convection and upwelling). Because the magnitude of an earthquake is largely a function of rupture area and stress drop, it seems plausible that similar faults, even though they occur in somewhat different tectonic regimes, may generate earthquakes of similar magnitude as long as fault-plane rupture areas are similar in size. Because the graben-bounding faults in the Great Basin are of the same type and size as those in the study region and have generated large events in historic time (1915 - 7.6, 1954 - 7.1, 1932 - 7.3), they may provide an indication of the size of earthquakes possible on major faults bounding the grabens in the Northern Aleutian back-arc region.

As discussed above, the major grabens on the Northern Aleutian shelf do not conform precisely to any existing back-arc basin, so it is difficult to assign earthquake magnitudes based on a comparison to these regions. However,

comparison of the size of normal **faults** that have been associated with large historic earthquakes in other parts of the world indicate that large earthquakes are possible on the major graben bounding faults north of the Aleutians. This is supported by the occurrence of the M=7.2 earthquake which occurred in the vicinity of the St. George graben. Based on these parameters, a maximum earthquake of about $M_s 7 \frac{3}{4}$ is postulated for major graben-bounding faults in the study area. This is believed to be a very conservative but necessary estimate to ensure that the subsequent engineering analyses account for all plausible conditions. It should also be noted that the recurrence intervals on these types of earthquakes can be very **long**, on the order of a few thousand years (Wallace, 1977; **Schell** and others, 1981; **Schell**, 1982), and therefore, the occurrence of such an event is quite remote during the life of facilities contemplated for the present phase of oil exploration.

5.4.2.3 Other Large Back-Arc Faults

Seismic-reflection data reveal a myriad of faults in the back-arc region, but understanding the nature of these faults is difficult based on the present, widely spread data. Shallow and intermediate-penetration data reveal faults near the surface (Plates V(A) and V(B)). Some of these appear to be growth-type **faults** related to the subsidence and gravity effects within the basin-fill sediments. As such, they have no connection to basement-involved deformation and probably do not represent a potential source of large earthquakes. Earthquakes in the Gulf of Mexico region where these types of faults are common are generally less than magnitude 6.

The relation to basement is not clear for some other faults in the back-arc region, and some of them appear to have significant lengths. Fault-length/

earthquake-magnitude relationships (Slemmons, 1977) suggest that earthquakes in the 6 to 6 1/2 magnitude range may be possible.

5.4.2.4 Aleutian Arc: Volcano and Associated Faults

Earthquakes associated with the Aleutian Arc may be caused by both volcanoes and fault movements. There are three primary sources of these earthquakes: 1) from the actual volcanic explosion, 2) from fault movements caused by expansion and contraction of the rocks surrounding the *magma* chambers, and 3) from sympathetic movements on nearby faults. Based on worldwide historic data, the first type does not seem capable of generating large earthquakes, but the second and third types may.

The largest earthquakes known to be associated with volcanism occurred in 1) Hawaii in 1975 where a magnitude 7.2 earthquake accompanied an eruption of **Mauna** Loa, and 2) Japan in 1914 with a magnitude estimated at 7. Hawaii is a rather unique tectonic environment, and it is not clear whether it should be considered as an analog of the Alaska-Aleutian subduction regime. The **1914** Japanese earthquake is poorly documented, and hence, is also of questionable use. Generally earthquakes associated with volcanic activity are no larger than magnitude 5 to 6. The largest historic event in the site region possibly associated with volcanism had a magnitude of less than 5. Based on these parameters, the maximum earthquake associated with volcanism in the site region is estimated at 6. This is believed to be a reasonably conservative estimate but is probably not as conservative as the estimate of the maximum event associated with the major graben-faulting faults.

Fault movement caused by sympathetic movements of nearby **faults** is **sub-**ject to considerable uncertainty in the Alaska Peninsula - **Unimak** Island

region due to lack of detailed geologic studies. Beikman (1975) shows several northeast-southwest trending faults along the southern coast of the Peninsula between Pavlof Bay and the Shelikof Strait. The shortest fault is about 40 km long; the longest one is about 70 km long. These faults do not cut Quaternary strata. On Unalaska Island, east-west and northwest-southeast trending faults cut Quaternary volcanics but these features are all relatively short (about 15 km).

Assuming that there are no major late Quaternary faults on the Aleutian Arc adjacent to the study area larger than those already mapped, the magnitude 6 earthquake postulated for the volcanogenic event should be sufficiently conservative to account for fault-related earthquakes.

5.4.2.5 Unknown Earthquake Sources - Random Earthquake

The earthquake hazard analysis must also consider a maximum random earthquake because earthquakes in the back-arc region do not appear to be restricted to the major grabens. However, the maximum random event need not be large because the major tectonic features in the area, the ones capable of generating large earthquakes, are known (Plates V(A), V(B), VI, VII and Figure 5-4). The source of random events could be faults, such as the small growth faults seen on geophysical profiles (Plates IV(A), IV(B) and VII) or faults that are too small or too deep to have been detected by the geophysical survey.

A reasonable random earthquake magnitude is estimated to be about a magnitude 5 1/2 event. This is consistent with earthquakes which have occurred in the region historically but cannot be associated with any known geologic structure.

5.4.3 Earthquake Ground Motions

Peak ground accelerations and scaled time histories were determined for the study area based on the probable and maximum earthquakes postulated for the region. These postulated events were obtained from an evaluation of the tectonics and the **seismicity** discussed in Sections 2.4.2, 2.4.3, 5.4.1, and 5.4.2. The strong motion **accelerograms** recorded in Japan and the United States were used to estimate the peak ground accelerations. Representative time histories were selected from this collection of recorded **accelerograms** and published artificial **accelerograms**. These time histories were scaled to the peak ground accelerations and subsequently used in the liquefaction **analyses** presented in Section 5.6.

The recommended ground motions reflect current understanding of the **earthquake** potential in the Northern Aleutian Shelf region and are considered adequate for liquefaction assessments on a regional scale. *The* motions are not intended for design purposes. More-detailed studies would be required to determine design criteria for specific sites.

5.4.3.1 Probable and Maximum Earthquakes

Based on the interpretations of the tectonic and seismological data, probable and maximum earthquakes were postulated for the study area. As summarized in Table 5-1, the largest earthquakes were postulated for the Aleutian subduction zone and the North Amak Fault Zone. The Aleutian subduction zone was assigned a magnitude Ms 8 3/4 shallow event and a magnitude Ms 7 3/4 deep event; the North Amak Fault Zone was assigned a magnitude Ms 7 3/4.

The maximum magnitude assignments for the Aleutian subduction zone were **also** considered probable events because of the frequent occurrence of large

magnitude earthquakes within this zone. Although the North Amak Fault Zone and other large back-arc faults were judged capable of producing **large-**magnitude earthquakes (see Section 5.4.2 and **Table 5-1**), the seismicity in **the** region and in similar tectonic environments throughout the world suggests that the recurrence intervals of large earthquakes in the back arc regions of subduction zones is long. Thus, earthquakes likely to occur on this feature during the life of the expected facilities would be **small**. For this study only maximum earthquakes were considered for the seismic sources in the study area. This conservative assumption should be noted when interpreting the results of this study.

5.4.3.2 Peak Ground Accelerations

Only three strong-motion **accelerograms** recorded in Alaska have been processed (USGS, 1976 and 1978). Two were recorded at the western tip of the Aleutian arc (May 2, 1971, $M = 7.0$); one was recorded in eastern Alaska (July 30, 1972, $M_L = 7.0$). Numerous strong-motion **accelerograms** recorded during earthquakes originating in the subduction zone along the coast of Japan have been processed and are available. Because similar tectonic conditions exist along the Aleutian arc near the study area, these Japanese records are well suited for estimating ground motions from earthquakes in the Aleutian subduction zone.

A number of the Japanese **accelerograms** were obtained and processed (**Mori and Crouse**, 1981), and an attenuation relationship based on these data was developed to estimate peak ground accelerations in the study area from earthquakes originating in the Aleutian subduction zone. The relationship expressed the peak ground acceleration in terms of earthquake magnitude and **hypocentral** distance. Similar types of attenuation relationships have been

developed with western U.S. **accelerogram** data. These relationships were used to estimate peak ground accelerations for the earthquakes originating within the study area. The implicit assumption *in* using these attenuation relationships is that the attenuation of ground motion from earthquakes in the Aleutian subduction zone and shallow earthquakes within the study area is very similar to ground-motion attenuation in Japan and in the western U.S. , **respectively.**

The results of these studies indicate that the peak ground acceleration would be approximately **0.1g** for all locations within the study area due to either the shallow ($M = 8 \frac{3}{4}$) or deep ($M = 7 \frac{3}{4}$) earthquakes postulated for the subduction zone. Therefore, ground motions of long duration, with peaks around **0.1g**, should be considered likely during the useful life of the lease areas. These motions also represent the maximum conditions from earthquakes in the Aleutian subduction zone because these postulated earthquakes are also the largest events that could reasonably occur.

The peak ground accelerations due to the occurrence of the maximum earthquake postulated on the seismic sources within the study area (Table 5-1) are shown in Figure 5-5. These accelerations vary from 0.4g to 0.7g for locations near the North Amak Fault Zone and diminish to **0.1g** for more distant locations. Ground accelerations on the order of **0.1g** to 0.2g can be expected near small magnitude ($M=5 \frac{1}{2}$) random events, which have been assumed as capable of occurring anywhere within the study area.

5.4.3.4 Time Histories

The **accelerograms** recommended for the liquefaction analyses are listed in Table 5-2. Because no **accelerograms** have been recorded during great **earth-**

quakes ($M > 8$), the Caltech artificial earthquake **Accelerogram** A-1 (Jennings and others, 1968) was selected for the magnitude $8 \frac{3}{4}$ event in the Aleutian Subduction Zone. **Accelerogram** A-1 has frequency characteristics commonly found in motions recorded on deep alluvial sites. Furthermore, its duration is representative of the duration of strong shaking to be expected from an earthquake of this magnitude.

The 1940 El Centro **accelerogram**, suitably scaled, was selected to approximate shaking near (within about 20 km) magnitude $7 \frac{3}{4}$ earthquakes on the North Amak Fault Zone. The properly-scaled 1952 Taft **accelerogram** which was recorded about 42 km from the White Wolf fault also approximates the shaking at distances greater than about 20 km. Neither **accelerogram** should be used outside their applicable distance range.

The same criterion applies to the records selected for the magnitude $6 \frac{1}{2}$ events for other possible large faults in the back-arc area. The Imperial Valley Array No. 8 **accelerogram** was recorded approximately 4 km from the fault rupture of the 1979 Imperial Valley earthquake. Therefore, this record is to be used at distances near (within 5 km) the other large back arc faults shown in Figure 5-5. The Holiday Inn **accelerogram**, recorded about 9 km from the fault rupture of the 1971 San Fernando earthquake, should be used, after scaling, to approximate the shaking at distances greater than 5 km from the fault zones. The records selected for the magnitude 6 and $5 \frac{1}{2}$ events can be used at any distance provided they are properly scaled.

As noted above, the recommended **accelerograms** will have to be scaled to obtain the proper peak accelerations. By definition, the scaling factor for each recommended **accelerogram** is the ratio of the peak ground acceleration

D estimated for a particular location in the study area to the peak acceleration of the recommended **accelerogram**. For example, the peak acceleration estimated at any location in the study area due to the magnitude 8 3/4 earthquakes is **0.1g**. Since the peak acceleration for **Accelerogram A-1** is **0.385g** (Jennings and others, 1968), the scaling factor applied to this record is $0.1/0.385 = 0.26$. The peak ground accelerations for the other maximum earthquakes can be obtained from Figure 5-5 and used to obtain the proper scaling factors for the other recommended time histories.

5.5 SEDIMENT CHARACTERISTICS

The results of the geological laboratory studies were used to provide a detailed description of the upper 1 to 2 m of sediment in the study area. Detailed discussions of the cores, as well as grain size, mineralogy, carbon content and engineering properties are provided in the following paragraphs.

5.5.1 Core Descriptions

Radiographs were taken of five vibracores to assess stratigraphic relationships, the presence of **bioturbation**, location of pebbles, and coring disturbance. Core locations and descriptions are presented in Appendix III.

Cores were generally bioturbated throughout their length and showed minimal bedding. Evidence of **bioturbation** included numerous discrete burrows, and more commonly, complete homogenization of the sediment with total absence of internal structure. Subrounded, 4-mm-long **clasts** were commonly observed throughout the cores. Because there is no evidence for significant Holocene glacial activity in the region, it is doubtful that these particles are the result of ice rafting. Rather they probably represent fecal pellets.

Radiographs indicate that the top 5 to 15 cm of sediment in most cores appears less dense and less well compacted than the rest of the core. This may be due to a higher water content in the **surficial** sediment and to almost annual storm reworking of this upper layer. Sample No. 58 (Station 1270/175) is different from **all** of the other cores in that its radiograph shows two well-stratified, non-bioturbated units at 15 to 23 cm and 120 to 130 cm. Specific conditions responsible for the preservation of these horizons are unknown.

Four cores have shell layers averaging **about** 2.5 cm in thickness. Each of these cores was collected from a water depth of approximately 90 m. The shell layers, found 50 to 90 cm beneath the sediment surface, may represent a storm lag deposit. Attempts to date these layers did not result in useable **radiometric** data.

5.5.2 Grain Size

The results **of** grain-size analyses indicate that most **surficial** sediments are silty sands and sands (Figure 5-6). Appendix I contains calculated grain size data and computed Folk (1980) sediment texture parameters. Analyses showed a mean grain size (M_z) distribution similar **to** that of **Sharma** (1975, **1979**). Close examination of the relationship between individual samples, however, revealed a much more complicated grain-size distribution (Figure 5-7).

The complex sediment texture within the study area is attributed to four factors: 1) water depth, 2) currents, 3) shelf morphology, and 4) modern source areas. The water depth of the area is important in determining the effective wave base. This is the depth at which storm-produced waves can transmit their energy to the sediment. The Bering Sea is one of the stormiest

regions of the world. Waves have an average height of 2 m, a period of 6 sec, and lengths of 50 m (Askren, 1972). The annual maximum storm waves predicted from synoptic surface wind charts have a height of 10 m (**Sharma** and others, 1972). By using Lamb's equation for estimating maximum horizontal bottom current velocity (Lamb, 1879), Askren determined that the maximum depth of wave-induced sediment transport in Bristol Bay is approximately 100 m. This suggests that the entire area is affected by storm-wave agitation.

Storm-wave-generated bottom agitation causes sediments finer than a certain size to erode leaving behind coarser size sediments. After repeated movements and depositions, each grain reaches a theoretical equilibrium position. The effects of this transport can best be seen in the mean grain size distribution within the study area. Sediments within Bristol Bay generally decrease in mean grain size with increase in water depth. This trend suggests that the mean grain size of the sediment has reached a crude textural equilibrium with prevailing conditions. This is in contrast to many other continental shelves throughout the world which still show sediment distribution patterns which indicate that they are **relicts** from times of Pleistocene lower sea level.

Sediment standard deviation (sorting) also reflects the influence of wave activity, plus the modifying influences of currents, shelf morphology, and source area (Figure 5-8). Sediments with a mean grain size of approximately 2.5 phi (equivalent to 0.18 mm) are the best sorted, as would be expected from **Inman's** predictive hydrodynamic studies (**Inman**, 1949). The coarser material near-shore (recent sediment input) as well as the finer sediments in deeper water, where less wave influence exists, have the poorest sorting.

Skewness (Figure 5-9) reflects the progressive sediment fining offshore. Coarse sediments are located over most of the area sampled during the Discoverer program, whereas fine-skewed sediments are concentrated in samples with mean grain size less than 2.5 . Kurtosis (Figure 5-10) increases and reaches a maximum in sediments with a mean grain size of 3.0 phi (0.125 mm).

5.5.3 Mineralogy

Mineralogic studies indicate that five minerals or mineral groups compose the majority of southeastern Bering Sea sediments. These are quartz, feldspar, hypersthene, hornblende, and the opaque minerals (Figures 5-11 to 5-16). Table 4-1 summarizes results of the microscopic mineral investigations.

Euhedral grains of each mineral were common, causing the sediments to appear angular to sub-angular with poor **sphericity**. Two types of hornblende were observed: 1) common hornblende, strongly **pleochroic** in green and brown; and 2) basaltine, a type of hornblende common in **basalts** or hornblende **andesites**, **pleochroic** in brown and dark brown.

The primary source of surface sediment in Bristol Bay appears to be the Alaska Peninsula and Unimak Island. The presence of unworn and unaltered hypersthene and opaque minerals suggests a nearby source of basic and **ultra-**basic rock. Both the Alaska Peninsula and **Unimak** Island are composed primarily of volcanic **flow** and **volcanoclastic** rocks, which are mostly porphyritic **basalts** and **andesites**. Areas of intrusive quartz diorite and **hornblende-**biotite granite are also present (Kennedy and **Waldron**, 1955; and **Waldron**, 1961; Burk, 1965).

The Amak Basin, just north of Unimak Island, has apparently served as a sink for the majority of heavy minerals from **Unimak** Island, for it is here that the greatest concentration of basaltine and opaque minerals are found. Another concentration of hornblende is found offshore from the **Black** Hills of the Alaska Peninsula. This hornblende is not **basaltine** (Figure 5-15), but rather, is from the Naknek Formation, the unit that makes up much of the **Black** Hills. The Naknek Formation is an **arkosic** sandstone that is composed of about 5 percent hornblende. The source for the Naknek sandstone is a **hornblende-biotite** granite (**Burk**, 1965). Following **fluvial** transport to shore, sorting by currents and wave action has concentrated the hornblende of the Naknek close to shore, while the remainder of the rock, quartz and feldspar, has been transported farther offshore.

Hypersthene in the area shows a steady decrease in abundance with increase in distance from shore (Figure 5-14), **while** quartz (Figure **5-11**) and feldspar (Figure 5-12) show significant increase in abundance as distance from shore and source area increases. The ratio of quartz and feldspar is nearly uniform throughout the area investigated (Figure 5-13). This suggests that little or no chemical weathering in the source terrain and little post-depositional modification of sediment in the Bristol Bay region.

Opaque minerals are concentrated north of Unimak Island and in the area surrounding Amak Island (Figure 5-16). The percentage of opaques decreases with increase in distance from shore; they are very rare offshore from the Black Hills. The distribution pattern of the heavy mineral fraction in the Bristol Bay region reflects present day sources and suggests that at least the heavy mineral fraction is contemporary.

The depositional pattern for the heavy mineral fraction, which is **similar** to that described by **Sharma, also** resembles sediment associations described by Gardner and others (1979) for the adjoining St. George Basin area. By using a Q-mode factor analysis of 58 variables related to sediment size and composition, Gardner and his colleagues determined three main sediment sources. These are the Alaskan mainland, the Aleutian Islands, and the **Pribilof** Islands. In the Bristol Bay region, the major present day source areas are the Alaska mainland, the **Alaska** Peninsula, and Amak Island.

5.5.4 Carbon Content

The percentages of total carbon, total inorganic carbon, **total** organic carbon, and total carbonate were analyzed **using a** LECO **WR-12** induction furnace and a modified **Kolpac** and Bell apparatus. These analyses were performed for 11 of the **surficial** sediment grab samples. Test specimens were chosen because of their fine mean grain size, on the assumption that the highest carbon values would be obtained from the samples containing the most clay.

All of the samples show low carbon concentrations when compared to average shelf values. Total organic carbon ranges from about 0.4 percent to 0.3 percent with an average of nearly 0.4 percent (Figure 5-17 and Table 4-2). These values are far below the average of 1.5 percent determined by Trask (1932) for lower latitude shelves, but similar to values displayed by **Sharma** (1975) for Bristol Bay. Measurements were made of the **CaCO₃** content from 11 grab samples. The maximum **CaCO₃** was about **0.3** percent, while the average was about 0.2 percent (Table 4-2).

There is a definite negative correlation between grain size and carbon content. A similar trend is well documented in the St. George Basin area by

Gardner and others (1979) and by other workers including Kemp (1971), working in Lake Ontario, and Bordovskiy (1965), working on Bering Sea sediments close to the Russian shore. **Sharma** (1975) suggests this same relationship for Bristol Bay.

Bordovskiy (1965) has explained this association between clay rich sediments and high organic content by identifying the major source of the organic material. The predominant form of carbon in sea water is as dissolved matter. This matter readily forms stable organic mineral compounds with clay particles. In other words, carbon is trapped and incorporated into the clay particles, thereby resulting in clay-size sediment high in carbon.

This mechanism explains the low carbon content observed in most of the sediments of the Bristol Bay area. Bristol Bay sediments contain no more than 11 percent clays, and generally contain 3 percent or **less (Sharma, 1975)**. Similar clay percentages were noted in the analyses of samples collected by this study.

5.5.5 Engineering Properties

The engineering characteristics of sediments on the North Aleutian Shelf were evaluated based on the results of a visual examination of the recovered samples, in situ shear strength measurements, and a series of engineering laboratory tests. Before presenting these data, it is essential that two limitations be noted.

The first limitation is associated with the depth of sampling. In every case these engineering characteristics were deduced from data gathered in the upper 1 to 2 m of the soil profile. Therefore, interpretations based on these data are appropriate only for the same depth range. In a strict sense this

restricts use of the data to a limited number of engineering applications such as pipeline stability calculations, small-foundation bearing capacity determinations and scour potential assessments. It is possible to extrapolate **surficial** properties to greater depths (>1 to 2 m) by judicious application of generalized **geotechnical** engineering relationships and by careful review of the geologic history for the area. However, this approach is subject to considerable uncertainty and definitely would be inappropriate for final design of key bottom-supported petroleum facilities.

A second limitation deals with the quality of data. The objective of this engineering evaluation was not to define precise engineering properties. Rather it was to obtain a general understanding of conditions over a large area. This philosophy led to use of the vibracore, Van Veen sampler, gravity core and drop **penetrometer**. The three types of soil sampling tools introduce considerable disturbance to the sediment during sampling; because of induced vibrations in the case of the **vibracore**, or volume change characteristics in the case of the Van Veen and gravity samplers. Likewise the drop penetrometer involves uncertainty but in its case through the interpretation process. Consequently some discrepancies between actual in-situ properties and the characteristics presented below must be anticipated.

5.5.5.1 Visual Classification

Examination of the recovered **surficial** sediments determined that the study area is covered by a **surficial** layer of granular sediments. From the following field observations, it was inferred that these sediments are generally very dense.

- 1) Penetration of the high resolution seismic profiling system (3.5 kHz) was limited. Typical acoustic penetration depths ranged from 0 to 22 m with average penetration less than 5 m.

- 2) Results of **in situ** testing using the drop penetrometer indicated that minimal penetration occurred.
- 3) Little or no penetration occurred during gravity sampling using either a 140 kg or 360 kg weight stand.
- 4) Attempts to sample the **in situ** sediments by **vibracorer** were not as successful as anticipated. **Vibracore** penetration was shallow and the core recoveries were short. Although this was partially due to equipment limitations, the dense nature of the sediment was considered to have been a significant contributing factor.

Visual examination of the recovered samples and the results of subsequent index property tests (settling tube and grain-size analyses) indicate that the **surficial** sediments in the **study** area can be divided into the following four types with respect to **geotechnical** engineering characteristics:

- 1) **Soil Type No. 1, SP(1)** - dark brown gravelly sand and dark gray coarse to medium sand with little or no fines. The gravelly sand is present near the coastline.
- 2) **Soil Type No. 2, SP(2)** - dark gray and relatively uniform fine sand with little or no fines.
- 3) **Soil Type No. 3, SP/SM(3)** - gray to brownish gray fine sand with some fine and occasional shell fragments. This is a transitional zone between Soil Type No. 2 sediments and Soil Type No. 4 sediments described below.
- 4) **Soil Type No. 4, SM(4)** - Brown gray fine silty sand with an appreciable amount of fine and occasional shell fragments.

The distribution of these sediments is shown in Figure 5-18.

5.5.5.2 In Situ Shear Strength Measurements

As summarized in Section 3.3.3, **in situ** penetration measurements were performed at 46 locations using a drop penetrometer device (Scott, 1967). Acceleration records obtained by the device were converted to penetration resistance values at various penetration depths by integrating the recorded

acceleration-time histories using the characteristics of the accelerometer and penetrometer assembly. Results of these analyses were used to obtain a resistance force versus penetration plot.

Sixteen records were selected for detailed evaluations. The remaining records were disregarded for one or more of the following reasons:

- 1) Illegible records where either the diamond-tipped stylus failed to register on the pressure sensitive paper or the traces were too faint to be accurately interpreted
- 2) Invalid records where the penetrometer assembly failed to penetrate into the soil due to inclined entry or operational difficulty, and
- 3) Multiple records of similar order of magnitudes obtained at one station (i.e., only one of the similar records was used).

The selected records were digitized and then double integrated using a computer program developed by Professor Scott. Relevant results are summarized in Table 5-3.

An estimate of the in situ friction angle was made by correlating the penetration resistance results with penetration resistance values calculated analytically using a method developed by Durgunoglu and Mitchell (1975). These individuals determined that penetration resistance depends on the soil type, penetrometer roughness, and the apex angle of the penetrometer cone (60° in this study). One of the major uncertainties in this method is the frictional value between the penetrometer and soil. In this study, an upper bound friction angle was estimated assuming that the penetrometer was completely smooth (i.e., friction at the penetrometer-soil interface was zero). Similarly, a lower bound estimate was made assuming that the penetrometer was completely rough (i.e., friction between the penetrometer and soil equal to the shear strength of the soil). The results of the soil friction angle estimate are shown in Table 5-3.

Based on the results shown in this table, the following friction angles (ϕ) estimates were made for the four types of **surficial** sediments in the study area:

- 1) Soil Type No. 1: $\phi = 43^\circ$ to 49°
- 2) Soil Type No. 2: $\phi = 43^\circ$ to 49°
- 3) Soil Type No. 3: $\phi = 44^\circ$ to 47°
- 4) Soil Type No. 4: $\phi = 36^\circ$ to 42°

The magnitude of these friction angles indicates that the **surficial sediments** in the study area are very dense. Equivalent relative densities would be in excess of 90 percent or more. Inasmuch as the above friction angles are representative of **surficial** sediments and correspond to low confining stress, a decrease in friction angle with depth might be expected, as the friction angle decreases with increasing confinement.

5.5.5.3 Index Properties

The laboratory test program was designed to characterize the sediments at the site and to provide **geotechnical** engineering properties for **use** in the **geotechnical** hazard assessments. The index property tests comprised

	<u>Number</u>	<u>ASTM Designation</u>
Grain Size Analyses	34	422
Unit Weights	46	
Water Contents	46	216
Specific Gravity of Solids	3	854
Maximum Dry Unit Weights	8	2049
Minimum Dry Unit Weights	8	2049

The results of grain size analyses for the 34 specimens are summarized in Appendix I. Average characteristics are summarized in Figure 5-19. As described above (Section 5.5.5.1), the **surficial** sediments in the study area can be divided into four types; the spatial distribution of these four sediment types is shown in Figure 5-18. With the exception of Soil Type No. 4, these sediments are relatively uniform with a coefficient of uniformity (D_{60}/D_{10}) ranging from **1.3 to** about 3.5.

Unit weight measurements were made on 46 samples. The results of these tests are summarized in Table 4-3. These results were plotted with respect to the mean grain size, D_{50} , and are shown in Figure 5-20. As can be seen from this figure, the results indicate a wide scatter in dry unit weight values. This was due to the varying extent of sample disturbance introduced during sampling and possibly during handling and transporting the samples. Because the sampling methods (gravity core, vibracore, and Van Veen) employed in this study are known to disturb sands and to change *their* engineering properties, most of these unit weights are suspect.

Moisture content tests were performed on 46 samples. The results of these tests are summarized in Table 4-3. Due to sample disturbance effects, these moisture content values are probably higher than the values **representative of** in situ conditions.

Specific gravity tests were performed on three bulk-sample specimens in accordance with ASTM D854. As tabulated in Table 4-4, the specific gravity values for Soil Type 1 and 4 are 2.74 and 2.69, respectively, and for Soil Type 2 is about 2.8.

Eight sets of maximum and minimum dry unit weight tests were performed in accordance with ASTM D2049. Results of these tests are summarized in Table 4-5. These results indicate that the maximum and minimum dry unit weights are highest for **the coarse-grained** soils (Soil Type 1) and lowest for the fine-grained soils (**Soil** Type 4).

5.5.5.4 Geotechnical Engineering Properties Tests

The engineering properties tests were performed on good quality gravity core specimens and on reconstituted specimens. One of the major difficulties **in** performing **tests** on reconstituted samples is that it requires **a** reliable estimate of in situ unit weights of the sediments. The results of in situ shear strength measurements with the drop penetrometer indicate that **surficial** sediments in the study area are very dense. As shown in Figure 5-21, **a** comparison of the estimated friction angle values from in situ measurements with **the** empirical correlation between friction angle and relative density (**DM-7**, 1971) indicates that the relative densities of sediments **in** the study are **close** to 100 percent. Likewise, the plot of dry unit weights versus the mean grain sizes (**D₅₀**) indicates that the average dry unit weights **are very close** to the maximum dry unit weights **as** determined by the laboratory **tests**. Again, this is indicative of the dense nature of the in situ sediments.

In this study, the 25 kg bulk samples obtained **at** Stations 1020/100, 1070/91, 1177/185 and 1262/185 (Sample Nos. 9, 24, 43 and 57) were selected to represent the four soil types **in** the study area. Based **on an** evaluation of the available **in** situ test results and index properties **as well as** engineering judgment, possible ranges of **insitu** dry unit weights of the sediments were estimated. They are shown **in** Table 5-4. In this table, the dry unit weights selected for preparing the reconstituted specimens are also indicated. These

dry unit weights were considered to be best estimates of unit weights for sediments within the study area with the exception of Soil Type No. 1 where the selected dry unit weight probably corresponds to the anticipated lower bound value in situ. Thus, the **geotechnical** properties obtained from tests on reconstituted specimens may be conservative for Soil Type No. 1, and probably correspond to lower bound values in situ.

Seven **oedometer** tests were performed on three gravity core specimens and four reconstituted specimens. A summary of the results from these tests is presented in Table 4-6. Plots of voids ratio versus the logarithm of consolidation stress are presented in Appendix II. These plots indicate that the sediments are relatively incompressible except where densities are low.

Six permeability measurements were performed on two gravity core specimens and four reconstituted specimens. The results of these tests are summarized in Table 4-7. As shown in this table, Soil Type Nos. 1 and 2 are relatively permeable with coefficients of permeability ranging from 10^{-3} to about 5×10^{-5} **cm/sec**. Soil Type Nos. 3 and 4 are less permeable due to the presence of appreciable fines content.

Isotropically consolidated-drained **triaxial** compression tests were performed on 12 reconstituted specimens and two gravity core specimens. Two of the test series were multistage, the rest were single stage. The results of these tests are summarized in Table 4-8. The **Mohr's** circles as well as the stress-strain and volumetric-change plots are provided in Appendix II. The results of tests on reconstituted specimen indicated that the effective **fric-**tion angles are about 39° , 40° , 41° , and 37° for Soil Types Nos. 1, 2, 3, and 4 respectively. The two multistage tests on gravity core specimens indicate that the effective friction angle is about 35° to 38° for **Soil Type No. 4**.

This range in effective friction angle for Soil Type No. 4 is slightly lower than what was estimated from the in situ shear strength measurements. This may be indicative of sample disturbance and other factors such as the procedures utilized in interpreting the **in situ** strength measurements.

Cyclic simple shear tests were performed on five gravity core specimens and **12 reconstituted** specimens. The results of these tests are summarized in Table 4-9 and in Figure 5-22. An examination of these results indicates that the cyclic shearing strengths determined from the gravity core specimens are either higher than or of the same order of magnitude as the **reconstituted** specimens, which were prepared at higher unit weights than the gravity core specimens. This apparent contradiction is thought to be indicative of the significant effects of **soil** grain-structure arrangement in situ that is not accounted for by reconstituted samples duplicating only the dry unit weight. Data presented in Figure 5-22 were subsequently adjusted to likely field conditions based upon the age of the deposits (Seed, 1976). Age dating studies (Section 4.2.,4) suggest that sediments at the site below a depth of 0 to 3 m are at least 11,000 years old. A correlation of this information with the data presented by Seed (1976) indicates that the **cyclic** shearing strengths of the in situ sediments excluding the agitated **surficial** veneer would be at least 50 percent higher than strengths measured **in** the laboratory. The cyclic **simple** shear test results from the gravity core specimens also indicate that limiting shearing strains develop regardless of the magnitude or duration of the applied cyclic shearing stress (Appendix II). This is indicative of dense soils where the effects of dilation prevent a complete loss of shearing resistance.

Modulus and damping characteristics were determined for four **reconstituted** specimens utilizing a Hardin type resonant column test device for low strain amplitudes (10^{-4} to 10^{-2} percent shearing strain) and an MTS Model 810 **cyclic triaxial** loading system operating in strain-controlled mode for higher strain amplitudes (10^{-2} to 1 percent shearing strain). A summary of test results is provided in Tables 4-10 and 4-11; Appendix II contains individual test data. Based on the same reasoning stated in the previous section, the stiffness of an in situ deposit is expected to be higher than these laboratory data. Data presented by Anderson and Stokoe (1978) suggest that the in situ modulus curves could be best represented by multiplying the laboratory modulus values presented in Appendix II by 1.5 (i.e., a 50 percent increase).

5.6 GEOTECHNICAL ANALYSIS

Information presented in the preceding sections of this chapter were integrated to provide basic site characterization data necessary for an engineering evaluation of soil behavior. This evaluation considered the **geotechnical** behavior of soils under (1) gravity loading, (2) storm-wave loading, and (3) earthquake loading. Results from these analyses formed the basis for identifying potential geologic hazards on the Northern Aleutian Shelf.

A considerable degree of judgment must be used when interpreting the meaning or significance of the following analyses. These analyses were often based on information which was insufficient or inferred. For example, **only surficial** sediment data (upper 1 to 2 m) were obtained; hence, **soil** profiles had to be inferred from existing geologic data and judgment. Despite these limitations, the **geotechnical** analyses provide a framework for judging the potential severity of certain hazards. Future site-specific studies should address these hazards carefully before installation of any important structure.

5.6.1 Gravity Loading

Gravity loading refers to loading which results from the buoyant weight of the structure or the soil mass. The principal **geotechnical** considerations associated with gravity loading include vertical bearing capacity and settlement, when the load results from structures, and slope instability in areas where the seafloor slopes substantially. Most **geotechnical** problems related to gravity loading result where soft sediments exist and as noted in Section 5.5, the limited data available for the study area definitely suggest that soils are dense.

5.6.1.1 Bearing Capacity

Bearing capacities for **surficial** sediments should be high in view of the high frictional angles characterizing **surficial** sands. For most locations the effective angle of internal friction **will** be greater than 36° . The associated design bearing capacity for a surface foundation with this friction angle will be in excess of 150 kN/m^2 for a footing with a 2 m width. Appropriate adjustments must be made to this value if horizontal forces exist concurrent with vertical loading forces.

This bearing capacity estimate is most applicable for the design of pipelines and small mat foundations, with a diameter or width less than 1 to 2 m. The absence of **geotechnical** information at greater depths creates a degree of uncertainty about **the** use of friction angles determined in this study to compute bearing capacity for larger foundations, such as might exist with an exploratory **jackup** rig. Although softer layers were not interpreted from geophysical records, the occurrence of an underlying weaker layer which could cause "punch-through" of a heavily-loaded, large foundation cannot be ruled out. Given this uncertainty, it is evident that more detailed site-specific

studies will be warranted when potentially critical structures are being placed on the seafloor.

5.6.1.2 Settlement

The settlement of sandy soils under static (or gravity) loading is generally **small**, as compared to clayey soils. The results of oedometer tests (Section **5.5.5**) confirm this behavior. Compression indices for tests on reconstituted samples were typically an order of magnitude less than the values normally associated with clays. Higher values recorded for **gravity-core** samples are attributed to sample looseness near the **seabottom**.

These low compression indices imply that settlements will be small as long as the foundation size is small and loads are within normal limits. Most of the settlement should occur rapidly as immediate (or *elastic*) compression of the soil structure. Much of the site is covered with relatively fine to medium sands ($D_{10} > 0.05$ mm); hence, permeability will be relatively high and consolidation will be rapid. Consequently, any time-dependent settlement is expected to occur rapidly.

The uncertainties associated with soil conditions at depth means that the above interpretations are most appropriate for small foundations. Although deeper soils are expected to be either dense sands or stiff clays, **site-specific** studies will have to be conducted to verify this premise, particularly where critical structures are to be emplaced.

5.6.1.3 Slope Stability

Available bathymetric information indicates that the natural slope of the seafloor in the study area is gentle with a maximum gradient on the order of

0.5 percent near the coastline and with a gradient of about 0.02 percent or less over much of the study area.

The **surficial** sediments encountered in the study area are characterized by dense sandy materials. These types of materials have adequate shearing resistance so **that** the potential for slope instability under gravity loading *is* very low. The sediments below the **surficial** sediments are expected to have similar or greater shearing resistance. Thus, no unusual slope instability problems are anticipated in the study area unless man-made, large gradients are created. **At** these locations **slope** stability should be investigated on a site-specific basis.

5.6.2 Storm-Wave Loading

Storms generated in the Gulf of Alaska and the Bering Sea will occur in the study area at fairly frequent intervals, as noted in Section 2.2.3. The consequence of these storms will be large storm waves having significant wave heights from 15 to 25 m. These large waves potentially can cause scour of fine-grained sands and silts, liquefaction of sands in shallow water, and slope instabilities due to hydrodynamic pressure oscillation. Storm waves can also indirectly affect the soil as they load pipelines and other bottom-supported structures. Treatment of these indirect loading effects is, however, beyond the scope of this regional analysis. Detailed evaluations of wave-structure interaction should be anticipated during site-specific investigations.

5.6.2.1 Scour

Wave-induced currents in combination with local bottom currents acting on fine silts and sands can result in scour of the seafloor (e.g. Kuenen, 1950). As summarized in Section 2.2.4, maximum bottom currents are expected to be on the order of about 100 **cm/sec** in the coastal region and slightly less in

deeper water. In proximity to an offshore structure, these currents **would** likely be even higher, due to hydrodynamic interaction effects. According to empirical relationships developed by **Kuenen** (1950), these velocities are sufficiently high to transport **surficial** sediments in the area. This indicates a potential for scouring **in** a major portion of the area, particularly along the coastal region and in proximity to an offshore structure.

The possibility of scour presents no significant problem to the design of offshore structures. Various remedial measures can be taken to mitigate the scour effects. These remedial measures should be developed for each specific case taking the type and configuration of the offshore structure into consideration.

5.6.2.2 Wave-Induced Liquefaction

The passage of storm waves can generate a transient pore pressure and a permanent excess pore-water pressure buildup in **cohesionless** sediments (Finn and others, 1980). The magnitude of the transient and permanent pore pressures depends on a number of factors, including the wave height and length, the water depth, and the soil type. Where conditions are suitable, the transient pore pressures develop instantaneously in a one-to-one relationship with the applied wave loading while the excess pore pressure buildup accumulates in proportion to the number of wave-induced shearing stress reversals. **As** the pore pressure increases, the effective resistance of **cohesionless** soil can decrease, which can lead to potential instability of the seafloor.

The interaction of a storm wave with the seafloor sediments and its associated effects on the seafloor stability involve many important individual elements. Rational frameworks for evaluating these types of problems have

been provided by various investigators (e.g., Seed and Rahman, 1977; Finn and others, 1980). In this analysis the potential for wave-induced liquefaction within the study area was evaluated using the method recommended by Seed and Rahman, (1977). The following maximum wave characteristics were considered.

- o maximum wave height = 30 m
- o period = 15 seconds
- o water depth = 76 m

This analysis also required use of a wave-height/occurrence histogram. The distribution shown in Table 5-5 was assumed for this study. The **values** shown in this table were based on engineering judgment and unpublished **data** for the area. Site-specific information and evaluation are necessary for further refinement of these values.

This analysis involved **the** following steps:

1. Evaluate the storm-wave-induced shear stress in the soil profile.
2. Establish **an** equivalent uniform storm.
3. Estimate the excess pore pressure increase.

The induced shear stress for each wave cycle (component) was calculated using the theory of elasticity as formulated by Seed and **Rahman** (1979). The equivalent uniform storm was then established using their shear stress ratio at the top of soil profile induced and the liquefaction strength curves (Figure 5-23) in accordance with the procedures developed by Lee and Chan (1972).

The third step in the analysis involved an estimate of the excess (or permanent) pore-water pressure increase. In this study, simplified procedures were used to estimate the excess pore pressure in accordance with the following equation given by Seed and **Rahman** (1977):

$$\frac{\Delta u_g}{\sigma'_{Vo}} = \frac{2}{\pi} \sin^{-1} \left(\frac{N}{N_1} \right)^{1/2\Theta} \dots \dots \dots (5-2)$$

where

σ'_{Vo} = initial effective vertical stress

Δu_g = excess pore pressure

N = equivalent number of cycles of a specific wave height that produces same effect as the storm wave

N_1 = number of cycles of a given cyclic shearing stress ratio (ratio of cyclic shearing stress to σ'_{vo}) that produces liquefaction of the soil. N_1 can be obtained from liquefaction strength curves.

Θ = empirical factor, a value of $\Theta = 0.7$ is typical (Seed and Rahman, 1977) and was assumed in this study.

The use of Equation 5-2 to estimate the excess pore pressure is conservative inasmuch as the effects of pore pressure dissipation and redistribution are not considered. This equation was adopted in lieu of a more complicated analysis (e.g. , Finn and others, 1980; Clukey and Sangrey, 1980). The excess pore pressure values obtained on the basis of the above equation represent conservative upper bound estimates. The calculated excess pore pressure ratio ($\Delta u/\sigma'_{vo}$) was found to be negligible (less than 0.02). Thus, the potential for wave-induced liquefaction is extremely low.

5.6.2.3 Wave-Induced Transient Porewater Pressure

The passage of storm waves also induced transient porewater pressure which imposes transient seepage forces and reduced effective stress in the soils. This must be considered in evaluating the storm-wave-induced instability.

In this study the amplitude of the transient pore pressure (Δu_t) was calculated by the following simplified formula (Liu and others, 1979):

$$\Delta u_t = P_0 \frac{\cosh \left[\frac{2}{L} \pi (d_s - z) \right]}{\cosh \left(\frac{2}{L} \pi d_s \right)} \dots \dots \dots (5-3)$$

where

P_0 = amplitude of wave pressure on the seafloor

$$= \frac{\gamma_w \times H}{2 \cosh \left(\frac{2\pi d}{L} \right)} * \cosh \left(\frac{2}{L} x - \omega t \right)$$

L = wave length

d = water depth

γ_w = unit weight of seawater

H = wave height

d_s = thickness of soil profile overlying an impermeable layer

z = depth at any point along the soil profile

x = horizontal distance from wave crest

t = time

ω = circular frequency of wave train

The vertical and horizontal hydraulic gradients can be calculated by partial differentiation with respect to z and x . With the given condition, the maximum hydraulic gradient was found to be less than 0.15 m/m (meter of water column per meter length). This small transient hydraulic gradient is not critical to the stability of seafloor slope; however, it should be considered in the design of pipelines and man-made slopes in the area.

The results of the above evaluation indicate that the storm-wave induced liquefaction potential is extremely low for locations where the water depth is 76 m or more. More critical conditions potentially develop as the water depth decreases. However, even at a depth of 25 m, the analysis predicts minimal

pore pressure buildup. As with any coastal regime, some sediment movements might be anticipated at less than 25 m of water because of the combined action of wave-induced excess and transient pressure. Most sediments in this depth regime are very coarse sands and gravels, and hence, should be very resistant to wave-induced instability. Nevertheless, localized deposits of finer sediments may occur and the bearing support of these materials will be potentially reduced or temporarily lost.

5.6.2.4 Slope Stability Under Wave Loading

As described previously, the natural slopes of the study area are gentle with gradients generally less than 0.5 percent. The preceding pore pressure evaluation indicates that the buildup in pore pressure will be minimal, and hence, the effects of storm-waves on slope stability will be small, i.e., the potential for seafloor slope instability under storm-wave loading will be extremely low.

5.6.3 Earthquake Loading

The Northern Aleutian Shelf study area has a high level of seismic activity. Results presented in Section 5.4.3 indicate that ground accelerations equal to at least **0.1g** can be expected throughout the area; peak accelerations between 0.4 and 0.7g are predicted near the North Amak Fault Zone. The consequence of earthquake-induced ground shaking can be liquefaction and settlement of sandy soils, seafloor slumping or inertial loading of any bottom-supported structures. Inertial loading of a structure results in both added forces on structural members and connections as well as added loading to the soil as the structure responds at some damped natural frequency of vibration.

This analysis considered only the "free-field" loading associated with liquefaction, settlement, and slope instability. The inertial response of structures, whether the structure is a platform or pipeline, warrants special consideration on a project-specific basis. Procedures outlined in API RP2A (API, 1982) and ATC (1980) provide guidelines for treating these loading phenomena.

5.6.3.1 Liquefaction and Settlement

For granular soils, earthquake-induced cyclic shearing stresses cause a temporary progressive buildup **in** pore-water pressure within the soil. For loose sands, when the pore pressure reaches the effective overburden pressure, the sediments temporarily become fluid-like in consistency and are said to have liquefied. In the case of loose sands at or near this condition, the soil may temporarily lose its ability to support a structure or resist lateral loading. However, for medium dense **to** dense sandy soils such as those in the study area, the tendency of the sand to increase in volume as shear deformations occur (called dilation) increases the undrained shearing resistance of the soil even if the earthquake-induced excess pore pressures increase to **values** approaching effective vertical stresses. This results in a stable, limiting deformation state (or residual undrained strength) which inhibits large shear deformation or failure. Thus, either "seismically-induced **pore-pressure** buildup" or "cyclic mobility" (e.g., Seed, 1976; Castro and Poulos, 1976) are probably more appropriate terms to describe the earthquake loading effects for the study area even though the term "liquefaction" is widely used in engineering practice. The term "liquefaction" is used in this study to describe the state of earthquake-induced excess pore pressure reaching the initial (prior to seismic loading) effective overburden of the soil.

From the onset of this study, it was recognized that "liquefaction" in the traditional sense of fluid-like failure would be improbable for the study area. Simplified total (undrained) analyses such as those described by Seed and Idriss (1971) and Seed (1976) would not properly describe the effects of earthquake loading. Upon consultation with NOAA representatives a mutual agreement was reached to evaluate the study area using an effective-stress computer program called **DESRA II** (Martin and others, 1976; Lee and Finn, 1977). This program features an algorithm for estimating the increase in pore-water pressures resulting from earthquake-induced cyclic shearing stresses. The program also models the effects of pore-pressure redistribution and dissipation within the soil deposit during and immediately after earthquake loading. Both features provide improved liquefaction potential evaluations.

To perform the **DESRA** analyses, a number of specific soil parameters were estimated on the basis of laboratory test data and published empirical soil property correlations. These parameters included the low-strain shear modulus and maximum soil shearing strength, the one-dimensional rebound characteristics, the liquefaction strength and the permeability of the soil. The low-amplitude shear moduli (G_{\max}) were estimated using the following relationship (Seed and Idriss, 1971):

$$G_{\max} = 1000 k_2 \sigma'_0{}^{0.5} \dots \dots \dots (5-4)$$

where

- k_2 = a constant which varies with soil type and density,
- σ'_0 = the mean effective confining pressure at the depth of interest.

The k_2 values utilized in this study were based on the results of resonant column tests adjusted to represent closely in situ conditions (Figure 5-24). Values of G_{\max} and associated maximum shearing strength, τ_{\max} , were used to define a hyperbolic stress-strain relationship (Duncan and Chan, 1970) which characterized the soil response throughout earthquake loading. The τ_{\max} values were estimated from the results of static triaxial tests assuming that the effective friction angles of 39° , 41° , 41° , and 37° appropriately represent the four soil profiles at Stations 1177/185, 1262/185, 1070/91, and 1020/100, respectively.

For saturated sands, cyclic loading causes an incremental change (increase) in excess pore pressure of, A_u , in accordance with the following expression of Finn and others (1976):

$$A_u = \bar{E}_r \Delta \epsilon_{vd} \dots \dots \dots (5-5)$$

where

$$\bar{E}_r = \text{one-dimensional rebound modulus}$$

$$\Delta \epsilon_{vd} = \text{incremental change in volumetric strain}$$

The rebound modulus, \bar{E}_r , is expressed (Martin and others, 1975) as:

$$\bar{E}_r = \frac{(\sigma'_v)^{1-m}}{Mk(\sigma'_{v0})^{n-m}} \dots \dots \dots (5-6)$$

where

$$\sigma'_{v0} = \text{initial effective vertical stress}$$

$$\sigma'_v = \text{effective vertical stress at any time}$$

k, m, n experimental rebound parameters determined by one-dimensional loading and unloading tests.

The liquefaction strengths of the four soil profiles were obtained from the results of cyclic simple shear tests with appropriate corrections to account for **in.situ** conditions (Figure 5-23). The permeability characteristics of the site soils were obtained from laboratory data. These characteristics were required to account for pore pressure redistribution and dissipation during earthquake loading. Best-estimate soil properties utilized in this study are presented **in** Table 5-6.

In this liquefaction evaluation, the earthquake time histories identified in Table 5-2 were utilized as seismic input. These earthquake time histories were scaled to the peak ground acceleration levels shown in Figure 5-5. The seismic record was introduced at the bottom of the soil profile; a transmitting boundary at the base apporitions the input motion such that energy radiates upward and downward from the input point in a manner consistent with the **rela-**tive compliance of the soil column above and below the point of input.

Forty-six liquefaction analyses were performed to evaluate pore pressure buildup in the study area during various earthquake loadings. Table 5-7 provides a summary of the results of various cases analyzed. Appendix IV presents both calculated profiles of maximum earthquake-induced excess pore pressure and selected pore pressure profiles at various time intervals during earthquake loading.

The results presented in Table 5-7 and Appendix IV were plotted to show the potential for earthquake-induced liquefaction within the study area. This interpretation is presented in Figure 5-25. **In** this figure liquefaction potential is subdivided into the following three categories:

- 1) High potential area where excess pore pressure buildup approaching effective overburden pressures is considered highly likely.
- 2) Moderate potential area where high pore pressure buildup is possible but is not considered likely.
- 3) Lower potential area where high pore pressure buildup is considered to be highly unlikely.

The liquefaction potential contours shown in Figure 5-25 were based on broad extrapolations and assumptions necessary for the preliminary and regional nature of this study. It was not intended to provide detailed assessment for a specific structure. Such an analysis requires further detailed site specific evaluations which take into account the possible effects of soil-structure interaction.

The consequence of "liquefaction", should it occur, will be controlled by the denseness of the sands. As noted previously, the **surficial** sediments in the study area are apparently very dense. Laboratory cyclic simple shear test data on these dense samples indicate that limiting strains develop regardless of the magnitude or duration of the applied cyclic shearing stresses. Thus, even in areas of high liquefaction potential, flow failure such as that experienced by the foundation of Sheffield Dam during the 1926 Santa Barbara earthquake (Seed and others, 1969) is unlikely. However, small permanent deformations during shaking are possible, with additional vertical displacements occurring as excess pore pressures dissipate. The magnitude of this post-earthquake settlement is also expected to be small.

The above liquefaction analyses were performed for a free field stress condition. Past experience indicates that the liquefaction potential for the soil beneath an offshore gravity-base structure is likely to be less than that of the free field. This primarily results from the effect of preshearing

(static horizontal shearing stress) and increases in confining pressure due to the structure loading, which usually more than offset the effects of additional **cyclic** shearing stresses induced by inertial response of the structure.

5.6.3.2 Slope Stability During Earthquakes

The potential for earthquake-induced slope failures is expected to be very **low** in most locations because of the relatively flat nature of the seafloor and the denseness of the seafloor sediments. In those areas where high excess pore-water pressures are predicted, some slope deformation might be anticipated during design earthquake accelerations. However the tendency for dilation should preclude any flow-type failures or the initiation of turbidity flows.

These conclusions assume that no local deposits of loose Holocene sands occur. Such materials are susceptible to large movement on slopes with angles less than 0.5 percent. Although such sediments are not anticipated, more detailed site investigations will ultimately be required in the area prior to development to verify this assumption.

Table 5-1 Estimates of Maximum Earthquakes **in**
the Northern Aleutian Shelf Region

Earthquake Sources	Maximum Earthquake (Ms)
ALEUTIAN SUBDUCTION ZONE	
Thrust Event-Shallow (above 40 to 50 km)	8 3/4
Thrust or Normal Event-Deep (below 40 to 50 km)	7 3/4
MAJOR GRABEN-BOUNDING FAULTS	
North Amak Fault Zone	7 3/4
OTHER LARGE BACK ARC FAULTS	
ALEUTIAN ARC	
Volcanic Event and Associated Faults	6
RANDOM EARTHQUAKE	5 1/2

Table 5-2 Recommended Time Histories for Earthquake Sources

Earthquake Source	Earthquake Magnitude	Recommended Time History
Aleutian Subduction Zone	8 3/4	A-1 (Jennings and others, 1968)
Major Graben-Bounding	7 3/4	1952 Taft 1940 El Centro
Other Large Back-arc Faults	6 1/2	1971 Holiday Inn 1979 Imperial Valley Array No. 8
Aleutian Arc	6	1966 Parkfield No. 5
Random Event	5 1/2	1957 San Francisco State Bldg. 1941 Long Beach Public Utilities

Table 5-3 Summary of Results From Drop Penetrometer Tests

Corre- sponding Sample Number	Soil ¹⁾ Type	Maximum Penetration d _{max} (cm)	Acceleration (g)/Penetration Resistance (kg) ²⁾					Estimated Minimum Friction Angle
			at d=0 ³⁾	d=5	d=10	d=15	d=30	
2	SM(4)	25	0.8/35	1.0/50	1.2/65	1.1/57		39
3	SM(4)	43	0.9/43	1.0/50	1.2/65	1.3/72	1.6/94	36
6	SM(4)	23	0.7/28	1.0/50	1.1/57	1.2/65		40
9	SM(4)	20	0.8/35	1.1/57	1.3/72	1.3/72		41
9	SM(4)	41	0.8/35	1.3/72	1.5/86	1.4/79	1.4/79	36
11	SM(4)	23	0.8/35	1.1/57	1.5/86	1.5/86		40
17	SP/SM(3)	15	0.8/35	1.2/65	2.0/123	1.0/50		43
20	SP(2)	13	0.8/35	1.3/72	1.0/50	-		43
20	SP(2)	17	0.9/43	1.5/86	1.0/50	4.1/275		42
24	SP/SM(3)	11	0.9/43	2.2/137	1.3/72	-		44
24	SP/SM(3)	8	0.7/28	2.2/137	-	-		46
35	SP(2)	14	0.8/35	1.2/65	1.2/65	-		43
40	SP(1)	18	0.8/	1.2/65	1.7/100	1.7/100		42
43	SP(1)	6	0.8/35	2.1/130	-	-		49
46	SP(2)	4	0.8/35					49
59	SP(1)	4	0.8/35					49

Notes:

- 1) Refer to Table 4-3
- 2) penetration Resistance (kg)
- 3) d = penetration Depth (cm)

Table 5-4 Expected Range of Dry Unit Weights

Soil Type ¹⁾	Expected Range of Dry Unit Weight (kN/m ³)	Selected for Test Specimen Preparation (kN/m ³)
SP (1)	15.0 to 17.5	16
SP (2)	15.0 to 17.0	16
SP/SM(3)	15.0 to 17.0	16
SM (4)	13.5 to 15.0	15

Notes:

1) Refer to Table 4-3

Table 5-5 Wave-Height Histogram Used in Liquefaction Studies

Wave Height (m)	Number of Occurrences
30.0	1
28.0 to 29.3	1
26.7 to 28.0	2
25.3 to 26.7	3
24.0 to 25.3	7
22.7 to 24.0	16
21.3 to 22.7	24
20.0 to 22.3	31
18.7 to 20.0.	35
17.3 to 18.7	39
16.0 to 17.3	75
14.7 to 16.0	103
13.3 to 14.7	141
12.0 to 13.3	176
10.7 to 12.0	220
9.3 to 10.1	270
8.0 to 9.3	325

Note: The total storm duration was estimated to be about 6.1 hours assuming an average period **of** about 15 seconds.

Table 5-6 Soil Properties for Liquefaction Analyses

Geotechnical Properties	Values Used For Soil Type ¹⁾				Remarks
	SP(1)	SP(2)	SP/SM(3)	SM(4)	
Total Unit Weight (kN/m ³)	20.5	20.0	20.0	19.0	
Effective Friction Angle (Degrees)	39	41	41	37	
Rebound Parameter k	0.043	0.105	0.134	0.051	
Rebound Parameter m	0.464	0.358	0.357	0.415	
Rebound Parameter n	0.067	0.063	0.05	0.067	
Coefficient of Permeability (cm/see)	10⁻³	5X10⁻³	5X10 ⁻⁵	ZX10 ⁻⁵	
Shear Modulus Coefficient, K2	1.5 Times Lab Data	1.5 Times Lab Data	1.5 Times Lab Data	1.5 Times Lab Data	Figure 5-23
Damping Ratio	Figure 11-41	Figure 11-40	Figure II-42	Figure II-39	
Liquefaction Strength	Figure 5-23	Figure 5-23	Figure 5-23	Figure 5-23	

Note: ¹⁾Refer to Table 4-3

Table 5-7 Summary of Results from Liquefaction Analyses *

Earthquake Source	Earthquake Record	Maximum Ground Acceleration(g)	Liquefaction Results for Profile in Soil Type ¹⁾			
			SP(1)	SP(2)	SP/SM(3)	SM(4)
Aleutian Subduction Zone	A-1	0.16	No Liq.	No Liq.	No Liq.	No Liq.
		0.19	No Liq.	No Liq.	No Liq.	No Liq.
Major Grabens	Taft, 1952	0.4	No Liq.	No Liq.	No Liq.	No Liq.
		0.5	Liq. in Top 8m	Liq. in Top 8m	No Liq.	Liq. in Top 3m
		0.6			Liq. in Top 4m	
	0.7	Liq. in Top 12m	Liq. in Top 14m	Liq. in Top 8m	Liq. in Top 8m	
	El Centro, 1940	0.4	No Liq.	No Liq.	No Liq.	No Liq.
		0.5	No Liq.	No Liq. between 2m to 3m	No Liq.	No Liq.
		0.6			No Liq.	
0.7		Liq. in Top 12m	Liq. in Top 14m	Liq. in Top 8m	Liq. in Top 9m	
Other Large Back Arc Faults	El Centro, 1979.	0.3	No Liq.	No Liq.	No Liq.	No Liq.
		0.6	No Liq.	No Liq.	No Liq.	No Liq.
Aleutian Arc	Parkfield, 1966	0.4	No Liq.	No Liq.	No Liq.	No Liq.
Random ²⁾ Events						

Notes: 1) Refer to Table 4-3 for soil types.

2) Random events were considered least critical and thus, not analyzed. No liquefaction would be expected during these events.

* In this study "liquefaction" refers to the condition when earthquake-induced excess pore pressure equals the initial effective overburden.

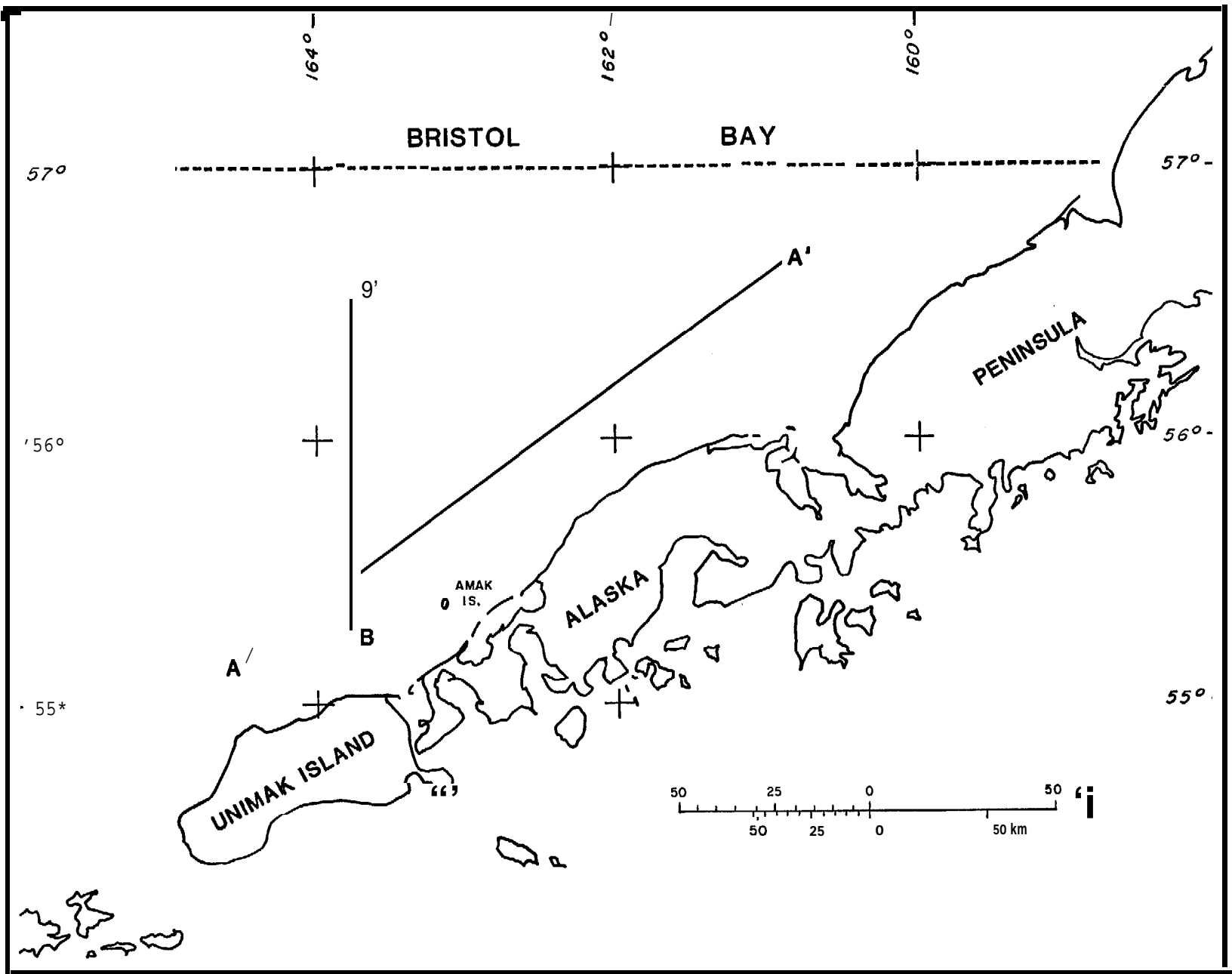


FIGURE 5-1 LOCATION MAP FOR CROSS-SECTIONS A-A' AND B-B'

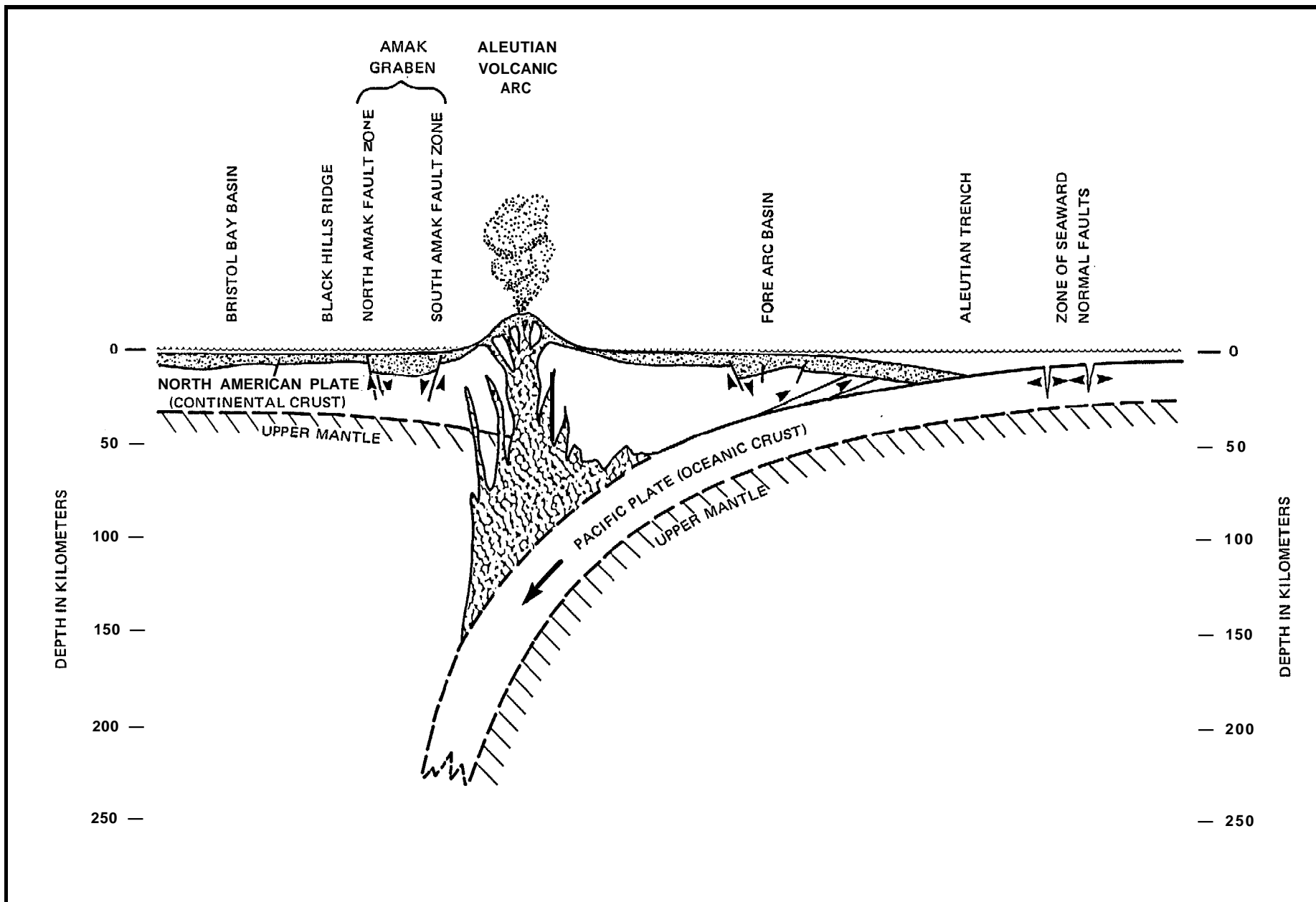


FIGURE 5-2 SCHEMATIC GEOLOGIC CROSS-SECTION OF NORTHERN ALEUTIAN SHELF REGION

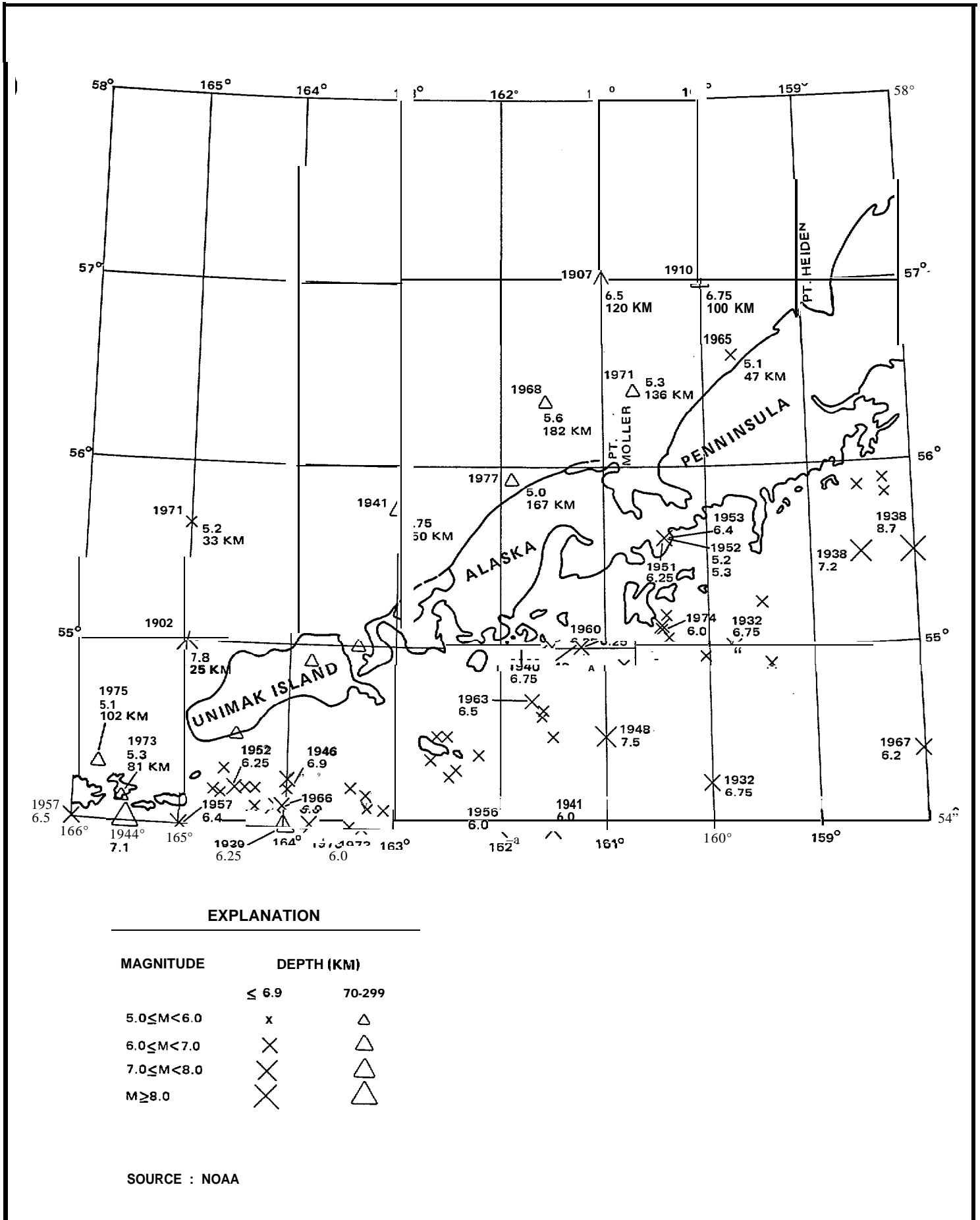
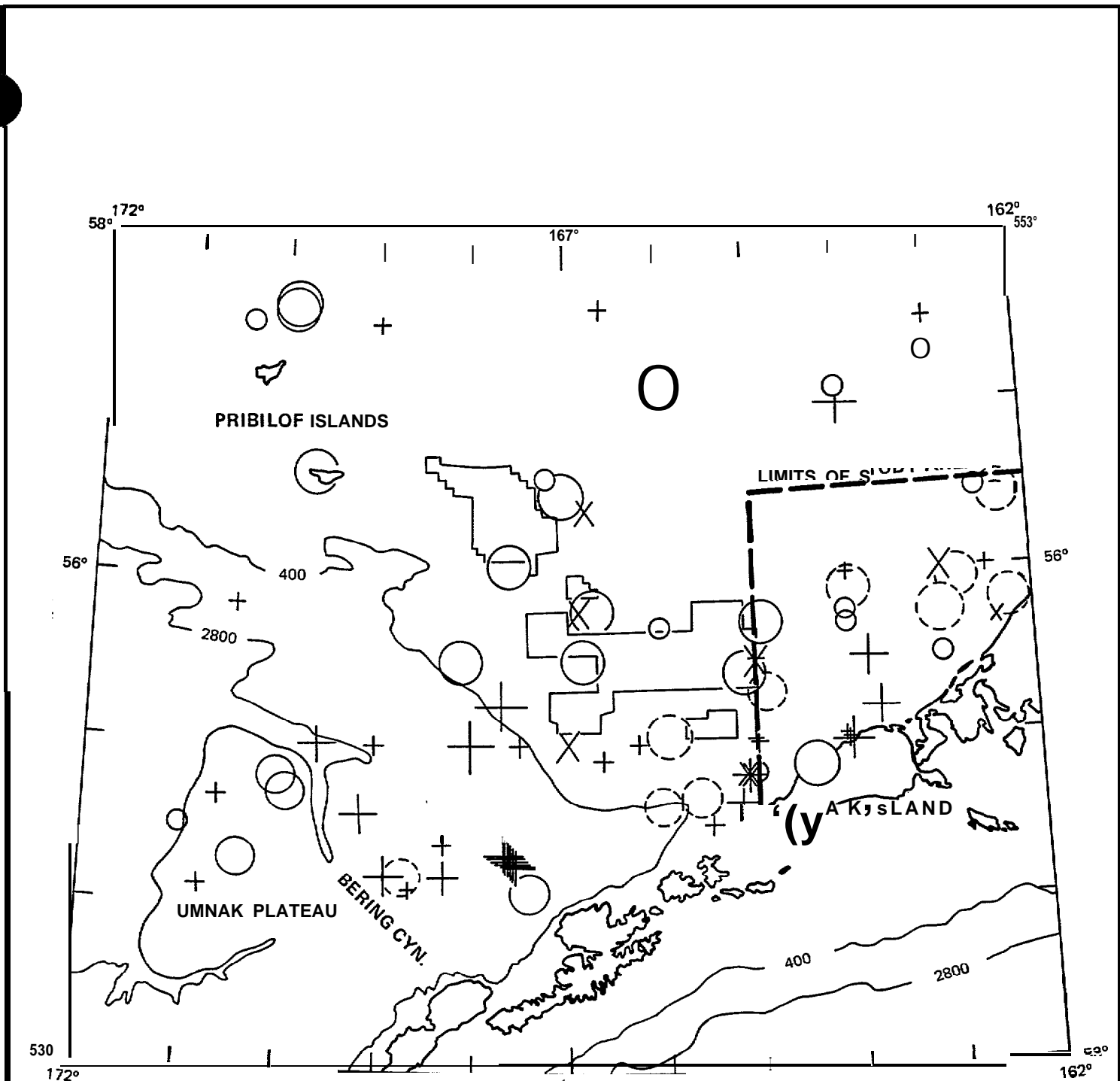


FIGURE 5-3 MAP OF MODERATE TO LARGE MAGNITUDE EARTHQUAKES IN THE NORTHERN ALEUTIAN SHELF REGION



SOURCE: DAVIES, 1981
 MINERALS MANAGEMENT SERVICE, 1982.

EXPLANATION

Epicenter symbols are scaled by magnitude according to height (seconds of latitude) = $6.5 + 1.66 M_{sg}$.:
 crosses represent events with unknown depth; x's those with depths inferred to be shallow; solid circles,
 those known to be shallow ($Z \leq 75$ km); dashed circles, those known to be deep ($Z \geq 113$ km).

**FIGURE 5-4 MAP OF EARTHQUAKES IN THE ST. GEORGE BASIN REGION,
 1925 THROUGH 1978**

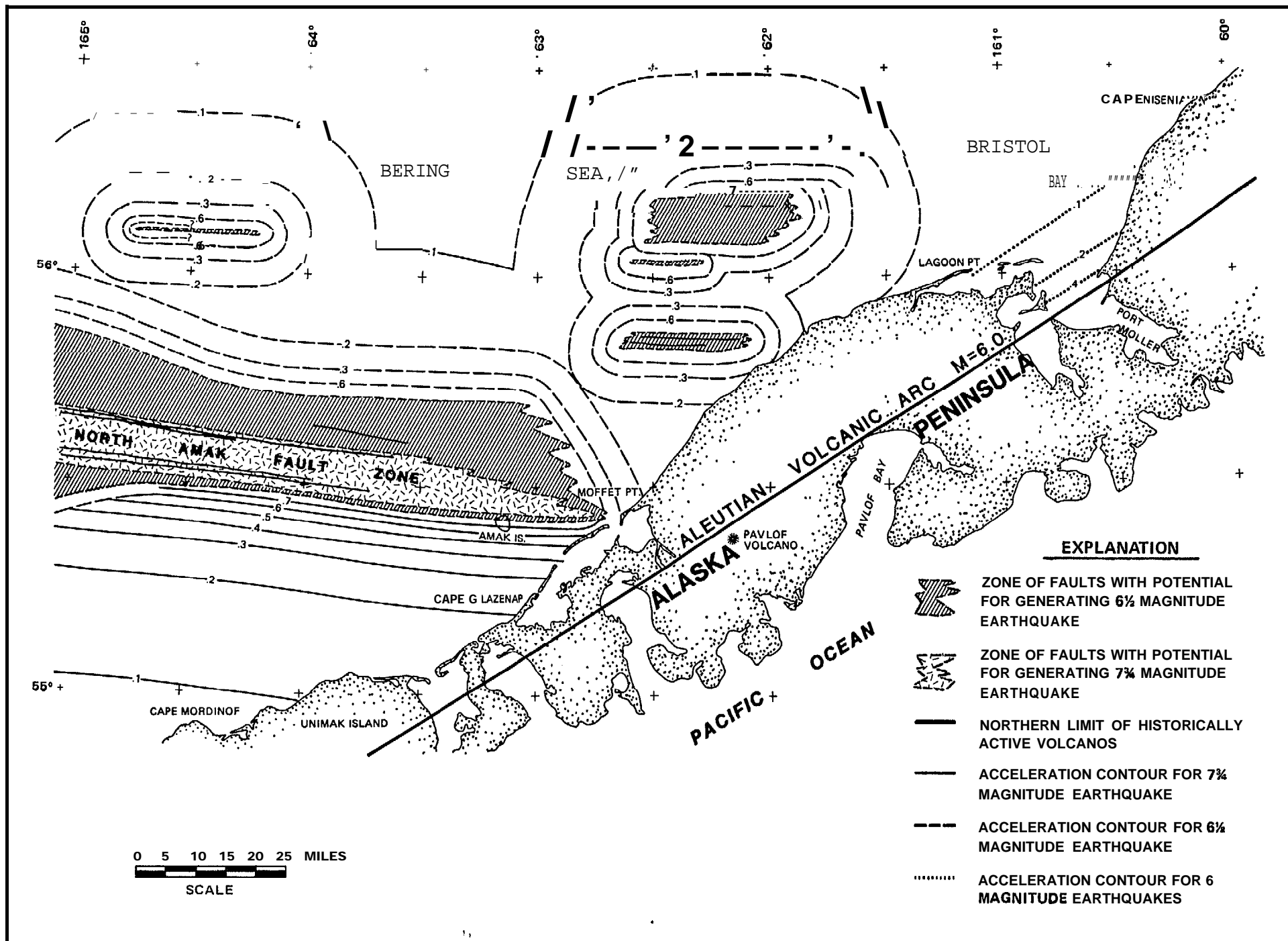


FIGURE 5-5 SOURCES OF POSTULATED MAXIMUM EARTHQUAKES, NORTHERN ALEUTIAN SHELF REGION

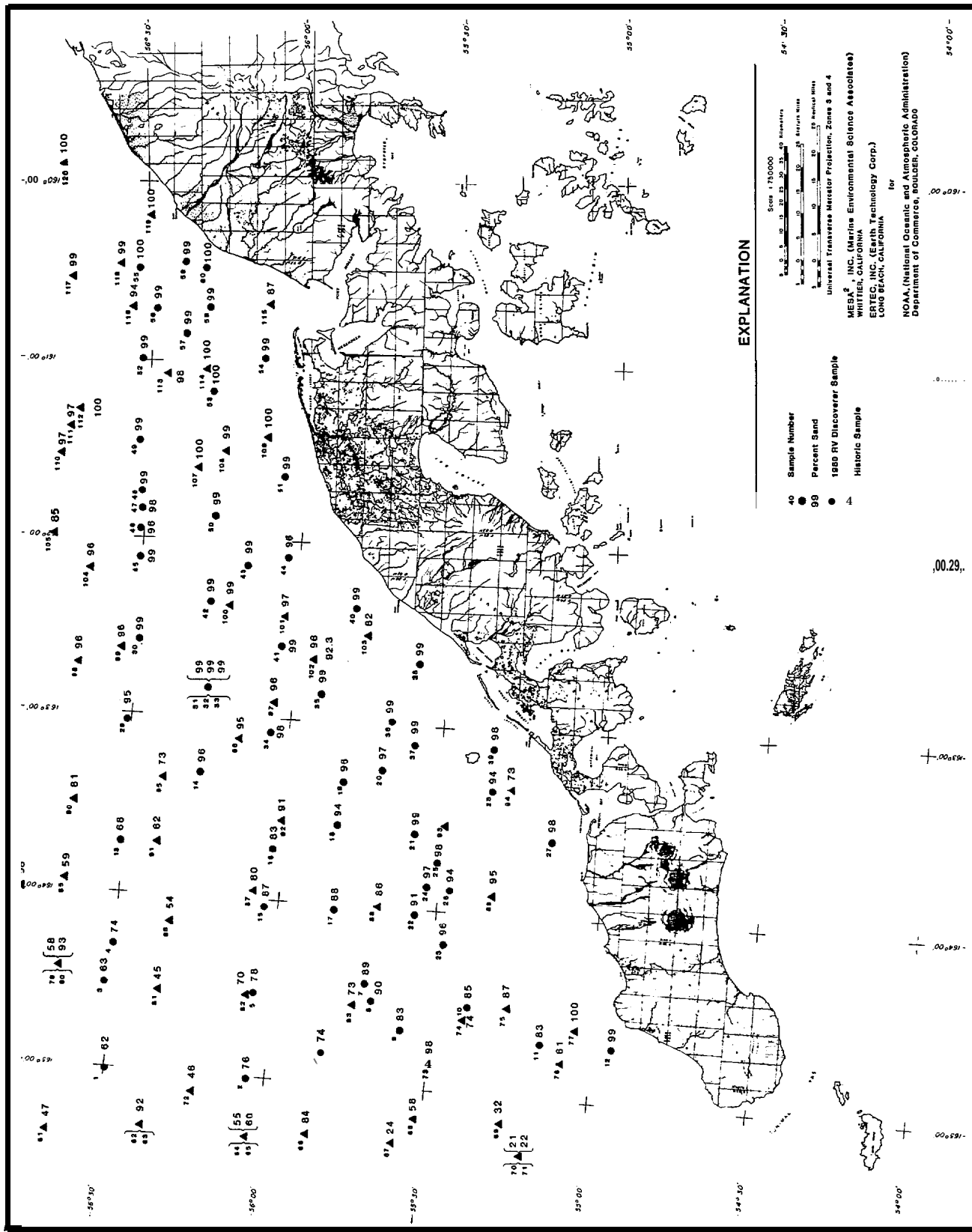


FIGURE 5-6 PERCENT SAND IN SURFACE SEDIMENTS

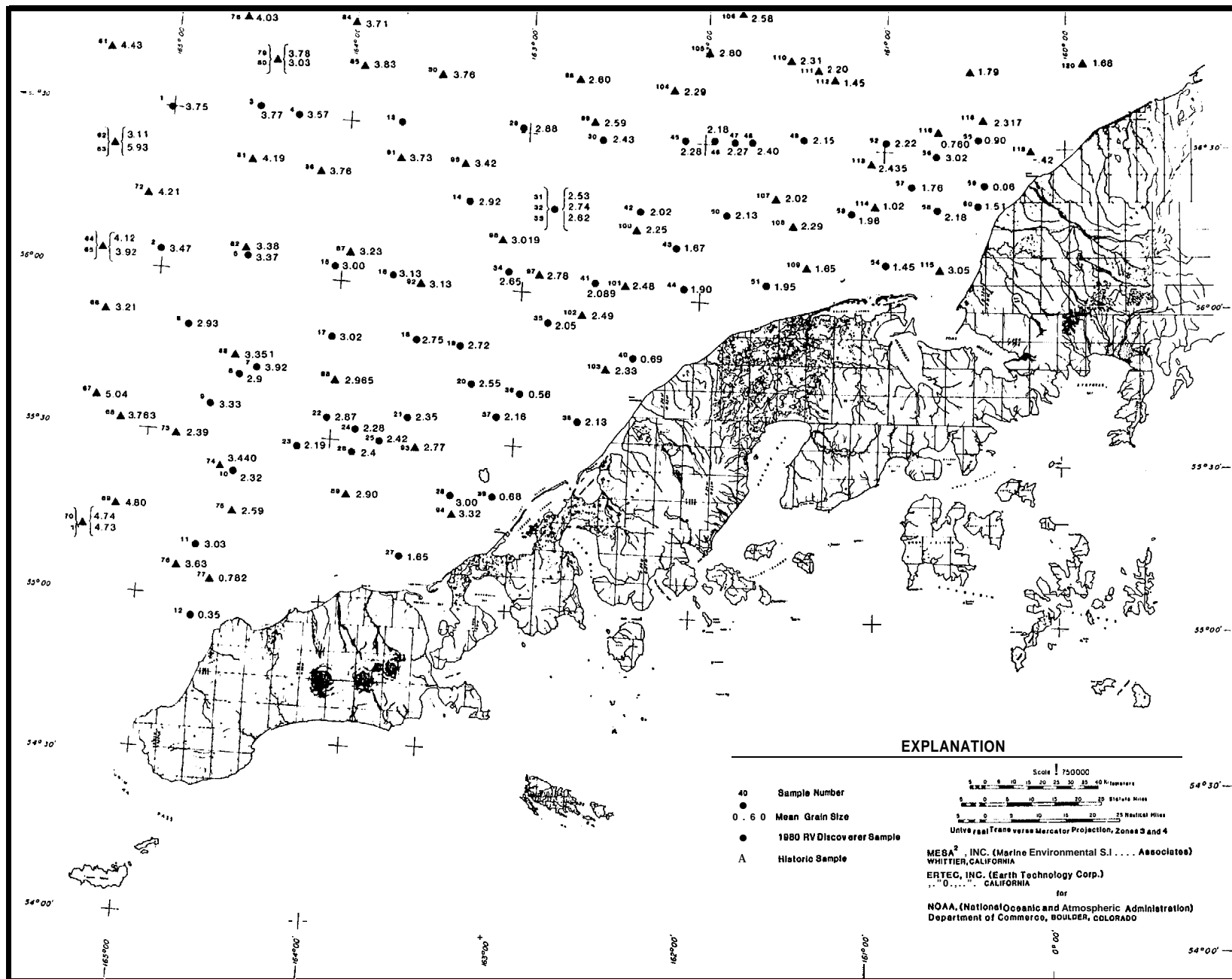


FIGURE 5-7 MEAN GRAIN SIZE OF SURFACE SEDIMENTS

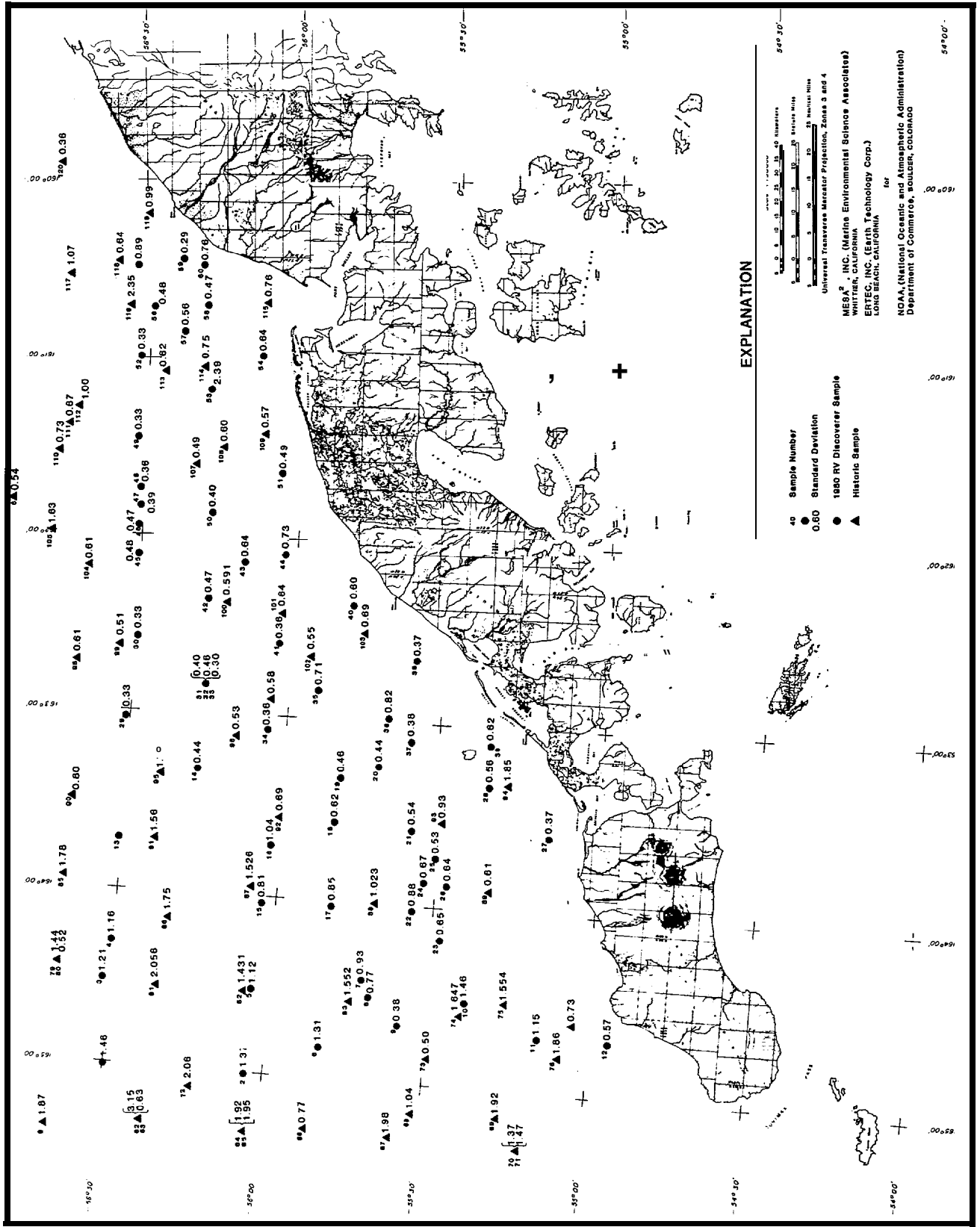


FIGURE 5-8 GRAIN SIZE STANDARD DEVIATION OF SURFACE SEDIMENTS

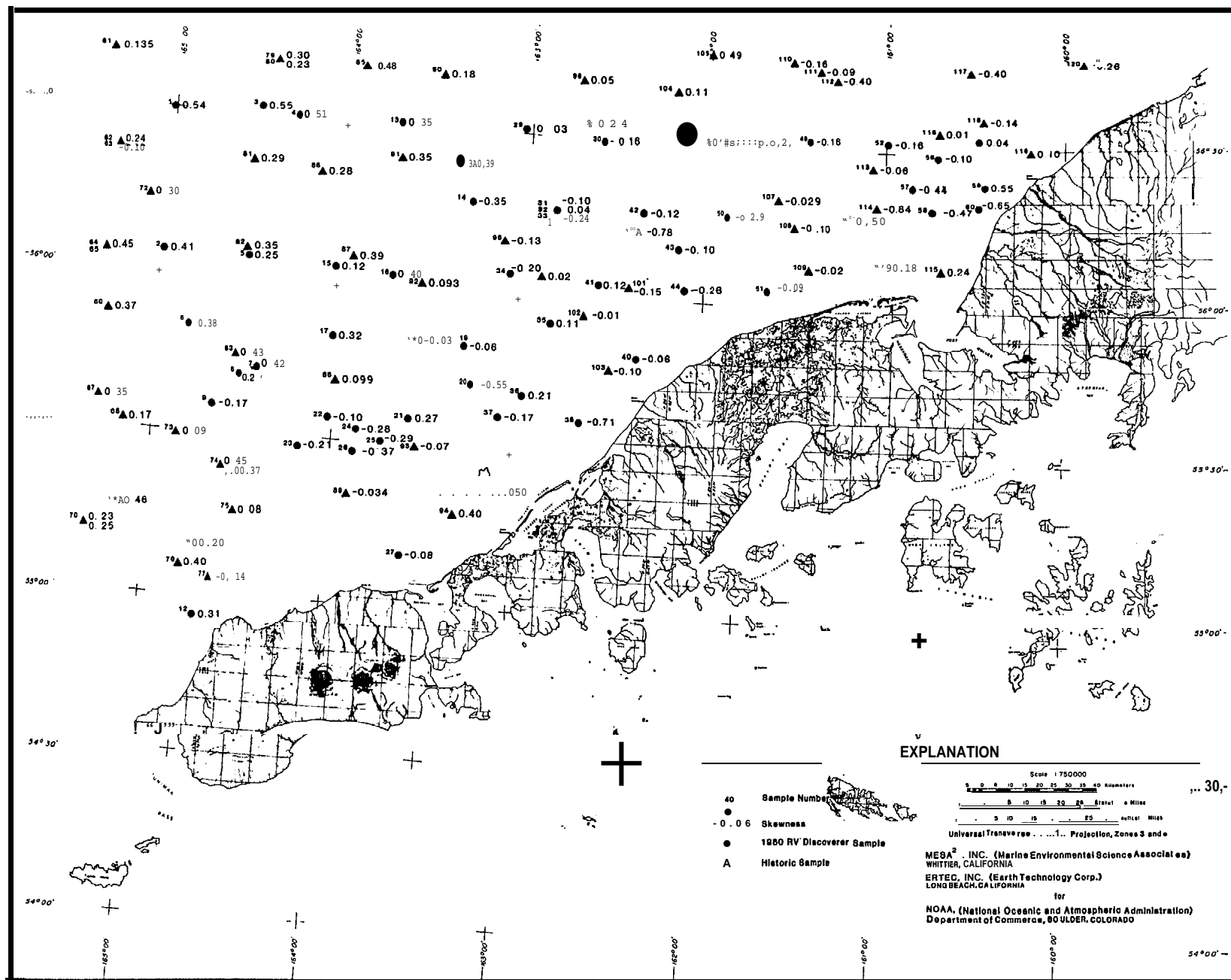


FIGURE 5-9 SEDIMENT SKEWNESS

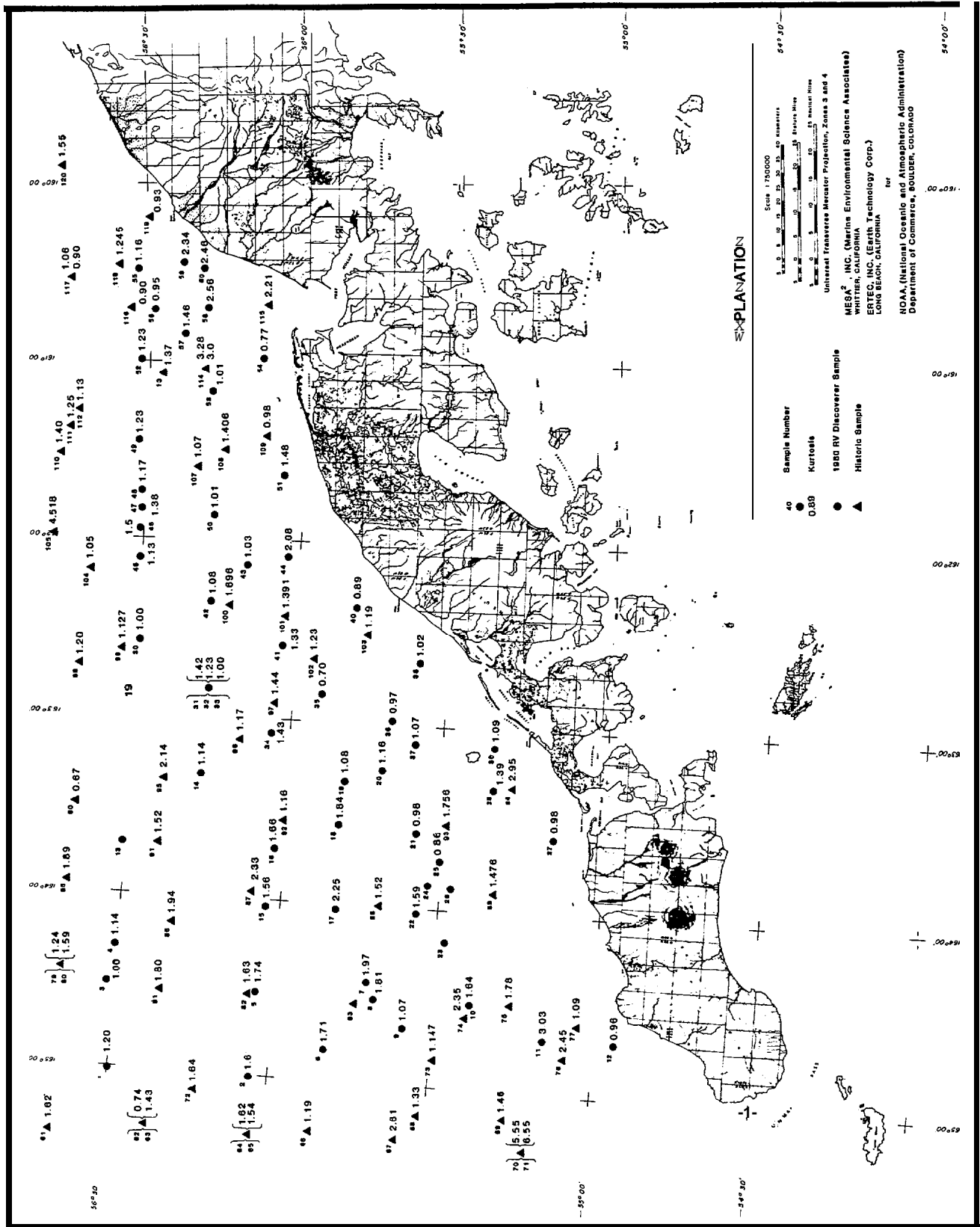


FIGURE 5-10 SEDIMENT KURTOSIS

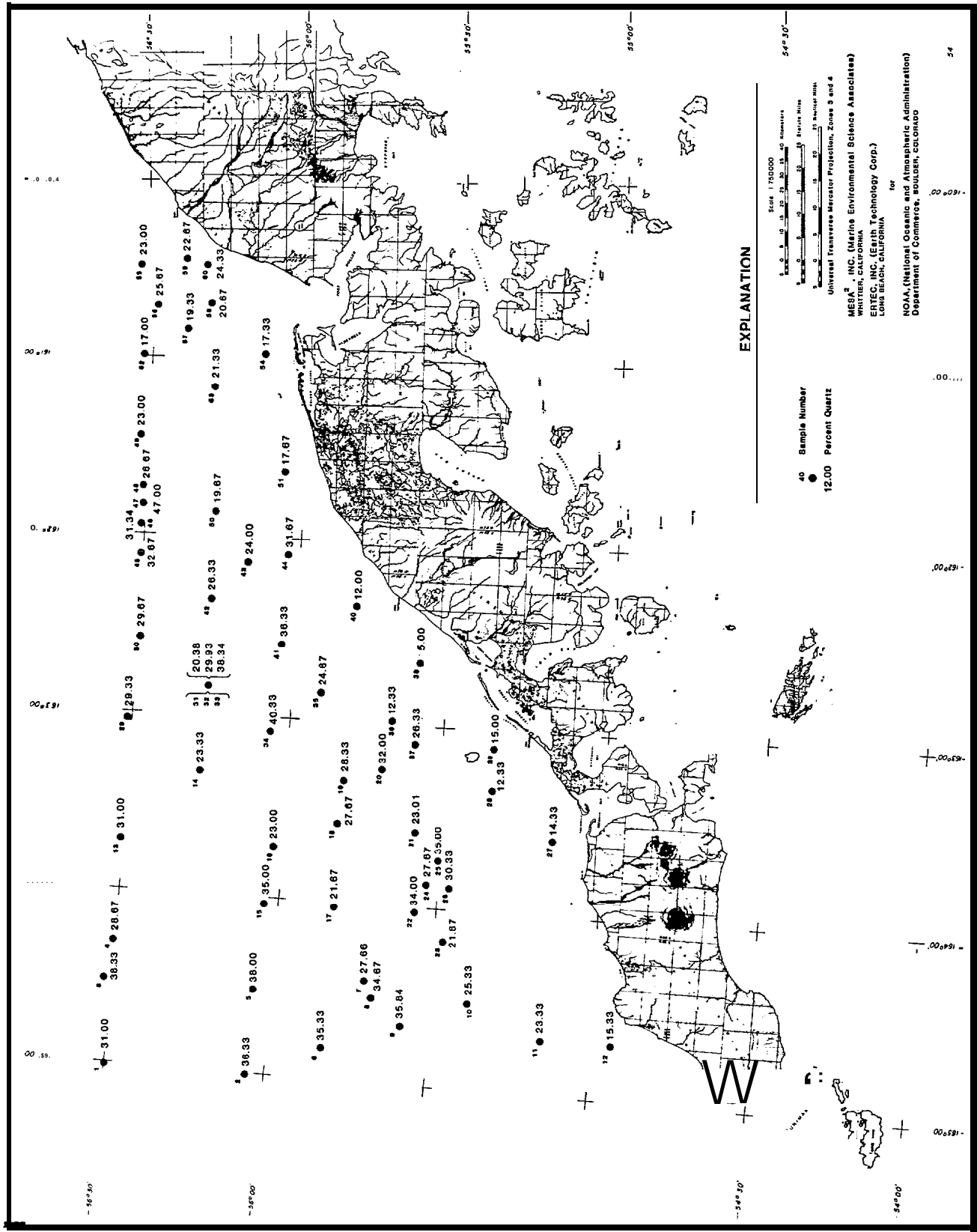


FIGURE 5-11 PERCENT QUARTZ IN SURFACE SEDIMENTS

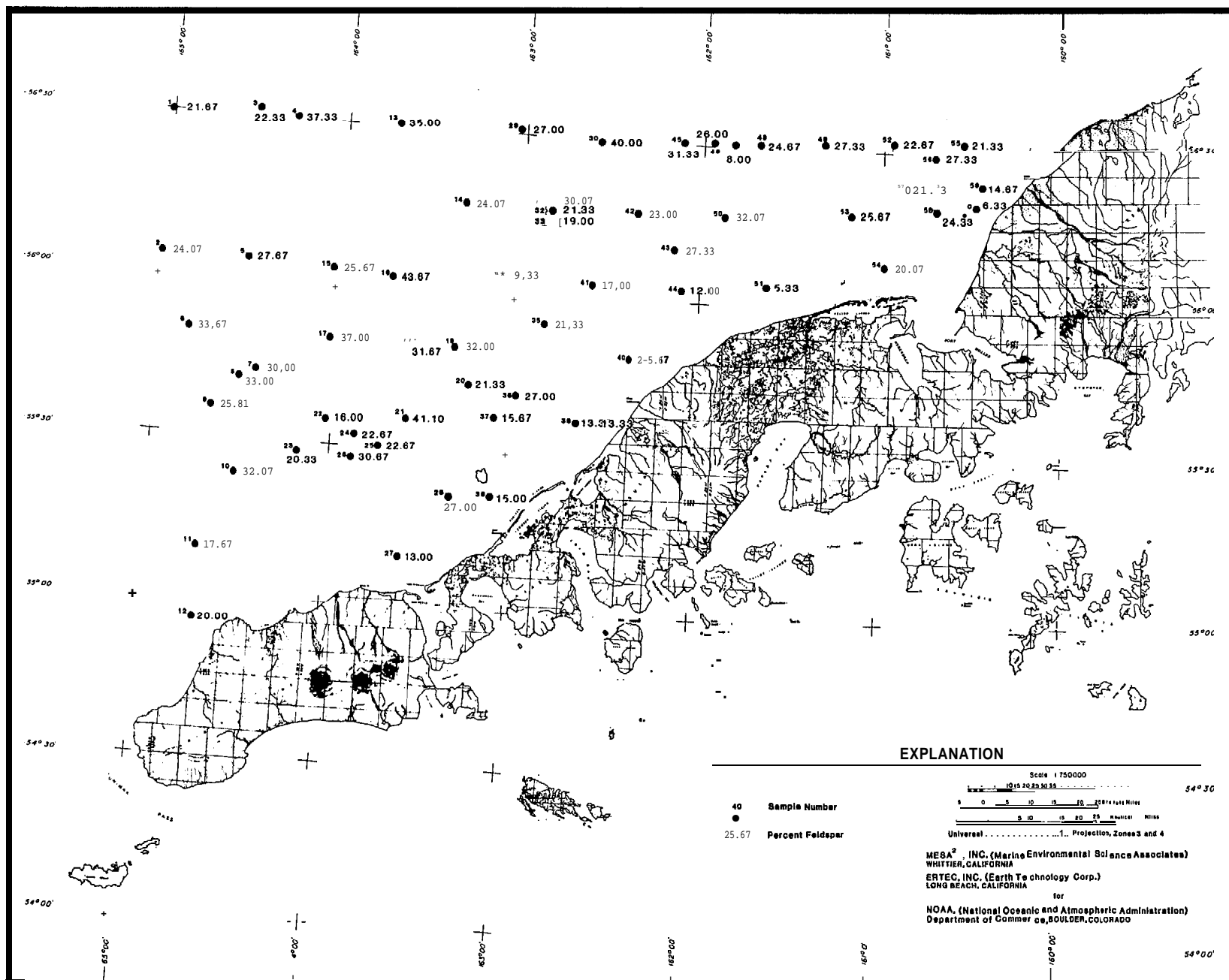


FIGURE 5-12 PERCENT FELDSPAR IN SURFACE SEDIMENTS

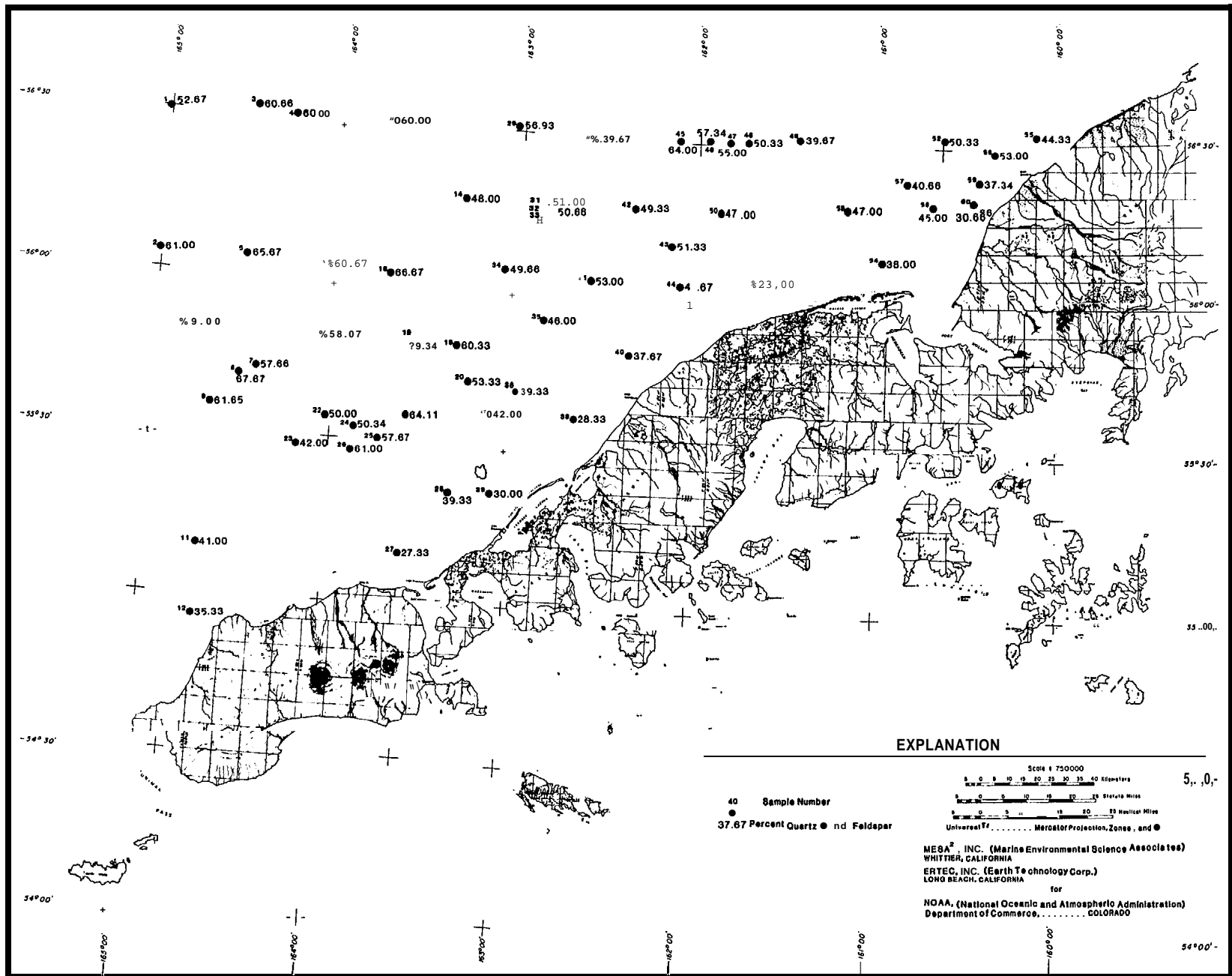


FIGURE 5-13 RATIO OF QUARTZ TO FELDSPAR IN SURFACE SEDIMENTS

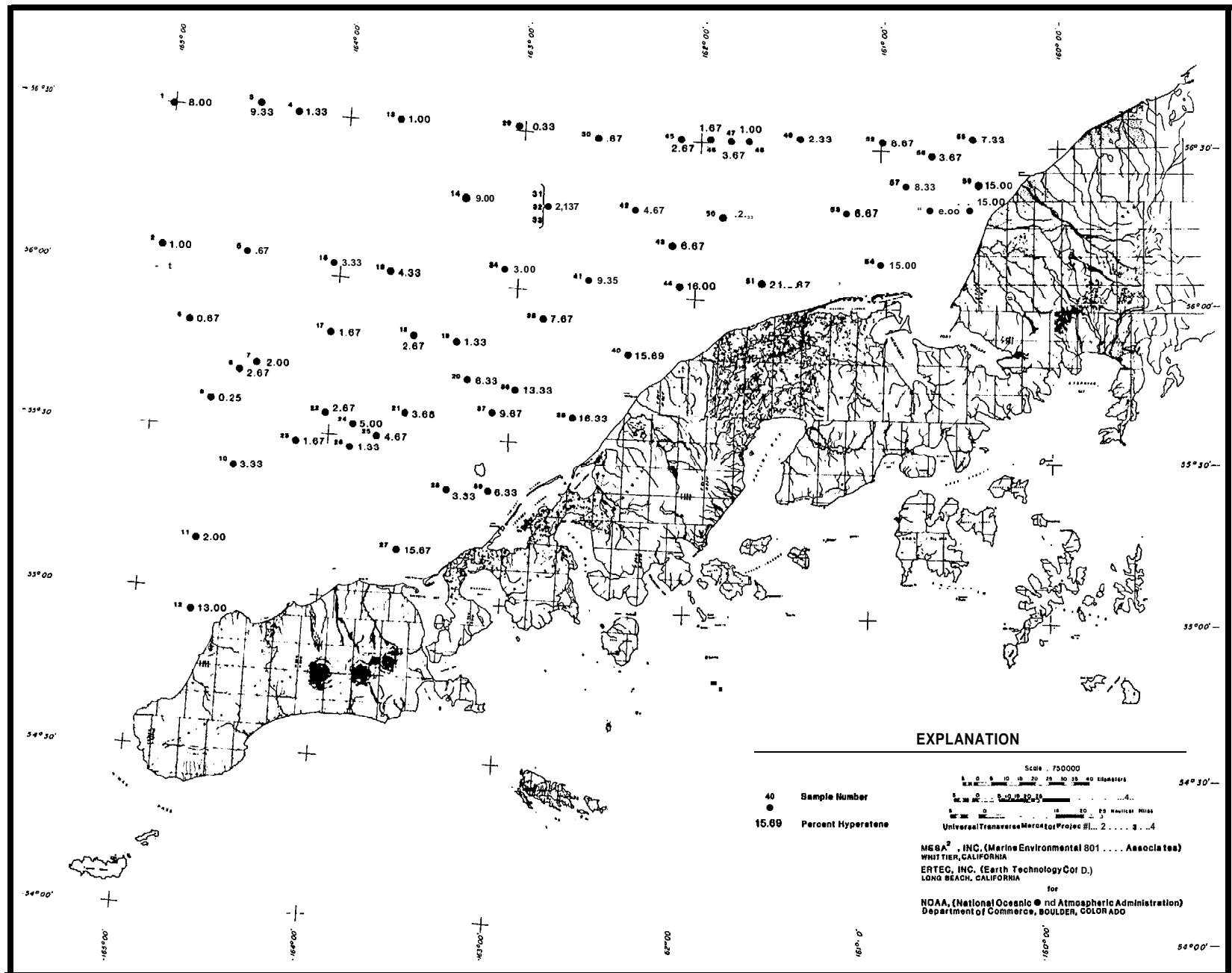


FIGURE 5.14 PERCENT HYPERSTHENE IN SURFACE SEDIMENTS

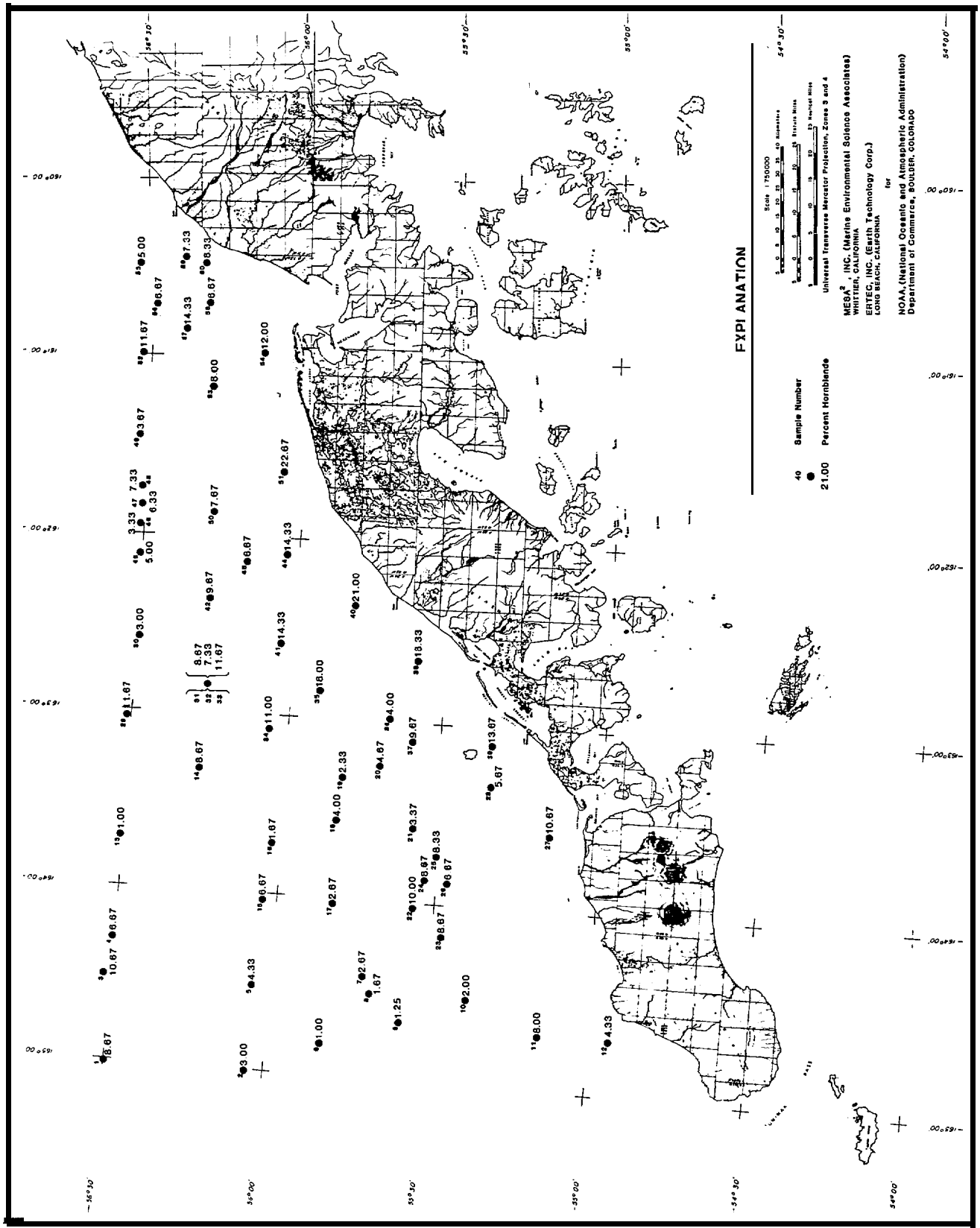


FIGURE 5-15 PERCENT HORNBLLENDE IN SURFACE SEDIMENTS

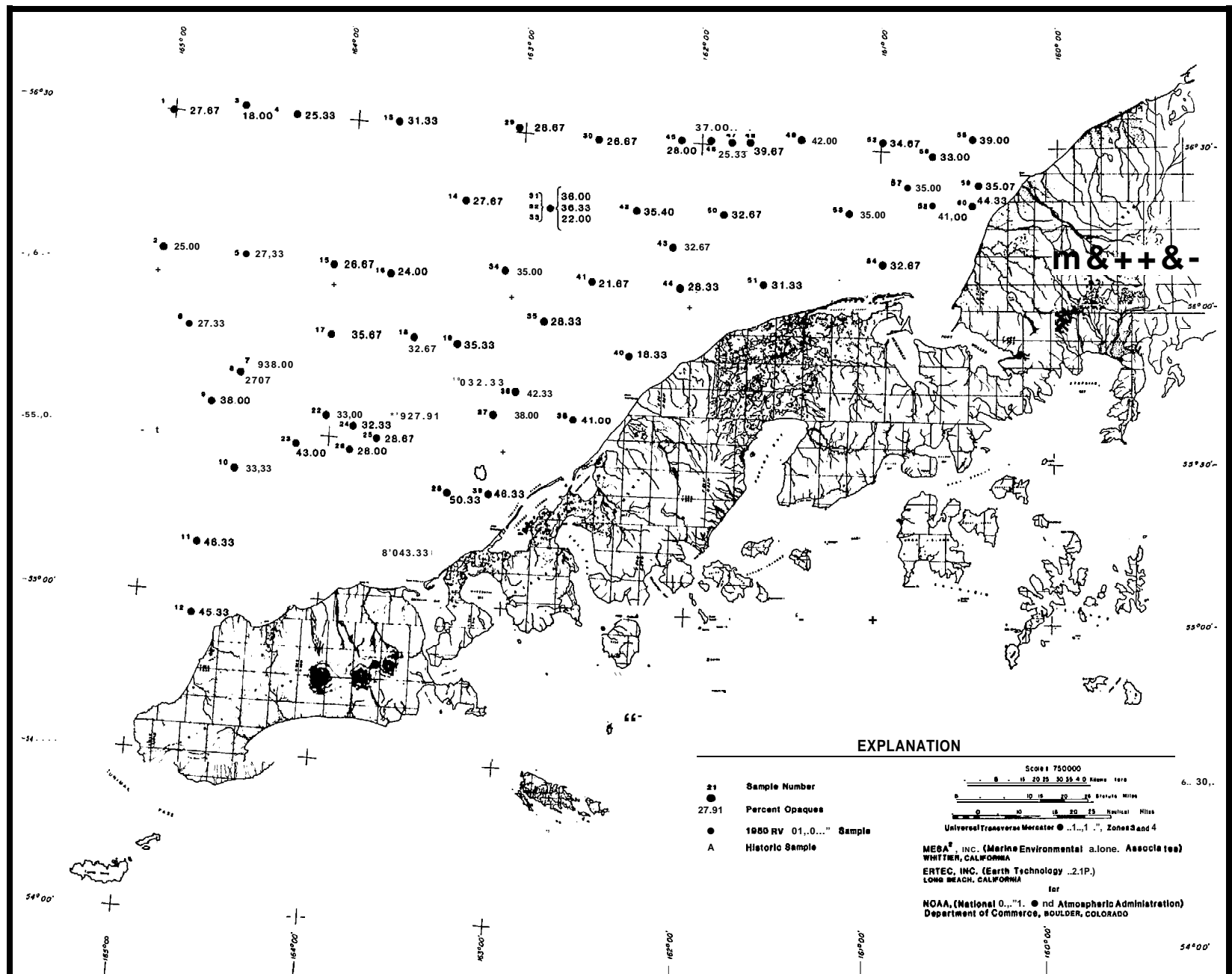


FIGURE 5-16 PERCENT OPAQUES IN SURFACE SEDIMENTS

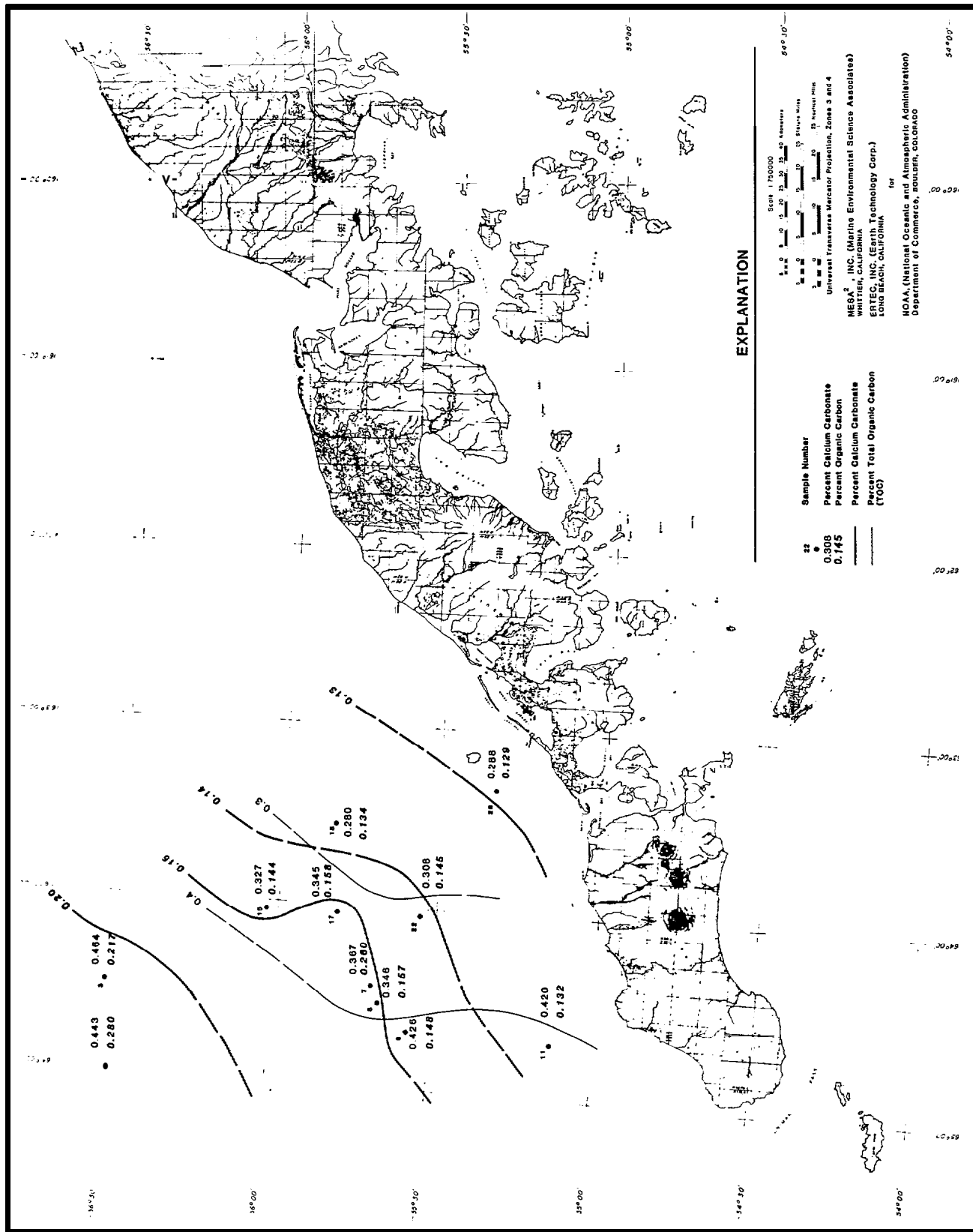


FIGURE 5-17 TOTAL ORGANIC CARBON AND PERCENT CALCIUM CARBONATE IN SURFACE SEDIMENTS

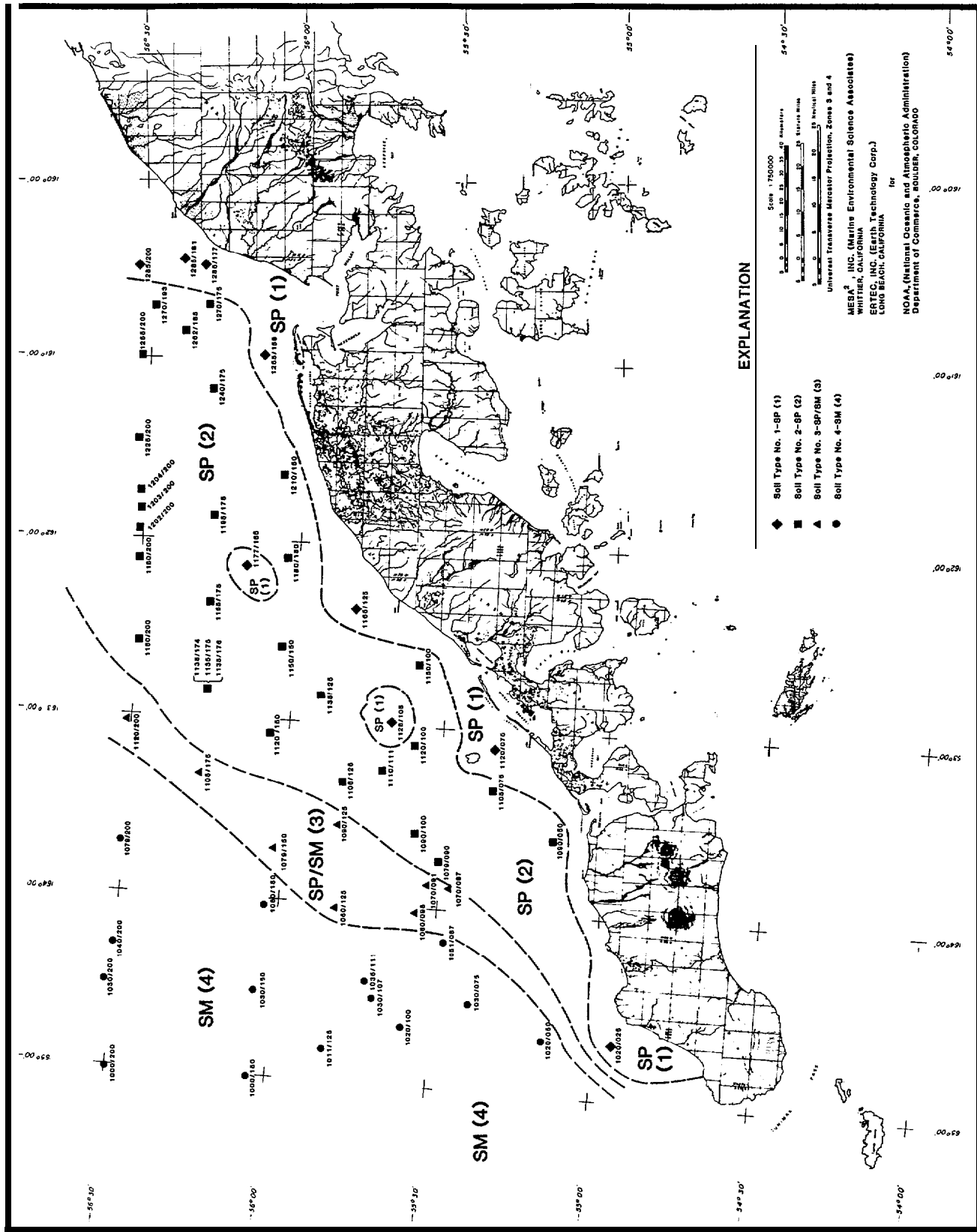
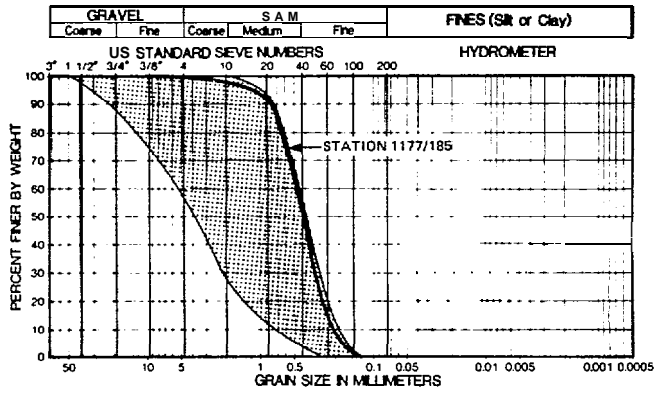
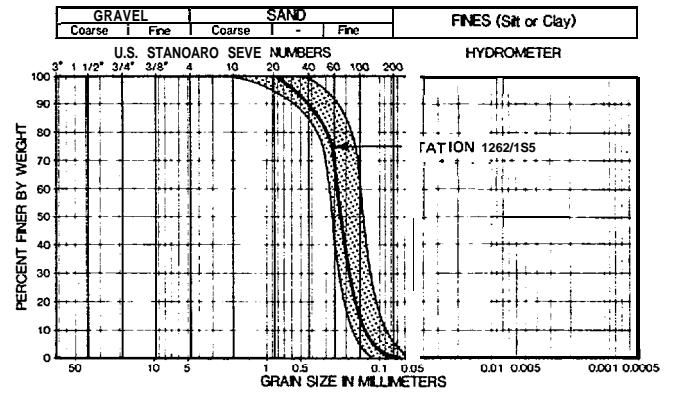


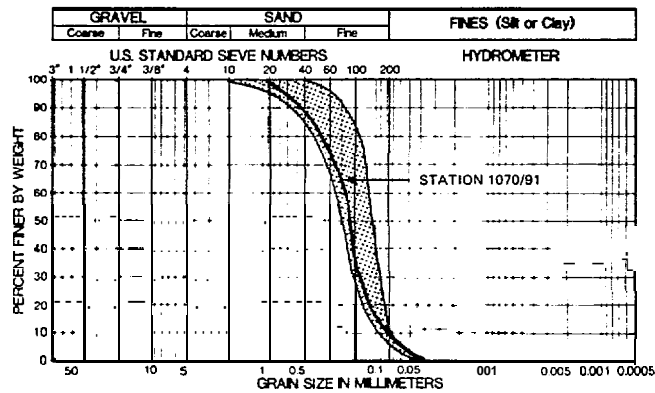
FIGURE 5-18 DISTRIBUTION OF SOIL TYPES



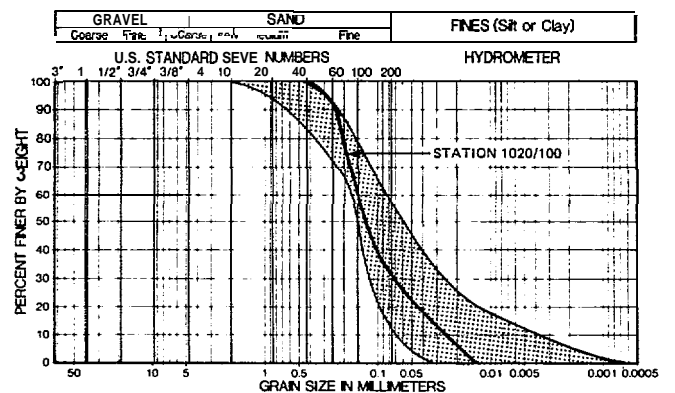
SOIL TYPE NO. 1-SP (1)



SOIL TYPE NO. 2-SP (2)

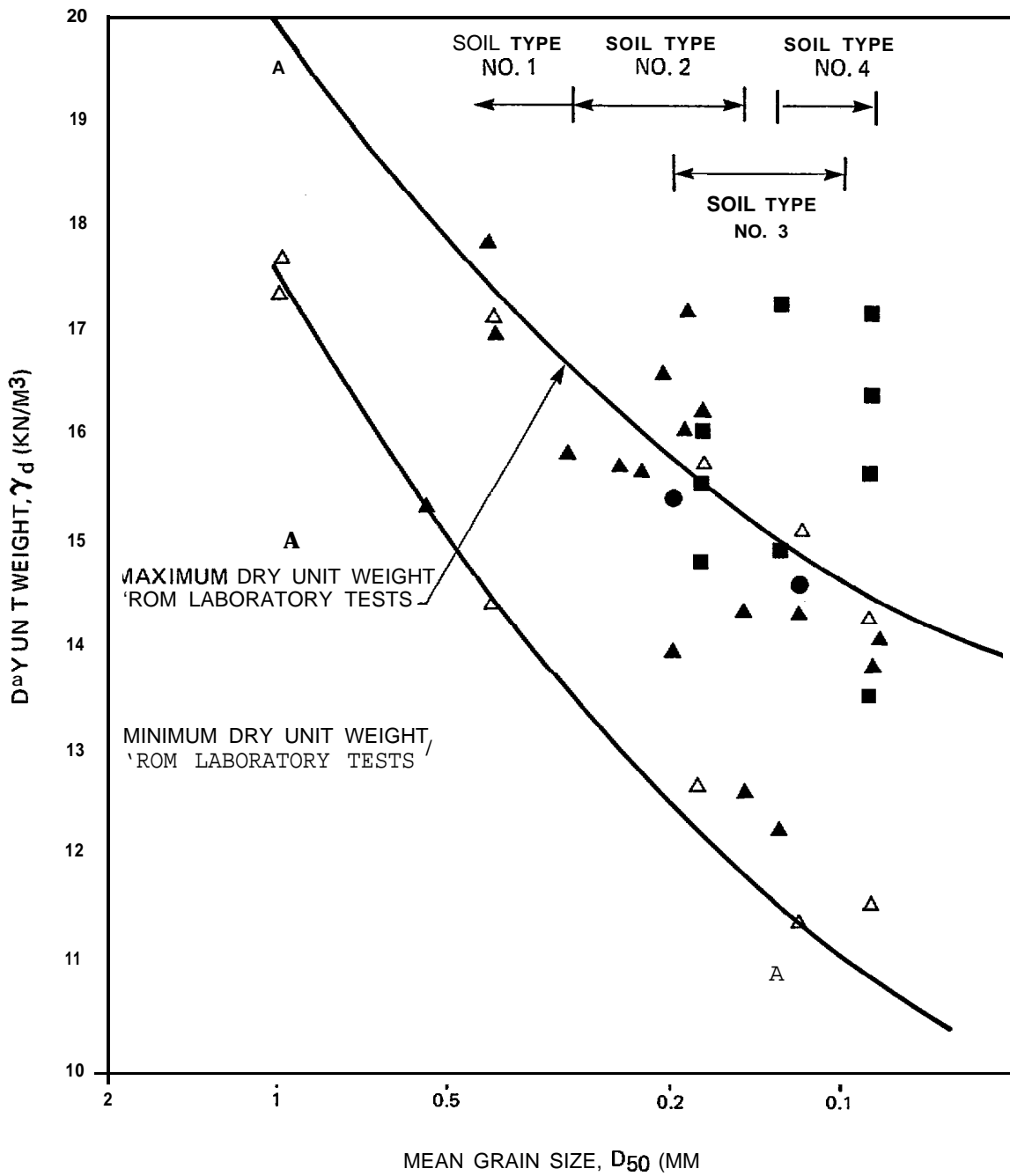


SOIL TYPE NO. 3-SP/SM (3)



SOIL TYPE NO. 4-SM (4)

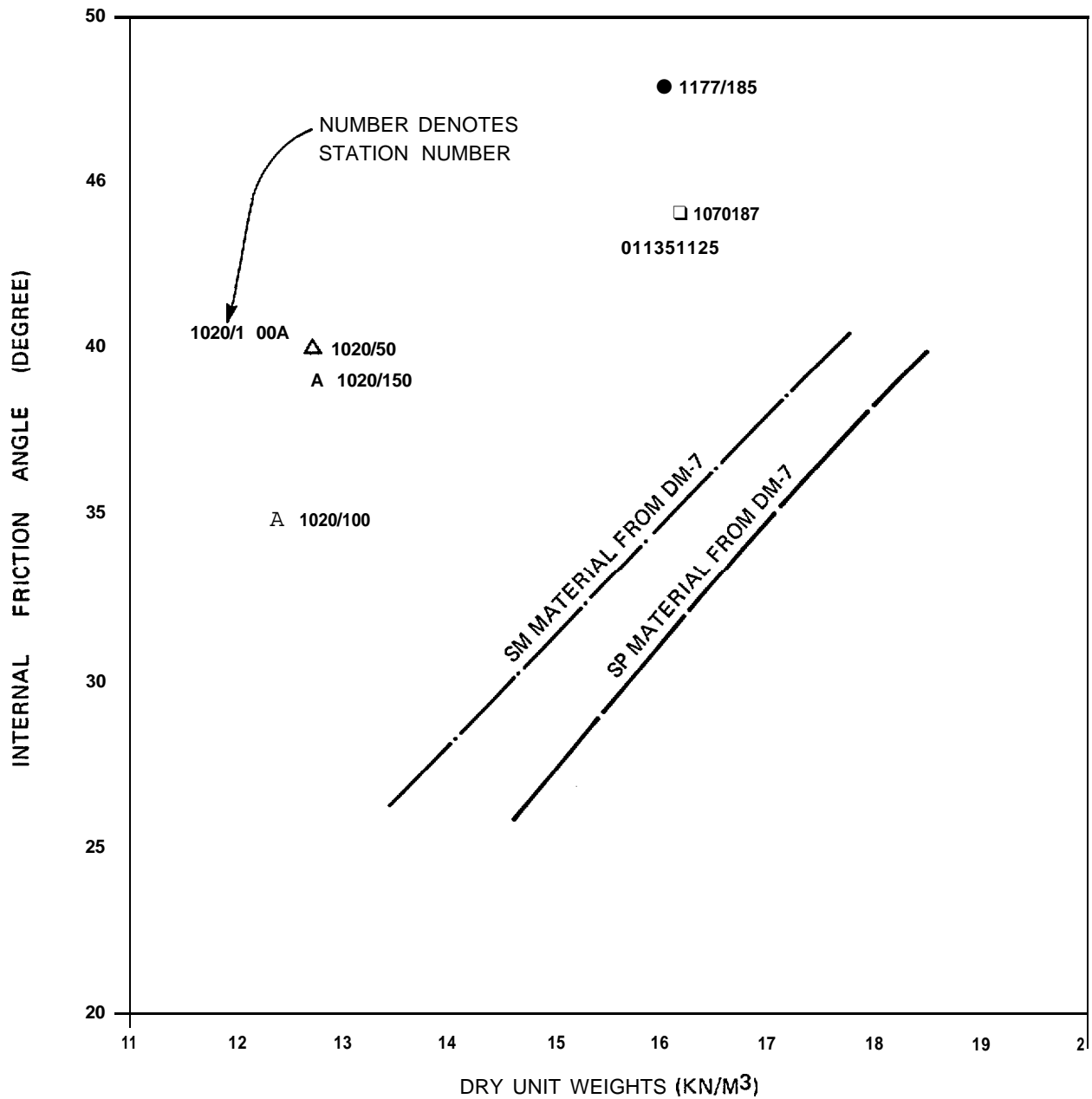
FIGURE 5-19 RANGE OF GRAIN-SIZE CONDITIONS



EXPLANATION

- A** V.V. SUBSAMPLE
- GRAVITY CORE
- VIBRACORE
- A RESULTS OF MAXIMUM/MINIMUM DENSITY

FIGURE 5-20 VARIATION OF DRY UNIT WEIGHT WITH MEAN GRAIN SIZE



NOTES: DATA POINTS ARE BASED ON:

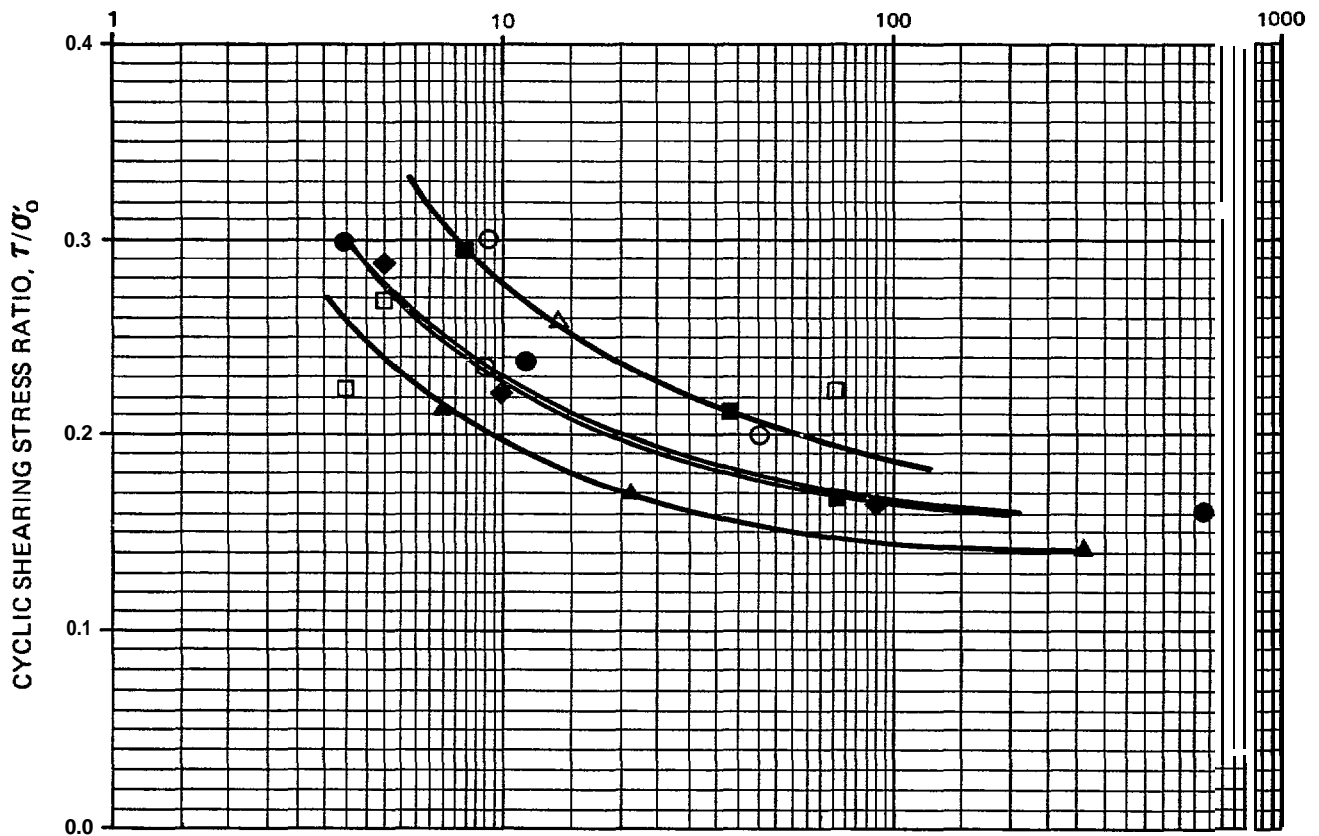
1. MINIMUM INTERNAL FRICTION ANGLE FROM INTERPRETATION OF PENETROMETER DATA
2. DRY UNIT WEIGHT FROM VAN VEEN SUBSAMPLES (TABLE 4-3)

SYMBOLS

- | | |
|---|-------------------------|
| ● | SOIL TYPE 1 – SP (1) |
| ○ | SOIL TYPE 2 – SP (2) |
| • | SOIL TYPE 3 – SP/SM (3) |
| A | SOIL TYPE 4 – SM (4) |

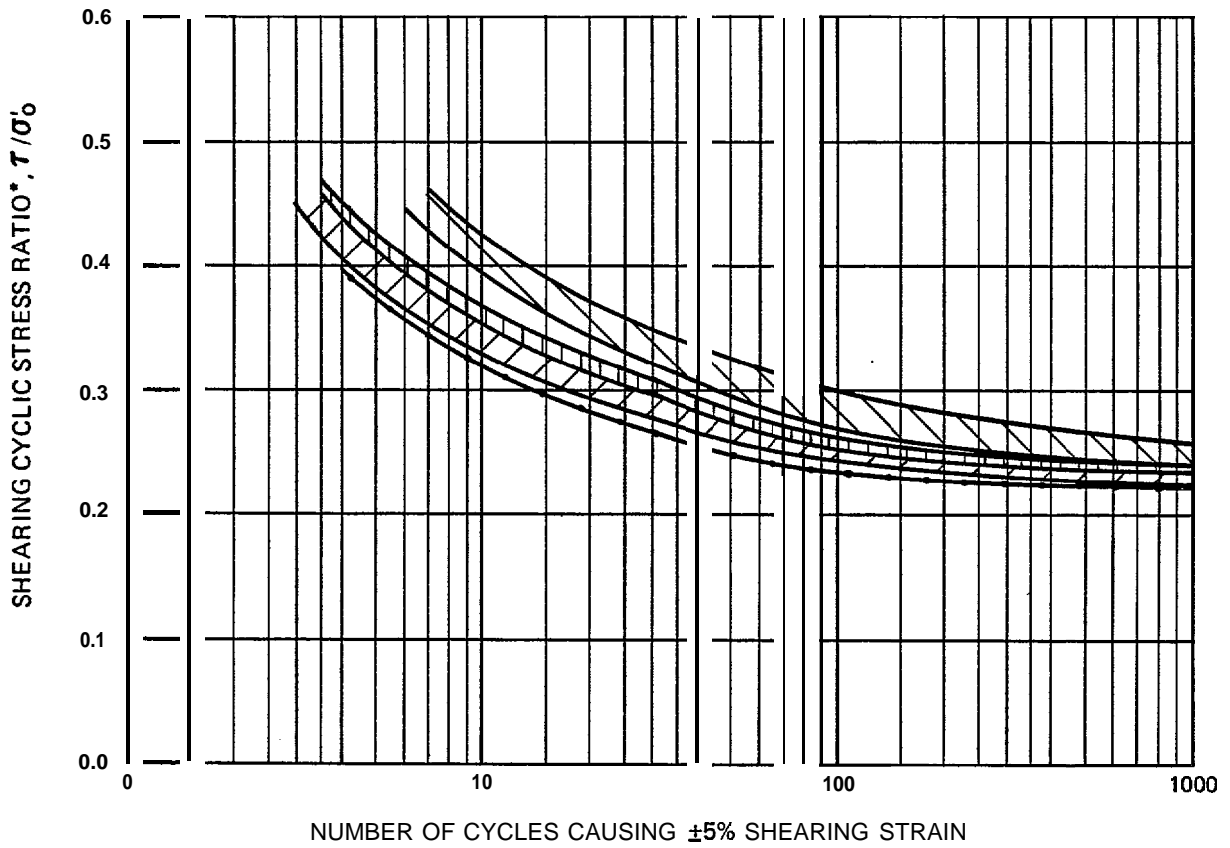
FIGURE 5-21 VARIATION OF FRICTION ANGLE WITH DRY UNIT WEIGHT

NUMBER OF CYCLES TO CAUSE 5% SHEAR STRAIN



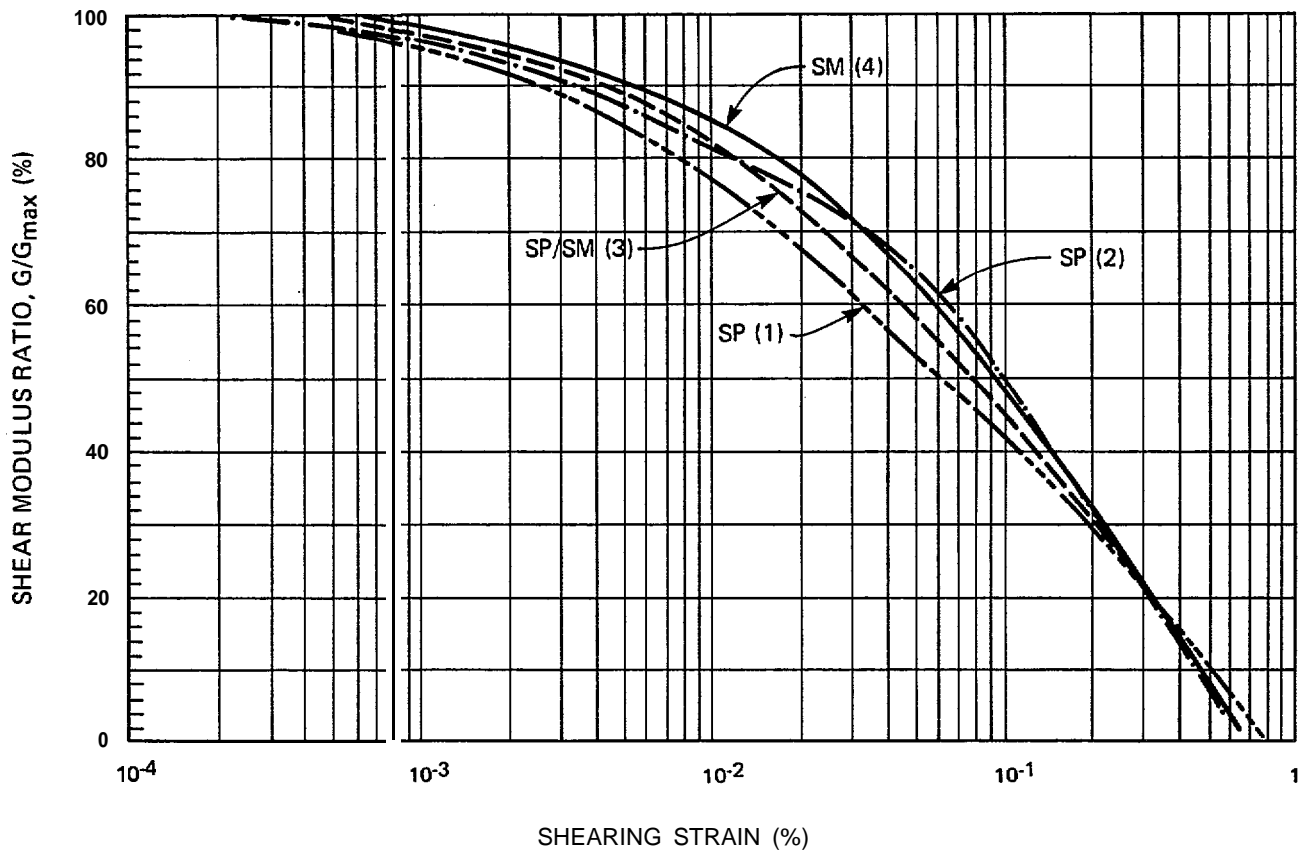
<u>SYMBOL</u>	<u>SAMPLE NO.</u>	<u>SAMPLE TYPE</u>	<u>SOIL TYPE</u>	<u>γ_d KN/M³</u>	<u>WATER CONTENT (%)</u>
□	2	UNDISTURBED	SM-ML	14.4	31
△	11	UNDISTURBED	SM	15.5	28
○	23	UNDISTURBED	SM	14.7	30
●	9	RECONSTITUTED	SM	15.1	30
■	24	RECONSTITUTED	SP-SM	15.7	27
◆	43	RECONSTITUTED	SP	16.3	24
▲	57	RECONSTITUTED	SP	16.1	23

FIGURE 5-22 RESULTS OF CYCLIC SIMPLE SHEAR TESTS



● DEFINED AS RATIO OF CYCLIC SHEARING STRESS (τ) TO INITIAL EFFECTIVE VERTICAL STRESS (σ'_{0})

FIGURE 5-23 ESTIMATED LIQUEFACTION STRENGTH IN THE FIELD



SOIL TYPE	K2
SP (1)	16
SP (2)	15
SP/SM (3)	14
SM (4)	10

J

$$G_{max} = 1000 * K_2 \sqrt{\sigma'_o}$$

WHERE G_{max} = MAXIMUM SHEAR MODULUS (KN/M2)

G = SHEAR MODULUS (KN/M²) AT SPECIFIC SHEARING STRAIN LEVEL

σ'_o = MEAN EFFECTIVE CONFINING STRESS (KN/M²)

FIGURE 5-24 SHEAR MODULUS VALUES USED IN LIQUEFACTION ANALYSES

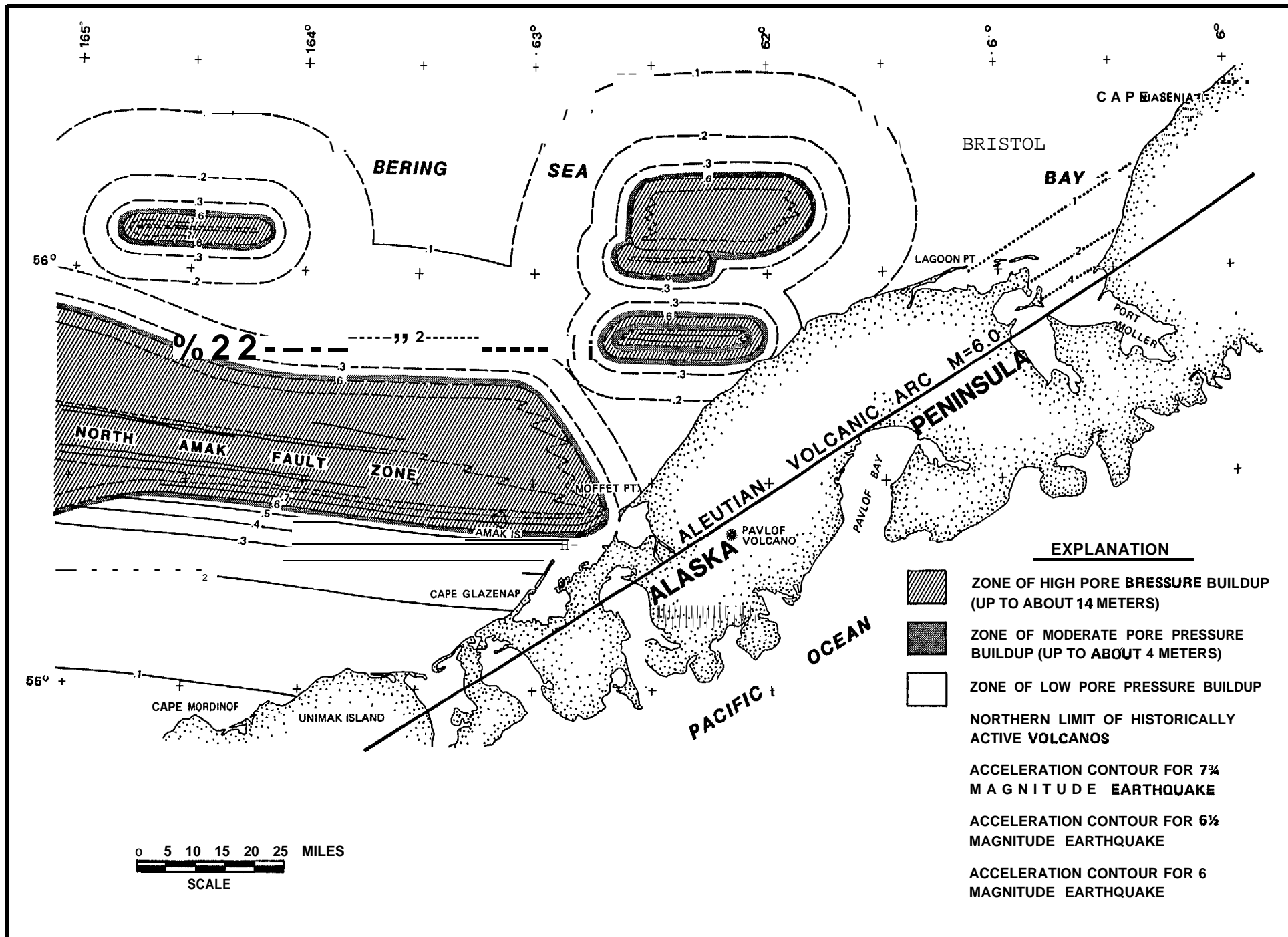


FIGURE 5-25 POTENTIAL FOR EARTHQUAKE-INDUCED PORE PRESSURE BUILDUP

6.0 POTENTIAL GEOLOGIC HAZARDS

6.1 EARTHQUAKES

The study region is in proximity to one of **the** more tectonically active regions of the world with a high rate of seismic activity. The major source **of** large earthquakes is the Alaska-Aleutian subduction zone which has generated several earthquakes in excess of magnitude **8** in historic times. Earthquakes of similar magnitude can be expected in the future and are capable of causing peak ground accelerations of about **0.1g** in the study region.

A less-well known source of possible large earthquakes is the large faults that form the margins of the basins behind (north of) the Aleutian arc such as the North Amak Fault Zone. This fault zone extends westerly through the study region and beyond for a distance of more than 150 km (Plate IV(A)). The largest earthquake possible on this large normal fault zone must be estimated due to the short earthquake records in the area. Empirical data from similar * faults throughout the world suggest that an earthquake of up to magnitude Ms 7 3/4 is plausible for this zone, but that such an event would probably have very long recurrence intervals, and hence, would not be very likely during the time span over which oil exploration and recovery are presently envisaged. If such an earthquake were to occur, peak ground accelerations could reach 0.4 to 0.7g in the vicinity of the fault zone (Figure 5-5).

Moderate-magnitude earthquakes could emanate from other faults within the area. Some of these faults extend upward to near the seafloor and a few even have seafloor expression in the form of **surficial** sags (Plates V(A) and V(B)).

Present data are not of sufficient resolution or density of spacing to completely characterize the nature of these faults; therefore, they are conservatively estimated to be capable of producing magnitude 6 1/2 earthquakes. Still other small faults may exist where geophysical data have not yet been collected. To account for these types of faults, a random earthquake of magnitude 5 1/2 is postulated.

6.2 SURFACE FAULTING

Surface faulting may also be a significant geologic hazard in specific locations. Faults disrupt the seafloor in two areas (Plates VIII(A) and VIII(B)) of the study region and approach the surface to within 150 to 300 m in three other areas (Plates V(A) and V(B)). Engineered facilities in these regions could be subject to vertical fault displacement or tilting of the seafloor and strong earthquake shaking. Data are presently not sufficient to estimate the amount of surface displacement which might be associated with these faults. Empirical fault-displacement/earthquake-magnitude data (Slemmons, 1977) for normal faults indicate that magnitude Ms 7 3/4 earthquakes can generate surface displacements of about 5 to 15 m.

6.3 VOLCANOES

The study area is bounded on the southeast by the volcanically active Aleutian Islands and Alaska Peninsula. Three major potentially active volcanoes are adjacent to the study region: **Shishaldin, Pavlof, and Veniaminoff.** The primary hazard from these volcanoes appears to be ash fall. The controlling factor in ash dispersal is wind direction. In the summer when the prevailing winds are from the south, volcanic ejects could be carried into the site region.

Earthquakes associated with volcanic eruptions are generally less than magnitude 6 and thus ground shaking **would** probably attenuate rapidly enough that peak accelerations would generally be less than about **0.1g** in the study region (Figure S-5). The hazard from volcano-induced earthquakes is, therefore, regarded to be low.

6.4 SOIL INSTABILITY

Geotechnical studies indicate that geologic hazards due to soil **instabil-**ity will generally be related to storm-wave and earthquake loading. Soils appear to be dense or hard, and slopes are relatively flat (less than 0.5 percent); hence, many of the hazards commonly associated with weak sediments or slope instabilities do not exist. This suggests that bearing support for foundations will be acceptable under gravity (or static) loading (no **storm-**waves or earthquakes) as long as normal **geotechnical** design procedures are followed.

Wave-induced soil instabilities may be of potential concern at shallow water locations (e.g., water depths less than 25 m) where, during intense storm waves, bearing support for pipelines or other small, bottom supported structures could decrease or be temporarily lost. Whereas a possibility exists for wave-induced instability in shallow water, the likelihood generally appears to be **low** due to denseness and coarse-particle size of **surficial** sediment.

A more serious wave-induced instability potentially results from sediment scour. The sandy sediments in the study area have a grain-size distribution which is potentially susceptible to scour. Furthermore, maximum bottom currents on the seafloor in the study area are expected to be on the order of

about 100 **cm/sec in** the coastal region and slightly less in deeper water. Higher velocities may also occur **in** proximity to a particular offshore structure because of hydrodynamic interaction effects. Published correlations indicate that these currents are sufficiently high to scour and transport the **surficial** sediment on the shelf.

Earthquake-induced soil instabilities form another potential geologic hazard for the shelf. This hazard was evaluated by conducting laboratory tests to evaluate the cyclic strength of the soil and then using this information to predict analytically the tendency for excess pore-pressure buildup at different locations. Results of these analyses were used to identify three levels of hazard:

- 1) High-potential area where high excess pore-pressure buildup is considered very likely.
- 2) Moderate-potential area where high pore-pressure buildup is possible but is not considered likely.
- 3) Lower-potential area where high pore-pressure buildup is considered very unlikely.

Figure 5-25 identifies areas on the North Aleutian shelf having these rankings.

It should be again noted, that "liquefaction" **resulting in fluid-like** failure is highly improbable for the study area. The term of "liquefaction" utilized in this report refers to the condition of excess pore pressure reaching the **intital** effective overburden value. The results of the earthquake-related seismic analysis also indicate that the potential depth of sediment liquefaction is very shallow (less than 15 m) even in zones of high pore-pressure buildup. In addition, the sediments in the study area are

apparently quite dense. Data from laboratory cyclic simple shear tests indicate that certain limiting strains developed regardless of magnitudes or duration of the applied cyclic shearing stress. The limiting strain capability as well as the gentle slope gradients of the seafloor in the study area lead to the conclusion that seafloor instability in the form of flow slides as a result of strong earthquake shaking is unlikely even in areas of high pore-pressure buildup or liquefaction. However, seismically-induced permanent settlements or subsidence may be possible.

6.5 SHALLOW GAS AND GAS SEEPS

There is no conclusive seismic evidence for the presence of gas seeps within the area. However, at a few locations bowed reflectors and anomalies in reflector intensity suggest the presence of near-surface shallow gas. No hydrocarbons were reported from any sediment sample locations. "Bright spots" and chaotic reflectors indicative of possible hydrocarbon occurrence were observed on deep-penetration seismic-reflection lines. These areas are located west of Amak Island and north of Unimak Island at depths generally greater than 800 m (Plates VA and VB).

Caution will be required in areas exhibiting a potential for shallow gas or gas-saturated sediments. In addition to the possibility of blowouts from shallow **formational** gas, accumulations of gas in sediments may result in low to negligible sediment strengths increasing the potential for soil instability. This hazard is important but not considered critical because of the infrequent occurrence.

6.6 SEDIMENT TRANSPORT

Numerous scours were identified from their distinctive signature on the side-scan sonar and 3.5 kHz data sets (Plates V(A) and V(B)). These results

suggest that significant sediment transport must be anticipated, particularly in shallow water areas. In some case, these scours are incised up to 5 m into the sandy seafloor.

Generally, most scours have asymmetric cross-sections. The scours often occur in groups with some groups containing more than 200 distinct linear scours. Some individual scours have minimum lengths of 800 m, which is the **limit** of the side-scan sonar coverage. The width of individual scours ranges from a few meters to more than 250 m. The orientation of the scour sets varies from parallel to shore to perpendicular to shore. Some areas appears to have been influenced by the transverse longitudinal ridge system that covers the southeastern portion of the shelf. Other areas possess individual sets of intersecting scours, or more intricate sets of scours having sinuous or free-form shapes. Many scours have rippled coarse sand or lag gravel in their troughs.

6.7 OTHER POSSIBLE HAZARDS

From intermediate-penetration seismic data, a probable extension of the Black Hills Uplift is noted on the Geologic Hazards Map (Plates VA and VB). This narrow basement rise ascends abruptly from a depth of approximately 1 km near its western edge to 130 m below the sea bottom within 10 km of the Peninsula. The possible effect of the shallow nature of the uplift should be considered during platform and pile design.

7.0 CONCLUSIONS AND RECOMMENDATIONS

7.1 CONCLUSIONS

Geological hazards on the Northern Aleutian Shelf have been evaluated during **this** study. The area encompassed by the **evaluation** extends from the Alaskan Peninsula and **Unimak** Island on the south to latitude 57° 00' on the north, and between Port **Moller** (159° 30' **W**) and Unimak Pass (165° W) on the east-west boundaries. The evaluation was accomplished by conducting a review of existing literature followed by a field investigation and laboratory studies. The following conclusions were formulated on the basis of information gathered during this evaluation.

Regional Setting.

The regional setting for the area involves

- 1) a very flat continental shelf with maximum water depths less than 110 m and with maximum slopes of less than 0.5 percent;
- 2) a dynamic and complex oceanographic environment with salinities from 31 to 33 ‰, water temperatures from 0.5 to 18° C, 100 year significant wave heights from 17 to 23 m, tides from 2 to 7 m, and current velocities up to 100 cm/sec;
- 3) severe meteorologic conditions where winds approach or exceed 55 knots , where significant accumulations of precipitation occur and where temperatures range +25° C to -25° C
- 4) complex geologic conditions which have evolved from a complex process of subduction, uplift, sedimentation, glaciation and **volcanism and** which presently are strongly influenced by active seismic and volcanic environments.

This regional setting governs the potential for geologic hazards either directly as in the case of seismicity and volcanism, or indirectly such as the effects of storm waves on the stability of a bottom-supported platform or pipeline.

Field Program.

The field program was performed from aboard the NOAA ship Discoverer and involved seismic profiling, sediment sampling and in **situ** testing. Over 4000 km of seismic profile were collected; sediment samples were obtained at 60 stations. From this program it was concluded that

- 1) high quality geophysical data can be obtained using 3.5 kHz, **uniboom**, air gun, sparker and **sidescan** equipment during calm weather periods;
- 2) extreme care must be used during profiling due to the prevalence of crab pots in the survey area;
- 3) **surficial** sediments can be sampled with grab samplers, gravity coring methods and **vibracore**s, but penetration is limited to the upper 1 to 2 m due to the dense sandy characteristics of the soil; and that
- 4) drop penetrometer testing provides an efficient means of obtaining information about **surficial** soil conditions **in situ**, without necessitating elaborate deployment equipment, but as with sediment sampling, the depths of penetration are limited.

Laboratory Program.

Laboratory testing was conducted in shore-based testing facilities. The scope of these tests ranged from geological descriptions through cyclic testing. Results of this program indicated that

- 1) sediments on the shelf are silty sands and sands with mean grain sizes which decrease from 1 to 5 phi (0.5 to 0.0625 mm) as water depth increases, and with poorest sorting in shallow and deep waters;
- 2) the majority of the samples are composed of varying amounts of quartz, feldspar, hypersthene, hornblende and opaque minerals;
- 3) carbon concentrations are low with total organic carbon ranging from 0.3 to 0.5 percent and **CaCO₃** averaging 0.2 percent;
- 4) four general soil types can be delineated from an engineering standpoint with each type being distinguished by decreasing percentages of coarse material and increasing percentages of silts;
- 5) the dry unit weight water content of **surficial** sediments range from 12 to 18 kN/m³ and 10 to 40 percent, respectively;

- 6) apparent specific gravities of sediment particles vary from 2.67 to 2.80;
- 7) maximum and minimum dry unit weights range from 14 to 20 kN/m^3 and 12 to 18 kN/m^3 , respectively;
- 8) compressibility is low with compression indices varying from 0.03 to **0.19** and recompression indices ranging from 0.003 to 0.012;
- 9) materials are relatively permeable with coefficients of permeability ranging from 1×10^{-3} to 5×10^{-5} cm/sec;
- 10) frictional characteristics of the sediments are high with effective friction angles from **isotropically** consolidated-drained **triaxial** tests ranging from 37° to 41° ;
- 11) liquefaction strengths when normalized by the effective vertical stress during cyclic loading are from 0.32 to 0.40 for 10 cycles of loading and from 0.24 to 0.34 for 30 cycles of loading and exhibit low strain potential due to material denseness; and
- 12) low amplitude shear **moduli** vary from $1.1 \times 10^4 \text{ kN/m}^2$ to $1.8 \times 10^5 \text{ kN/m}^2$, damping values range from 2 to 5 percent, and strain effects are similar to those recorded for other sands.

Data Interpretation and Results.

Data gathered during the literature review, field program and laboratory testing were interpreted collectively to develop a regional framework for geological conditions within the study area. The results of this evaluation indicate that

- 1) **bathymetry** is flat with maximum slopes near the coastline of 0.5 percent or less and slopes beyond the 90 m **isobath** equal to 0.02 percent or less;
- 2) three sediment-filled basins (St. George, Amak and Bristol Bay) dominate the geologic structure within the study area;
- 3) complex basement-involved faulting occurs in proximity to the edges of St. George Basin and the Amak Basin and some of these faults are associated with **surficial** sag zones;
- 4) the upper 0 to 20 m of sediment originated in the late Quaternary (Wisconsinan and Holocene) and have an age of 11,000 to 12,000 years **B.P.** at a depth of 1 m;

- 5) The area is seismically active and has a potential for large earthquakes with the most likely sources of strong ground motion being the Alaska-Aleutian subduction zone. A less frequent source of large earthquakes is the major faults bounding the Amak and St. George basins .
- 6) maximum earthquake magnitudes can range from $8 \frac{3}{4}$ for the Aleutian subduction zone down to $5 \frac{1}{2}$ for a random event;
- 7) peak ground accelerations during earthquake loading will likely be equal to **0.1g** for the overall study area and could reach 0.4 to 0.7g on a less frequent basis near the North Amak Fault Zone.
- 8) sediments are sands and silty sands with relative densities near 100 percent and in situ friction angles from drop penetrometer tests of 36° to 50° ;
- 9) **geotechnical** performance of the sediments under gravity loading will be adequate and conventional analytical methods can be used in establishing foundation design methods;
- 10) storm-wave loading may create some engineering concerns in. **shallow-water** depths by scour or wave-induced instability and these concerns should be addressed in site specific design; and that
- 11) **surficial** sediments may "liquefy" during large earthquakes near the major fault zones but consequences will-likely be limited to settlement and inertial loading to the structure.

Potential Geologic Hazards.

Potential geologic hazards on the North Aleutian Shelf which will require special consideration during siting of exploratory and production facilities include:

- 1) earthquakes which can cause ground accelerations of 0.1 to 0.7g depending on the specific location of the facility;
- 2) surface faulting which could result in vertical offsets of 5 to 15 m;
- 3) volcanoes which could inundate a facility with volcanic ejects if prevailing winds are from the south;
- 4) soil instability during storm-wave loading as sediments scour or liquefy under the action of hydrodynamic pressure fluctuations or bottom currents;
- 5) soil instability during earthquake loading as **surficial** sediments (0 to 15 m) in proximity to the earthquake source liquefy;

- 6) shallow gas and gas seeps which may cause blowouts or weakened soil conditions; and
- 7) sediment transport which can either bury, expose or undermine bottom supported structures.

Whereas the potential impact of these hazards is serious, all can generally be handled with existing technology either by relocating the site to avoid the hazard (*faults* or gas seeps) or by designing the facility to withstand the effects of the hazard. For example, the potentially harmful effects of earthquakes can be mitigated by adequate structural and foundation design followed by judicious use of protection systems.

7.2 RECOMMENDATIONS

This geologic hazards assessment was performed to obtain a regional understanding of geologic conditions on the Northern Aleutian **Shelf** which may impact lease development. Results of the study indicate that **certain** geologic hazards exist and must be addressed in any development of the area. It is recommended that these developments be approached on a site-specific basis and that they include as a minimum

- 1) additional oceanographic and meteorologic studies to enhance present understanding of currents, waves and wind conditions **at** a site;
- 2) additional high resolution sub-bottom seismic profiling and side-scan sonar surveying to define surface and near-surface geology in more detail;
- 3) **geotechnical** borings to a depth of 100 m or more for the purpose of obtaining high quality **soil** samples and in situ test data (vane shear or cone penetrometer);
- 4) specialized laboratory testing of high quality samples to establish design parameters for engineering studies;
- 5) further engineering studies to evaluate soil and foundation stability under gravity, storm-wave and earthquake loading conditions; and
- 6) field monitoring of foundation performance to ensure that behavior is consistent with expectation.

8.0 REFERENCES CITED

- Alaska Geological Society, 1975, Composite **stratigraphic** section, Bristol Bay and Alaska Peninsula regions, Alaska: The Alaska Geological Society, 1 sheet.
- American Petroleum Institute (API), 1982, **RP 2A**: Recommended Practice for Planning, Designing, and Constructing Fixed Offshore Platforms, 13th Edition, Dallas, Texas.
- Anderson, D. G., and **Stokoe**, K. H., II, 1978, Shear modulus: A time dependent material property: ASTM Symposium on Dynamic Soil and Rock Testing, Denver, Colorado.
- ATC, 1980, Tentative Provisions for the Development of Seismic Regulations for Buildings: Applied Technology Council, San Francisco, California.
- Armstrong, R. L. , **Harakal**, J. E., and **Hollister**, V. F., 1976, Age determination of late Cenozoic porphyry deposits of the North American **Cordillera**: in Institution of Mining and Metallurgy: Applied Earth Science, **Institution of Mining and Metallurgy Transactions**, Section B. V. 85, p. **B239-B244**.
- Arsen'ev**, V. S., 1967. The currents and water masses of the Bering Sea: (**Transl.** , 1968 National Marine Fisheries Center, Seattle), 146 p.
- Askren, D. R., 1972, Holocene **Stratigraphic** Framework Southern Bering Sea Continental shelf: Master's Thesis, University of Washington, 104 p.
- Baily**, K. A., Cooper, A. K., Marlow, M. S., and Scholl, D. W., 1976, Preliminary residual magnetic map of the eastern Bering Shelf and parts of western Alaska: U.S. Geological Survey, Miscellaneous Field Studies Map **MF-716**.
- Baranov. B. V., and Lobkovskii, L. I., 1980, Shallow seismicity in the **back-arc** of the **Kurile** Island arc and its connection with the **Benioff** zone; **Dokl. Akad. Nauk. USSR**, V. 255, no. 1.
- Beikman, H., 1975, Preliminary geologic map of the Alaska Peninsula and Aleutian Islands: U.S. Geological Survey, Miscellaneous Field Studies Map **MF-674**, 2 sheets.
- Berryhill**, R. V., 1963, Reconnaissance of beach sands, Bristol Bay, Alaska: U.S. Bureau of Mines, Report of Investigations 6214, 48 p.
- Bordovskiy, O. K., 1965, Accumulation and transformation of organic substances in marine sediment: **Marine Geology**, V. 3, p. 3-114.
- Brewer, W. A., Jr., **Sezrby**, H. W., Wise J. L., Davis, H. F., and **Prechtel**, A, s., 1977, Climatic Atlas of the outer continental shelf waters and coastal regions of Alaska: Arctic Environmental Information and Data Center, Anchorage, 443 p.

- Burk, C. A., 1965, Geology of the Alaskan Peninsula Island" Arc and Continental Margin: Geological Society of America, Memoir 99, 250 p.
- Casagrande, A.**, 1976, Liquefaction and cyclic deformation of sands - a critical review: Harvard Soil Mechanics Series No. 88, Harvard University, Cambridge, Mass.
- Castro, G., and **Poulos, S. J.**, 1976, Factors affecting liquefaction and cyclic mobility: Preprint, ASCE Annual Convention and Exposition, Philadelphia, Pennsylvania, Sept 27-Ott 1.
- Clukey, E. C.**, and **Sangrey, D. A.**, 1980, Evaluating submarine slope instability in Alaska: Paper presented at the ASCE Annual Meeting, Hollywood, Florida, October 27-31.
- Cobb, E. H., 1972, Metallic mineral resources of the Cold Bay Quadrangle, Alaska; U.S. Geological Survey, Miscellaneous Field Studies Map **MF-441**, 1 sheet.
- Cooper, A. K., Marlow, M. S., Parker A. W., and **Childs, J. R.**, 1979, Structure-contour map on acoustic basement in the Bering Sea: U. S. Geological Survey, Miscellaneous Field Studies Map **MF-1165**.
- Cooper, A. K., Scholl, D. W., and Marlow, M. S., 1976, Plate tectonic model for the evolution of the eastern Bering Sea Basin: Geological Society of America Bulletin, **V. 87**, p. 1099-1126.
- Curray, J. R., 1965, Late Quaternary history, continental shelves of the United States, in Wright, H. E., and Frey, D. G., (editors). The Quaternary of the United States, Princeton, New Jersey, Princeton University Press, p. 723-735.
- Davies, J. N., 1981, Seismic and volcanic risk in the St. George Basin and adjacent Aleutian arc, in Environmental assessment of the Alaskan Continental shelf: **Combellick, R. E.**, and **Sackinger, W. M.**, eds.,; Fairbanks and Juneau, Alaska, U.S. Dept. of Commerce, NOAA, ocs Environmental Assessment Prog., Chap. 3.
- DM-7**, 1971, Design Manual for Soil Mechanics, Foundations and Earth Structures, U. S. Navy, Bureau of Yards and Docks.
- Dodimead, A. J., Favorite, F. and Hirano, T., 1963, Salmon of the North Pacific Ocean, Part II. Review of oceanography of the subarctic Pacific Region: International North Pacific Fisheries Committee, Bulletin No. 13, p. 1-11 and 177-187.
- Duncan, J. M., and **Chang, Y.**, 1970, Non linear analysis of stress and strain in soils: ASCE Journal, Soil Mechanics and Foundation Engineering Division, V. 96, No. SM5.

- Durgunglu H., and Mitchell, J. K., 1975, Static penetration resistance of soils. I-Analysis, II-Evaluation of Theory and Implications for Practices: In Proceedings, In Situ Measurement of Soil Properties, V. I, Raleigh, North Carolina.
- Emery, K. O., 1938, Rapid method of mechanical analysis of sands: *Journal of Sedimentary Petrology*, V. 8, p. 105-11.
- Favorite, F., Ahantz, J. W., and Hebard, C. P., 1961, **Oceanographic** Observations in Bristol Bay and the Bering Sea 1939-1941 (**USCGT Redwing**): U. S. Fish and Wildlife Service, Special Scientific Report - Fisheries, No. 381.
- Felix, F., 1969, Origin and recent history of Newport submarine canyon, California Continental Borderland: Office of Naval Research, Geophysics Branch, Tech. Report **NR083-144**, 52 p.
- Finn, W. D. Lian, Siddharthan, R., and Martin, G. R., 1980, **Wave-induced** instability in ocean floor sands, Preprint, ASCE Convention and Exposition, Miami, Florida.
- Folk, R. L., 1980, *Petrology of Sedimentary Rocks*: **Hemphill Publishing**, Austin, Texas, p. 41-45.
- Folk, R. L., 1974, *Petrology of Sedimentary Rocks*: **Hemphill Publishing**, Austin, Texas, 182 p.
- Folk, R. L., and Ward, W. C., 1957, Brazes river bar - a study in the significance of grain-size parameters: *Journal of Sedimentary Petrology*, V. 27, p. 3-26.
- Gardner, J. V., Vallier, T. L., Dean, W. E., Kvenvolden, K. A., and Redden, G. D., 1979, **Sedimentology** and geochemistry of surface sediments and the distribution of faults and potentially unstable sediments, St. George Basin region of the outer continental shelf, southern Bering Sea: U. S. Geological Survey, Open File Report 79-1562, 88 p.
- Gershanovich, D. E., 1968, New data on **geomorphology** and recent sediments of the Bering Sea and the Gulf of Alaska: *Marine Geology*, V. 6, p. 281-296.
- Gibbs, R. J., 1974, A settling tube system for sand-size analysis, *Journal Sedimentary Petrology*, V. 44, p. 583-588.
- Gibbs, R. J., Mathews, M. D., and Lindk, D. A., 1971, The relationship between sphere size and settling velocity, *Journal Sedimentary Petrology*, V. 41, p. 7-18.
- Grow, J. A., and Atwater, T. A., 1970, Mid-Tertiary tectonic transition in the Aleutian Arc: *Geological Society of America Bulletin*, V. 81, p. 3715-3722.
- Hand, B. M., 1964, Hydrodynamics of beach and dune sedimentation (**Ph.D Thesis**): Pennsylvania State University, University park, Pennsylvania, 163 p.

- Hebard, J. F., 1961, Currents in the southeastern Bering Sea: International North Pacific Fisheries Committee, Bulletin No. 5, p. 9-15.
- Hebard, J. F., 1959, Currents in the southeastern Bering Sea and possible effects upon King Crab Larvae: U. S. Fish and Wildlife Service, Special Scientific Report - Fisheries, No. 293.
- Hsui, A. T., and Toksoz, M. N., 1981, Back-arc spreading: trench migration, continental pull or induced convection?: Tectonophysics, V. 74, p. 89-98.
- Hunter, R. E. **Sallenger**, A. H., and **Dupre'**, W. R., 1979, Maps showing directions of longshore sediment transport along the Alaska Bering Sea Coast: U.S. Geological Survey, Miscellaneous **Field** Investigations Map, MF-1049.
- Inman**, D. L., 1949, Sorting of sediments in the light of fluid mechanics: Journal of Sedimentary Petrology, V. 19, p. 51-70.
- Jennings, P. C., Housner, G. W., and Tsai, N. C., 1968, Simulated earthquake motions, Earthquake Engineering Research Laboratory Report, California Institute of Technology, April.
- Katili**, J. A., and Soetadi, 1971, Neotectonics and seismic zones of **Indonesia**: Proceedings of Royal Society of New Zealand.
- Kemp, A. L. W., 1971, Organic carbon and nitrogen in the surface sediments of Lake Ontario, **Erie, and Huron**: Journal of Sedimentary Petrology, V. 41, p. 537-548.
- Kennedy, G. C., and **Waldron**, H. H., 1955, Geology of **Pavlof** Volcano and vicinity, Alaska: U.S. Geological Survey Bulletin, 1028-A, p. 1-19.
- Kinder, T. H., 1977, The hydrographic structure over the continental shelf near Bristol Bay, Alaska, June 1976: Department of Oceanography of Washington Technical Report, **Ref-** M77-3, 61 p.
- Kinder, T. H., and Schumacher, J. D., 1980, Hydrographic structure over the continental shelf of the southeastern Bering Sea, **in** Coachman, L. K., and Tripp, R. B., (editors), Fifth annual report Bristol Bay Oceanographic Processes: Pacific Marine Environmental Lab., Environmental Research Laboratory, NOAA, p. 25-79.
- Kolpack**, R. L., and Bell, S. A., 1968, Gasometric determination of carbon in sediments by hydroxide absorption, Journal Sedimentary Petrology, V. 38, No. 2, p. 617-620.
- Komar**, P. D., 1976, Beach Processes and Sedimentation: Prentice-Hall Inc., Englewood Cliffs, New Jersey, 429 p.
- Kuenen, P. H., 1950, Marine Geology, New York, **Wiley**.
- Lamb, Horace, 1879, Hydrodynamics: Dover Publications, New York, p. 367., 1945.

D

- Lee, R. L., and **Chan, K.**, 1972, Number of equivalent significant cycles in strong motion earthquakes: Proceedings, International Conference on **Microzonation**, Seattle, Washington, October.
- Lee, M. K. W., and Finn, W. D., **Liam**, 1977, **DESRA**, program for the dynamic effective stress response analysis for soil deposits: **Soil Mechanics** Series No. 36, Dept. of Civil Engineering, University of British Columbia, Vancouver, B. C. Canada.
- Lisitzin, A. P.**, 1972, Sedimentation in the **world** oceans: Society of Economic Paleontologists and Mineralogists Special Publication No. 17, p. 77.
- _____, 1966, Recent sedimentation in the Bering Sea (in Russian); Inst. **Okenol. Akac. Nauk U.S.S.R.**, (translated by Israel Program for Scientific Translation), from U.S. Department of Commerce, Clearinghouse for **Federal Scientific and Technologic** Information, 614 p.
- Liu, P. L. F., Timothy, P., and O'Donnell, R., 1979, Wave-induced forces on buried pipelines in permeable seabeds: proceedings, 4th Conference on Civil Engineering in the Ocean, San Francisco, California.
- Marlow, M. W.**, and Cooper, A. K., 1980a, Mesozoic and Cenozoic structural trends beneath the southern Bering Sea shelf: American Association Petroleum Geologists Bulletin, **V. 64**, p. 2139-2155.
- Marlow, M. S.**, and Cooper, A. K., 1980b, Multichannel seismic-reflection profiles collected in 1976 in the southern Bering Sea shelf: U.S. **Geological** Survey, Open File Report OF 80-389.
- Marlow, M. S.**, McLean, Hugh, Cooper, A. K., **Vallier, T. L.**, Gardner, **J. V.**, **McMullin, R.**, and Lynch, M. B., 1980; A preliminary summary of Regional Geology, Petroleum Potential, Environmental Geology, and Technology for Exploration and Development for proposed OCS Lease Sale No. 7, Northern Aleutian Shelf, Bering Sea, Alaska: U.S. Geological Survey, Open File Report, OF 80-653, 53 p.
- Marlow, M. S.**, Gardner, **J. V.**, **Vallier, T. L.** McLean H., Scott, E. W., and Lynch, M. B., 1979, Resource report for proposed OCS Lease Scale No. 70, St. George Basin, Shelf Area, Alaska: U.S. Geological Survey, Open File Report OF 79-1650, 79 p.
- Marlow, M. S., McLean H., **Vallier, T. L.**, **School, D. W.**, Gardner, **J. V.**, and Powers, R., 1976a, Preliminary report on the regional geology, oil and gas potential and environmental hazards of the Bering Sea shelf south of St. Lawrence, Island, Alaska: U. S. Geological Survey Open File Report OF 76-785, 98 p.
- Marlow, M. S., Scholl, D. W., Cooper, A. K., and Buffington, E. C., 1976b, Structure and evolution of Bering Sea shelf south of St. Lawrence Island: American Association of Petroleum Geologists Bulletin, **V. 60**, No. 2, 161-183.

- Martin, G. R., Finn, W. D. L., and Seed, H. B., 1975, Fundamentals of liquefaction under cyclic loading, Journal of **Geotechnical Engineering** Division, ASCE, **Vol.** 101, NO. GT5, pp. 423-438.
- Martin G. R., Finn, **Liam**, W. D., and Seed, H. B., 1976, Fundamentals of liquefaction under cyclic loading, ASCE Journal, **Geotechnical Engineering** Division, V. 101, No. GT5.
- McGeary**, S. E., and **Ben-Avraham**, Z., 1981, **Allochthonous terranes** in Alaska: Implications for the structure and evolution of the Bering Sea shelf: *Geology*, v. 9, p. 608-614.
- McIntyre, D. D., 1969, The hydraulic equivalence and size distribution of some mineral grains from a beach, *Journal of Geology*, V. 67, p. 278-301.
- McLean, H. 1979, Observations on the geology and petroleum potential of the Cold Bay-False Pass Area, Alaska Peninsula: U.S. Geological Survey Open File Report OF 79-1605.
- _____, 1977, Organic geochemistry, **lithology** and paleontology of Tertiary and Mesozoic rocks from wells on the Alaska Peninsula: U.S. Geological Survey, Open File Report OF 77-813, 62 p.
- McLean, **H.**, **Englehardt**, C. L., and **Howell**, D. G., 1978, Reconnaissance **map of** the Cold Bay and False Pass quadrangles, Alaska: U.S. Geological Survey, Open File Report OF 78-813, 62 p.
- Minerals Management Service (**MMS**), 1982, St. George Basin final environmental impact statement: U.S. Dept. Interior.
- Molnia**, B. F., Schwab, W. C., Austin, W. A., and Hoose, **p. J.**, 1982, **Map of** potential geologic hazards on North Aleutian Shelf (Lease Scale 92), U.S. Geological Survey, Open File Report OF 82- in press.
- Moore, D. G., 1972, Reflection profiling studies of the California Continental Borderland: Structure and Quaternary Turbidite Basins: Geological Society of America, Special paper 197, 142 p.
- Mori**, A. W., and **Crouse**, C. B., 1981, Strong motion data from Japanese earthquakes: World Data Center A for Solid Geophysics, Report SE-29, NOAA, December.
- Nakamura**, K., Jacob, K., **Daives**, J., 1977, Volcanoes as possible indicators Or tectonic stress orientations - **Aleutians** and Alaska, **in** **Island Arcs, Deep Sea Trenches and Back-Arc Basins**; American **Geophysical** Union, Maurice Ewing Series V. 1, p. 1-14.
- Nelson, C. H., Hopkins, D. M., and School, D. W., 1974, Cenozoic Sedimentary and Tectonic History of the Bering Sea: **in** Hood, D. W., and **Kelly**, B. J., (**eds.**),
- Ohtani, K., 1973, Oceanographic structure in the Bering **Sea**: Memoirs of the Faculty of Fisheries, **Hokkaido** University, V. 21, p. 65-106.

- Pearson, C. A. **Mofjeld**, H. O., and Tripp, R. B., 1981, Tides of the Eastern Bering Sea Shelf: in Hood, D. W. and **Calder**, J. A., eds., **The Eastern Bering Sea Shelf: Oceanography and Resources**: Office of Marine Pollution Assessment of the National Oceanic and Atmospheric Administration, V. 1, p. 111-130.
- Quayle**, R. G., and **Fulbright**, D. C., 1975, Extreme wind and wave return periods for the U.S. Coast: *Mariner's Weather Log*, V. **19**, p. 67-70.
- Reed, W. E., LeFever, R., and Moir, G. 1976, Depositional environment interpretations using settling velocity (Psi) distribution, *Geological Society of America Bulletin*, V. 87, No. 5.
- Sanford, R. B., and Swift, D. J., 1971, Comparison of sieving and settling techniques for size analysis using a **Benthos** Rapid Sediment Analyzer: *Sedimentology*, V. 17, p. 257-264.
- Schell**, B. A., **1982**, **Distribution** and style of faults in the Great Basin and their relationship to the magnitude and frequency of earthquakes: American Geophysical Union, Chapman Conference, Snowbird, Utah.
- Schell**, B. A., **Farley**, T., and Muir, S. G., 1981, Fault rupture and earthquake hazards in east-central Nevada and west central Utah: Association of Engineering Geologists, Meeting Program with Abstracts, p. 52.
- Schlee**, J., 1966, A modified Woods Hole Rapid Sediment Analyzer: *Journal of Sedimentary Petrology*, V. 36, p. 403-413.
- Scholl, D. W., Buffington, E. C., and Hopkins, D. M., **1966**, Exposure of basement rock on the continental slope of the Bering Sea: *Science*, v. **153.**, p. 992-994.
- Schumacher, J. D., Kinder, **T.H.** Pashinski, D.J., and **Charnell**, R. L., **1979**, A - structural front over the continental shelf of the eastern Bering Sea: *Journal Physical Oceanography*, V. 9, p. 79-87.
- Scott**, R. S., 1967, In-place measurement of the strength of ocean floor **soils** by accelerometer: *Proceedings, Civil Engineering in the Oceans*, ASCE Conference, San Francisco, California, p. 419-444.
- Seed, H. B., **1976**, **Evaluation** of soil liquefaction effects on level ground during earthquakes: *Preprints, ASCE Annual Convention and Exposition*, Philadelphia, PA.
- Seed, H. B., Lee, K. L., and **Idriss**, I. M., 1969, An analysis of the Sheffield Dam failure: *ASCE Journal, Soil Mechanics and Foundation Division*, V. 95, No. SM6.
- Seed, H. B., and **Rahman**, M. S., 1977, Analysis for wave-induced liquefaction in relation to ocean floor stability: Report No. **UCB/TE 77/02**, Department of Civil Engineering, Institute of Transportation and Traffic Engineering, University of California at Berkeley.

- Seed, H. B., and Idriss, I. M., 1971, Simplified procedures for evaluating soil liquefaction potential: ASCE Journal, Soil Mechanics and Foundation Division, V. 93, No. SM3.
- Sengupta, S., and Veenstra, H. J., 1968, On sieving and settling techniques for sand analysis: **Sedimentology**, V. 11, p. 83-98.
- Sharma**, G. D., 1979, The Alaska Shelf: Springer-Verlag, New York, 498 p.
- Sharma**, G. D., 1975, Contemporary epicontinental sedimentation and shelf grading in the southeast Bering Sea: in Forbes, R. B., (editor), Contributions to the Geology of the **Bering** Sea Basin and Adjacent Regions; Geologic Society of America, Special Paper 151, p. 33-48.
- Sharma**, G. D., 1974, Contemporary deposition environmental of the eastern Bering Sea: in Hood, D. W., and Kelly, E. J. (editors), Oceanography of the Bering Sea, p. 517-552.
- Sharma**, G. D., **Naidu**, A. S., and Hood, D. W., 1972, Bristol Bay: A model of a contemporary graded **shelf**, American Association of Petroleum Geologists. Bulletin, V. 56, p. 2000-2012.
- Slemmons**, D. B., 1977, State-of-the-art for assessing earthquake hazards in the United States, Report 6: Faults and Experiment Station Miscellaneous Paper S-73-1.
- Spence, W., 1977, The Aleutian arc: Tectonic blocks, episodic subduction, strain diffusion, and magma generation: Journal of Geophysical Research, V. 82, p. 213-230.
- Takenouti, A. Y., and Ohtani, K., 1974, Currents and water masses in the Bering Sea: A review of Japanese Work, in Hood, D. W., and **Kelley**, E. J. (editors), Oceanography of the Bering **Sea**, Institute of Marine Science, University of Alaska Occasional Publication 2, p. 39-57.
- Thorn, E. C., 1973, Extreme wave height distributions over oceans: **ASCE** Journal, Waterways, Harbors and Coastal Engineering Division, V. 99, p. 355-374.
- Trask, P. D., 1932, Origin and environment of source beds of petroleum: Gulf Publishing Company, Houston, 323 p.
- U.S. Army, Corps of Engineers, 1974, The Bristol Bay environment, A background study of available knowledge: Arctic Environmental Information and Data Center, University of Alaska, Anchorage, 858 p.
- U.S. Department of Commerce, 1979, Coastal **Pilot** #9, Pacific and Arctic Coasts, U.S. Department of Commerce, National Oceanic and Atmospheric Administration, National Ocean Survey, Washington, D. C.
- USGS, 1976, Seismic engineering data report: strong-motion earthquake **accelerograms**, digitization and analysis, 1971 records: Open File Report No. 76-609, **July**.

- USGS, 1978 Seismic engineering data report: strong-motion earth records:
Open File Report No. 78-941, October.
- Uyeda, S. 1977, Some basic problems in the trench-arc-back-arc system, in
Island Arcs, Deep Sea Trenches and Back-Arc Basins: American Geophysical
Union, Maurice Ewing Series, V. 1, p. 1-14.
- Uyeda, S., Kanomori, H., 1979, Back-arc opening and the moe of subduction:
Journal of Geophysical Research, V. 84, p. 1049-1061.
- Von Huene, R. and Shor, G. G., 1969, The structure and tectonic history of the
eastern Aleutian Trench: Geologic Society of America Bulletin, V. 80, p.
1889-1902.
- Waldron, H. H., 1961, Geologic reconnaissance of Frosty Peak Volcano and
vicinity, U.S. Geological Survey Bulletin, 1028-T, p. 677-708.
- Wallace, R. E., 1977, Profiles and ages of young **fault** scarps, north-central
Nevada: Geological Society of America Bulletin, V. 88, p. 1267-1281.
- Wilcox, R. E., 1959, Some effects of recent volcanic ash falls with special
reference to Alaska: U.S. Geological Survey Bulletin, 1028-N, p.
409-476.
- Wilson, F. H., 1981, Map and table showing **radiometric** ages of rocks in the
Alaska Peninsula: U.S. Geological Survey Open-File Report **OF81-471**, 23 p.
- Zonenshain, L. P., and Savostin, L. A., 1981, Movement of **lithospheric** plates
relative to subduction zones: formation of marginal seas and active
continental margins: **Tectonophysics**, V. 74, p. 57-87.

APPENDIX I

SAMPLE LOCATIONS AND GRAIN-SIZE
DISTRIBUTIONS

1.0 DEFINITIONS

Most of the grain size data for sediments obtained during the field program are reported in phi (ϕ) units. The equivalence between phi units and mean grain diameter is shown below.

Millimeters	Phi (ϕ)	Wentworth Size Class
2.4 - 2.0	-1.0	Granule
2.0 - 1.0	0.0	Very coarse <u>sand</u>
1.0 - 0.50	1.0	Medium <u>sand</u>
0.50 - 0.25	2.0	Fine <u>sand</u>
0.25 - 0.125	3.0	Very fine <u>sand</u>
0.125 - 0.0625	4.0	Coarse <u>silt</u>
0.0625 - 0.031	5.0	Medium <u>silt</u>
0.031 - 0.0156	6.0	Fine <u>silt</u>
0.0156 - 0.0078	7.0	Very fine <u>silt</u>
0.0078 - 0.0039	8.0	Coarse <u>clay</u>
0.0039 - 0.0020	9.0	Medium <u>clay</u>
0.0020 - 0.00098	10.0	Fine <u>clay</u>

Results of sediment analyses are also reported in terms of mean grain size, standard deviation, skewness, and **kurtosis**. These statistical parameters are described by Folk and Ward (1957) in the following manner:

1) Mean Grain Size:

The mean grain size is a measure of the average value of grain diameter as described by the following formula

$$M = \frac{\phi_{16} + \phi_{50} + \phi_{84}}{3}$$

where ϕ indicates a ϕ percentile.

2) Standard Deviation:

The standard deviation is a measure of sediment sorting with 68 percent of the distribution lying within + 1 standard deviation of the mean.

3) Skewness and Kurtosis:

Skewness and kurtosis tell how closely the grain size distribution approaches the normal Gaussian probability curve. Skewness defines the asymmetry of a grain size distribution and is determined from the following formula

$$SK = \frac{\phi_{16} + \phi_{84} - 2\phi_{50}}{2(\phi_{84} - \phi_{16})} + \frac{\phi_5 + \phi_{95} - 2\phi_{50}}{2(\phi_{95} - \phi_5)}$$

where ϕ indicates a ϕ percentile. Kurtosis defines the degree of peakedness of sediment size distribution and is determined from the following formula

$$K = \frac{\phi_{95} - \phi_5}{2.44 (\phi_{75} - \phi_{25})^2}$$

where ϕ indicates a ϕ percentile.

Table I-1. Sample Data

Sample ⁽¹⁾ Station		Sediment Parameters (Folk and Ward)										
Number	Number	Latitude(N)	Longitude(W)	Depth(m)	%			Standard		Skewness	Kurtosis	
					sand	silt	clay	Mean(\$)	Deviation(\$)			
1	1000/200	56° 29.9'	164° 59.3'	82	62	36	2	3.75	1.46	0.54	1.20	
2	1000/150	56° 03.5'	164° 59.6'	93	76	22	2	3.47	1.37	0.41	1.61	
3	1030/200	56" 31.0'	164° 30.0'	82	63	34	3	3.77	1.21	0.55	1.00	
4	1040/200	56° 30.4'	164° 16.7'	82	74	24	2	3.57	1.16	0.51	1.14	
5	1030/150	56° 03.0'	164° 31.0'	93	78	10	2	3.37	1.12	0.25	1.74	
6	1011/125	55° 50.2'	164° 48.4'	95	74	24	2	3.53	1.31	0.38	1.71	
7	1035/111	55° 42.8'	164° 26.5'	95	89	9	2	2.93	0.93	0.42	1.97	
8	1030/107	55° 41.0'	164° 31.0'	95	90	8	2	2.90	0.77	0.21	1.81	
9	1020/100	55° 36.4'	164° 40.2'	100	83	14	3	2.16	0.38	-0.17	1.07	
10	1030/75	55° 23.0'	164° 31.0'	100	85	14	1	2.32	1.46	0.37	1.64	
11	1020/50	55° 09.6'	164° 41.4'	99	83	15	2	3.03	1.15	0.20	3.03	
12	1020/25	54" 56.5'	164" 41.0'	60	99	1	0	0.35	0.57	0.31	0.96	
13	1079/200	56° 30.0'	163" 42.0'	82	--	.-		----	----	----	----	
14	1105/175	56° 16.0'	163° 18.0'	89	96	4	0	2.92	0.44	-0.35	1.14	
15	1060/150	56° 03.0'	164° 02.0'	92	87	11	2	3.00	0.81	0.12	1.56	
16	1079/150	56° 03.0'	164° 43.0'	93	83	16	1	3.13	1.04	0.40	1.66	
17	1060/125	55° 49.6'	164° 02.2'	94	88	10	2	3.05	0.85	0.32	2.25	
18	1090/125	55° 50.0'	163° 33.0'	94	94	4	2	2.75	0.62	-0.03	1.84	
19	1105/125	55° 49.0'	163° 19.0'	90	96	4	0	2.72	0.46	-0.06	1.08	
20	1110/111	55° 42.2'	163° 14.8'	83	97	3	0	2.55	0.44	-0.55	1.16	
21	1090/100	55" 35.0'	163° 35.0'	83	99	1	0	2.35	0.54	0.27	0.98	
22	1060/98	55° 35.1'	164° 03.0'	98	91	7	2	2.87	0.88	-0.10	1.59	
23	1051/87	55° 29.2'	164° 11.1'	97	96	4	0	2.19	0.65	-0.21	0.77	
24	1070/91	55" 31.9'	163° 53.9'	84	97	3	0	2.28	0.67	-0.28	1.11	
25	1079/90	55° 30.9'	163" 44.1'	84	98	2	0	2.42	0.53	-0.29	0.86	
26	1070/87	55° 29.4'	163° 52.2'	89	94	4	2	2.40	0.64	-0.37	1.07	
27	1090/50	55° 09.0'	163° 35.0'	39	98	2	0	1.64	0.37	-0.08	0.98	
28	1105/75	55° 22.4'	163° 20.3'	51	94	4	2	3.00	0.56	-0.17	1.39	
29	1120/200	56° 30.1'	163° 02.3'	81	95	5	0	2.88	0.33	0.03	1.19	
30	1150/200	56° 29.1'	162° 33.5'	81	99	1	0	2.43	0.33	-0.16	1.00	
31	1135/174	56" 15.0'	162° 49.7'	80	99	1	0	2.53	0.40	-0.10	1.42	
32	1135/175	56° 15.0'	162° 49.7'	80	99	1	0	2.74	0.46	0.04	1.23	
33	1135/176	56° 15.0'	162" 49.7'	80	99	1	0	2.62	0.30	-0.24	1.00	

NOTES: (1) Samples 1 through 60 are from this study; samples 61 through 120 are from previous studies.

Table I-1. Sample Data (Continued)

Sample ⁽¹⁾ Number	Station Number	Latitude(N)	Longitude(W)	Depth(m)	Sediment Parameters (Folk and War-d)							
					% sand	% silt	% clay	Mean(\$)	Standard Deviation(\$)	Skewness	Kurtosis	
34	1120/150	56° 03.1'	163° 04.5'	86	98	2	0	2.65	0.36	-0.20	1.43	
35	1135/125	55" 49.3'	162° 50.0'	80	99	1	0	2.05	0.81	0.11	0.70	
36	1128/108	55° 40.0'	162° 58.7'	62	99	1	0	0.56	0.82	0.21	0.97	
37	1120/100	55° 36.0'	163° 06.0'	62	99	1	0	2.16	0.38	-0.17	1.07	
38	1150/100	55° 35.5'	162° 37.9'	40	99	1	0	2.13	0.37	-0.71	1.02	
39	1120/75	55° 20.8'	163" 07.9'	36	98	2	0	0.68	0.62	0.50	1.09	
40	1165/125	55" 48.4'	162" 22.3'	46	99	1	0	0.69	0.60	-0.06	0.89	
41	1150/150	56" 01.9'	162° 35.3'	77	99	1	0	2.48	0.36	0.12	1.33	
42	1165/175	56° 15.0'	162° 20.7'	82	99	1	0	2.20	0.47	-0.12	1.08	
43	1177/185	56° 08.2'	162° 09.7'	80	99	1	0	1.67	0.64	-0.10	1.03	
44	1180/150	56° 01.2'	162° 06.4'	72	99	1	0	1.90	0.73	-0.26	2.08	
45	1180/200	56° 28.0'	162° 05.1'	72	99	1	0	2.28	0.48	-0.11	1.13	
46	1202/200	56° 28.9'	161° 50.7'	81	96	4	0	2.18	0.47	-0.27	2.10	
47	1203/200	56° 28.9'	161° 48.1'	93	98	2	0	2.27	0.39	-0.34	1.38	
48	1204/200	56° 28.9'	161° 42.8'	91	98	2	0	2.40	0.36	-0.26	1.17	
49	1225/200	56° 29.3'	161" 25.8'	75	99	1	0	2.15	0.33	-0.16	1.23	
50	1195/175	56° 14.0'	161° 51.4'	72	99	1	0	2.13	0.40	-0.28	1.01	
51	1210/150	56" 02.0'	161" 37.9'	40	99	1	0	1.95	0.49	0.09	1.48	
52	1255/200	56° 29.7'	160° 57.8'	68	99	1	0	2.15	0.33	-0.16	1.23	
53	1240/175	56° 15.8'	161° 09.6'	52	100	0	0	1.96	0.75	-0.50	1.01	
54	1255/158	56° 06.9'	160° 55.8'	33	99	1	0	1.45	0.64	0.18	0.77	
55	1285/200	56" 30.4'	160° 27.6'	44	100	0	0	0.90	0.89	0.04	1.16	
56	1270/193	56° 27.5'	160° 42.0'	55	99	1	0	3.02	0.48	-0.10	0.95	
57	1262/185	56° 22.5'	160° 49.5'	49	100	0	0	1.76	0.56	-0.44	1.46	
58	1270/175	56° 17.0'	160° 42.0'	33	99	1	0	2.18	0.47	-0.47	2.56	
59	1285/181	56" 22.2'	160 ⁴ 26.1'	34	99	1	0	0.06	0.29	0.55	2.34	
60	1285/177	56° 17.5'	160° 28.0'	22	100	0	0	1.57	0.76	-0.65	2.46	

NOTES: (1) Samples 1 through 60 are from this study; samples 61 through 120 are from previous studies.

Table I-1. Sample Data (Continued)

Sample ⁽¹⁾ Station		Sediment Parameters (Folk) and Ward)									
Number	Number	Latitude(N)	Longitude(W)	Depth(m)	% sand	% silt	% clay	Mean(\$)	Standard Deviation(ϕ)	Skewness	Kurtosis
61	146	56° 40.3'	165° 22,9'	77	47.0	47.0	6.0	4.431	1.868	0.135	1.615
62	149	56° 23.8'	165° 18.2'	85	30.0	43.0	27.0	5.928	3.148	-0.104	0.739
63	150	56° 23.8'	165° 18.2'	85	92.0	7.0	1.0	3.113	0.626	0.244	1.434
64	152	56° 03.5'	165° 18.9'	97	55.0	38.0	7.0	4.118	1.927	0.446	1.615
65	153	56° 03.5'	165° 18.9'	97	60.0	33.0	7.0	3.921	1.946	0.496	1.540
66	D-5	55° 52.0'	165° 16.0'	--	84.0	13.0	3.0	3.207	0.767	0.365	1.188
67	155	55° 36.0'	165° 17.3'	111	10.0	66.0	10.0	5.037	1.970	0.354	2.613
68	c-5	55° 32.0'	165° 09.0'	--	58.0	39.0	3.0	3.763	1.039	0.166	1.328
69	B-5	55° 16.0'	165° 08.0'	--	31.7	56.9	11.4	4.798	1.923	0.455	1.456
70	156	55° 12.2'	165° 17.9'	114	22.0	71.0	7.0	4.737	1.365	0.231	5.547
71	157	55° 12.2'	165° 17.9'	114	21.0	72.0	7.0	4.726	1.466	0.251	6.548
72	E-5	56° 16.0'	165° 0500'	--	46.0	47.0	7.0	4.206	2.061	0.302	1.644
73	G-n	55° 30.6'	164° 50.2'	101	----	----	----	-----	-----	-----	-----
74	B-6	55° 24.0'	164° 35.0'	--	74.2	19.5	6.3	3.440	1.647	0.449	2.351
75	002	55° 16.0'	164° 30.0'	91	87.2	9.5	3.3	2.592	1.554	0.082	1.781
76	13	55° 05.5'	164° 47.0'	102	61.0	30.7	8.3	3.633	1.861	0.400	2.445
77	A-6	55° 03.0'	164° 35.0'	--	99.8	0.2	0.0	0.782	0.733	-0.135	1.089
78	F-6	56° 45.0'	164° 36.0'	--	54.2	35.6	10.1	4.027	1.976	0.463	1.911
79	065	56° 40.3'	164° 26.6'	74	58.0	37.0	5.0	3.778	1.443	0.304	1.242
80	067	56° 40.3'	164° 26.6'	74	93.0	6.0	1.0	3.029	0.523	0.231	1.588
81	E-6	56° 22.0'	164° 32.0'	--	45.1	46.0	8.9	4.186	2.056	0.289	1.803
82	D-6	56° 05.0'	164° 32.0'	--	70.0	25.0	5.0	3.373	1.431	0.353	1.626
83	c-6	55° 45.0'	164° 33.0'	--	73.0	21.0	6.0	3.351	1.552	0.430	1.932
84	F-7	56° 48.0'	164° 00.0'	--	57.7	36.5	5.8	3.714	1.628	0.366	1.687
85	19	56° 40.0'	163° 57.6'	77	59.3	33.3	7.4	3.833	1.777	0.482	1.888
86	E-7	56° 20.0'	164° 08.0'	--	54.0	40.0	6.0	3.763	1.751	0.282	1.936
87	D-7	56° 05.0'	163° 56.0'	--	79.8	14.7	5.5	3.227	1.526	0.391	2.327
88	c-7	55° 42.0'	164° 00.0'	--	86.4	11.0	2.6	2.965	1.023	0.099	1.523
89	B-7	55° 21.0'	163° 54.0'	--	95.3	2.5	2.3	2.895	0.605	-0.034	1.476
90	F-8	56° 39.0'	163° 29.0'	--	80.9	17.5	1.6	3.176	0.804	0.179	0.876

NOTES : (1) Samples 1 through 60 are from this study; samples 61 through 120 are from previous studies.

Table I-1. Sample Data (Continued)

Sample ⁽¹⁾ Station		Sediment Parameters (Folk) and Ward										
Number	Number	Latitude(N)	Longitude(W)	Depth(m)	% sand	% silt	% clay	Mean(\$)	Standard Deviation(\$)	Skewness	Kurtosis	
91	068	56" 24.2'	163° 42.0'	83	62.0	33.0	5.0	3.729	1.559	0.345	1.520	
92	D-8	56" 00.0'	163° 33.0'	--	91.4	5.9	2.6	3.131	0.689	0.093	1.158	
93	003	55° 30.0'	163° 32.0'	64	92.3	5.9	1.8	2.769	0.925	-0.069	1.756	
94	1	55° 17.7'	163° 18.9'	48	73.0	19.3	7.7	3.317	1.851	0.401	2.951	
95	E-8	56° 20.0'	163° 20.0'	· ·	5.8	21.1	5.8	3.415	0.504	0.389	1.139	
96	070	56° 09.3'	163° 08.2'	86	95.0	3.0	2.0	3.019	0.533	-0.134	1.172	
97	D-9	56° 03.0'	162° 54.0'	· -	96.0	1.0	3.0	2.778	0.579	0.018	1.444	
98	F-9	56° 40.0'	162° 42.2'	--	95.7	1.9	2.4	2.599	0.607	0.054	1.195	
99	076	56° 32.2'	162° 37.8'	73	96.0	2.0	2.0	2.593	0.506	0.237	1.127	
100	075	56° 11.7'	162° 22.7'	68	99.0	0.0	1.0	2.252	0.591	-0.068	1.696	
101	D-10	55° 58.0'	162° 25.0'	--	97.0	1.0	2.0	2.079	0.637	-0.153	1.391	
102	072	55° 56.5'	162° 38.0'	75	96.0	3.0	1.0	2.487	0.551	-0.012	1.232	
103	004	55° 46.0'	162° 29.5'	57	87.0	1.7	1.3	2.329	0.688	-0.098	1.188	
104	F-10	56° 38.0'	162° 12.0'	--	96.0	2.0	2.0	2.290	0.612	0.107	1.048	
105	11	56° 45.5'	161° 59.7'	71	84.7	5.7	9.7	2.800	1.625	0.485	4.508	
106	118	56° 53.8'	161° 47.1'	72	97.0	1.0	2.0	2.577	0.540	0.010	1.101	
107	E-n	56° 17.0'	161° 35.0'	--	99.9	0.1	0	2.018	0.491	-0.029	1.068	
108	005	56" 14.0'	161° 30.0'	88	98.6	0.4	1.0	2.287	0.602	-0.098	1.406	
109	BB-1	56° 06.0'	161° 25.5'	--	99.9	0.1	0.0	1.647	0.567	-0.022	0.983	
110	116	56° 43.9'	161° 31.3'	83	97.0	1.0	2.0	2.317	0.727	-0.157	1.402	
111	F-n	56" 43.0'	161° 21.0'	--	97.4	1.0	1.6	2.203	2.667	-0.085	1.245	
112	F-13	56° 41.0'	161° 14.0'	--	100.0	0.0	0.0	1.448	1.002	-0.402	1.132	
113	114	56° 25.3'	161° 04.0'	63	98.0	1.0	1.0	2.435	0.615	-0.058	1.370	
114	3	56° 17.4'	161° 02.3'	52	99.7	0.3	0.0	1.020	2.390	-0.840	3.280	
115	111	56° 06.4'	160° 41.0'	19	87.0	10.0	3.0	3.047	0.763	0.239	2.211	
116	110	56° 31.5'	160° 41.5'	61	94.0	2.0	4.0	0.760	2.353	0.005	0.895	
117	007	56° 43.0'	160° 31.0'	64	99.0	0.0	1.0	1.789	1.070	-0.402	1.063	
118	006	56° 34.0'	160' 26.0'	64	99.0	0.7	0.3	2.317	0.639	-0.142	1.245	
119	BB-12	56° 28.5'	160° 10.0'	--	100.0	0.0	0.0	-0.423	0.994	0.096	0.928	
120	F-14	56" 45.0'	159° 50.0'	· -	100.0	0.0	0.0	1.676	0.658	-0.261	1.554	

NOTES: (1) Samples 1 through 60 are from this study; samples 61 through 120 are from previous studies.

Table I-2. Engineering Data

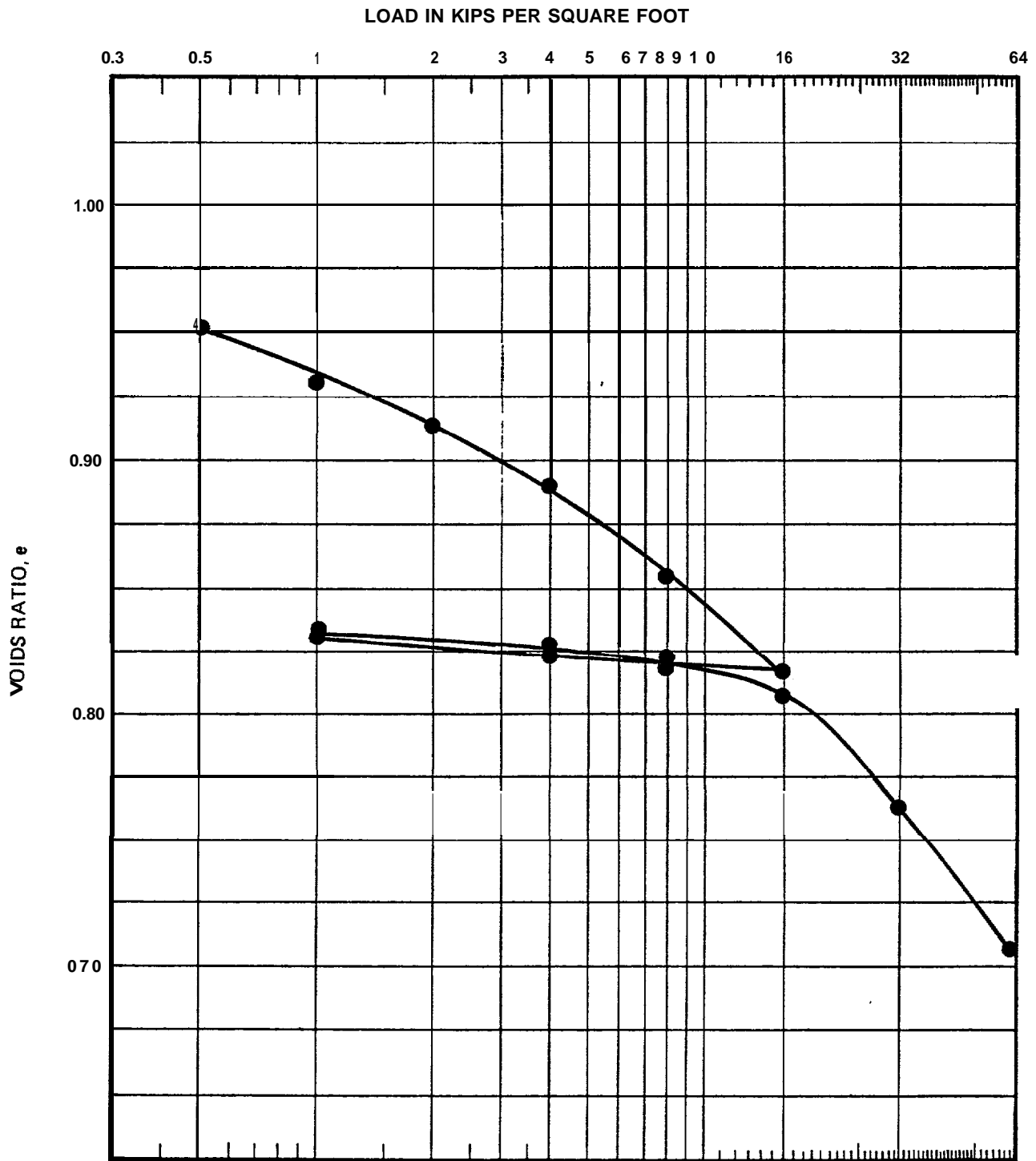
Station	Sample Type	Soil Type	D ₁₀ (mm)	D ₅₀ (mm)	D ₆₀ (mm)	Cu	%Finer #200
120/200		SP/SM (3)	.08	.10	.11	1.4	10
128/108	Bag	SP (2)	.42	1.00	1.10	2.6	1
135/175		SP (2)	.10	.14	.15	1.5	1
150/100		SP (2)	.12	.18	.19	1.6	1
150/150		SP (2)	.12	.19	.20	1.67	1
165/125		SP (1)	.34	.70	.84	2.47	1
177/185	Bag	SP (1)	.20	.42	.45	2.25	1
180/200		SP (2)	.11	.20	.21	1.91	1
210/150		SP (2)	.16	.25	.27	1.69	1
255/158		SP (1)	.19	.43	.52	2.74	1
255/200		SP (2)	.12	.20	.22	1.83	1
262/185		SP (2)	.17	.28	.30	1.76	2
270/193		SP (2)	.12	.25	.26	2.17	2
285/181		SP (1)	*50	1.20	1.50	3.00	1
285/181		SP (1)	.60	1.00	1.00	0.66	1
285/200		SP (1)	.20	.55	.70	3.50	1

Table I-2. Engineering Data (Continued)

Station	Sample Type	Soil Type	D ₁₀ (mm)	D ₅₀ (mm)	D ₆₀ (mm)	CU	%Finer #200
0/150	Gravity Core @ 22 cm	SM (4)	0.01	0.07	0.09	9.0	51
0/150	Gravity Core @ 50 cm	SM (4)	0.004	0.06	0.08	20.0	59
0/150	Gravity Core @ 64 cm	SM (4)	0.006	0.07	0.09	15.0	53
0/200		SM (4)		0.16	0.20		20
20/25		SP (1)	0.7	1.4	1.5		1
20/50	Gravity Core @ 8 cm	SM (4)	0.05	0.09	0.11	2.2	25
20/100		SM (4)		0.13	0.15		30
30/200		SM (4)		0.10	0.11		26
35/111		SM (4)		0.11	0.12		30
51/87	Gravity Core @ 11 cm	SM (4)		0.12	0.15		26
51/87	Gravity Core @ 21 cm	SM (4)	0.03	0.14	0.16	5.3	23
51/87	Gravity Core @ 33 cm	SM (4)	0.008	0.12	0.18	22.5	33
51/87	Gravity Core @ 64 cm	SM (4)	0.007	0.09	0.11	15.7	39
70/91		SP/SM (3)	.08	.20	.21	2.6	7
79/200		SM (4)		.09	.10		32
90/50		SP (2)	.19	.30	.35	1.8	1 "
90/125		SP/SM (3)	.08	.10	.11	1.4	8
120/100		SP (2)	.12	.19	.20	1.7	1

APPENDIX **II**

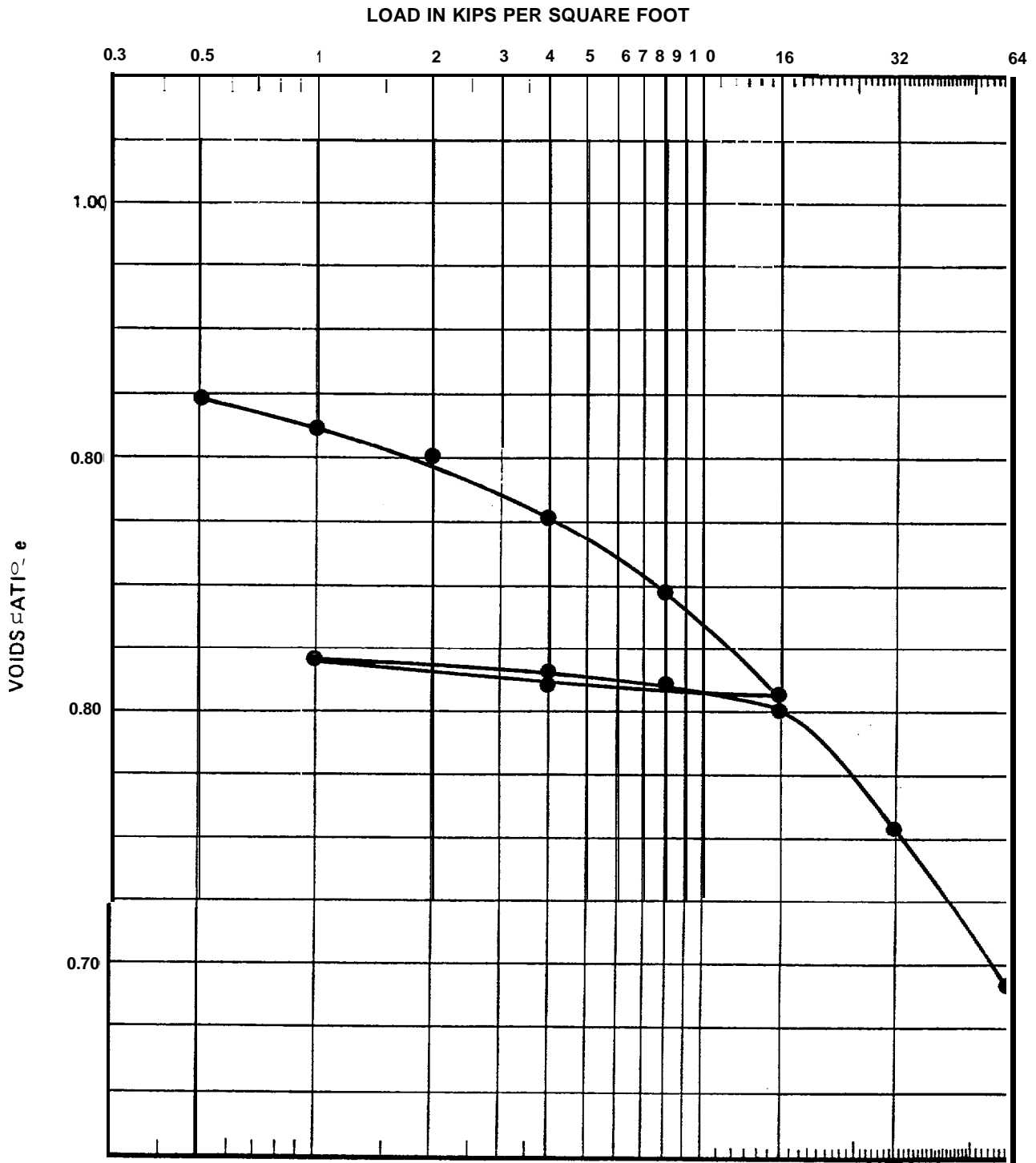
SUMMARY OF LABORATORY TEST RESULTS



SAMPLE NO.: 2
 WATER DEPTH (METERS): 93
 DEPTH INTERVAL (CM): 5-10
 TYPE OF SAMPLE: GRAVITY CORE

INITIAL VOIDS RATIO: 1.0
 COMPRESSION INDEX: 0.2
 RECOMPRESSION INDEX: 0.01

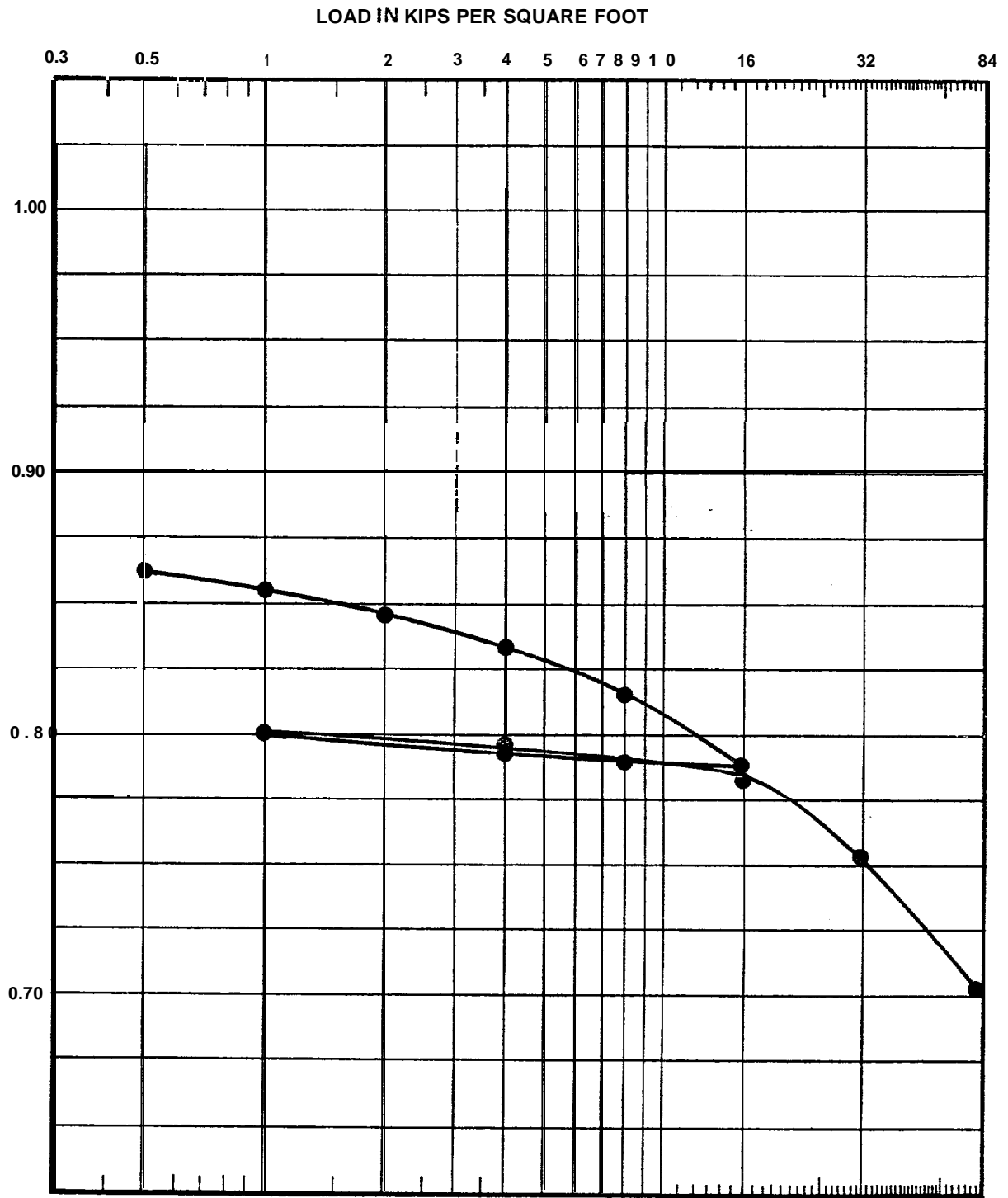
FIGURE 11-1 CONSOLIDATION TEST RESULTS - SAMPLE 2



SAMPLE NO.: 2
 WATER DEPTH (METERS): 93
 DEPTH INTERVAL (CM): 30-35
 TYPE OF SAMPLE: GRAVITY CORER

INITIAL VOIDS RATIO: 1.0
 COMPRESSION INDEX: 0.2
 RECOMPRESSION INDEX: 0.01

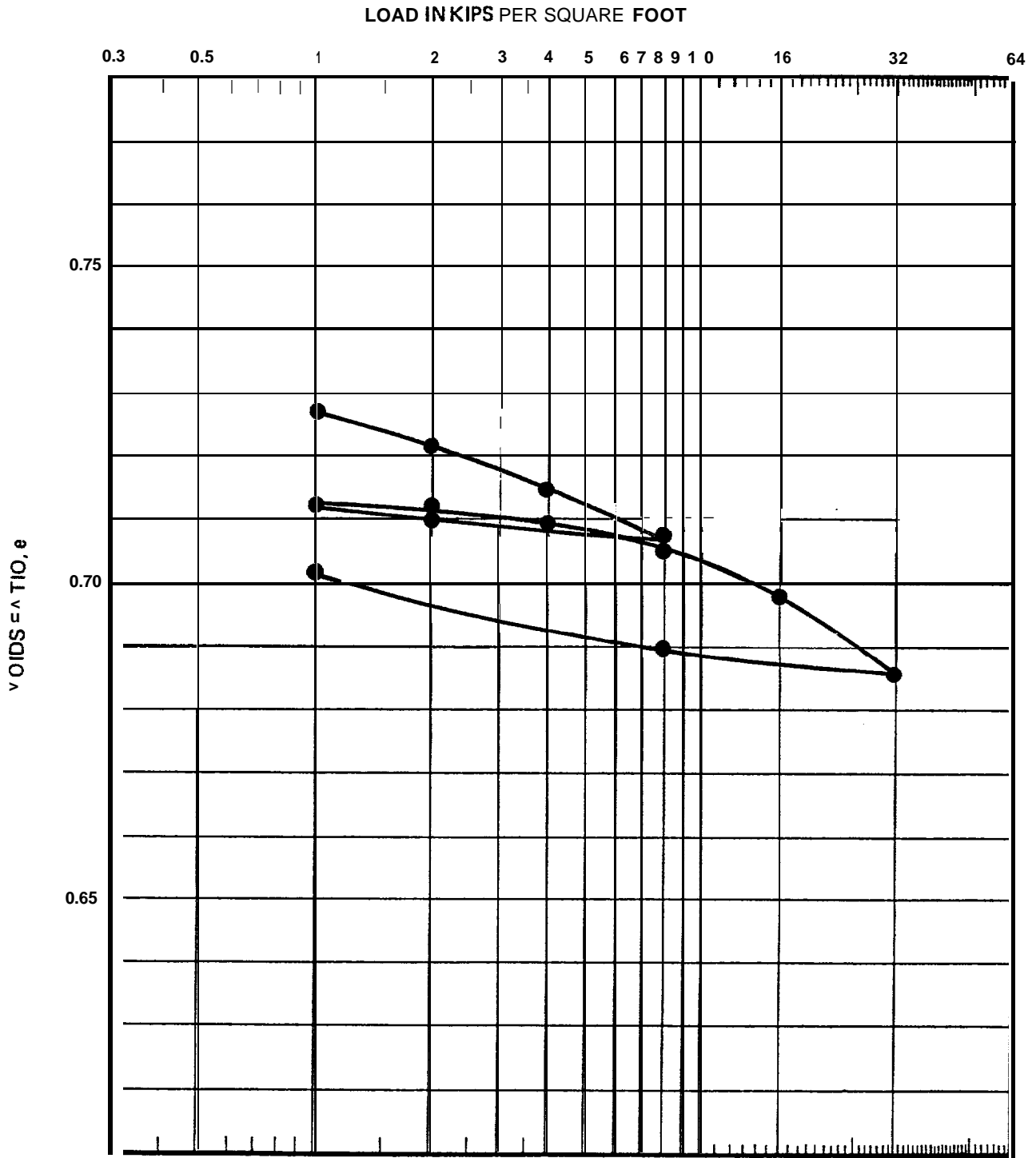
FIGURE I I-2 CONSOLIDATION TEST RESULTS - SAMPLE 2



SAMPLE NO.: 23
 WATER DEPTH (METERS): 97
 DEPTH INTERVAL (CM): 15-20
 TYPE OF SAMPLE: GRAVITY CORE

INITIAL VOIDS RATIO: 0.9
 COMPRESSION INDEX: 0.15
 RECOMPRESSION INDEX: 0.008

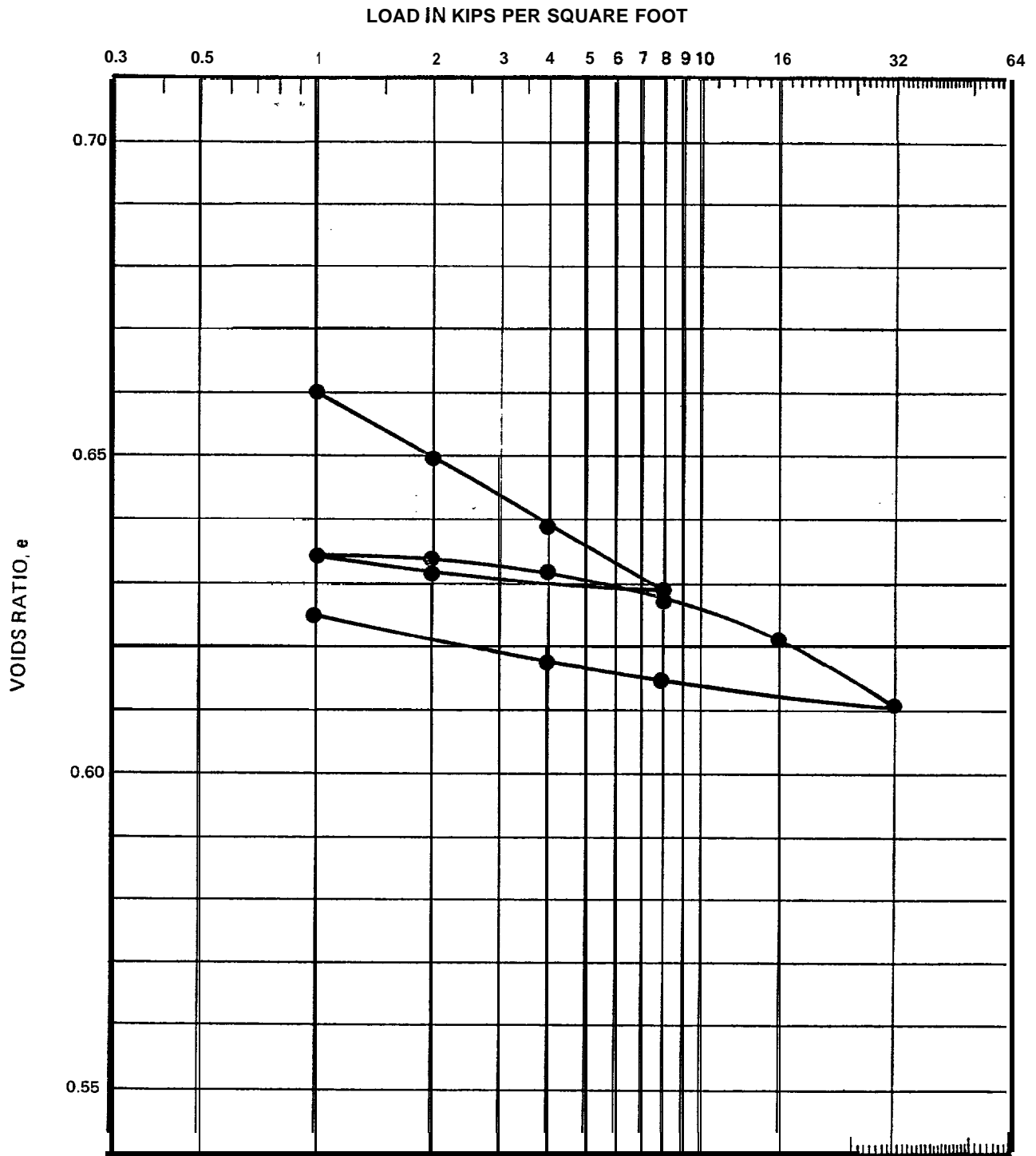
FIGURE II-3 CONSOLIDATION TEST RESULTS – SAMPLE 23



SAMPLE NO.: 9
 WATER DEPTH (METERS): 100
 DEPTH INTERVAL (CM): SURFICIAL
 TYPE OF SAMPLE: RECONSTITUTED

INITIAL VOIDS RATIO: 0.7
 COMPRESSION INDEX: 0.035
 RECOMPRESSION INDEX: 0.005

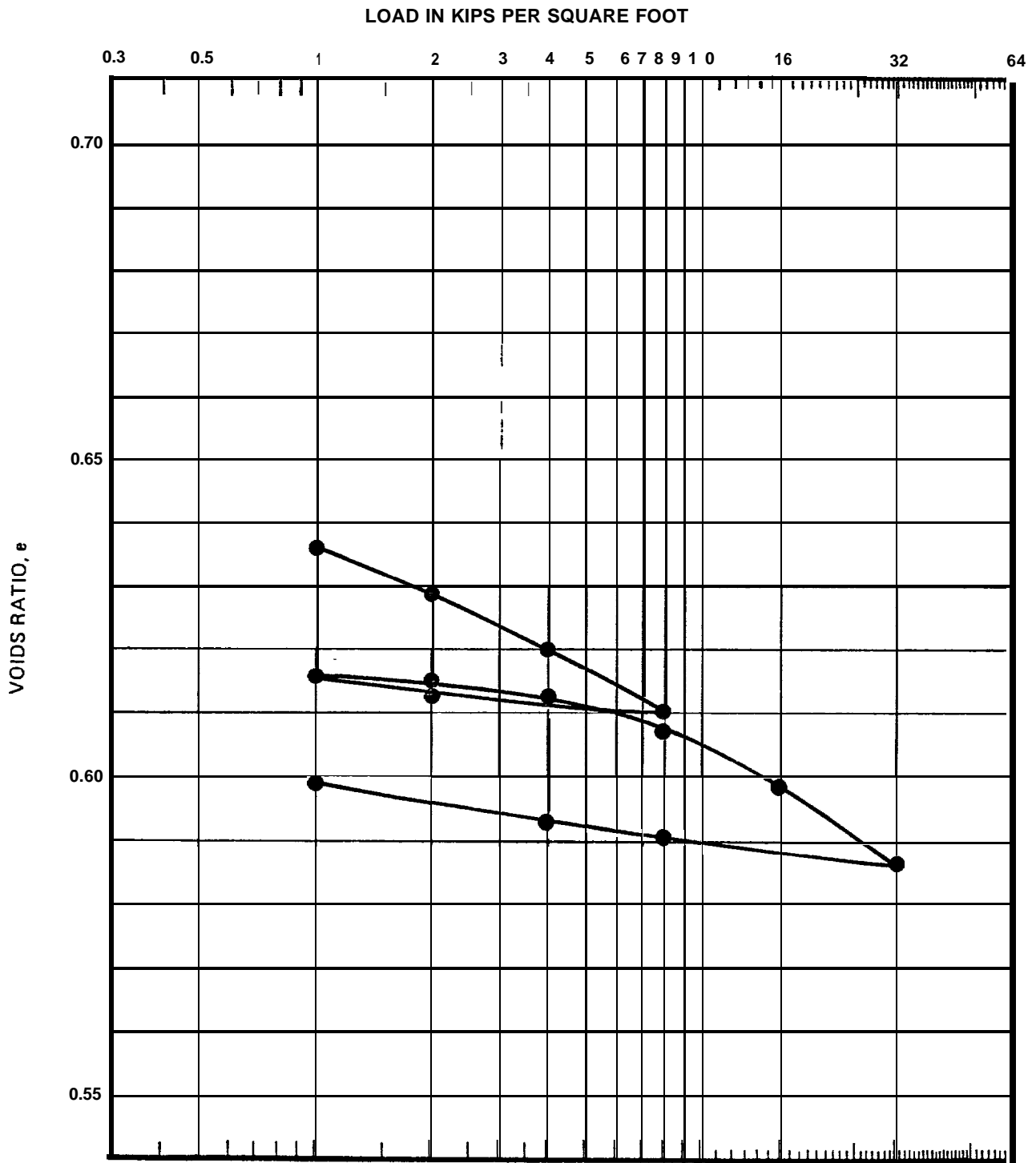
FIGURE II-4 CONSOLIDATION TEST RESULTS - SAMPLE 9



SAMPLE NO.: 24
 WATER DEPTH (METERS): 84
 DEPTH INTERVAL (CM): SURFICIAL
 TYPE OF SAMPLE: RECONSTITUTED

INITIAL VOIDS RATIO: 0.7
 COMPRESSION INDEX: 0.03
 RECOMPRESSION INDEX: 0.005

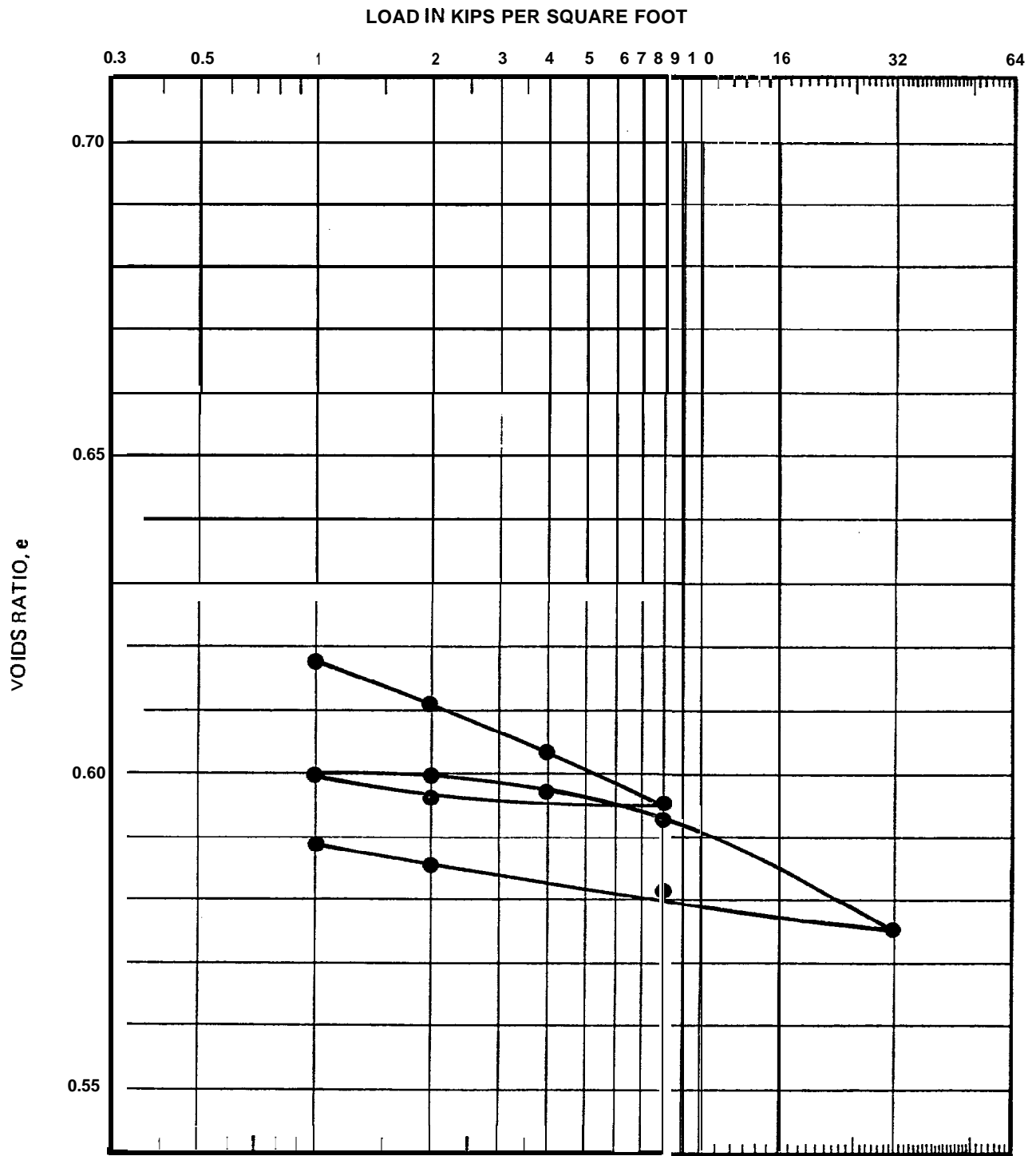
FIGURE II-5 CONSOLIDATION TEST RESULTS - SAMPLE 24



SAMPLE NO.: 43
 WATER DEPTH (METERS): 80
 DEPTH INTERVAL (CM): SURFICIAL
 TYPE OF SAMPLE: RECONSTITUTED

INITIAL VOID RATIO: 0.65
 COMPRESSION INDEX: 0.04
 RECOMPRESSION INDEX: 0.005

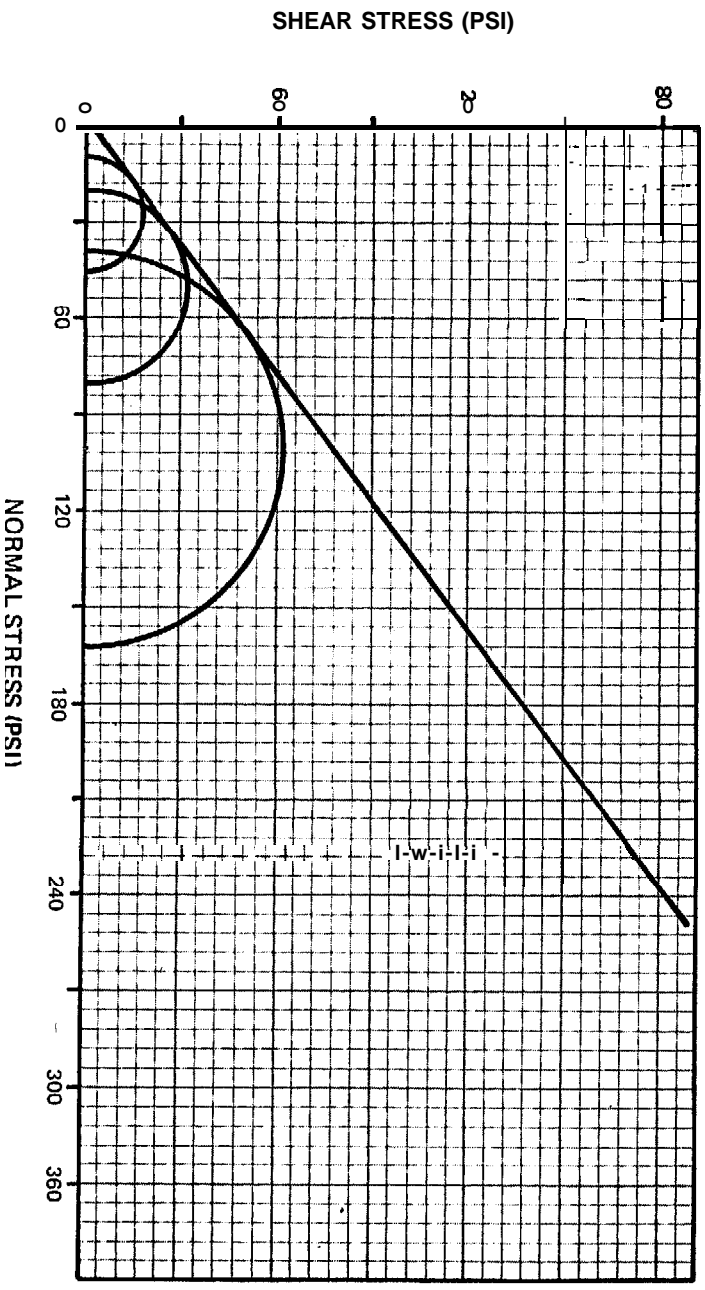
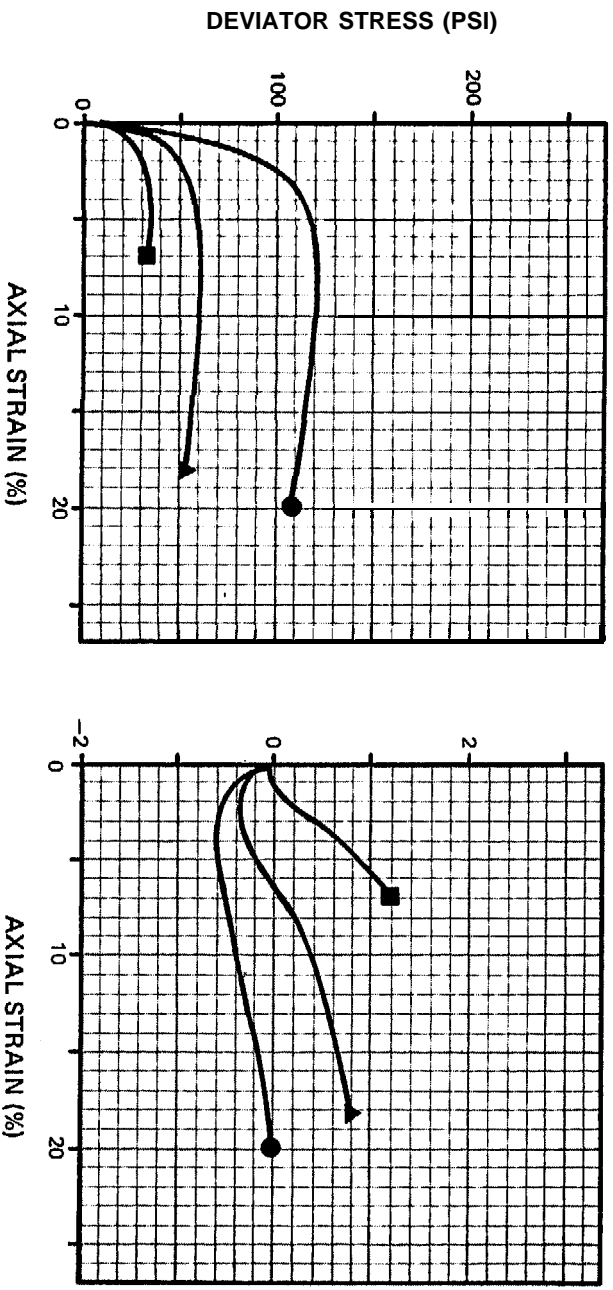
FIGURE II-6 CONSOLIDATION TEST RESULTS - SAMPLE 43



SAMPLE NO.: 57
 WATER DEPTH (METERS): 49
 DEPTH INTERVAL (CM): SURFICIAL
 TYPE OF SAMPLE: RECONSTITUTED

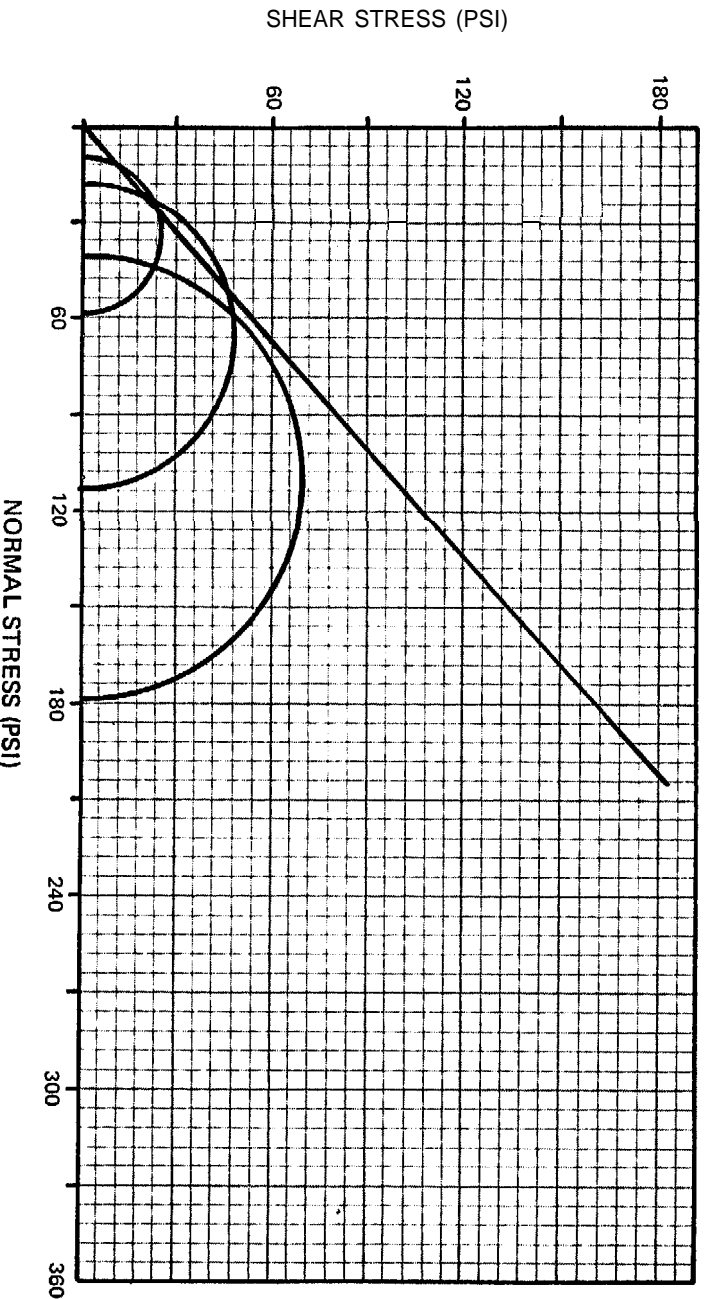
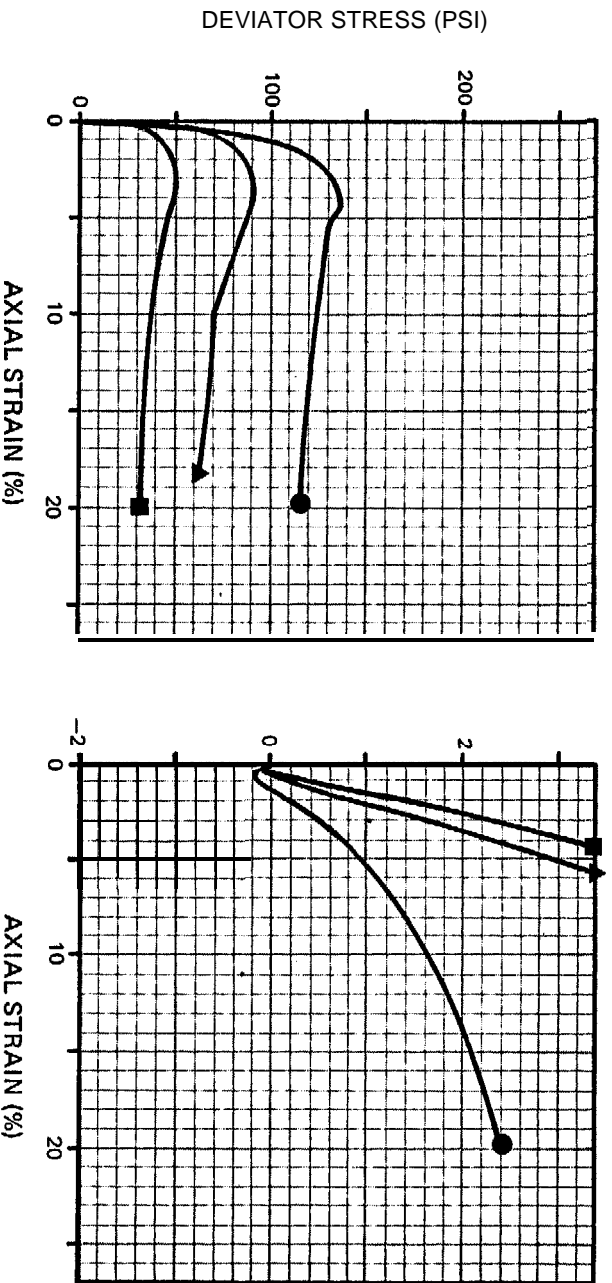
INITIAL VOID RATIO: 0.6
 COMPRESSION INDEX: 0.03
 RECOMPRESSION INDEX: 0.003

FIGURE II-7 CONSOLIDATION TEST RESULTS - SAMPLE 57



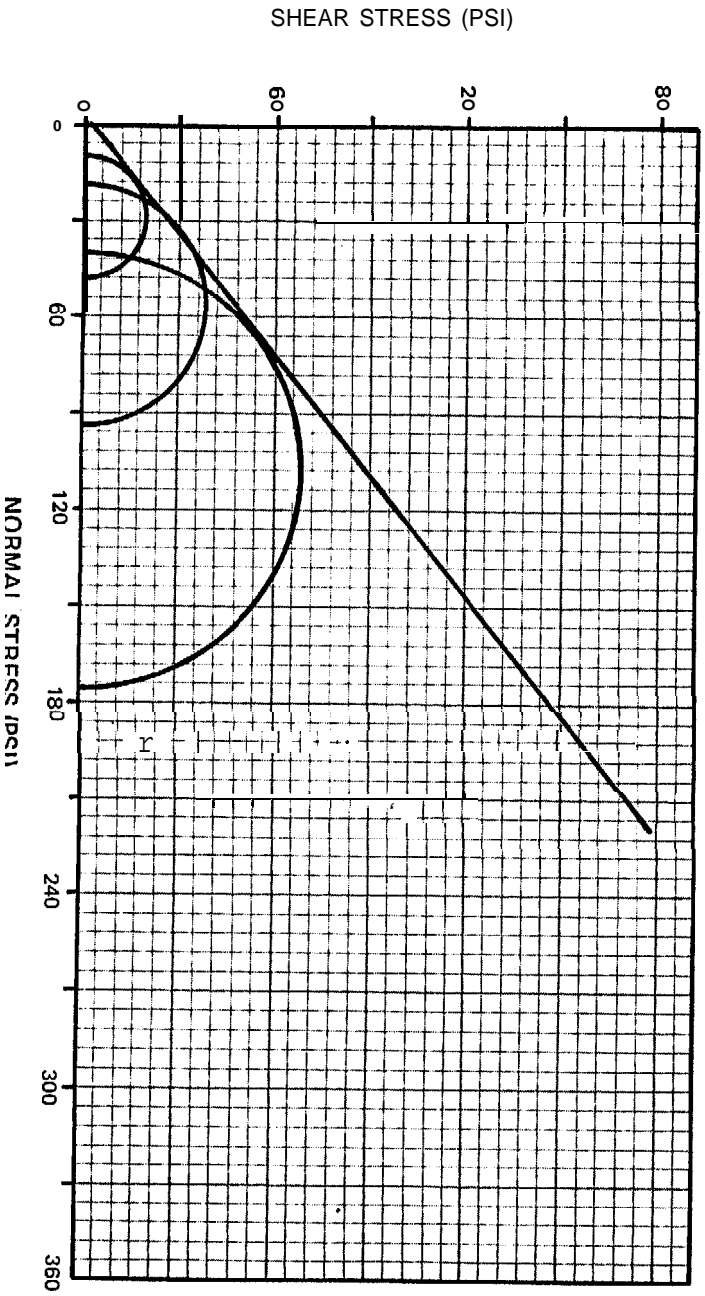
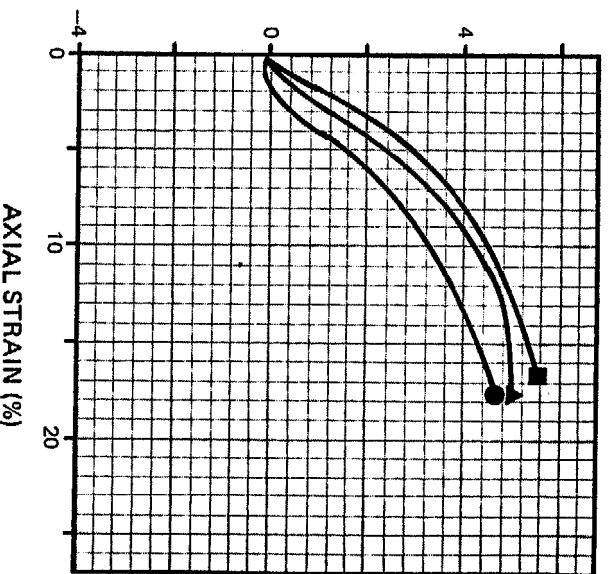
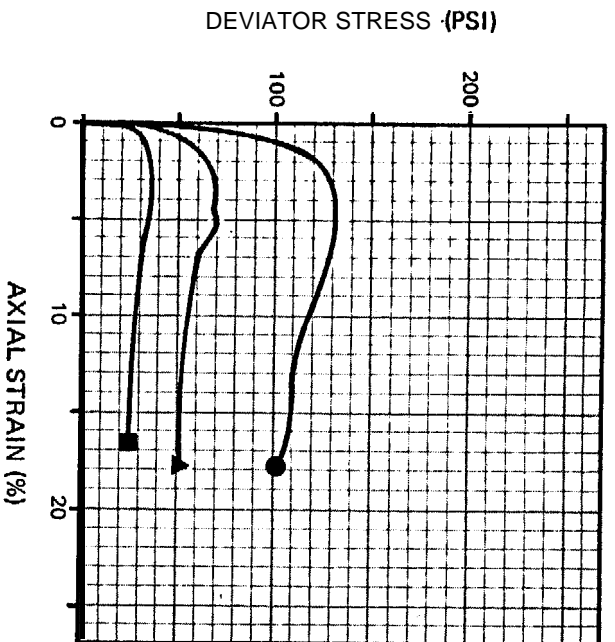
SYMBOL	BORING NUMBER	SAMPLE NUMBER	SAMPLE INTERVAL	TYPE OF SAMPLE	SOIL TYPE	TYPE OF TEST	DRY DENSITY (PCF)	MOISTURE CONTENT (%)	CONFINING PRESSURE (PSI)	MAXIMUM DEVIATOR STRESS $\sigma_1 - \sigma_3$ (PSI)	STRAIN RATE (%/MIN)	BACK PRESSURE
	10ZU/100	9	N/A	R	SM4	CD	95	15	40	121	0.08	
	10Z0/100	9	N/A	R	SM4	CD	95	15	20	60		
	10ZU/100	9	N/A	R	SM4	CD	95	15	10	35	0.08	

FIGURE II-8 STATIC TRIAXIAL TEST RESULTS FROM RECONSTITUTED TESTS ON SAMPLE 9



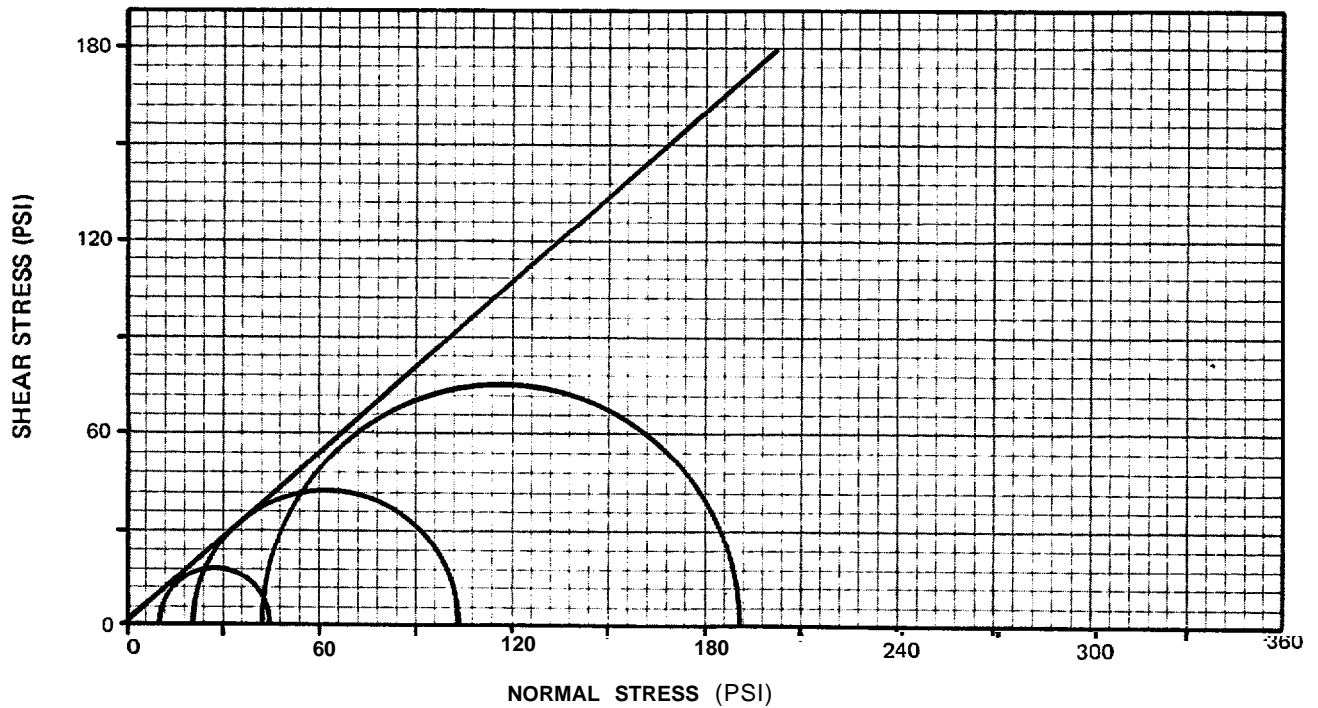
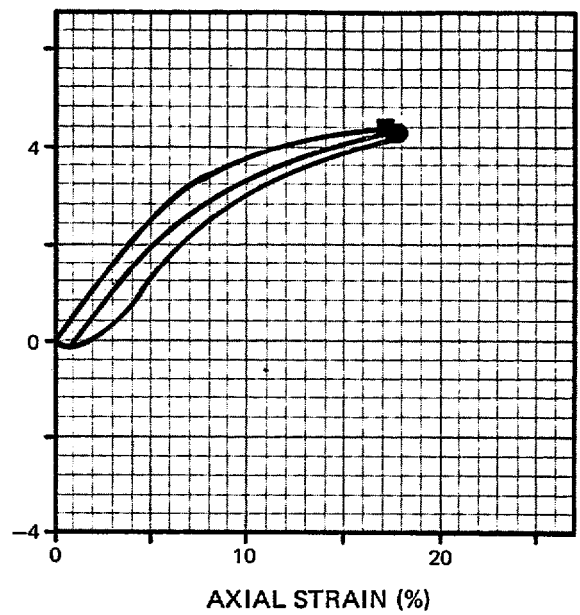
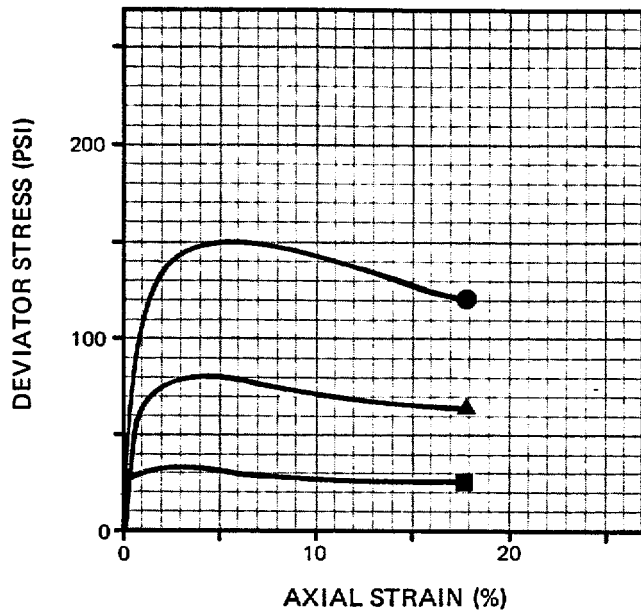
SYMBOL	BORING NUMBER	SAMPLE NUMBER	SAMPLE INTERVAL	TYPE OF SAMPLE	SOIL TYPE	TYPE OF TEST	DRY DENSITY (PCF)	MOISTURE CONTENT (%)	CONFINING PRESSURE (PSI)	MAXIMUM DEVIATOR STRESS (PSI)	STRAIN RATE (IN/IN/HR)	BACK PRESSURE
	107/U/91	24	N/A	R	SP/SM	CD	99	15	40	138	0.08	
	1V7/U/91	24	N/A	R	SP/SM	CD	99	15	20	91	0.08	
	107/O/91	24	N/A	R	SP/SM	CD	99	15	10	50	0.08	

FIGURE II-9 STATIC TRIAXIAL TEST RESULTS FROM RECONSTITUTED TESTS ON SAMPLE 24



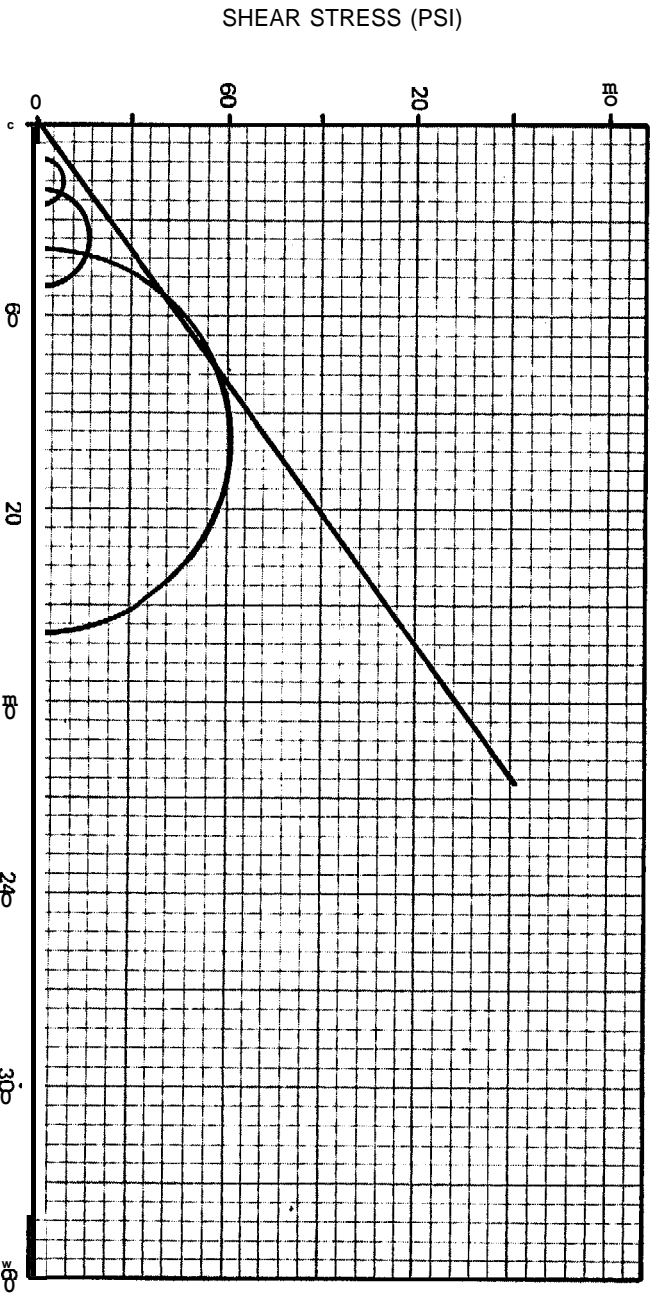
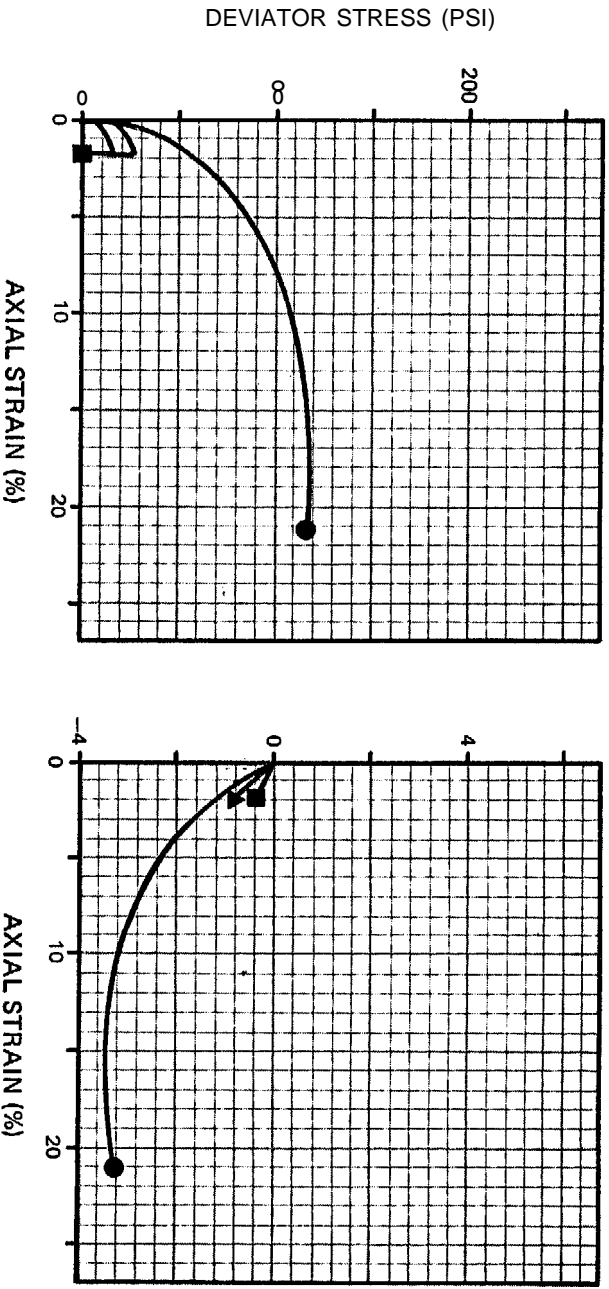
SYMBOL	BORING NUMBER	SAMPLE NUMBER	SAMPLE INTERVAL	TYPE OF SAMPLE	SOIL TYPE	TYPE OF TEST	DRY DENSITY (PCF)	MOISTURE CONTENT (%)	CONFINING PRESSURE (PSI)	MAXIMUM DEVIATOR STRESS (1-2-3 (PSI))	STRAIN RATE (%/MIN)	BACK PRESSURE
			N/A	n	SP1	UD	103	10	40	100	1.000	
	1177/185	43	N/A	R	SP1	CU	103	10	20	20	0.08	
	1177/185	43	N/A	R	SP1	CU	103	10	20	20	20	

FIGURE II-10 STATIC TRIAXIAL TEST RESULTS FROM RECONSTITUTED TESTS ON SAMPLE 43



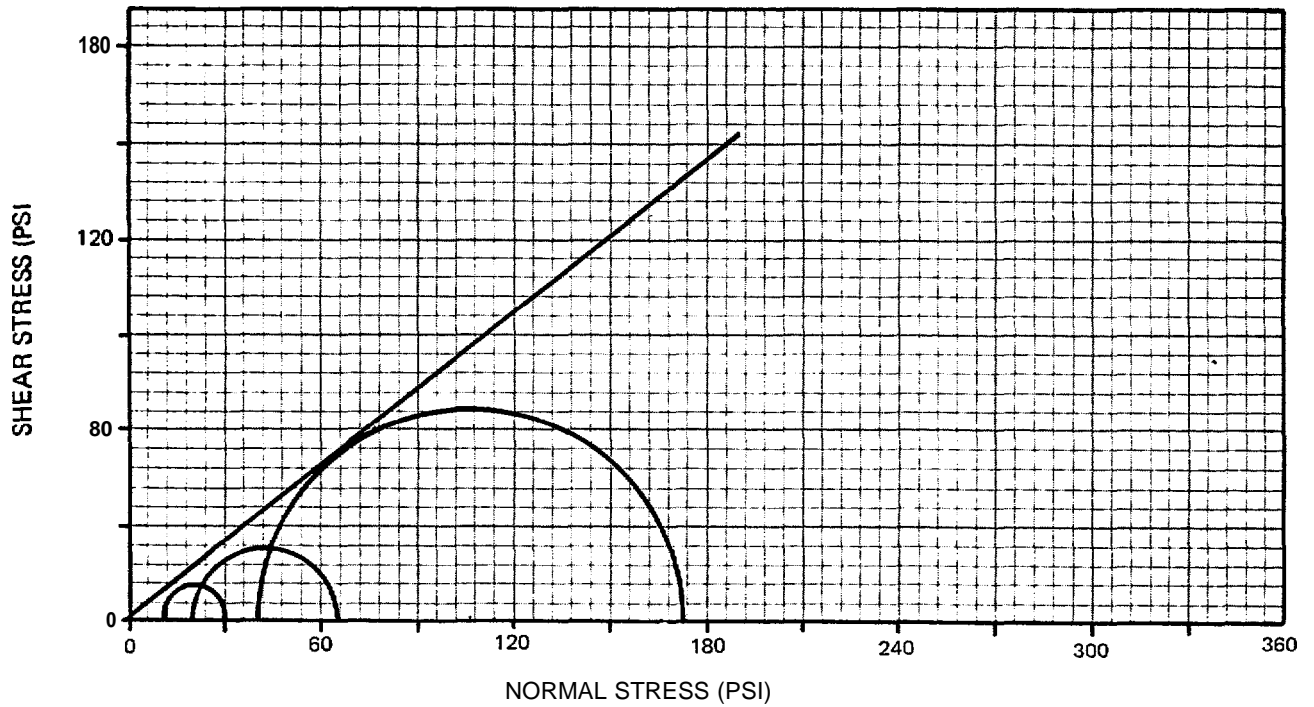
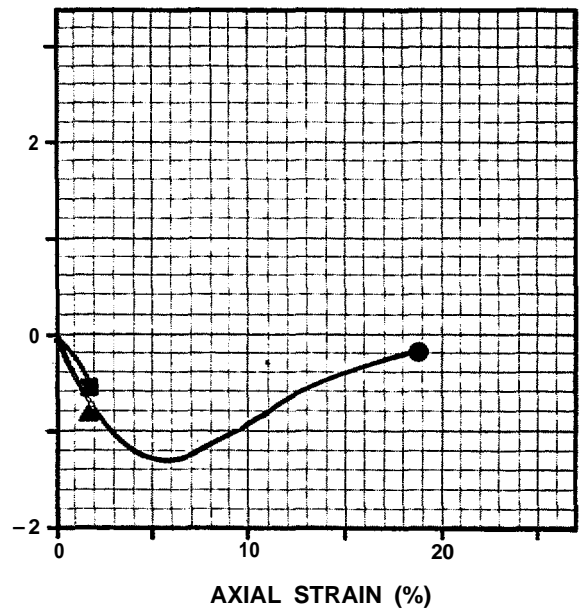
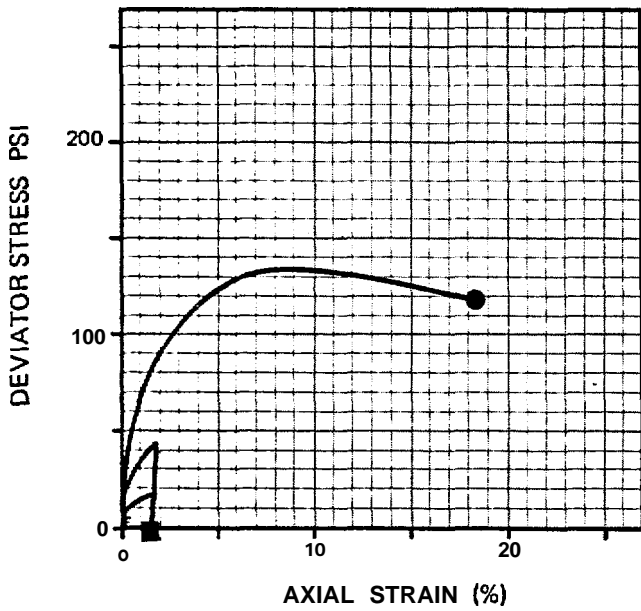
SYMBOL	BORING NUMBER	SAMPLE NUMBER	SAMPLE INTERVAL	TYPE OF SAMPLE	SOIL TYPE	TYPE OF TEST	DRY DENSITY (PCF)	MOISTURE CONTENT (%)	CONFINING PRESSURE (PSI)	MAXIMUM DEVIATOR STRESS $\sigma_1 - \sigma_3$ (PSI)	STRAIN RATE (%/MIN)	BACK PRESSURE
	1262/185	57	N/A	R	SP2	CD	102	10	40	151	0.08	
	1262/185	57	N/A	R	SP2	CD	102	10	20	82	0.08	
	1262/186	57	N/A	R	SP2	CD	102	10	10	34	0.08	

FIGURE 11-11 STATIC TRIAXIAL TEST RESULTS FROM RECONSTITUTED TESTS ON SAMPLE 57



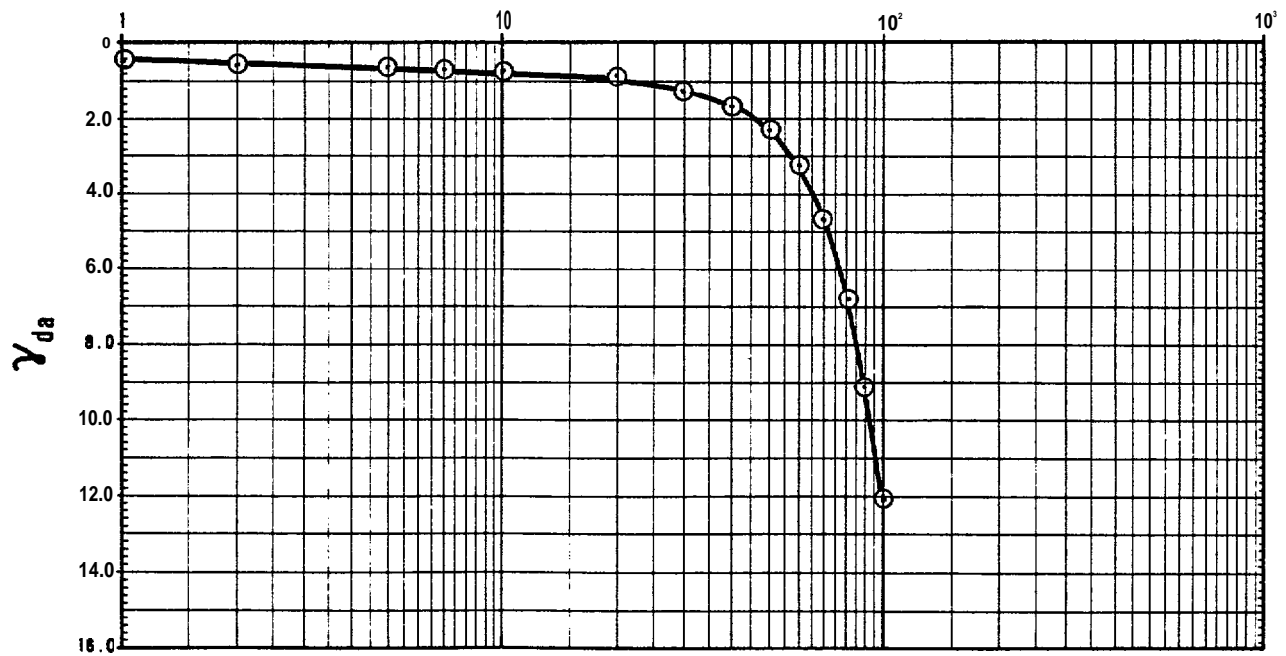
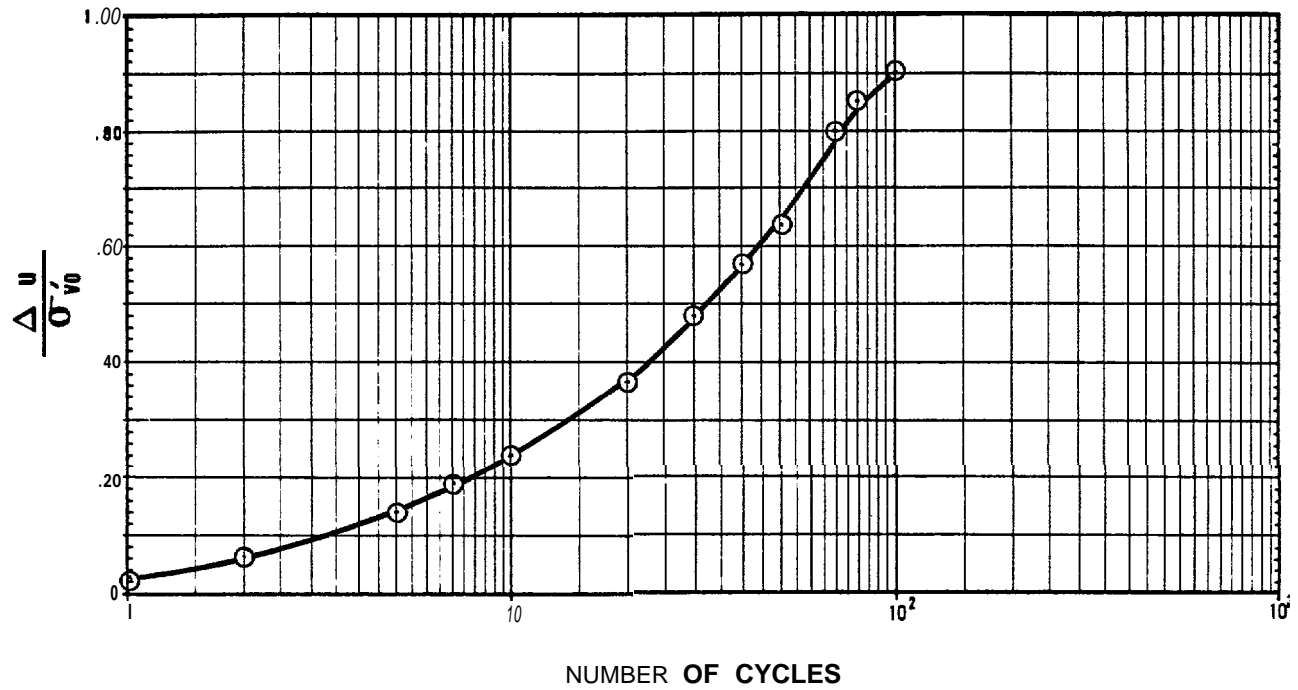
SYMBOL	BORING NUMBER	SAMPLE NUMBER	SAMPLE INTERVAL	TYPE OF SAMPLE	SOIL TYPE	TYPE OF TEST	DRY DENSITY (PCF)	MOISTURE CONTENT (%)	CONFINING PRESSURE	MAXIMUM DEVIATOR STRESS	STRAIN RATE	BACK PRESSURE
	50	2	9	GC	SM4	CU	88	37	20	31	0.08	
	1000/150	2	13-19	GC	SM4	CD	88	37	10	16	0.08	

FIGURE II-12 MULTISTAGE STATIC TRIAXIAL TEST RESULTS FROM GRAVITY CORE SAMPLE NO. 2



SYMBOL	BORING NUMBER	SAMPLE NUMBER	SAMPLE INTERVAL	TYPE OF SAMPLE	SOIL TYPE	TYPE OF TEST	DRY DENSITY (PCF)	MOISTURE CONTENT (%)	CONFINING PRESSURE (PSI)	MAXIMUM DEVIATOR STRESS $\sigma_1 - \sigma_3$ (PSI)	STRAIN RATE (%/MIN)	BACK PRESSURE
	1051187	23	14-20	GC	SP/SM	CD	93	29	40	133	0,08	
	1051/87	23	14-20	GC	SP/SM	CD	93	29	20	46	0.08	
	1051187	23	14-20	GC	SP/SM	CD	93	29	10	21	0.08	

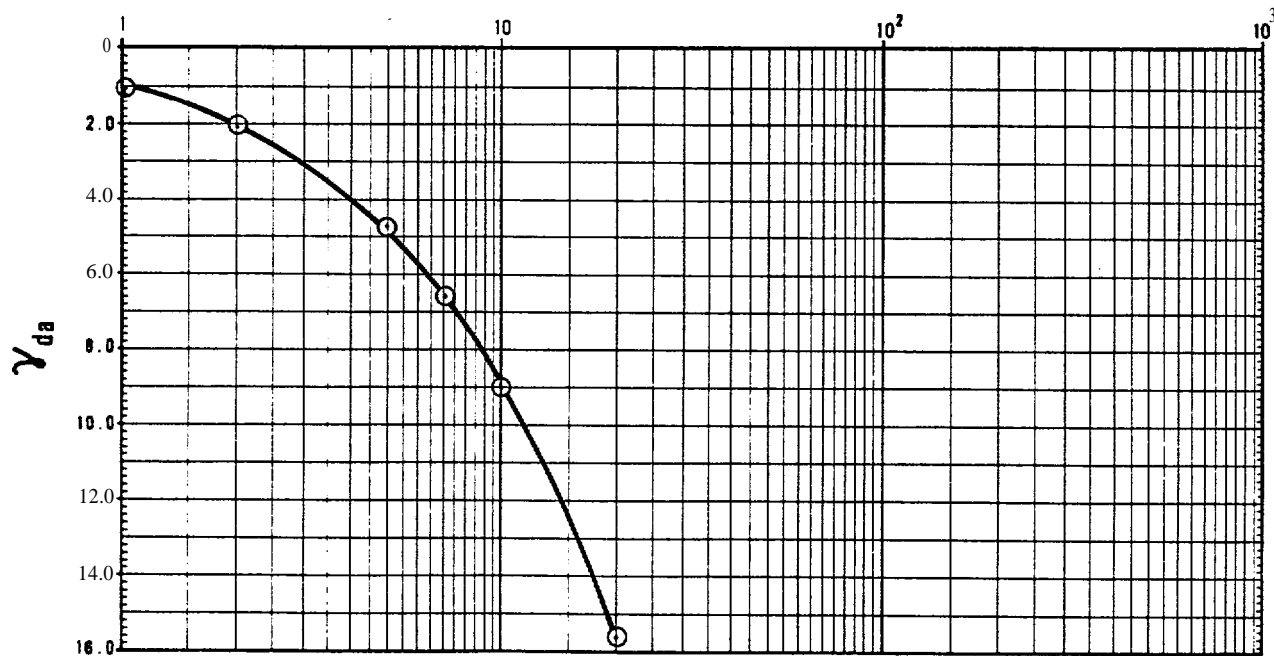
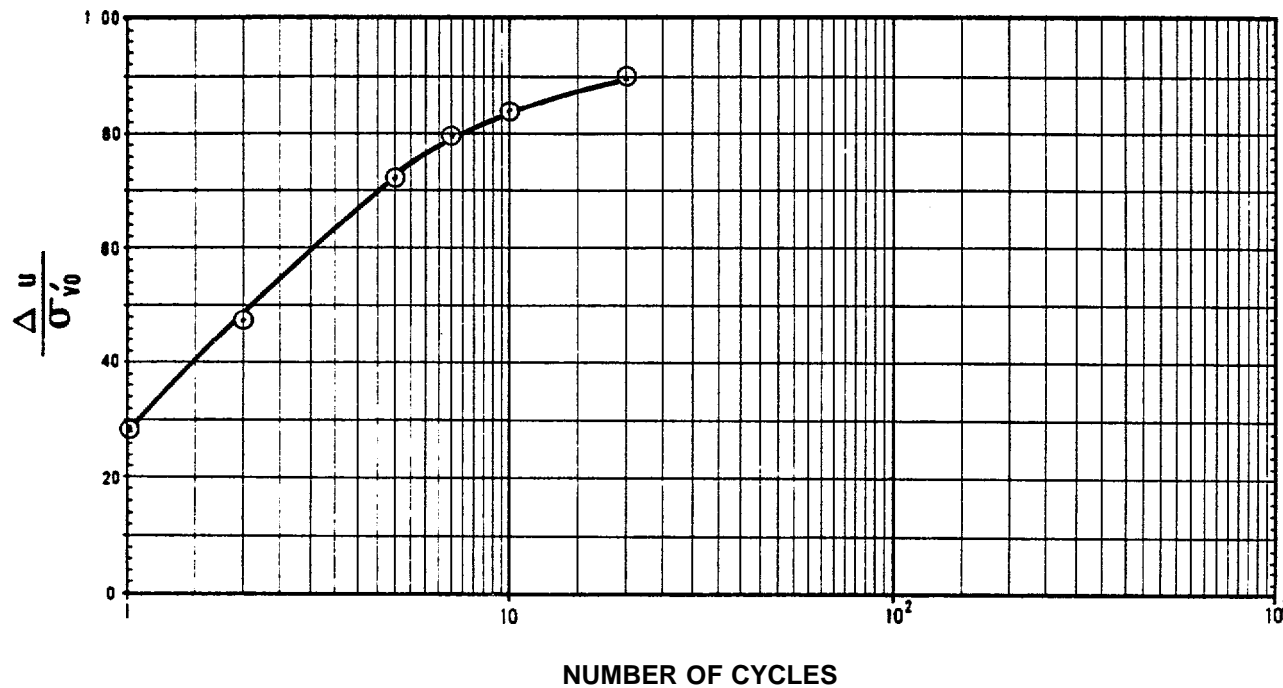
FIGURE II-13 MULTISTAGE STATIC TRIAXIAL TEST RESULTS FROM GRAVITY CORE SAMPLE NO. 23



TEST NO.	SAMPLE NO.	SAMPLE DEPTH (cm)	σ'_{v0} *	τ_h / σ'_{v0}	SOIL TYPE
1	2	48-51	70	0.22	SM

*KN/M²

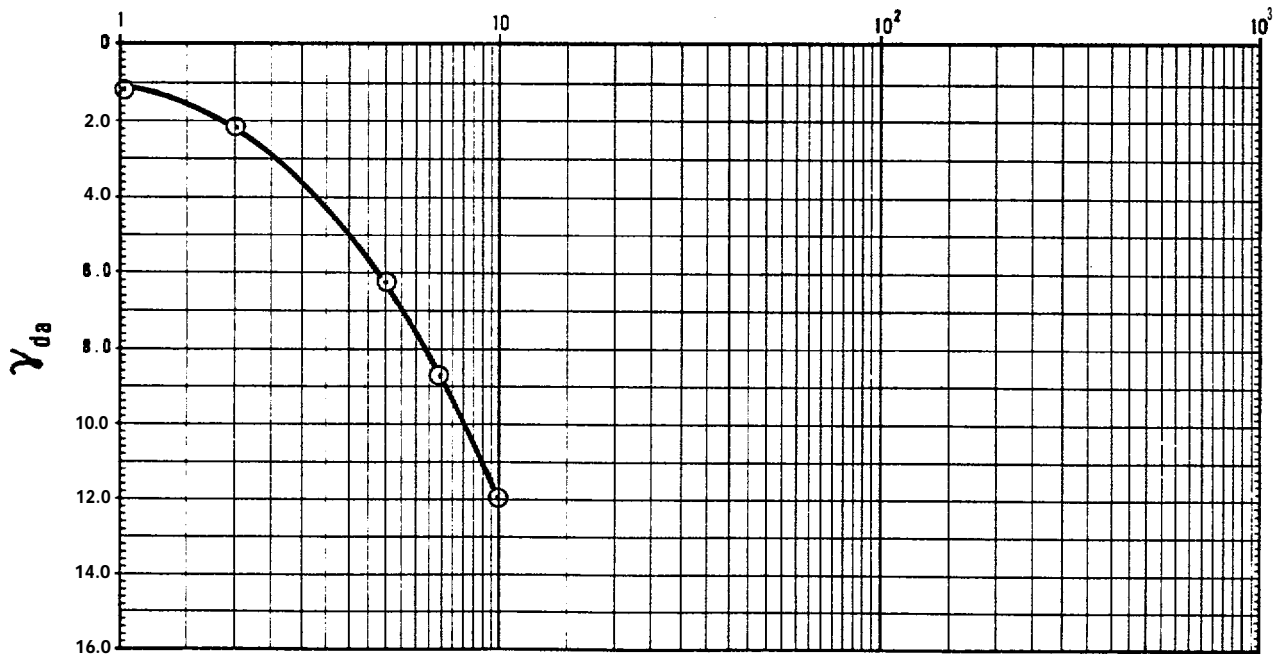
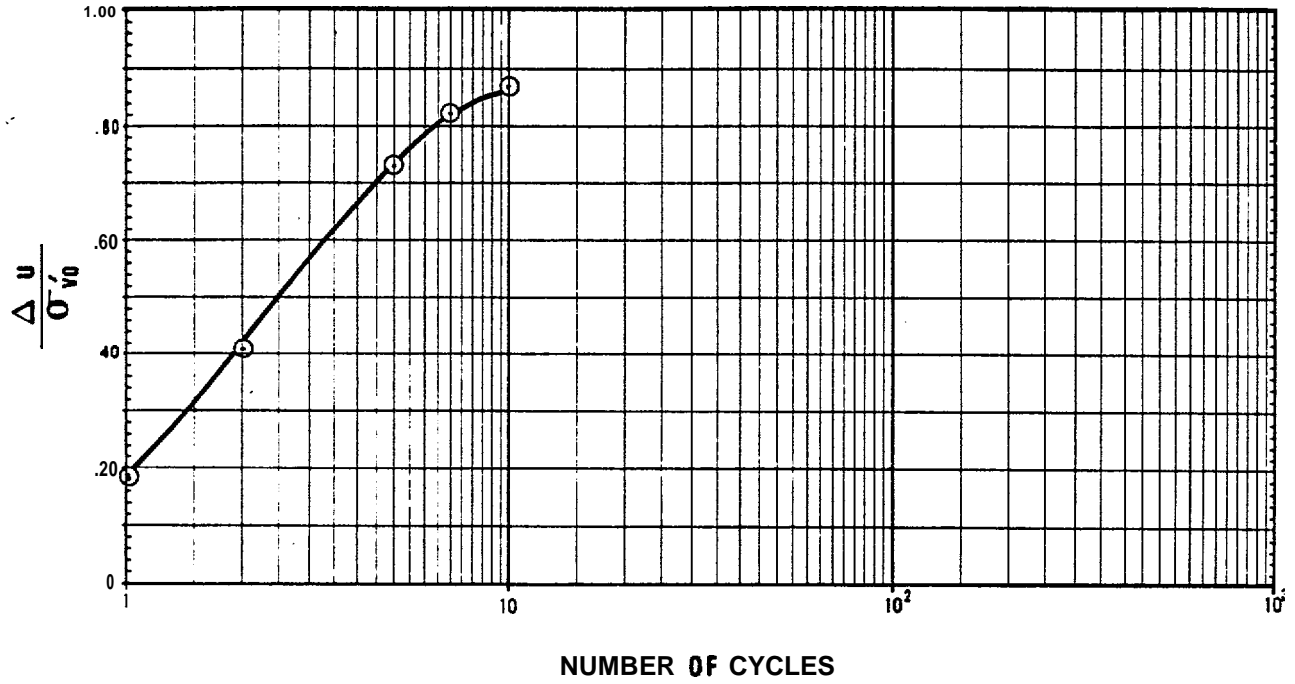
FIGURE II-14 LIQUEFACTION TEST RESULTS FROM GRAVITY CORE - SAMPLE 2-1



TEST NO.	SAMPLE NO.	SAMPLE DEPTH (cm)	$\sigma'_{v0} *$	τ_v / σ'_{v0}	SOIL TYPE
2	2	65-68	70	0.27	SM

● KN/M2

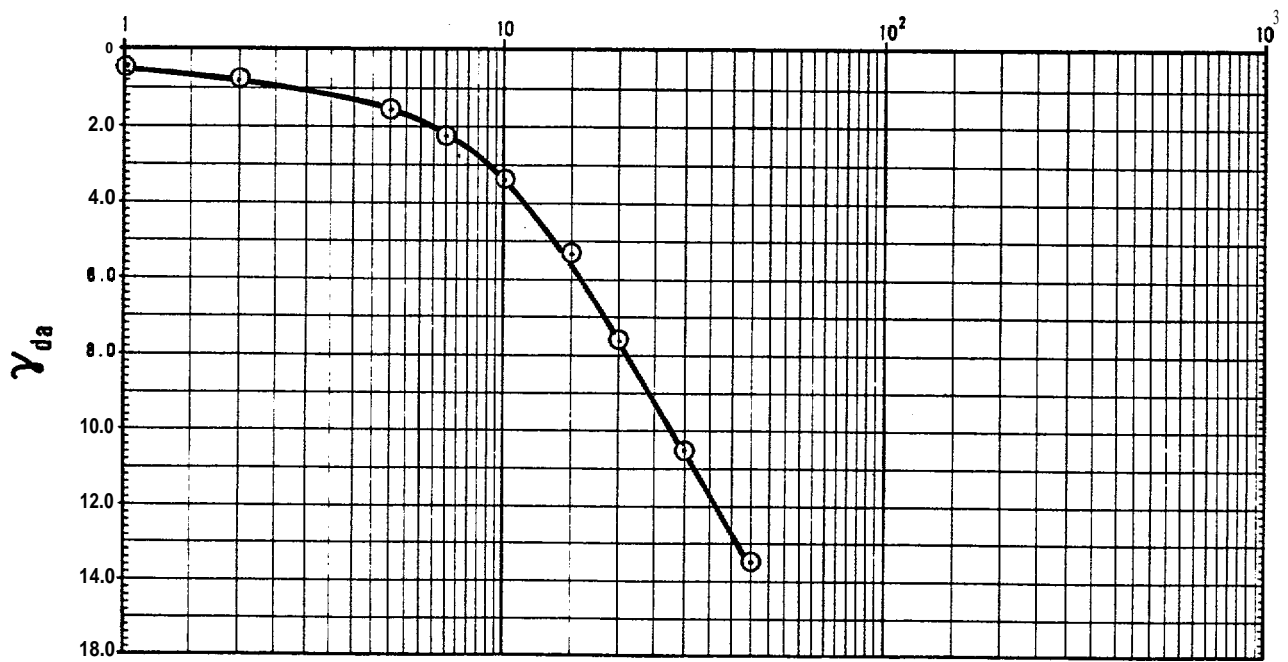
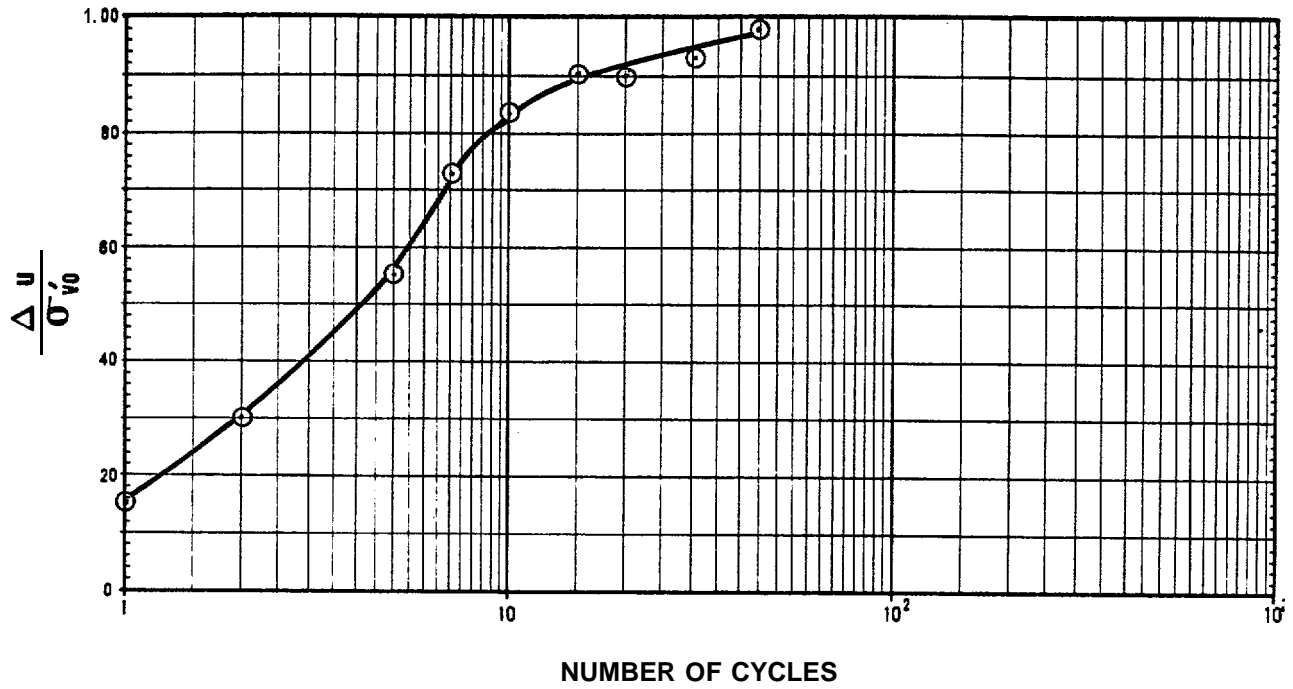
FIGURE II-15 LIQUEFACTION TEST RESULTS FROM GRAVITY CORE - SAMPLE 2-2



TEST NO.	SAMPLE NO.	SAMPLE DEPTH (cm)	σ'_{v0}	τ_1 / σ'_{v0}	SOIL TYPE
3	2	20-23	70	0.22	SM

*KN/M²

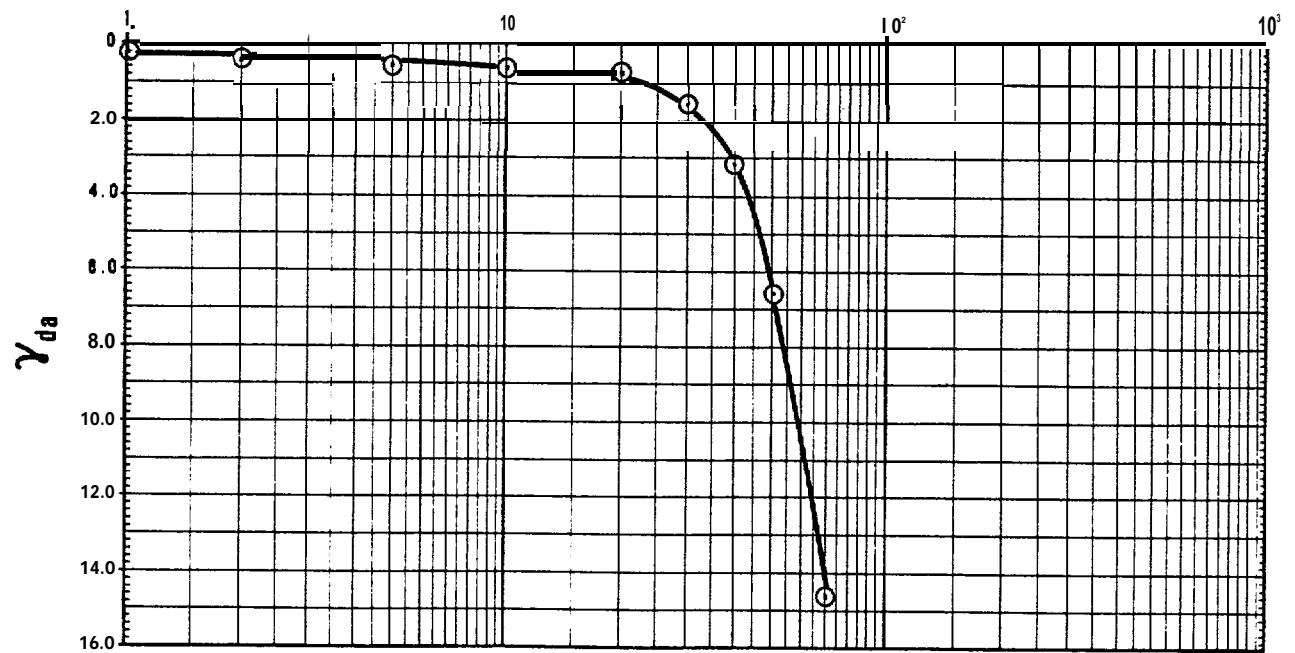
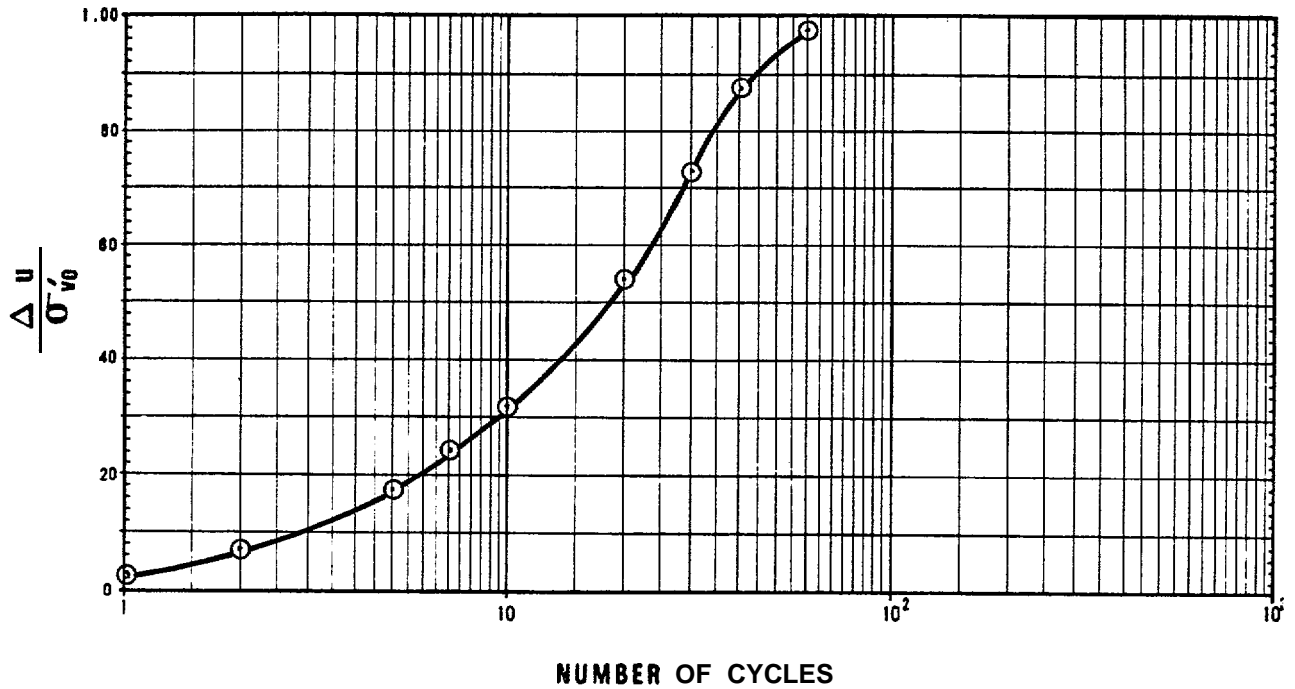
FIGURE II-16 LIQUEFACTION TEST RESULTS FROM GRAVITY CORE – SAMPLE 2-3



TEST NO.	SAMPLE NO.	SAMPLE DEPTH (cm)	σ'_{v0} •	τ_v / σ'_{v0}	SOIL TYPE
1	11	5 - 8	70	0.26	SM

● KN/M2

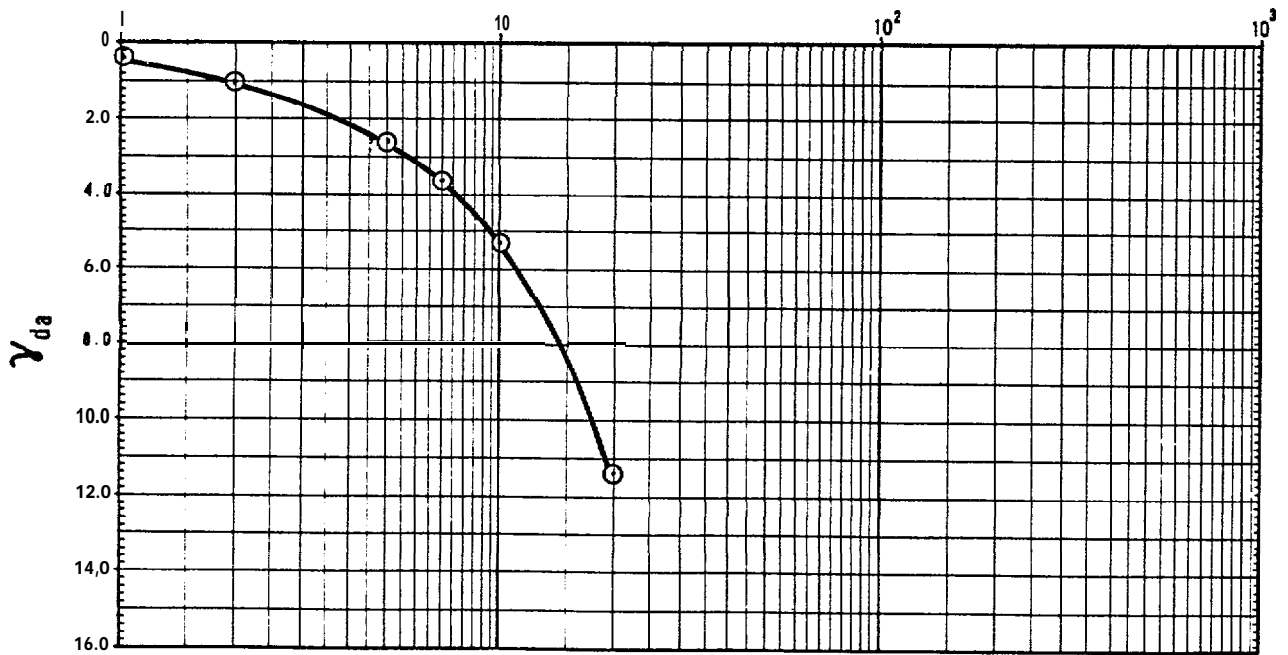
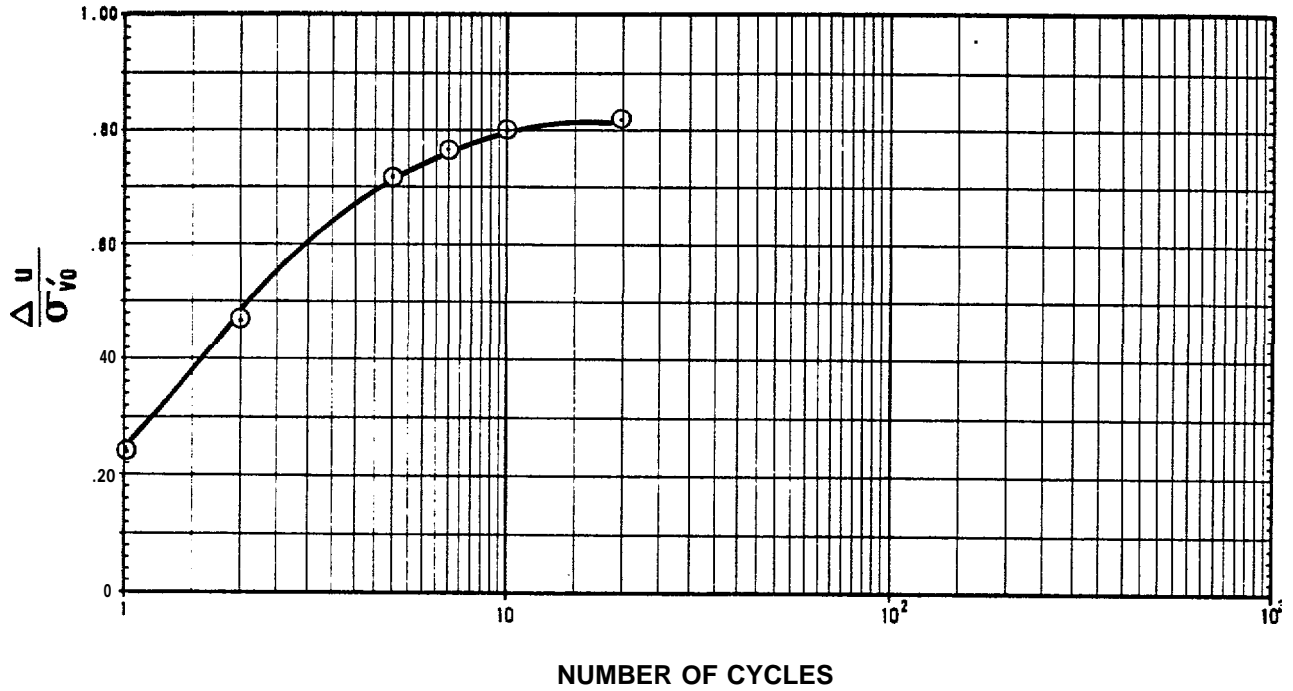
FIGURE II-17 LIQUEFACTION TEST RESULTS FROM GRAVITY CORE - SAMPLE 11-1



TEST NO.	SAMPLE NO.	SAMPLE DEPTH (cm)	σ'_{v0} ●	τ_1 / σ'_{v0}	SOIL TYPE
1	23	32-35	70	0.20	SM

● KN/M2

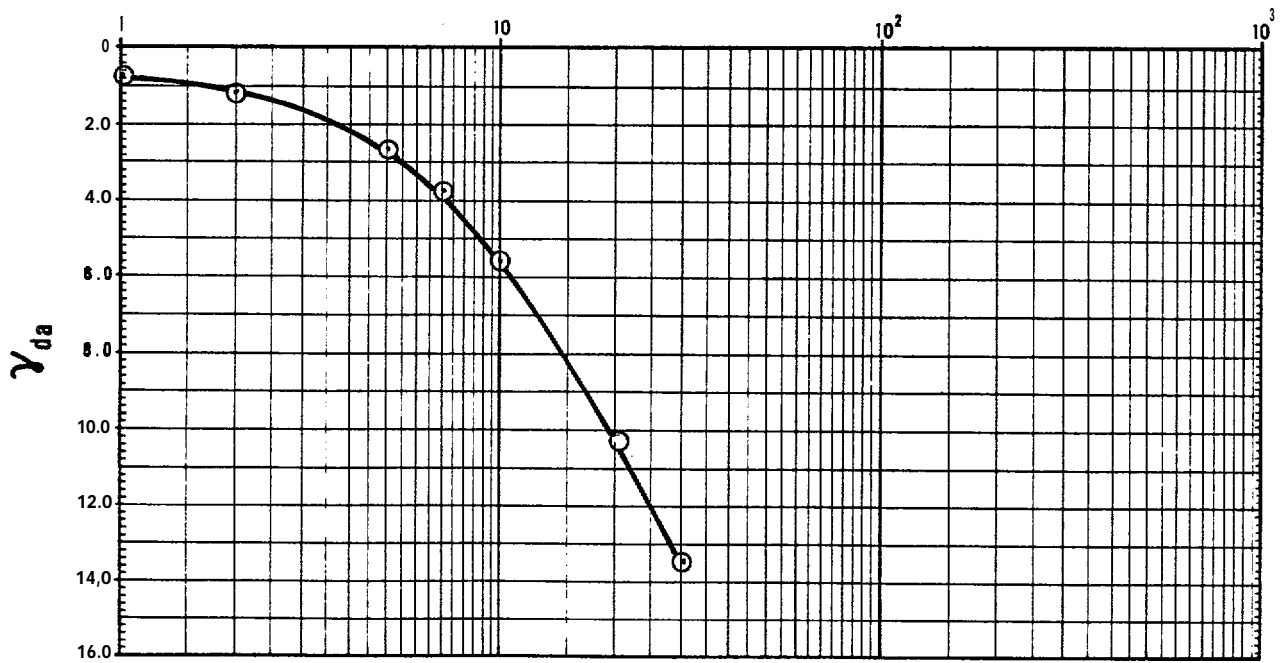
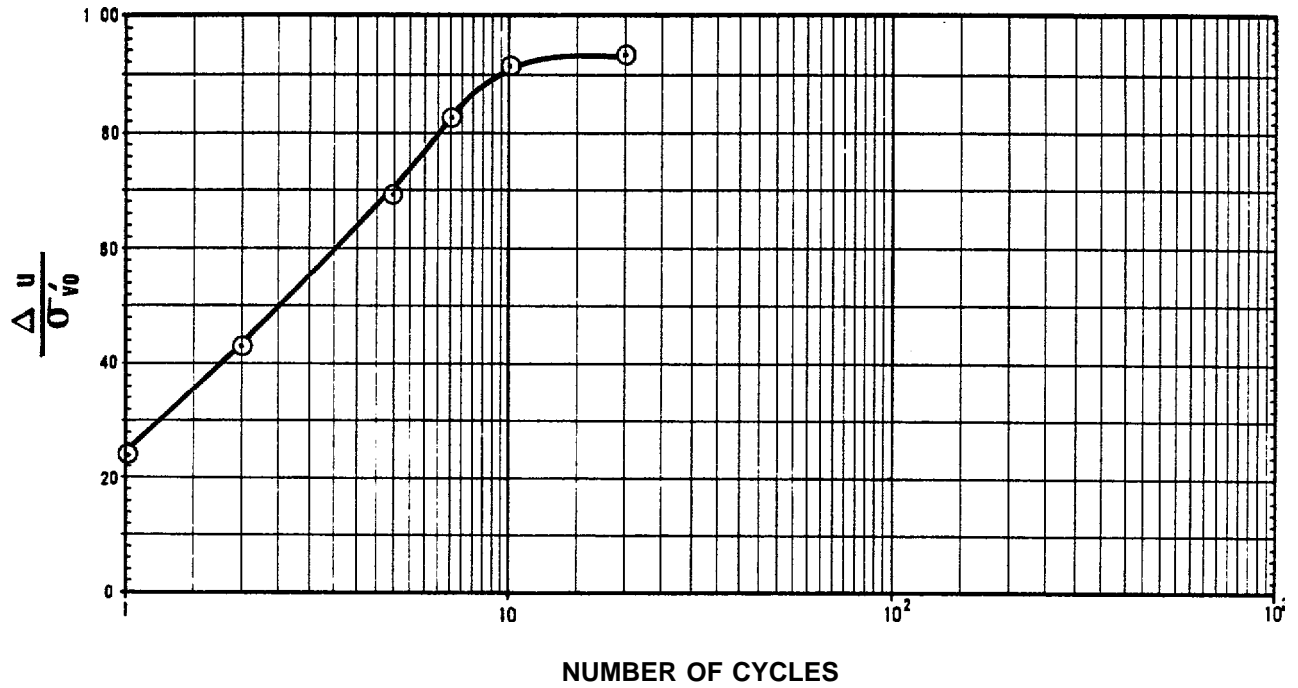
FIGURE II-18 LIQUEFACTION TEST RESULTS FROM GRAVITY CORE - SAMPLE 23-1



TEST NO.	SAMPLE NO.	SAMPLE DEPTH (cm)	σ'_{v0} •	τ_h/σ'_{v0}	SOIL TYPE
2	23	62-65	70	0.23	SM

*KN/M²

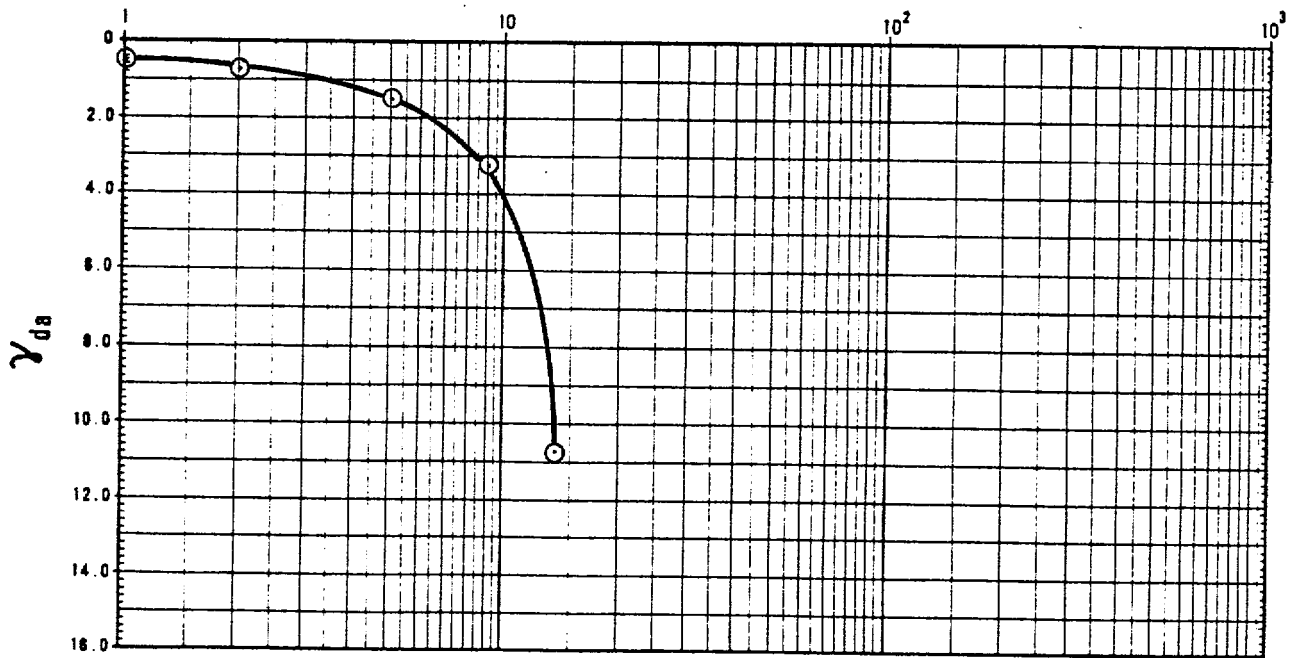
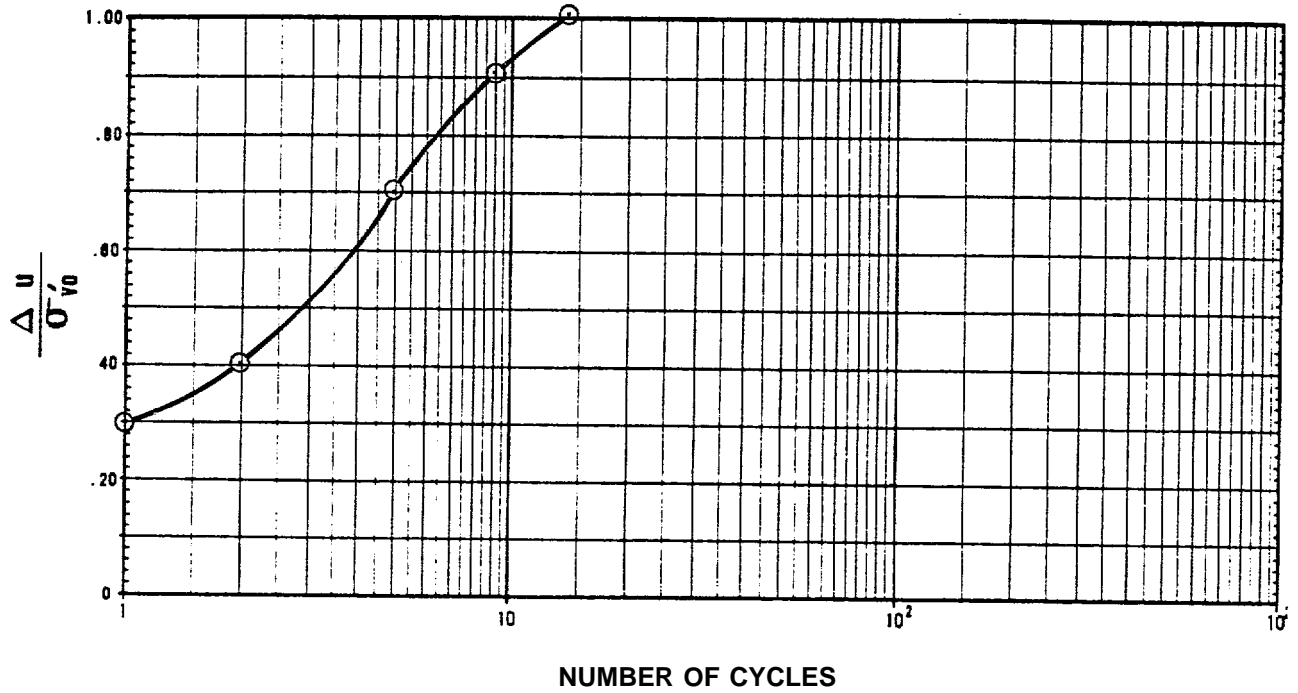
FIGURE II-19 LIQUEFACTION TEST RESULTS FROM GRAVITY CORE – SAMPLE 23-2



TEST NO.	SAMPLE NO.	SAMPLE DEPTH (cm)	σ'_{v0} *	τ_h/σ'_{v0}	SOIL TYPE
2	3	20-23	70	0.30	SM

*KN/M²

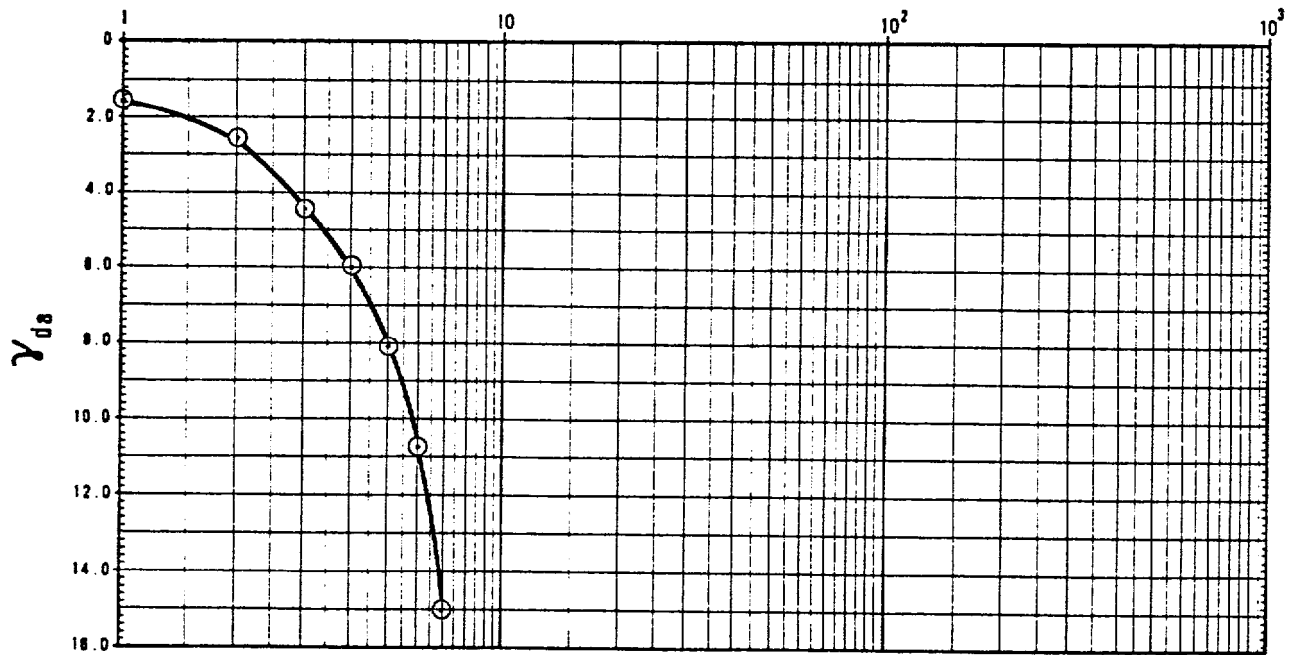
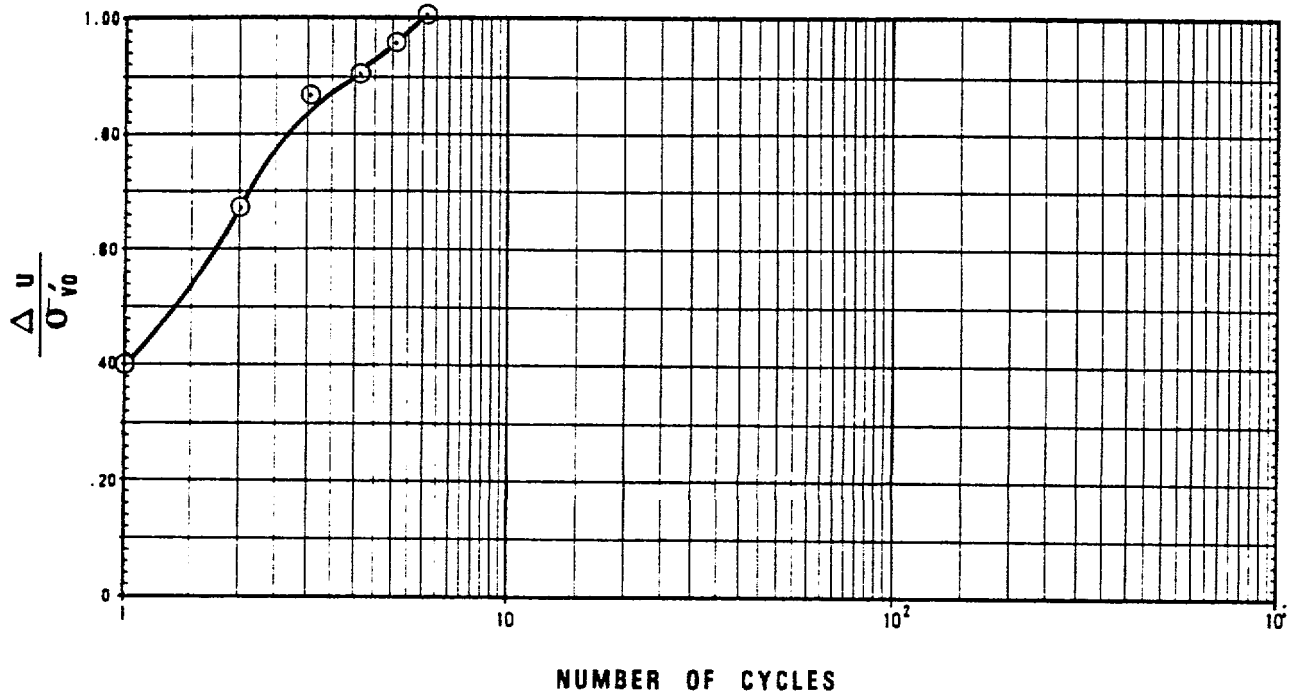
FIGURE II-20 LIQUEFACTION TEST RESULTS FROM GRAVITY CORE - SAMPLE 23-3



TEST NO.	SAMPLE NO,	SAMPLE TYPE	σ_v''	τ/σ_v	SOIL TYPE
1	9	RECONSTITUTED	70	0.24	SM

*KN/M²

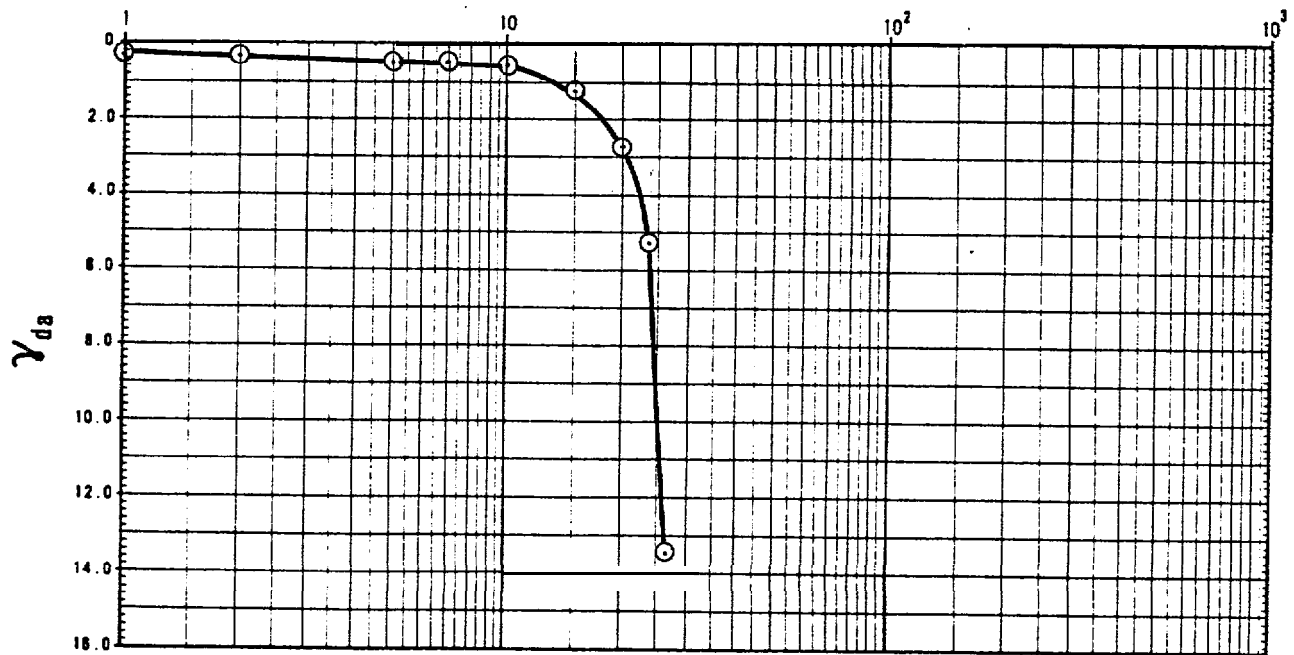
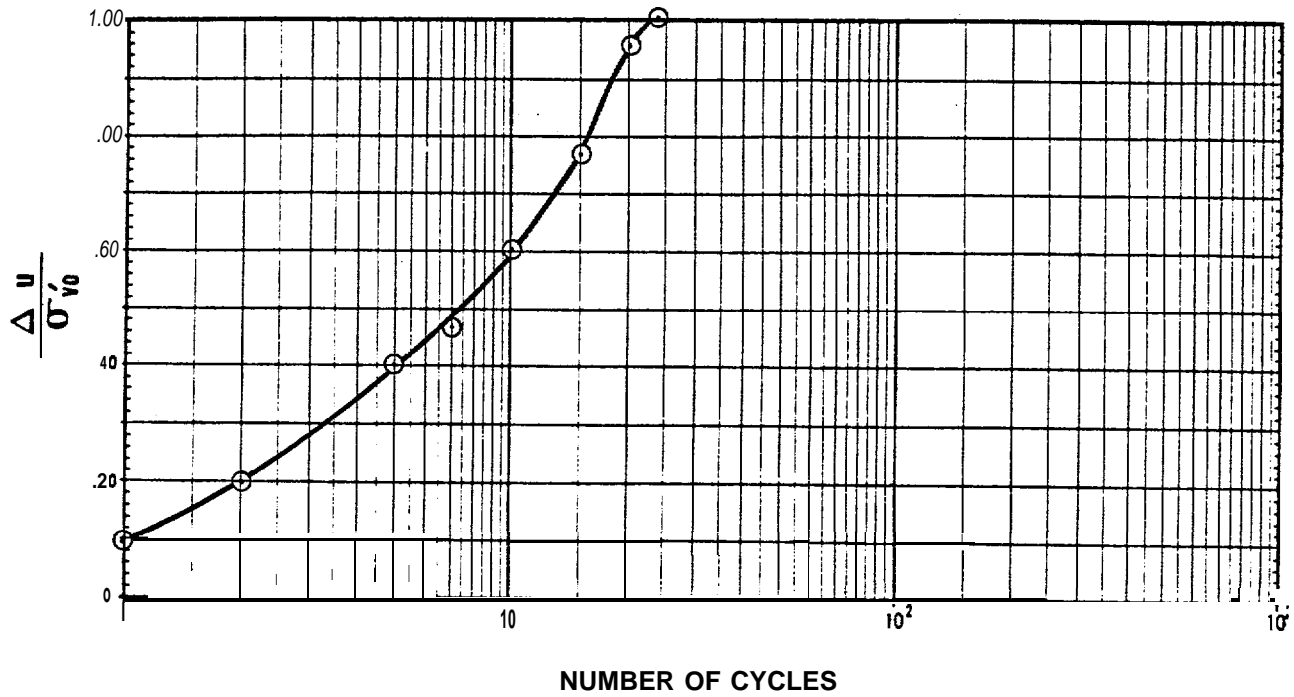
FIGURE 11-21 LIQUEFACTION TEST RESULTS FOR RECONSTITUTED SAMPLE 9-1



TEST NO.	SAMPLE NO.	SAMPLE TYPE	σ_v^*	τ/σ_v	SOIL TYPE
2	9	RECONSTITUTED	70	0.29	SM

● KN/M2

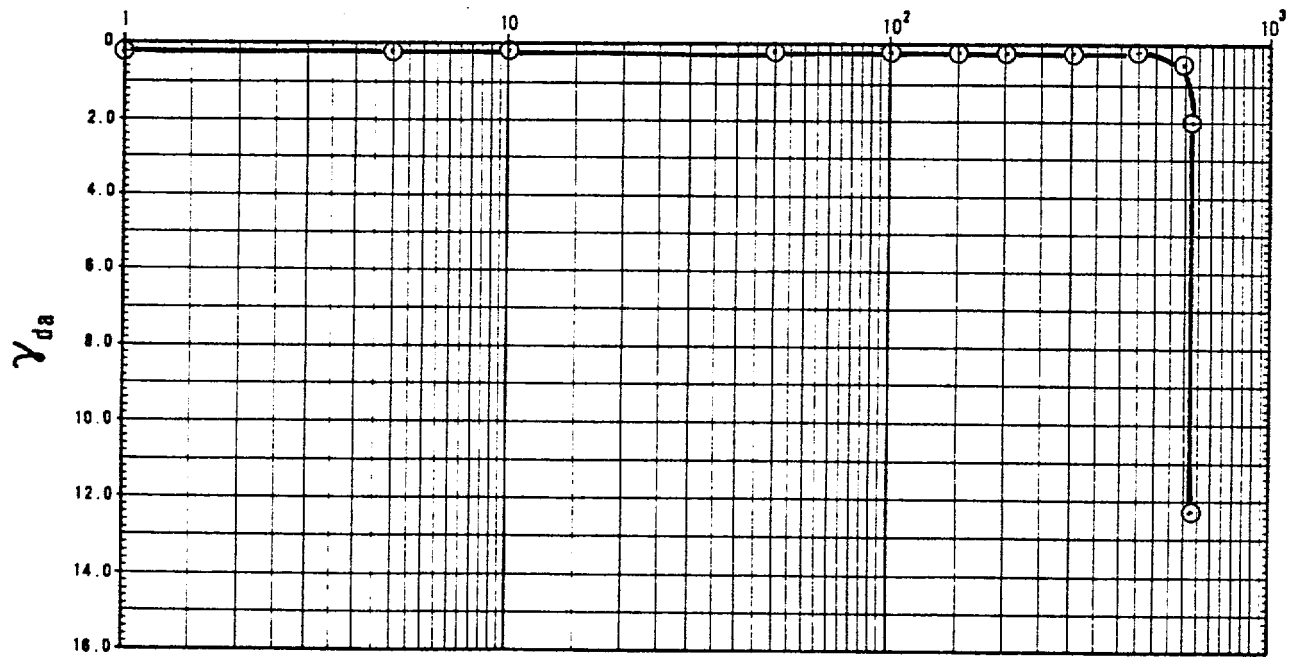
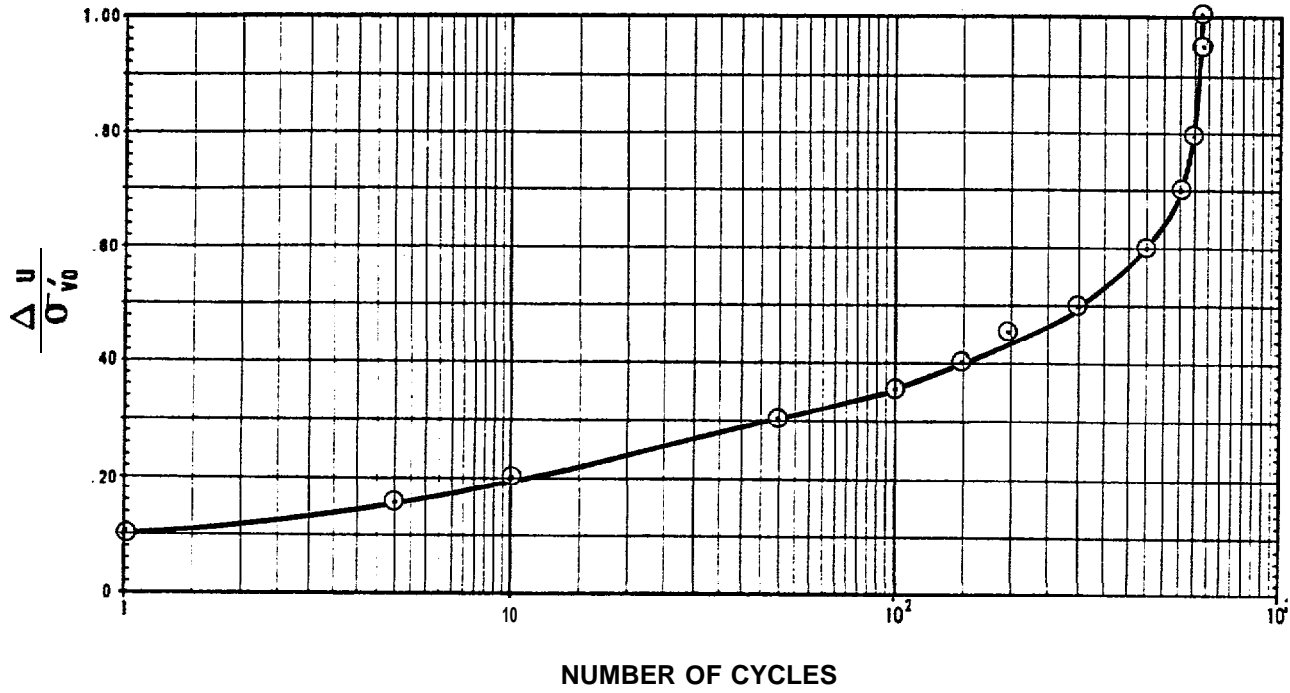
FIGURE II-22 LIQUEFACTION TEST RESULTS FOR RECONSTITUTED SAMPLE 9-2

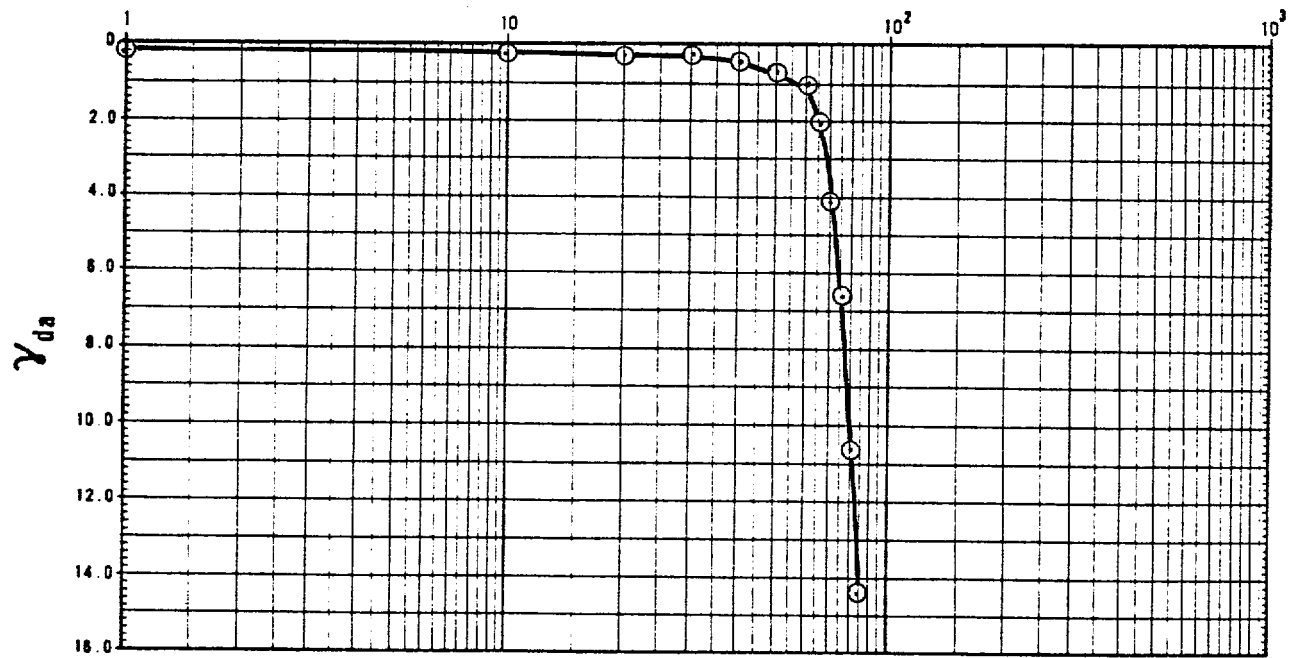
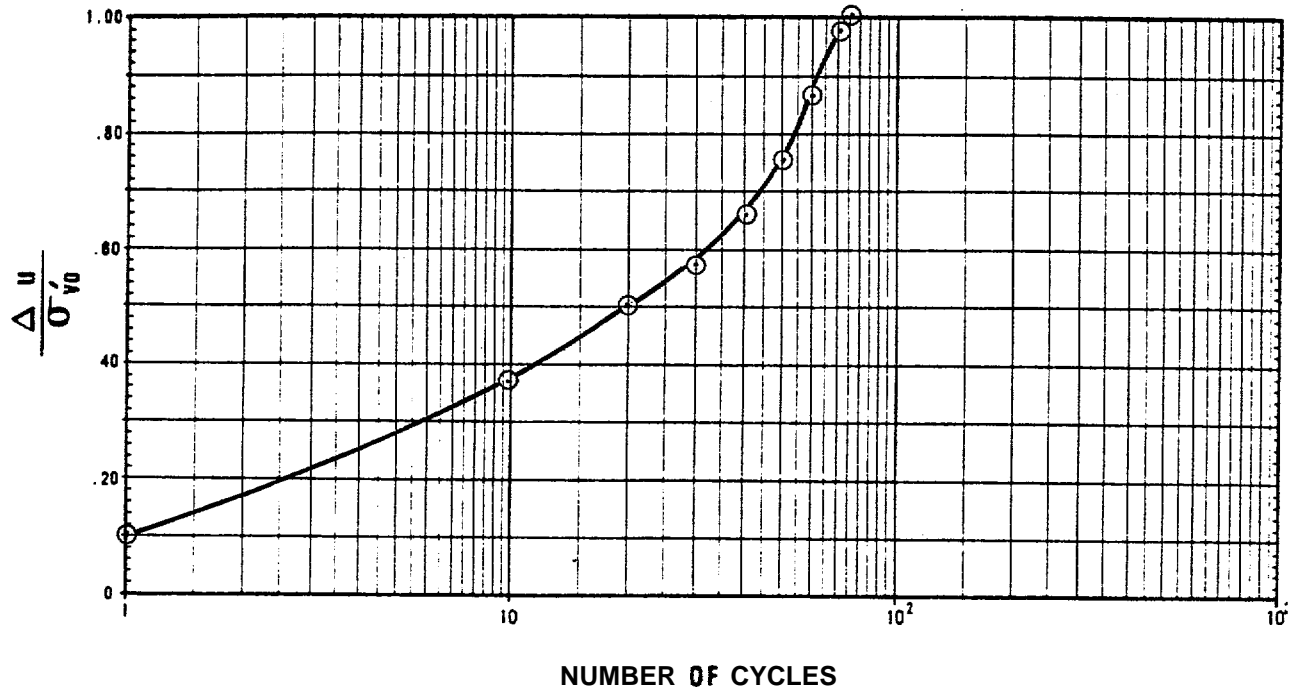


TEST NO.	SAMPLE NO.	SAMPLE TYPE	$\sigma'_{v'}$	τ/σ_v	SOIL TYPE
3	9	RECONSTITUTED	70	0.19	SM

● KNIM2

FIGURE II-23 LIQUEFACTION TEST RESULTS FOR RECONSTITUTED SAMPLE 9-3

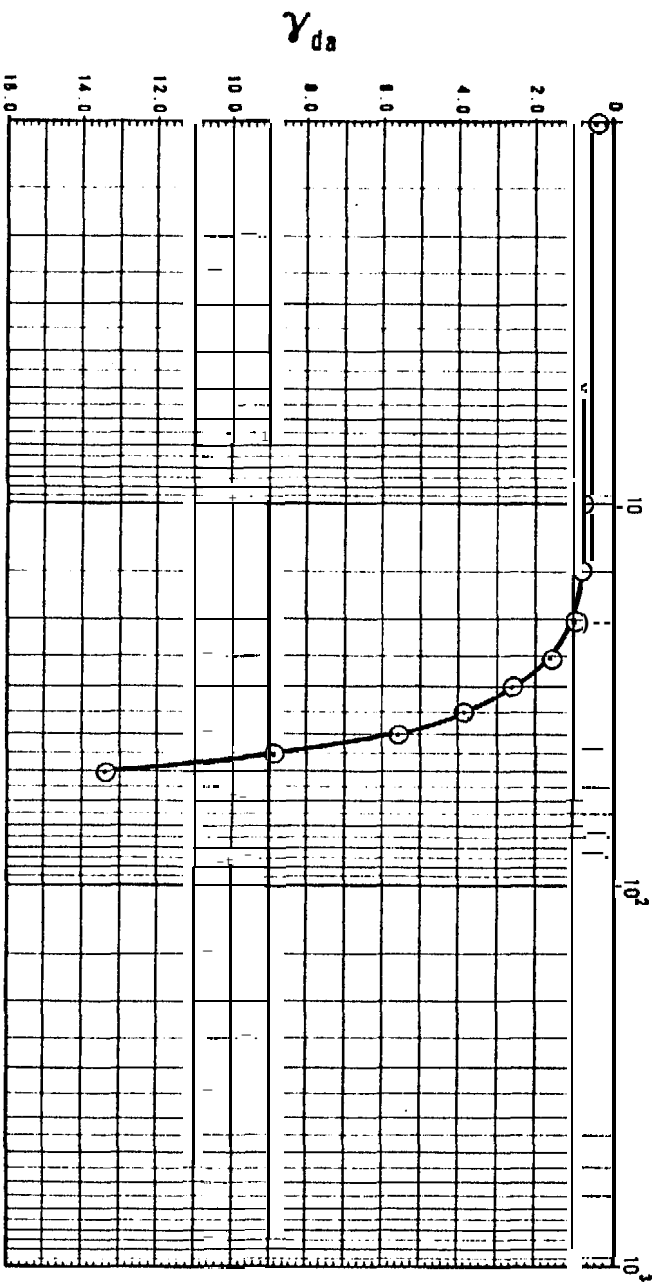
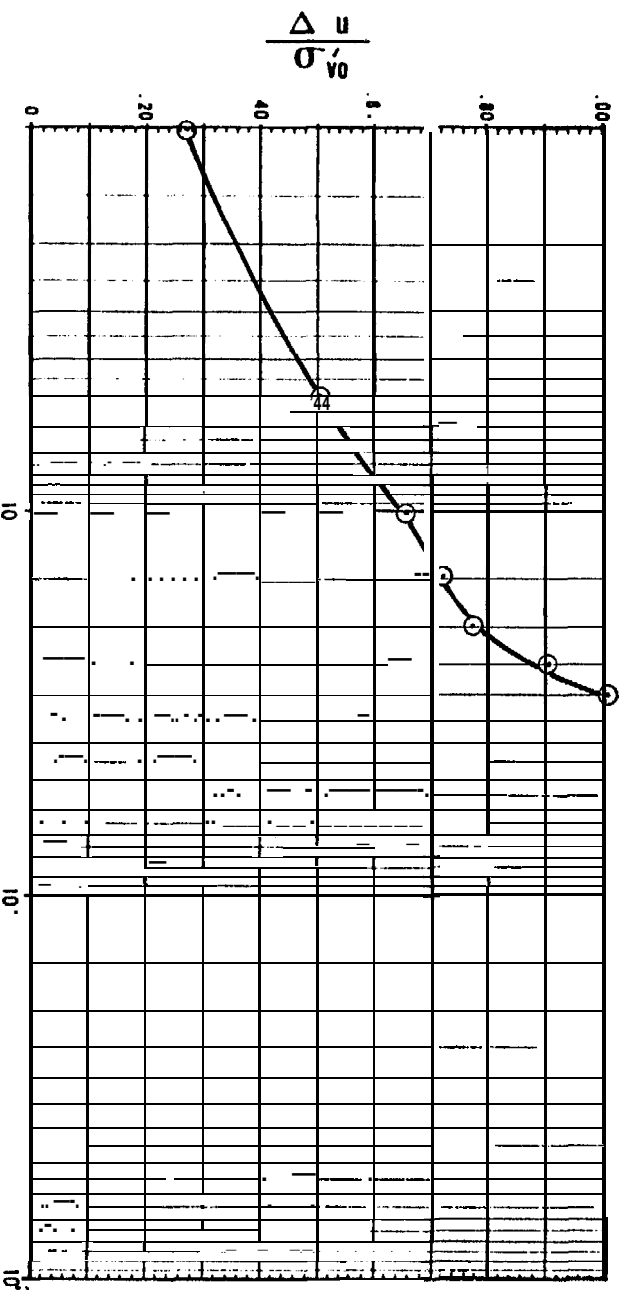




TEST NO.	SAMPLE NO.	SAMPLE TYPE	$\sigma_{v\bullet}$	τ/σ_v	SOIL TYPE
1	24	RECONSTITUTED	70	0.17	SP-SM

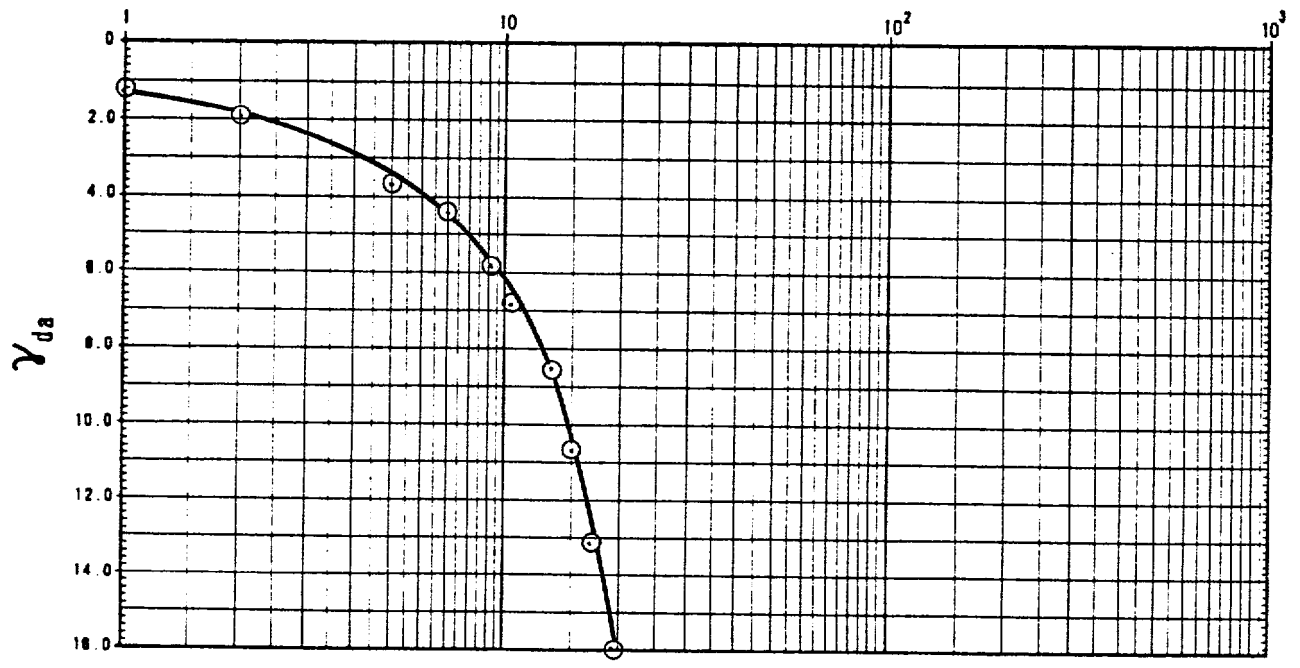
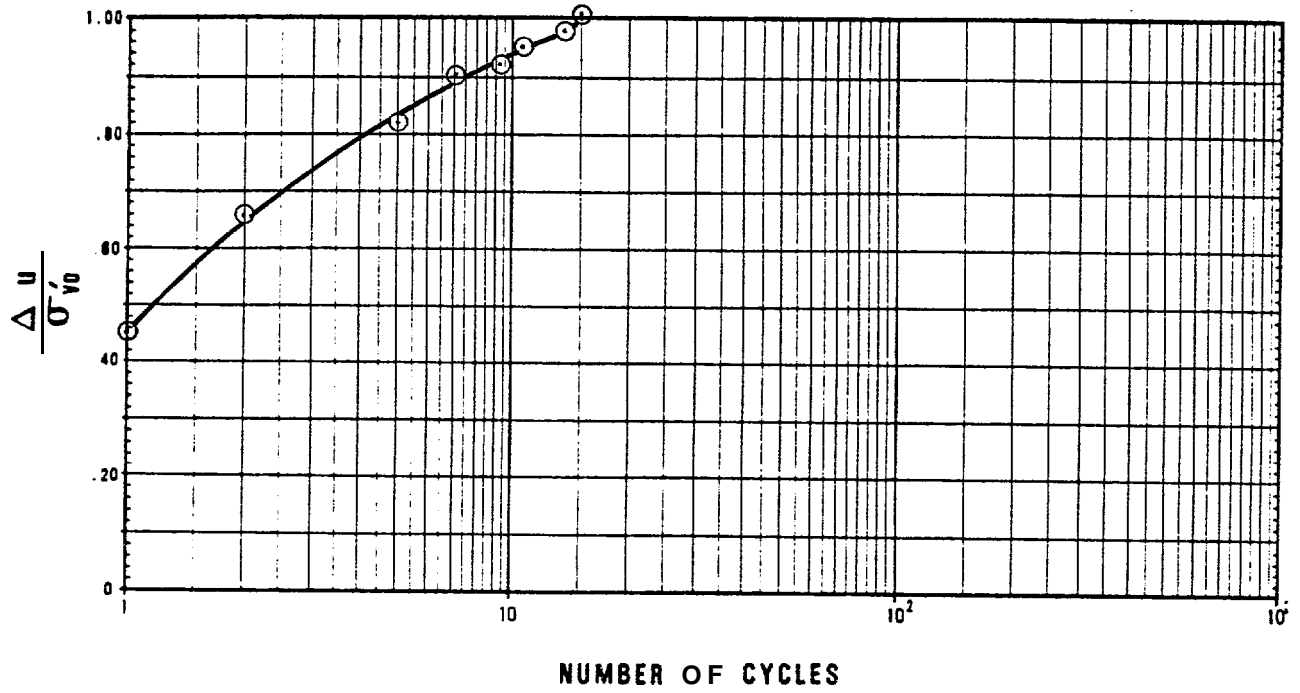
● KN/M2

FIGURE II-25 LIQUEFACTION TEST RESULTS FOR RECONSTITUTED SAMPLE 24-1



TEST NO.	SAMPLE NO.	SAMPLE TYPE	σ'_v	T/σ'_v	SOIL TYPE
2	24	RECONSTITUTED	70	0.21	SP-SM

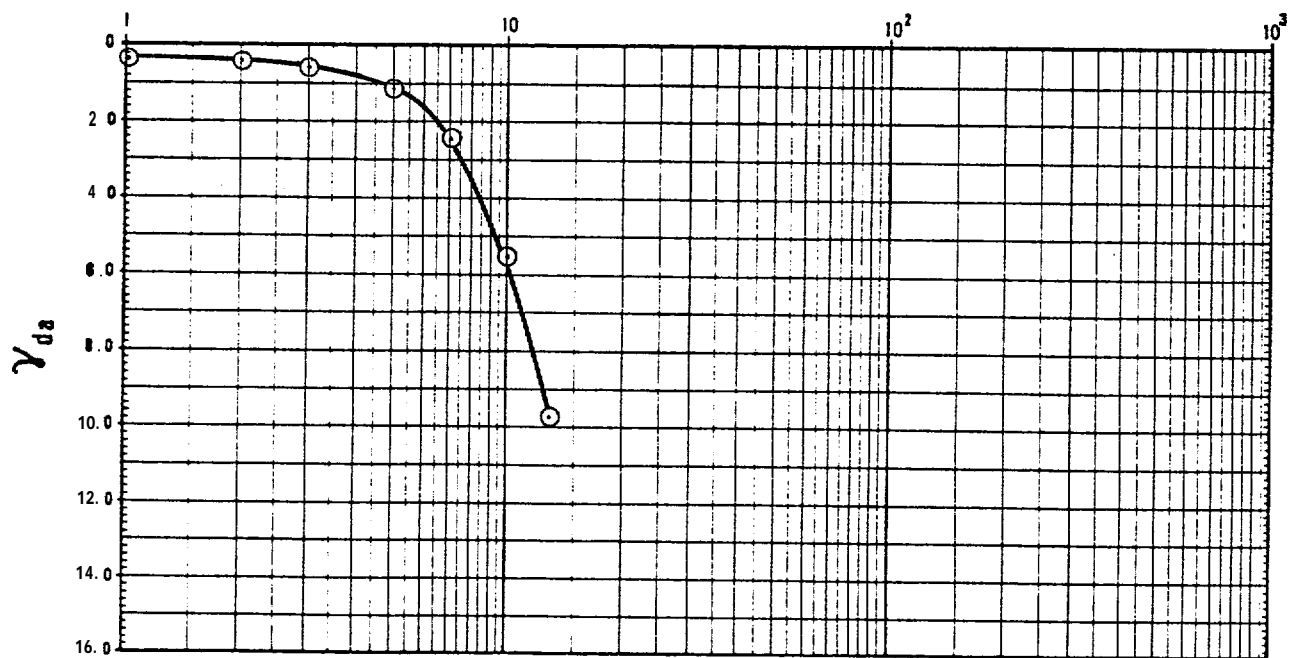
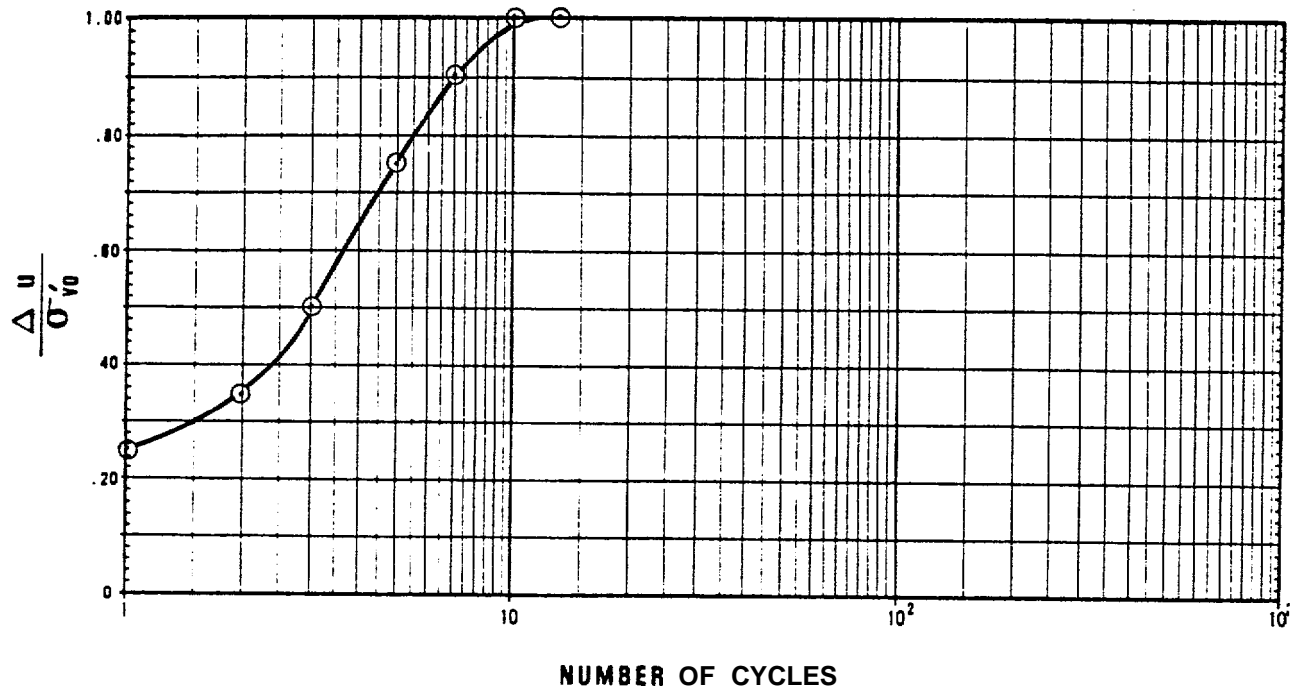
FIGURE 11-26 L QUAEFACTION TEST RESULTS FOR RECONSTITUTED M 24-2



TEST NO.	SAMPLE NO.	SAMPLE TYPE	σ'_{v0} *	τ/σ_v	SOIL TYPE
3	24	RECONSTITUTED	70	0.30	SP-SM

● KN/M2

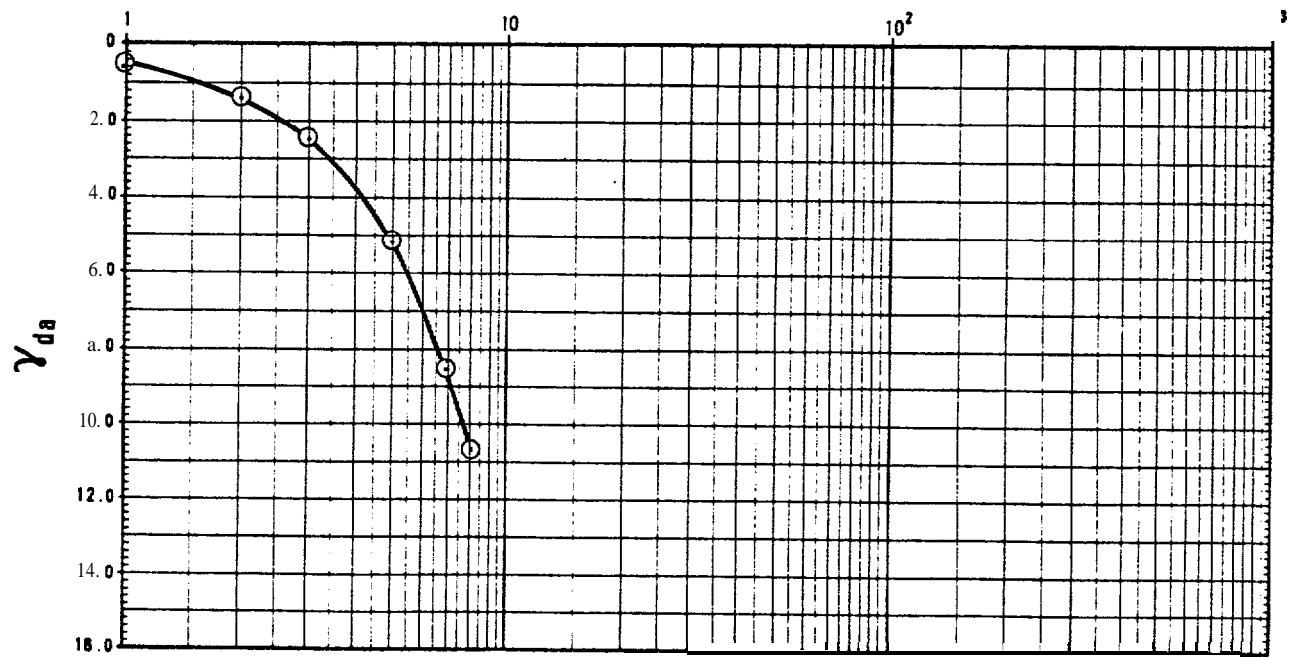
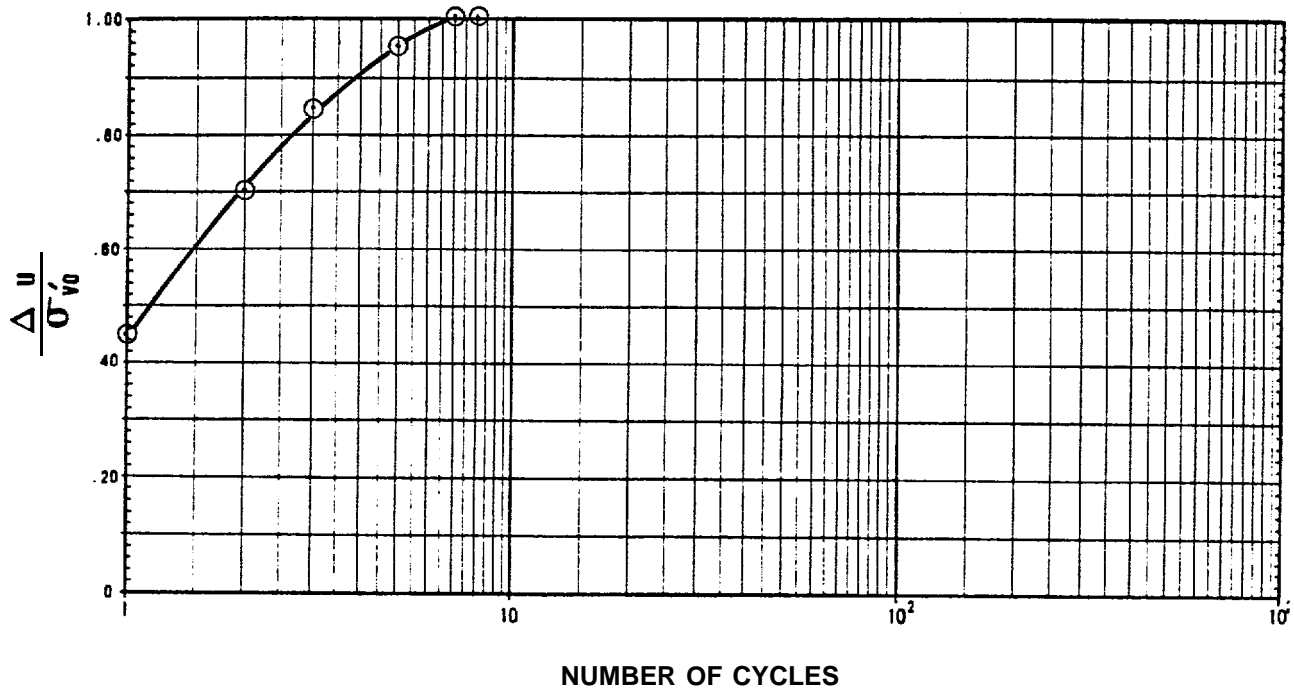
FIGURE II-27 LIQUEFACTION TEST RESULTS FOR RECONSTITUTED SAMPLE 24-3



TEST NO.	SAMPLE NO.	SAMPLE TYPE	σ_v^*	τ/σ_v	SOIL TYPE
3	43	RECONSTITUTED	70	0.22	SP

● KN/M2

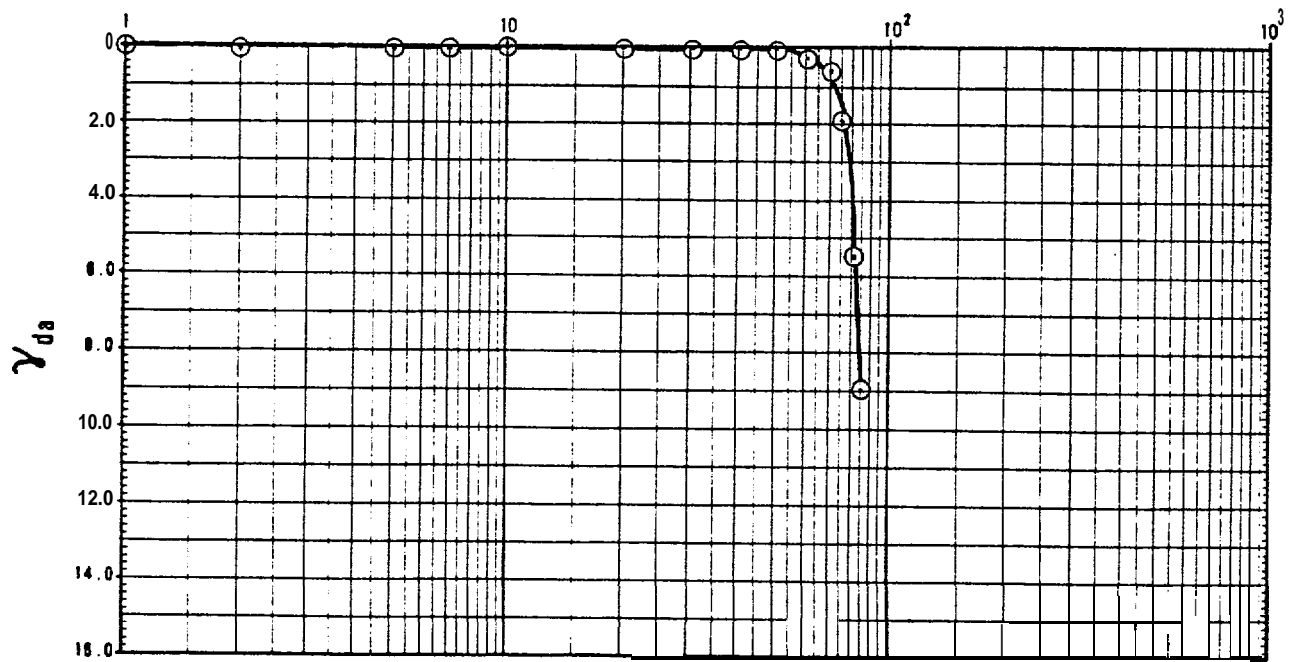
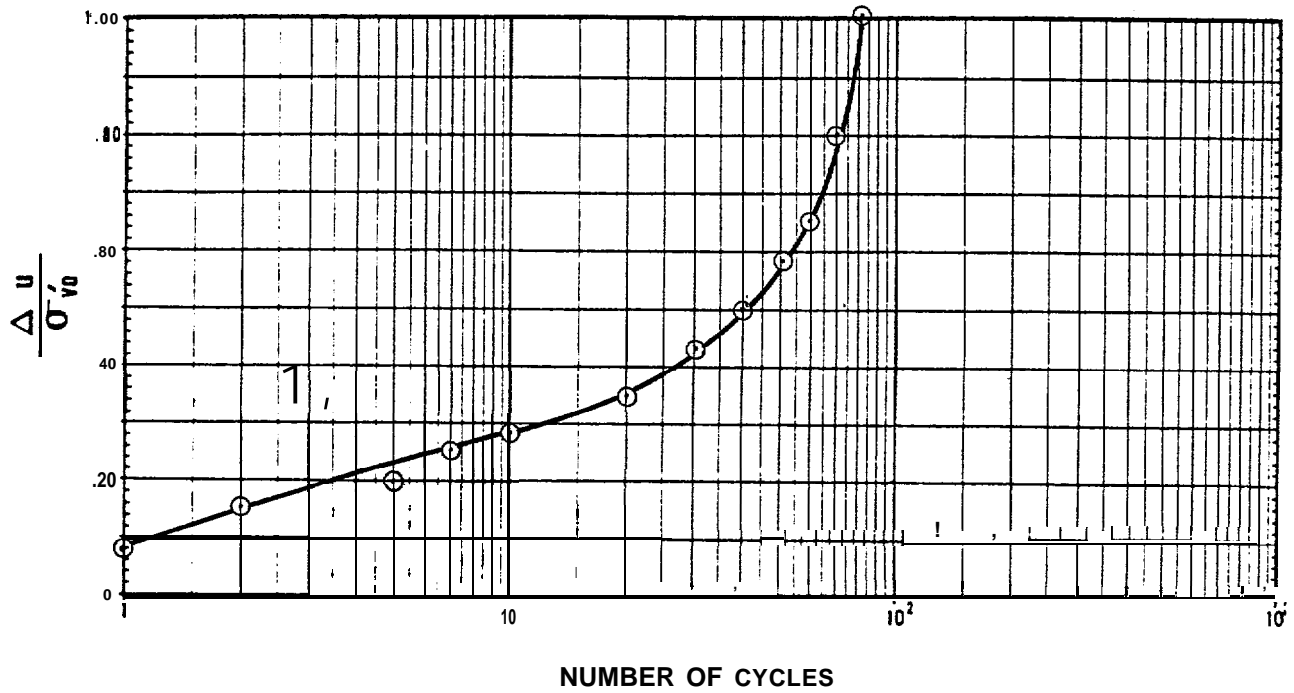
FIGURE II-28 LIQUEFACTION TEST RESULTS FOR RECONSTITUTED SAMPLE 43-3



TEST NO.	SAMPLE NO.	SAMPLE TYPE	σ_v^*	τ/σ_v	SOIL TYPE
4	43	RECONSTITUTED	70	0.29	SP

•KN/M²

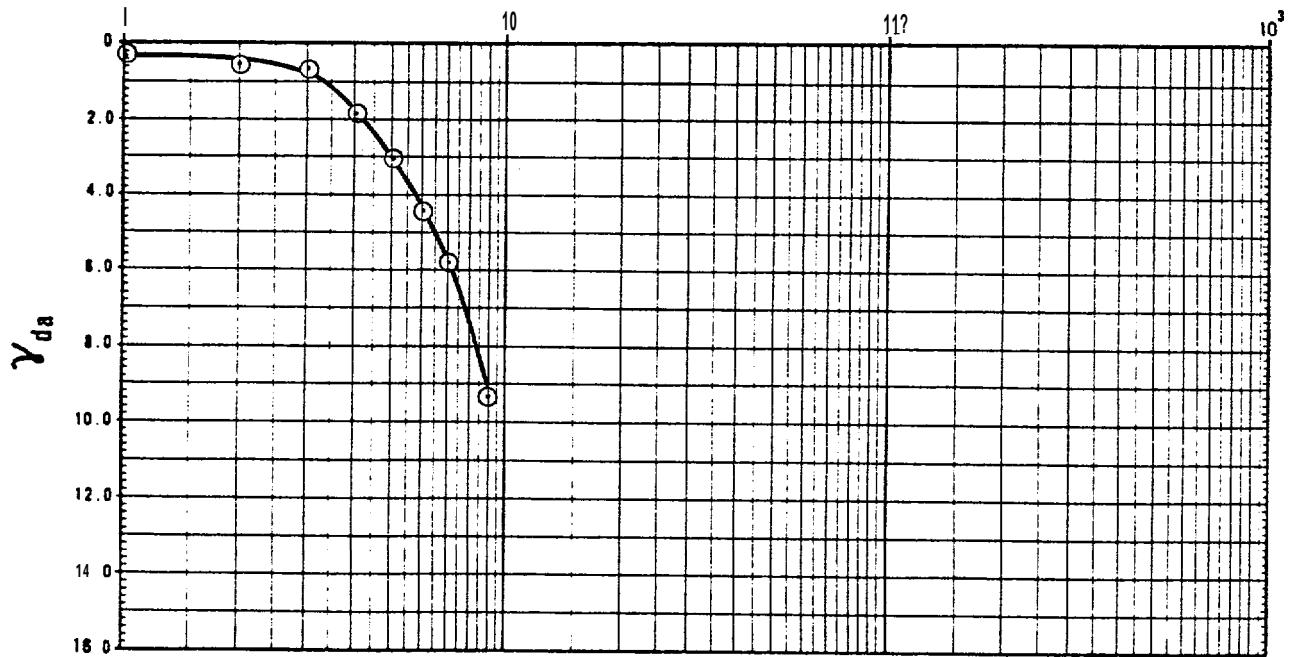
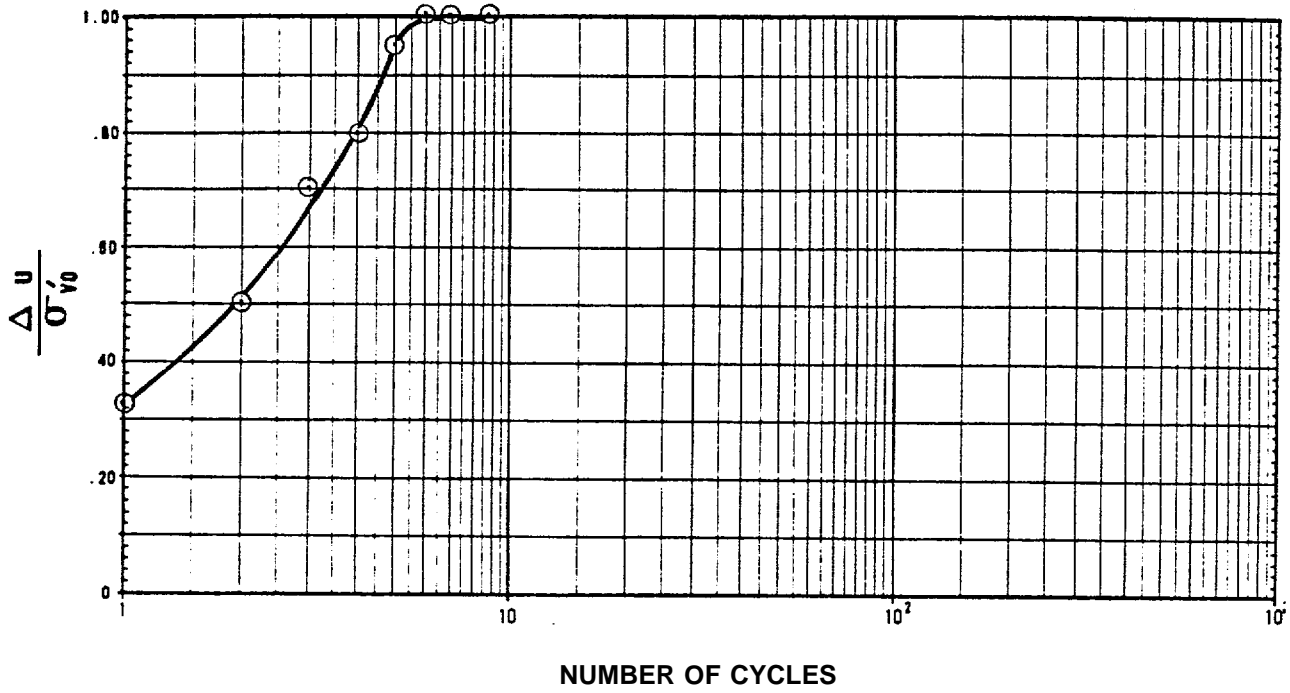
FIGURE II-29 LIQUEFACTION TEST RESULTS FOR RECONSTITUTED SAMPLE 43-4



TEST NO.	SAMPLE NO.	SAMPLE TYPE	σ_v	τ/σ_v	SOIL TYPE
5	43	RECONSTITUTED	70	0.17	SP

*KN/M²

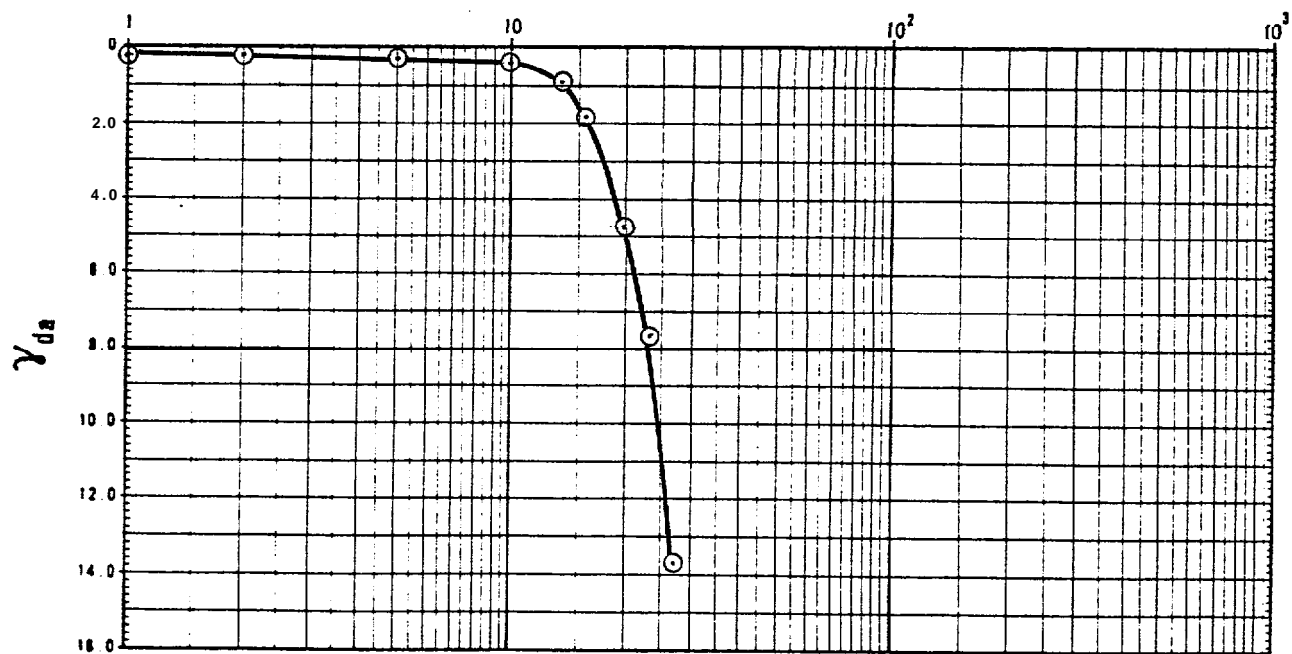
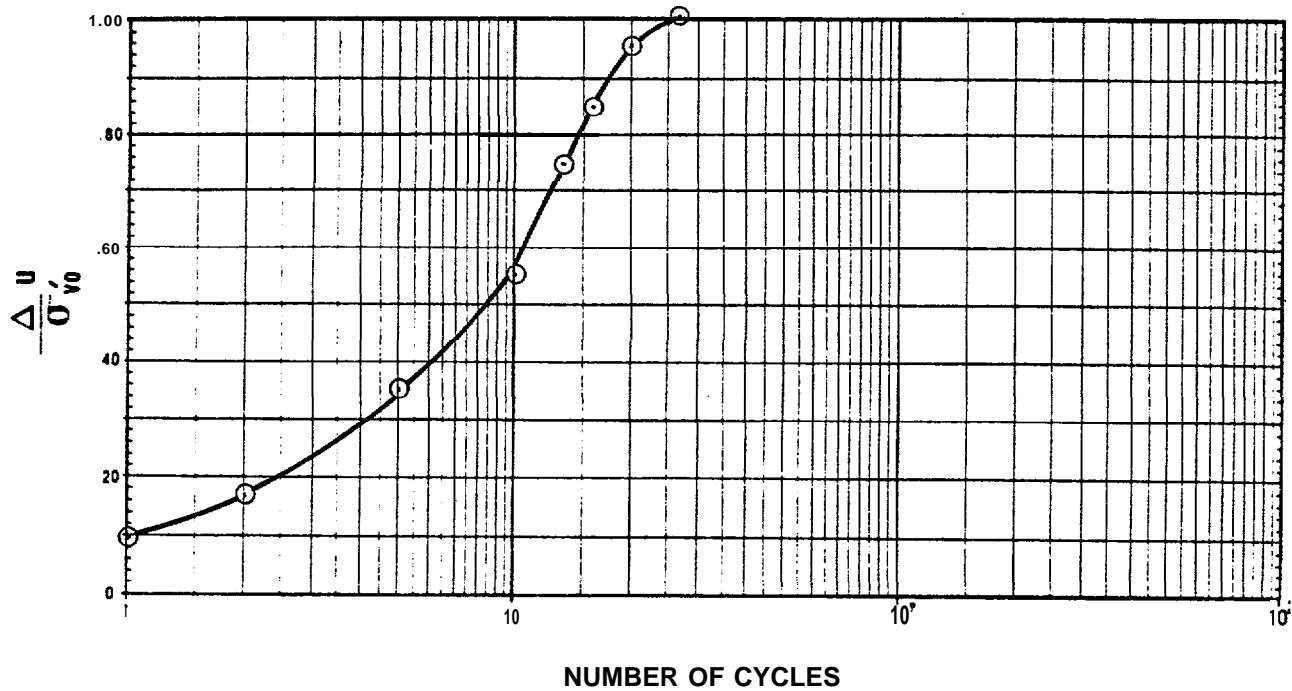
FIGURE II-30 LIQUEFACTION TEST RESULTS FOR RECONSTITUTED SAMPLE 43-5



TEST NO.	SAMPLE NO,	SAMPLE TYPE	σ_v^*	τ/σ_v	SOIL TYPE
1	57	RECONSTITUTED	70	0.21	SP

*KN/M²

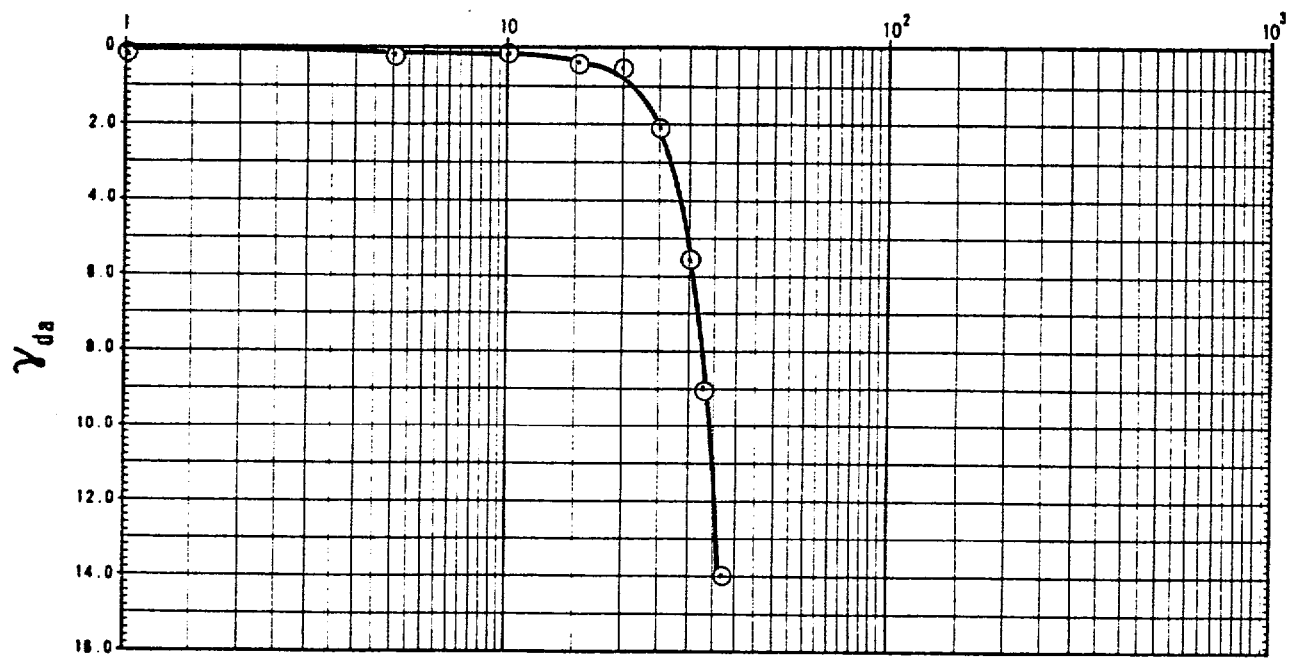
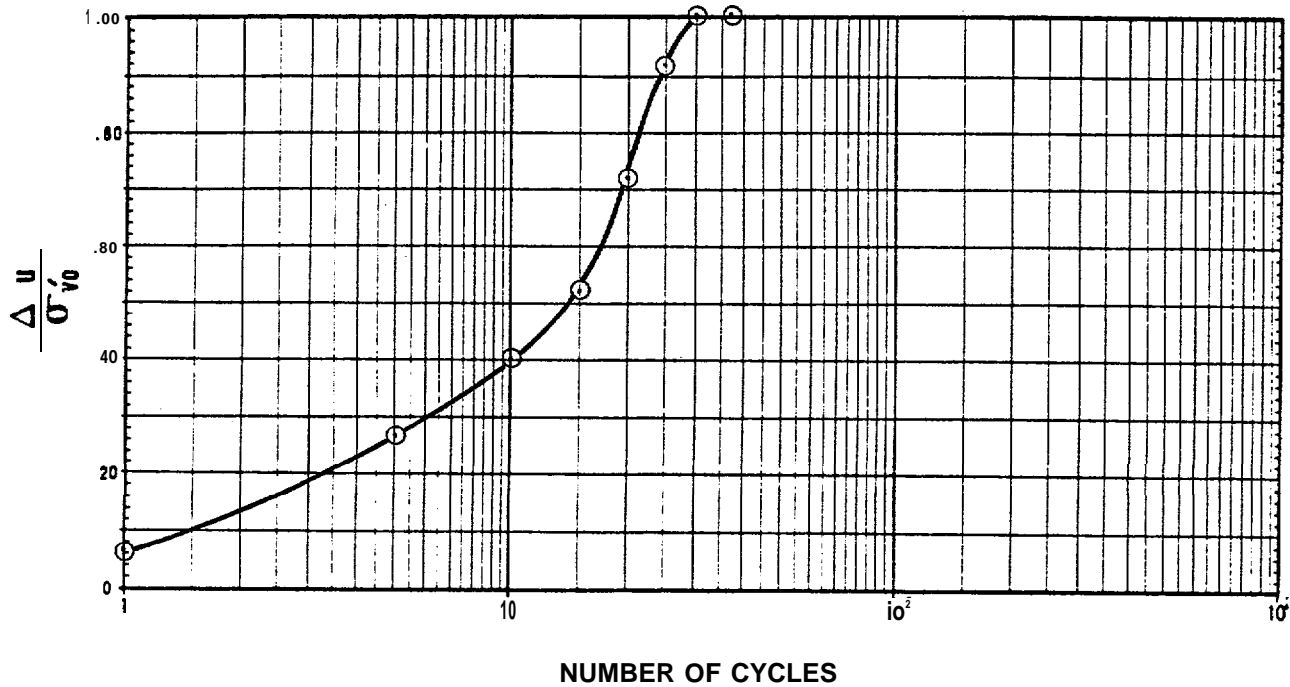
FIGURE II-31 LIQUEFACTION TEST RESULTS FOR RECONSTITUTED SAMPLE 57-1



TEST NO.	SAMPLE NO.	SAMPLE TYPE	$\sigma_{v\cdot}$	τ/σ_v	SOIL TYPE
2	57	RECONSTITUTED	70	0.17	SP

● KN/M2

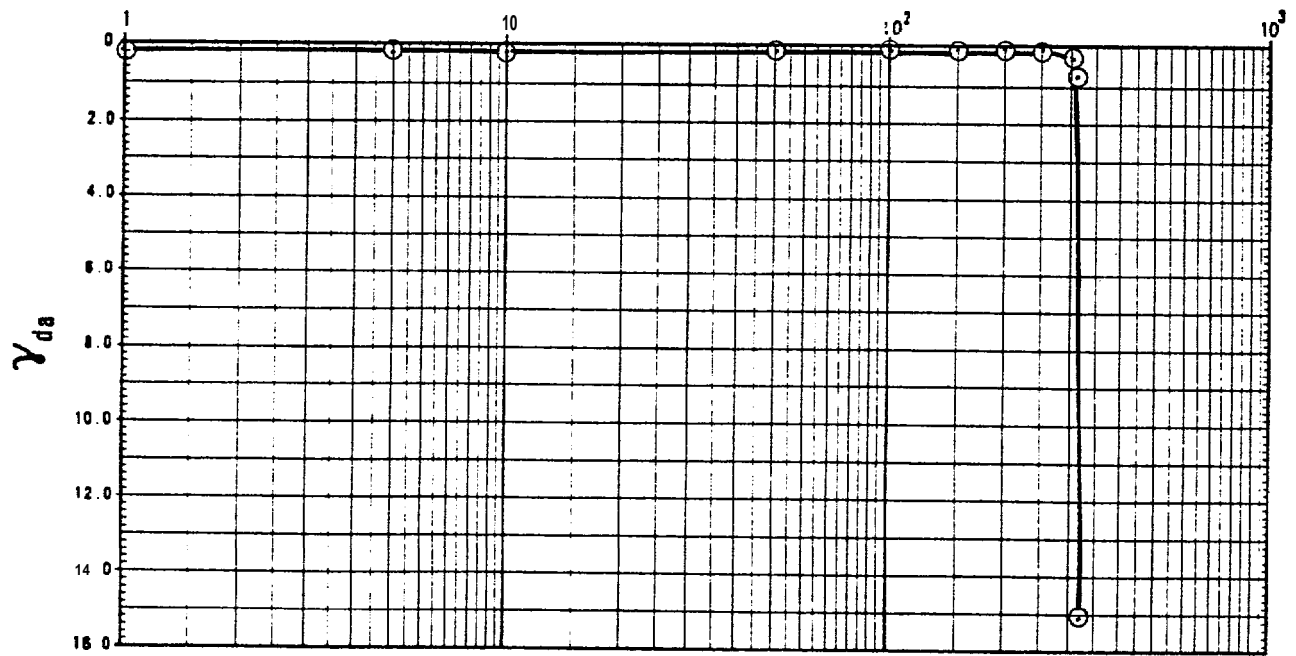
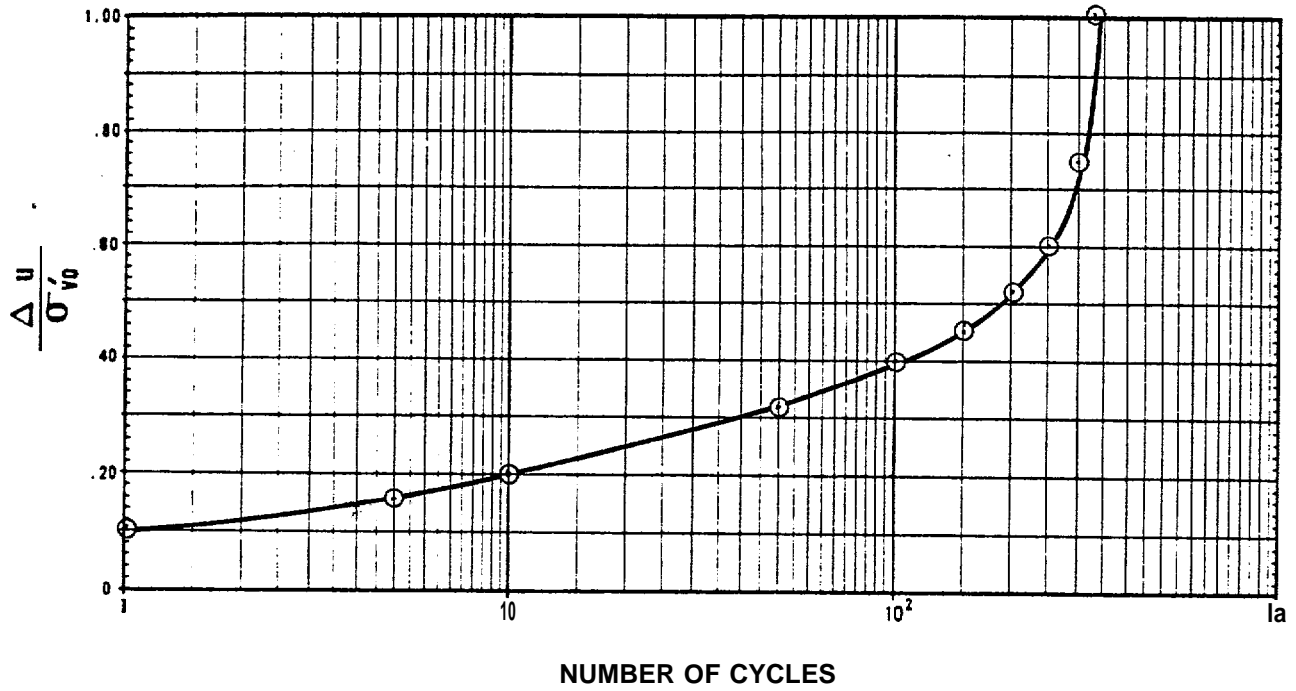
FIGURE II-32 LIQUEFACTION TEST RESULTS FOR RECONSTITUTED SAMPLE 57-2



TEST NO.	SAMPLE NO.	SAMPLE TYPE	σ_v'	τ/σ_v	SOIL TYPE
3	57	RECONSTITUTED	70	0.14	s?

● KNIM2

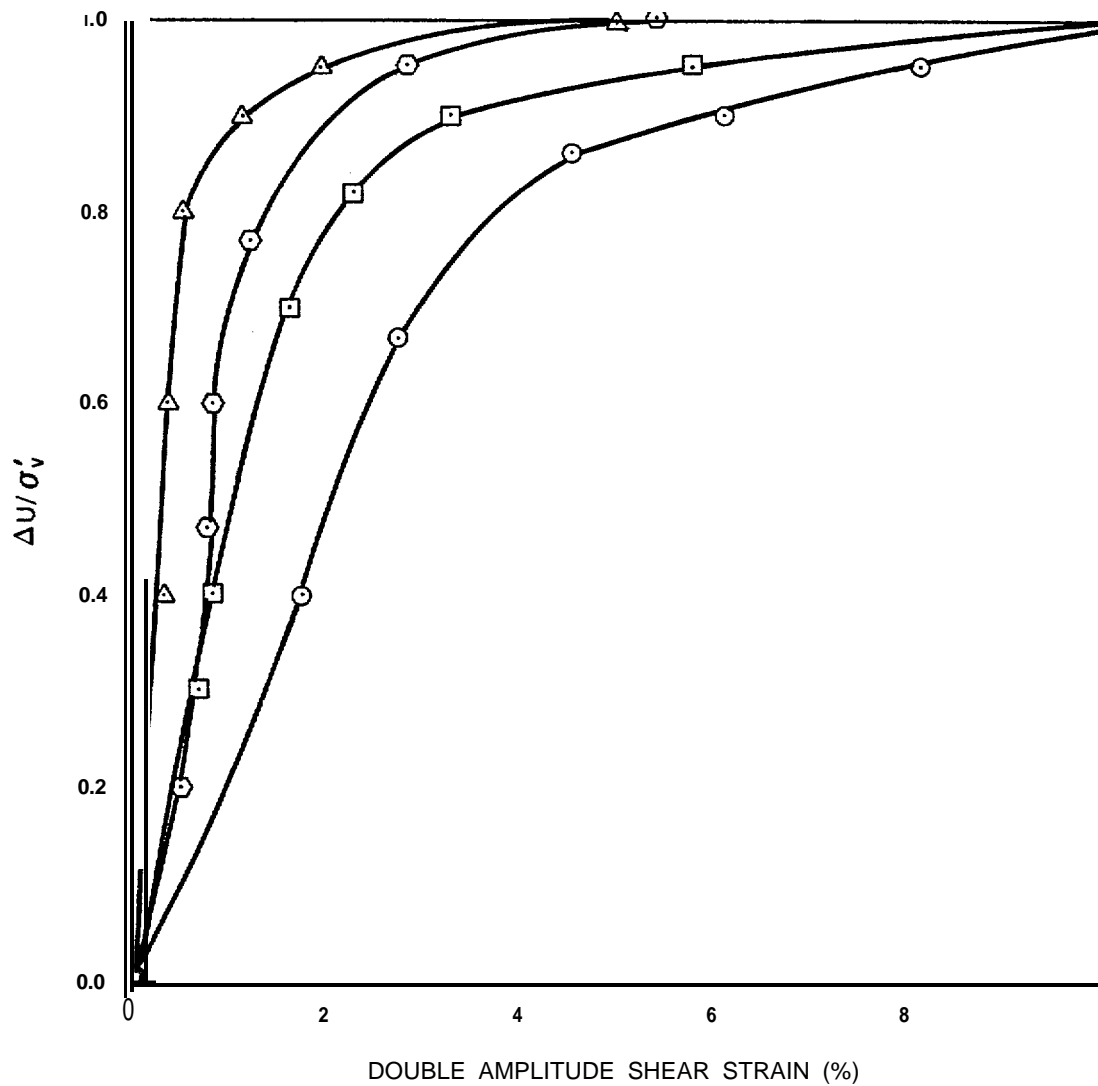
FIGURE II-33 LIQUEFACTION TEST RESULTS FOR RECONSTITUTED SAMPLE 57-3



TEST NO.	SAMPLE NO.	SAMPLE TYPE	σ'_{v0}	τ/σ_v	SOIL TYPE
4	57	RECONSTITUTED	70	0,13	SP

*KN/M²

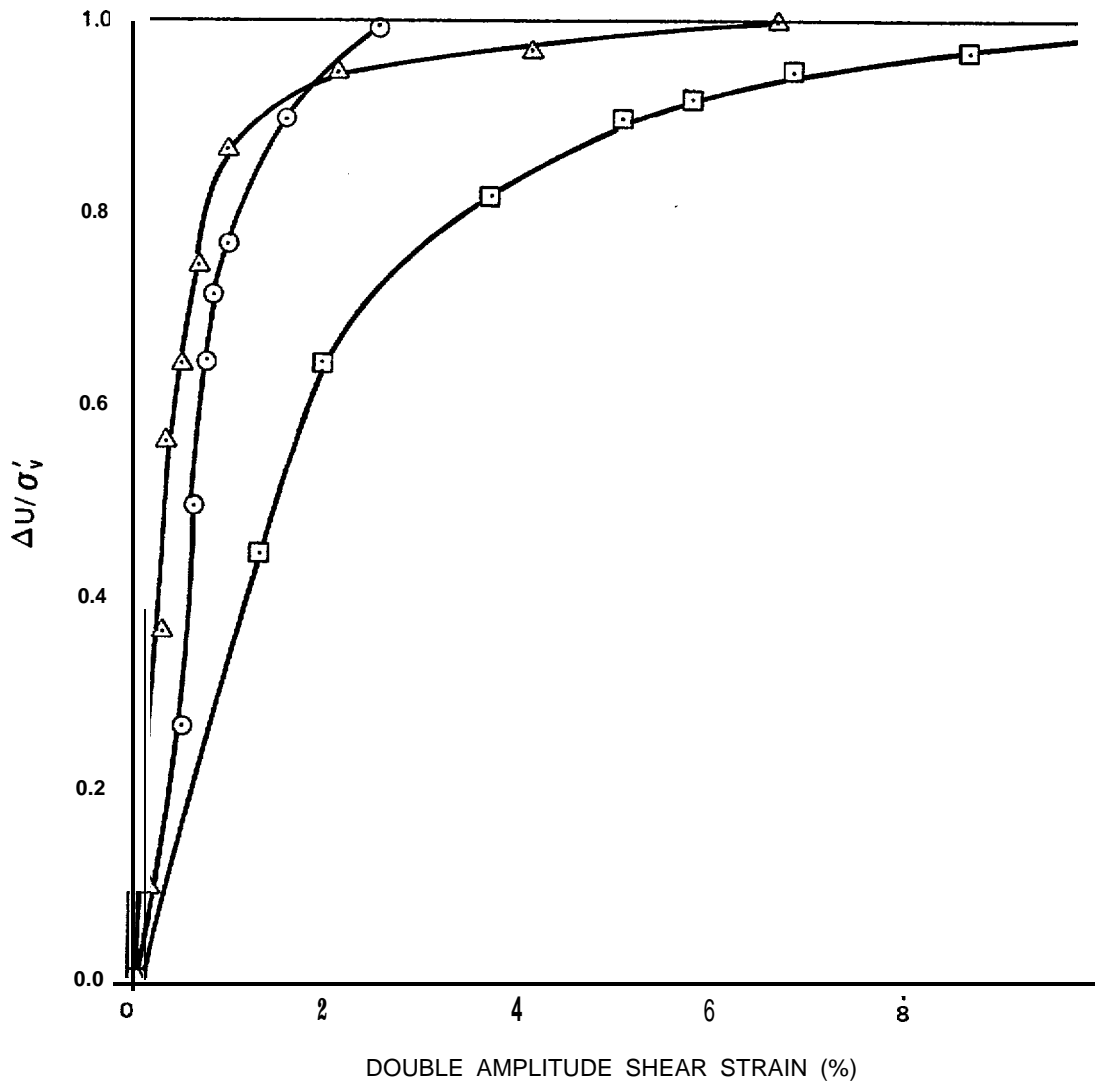
FIGURE II-34 LIQUEFACTION TEST RESULTS FOR RECONSTITUTED SAMPLE 57-4



SAMPLE NO.: 9
 DRY DENSITY (KN/M³): 15.1
 WATER CONTENT (%) : 30

SYMBOL	STRESS RATIO τ / σ'_v
○	0.29
□	0.24
○	0.19
△	0.16

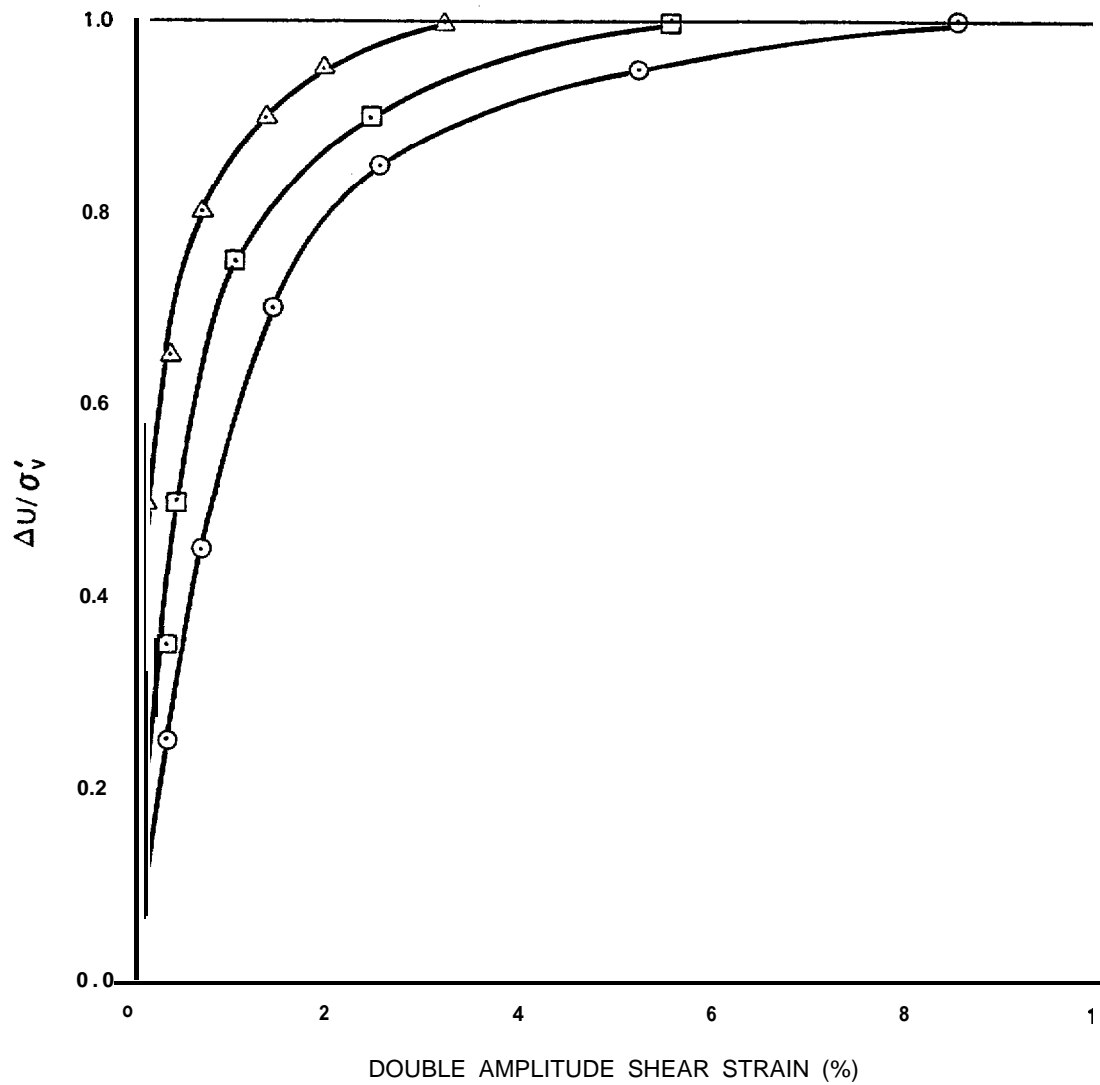
FIGURE II-35 PORE PRESSURE/STRAIN RESPONSE CURVES FOR RECONSTITUTED SAMPLE 9



SAMPLE NO.: 24
 DRY DENSITY (KN/M³): 15.7
 WATER CONTENT (%): 27

SYMBOL	STRESS RATIO τ / σ'_v
O	0.21
□	0.30
△	0.17

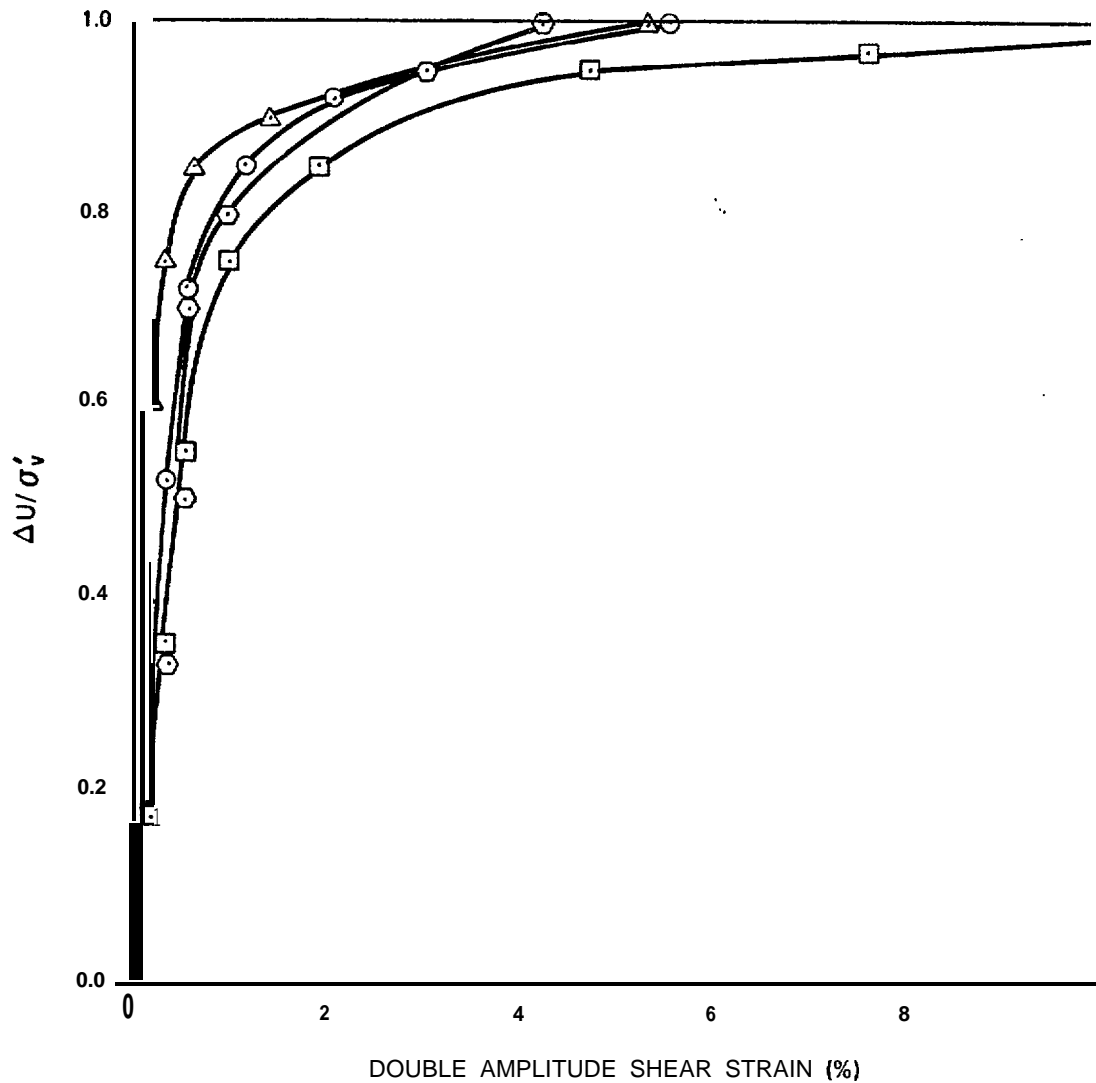
FIGURE II-36 PORE PRESSURE/STRAIN RESPONSE CURVES FOR RECONSTITUTED SAMPLE 24



SAMPLE NO.: 43
 DRY DENSITY (KN/M³): 16.3
 WATER CONTENT (%): 24

SYMBOL	STRESS RATIO τ / σ'_v
○	0.29
◻	0.22
△	0.17

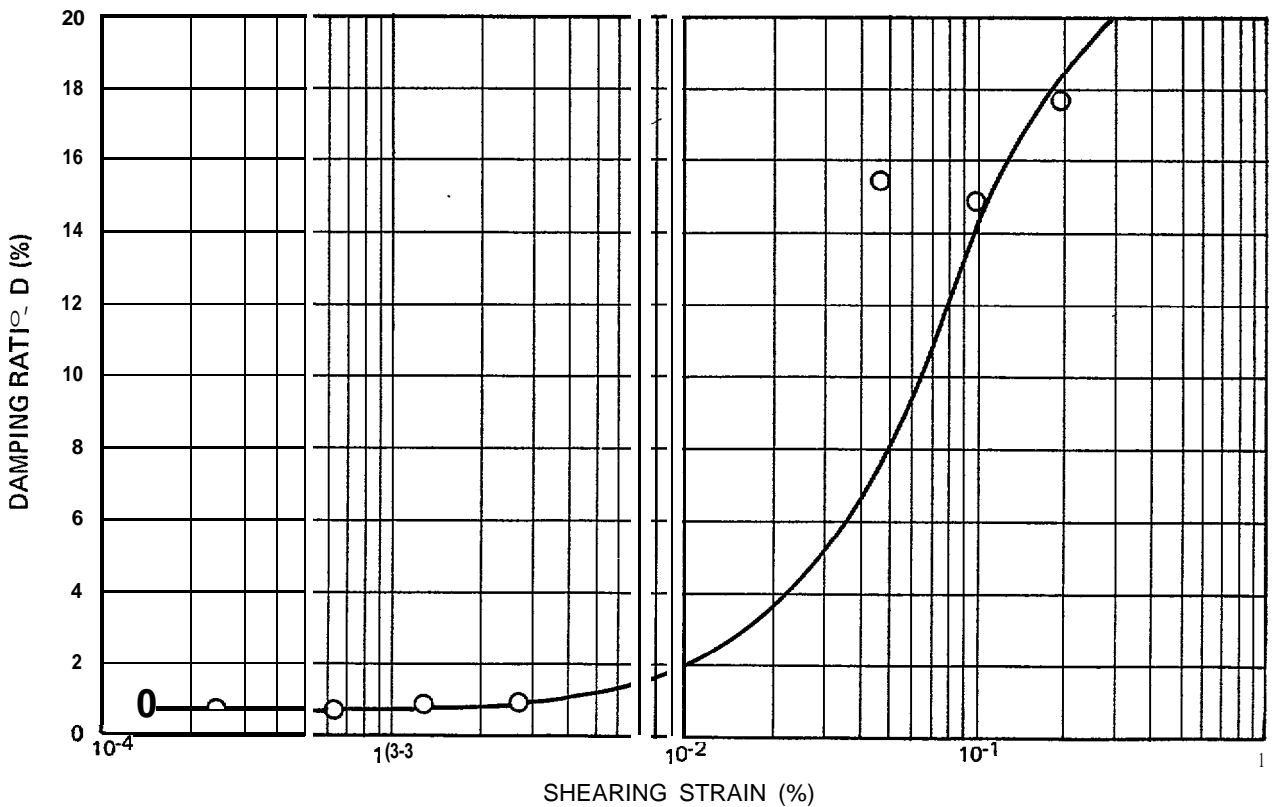
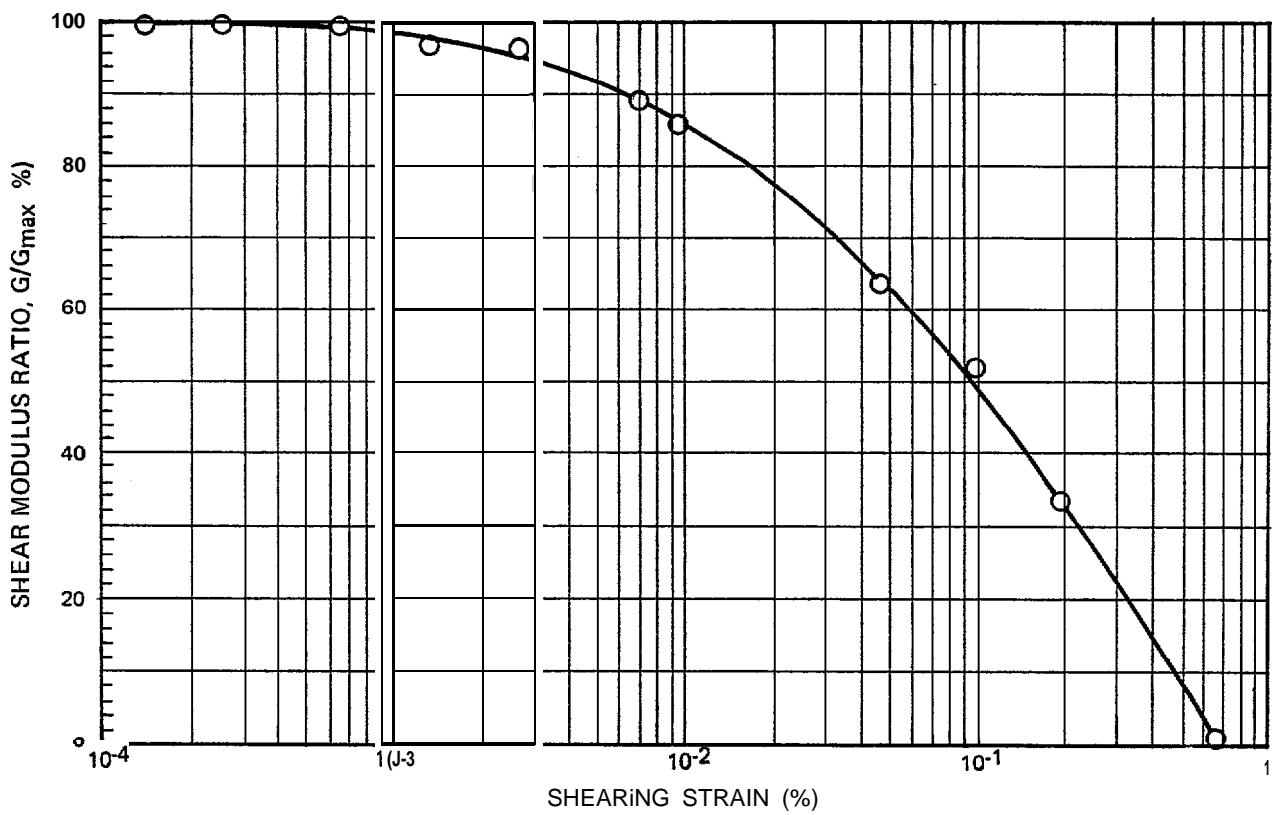
FIGURE II-37 PORE PRESSURE/STRAIN RESPONSE CURVES FOR RECONSTITUTED SAMPLE 43



SAMPLE NO.: 57
 DRY DENSITY (KN/M³): 16.2
 WATER CONTENT (%) : 24

SYMBOL	STRESS RATIO τ / σ'_v
○	0.21
□	0.17
△	0.14
○	0.13

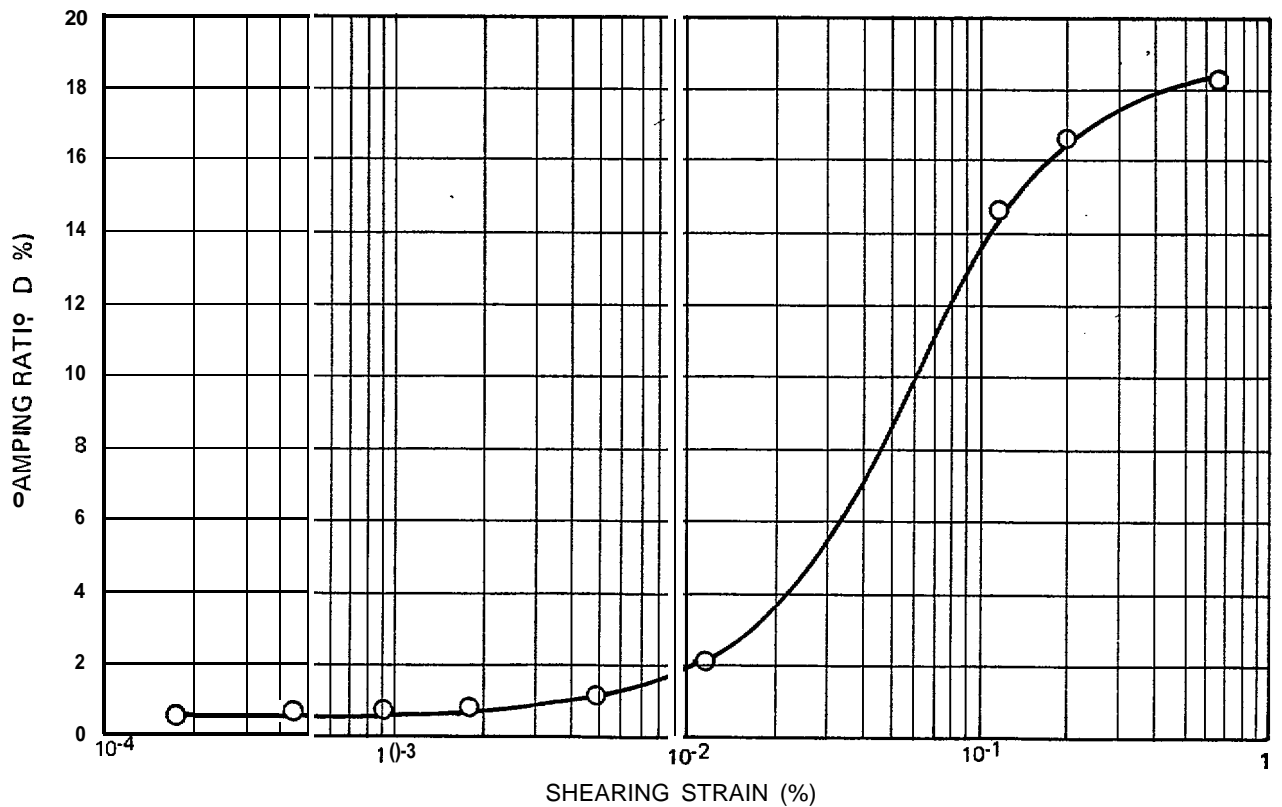
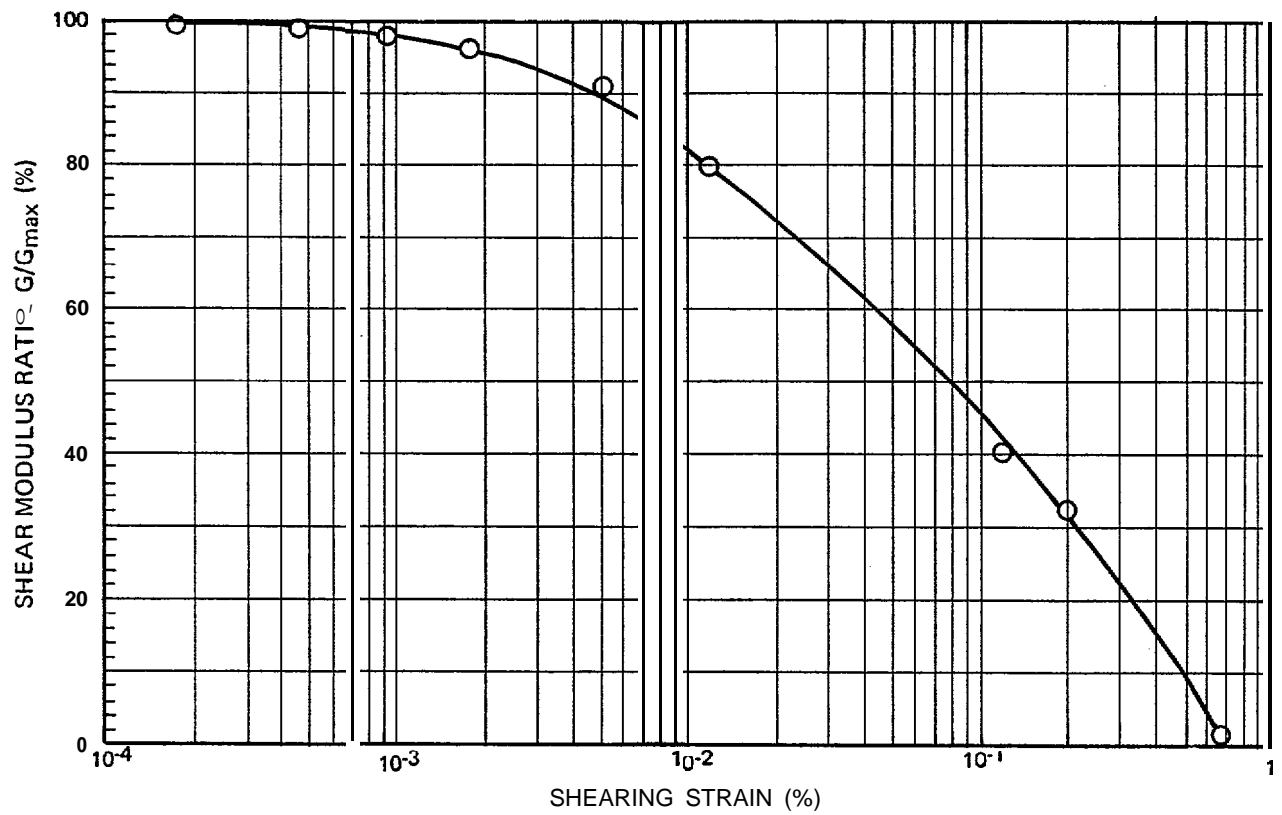
FIGURE 11-38 PORE PRESSURE/STRAIN RESPONSE CURVES FOR RECONSTITUTED SAMPLE 57



SAMPLE NO.: 9
 WATER DEPTH (METERS): 100
 DEPTH INTERVAL: SURFICIAL
 SAMPLe TYPE : RECONSTITUTED (SM)

DRY UNIT WEIGHT (KN/M³): 15
 WATER CONTENT [%]: 14
 CONFINING PRESSURE (KN/M²): 140
 G_{max} (KN/M²): 0.8 x 10⁵

FIGURE II-39 MODULUS AND DAMPING RATIO CURVES FOR SAMPLE 9



SAMPLE NO.: 24

WATER DEPTH (METERS): 84

DEPTH INTERVAL: SURF ICIAL

SAMPLE TYPE : RECONSTITUTED (SP/SM)

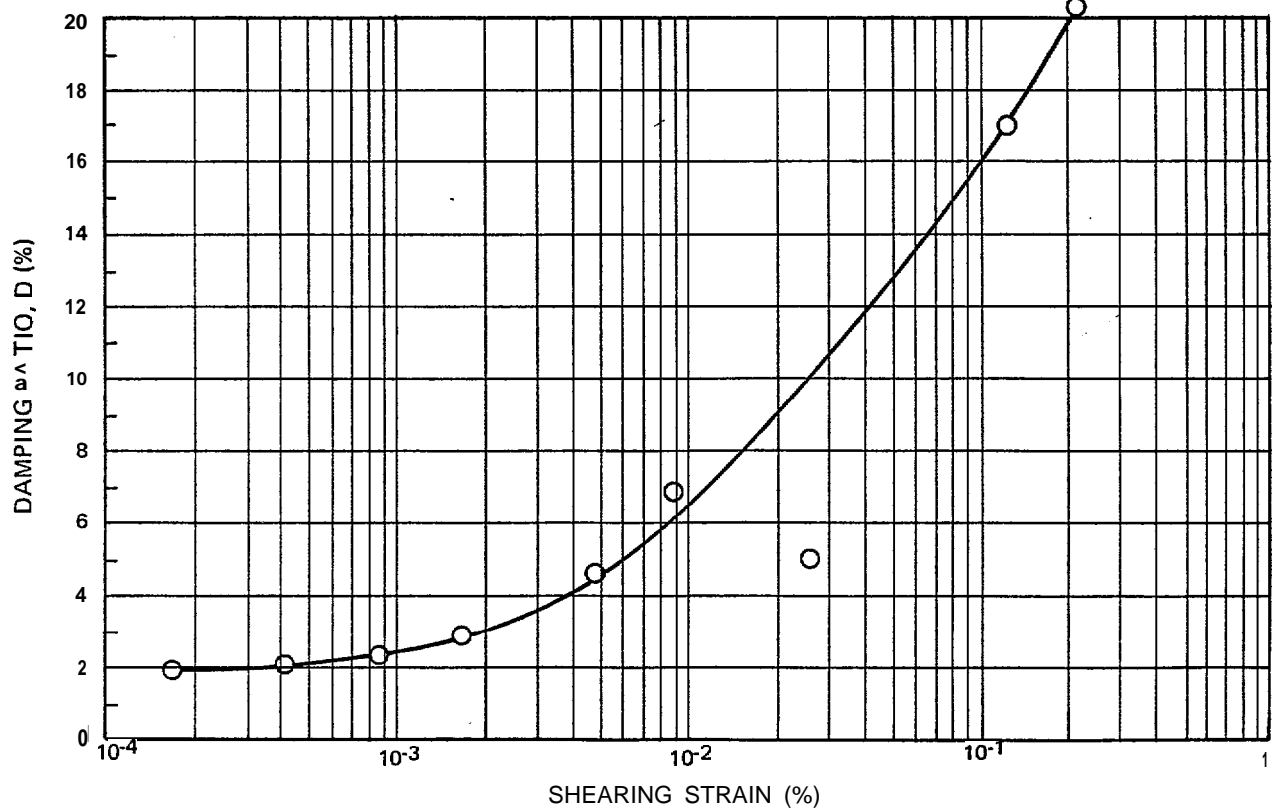
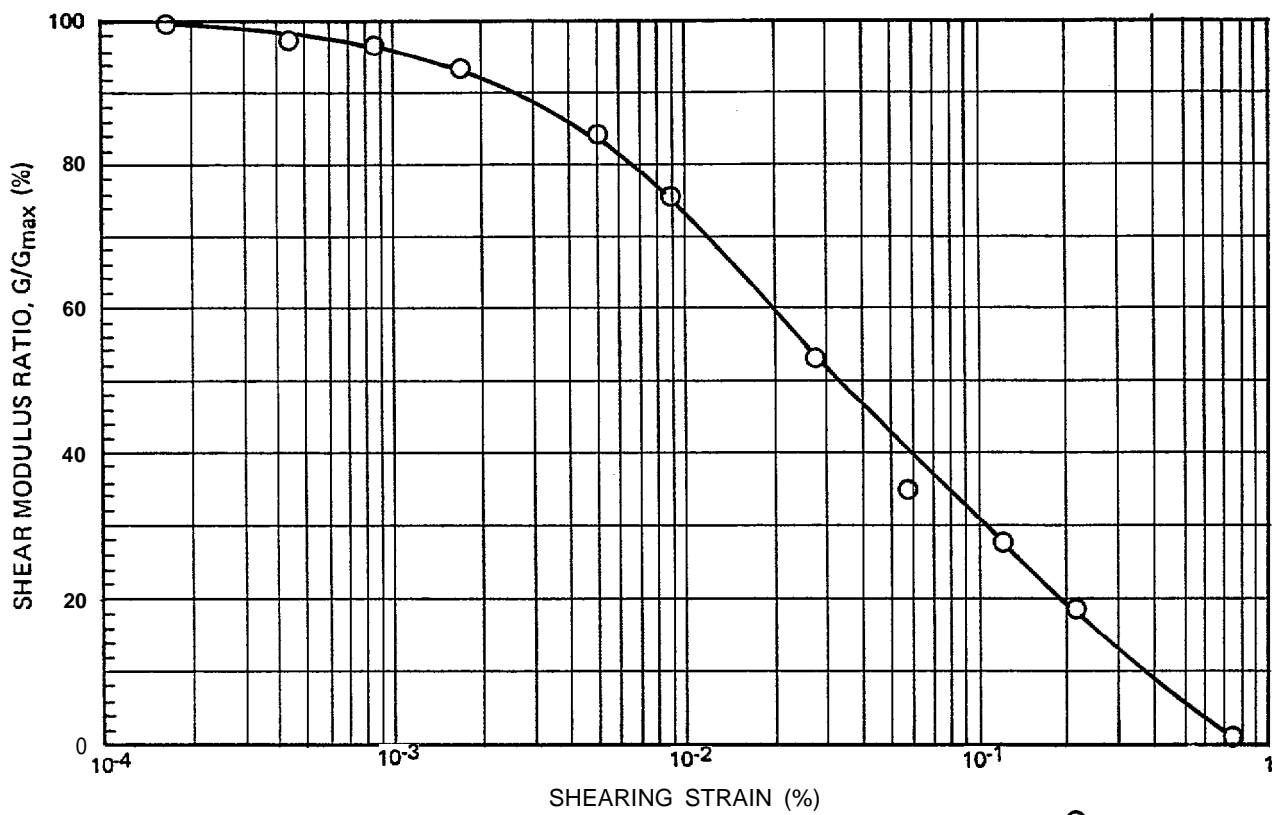
DRY UNIT WEIGHT (KN/M^3): 16

WATER CONTENT (%): 15

CONFINING PRESSURE (KN/M^2): 140

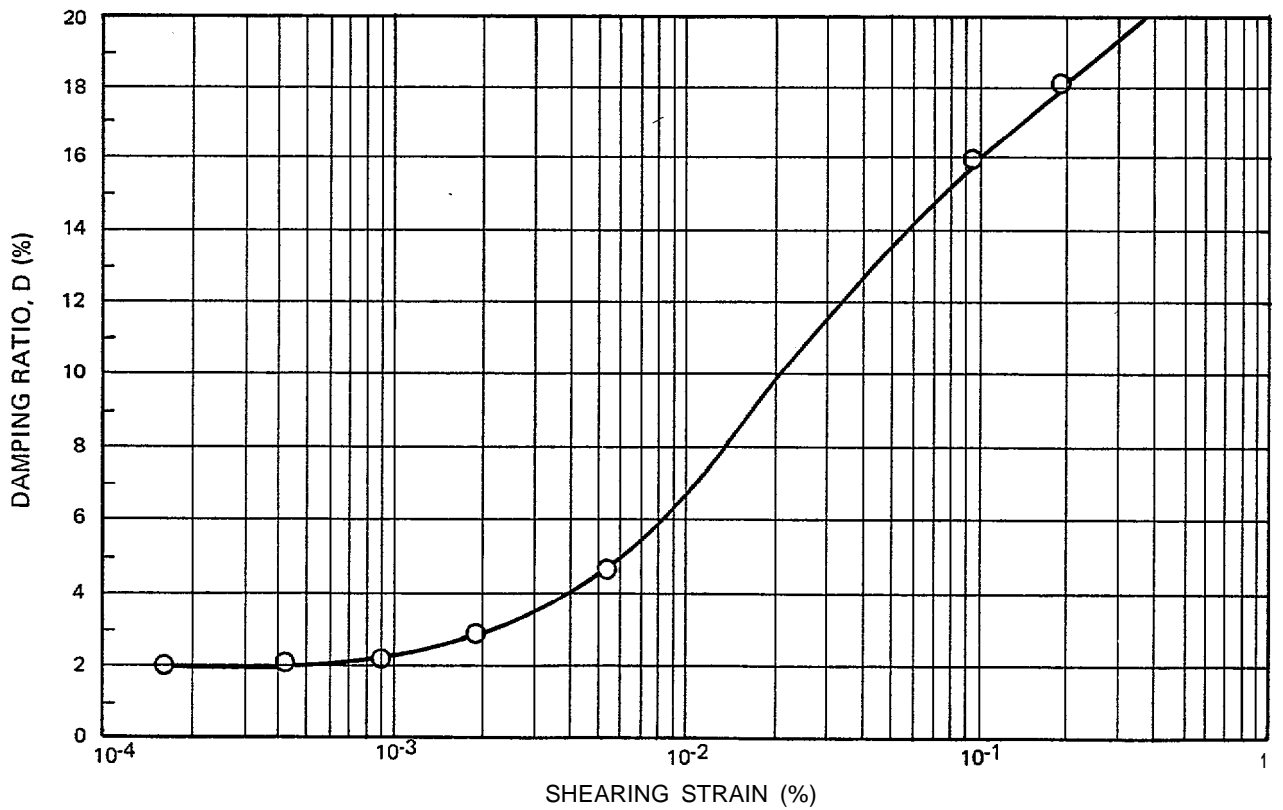
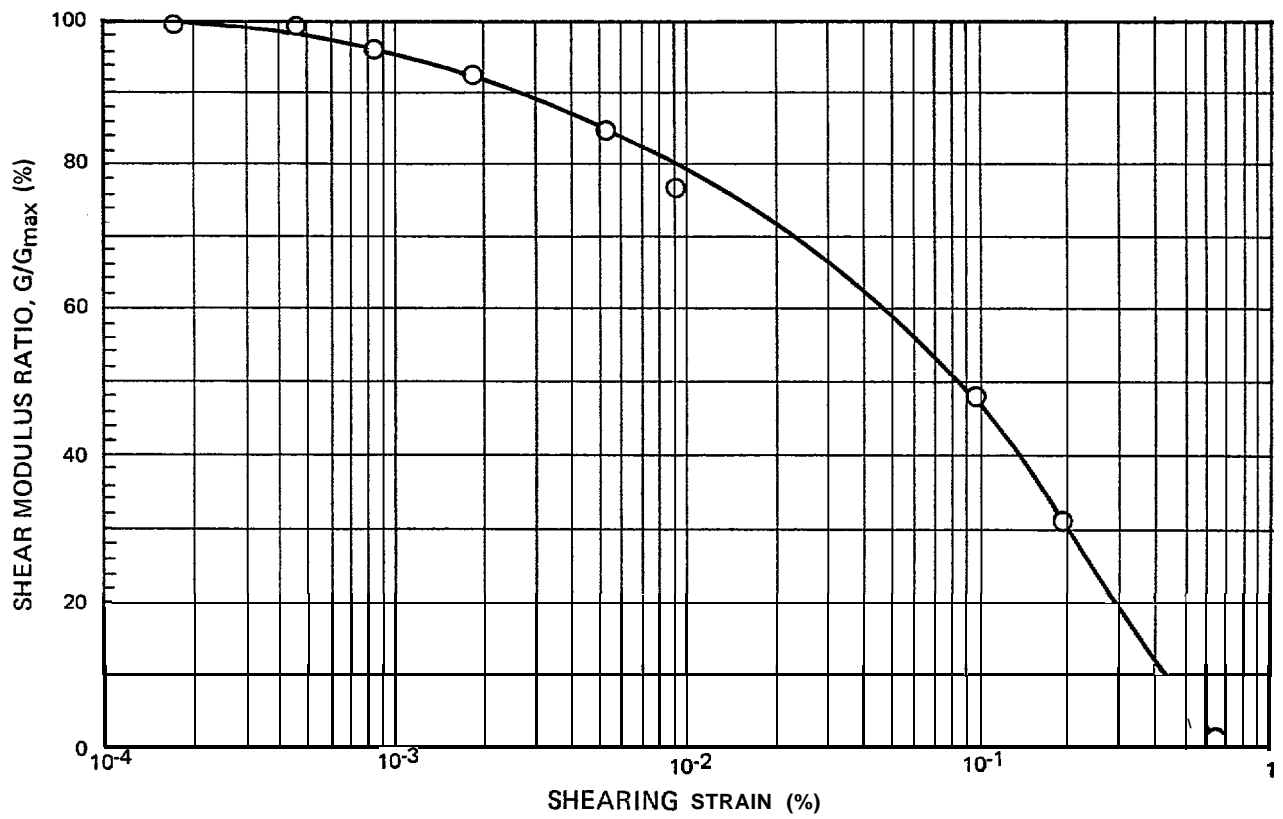
G_{max} (KN/M^2): 1.1×10^5

FIGURE II-40 MODULUS AND DAMPING RATIO CURVES FOR SAMPLE 24



SAMPLE NO.: 43	DRY UNIT WEIGHT (KN/M^3): 16
WATER DEPTH (METERS) :80	WATER CONTENT (%): 10.5
DEPTH INTERVAL: SURFICIAL	CONFINING PRESSURE (KN/M^2): 140
SAMPLE TYPE : RECONSTITUTED (SP)	G_{max} (KN/M^2): 1.2×10^5

FIGURE II-41 MODULUS AND DAMPING RATIO CURVES FOR SAMPLE 43



SAMPLE NO.: 57

WATER DEPTH (M ETERS):49

DEPTH INTERVAL: SURFICIAL

SAMPLE TYPE : RECONSTITUTED (SP)

DRY UNIT WEIGHT (KN/M^3): 16

WATER CONTENT (%): 9.5

CONFINING PRESSURE (KN/M^2): 140

G_{max} (KN/M^2): 1.2×10^5

FIGURE II-42 MODULUS AND DAMPING RATIO CURVES FOR SAMPLE 57

APPENDIX III

VIBRACORE DESCRIPTIONS



Marine Environmental Science Associates

VISUAL CORE DESCRIPTION

LEGEND

CENTIMETERS	COLOR : MPI	Su E	DESCRIPTION
0			Fine and Very Fine Sand
			Medium Sand
			Coarse Sand
			Silty Sand
			Sandy Silt
			Silt
			Gradational color change
			Mottling
			Burrows
			Pelecypods
			Shell fragments
			Rock fragments



VISUAL CORE DESCRIPTION

PROJECT NOAA - Bristol Bay

STATION 0/200 A Section 1

LOGGED BY E. Johnson DATE 15 Jan 82

LOCATION 56°29.9'N 164°59.3'W

LENGTH 86 cm

WATER DEPTH 82 m

SECTION 1 OF 2

VESSEL Discoverer DATE 279 JD 1980

LENGTH 86 cm TYPE CORE Vibracore

	COLOR	JB PI	DESCRIPTION
0			
10	5y5/2	X	0-8 cm: Geotechnical and grain size analysis light olive grey, silty fine sand
20			
30	5y3/2		olive grey, silty fine sand mottled with dusky yellow green silty sand
40			
50			
60	5gy3/2		Greyish olive green silty fine sand with slight netting
70	5y3/2		Olive grey fine sand with scattered whole pelecypod shells, 1 cm in diameter, and a pebble, 1 cm in diameter
80	5y3/2	X	Olive grey silty sand 78-86 cm: Geotechnical and grain size analysis 86cm: Bottom of section 1.
90			

Note: Section 2 was lost in shipping from Discoverer.



Marine Environmental Science Associates

VISUAL CORE DESCRIPTION

PROJECT NOAA Bristol Bay

STATION 0/200B Section 1

LOGGED BY E. Johnson DATE 15Jan82

LOCATION 56°29.9'N 164°05'W

LENGTH 91 cm

WATER DEPTH 82 m

SECTION 1 OF 2

VESSEL Discoverer DATE 279JD1980

LENGTH 91cm TYPE CORE Vibracore

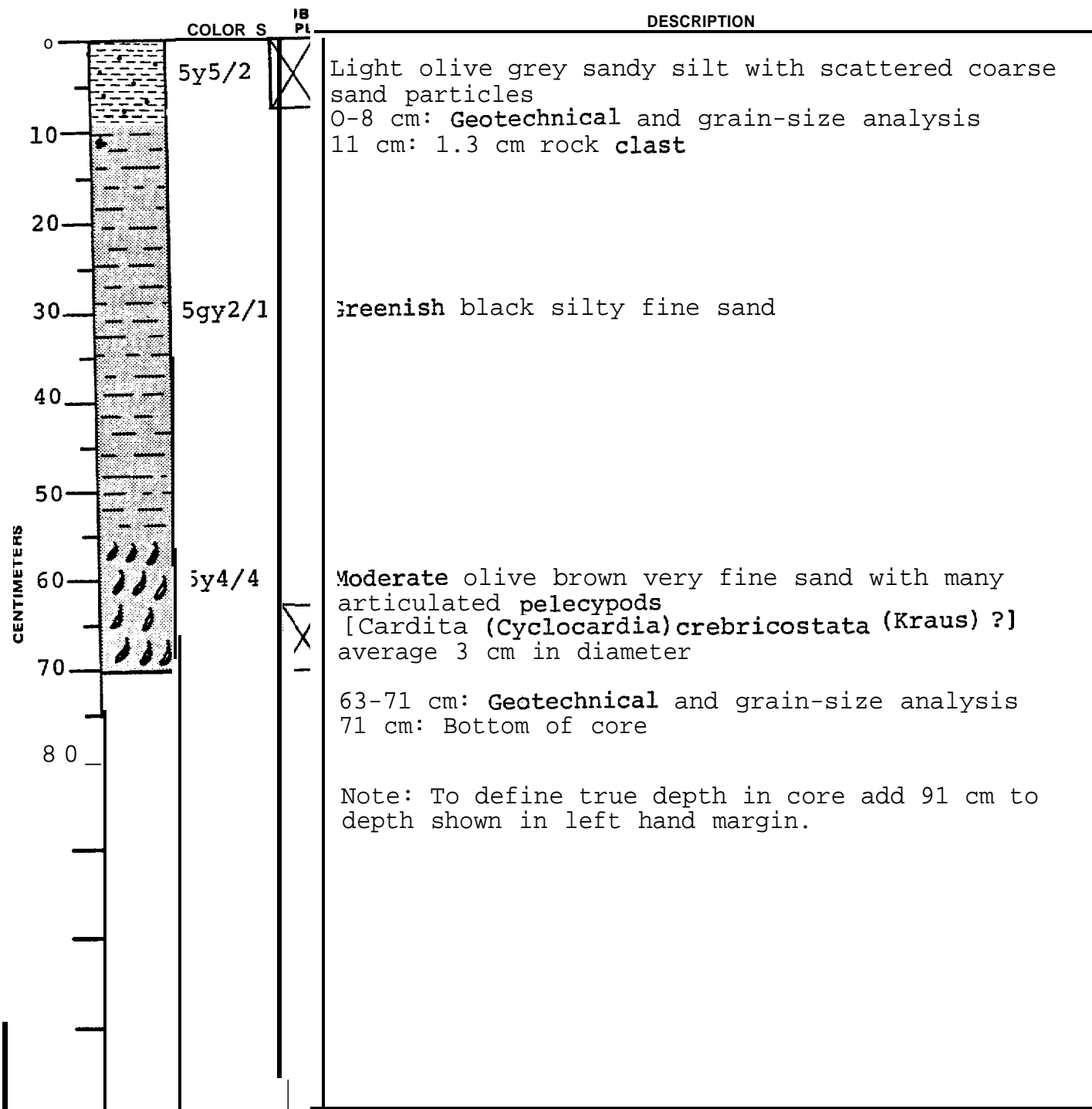
CENTIMETERS	COLOR & M	DESCRIPTION
0	5y5/2	Light olive grey very fine sand 0-8 cm: Geotechnical and grain-size analysis
10	5y3/2	Olive grey fine sand
20	5y5/2	Light olive grey silty fine sand
	5gy2/1	Greenish Black silty fine sand
30	5y5/2	Light olive grey silty fine sand
	5g2/1	Greenish black silty fine sand
40		
	5y5/2	Light olive grey silt mottled with greenish black silt
50		
	5g2/1	Greenish black silty fine sand
60		
	5b5/1	Bluish grey silty fine sand with thin black silt stringers
70		
	5y5/2	Light olive grey silty fine sand with thin black and brown silt stringers
80		
		83-91 cm : Geotechnical and grain-size analysis
90		91 cm: Bottom of section 1



Marine Environmental Science Associates

VISUAL CORE DESCRIPTION

PROJECT NOAA - Bristol Bay
 STATION 0/200B section 2 LOGGED BY E. Johnson DATE 15Jan82
 LOCATION 56°29.9'N 164°59.3'W LENGTH 71cm
 WATER DEPTH 82 m SECTION 2 OF 2
 VESSEL Discoverer DATE 279 JD 1980
 LENGTH 71 cm TYPE CORE Vibracore





Marlin **Environmental Science Associates**

VISUAL CORE DESCRIPTION

PROJECT NOAA-BRISTOL BAY

STATION 20/100

LOGGED BY E. Johnson DATE 15Jan82

LOCATION 55°36.4'N 164° 0.7'W

LENGTH 80 cm

WATER DEPTH 100 m

SECTION 1 OF 1

VESSEL Discoverer DATE 282 JD 1980

LENGTH 80 cm TYPE coRE Vibracore

	COLOR	SUB	DESCRIPTION
0	5y5/2	X	Lt. Olive Grey very fine sand 0-8 cm: Geotechnical and grain size analysis
10	5gy3/2		Grayish olive green fine sand
20			19cm : .5 cm rounded rock particle 23cm : .3 cm rounded rock particle 27cm : .18 cm rounded rock particle 34cm : .45 cm rounded rock particle
30			39cm : 1.0 cm rounded rock particle
40	5y2/1		Greenish Black fine sand
50			55cm : Shell fragment, 3 cm long
60			
70	gy3/2	X	Grayish olive green fine sand with shell hash. Shells average length is .5 cm. Fragments decrease in size and frequency downward in core.
80			72-80 cm: Geotechnical and grain size analysis 80 cm: Bottom of core



VISUAL CORE DESCRIPTION

PROJECT 03AA - Bristol Bay

STATION 70/87 A LOGGED BY Johnson DATE 15 Jan 82

LOCATION 55°29'4"N 163°52'7"W LENGTH 65 cm

WATER DEPTH 89 m SECTION 1 OF 1

VESSEL Discoverer DATE 283JD 1980

LENGTH 65 cm TYPE CORE Vibracore

	COLOR :	SUB IPI	DESCRIPTION
0	5y5/2	X	Lt. Olive grey fine sand
10	y4/4)-8 cm :Geotechnical and grain size analysis 11 cm :burrow
20	y3/2		Moderate olive brown silty sand
30	gy2/1		Olive grey very fine sand with mottling
40	y3/2		Greenish black very fine sand
50	gy2/1		Olive grey very fine sand with mottling
60	gy4/1	X	Greenish black very fine sand 56 cm: shell fragments
70			Dark greenish grey very fine sand 57-65 cm :Geotechnical and grain size analysis 65 cm Bottom of core
			Note: Additional core from catcher not described



Marine Environmental Science Associates

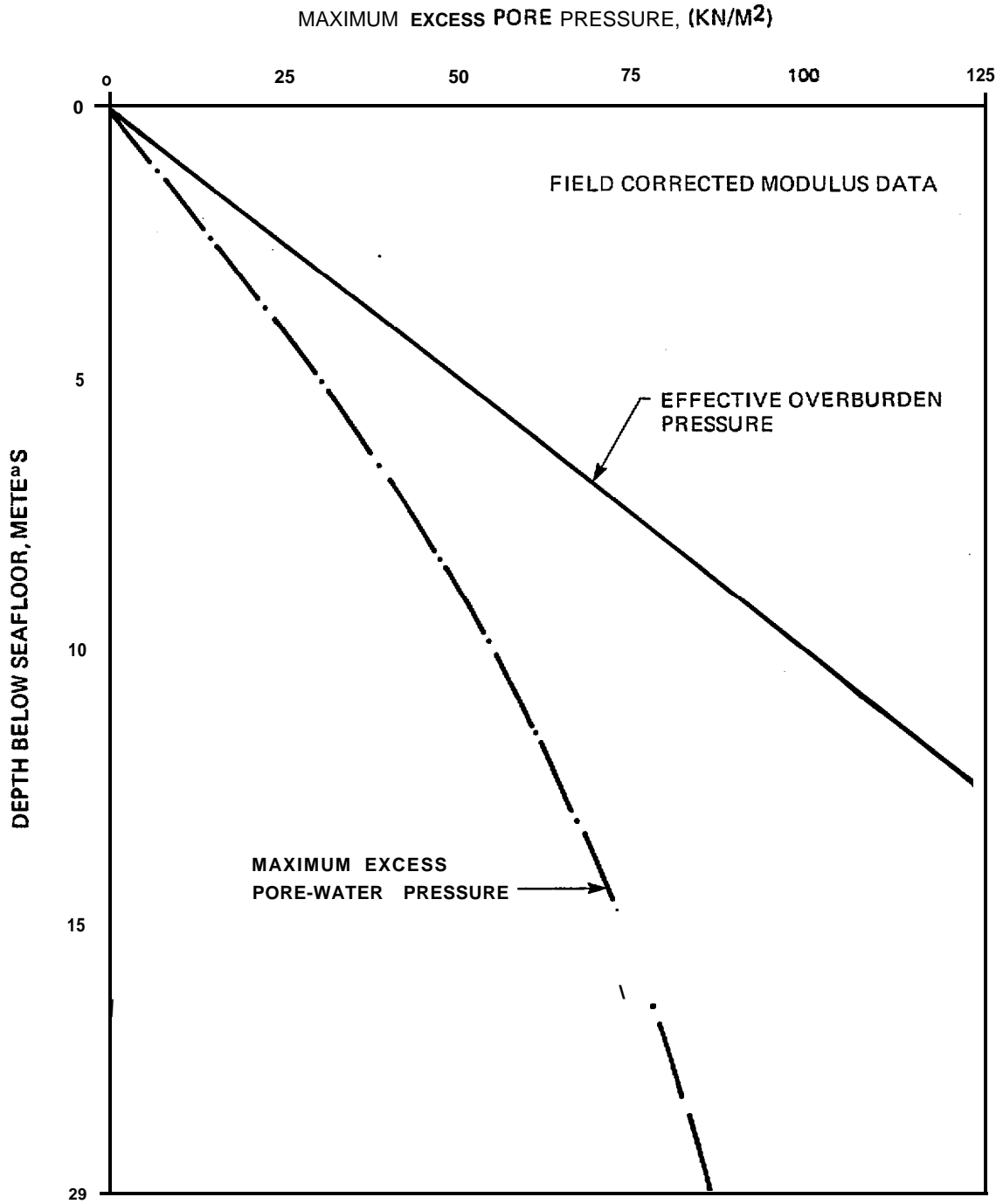
VISUAL CORE DESCRIPTION

PROJECT NOAA - Bristol Bay
 STATION 70/87 B LOGGED BY E. Johnson DATE 15 Jan 82
 LOCATION 55° 26.4' N 163° 2.2' W LENGTH 68 cm
 WATER DEPTH 89 m SECTION 1 OF 1
 VESSEL Discoverer DATE 283 JD 1980
 LENGTH 68 cm TYPE CORE Vibracore

	COLOR S	H P	DESCRIPTION
0	5y5/2	X	1. Olive grey fine sand 1.8 cm: Geotechnical and grain size analysis cm: burrow
10	5y3/2 & 5g2/1		1. Olive grey and greenish black fine sand cm: volcanic pebble
20	5y 3/2		1. Olive grey medium sand unit 1 cm thick 3 cm clast
30	5g2/1		1. Greenish black silty sand with mottling 1 cm shell fragments
40	5y3/2		1. Olive grey fine sand 5.6 cm: shell fragment
50	NI		1. Black coarse sand 5.9 cm: rock and shell fragments, 1 cm average length
60	5gy4/1		1. One shell fragment appears to be <u>Cardium (Cerastoderma) ciliatum</u>
70			1. Dark greenish grey fine sand 5.8 cm: Bottom of core

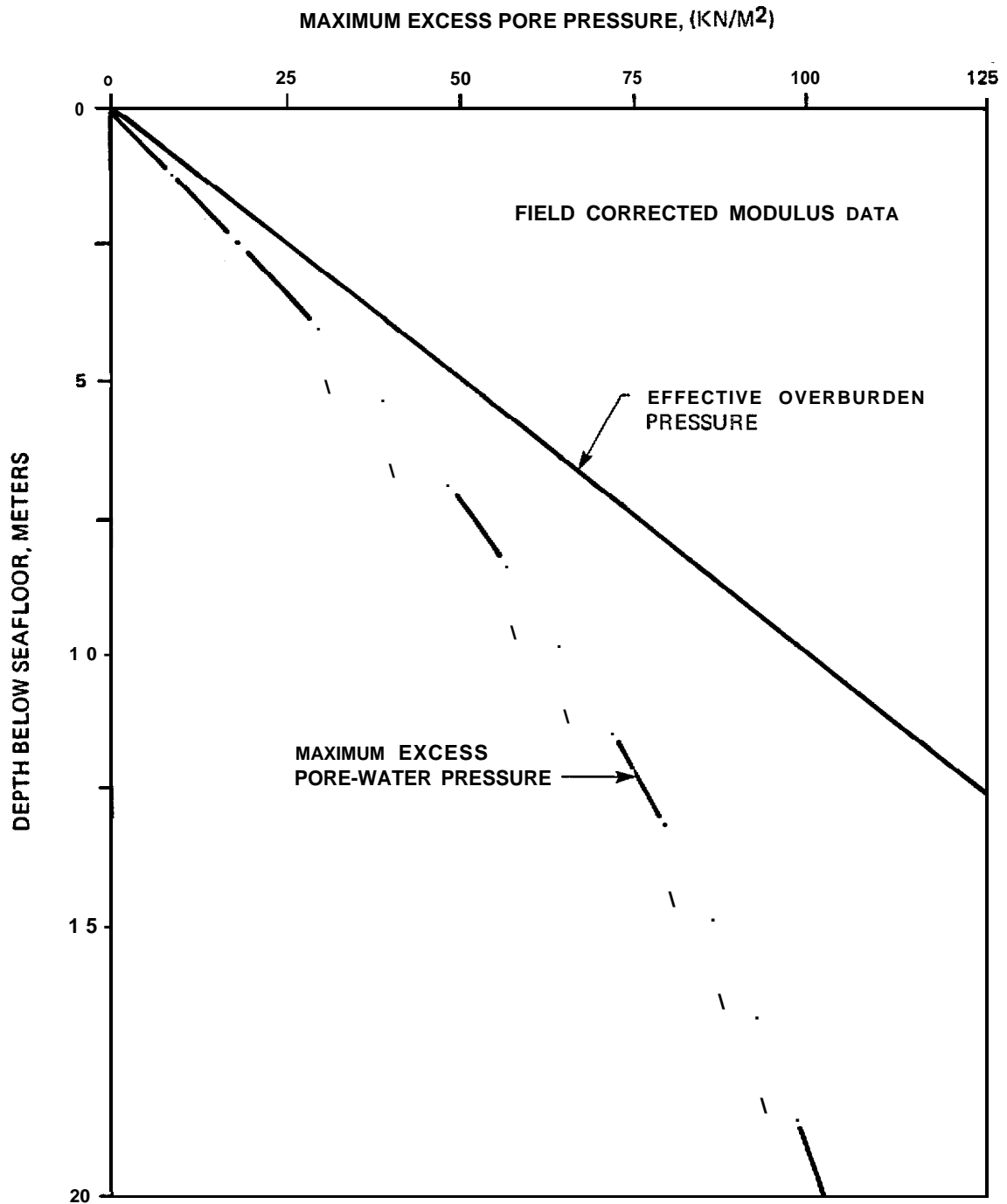
APPENDIX **IV**

RESULTS OF LIQUEFACTION ANALYSES



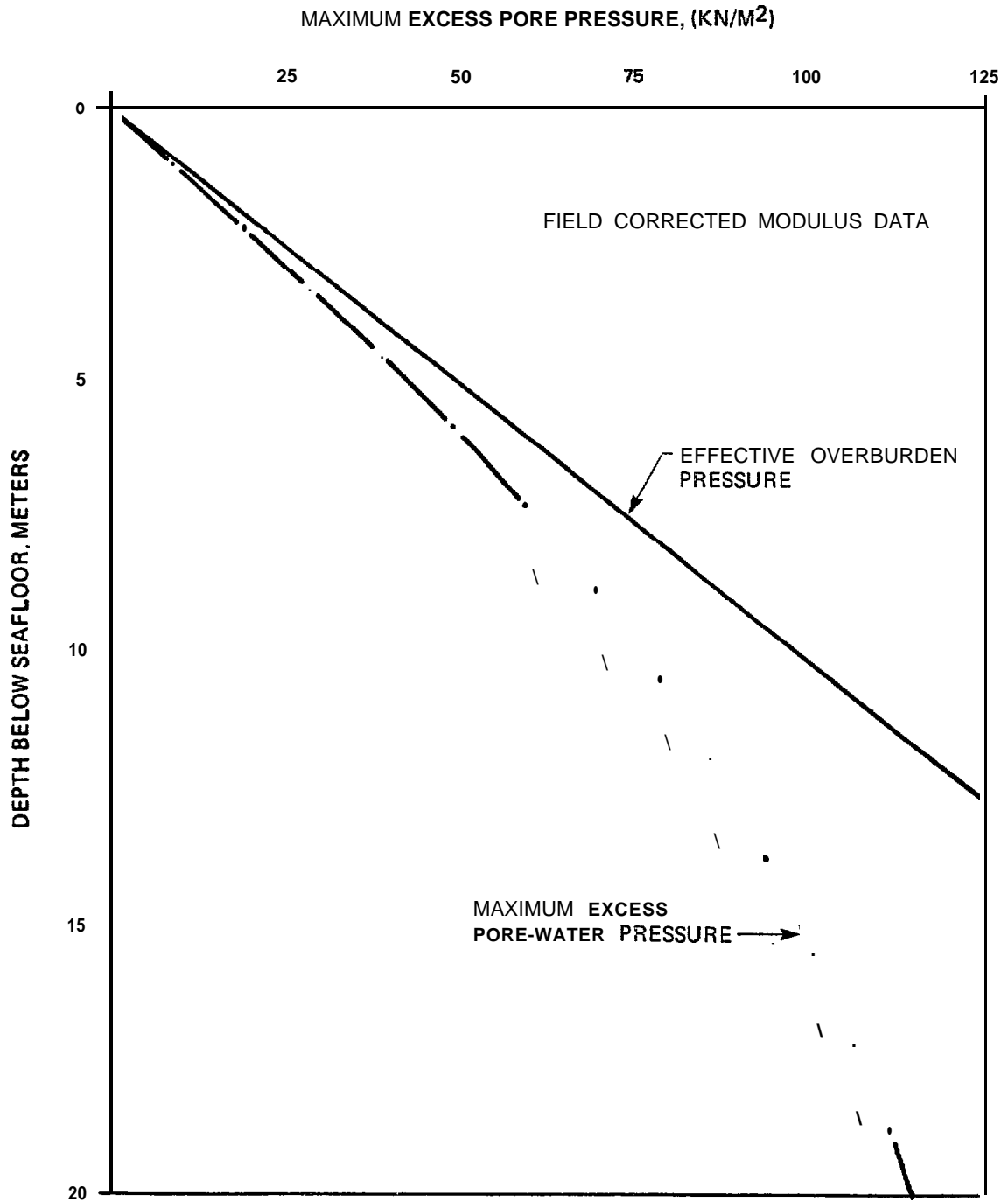
SOIL TYPE SP(1)
 EARTHQUAKE SOURCE SUBDUCTION ZONE
 EARTHQUAKE RECORD (NOR MALIZED TO $A_{max} = 0.16g$) CAL TECH A-1
 MAXIMUM GROUND ACCELERATION A_{max}
 CONCLUSION: NO LIQUEFACTION

FIGURE IV-I MAXIMUM EXCESS PORE PRESSURE RESPONSE CURVE
 (SP1, SUBDUCTION ZONE, 0.16g)



SOIL TYPE SP⁽¹⁾
 EARTHQUAKE SOURCE SUBDUCTION ZONE
 EARTHQUAKE RECORD (NORMALIZED TO A_g0.19g) CAL TECH A-1
 MAXIMUM GROUND ACCELERATION A_{max}
 CONCLUSION : NO LIQUEFACTION

FIGURE IV-2 MAXIMUM EXCESS PORE PRESSURE RESPONSE CURVE'
 (SPI , SUBDUCTION ZONE, 0.19g)



SOIL TYPE SP(1)

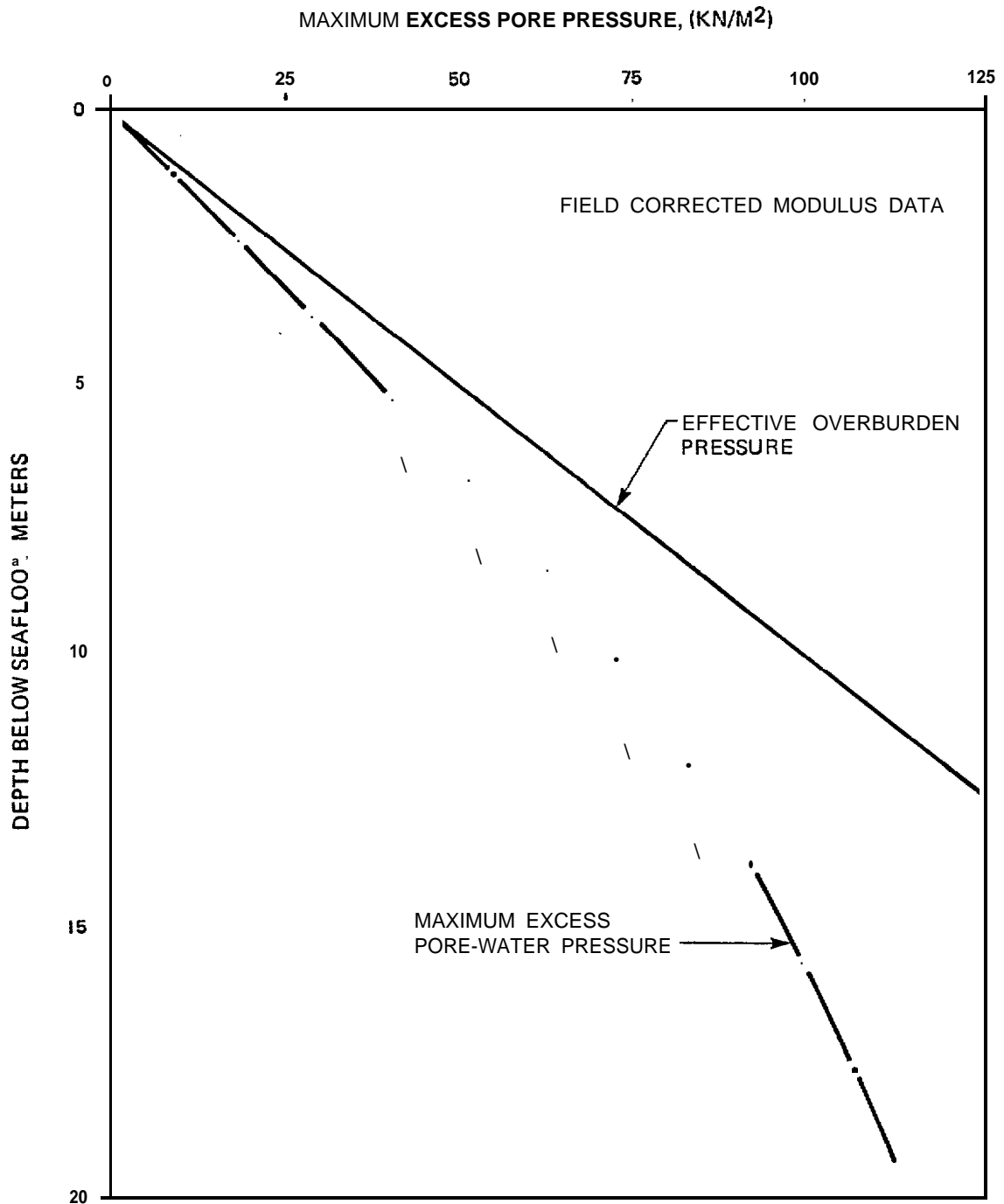
EARTHQUAKE SOURCE MAJOR GRABENS

EARTHQUAKE RECORD (NORMALIZED TO $A_{max} = 0.49$) TAFT 1952

MAXIMUM GROUND ACCELERATION A_{max}

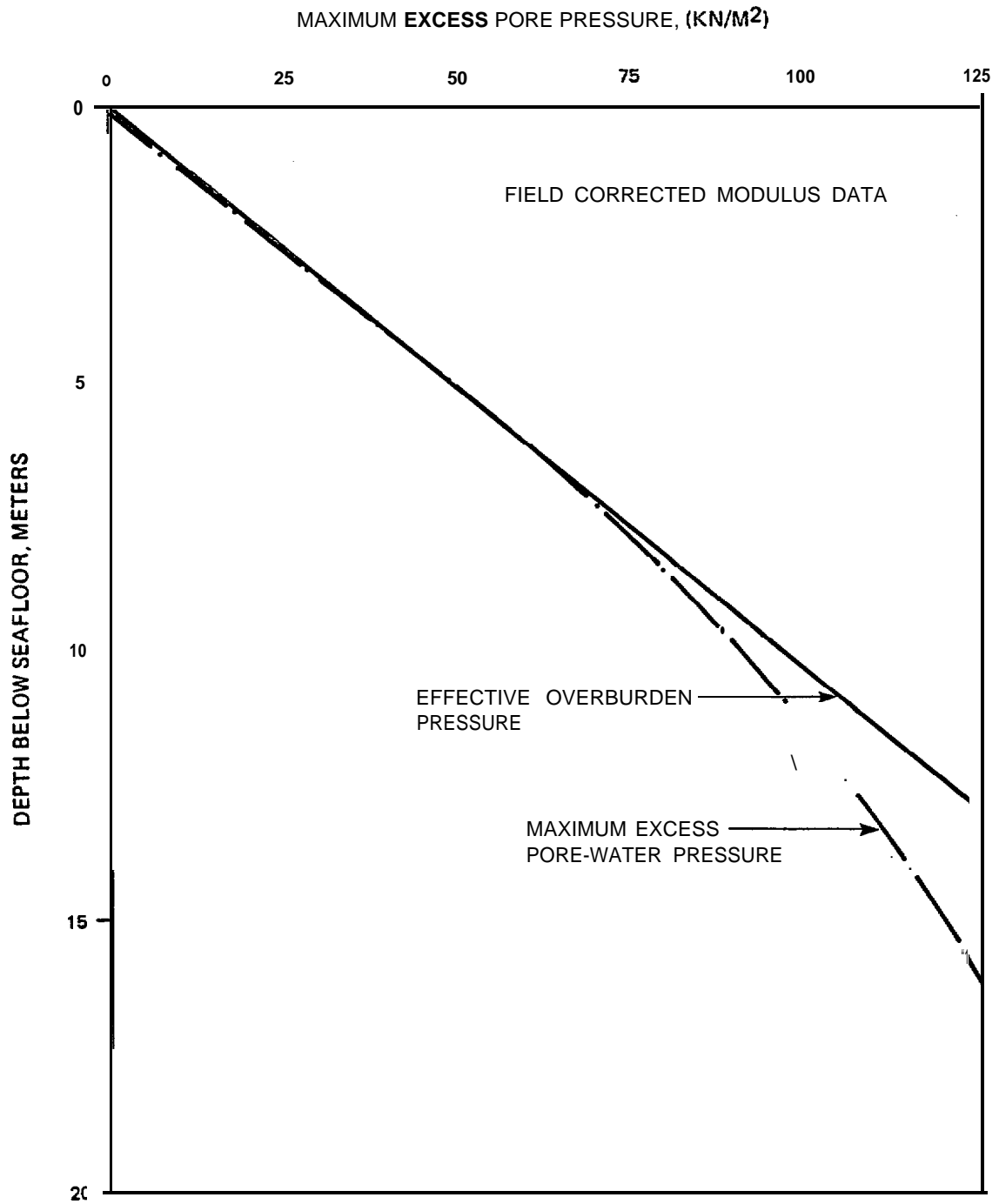
CONCLUSION: NO LIQUEFACTION

FIGURE IV-3 MAXIMUM EXCESS PORE PRESSURE RESPONSE CURVE
(SP1, MAJOR GRABENS, 0.4g)



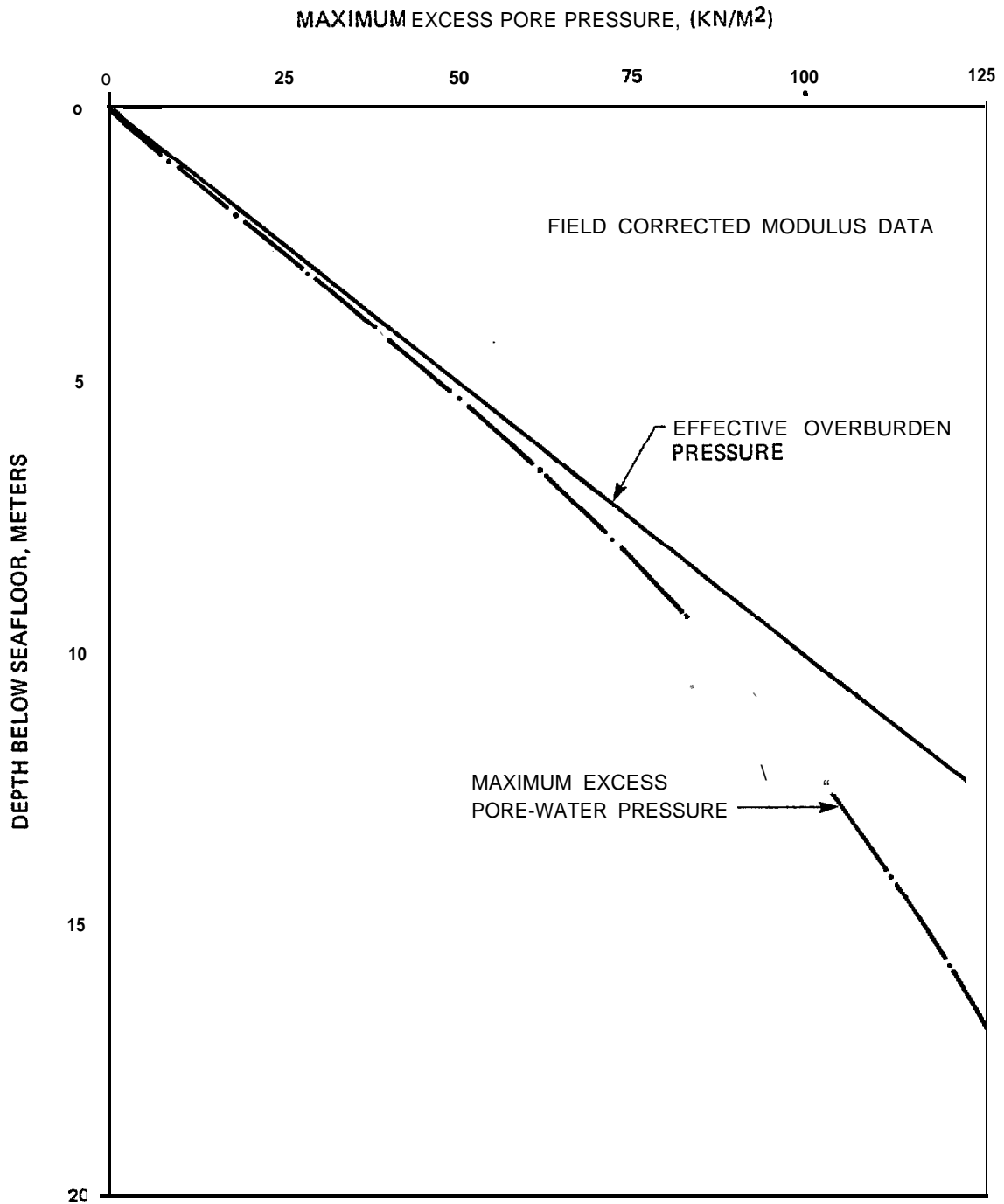
SOIL TYPE SP(1)
 EARTHQUAKE SOURCE MAJOR GRABENS
 EARTHQUAKE RECORD (NORMALIZED TO A_{max}) EL CENTRO 1940
 MAXIMUM GROUND ACCELERATION "A_{max}"
 CONCLUSION: NO LIQUEFACTION

FIGURE IV-4 MAXIMUM EXCESS PORE PRESSURE RESPONSE CURVE
 (SPI, MAJOR GRAB ENS, 0.4g)



SOIL TYPE SP (1)
 EARTHQUAKE SOURCE MAJOR GRABENS
 EARTHQUAKE RECORD (NORMALIZED TO $A_{max} = 0.5g$) TAFT 1952
 MAXIMUM GROUND ACCELERATION 0.5g
 CONCLUSION: LIQUEFACTION TO 8 M

FIGURE IV-5 MAXIMUM EXCESS PORE PRESSURE RESPONSE CURVE (SP1, MAJOR GRABENS, 0.5g)



SOIL TYPE SP (1)

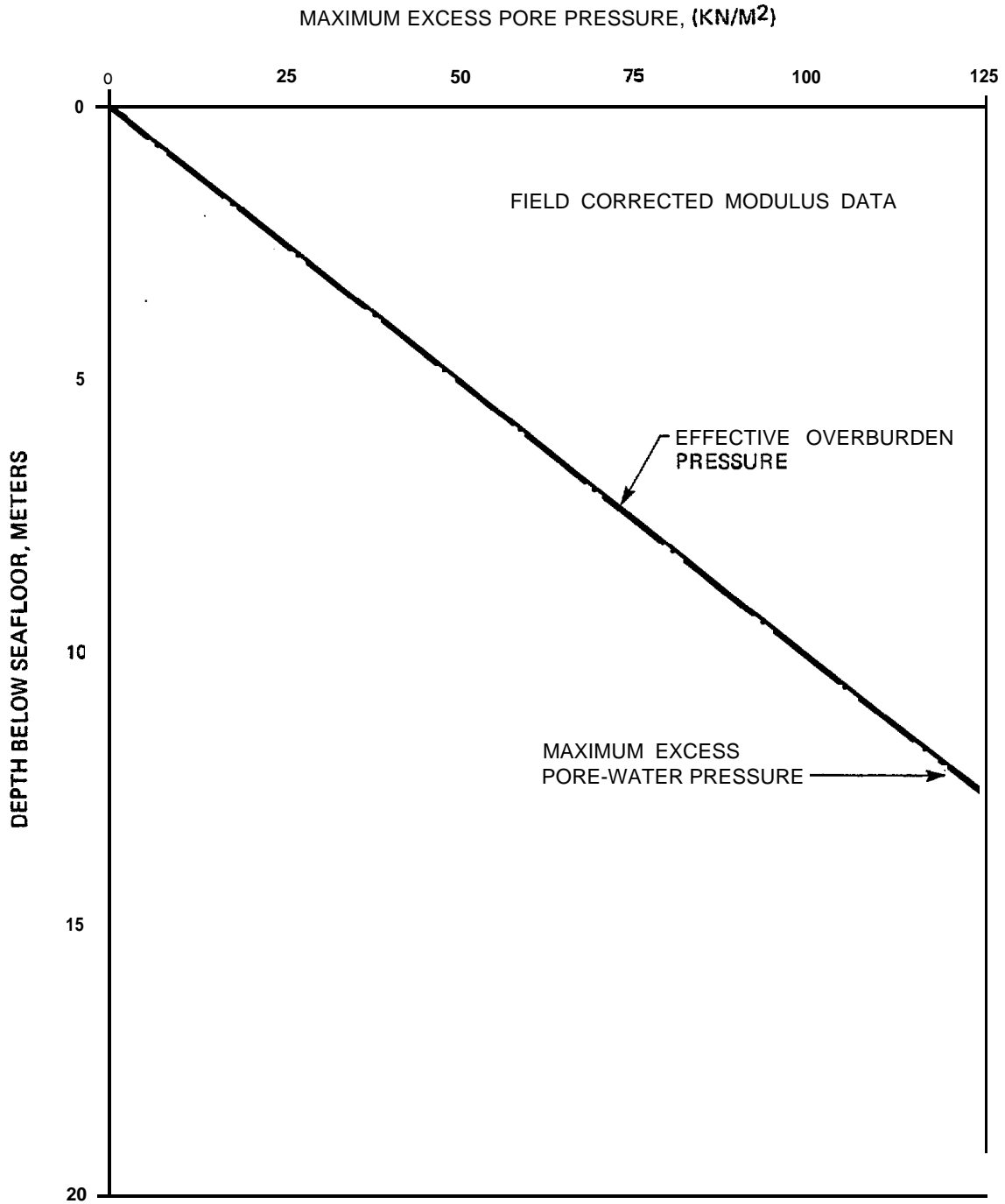
EARTHQUAKE SOURCE MAJOR GRABENS

EARTHQUAKE RECORD (NORMALIZED TO 0.5g) EL CENTRO 1940

MAXIMUM GROUND ACCELERATION 0.5g

CONCLUSION: NO LIQUEFACTION

**FIGURE IV-6 MAXIMUM EXCESS PORE PRESSURE RESPONSE CURVE
(SP1, MAJOR GRABENS, 0.5g)**



SOIL TYPE SP (1)

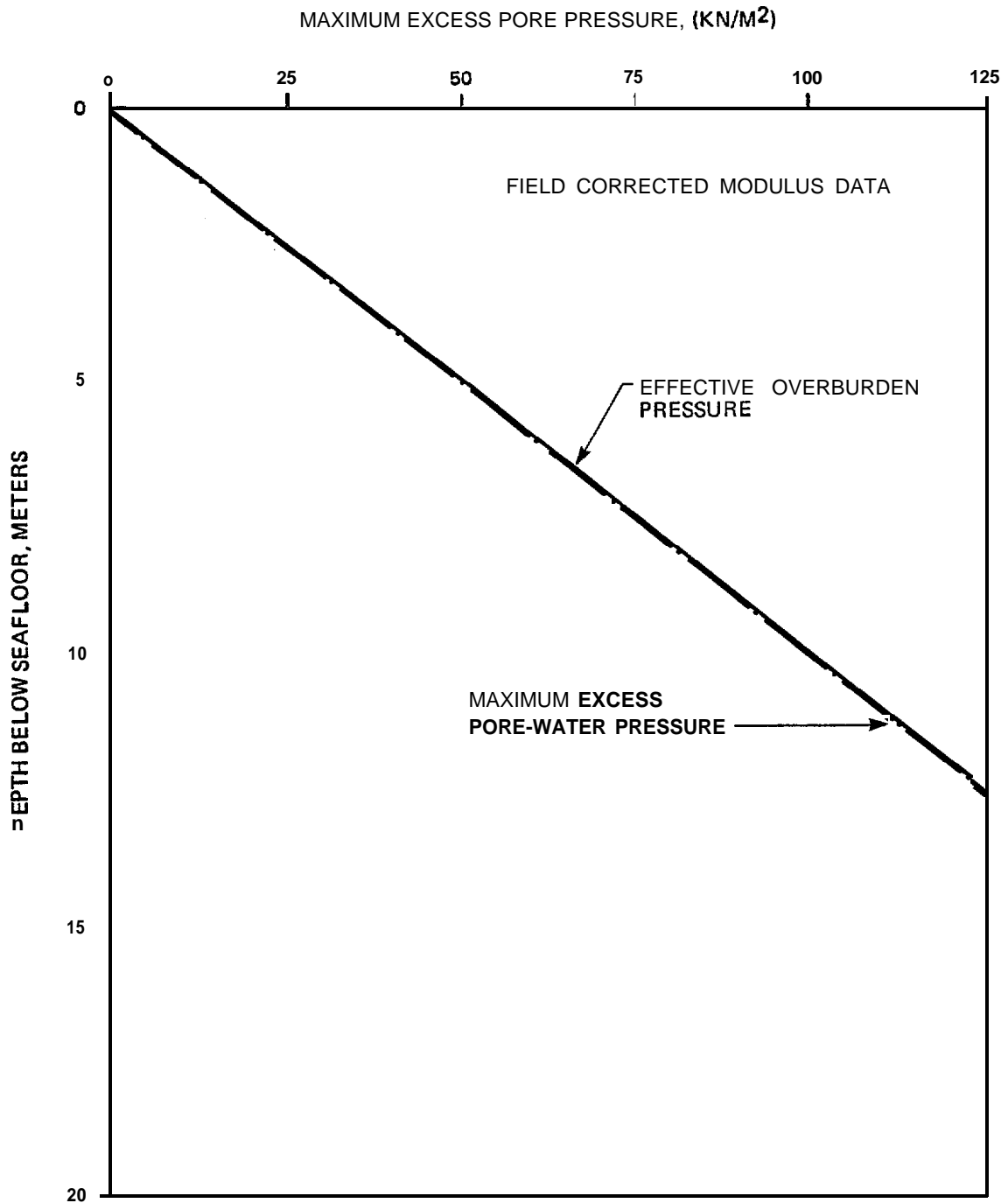
EARTHQUAKE SOURCE MAJOR GRABENS

EARTHQUAKE RECORD (NORMALIZED TO 0.7g) TAFT 1952

MAXIMUM GROUND ACCELERATION 0.7g

CONCLUSION: LIQUEFACTION TO 12 M

FIGURE IV-7 MAXIMUM EXCESS PORE PRESSURE RESPONSE CURVE
(SP1, MAJOR GRABENS, 0.7g)



SOIL TYPE SP (1)

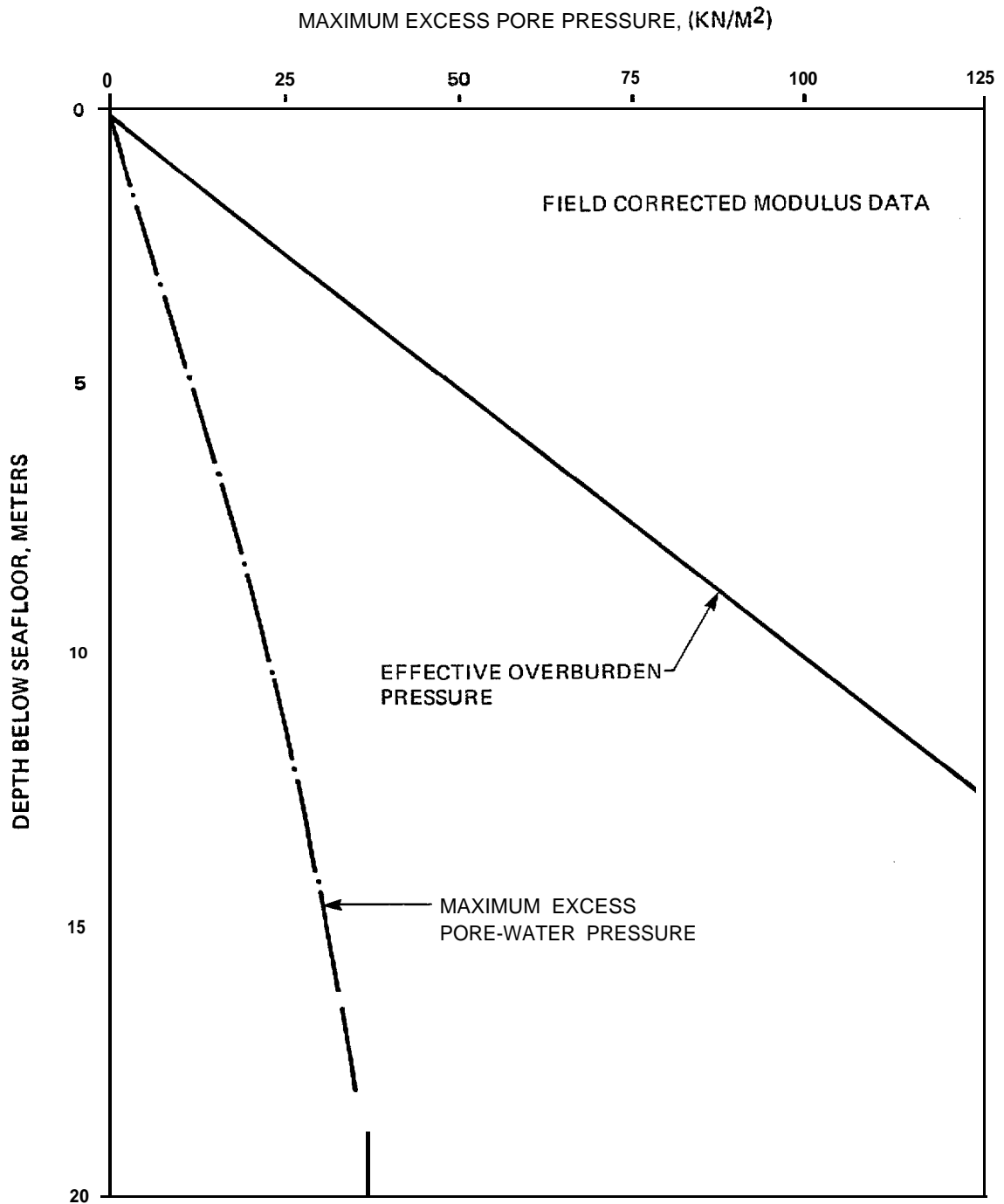
EARTHQUAKE SOURCE MAJOR GRABENS

EARTHQUAKE RECORD (NORMALIZED TO \hat{A}_{max}) EL CENTRO 1940

MAXIMUM GROUND ACCELERATION \hat{A}_{max} _____

CONCLUSION: Liquefaction TO 12 M

FIGURE IV-8 MAXIMUM EXCESS PORE PRESSURE RESPONSE CURVE
(SP1, MAJOR GRABENS, 0.7g)



SOIL TYPE SP (1)

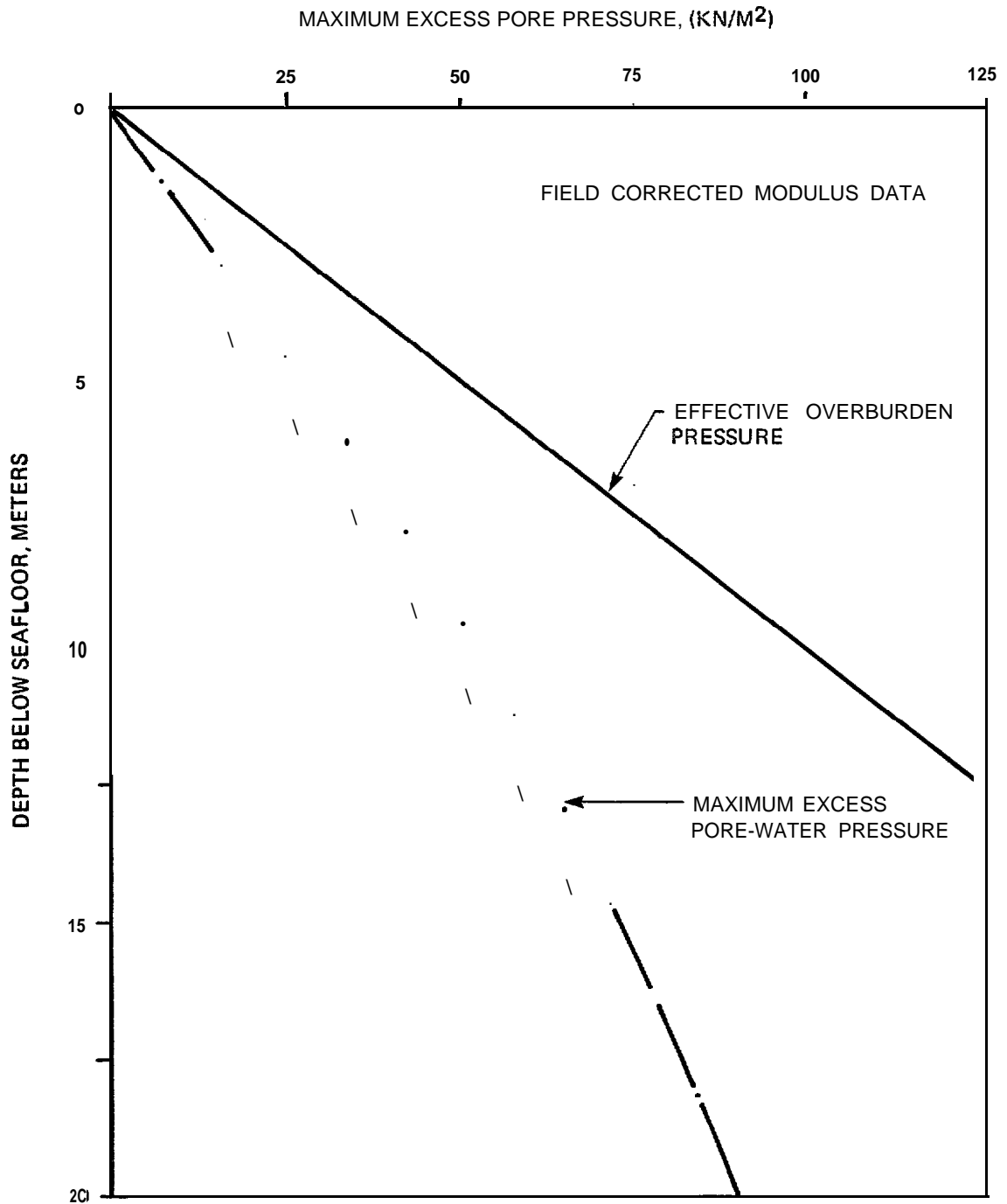
EARTHQUAKE SOURCE BACK ARC FAULTS

EARTHQUAKE RECORD (NORMALIZED TO $A_{max} \times 0.3g$) EL CENTRO 1979

MAXIMUM GROUND ACCELERATION = A_{max}

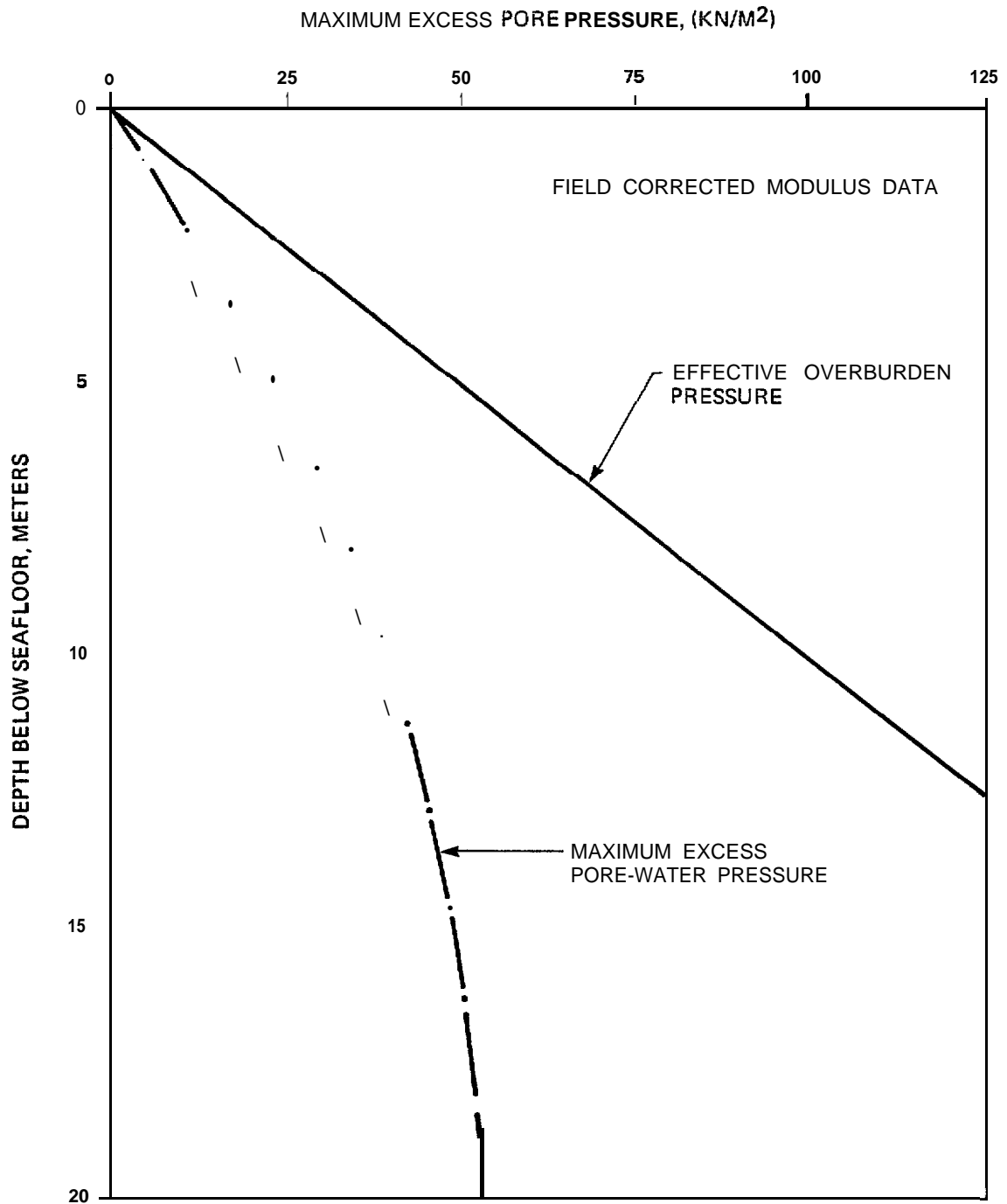
CONCLUSION: NO LIQUEFACTION

FIGURE IV-9 MAXIMUM EXCESS PORE PRESSURE RESPONSE CURVE
(SP1, BACK ARC FAULTS, 0.3g)



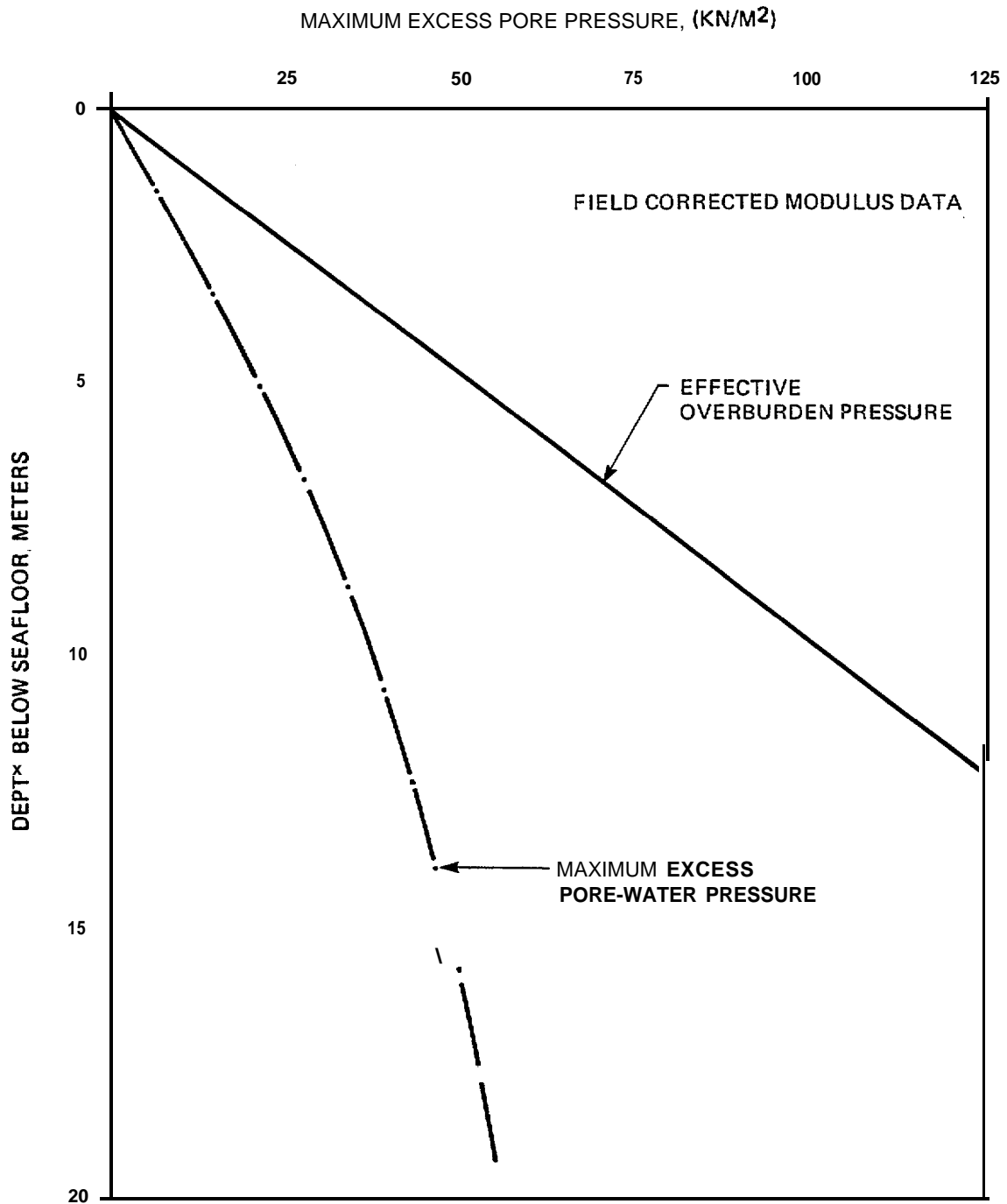
SOIL TYPE sp (1)
 EARTHQUAKE SOURCE BACK ARC FAULTS
 EARTHQUAKE RECORD (NORMALIZED TO $A_{max} = 0.6g$) EL CENTRO 1979
 MAXIMUM GROUND ACCELERATION A_{max}
 CONCLUSION: NO LIQUEFACTION

FIGURE IV-10 MAXIMUM EXCESS PORE PRESSURE RESPONSE CURVE
 (SP1, BACK ARC FAULTS, 0.6g)



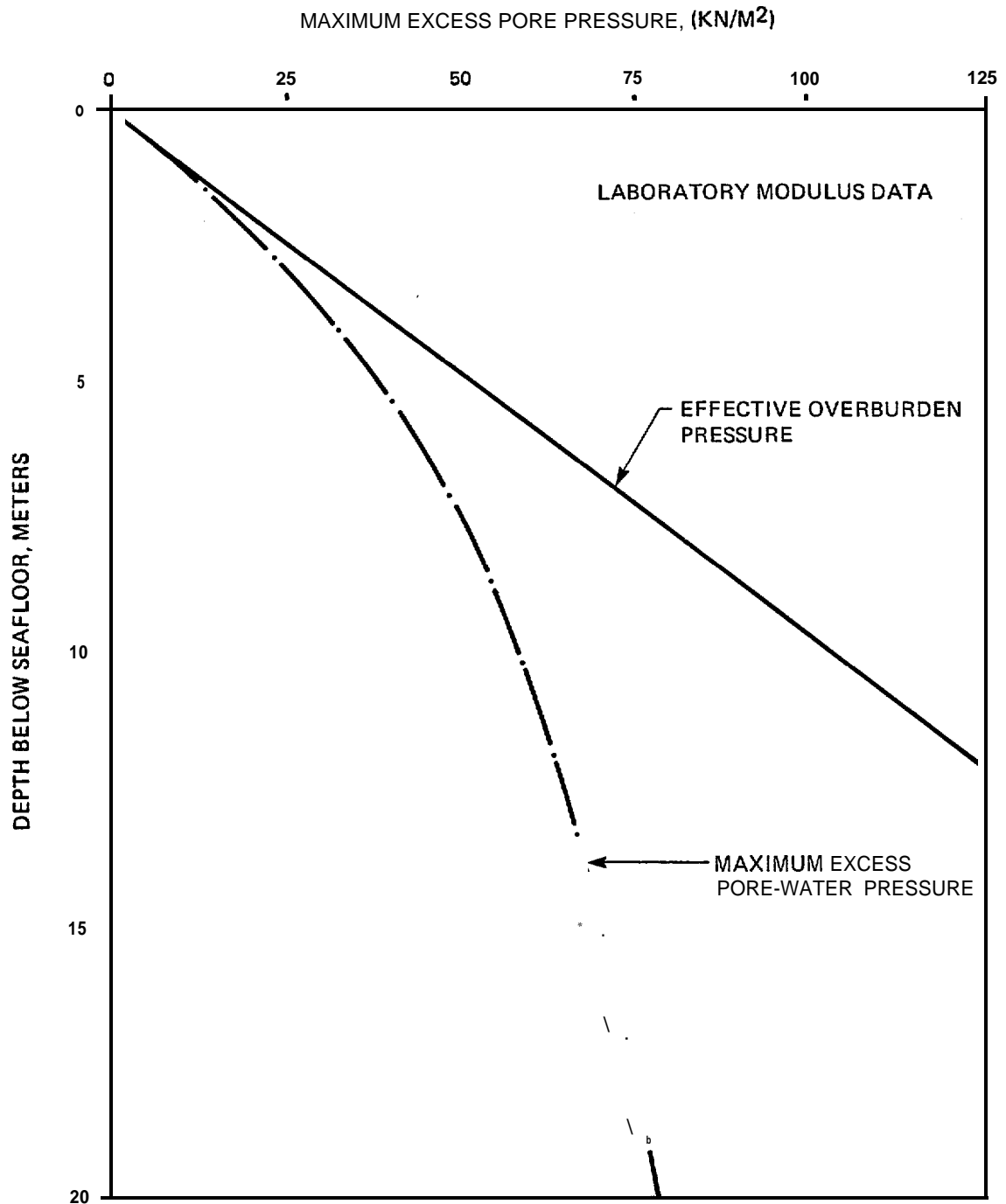
SOIL TYPE 'p'⁽¹⁾ _____
 EARTHQUAKE SOURCE ALEUTIAN ARC
 EARTHQUAKE RECORD (NORMALIZED TO $\frac{0.4g}{A_{max}}$) PARKFIELD 1966
 MAXIMUM GROUND ACCELERATION A_{max} _____
 CONCLUSION: NO LIQUEFACTION

FIGURE IV-I 1 MAXIMUM EXCESS PORE PRESSURE RESPONSE CURVE
 (SPI, ALEUTIAN ARC, 0.4g)



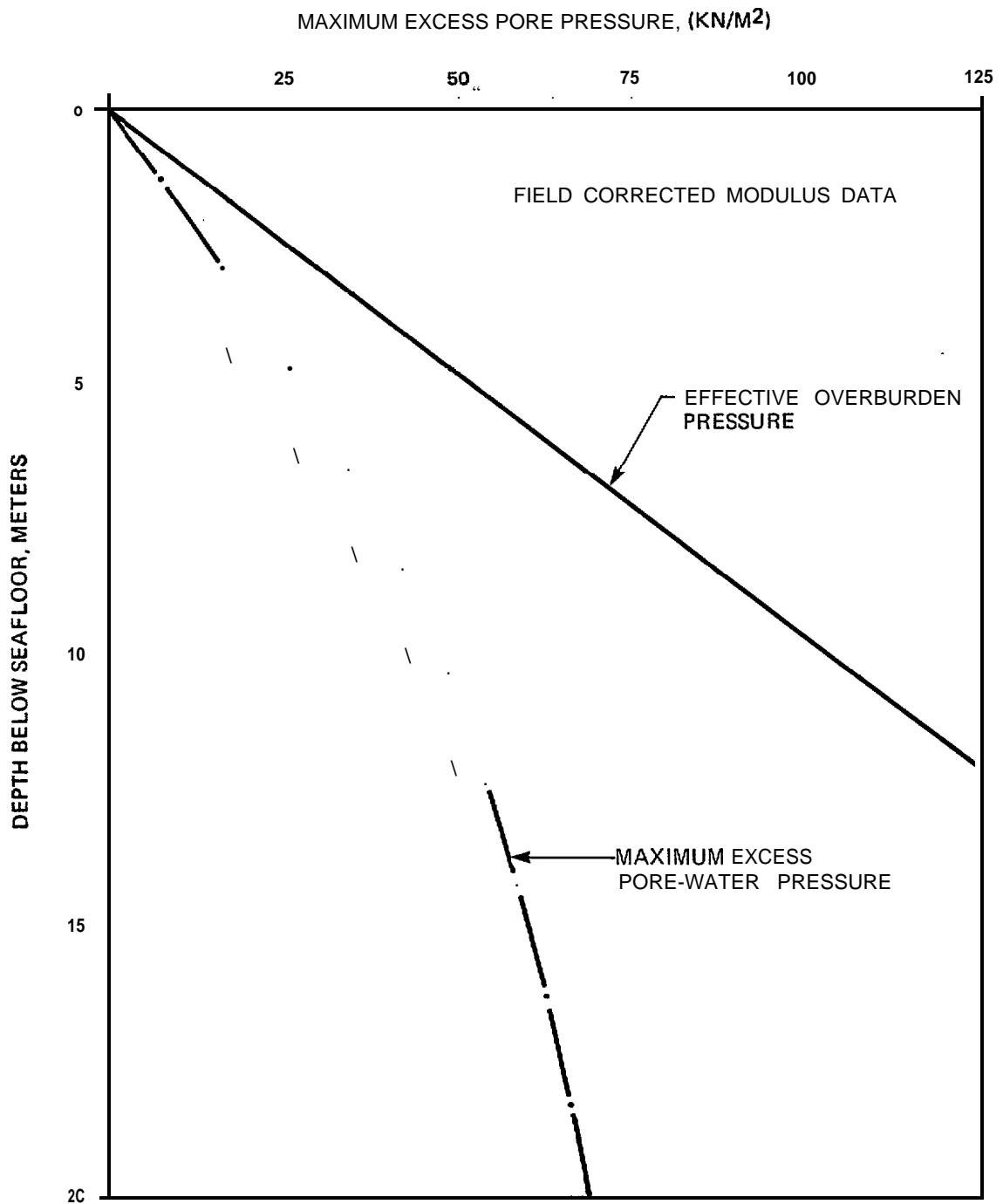
SOIL TYPE SP (2)
 EARTHQUAKE SOURCE subduction ZONE
 EARTHQUAKE RECORD (NORMALIZED TO A_g 0.16g) CAL TECH A-1
 MAXIMUM GROUND ACCELERATION A_{max}
 CONCLUSION: NO LIQUEFACTION

FIGURE IV-12 MAXIMUM EXCESS PORE PRESSURE RESPONSE CURVE
 (SP2, SUBDUCTION ZONE, 0.16g)



SOIL TYPE sp (2)
 EARTHQUAKE SOURCE SUBDUCTION ZONE
 EARTHQUAKE RECORD (NORMALIZED TO $A_{max} = 0.16g$) CAL TECH A-1
 MAXIMUM GROUND ACCELERATION A_{max}
 CONCLUSION: NO LIQUEFACTION

FIGURE IV-13 MAXIMUM EXCESS PORE PRESSURE RESPONSE CURVE
 (SP2, SUBDUCTION ZONE, 0.16g)



SOIL TYPE sp⁽²⁾

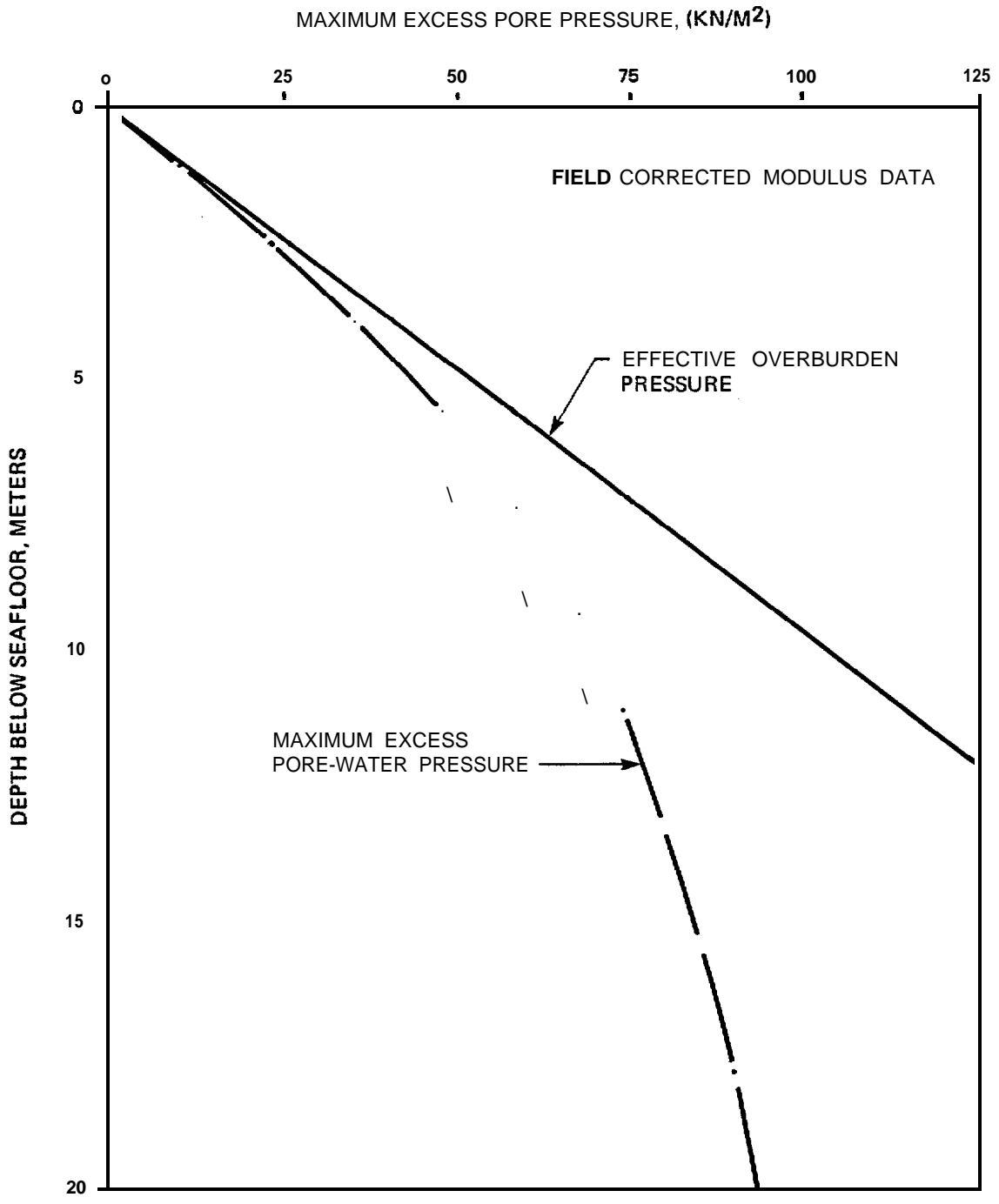
EARTHQUAKE SOURCE SUBDUCTION ZONE

EARTHQUAKE RECORD (NORMALIZE TO Amak = 0.19g) CAL TECH A-1

MAXIMUM GROUND ACCELERATION = Amak

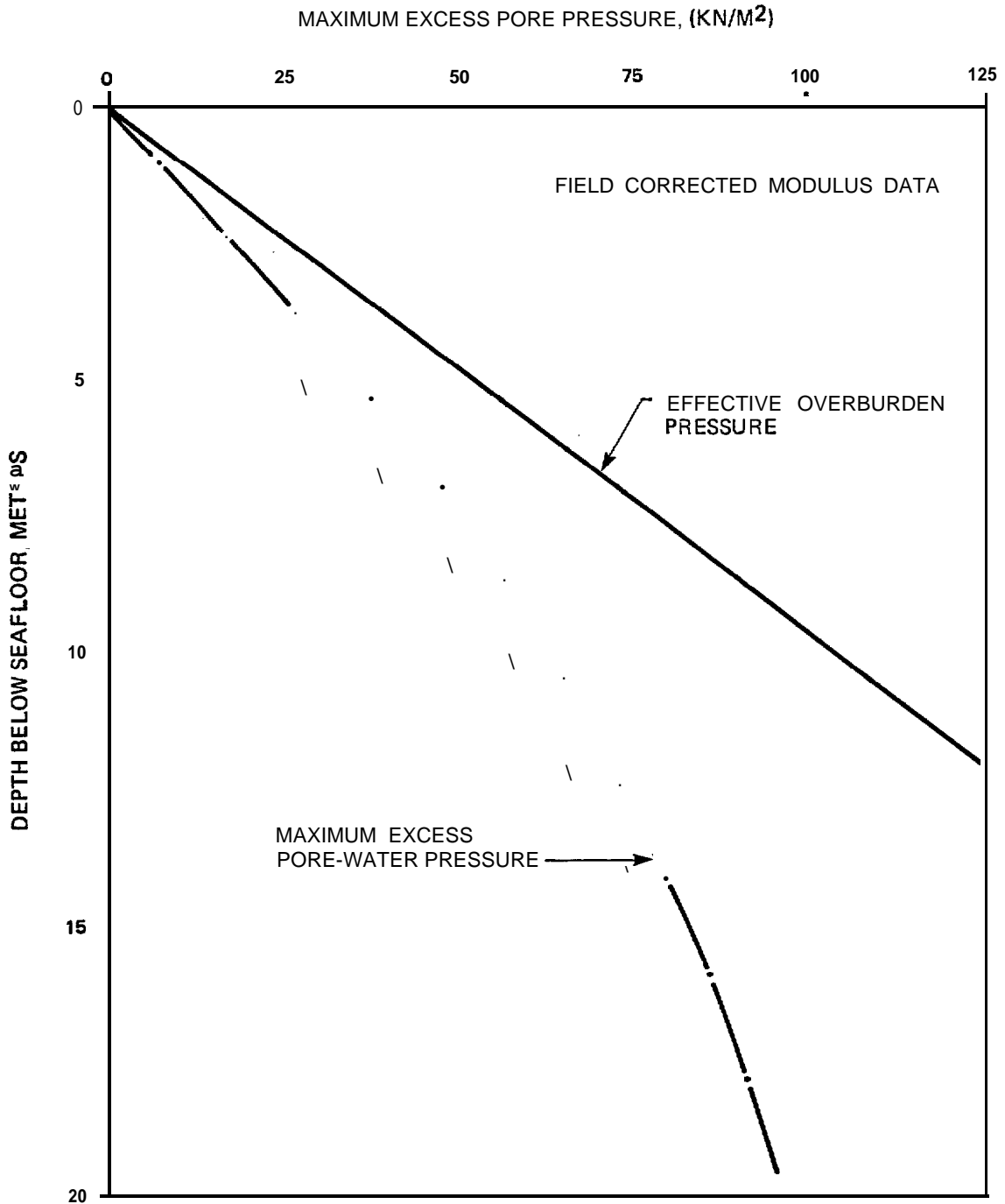
CONCLUSION: NO LIQUEFACTION

FIGURE IV-14 MAXIMUM EXCESS PORE PRESSURE RESPONSE CURVE
(SP2, SUBDUCTION ZONE, 0.19g)



SOIL TYPE SP (2)
 EARTHQUAKE SOURCE MAJOR GRABENS
 EARTHQUAKE RECORD INORMALIZED TO $A_{max} 0.4g$) TAFT 1952
 MAXIMUM GROUND ACCELERATION A_{max}
 CONCLUSION: NO LIQUEFACTION

FIGURE IV-15 MAXIMUM EXCESS PORE PRESSURE RESPONSE CURVE (SP2, MAJOR GRABENS, 0.4g)



SOIL TYPE sp⁽²⁾

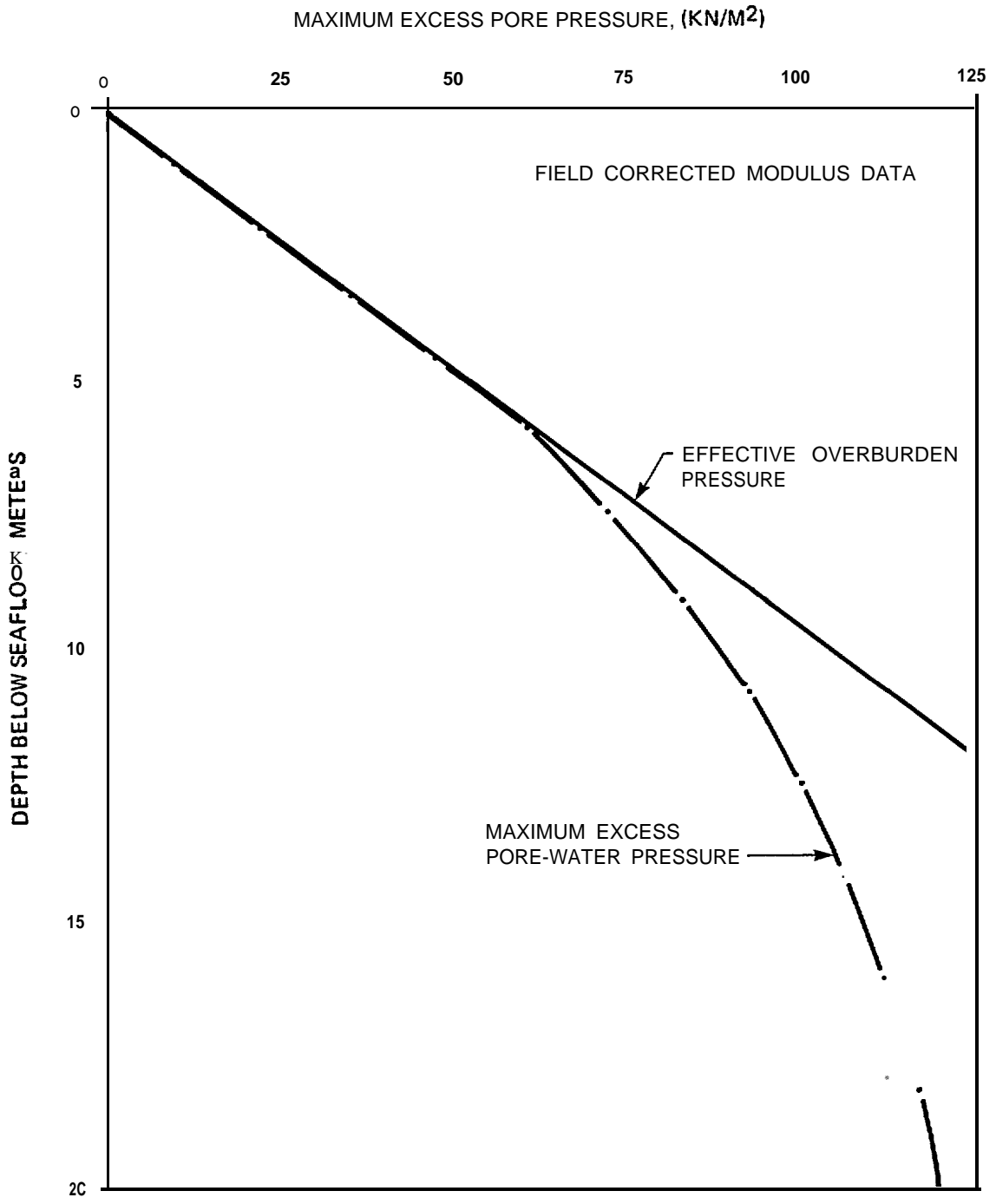
EARTHQUAKE SOURCE MAJOR GRABENS

EARTHQUAKE RECORD (NORMALIZED TO $A_{max} = 0.4g$) EL CENTRO 1940

MAXIMUM GROUND ACCELERATION A_{max}

CONCLUSION : NO LIQUEFACTION

FIGURE IV-16 MAXIMUM EXCESS PORE PRESSURE RESPONSE CURVE
(SP2, MAJOR GRABENS, 0.4g)



SOIL TYPE SP (2)

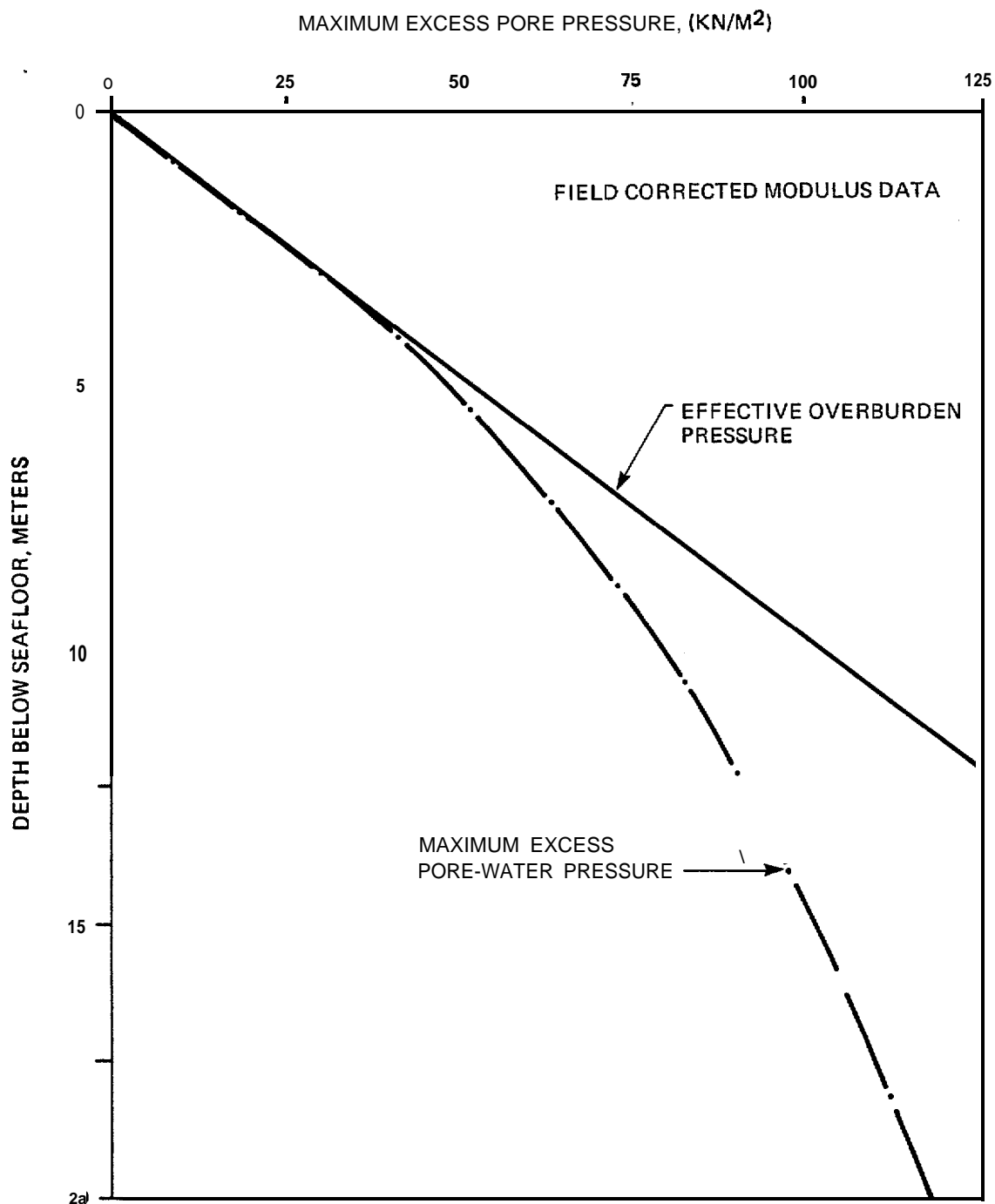
EARTHQUAKE SOURCE MAJOR GRABENS

EARTHQUAKE RECORD (NORMALIZED TO $A_{max} \leq 0.5g$) TAFT 1952

MAXIMUM GROUND ACCELERATION A_{max}

CONCLUSION: LIQUEFACTION TO 8 M

FIGURE IV-17 MAXIMUM EXCESS PORE PRESSURE RESPONSE CURVE
(SP2, MAJOR GRABENS, 0.%)



SOIL TYPE SP (2)

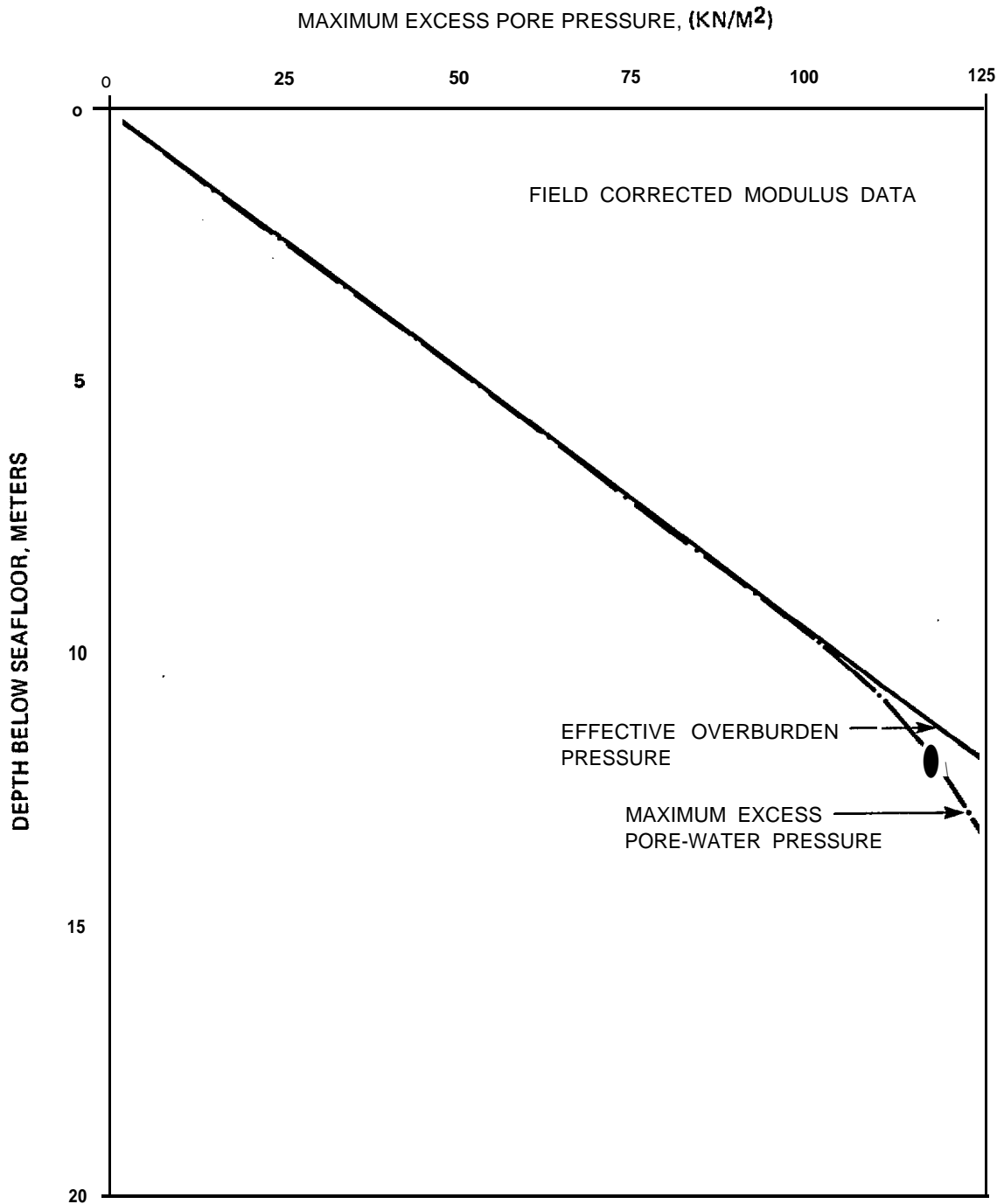
EARTHQUAKE SOURCE MAJOR GRABENS

EARTHQUAKE RECORD (NORMALIZED TO Am = 0.5g) EL CENTRO 1940

MAXIMUM GROUND ACCELERATION Am

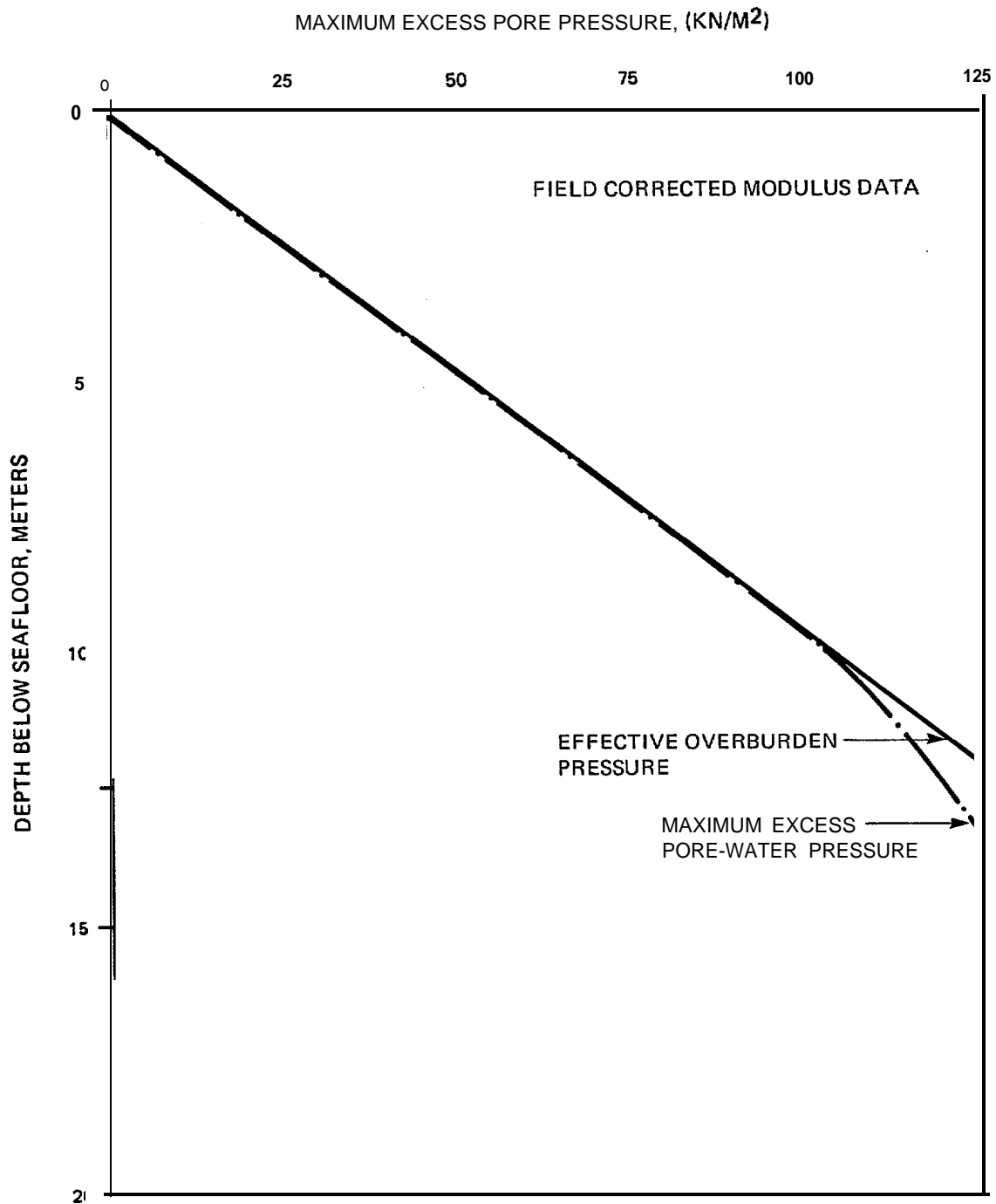
CONCLUSION: Liquefaction TO 3 M

FIGURE IV-18 MAXIMUM EXCESS PORE PRESSURE RESPONSE CURVE'
(SP2, MAJOR GRABENS, 0.5g)



SOIL TYPE 'p (2) _____
 EARTHQUAKE SOURCE MAJOR GRABENS _____
 EARTHQUAKE RECORD (NORMALIZED TO $A_m 0.7g$) EL CENTRO 1940 _____
 MAXIMUM GROUND ACCELERATION "Amax" _____
 CONCLUSION: LIQUEFACTION TO 14 M

FIGURE IV-19 MAXIMUM EXCESS PORE PRESSURE RESPONSE CURVE
 (SP2, MAJOR GRABENS, 0.7g)



SOIL TYPE ρ_p (2) _____

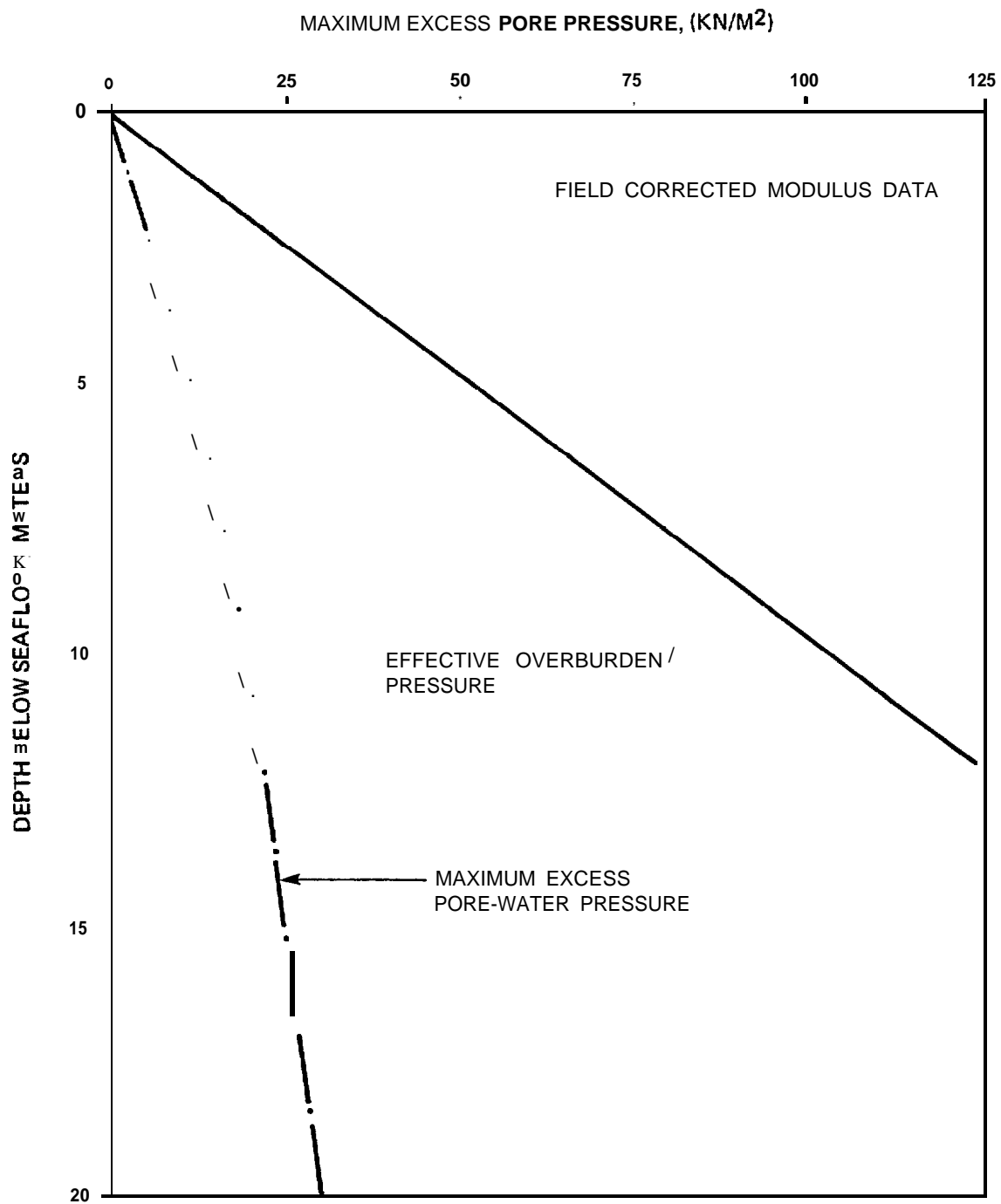
EARTHQUAKE SOURCE MAJOR GRABENS _____

EARTHQUAKE RECORD (NORMALIZED TO $A_{max} = \underline{0.7g}$) TAFT 1952 _____

MAXIMUM GROUND ACCELERATION $\underline{A_{max}}$ _____

CONCLUSION: LIQUEFACTION TO 14 M

FIGURE IV-20 MAXIMUM EXCESS PORE PRESSURE RESPONSE CURVE
(SP2, MAJOR GRABENS, 0.7g)



SOIL TYPE SP (2)

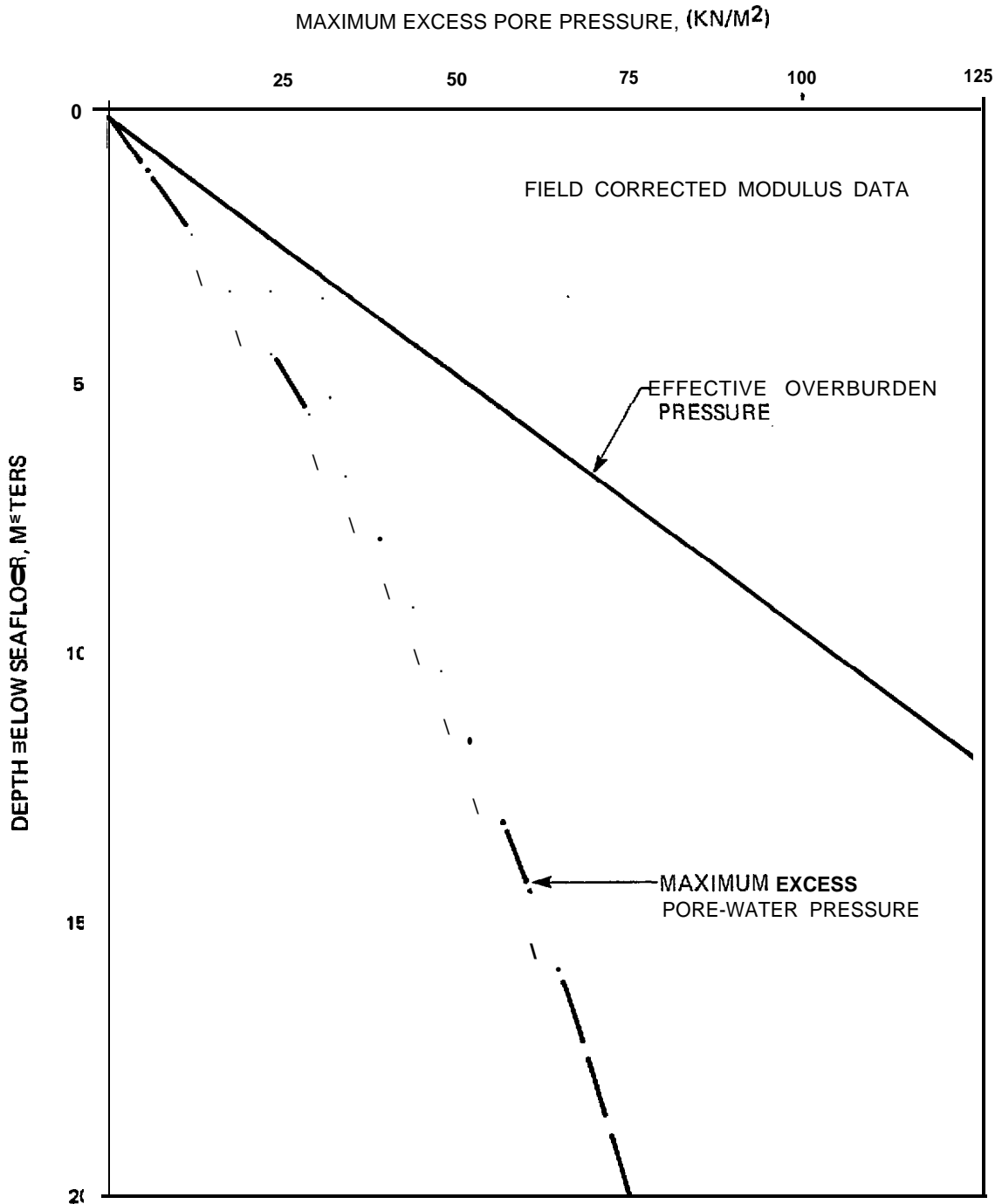
EARTHQUAKE SOURCE BACK ARC FAULTS

EARTHQUAKE RECORD (NORMALIZED TO $A_{max} = 0.3g$) EL CENTRO 1979

MAXIMUM GROUND ACCELERATION A_{max}

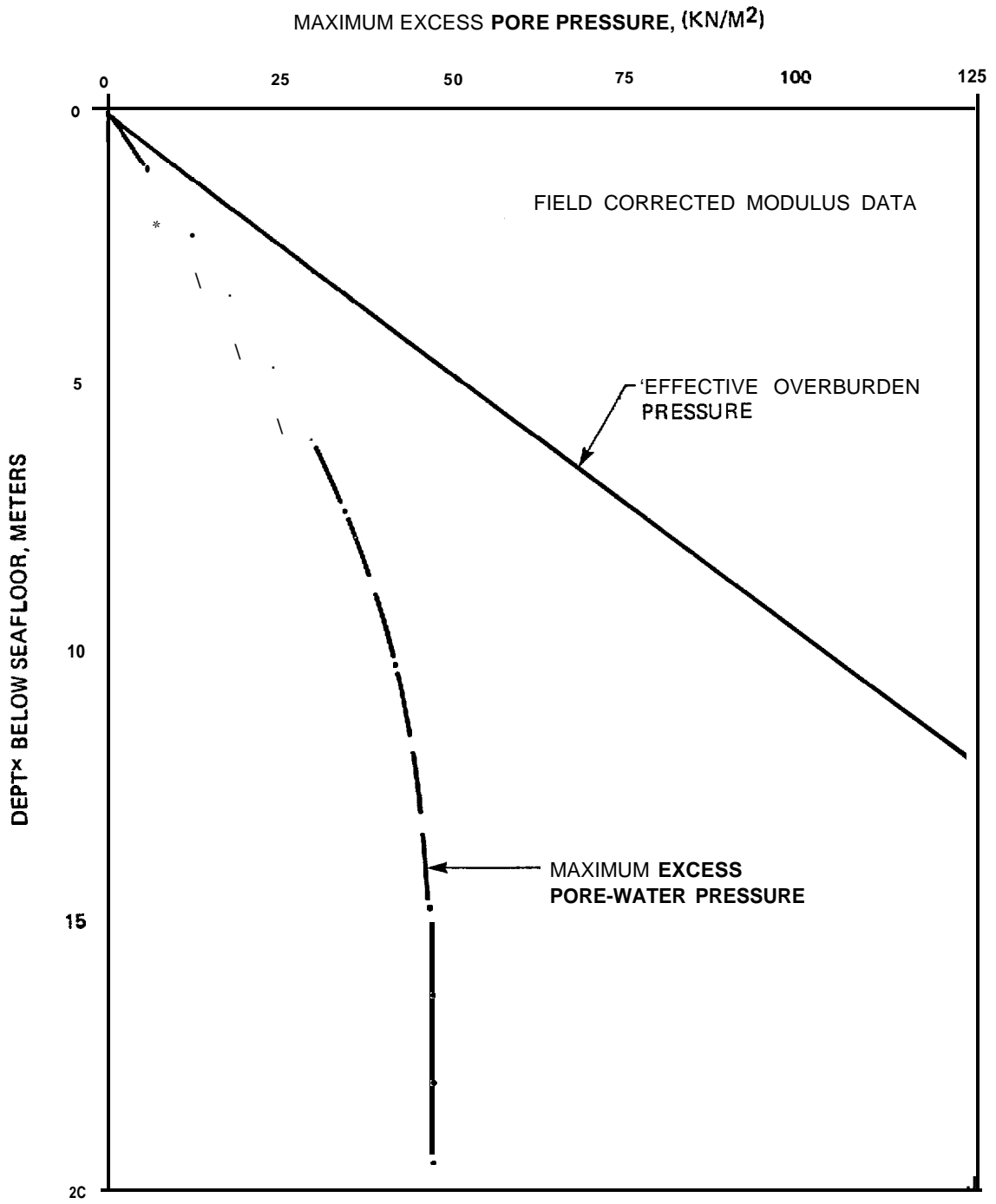
CONCLUSION: NO LIQUEFACTION

FIGURE IV-21 MAXIMUM EXCESS PORE PRESSURE RESPONSE CURVE
(SP2, BACK ARC FAULTS, 0.3g)



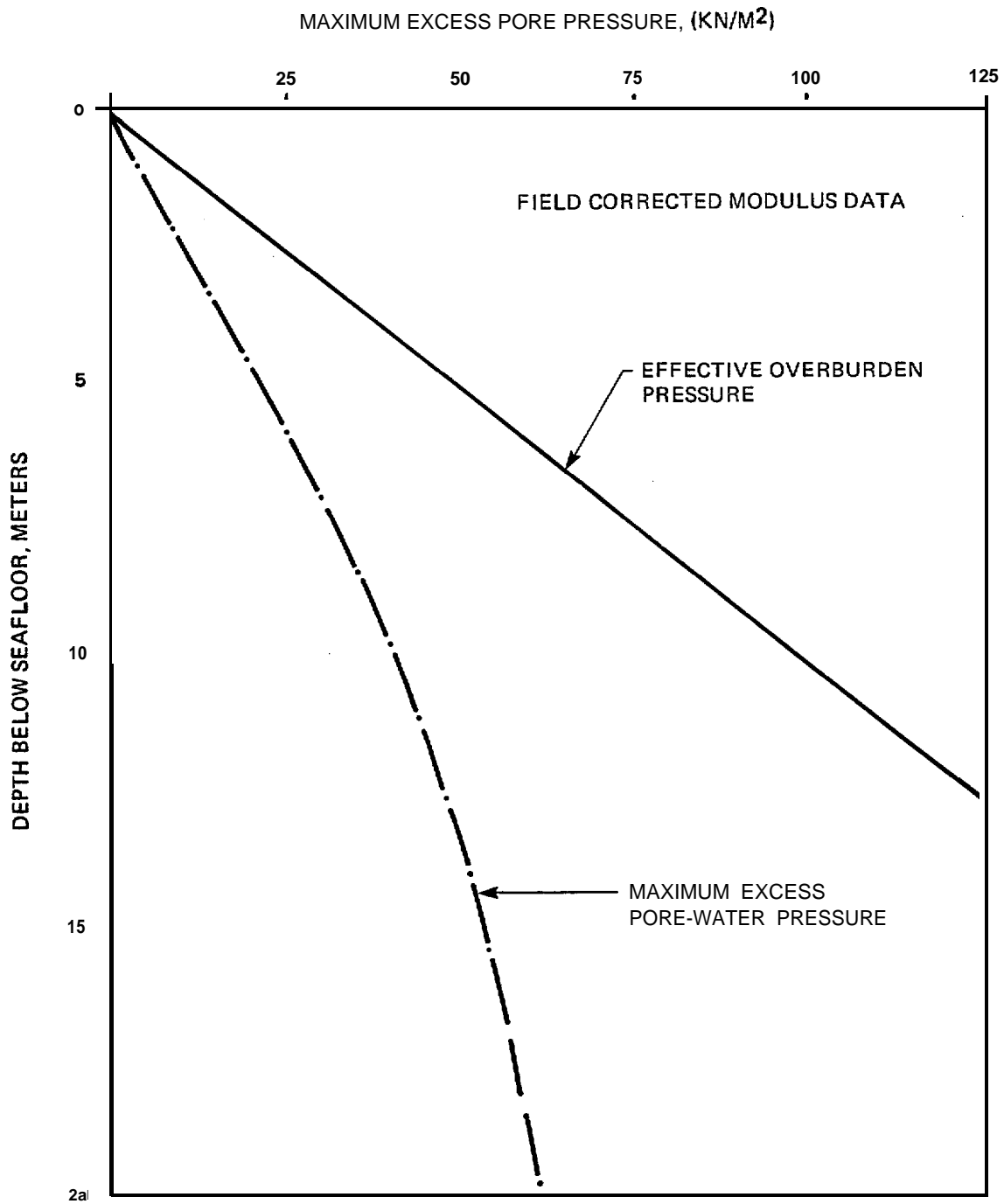
SOIL TYPE SP (2)
 EARTHQUAKE SOURCE BACK ARC FAULTS
 EARTHQUAKE RECORD (NORMALIZED TO A_{max} 0.6g) EL CENTRO 1979
 MAXIMUM GROUND ACCELERATION A_{max}
 CONCLUSION: NO LIQUEFACTION

FIGURE IV-22 MAXIMUM EXCESS PORE PRESSURE RESPONSE CURVE
 (SP2, BACK ARC FAULTS, 0.69)



SOIL TYPE SP (2)
 EARTHQUAKE SOURCE ALEUTIAN ARC
 EARTHQUAKE RECORD (NORMALIZED TO $A_{max}^{0.4g}$) PARKFIELD 1966
 MAXIMUM GROUND ACCELERATION A_{max}
 CONCLUSION: NO LIQUEFACTION

FIGURE IV-23 MAXIMUM EXCESS PORE PRESSURE RESPONSE CURVE
 (SP2, ALEUTIAN ARC, 0.4g)



SOIL TYPE SP/SM (3)

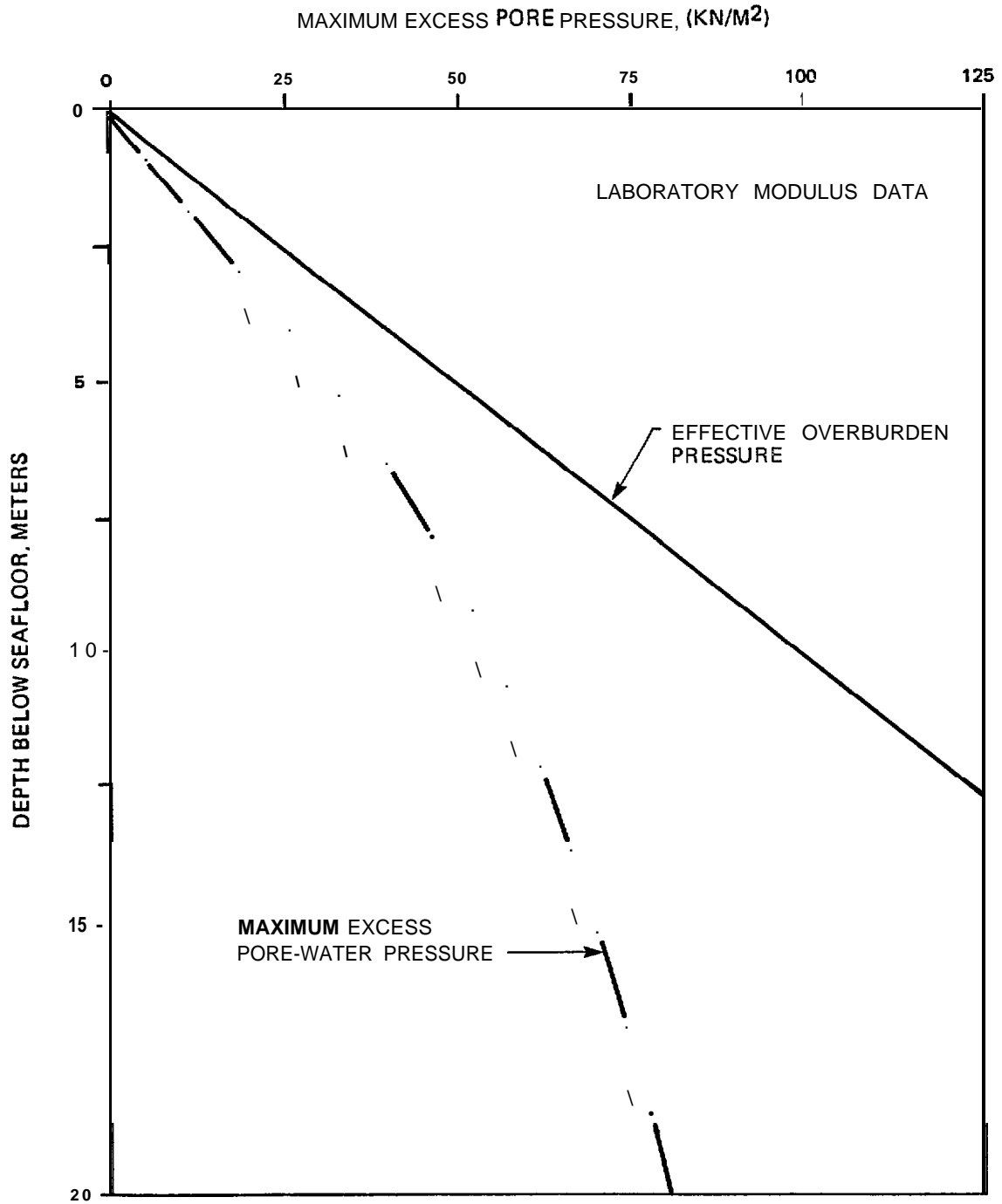
EARTHQUAKE SOURCE subduction ZONE

EARTHQUAKE RECORD INORMALIZED TO ($A_{1.0}$) CAL TECH A-1

MAXIMUM GROUND ACCELERATION A_{max}

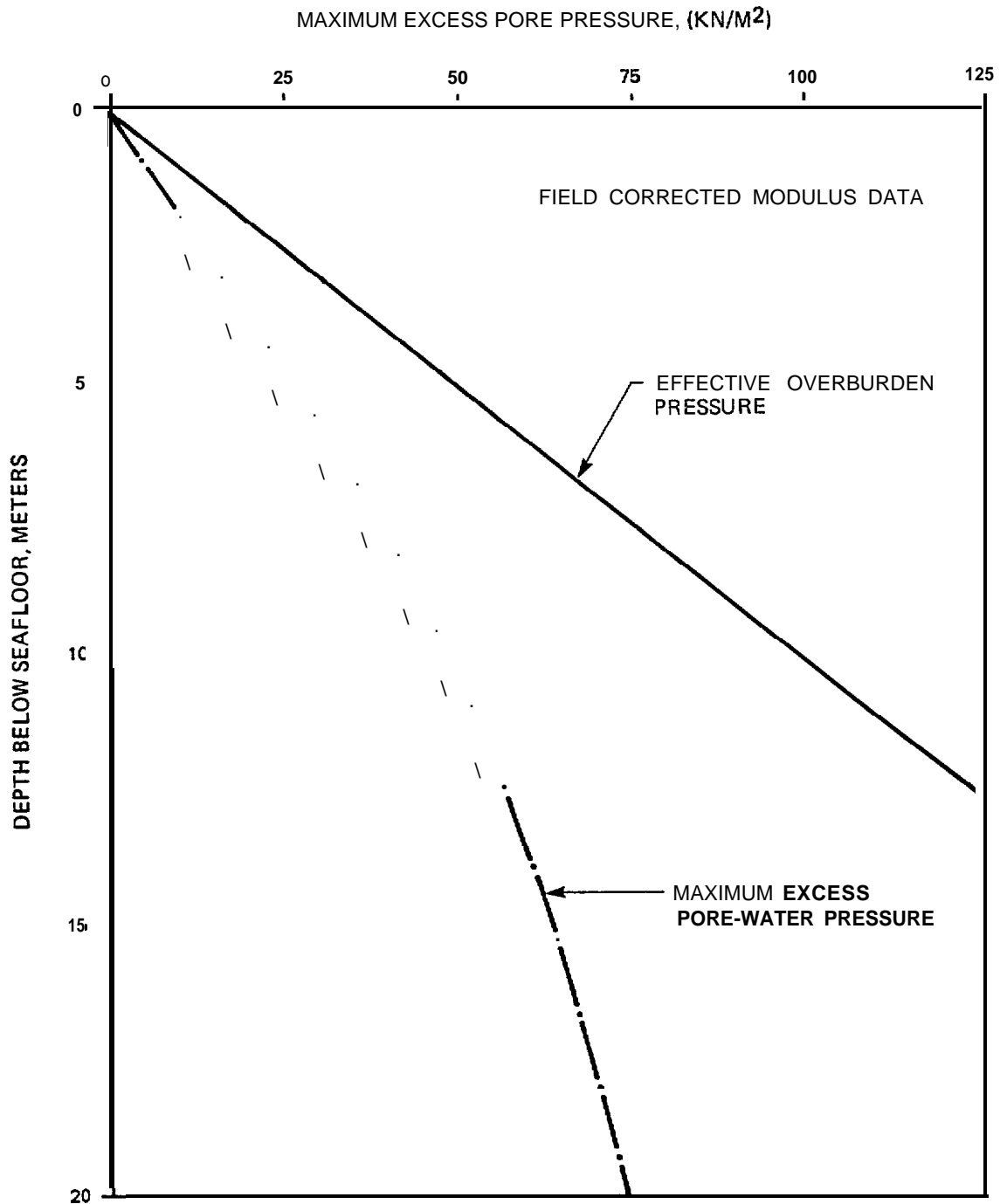
CONCLUSION: NO LIQUEFACTION

FIGURE IV-24 MAXIMUM EXCESS PORE PRESSURE RESPONSE CURVE (SP/SM3, SUBDUCTION ZONE, 0.16g)



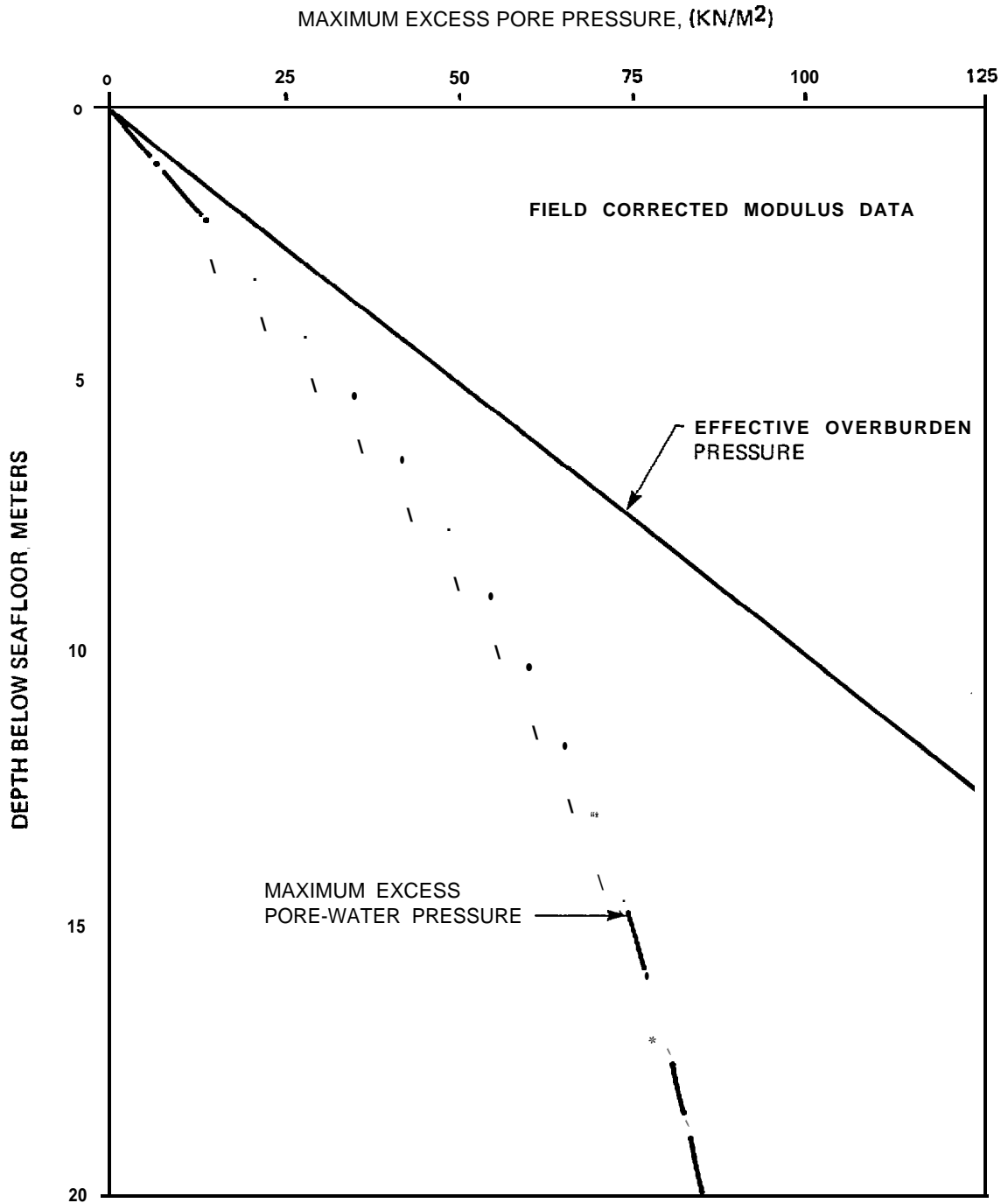
SOIL TYPE SP/SM(3)
 EARTHQUAKE SOURCE SUBDUCTION ZONE
 EARTHQUAKE RECORD (NORMALIZED TO A_{max} 0.16g) CAL TECH A-1
 MAXIMUM GROUND ACCELERATION A_{max}
 CONCLUSION : NO LIQUEFACTION

FIGURE IV-25 MAXIMUM EXCESS PORE PRESSURE RESPONSE CURVE
 (SP/SM3, SUBDUCTION ZONE, 0.16g)



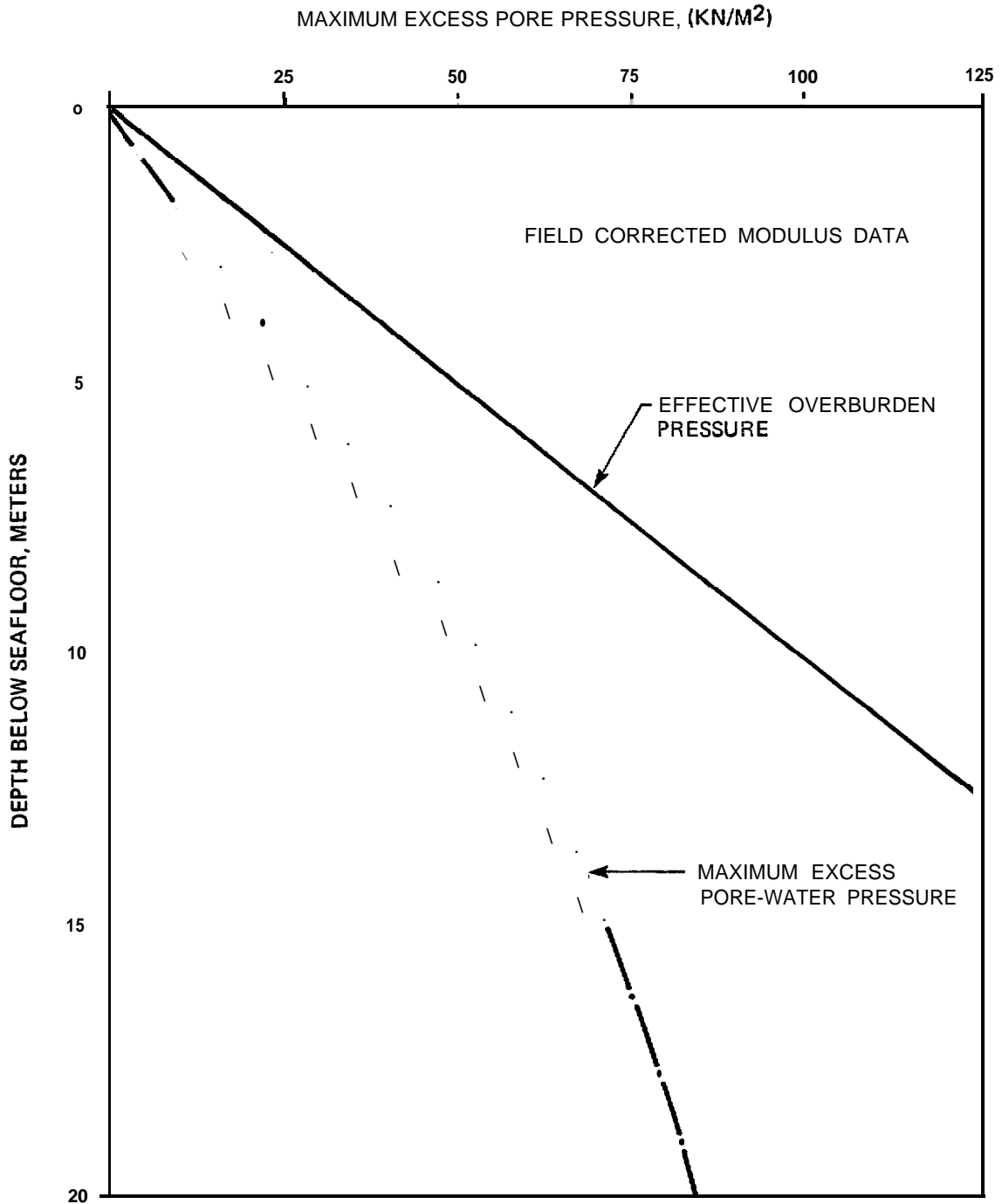
SOIL TYPE SP/SM (3)
 EARTHQUAKE SOURCE SUBDUCTION ONE
 EARTHQUAKE RECORD (NORMALIZED TO $A_{max} 0.19g$.) CAL TECH A-1
 MAXIMUM GROUND ACCELERATION $= A_{max}$
 CONCLUSION: NO LIQUEFACTION

FIGURE IV-26 MAXIMUM EXCESS PORE PRESSURE RESPONSE CURVE
 (SP/SM3, SUBDUCTION ZONE 0.19g)



SOIL TYPE SP/SM (3)
 EARTHQUAKE SOURCE MAJOR GRABENS
 EARTHQUAKE RECORD (NORMALIZE TO $A_{max} = 0.4g$) TAFT 1952
 MAXIMUM GROUND ACCELERATION A_{max}
 CONCLUSION: NO LIQUEFACTION

FIGURE IV-27 MAXIMUM EXCESS PORE PRESSURE RESPONSE CURVE
 (SP/SM3, MAJOR GRABENS, 0.4g)



SOIL TYPE SP/SM (3)

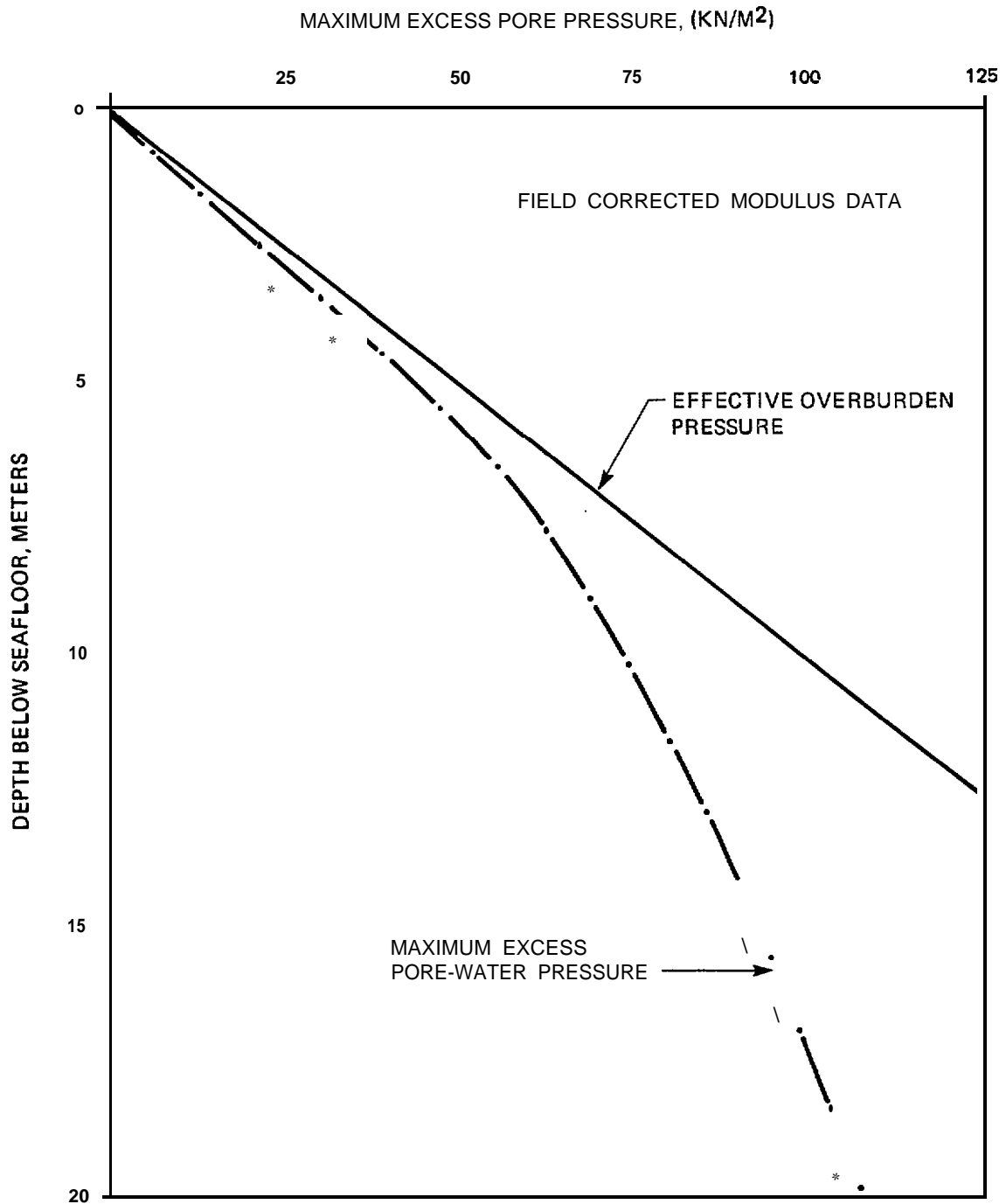
EARTHQUAKE SOURCE MAJOR GRABENS

EARTHQUAKE RECORD (NORMALIZED TO A_{max} 0.4g) EL CENTRO 1940

MAXIMUM GROUND ACCELERATION A_{max} _____

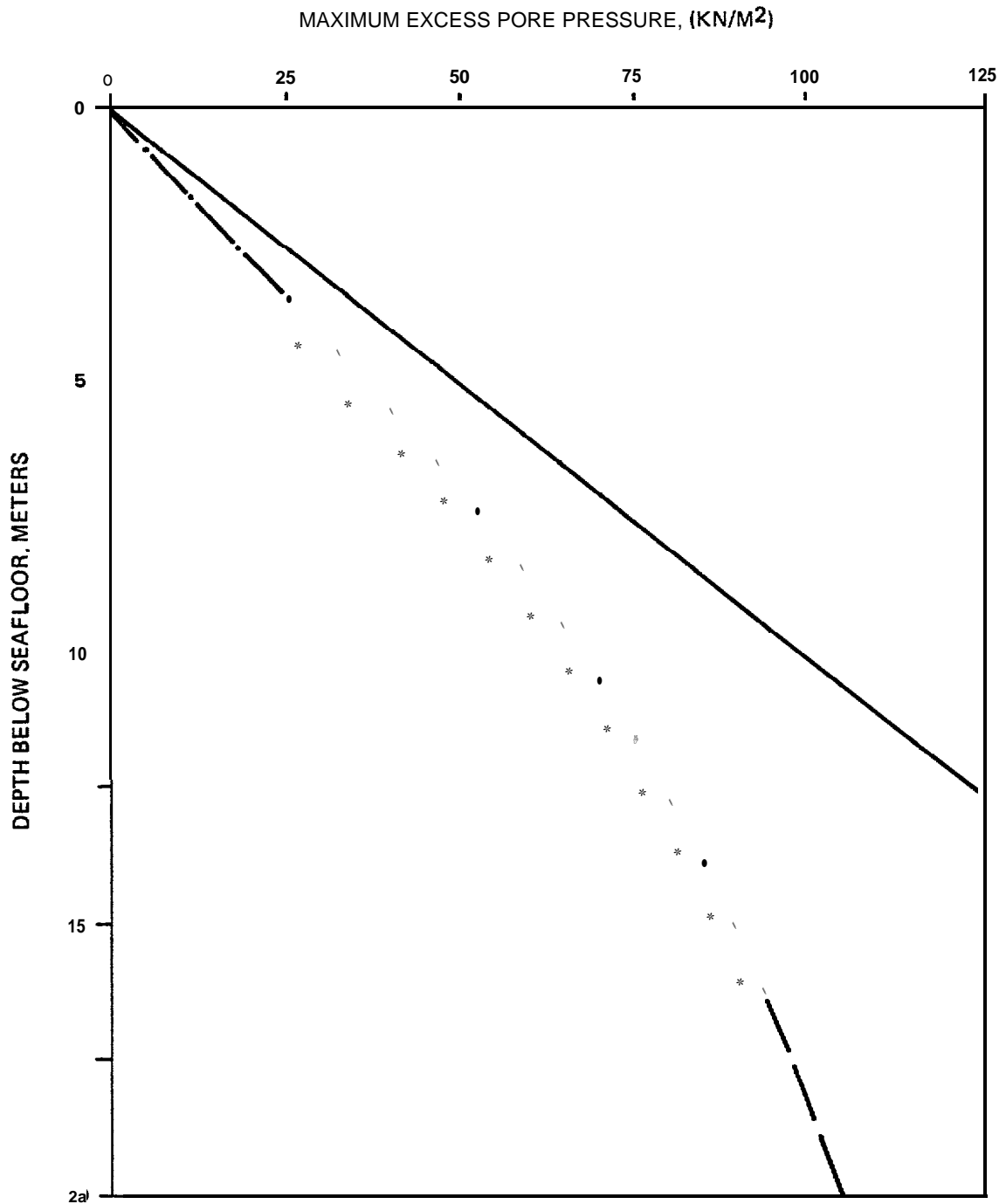
CONCLUSION: NO LIQUEFACTION

FIGURE IV-28 MAXIMUM EXCESS PORE PRESSURE RESPONSE CURVE
(SP/SM3, MAJOR GRABENS, 0.4g)



SOIL TYPE SP/SM (3)
 EARTHQUAKE SOURCE MAJOR GRABENS
 EARTHQUAKE RECORD (NORMALIZED TO $A_{max} = 0.5g$) TAFT 1952
 MAXIMUM GROUND ACCELERATION = A_{max}
 CONCLUSION: NO LIQUEFACTION

FIGURE IV-29 MAXIMUM EXCESS PORE PRESSURE RESPONSE CURVE
 (SP/SM3, MAJOR GRABENS, 0.5g)



SOIL TYPE SP/SM(3)

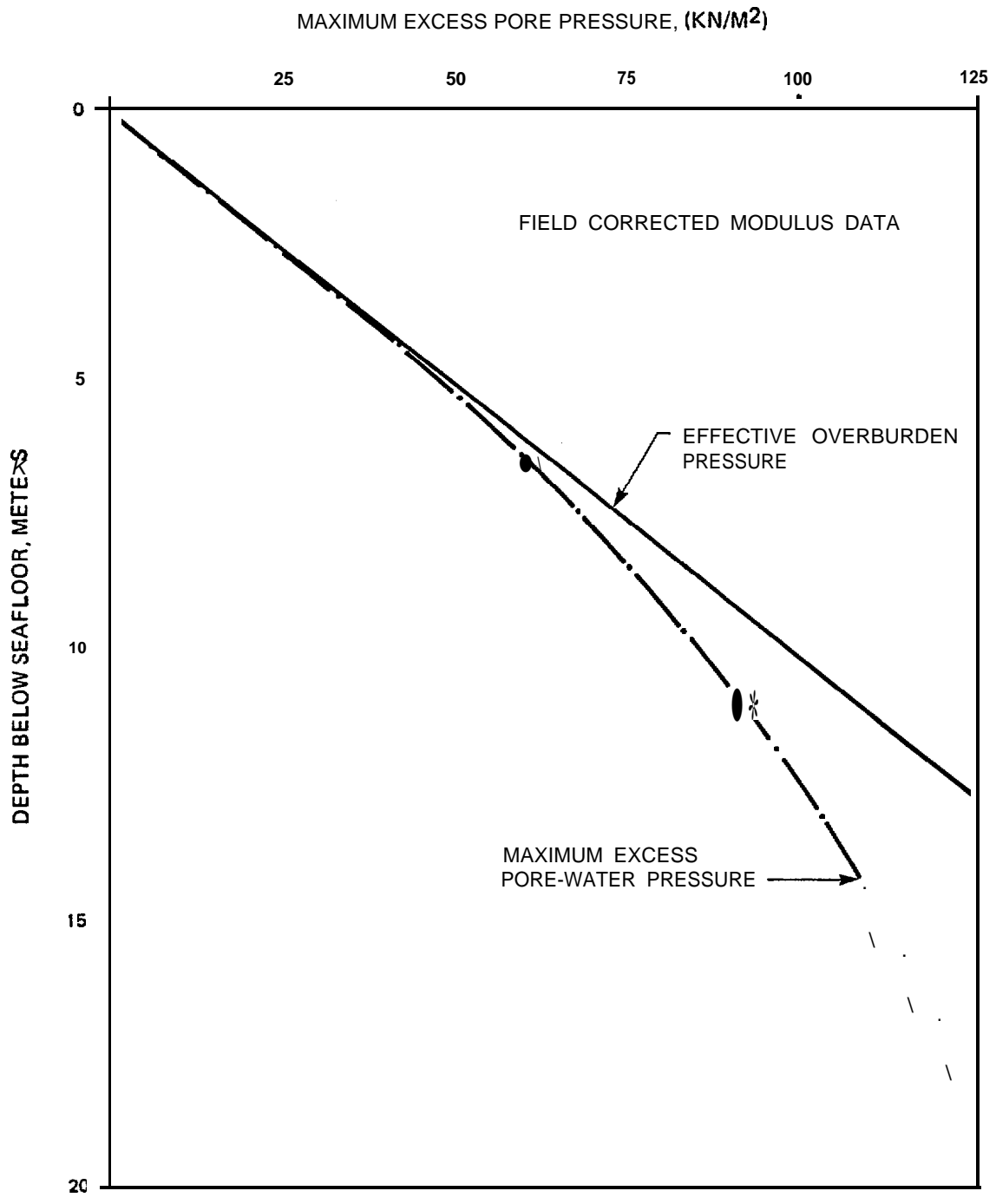
EARTHQUAKE SOURCE MAJOR GRABENS

EARTHQUAKE RECORD (NORMALIZED TO $A_{max} = 0.5g$) EL CENTRO 1940

MAXIMUM GROUND ACCELERATION A_{max}

CONCLUSION : NO LIQUEFACTION

FIGURE IV-30 MAXIMUM EXCESS PORE PRESSURE RESPONSE CURVE
(SP/SM3, MAJOR GRABENS, 0.5g)



SOIL TYPE SP/SM (c)

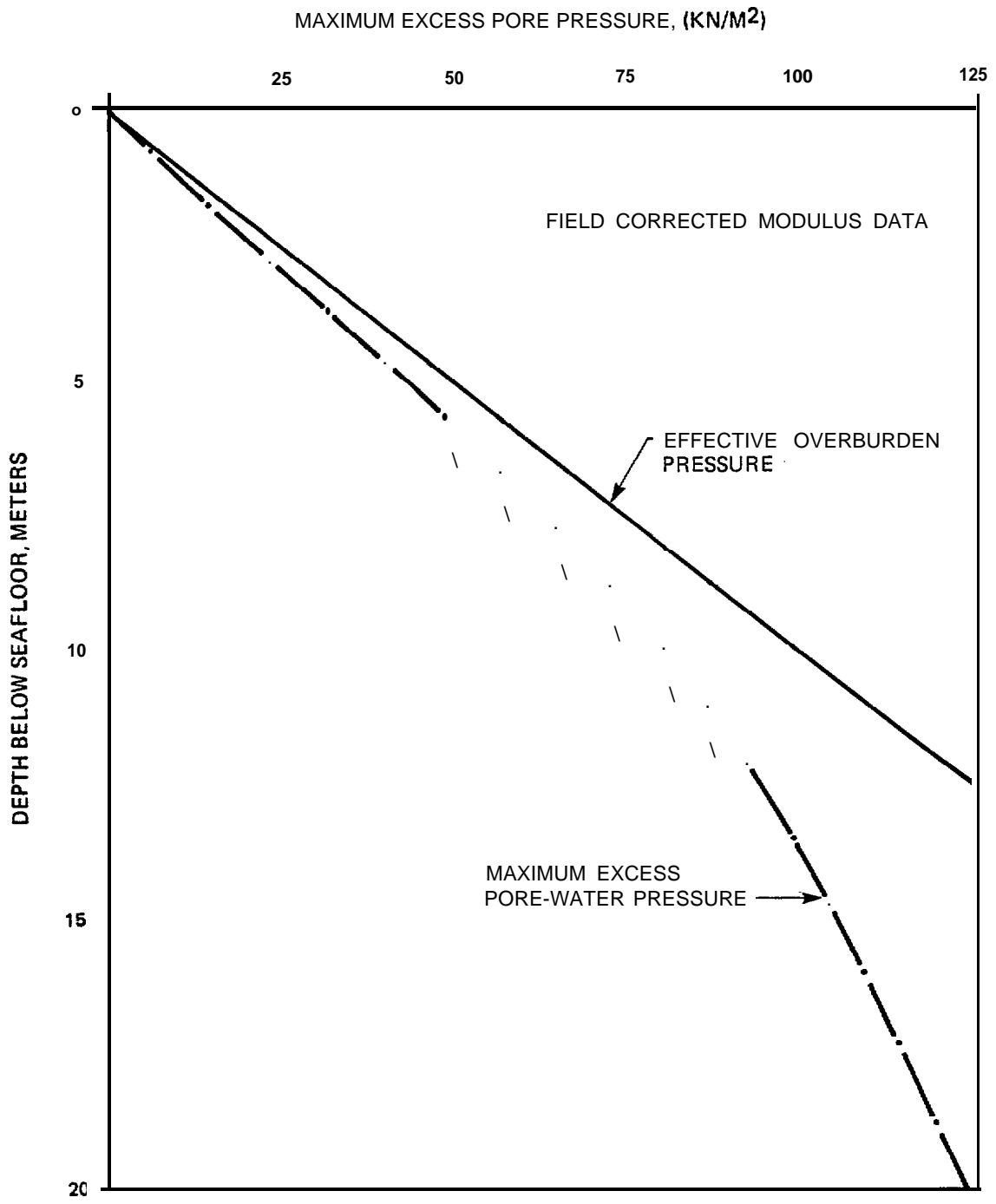
EARTHQUAKE SOURCE MAJOR GRABENS

EARTHQUAKE RECORD (NORMALIZED TO 0.6g) TAFT 1952

MAXIMUM GROUND ACCELERATION 0.6g

CONCLUSION : LIQUEFACTION TO 3.8 M

FIGURE IV-31 MAXIMUM EXCESS PORE PRESSURE RESPONSE CURVE
(SP/SM3, MAJOR GRABENS, 0.6g)



SOIL TYPE SP/SM (3)

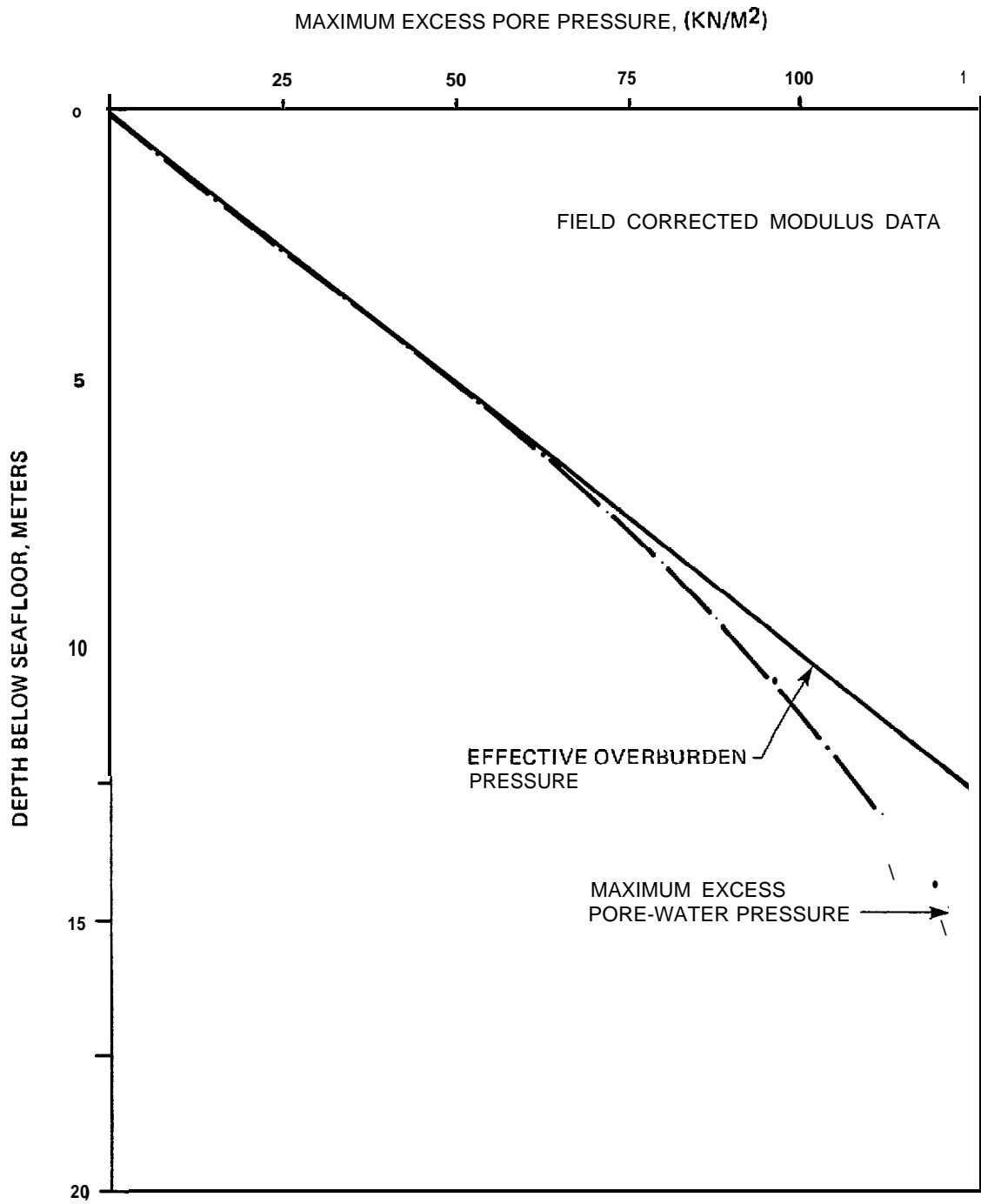
EARTHQUAKE SOURCE MAJOR GRABENS

EARTHQUAKE RECORD (NORMALIZED TO $A_{max} 0.6g$) EL CENTRO 1940

MAXIMUM GROUND ACCELERATION A_{max}

CONCLUSION: NO LIQUEFACTION

FIGURE IV-32 MAXIMUM EXCESS PORE PRESSURE RESPONSE CURVE
(SP/SM3, MAJOR GRABENS, 0.6g)



SOIL TYPE SP/SM (3)

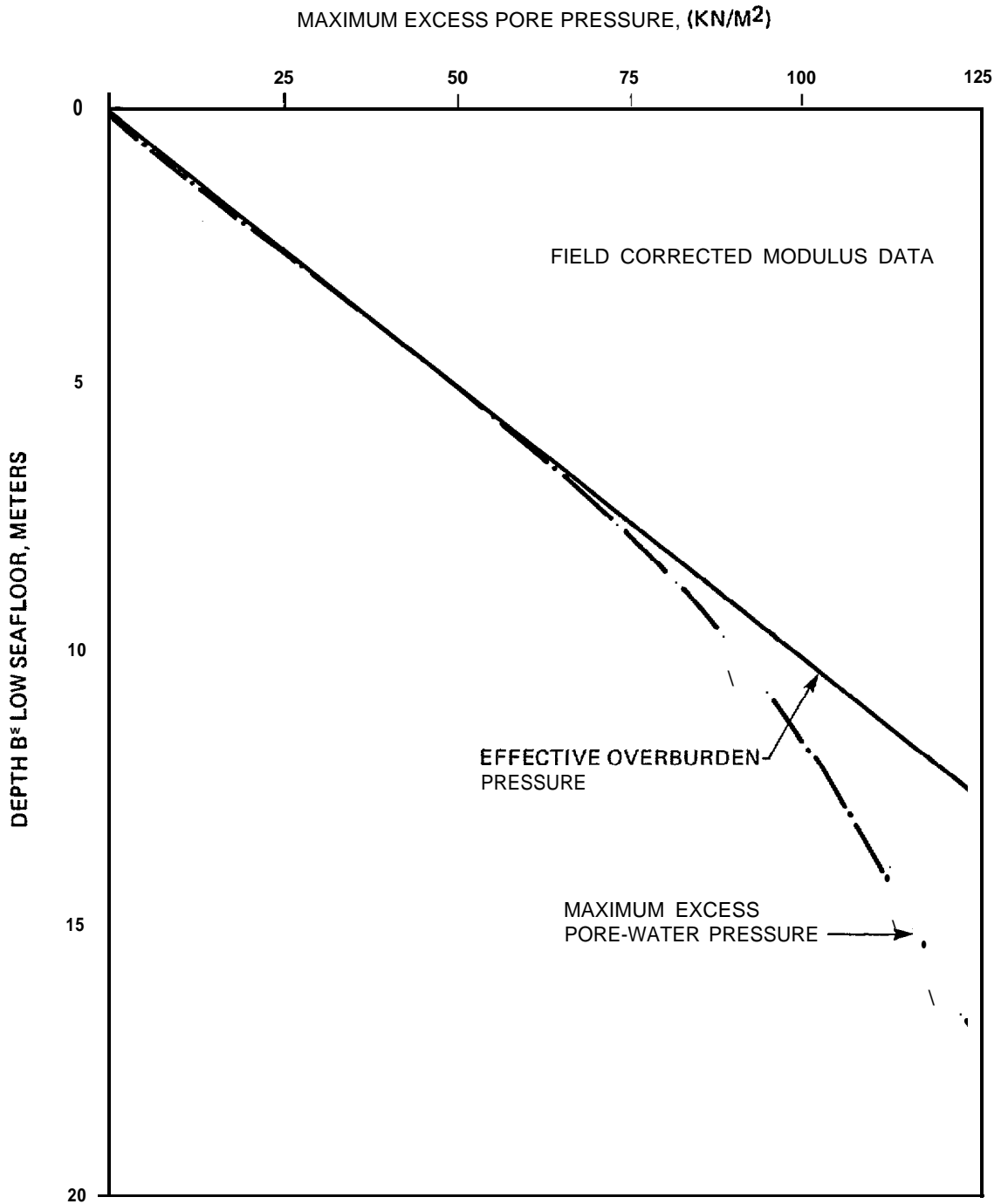
EARTHQUAKE SOURCE MAJOR GRABENS

EARTHQUAKE RECORD (NORMALIZED TO 0.7g) TAFT 1952

MAXIMUM GROUND ACCELERATION 0.7g

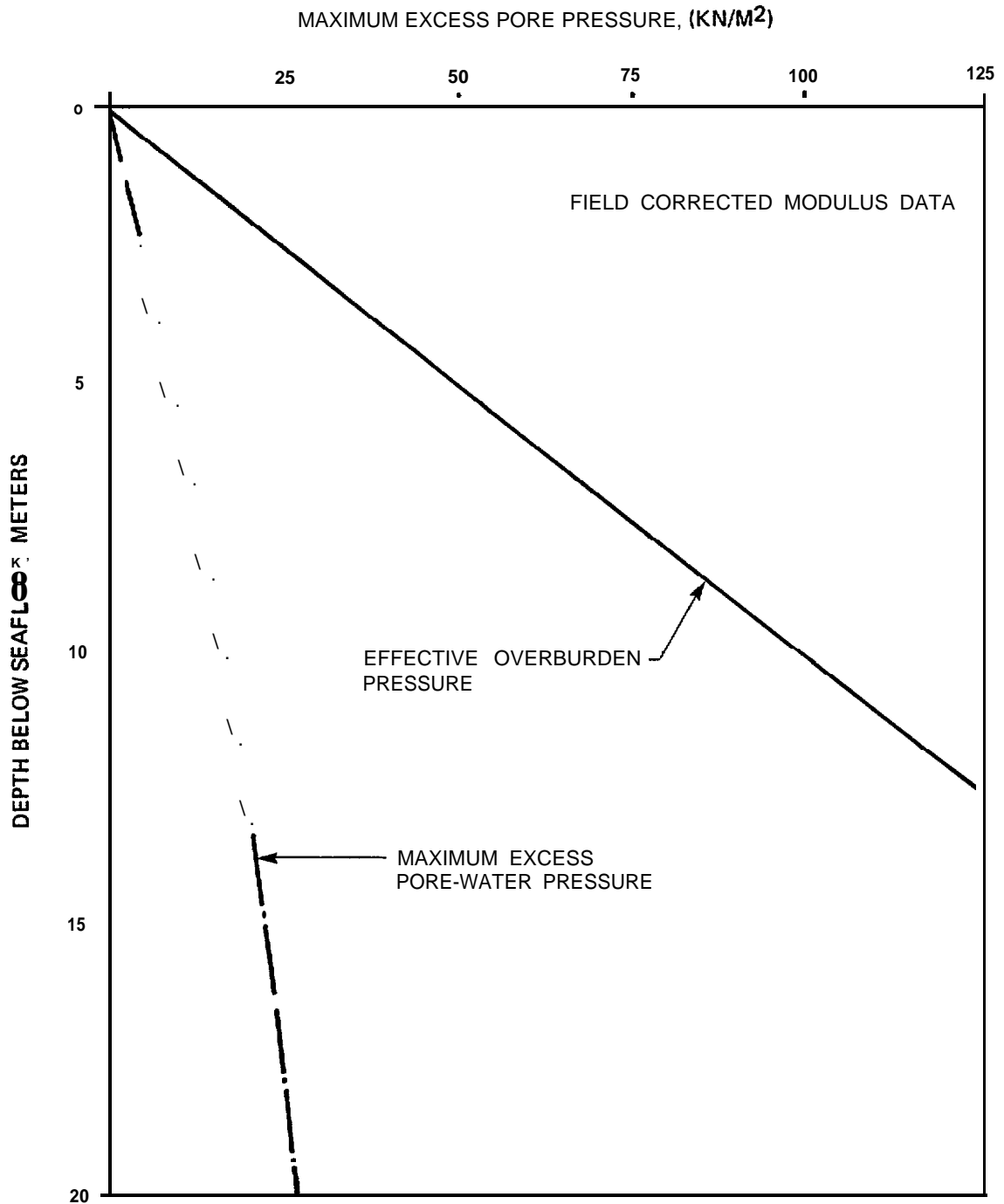
CONCLUSION : LIQUEFACTION TO 8 M

FIGURE IV-33 MAXIMUM EXCESS PORE PRESSURE RESPONSE CURVE
(SP/SM3, MAJOR GRABENS, 0.7g)



SOIL TYPE SP/SM (3)
 EARTHQUAKE SOURCE MAJOR GRABENS
 EARTHQUAKE RECORD (NORMALIZED TO $A_{max}^{0.7g}$) EL CENTRO 1940
 MAXIMUM GROUND ACCELERATION A_{max}
 CONCLUSION: LIQUEFACTION TO 8 M

FIGURE IV-34 MAXIMUM EXCESS PORE PRESSURE RESPONSE CURVE
 (SP/SM3, MAJOR GRABENS, 0.7g)



SOIL TYPE SP/SM (3)

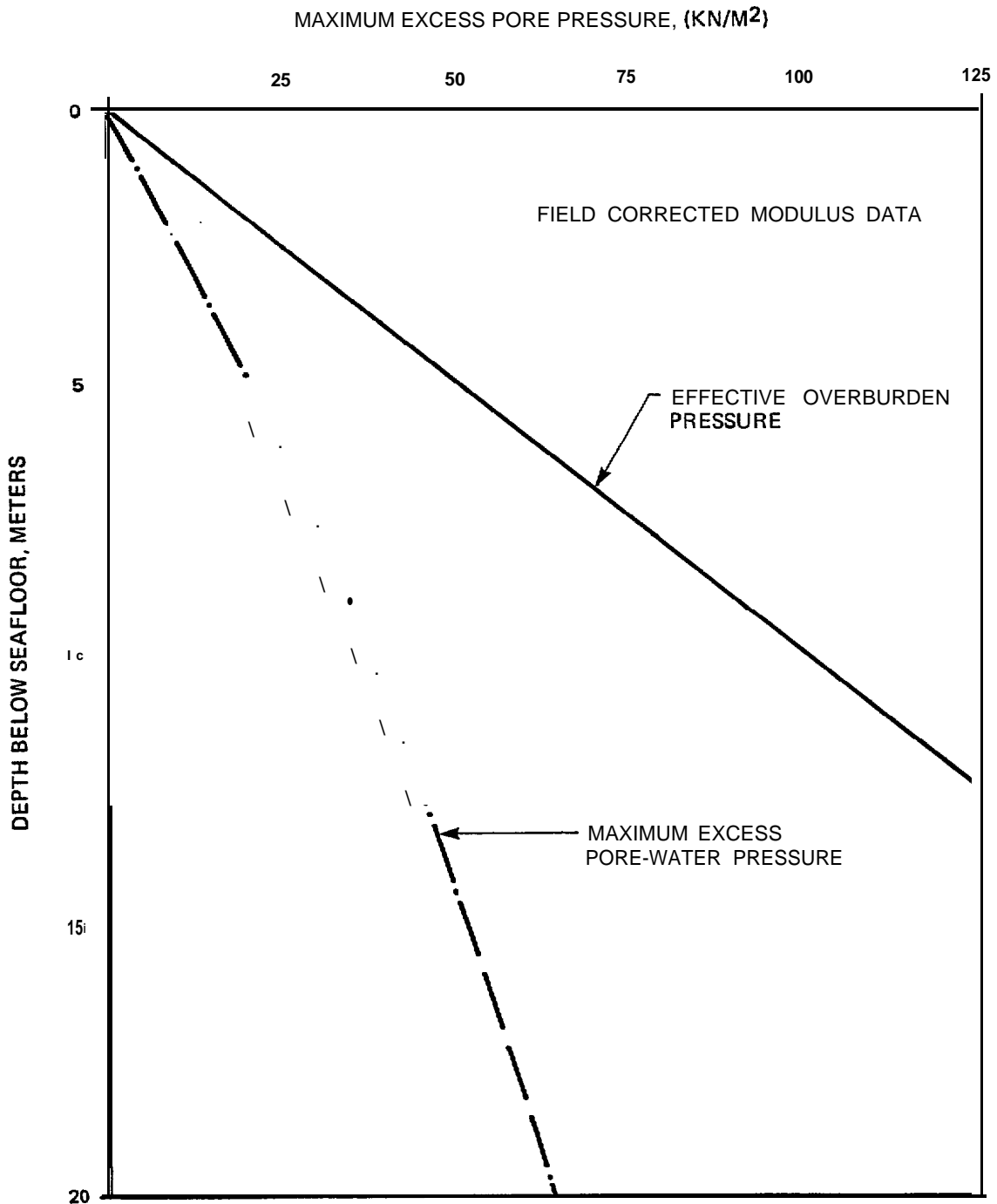
EARTHQUAKE SOURCE BACK ARC FAULTS

EARTHQUAKE RECORD (NORMALIZED TO $A_{max} = 0.3g$) EL CENTRO 1979

MAXIMUM GROUND ACCELERATION A_{max} _____

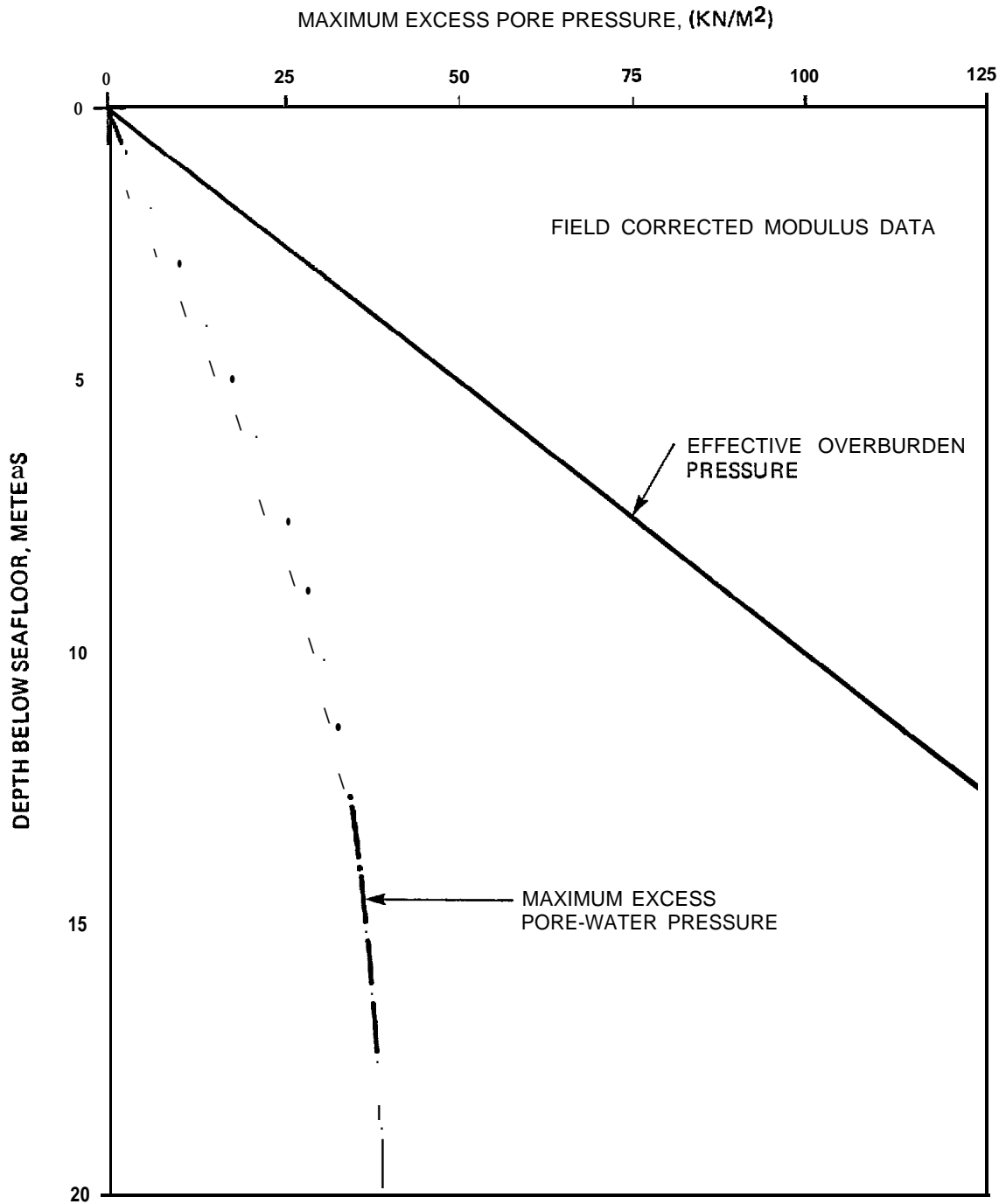
CONCLUSION: NO LIQUEFACTION

FIGURE IV-35 MAXIMUM EXCESS PORE PRESSURE RESPONSE CURVE
(SP/SM3, BACK ARC FAULTS, 0.3g)



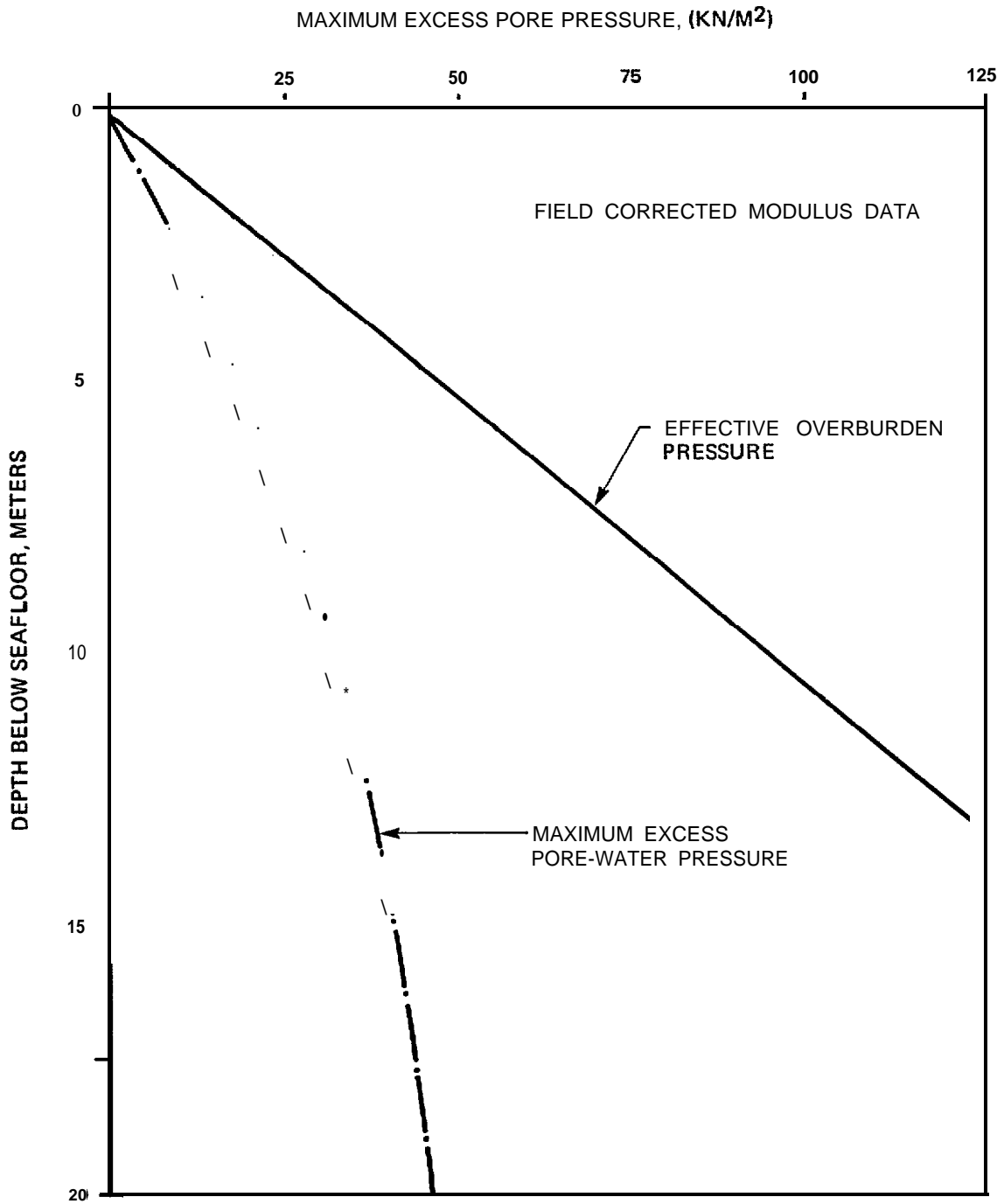
SOIL TYPE SP/SM (3)
 EARTHQUAKE SOURCE BACK ARC FAULTS
 EARTHQUAKE RECORD (NORMALIZED TO $A_{max} = 0.6g$) EL CENTRO 1979
 MAXIMUM GROUND ACCELERATION A_{max} _____
 CONCLUSION: NO LIQUEFACTION

FIGURE IV-36 MAXIMUM EXCESS PORE PRESSURE RESPONSE CURVE
 (SP/SM3, BACK ARC FAULTS, 0.6g)



SOIL TYPE SP/SM (3)
 EARTHQUAKE SOURCE ALEUTIAN ARC
 EARTHQUAKE RECORD (NORMALIZED TO $A_{max} = 0.4g$) PARKFIELD 1966
 MAXIMUM GROUND ACCELERATION A_{max}
 CONCLUSION: NO LIQUEFACTION

FIGURE IV-37 MAXIMUM EXCESS PORE PRESSURE RESPONSE CURVE
 (SP/SM3, ALEUTIAN ARC, 0.4g)



SOIL TYPE SM⁽⁴⁾

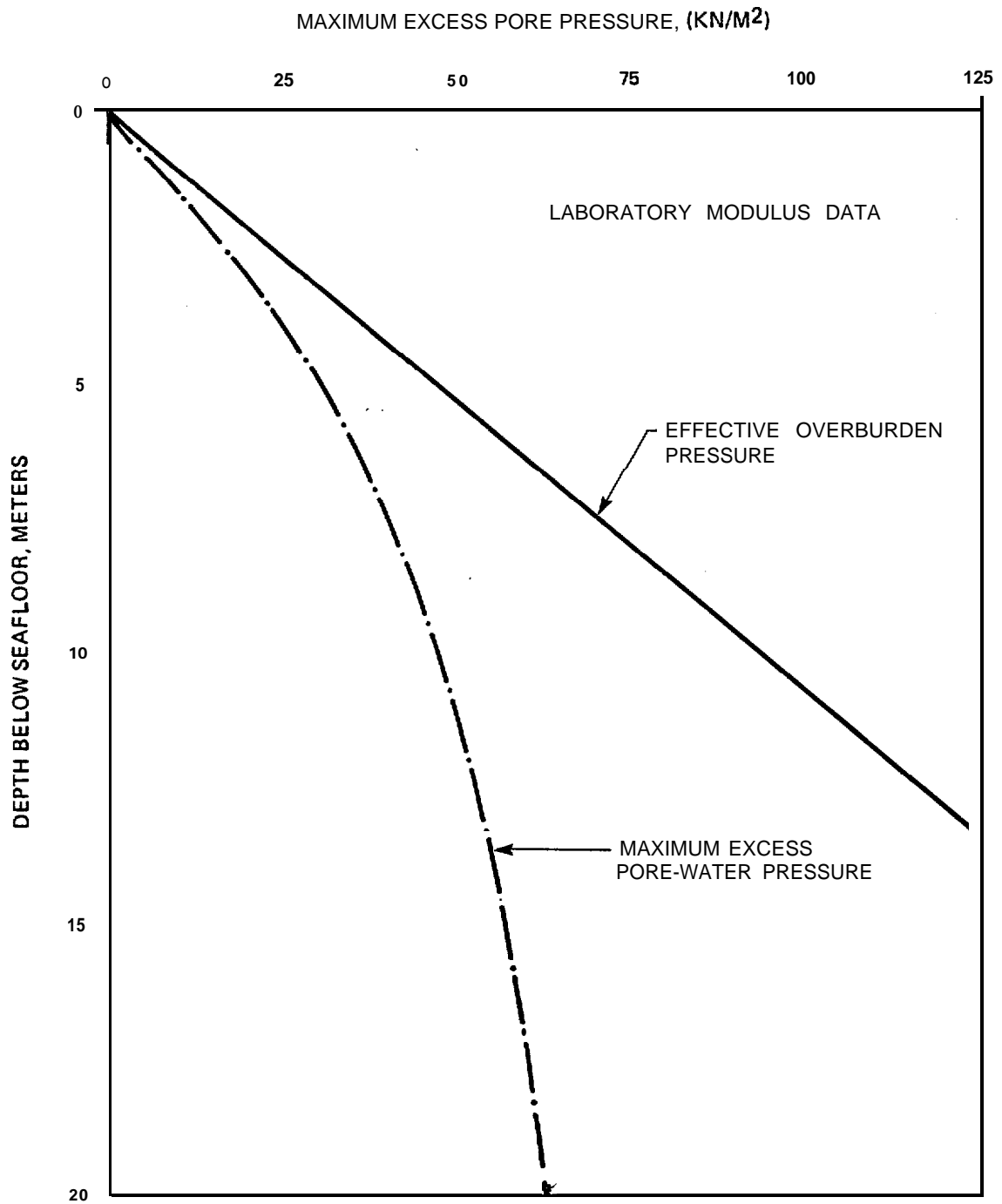
EARTHQUAKE SOURCE SUBDUCTION ZONE

EARTHQUAKE RECORD (NORMALIZED TO $A_{max}^{0.16g}$) CAL TECH A-1

MAXIMUM GROUND ACCELERATION A_{max}

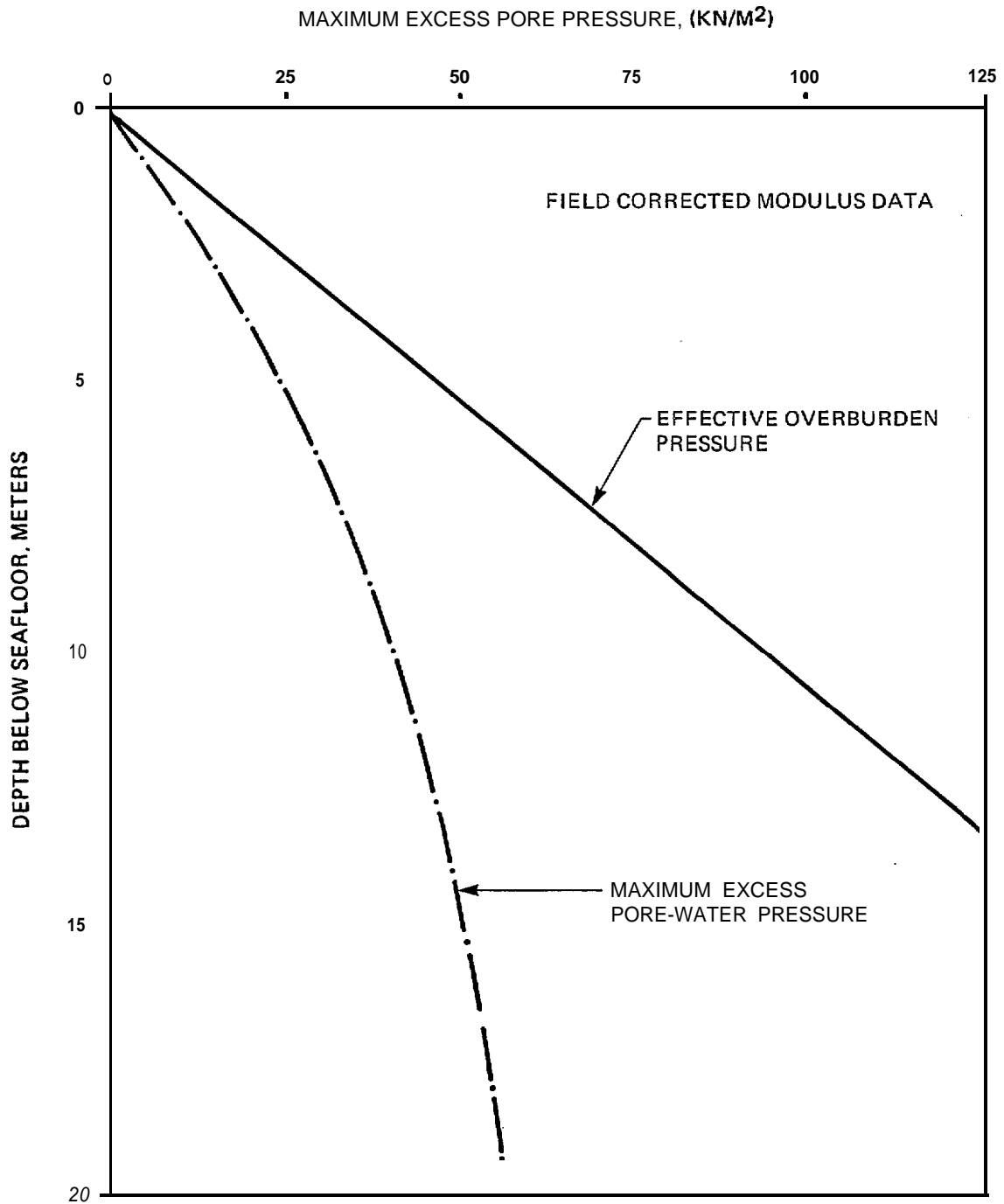
CONCLUSION: NO LIQUEFACTION

FIGURE IV-38 MAXIMUM EXCESS PORE PRESSURE RESPONSE CURVE
(SM4, SUBDUCTION ZONE, 0.16g)



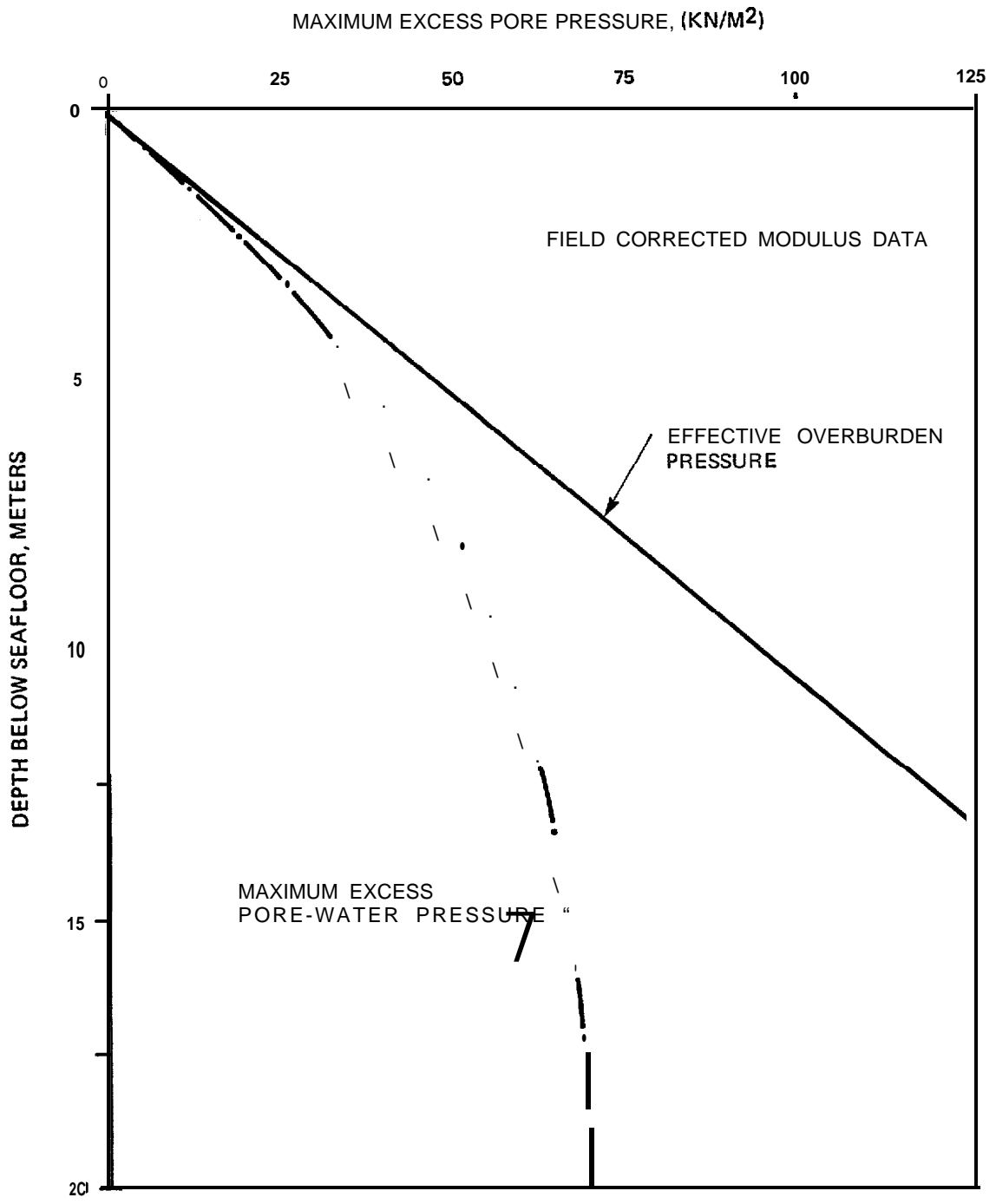
SOIL TYPE SM (4)
 EARTHQUAKE SOURCE SUBDUCTION ZONE
 EARTHQUAKE RECORD (NORMALIZED TO $A_{max} \cong 0.16g$) CAL TECH A-1
 MAXIMUM GROUND ACCELERATION A_{max}
 CONCLUSION: NO LIQUEFACTION

FIGURE IV-39 MAXIMUM EXCESS PORE PRESSURE RESPONSE CURVE
 (SM4, SUBDUCTION ZONE, 0.16g)



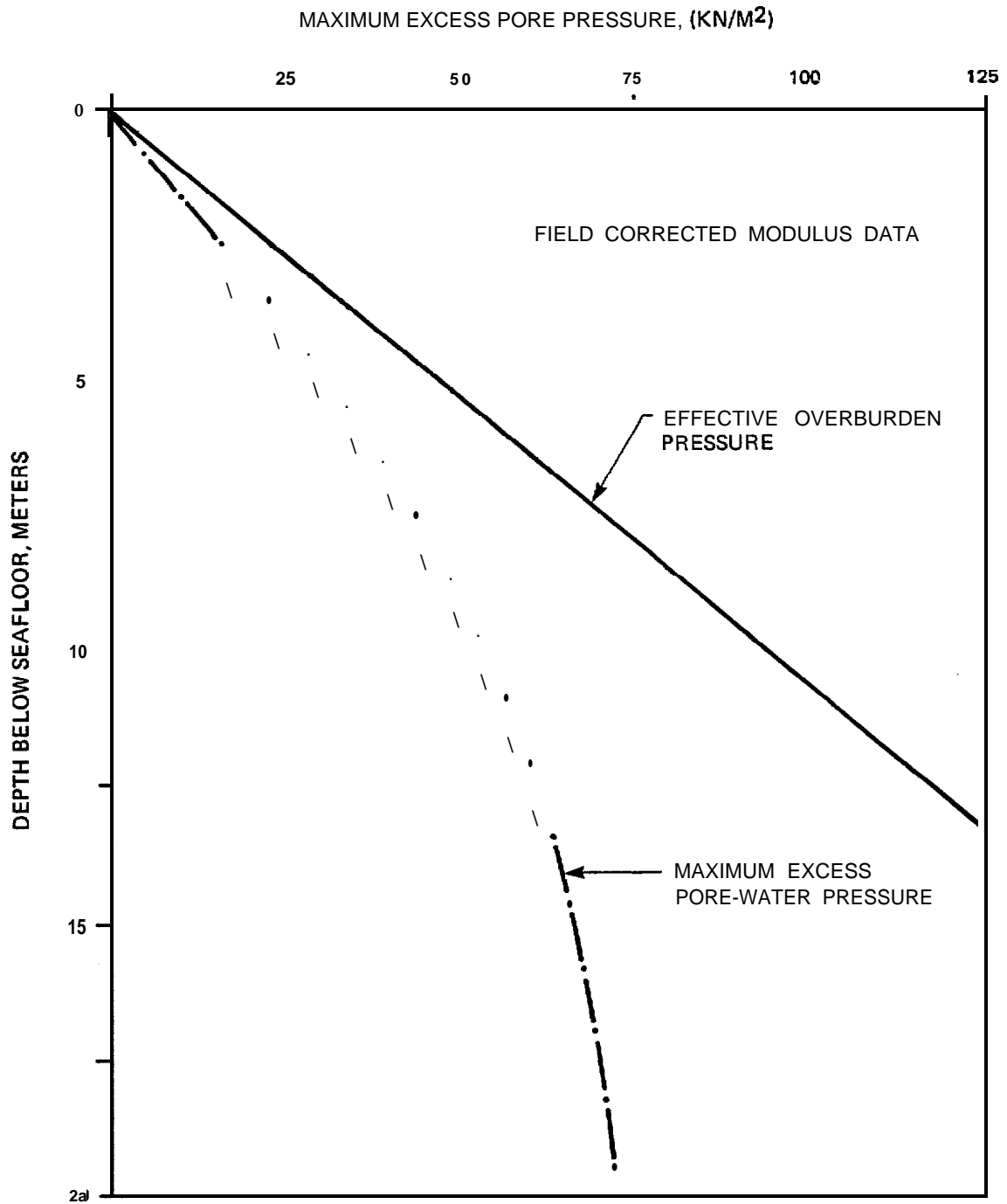
SOIL TYPE SM (4)
 EARTHQUAKE SOURCE SUBDUCTION ZONE
 EARTHQUAKE RECORD (NORMALIZED TO $A_{max} = 0.19g$) CAL TECH A-1
 MAXIMUM GROUND ACCELERATION $= A_{max}$
 CONCLUSION: NO LIQUEFACTION

FIGURE IV-40 MAXIMUM EXCESS PORE PRESSURE RESPONSE CURVE
 (SM4, SUBDUCTION ZONE, 0.19g)



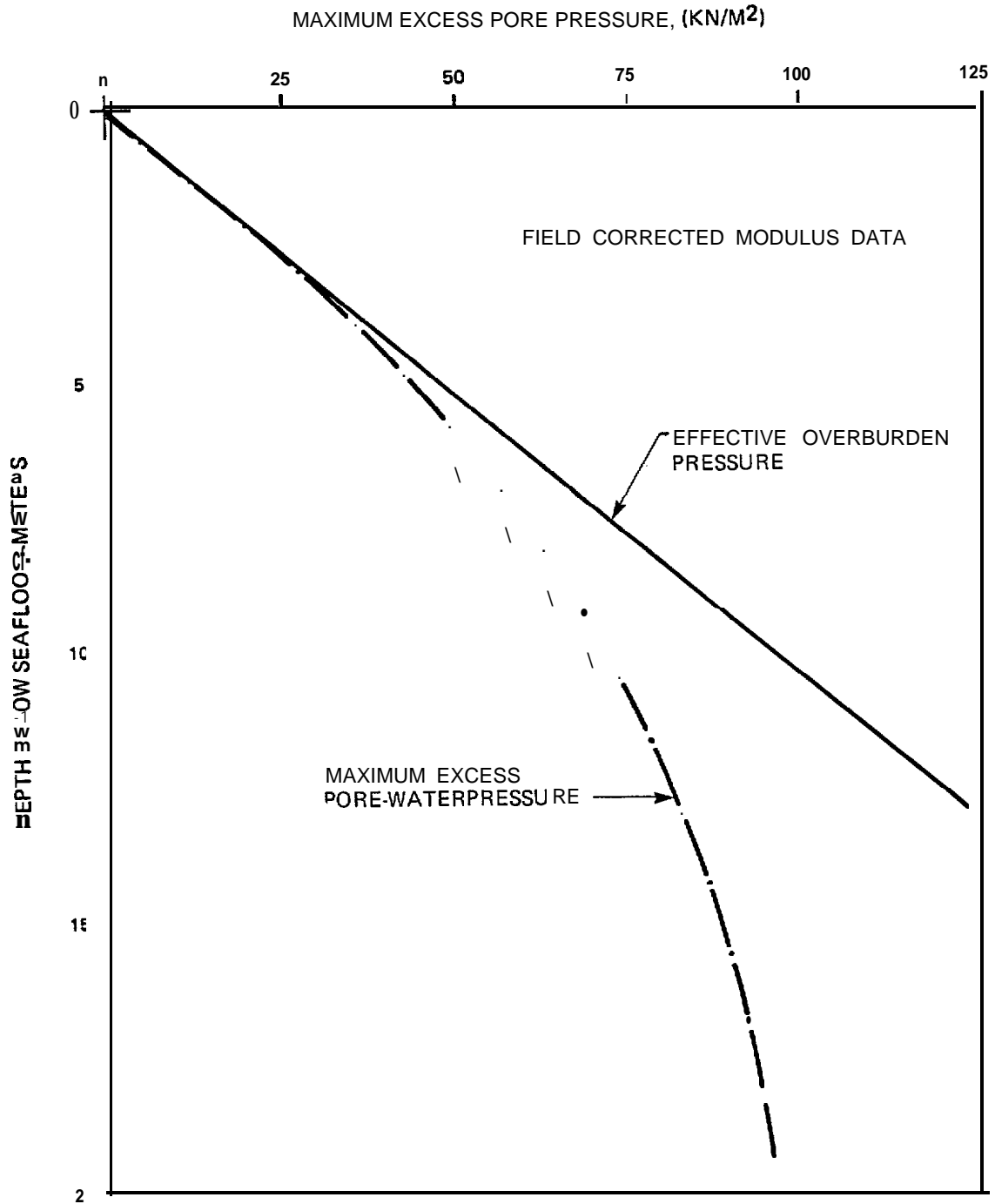
SOIL TYPE SM (4)
 EARTHQUAKE SOURCE MAJOR GRABENS
 EARTHQUAKE RECORD (NORMALIZED TO A_{max} 0.4g) TAFT 1952
 MAXIMUM GROUND ACCELERATION $= A_{max}$ _____
 CONCLUSION: NO LIQUEFACTION

FIGURE IV-41 MAXIMUM EXCESS PORE PRESSURE RESPONSE CURVE
 (SM4, MAJOR GRABENS, 0.4g)



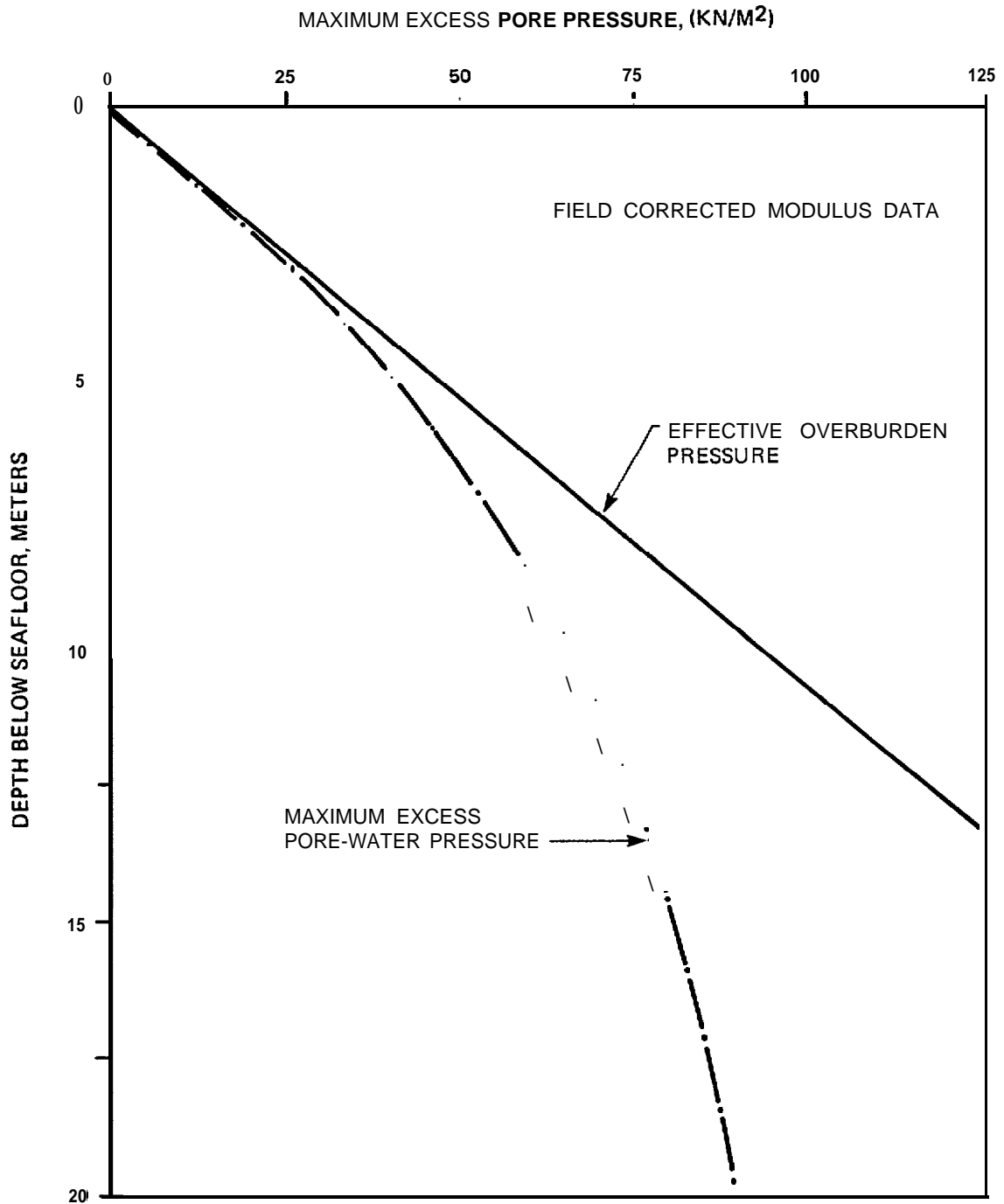
SOIL TYPE SM (s)
 EARTHQUAKE SOURCE MAJOR GRABENS
 EARTHQUAKE RECORD (NORMALIZED TO $A_{max} = 0.4g$) EL CENTRO 1940
 MAXIMUM GROUND ACCELERATION = A_{max}
 CONCLUSION: NO LIQUEFACTION

FIGURE IV-42 MAXIMUM EXCESS PORE PRESSURE RESPONSE CURVE
 (SM4, MAJOR GRABENS, 0.4g)



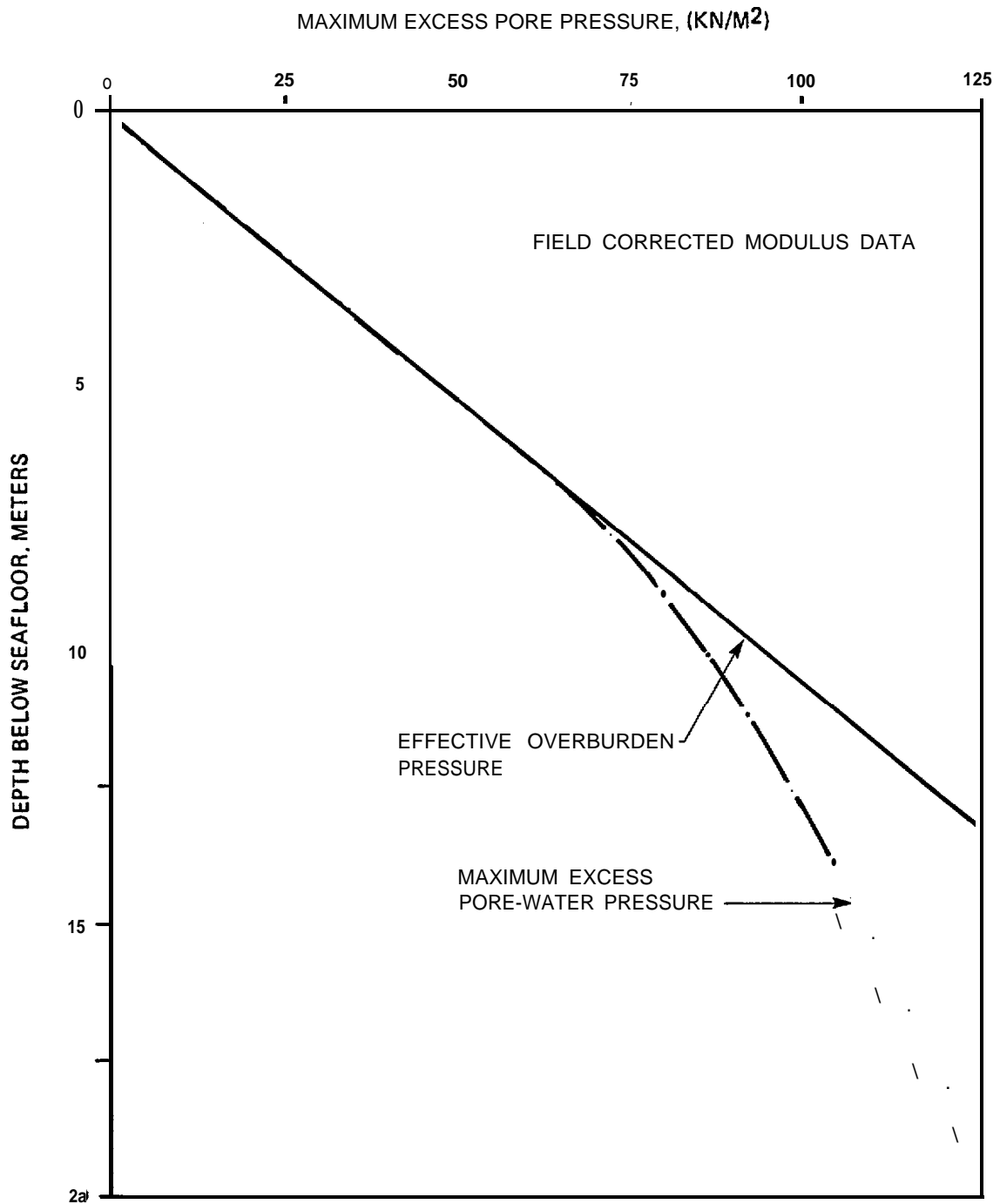
SOIL TYPE SM (4)
 EARTHQUAKE SOURCE MAJOR GRABENS
 EARTHQUAKE RECORD (NORMALIZED TO $A_{max} = 0.5g$) TAFT 1952
 MAXIMUM GROUND ACCELERATION $= A_{max}$
 CONCLUSION: LIQUEFACTION TO 3 M

FIGURE IV-43 MAXIMUM EXCESS PORE PRESSURE RESPONSE CURVE (SM4, MAJOR GRABENS, 0.5g)



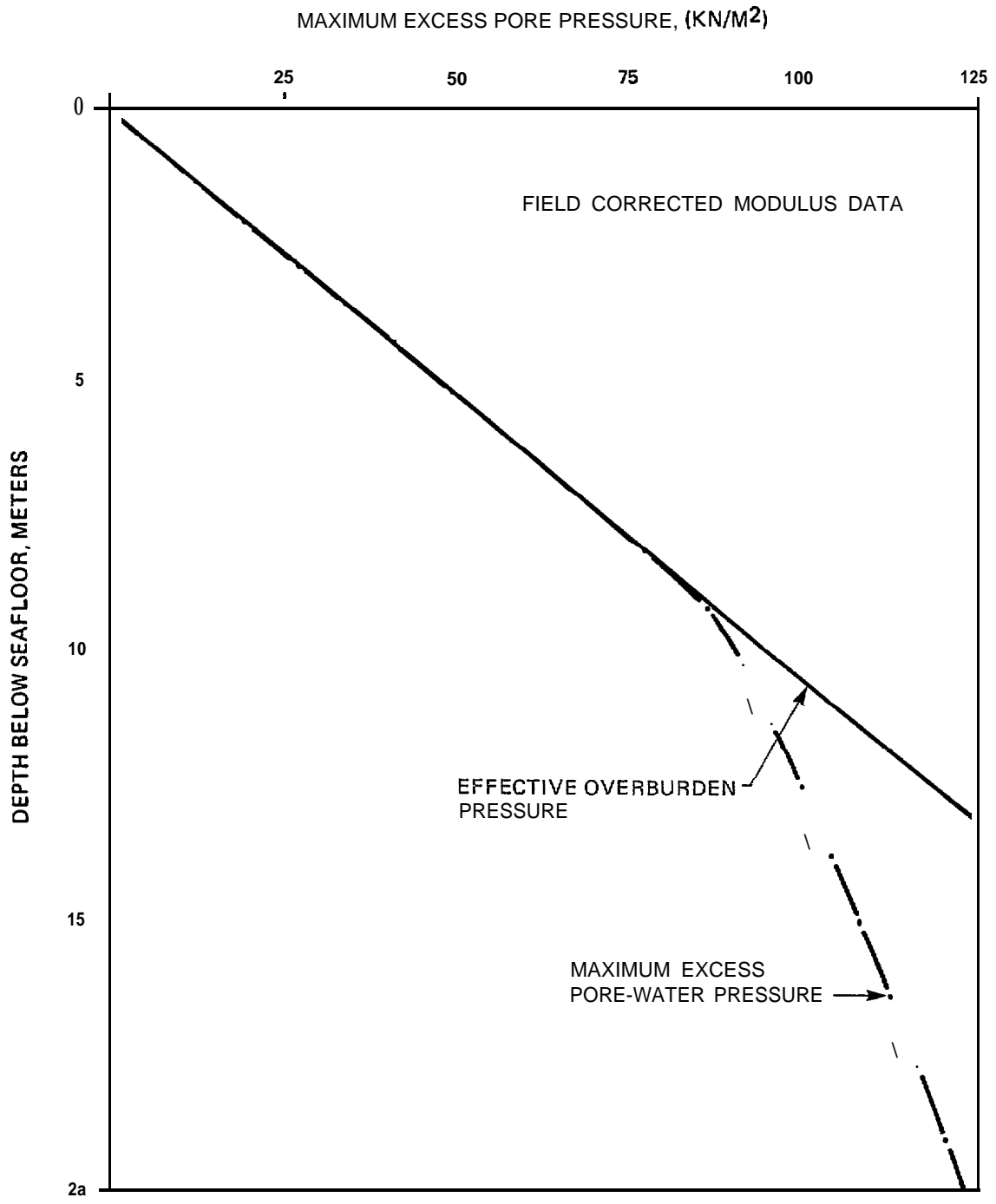
SOIL TYPE SM (4)
 EARTHQUAKE SOURCE MAJOR GRABENS
 EARTHQUAKE RECORD (NORMALIZED TO $A_{max} = 0.5g$) EL CENTRO 1940
 MAXIMUM GROUND ACCELERATION $\approx A_{max}$
 CONCLUSION: NO LIQUEFACTION

FIGURE IV-44 MAXIMUM EXCESS PORE PRESSURE RESPONSE CURVE
 (SM4, MAJOR GRABENS, 0.5g)



SOIL TYPE SM (4)
 EARTHQUAKE SOURCE MAJOR GRABENS
 EARTHQUAKE RECORD (NORMALIZED TO $A_{max} = 0.7g$) TAFT 1952
 MAXIMUM GROUND ACCELERATION A_{max}
 CONCLUSION: LIQUEFACTION TO' 8 M

FIGURE IV-45 MAXIMUM EXCESS PORE PRESSURE RESPONSE CURVE
 (SM4, MAJOR GRABENS, 0.7g)



SOIL TYPE SM (4)

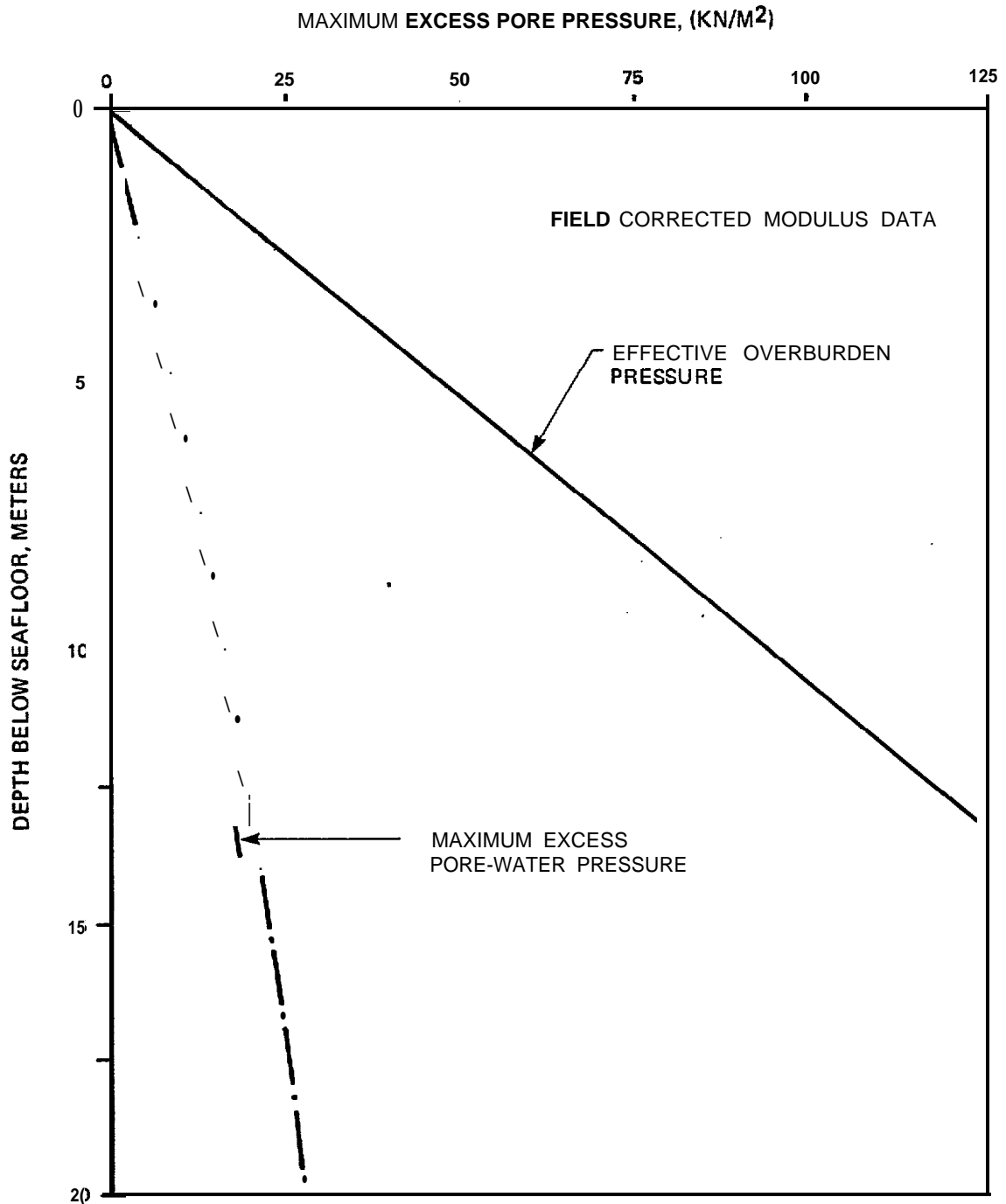
EARTHQUAKE SOURCE MAJOR GRABENS

EARTHQUAKE RECORD (NORMALIZED TO 0.7g) EL CENTRO 1940

MAXIMUM GROUND ACCELERATION = A_{max}

CONCLUSION: LIQUEFACTION TO 9 M

FIGURE IV-46 MAXIMUM EXCESS PORE PRESSURE RESPONSE CURVE
(SM4, MAJOR GRABENS, 0.7g)



SOIL TYPE SM (4)

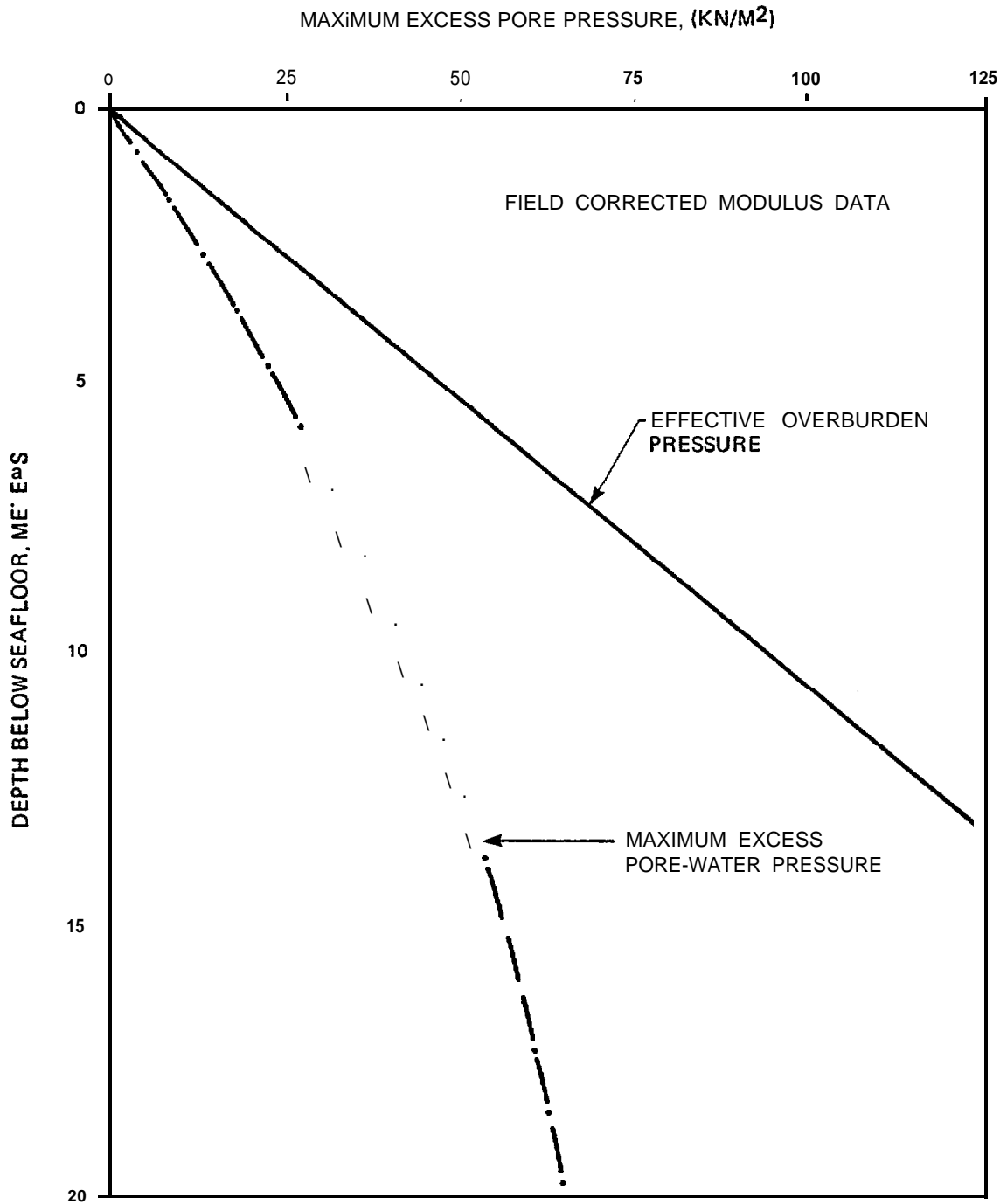
EARTHQUAKE SOURCE BACK ARC FAULTS

EARTHQUAKE RECORD (NORMALIZED TO $A_{max}^{0.3g}$) EL CENTRO 1979

MAXIMUM GROUND ACCELERATION A_{max}

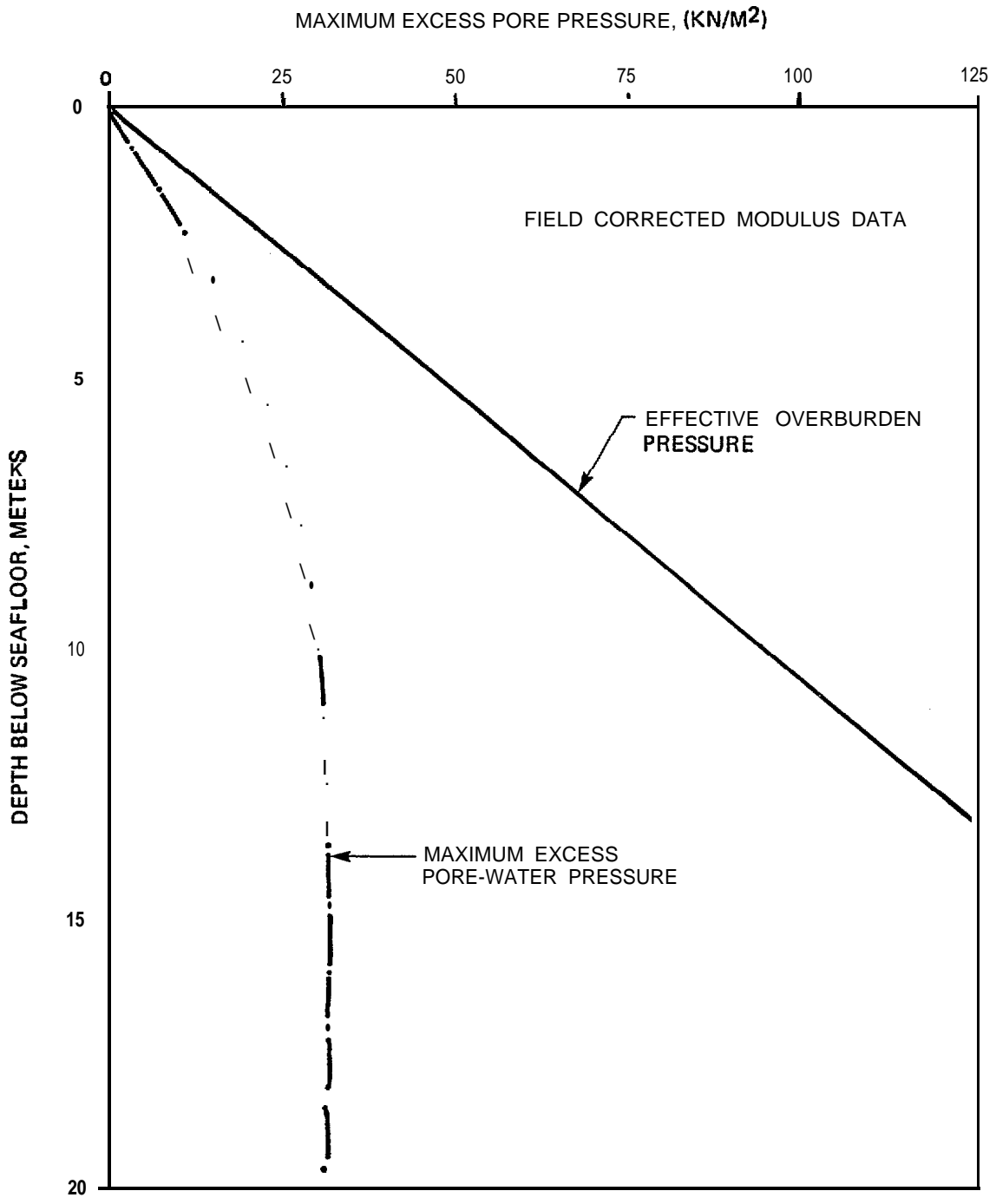
CONCLUSION: NO LIQUEFACTION

FIGURE IV-47 MAXIMUM EXCESS PORE PRESSURE RESPONSE CURVE
(SM4, BACK ARC FAULTS, 0.3g)



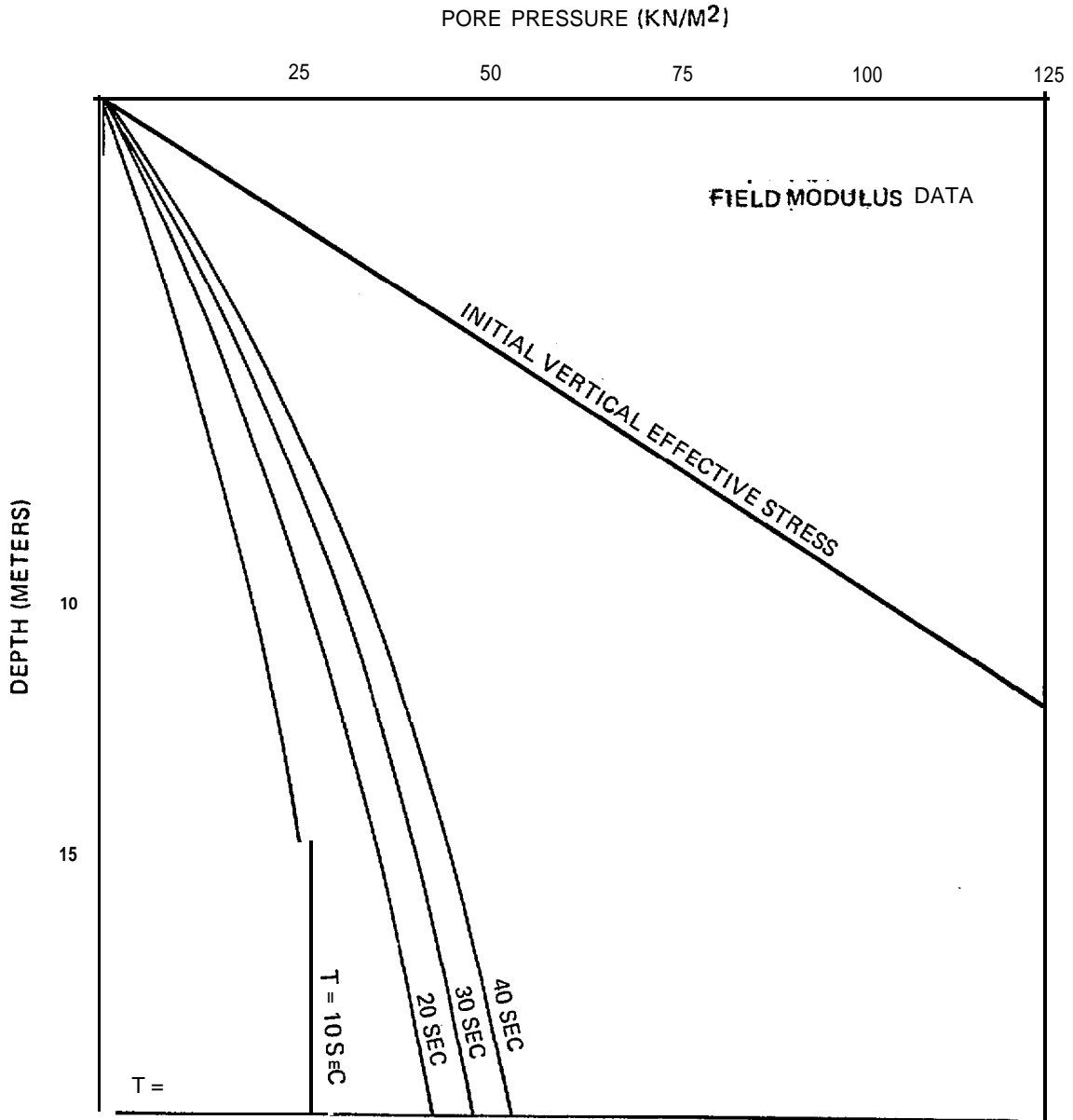
SOIL TYPE SM (4)
 EARTHQUAKE SOURCE BACK ARC FAULTS
 EARTHQUAKE RECORD (NORMALIZED TO $A_{max} = 0.6g$) EL CENTRO 1979
 MAXIMUM GROUND ACCELERATION " A_{max} "
 CONCLUSION: NO LIQUEFACTION

FIGURE IV-48 MAXIMUM EXCESS PORE PRESSURE RESPONSE CURVE
 (SM4, BACK ARC FAULTS, 0.6g)



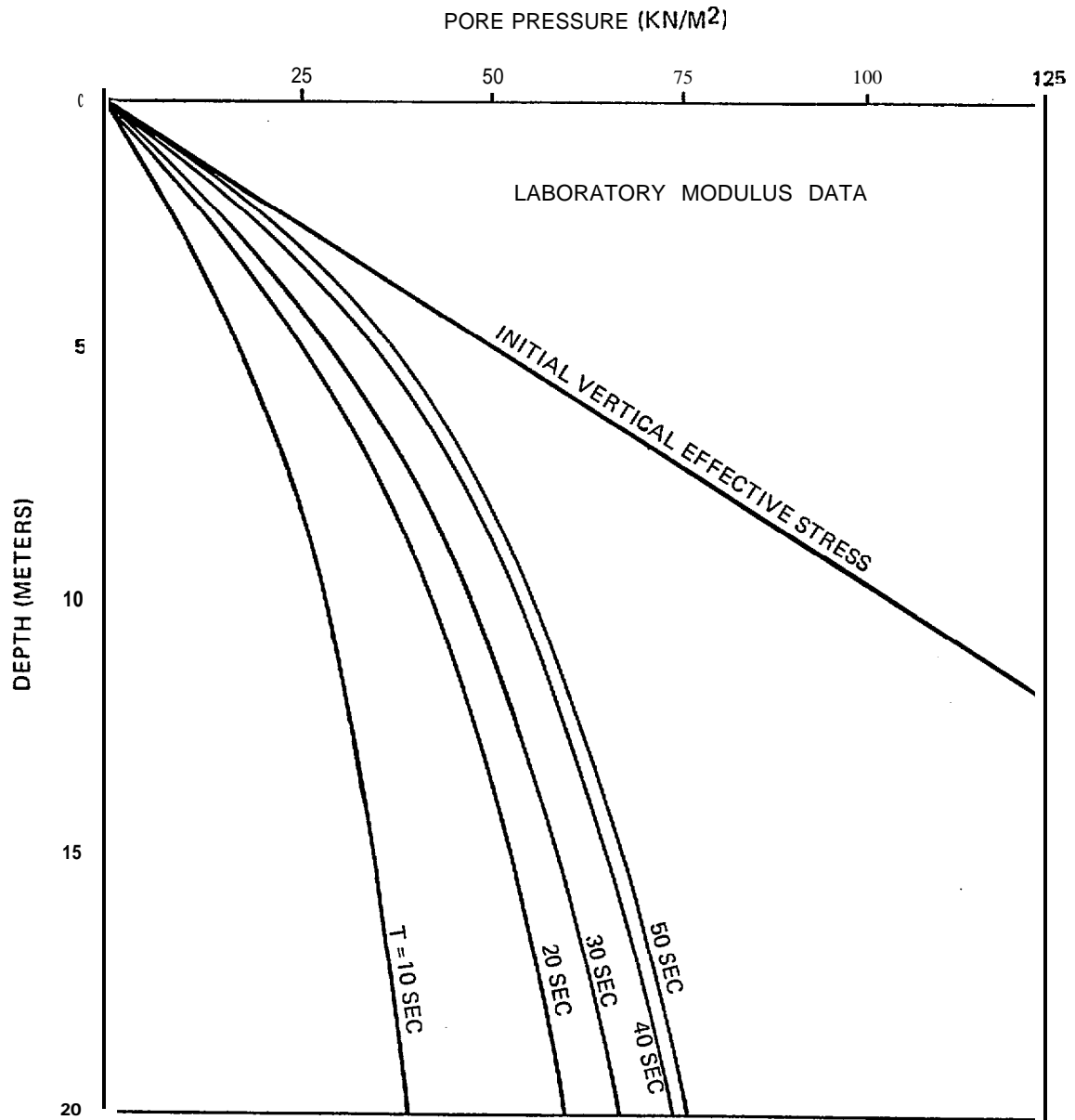
SOIL TYPE SM (4)
 EARTHQUAKE SOURCE ALEUTIAN ARC
 EARTHQUAKE RECORD (NORMALIZED TO $A_{max} = 0.49$) PARKFIELD 1966
 MAXIMUM GROUND ACCELERATION A_{max}
 CONCLUSION: NO LIQUEFACTION

FIGURE IV-49 MAXIMUM EXCESS PORE PRESSURE RESPONSE CURVE
 (SM4, ALEUTIAN ARC, 0.4g)



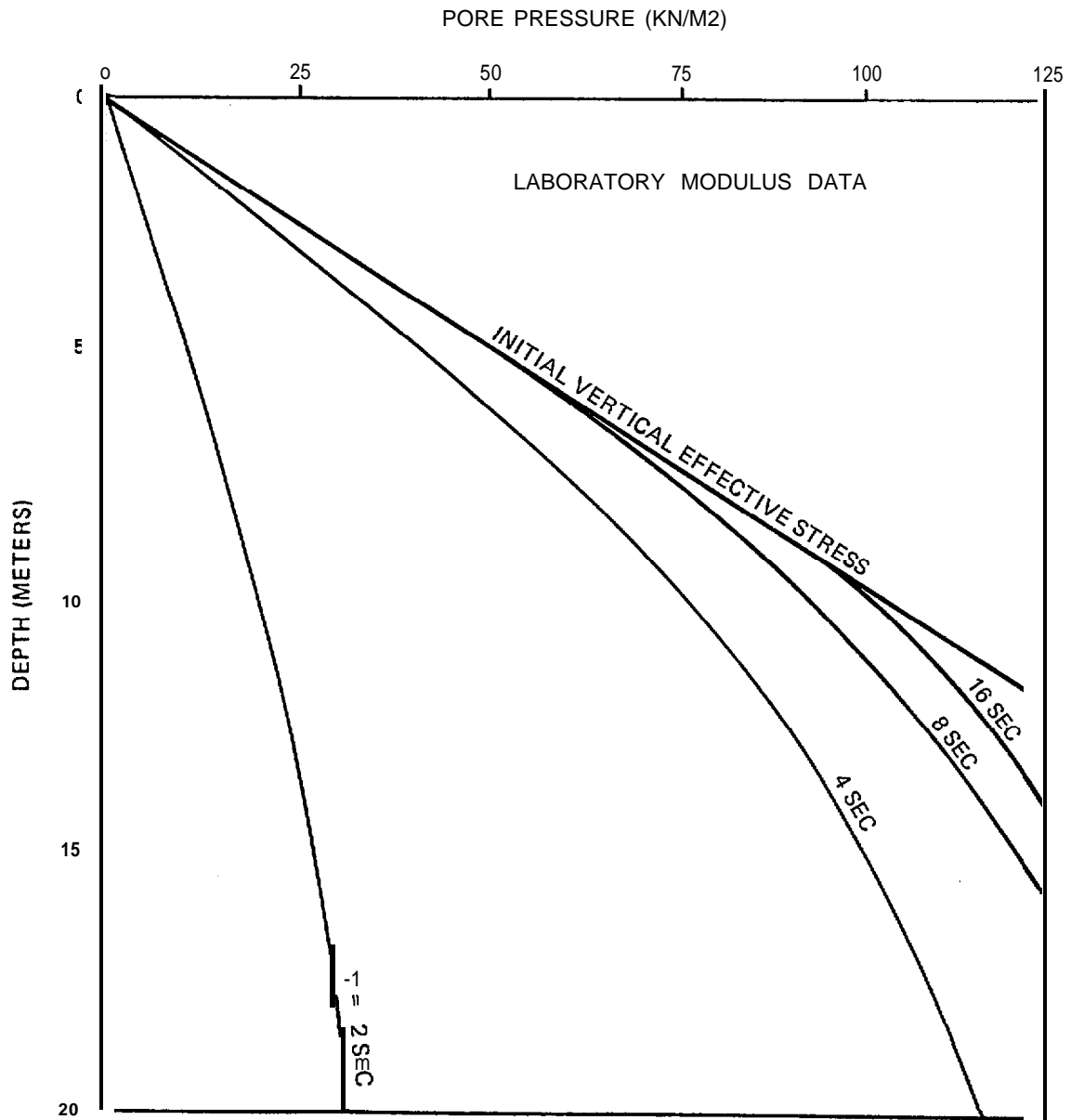
SOIL TYPE (PROFILE) sp (2)
 EARTHQUAKE SOURCE SUBDUCTION ZONE
 EARTHQUAKE RECORD (NORMALIZED TO $\hat{A}_{max} =$) CAL TECH A-1
 MAXIMUM GROUND ACCELERATION = \hat{A}_{max}
 CONCLUSION : NO LIQUEFACTION

FIGURE IV-50 PORE PRESSURE RESPONSE CURVES (SP2, SUBDUCTION ZONE, 0.16g)



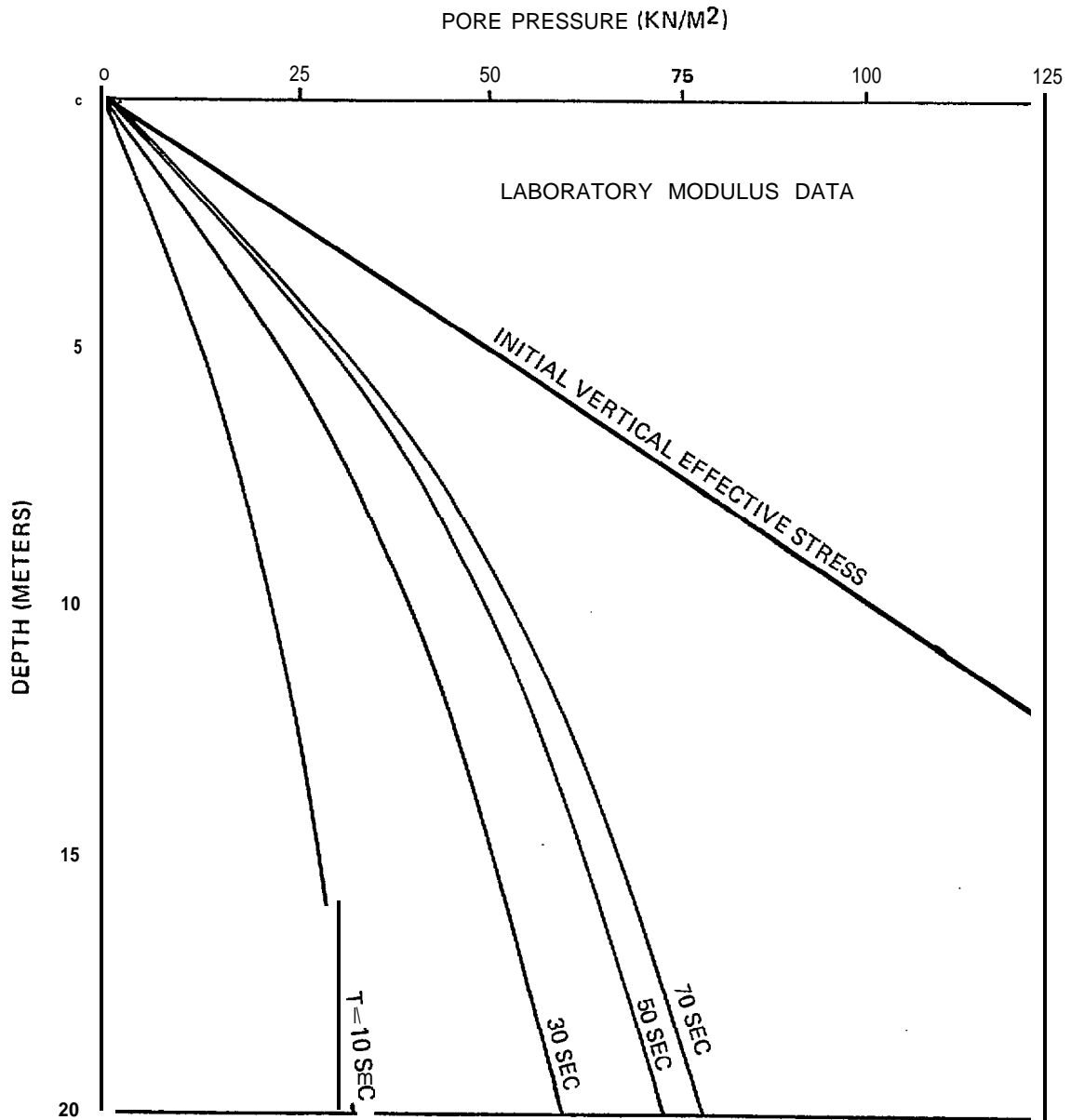
SOIL TYPE (PROFILE) sp (2)
 EARTHQUAKE SOURCE subduction ZONE
 EARTHQUAKE RECORD (NORMALIZED TO $A_{max} = 0.16g$) CAL TECH A-1
 MAXIMUM GROUND ACCELERATION = A_{max}
 CONCLUSION: LIQUEFACTION TO 1M

FIGURE IV-51 PORE PRESSURE RESPONSE CURVES (SP2, SUBDUCTION ZONE, 0.16g)



SOIL TYPE (PROFILE) sp (2)
 EARTHQUAKE SOURCE MAJOR GRABENS
 EARTHQUAKE RECORD (NORMALIZED TO $A_{max} = 0.7g$) EL CENTRO 1940
 MAXIMUM GROUND ACCELERATION A_{max}
 CONCLUSION: LIQUEFACTION TO > 8M

FIGURE IV-52 PORE PRESSURE RESPONSE CURVES (SP2, MAJOR GRABENS, 0.7g)



SOIL TYPE (PROFILE) SP/SM(3)

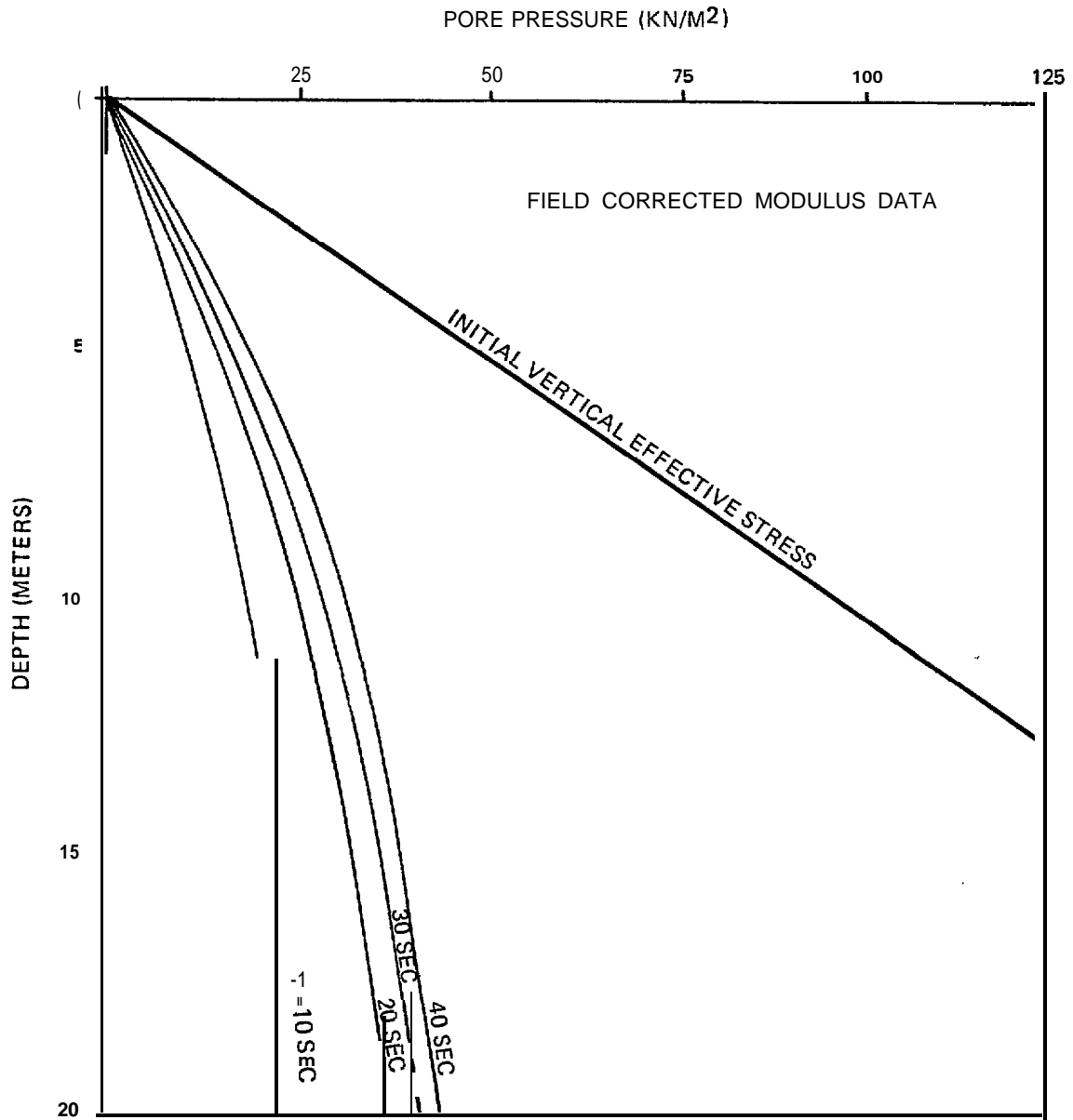
EARTHQUAKE SOURCE SUBDUCTION ZONE

EARTHQUAKE RECORD (NORMALIZED TO $A_{max} = 0.16g$) CAL TECH A-1

MAXIMUM GROUND ACCELERATION A_{max}

CONCLUSION: NO LIQUEFACTION

FIGURE IV-53 PORE PRESSURE RESPONSE CURVES (SP/SM3, SUBDUCTION ZONE, 0.16g)



SOIL TYPE (PROFILE) SM(4)

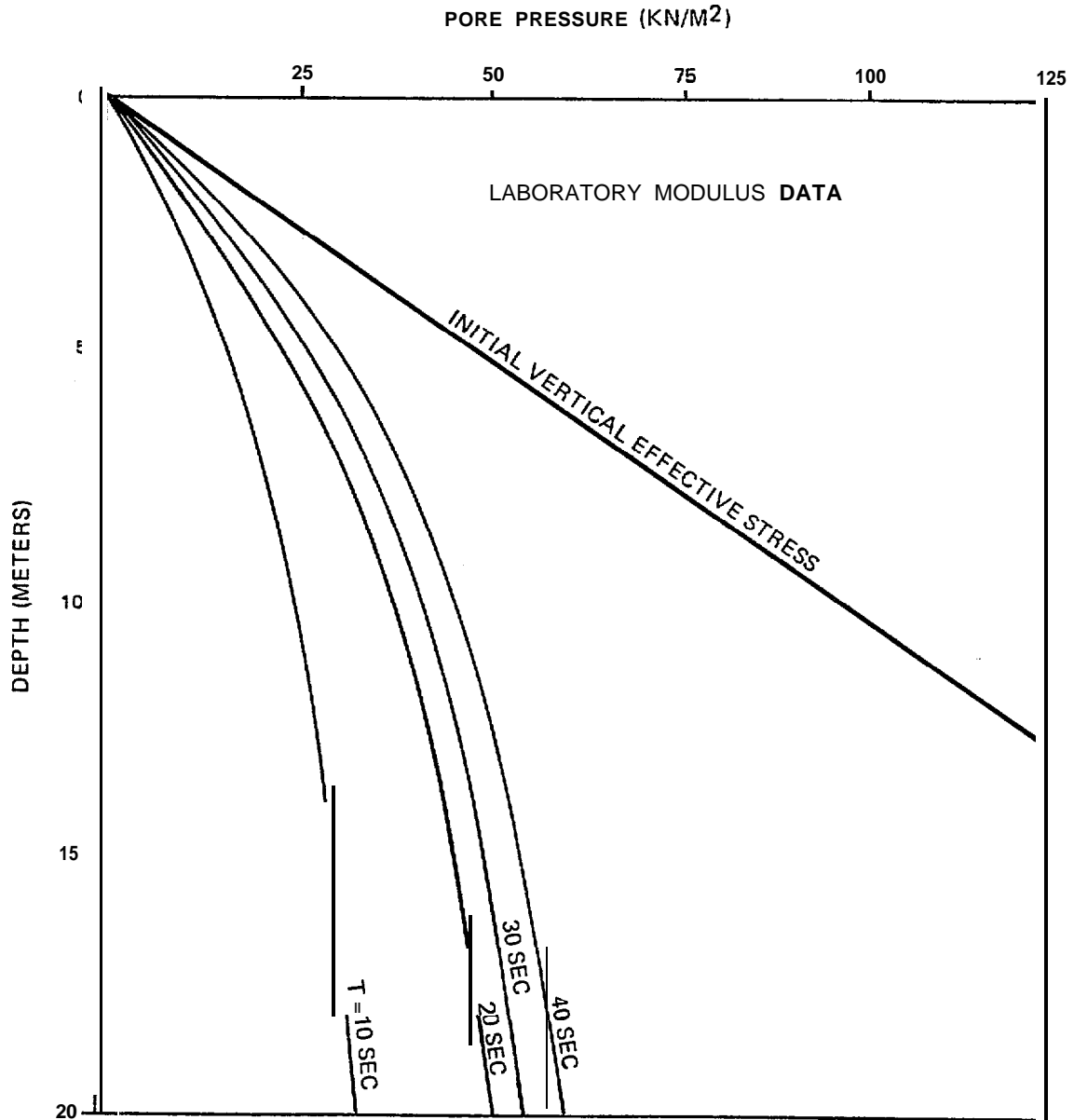
EARTHQUAKE SOURCE subduction ZONE

EARTHQUAKE RECORD (NORMALIZED TO $A_{max} = 0.16g$) CAL TECH A-1

MAXIMUM GROUND ACCELERATION " A_{max} "

CONCLUSION: NO LIQUEFACTION

FIGURE IV-54 PORE PRESSURE RESPONSE CURVES (SM4, SUBDUCTION ZONE, 0.16g)



SOIL TYPE (PROFILE) SM (4)

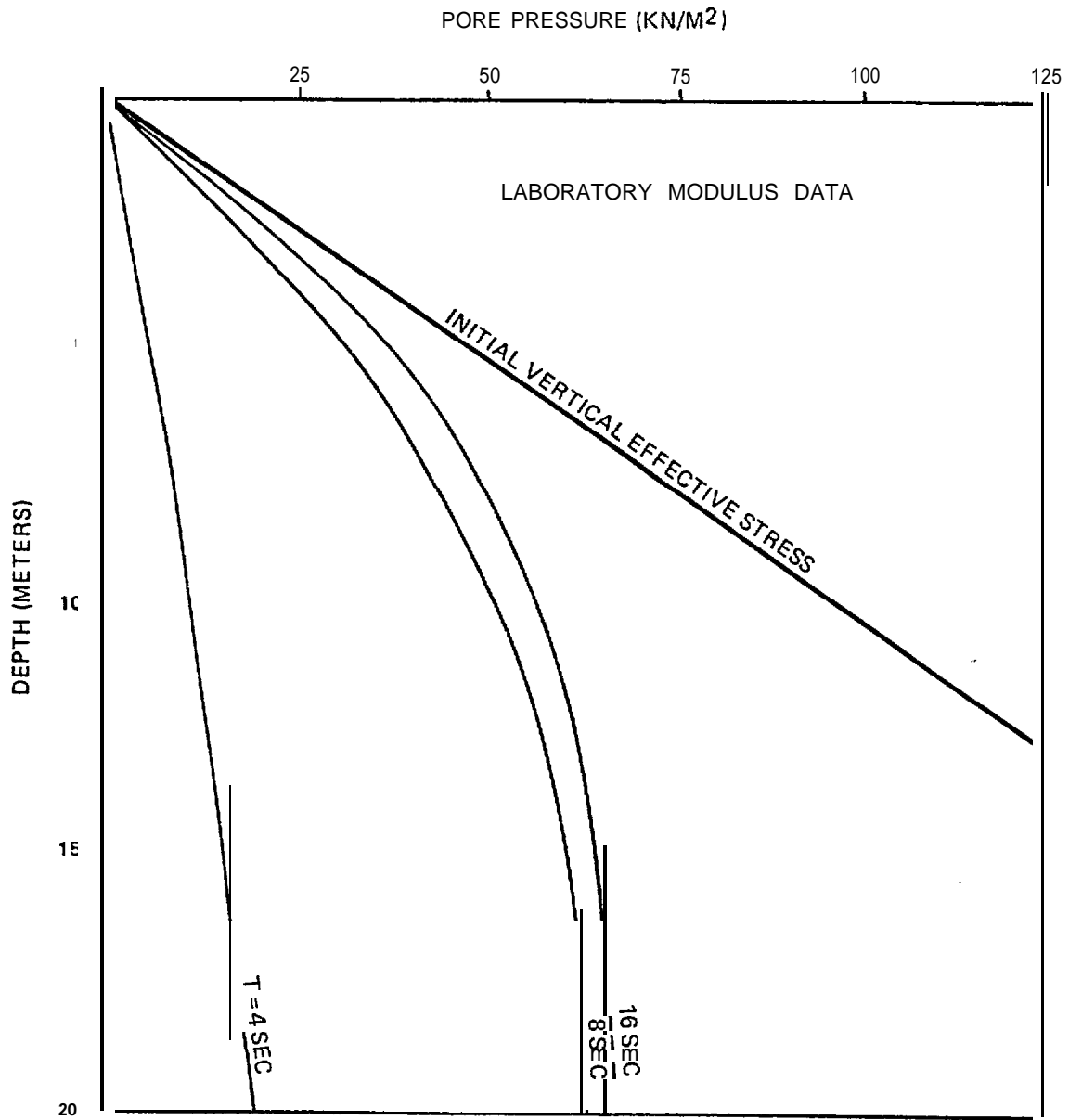
EARTHQUAKE SOURCE SUBDUCTION ZONE

EARTHQUAKE RECORD (NORMALIZED TO $A_{max} = 0.16g$) CAL TECH A-1

MAXIMUM GROUND ACCELERATION A_{max}

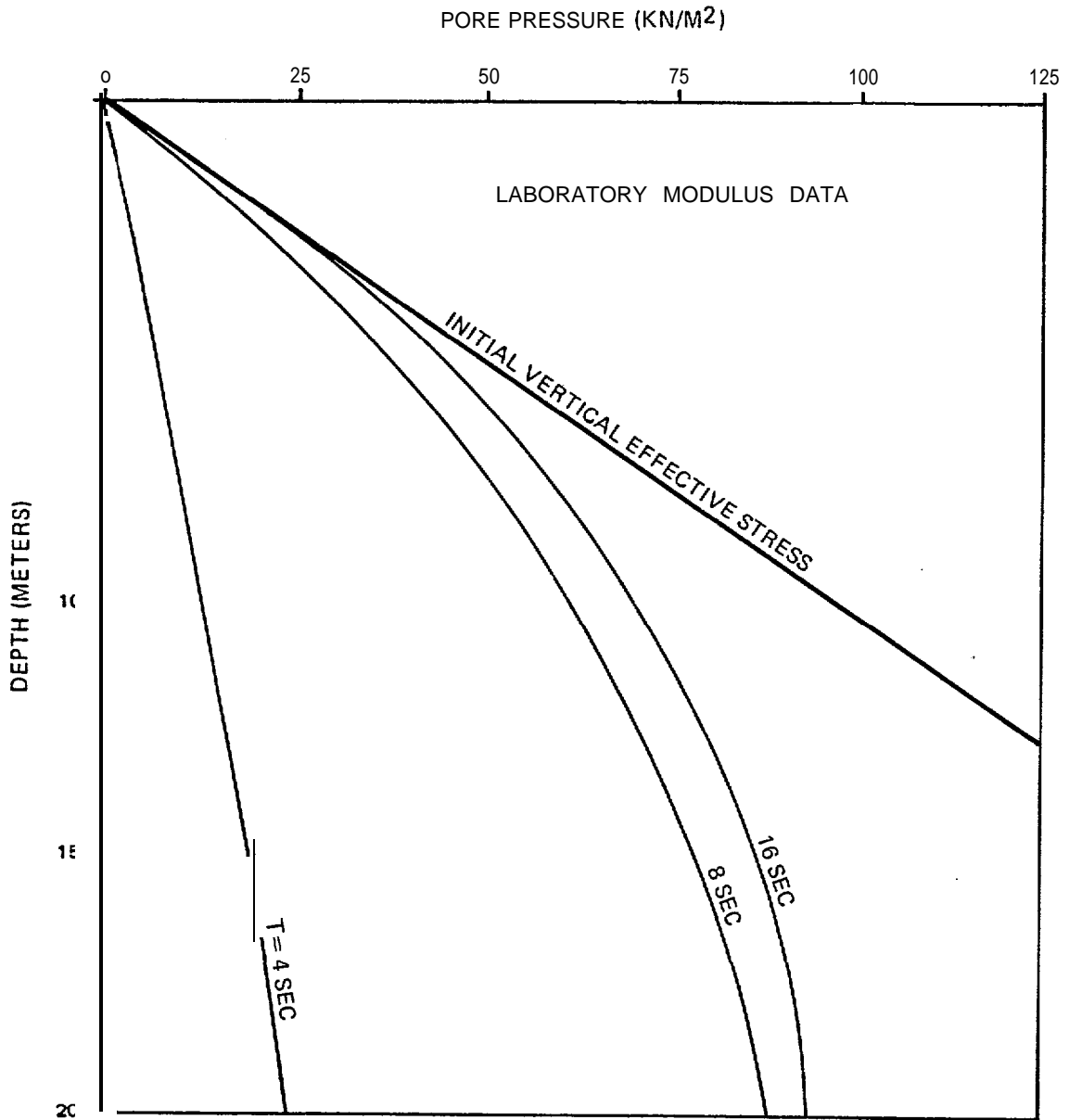
CONCLUSION: NO LIQUEFACTION

FIGURE IV-55 PORE PRESSURE RESPONSE CURVES (SM4, SUBDUCTION ZONE, 0.16g)



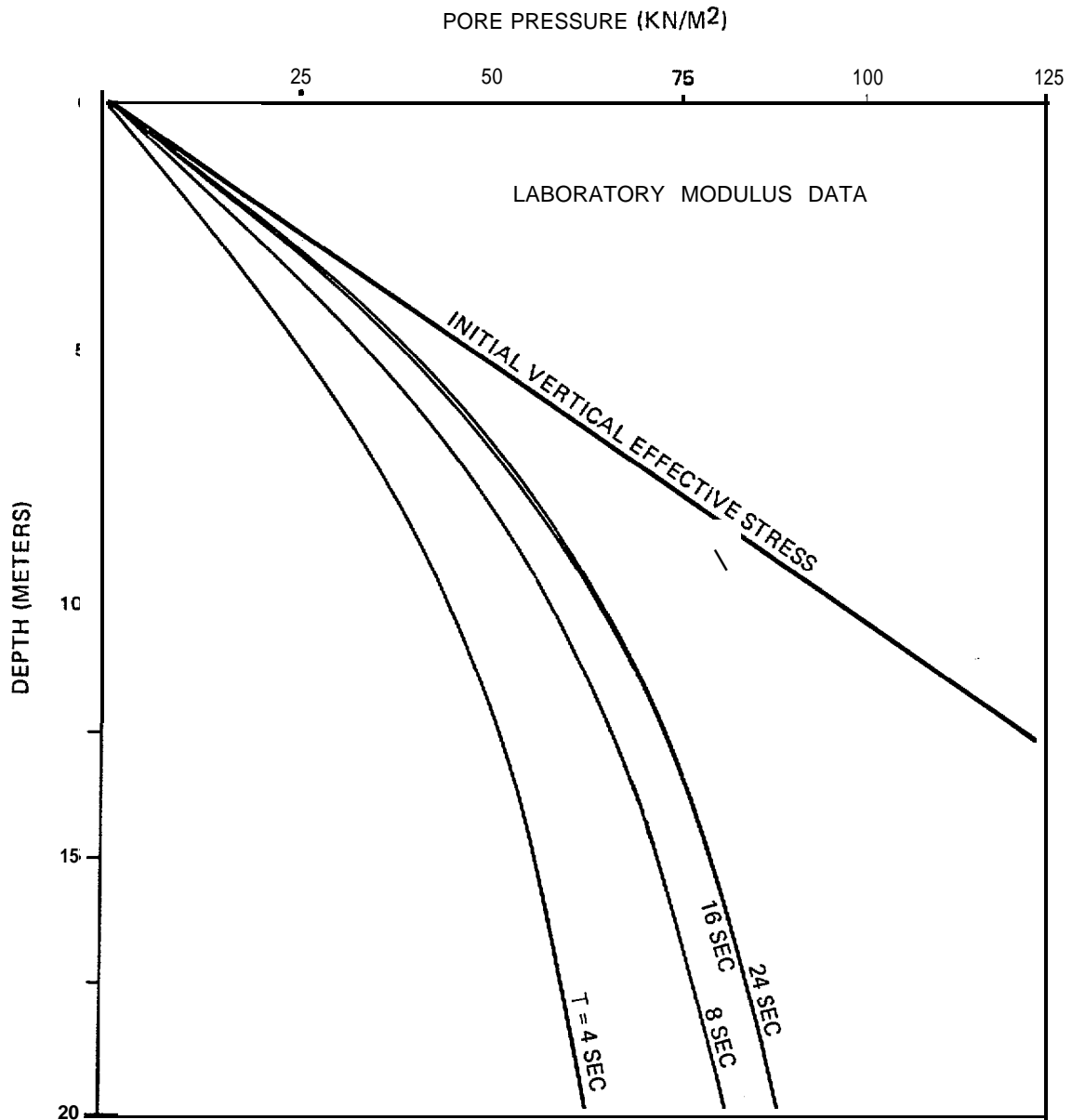
SOIL TYPE (PROFILE) SM (4)
 EARTHQUAKE SOURCE MAJOR GRABENS
 EARTHQUAKE RECORD (NORMALIZED TO $A_{max} = 0.49$) TAFT 1952
 MAXIMUM GROUND ACCELERATION A_{max}
 CONCLUSION: NO LIQUEFACTION .

FIGURE IV- 56 PORE PRESSURE RESPONSE CURVES (SM4, MAJOR GRABENS, 0.4g)



SOIL TYPE (PROFILE) SM (4)
 EARTHQUAKE SOURCE MAJOR GRABENS
 EARTHQUAKE RECORD (NORMALIZED TO $A_{max} = 0.5g$) TAFT 1952
 MAXIMUM GROUND ACCELERATION A_{max} _____
 CONCLUSION: LIQUEFACTION TO 3 M

FIGURE IV-57 PORE PRESSURE RESPONSE CURVES (SM4, MAJOR GRABENS, 0.5g)



SOIL TYPE (PROFILE) SM(4)

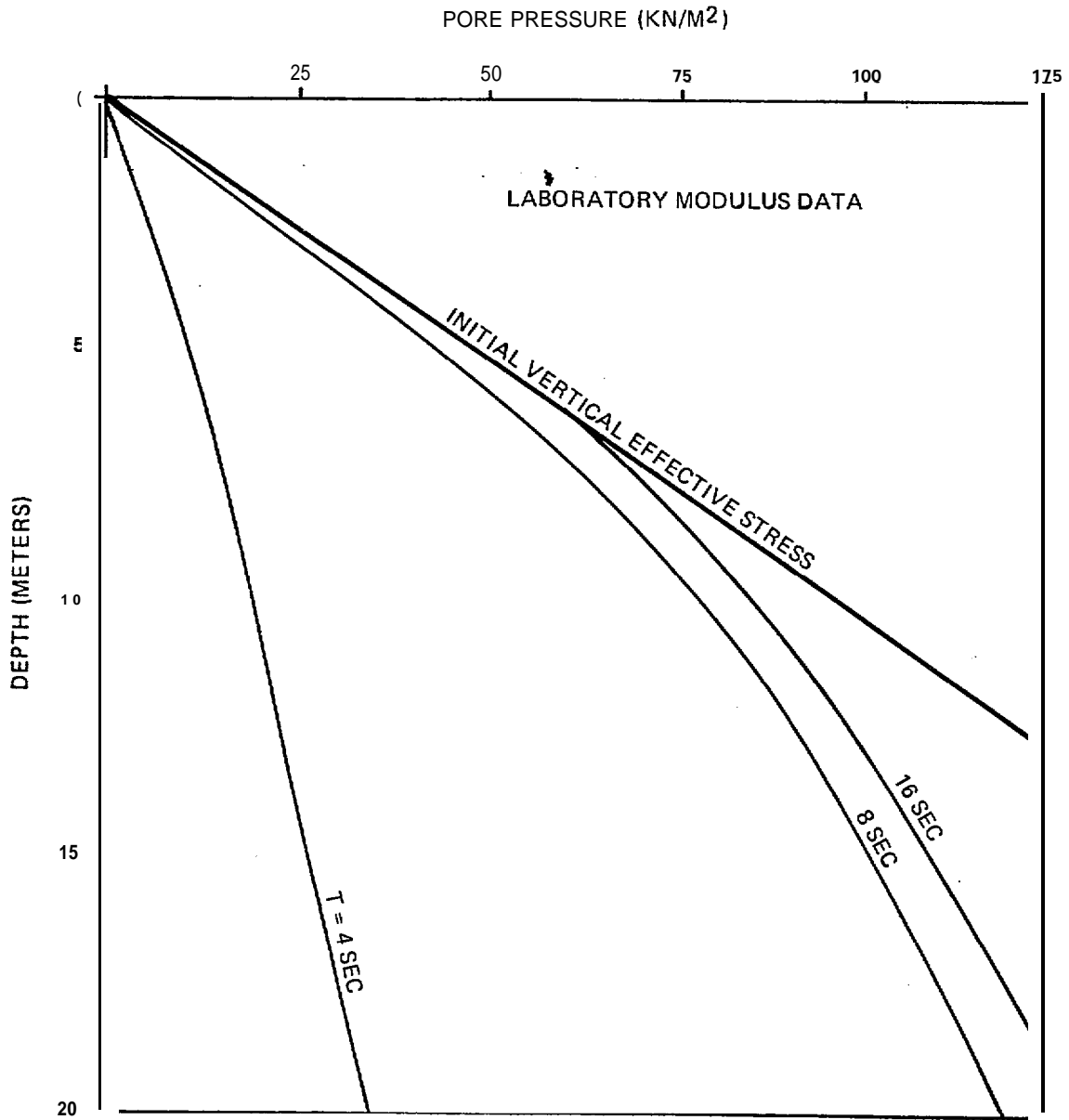
EARTHQUAKE SOURCE MAJOR GRABENS

EARTHQUAKE RECORD (NORMALIZED TO $A_{max} = 0.5g$) EL CENTRO 1940

MAXIMUM GROUND ACCELERATION A_{max}

CONCLUSION: NO LIQUEFACTION

FIGURE IV-58 PORE PRESSURE RESPONSE CURVES (SM4, MAJOR GRABENS, 0.5g)



SOIL TYPE (PROFILE) SM(4)

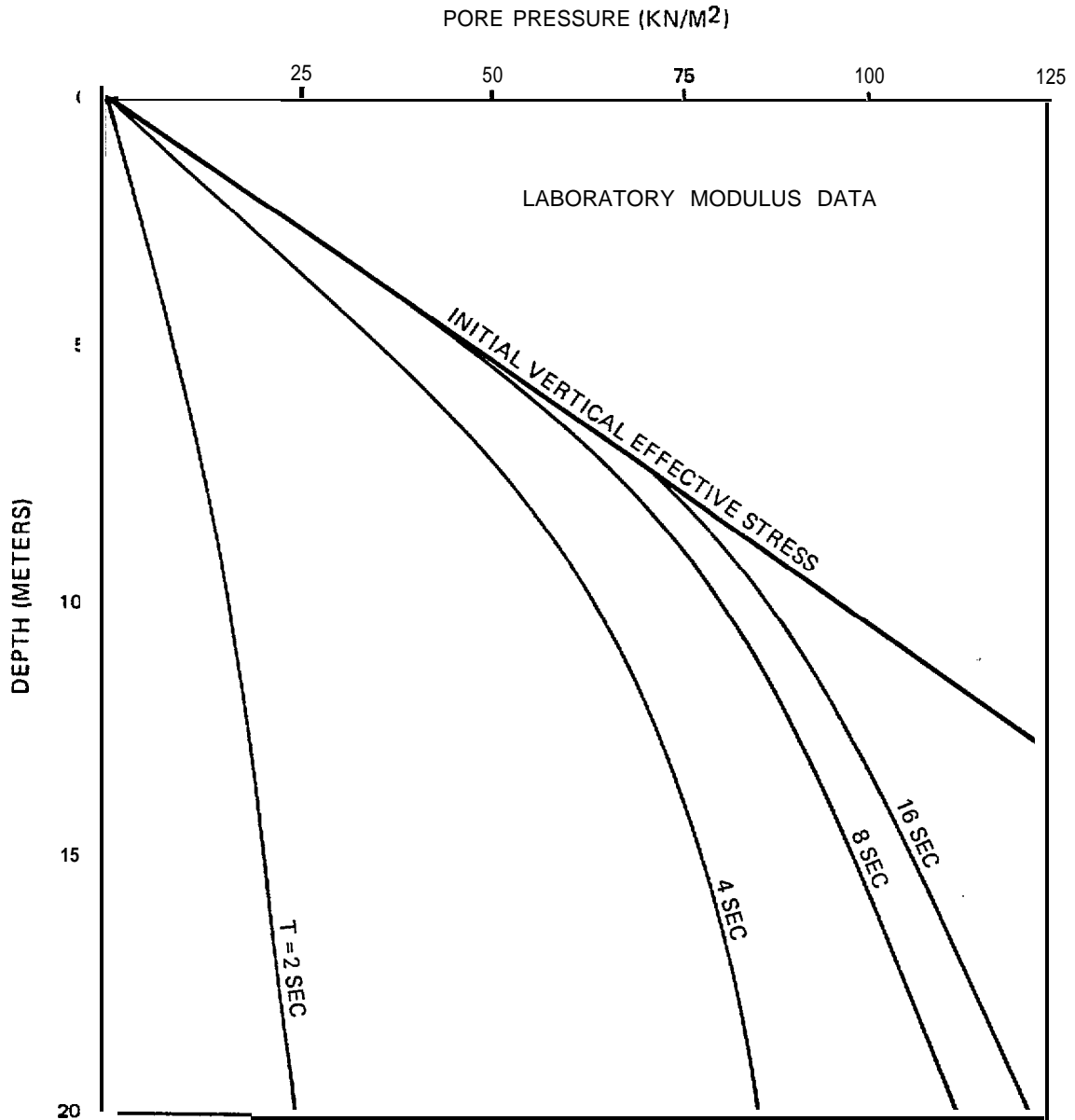
EARTHQUAKE SOURCE MAJOR GRABENS

EARTHQUAKE RECORD (NORMALIZED TO $A_{max} = 0.7g$) TAFT 1952

MAXIMUM GROUND ACCELERATION A_{max} _____

CONCLUSION: LIQUEFACTION TO >7M

FIGURE IV- 59 PORE PRESSURE RESPONSE CURVES (SM4, MAJOR GRABENS, 0.7g)



SOIL TYPE (PROFILE) SM (4)
 EARTHQUAKE SOURCE MAJOR GRABENS
 EARTHQUAKE RECORD (NORMALIZED TO $A_{max} = 0.7g$) EL CENTRO 1940
 MAXIMUM GROUND ACCELERATION A_{max} _____
 CONCLUSION: LIQUEFACTION TO $\geq 7M$

FIGURE IV-60 PORE PRESSURE RESPONSE CURVES (SM4, MAJOR GRABENS, 0.7g)